WARWICK
THE UNIVERSITY OF WARWICK

A Thesis Submitted for the Degree of PhD at the University of Warwick

Permanent WRAP URL:

http://wrap.warwick.ac.uk/181242

Copyright and reuse:
This thesis is made available online and is protected by original copyright.
Please scroll down to view the document itself.
Please refer to the repository record for this item for information to help you to cite it.
Our policy information is available from the repository home page.

For more information, please contact the WRAP Team at: wrap@warwick.ac.uk

warwick.ac.uk/lib-publications

WARWICK
THE UNIVERSITY OF WARWICK

Lessons in Photoprotection from Nature's Sunscreens: An Investigation of Photoactive Motifs in Synthetic Molecules

By

Adam Matthew Cowden

Thesis submitted for the degree of Doctor of Philosophy in Analytical Science

University of Warwick, Department of Chemistry

Molecular Analytical Science Centre for Doctoral Training

February 2023

i. Table of Contents

ii. Acknowledgements

iii. Declaration

iv. Abstract

v. List of Figures

vi. List of Tables

vii. Abbreviations

1. Introduction

1.1. Photochemistry, Sunscreens and Spectroscopy *1-2*

1.1.1 Historical perspective 2-4

1.1.2 Ultraviolet radiation 4

1.1.3 Solar radiation 4-5

1.1.4 Relationship between energy and wavelength 6-7

1.1.5 Laws of Photochemistry 7

1.1.6 Selection Rules and Principles of Electronic Spectroscopy 7-9

1.1.7 Relaxation from an Excited State 10-12

1.1.8 Internal Conversion and Conical Intersections 12-13

1.1.9 Intersystem Crossing and the Triplet State 13

1.1.10 Photostable process vs Bond-breaking/formation 14-15

1.1.11 Photosensitization 15

1.1.12 Effects of UVR in humans 15-16

1.1.13 Effects of UV on DNA 17-18

1.1.14 Notes on standards used in UV exposure 18-19

1.1.15 Sunscreens and Suncreams 19-20

1.1.16 Sunscreen safety 20-21

1.1.17 Natural sunscreens and photoprotectants 21-22

1.1.18 Mycosporine-like Amino Acids 23-26

1.1.19 Natural synthetic pathways of MAAs 26-27

1.1.20 Identifying MAAs by HPLC-MS 27

1.1.21 Bathochromic shifts in UV absorption spectra 27-28

1.1.22 The evolving definition of ultrafast 29

1.1.23 Transient Electron Absorption Spectroscopy (TEAS) (Solution-Phase) 29-31

1.1.24 Photochemical Processes as Signals on Electronic Transient Absorption Spectra 31-33

1.1.25 Transient Vibrational Absorption Spectroscopy (TVAS) 33

1.1.26 Defining an ideal and promising sunscreen molecule 33-34

1.1.27 In silico toxicology 34

1.2 Case studies on photochemistry of sunscreens

1.2.1 Photoprotection in Natural Product Mycosporine-like Amino Acids 35-37

1.2.2 Photoprotection in oxybenzone 38

1.2.3 Photoprotection in sinapoyl malate 39-40

1.2.4 Visualising photoprotection in 3 dimensions 40-42

1.3 Chapter summary 43

2. Materials and Methods (Synthesis)

2.1 General Synthesis Notes 44

2.2 Synthesis of singly substituted MAA derivatives based on oxo-mycosporines 45-51

2.3 Synthesis of substrates for biological assays

2.3.1. MAA-derivatives 52-53

2.3.2 Preparation of aminoacyl-SNACs (aminoacyl-N-acetylcysteamine thioesters) 54-55

2.4 Synthesis of doubly substituted MAA derivatives based on imino-mycosporines

2.4.1 General procedure and amino alcohols 56-64

2.4.2 NMR and LRMS characterisation of **DS1** and **DS2** 64-65

2.4.3 Characterisation of shinorine and porphyra-334 65-67

2.5 Synthesis of avobenzone/ octocrylene ("AVOCTOX") compounds

2.5.1 Precursors 68-75

2.5.2 DCC coupling in the synthesis of avobenzone/octocrylene ("AVOCTOX") compounds 76-81

2.5.3 Preparation of 1-(4-Chlorophenyl)-3-(4-methoxyphenyl)propane-1,3-dione 82

2.5.4 Preparation of 1-(4-(*Tert*-butyl)phenyl)-3-(4-methoxyphenyl)-2-methylpropane-1,3-dione 83

2.5.5 Preparation of (E)-3-(4-acetoxy-3,5-dimethoxyphenyl)acrylic acid 84

2.5.6 Preparation of 3-(4-(3-oxo-3-phenylpropanoyl)phenoxy)propyl (E)-3-(4-acetoxy-3,5-dimethoxyphenyl)acrylate (OAc-AVOCINN) 85

2.5.7 Deprotection (Deacetylation) of 3-(4-(3-oxo-3-phenylpropanoyl)phenoxy)propyl (E) 3-(4-acetoxy-3,5-dimethoxyphenyl)acrylate (AVOCINN) 86

2.6 Materials and Methods (Spectroscopy/Spectrometry)

2.6.1 'Ultraslow' Spectroscopies 87-88

2.6.2 Quantifying photostability 88-89

2.6.3 Ultrafast/Transient Absorption Spectroscopies 90

2.6.4 Transient Electronic Absorption Spectroscopy (TEAS) 90-93

2.6.5 Transient Vibrational Absorption Spectroscopy (TVAS) 93

2.6.6 FTIR Spectroscopy 94

2.6.7 Open-access LRMS and HRMS 94

2.6.8 Open-access NMR Spectrometry 95

2.6.9 Critical wavelength determination 95-96

2.6.10 Determination of extinction coefficients 96-97

2.7 Materials and Methods (Molecular Biology): Cloning, Expression and Purification of Moorea and Chlorogloeopsis C domain

2.7.1 Cloning summary 98-99

2.7.2 DNA Manipulation and Cloning Techniques 99-100

2.7.3 Preparation of Plasmid DNA 101

2.7.4 DNA quantification 102

2.7.5 Polymerase Chain Reaction 103

2.7.6 Agarose Gel Electrophoresis (Method 1) 103-104

2.7.7 Dpn1 digest 104

2.7.8 Purification of DNA from PCR reaction and restriction digests 104

2.7.9 Ligations 105

2.7.10 Preparation of plasmid DNA 105

2.7.11 Agarose Gel Electrophoresis (Method 2) 106

2.7.12 Restriction Digest 106

2.7.13 Sequencing 106

2.7.14 Transformation of plasmid into bacteria 107

2.7.15 Growing cells 107

2.7.16 Induction 107

2.7.17 Protein purification 108

2.7.18 Preparation of substrates for HPLC assay 109

2.7.19 Preparation of samples for HPLC assay 109-110

2.7.20 HPLC assay for detection of potential products 111

2.8 Materials and Methods (Computational Techniques)

2.8.1 Density Functional Theory 112-113

2.8.2 AVOCTO calculations 113-114

2.8.3 Submission to Alphafold via SCRTP and Phyre2 114

3. Synthetic Derivatives with MAA motifs

3.1 Background 115

3.1.1 Total synthesis 116-117

3.1.2 Bottom-up Approach 118

3.1.3 Exocyclic enaminones 118-120

3.1.4 Endocyclic enaminones 120-122

3.1.5 Amino-Cyclohexenimine unit 122-125

3.2 This work 126-128

3.2.1 Functionalisation of cyclic 1,3-diketones 129-130

3.2.2 Condensation of functionalised cyclic 1,3-diketones with amines 131-133

3.2.3 Condensation of enaminones with second equivalent of amine 133-135

3.2.4 Spectroscopy of the amino alcohol series 135-137

3.2.5 Photostability of the amino alcohol series 137-138

3.2.6 Ultrafast Spectroscopy of the amino alcohol series 138-142

3.2.7 Full experimental characterisation of DS1 and DS2 143-152

3.2.8 Power studies of DS1 and DS2 153-154

3.2.9 Investigating the response of the solvent to irradiation 155

3.2.10 Residuals 156

3.2.11 Fluorescence of DS1 and DS2 156-157

3.3 Chapter summary 158

4. Stabilisation of Avobenzone and Octocrylene in Composite Sunscreens (AVOCTOX and AVOCINN)

4.1.1 Background of avobenzone as a sunscreen ingredient 159-160

4.1.2 Photofragmentation patterns of avobenzone 160-162

4.1.3 Conformers present in avobenzone solutions 162-164

4.1.4 Ultrafast Photoprotective Properties of Avobenzone 164-165

4.1.5 Previous work on substituted dibenzoylmethane derivatives.....165-168

4.1.6 Interaction of avobenzone with other molecules 168

4.1.7 Background of octocrylene as a sunscreen ingredient..... 169

4.1.8 Photoprotective properties of octocrylene 169-170

4.1.9 Reactivity of octocrylene 170-171

4.1.10 Triplet energy transfer..... 172-174

4.1.11 Octocrylene as quencher (via triplet-triplet energy transfer) 174-175

4.1.12 Role of the *tert*-butyl and methoxy groups in para-substitution to the carbonyl 176-177

4.2 Design of AVOCTO molecules 177-179

4.2.1 Mechanism of the Steglich esterification 179-181

4.2.2 Expanding the Synthetic Scope.....182-185

4.3 Avobenzone stabilisation results 185

4.3.1 UV-visible properties of avobenzone in solution 186

4.3.2 Assessing stabilisation effects in binary mixtures in ethanol 187-190

4.3.3 Assessing stabilisation effects in binary mixtures in acetonitrile 191-195

4.4 Covalently linked dibenzoylmethane and cinnamate chromophores 196

4.4.1 Assessing the photostability of AVOCTO compounds 196-198

4.4.2 Ultrafast Spectroscopy of AVOCTO compounds..... 199-202

4.4.3 Assigning the features in the TAS at pump wavelength >350 nm 202-204

4.4.4 Assigning the features in the TAS at pump wavelength <290 nm 204-205

4.4.5 NMR study of AVOCTO5 photostability..... 205-206

4.4.6 Computational results (AVOCTO1, AVOCTO3 and AVOCTO5)..... 206-210

4.5 Chapter summary..... 211

5. Exploiting Genomics for Natural Product Synthesis

5.1.1 Background 212-213

5.1.2 Convergent pathways in Cyanobacteria 213-215

5.1.3 Mycosporine glycine synthesis in *A. variabilis* 215

5.1.4 NRPS enzymes 215-216

5.1.5 Mechanism of mycosporine glycine synthesis in *A. variabilis* 216-219

5.1.6 Metabolic potential of the genus *Moorea* 220

5.1.7 Aims and Objectives 220

5.2 Results

5.2.1 Cloning/purification 221-225

5.2.2 Computational modelling results for the *Moorea* C domain 226-227

5.2.3 Detection of potential products with an HPLC assay 228-238

5.3 Chapter conclusions 228-239

6. General discussion and Conclusion 240-241

7. Bibliography 242-270

8. Appendix

8.1 Spectra 271-318

8.2 MYCAS database 319-331

8.3 Amino acid sequences 332

ii. Acknowledgements

I would like to thank the PIs overseeing this project: Prof. Vas Stavros, Dr Christophe Corre and Prof. Martin Wills, for their supervision during the past 4 years. I thank Vas for conceiving the initial project and assembling a team that I joined through an MSc research project with the title "Microbial Sunscreens for a Better Life". I thank Martin for his guidance in chemical synthesis and for the rigour of fortnightly reports. I thank Christophe for support in experiments conducted in the School of Life Sciences and for introducing me to Molecular Biology and for the occasional espresso.

I would like to thank the wise and talented fellow PhDs in the Chemistry and Life Sciences departments at Warwick, in particular - Abbie from the Stavros group who conducted many of the ultrafast experiments in WCUS and provided invaluable support for data analysis, manuscript checking and presentation of the research; Emily, formerly of the Stavros Group, who ran computational studies on key molecules; and Jack and Dan for assistance in WCUS; Nazia, formerly of the Corre Group, who provided the plasmids used in this study; and Sopida, Paula, Sophie, Jinfan and Dan from the Corre Group for their guidance in carrying out the cloning, purification and expression protocols.

I would like to thank the MAS CDT members and staff who have been a supportive network at Warwick since 2019 through the PhD years 2020-2023 as well as a source of funding, training, and scientific expertise- In particular Christina Forbes, Naomi Grew and Eleanor Edwards who have been invaluable in dealing with the administrative side of the project. I thank course mates and friends Emma, Blane, Marlene, Hannah (and the whole 2019 CDT cohort) and Joel for their friendship and good times in Warwick and Coventry.

I thank my friends and my family (auntie Julie, my sister Rebecca, my granny Anne, my cousins Georgina and Robbie and my parents, Jackie and Jim) for their support. I also know that my late grandfather, Bumbush and late great-grandfather, Papa would be very proud. I thank my wonderful friends and Queen team (Nora, Roxanne, Fiona, Fern, Benny, Traian), who whether we won or not at the pub quiz, were an amazing group of people to spend my Monday evenings with (and in one case, to share a flat with) and made my stay in the Midlands all the more special. I want to thank Sixto, without whose encouragement and support this final year would have seemed a completely impossible feat.

This thesis is really a culmination of many years of education, so I also want to thank a handful of teachers from my school days at Campbell College Belfast who I believe nurtured my academic potential and encouraged me to aim high: Mrs. Hogg, Mr. McDowell, Dr. Reid and Mrs McNaught [names and titles are correct as of 2011]. I also want to thank Dr. Stephen Henderson who supported me in my progression at the University of Edinburgh and signed off my transfer to the Chemistry department from Modern Languages & Literature. I also thank the various yoga teachers I've practised with over recent years for helping me keep up my practice during the most stressful times, to keep on track and to honour the teacher within myself.

And to anyone who I appear to have forgotten, be assured I am most grateful, and the oversight is entirely my own.

iii. Declaration

This thesis is submitted to the University of Warwick in support of an application for the degree of Doctor of Philosophy. It has been composed by the author and has not been submitted in any previous application for any degree apart from some of the background material in Chapter 1 which was previously submitted for an MSc in Analytical Science degree by the same author.

The work presented (including data generated and data analysis) was carried out by the author except in the cases outlined below:

[1] Abbie Whittock, PhD acquired the data for the ultrafast experiments on AVOCTOX compounds (Chapter 4) and assisted with data acquisition and analysis for DS1 and DS2 (Chapter 2).

[2] Nurbolat Toktamys, MSc acquired the data and analysed the results for the ultrafast experiments of the five amino alcohol compounds (Chapter 2).

[3] Dr. Emily Holt ran the computations for the truncated AVOCTOX compounds (Chapter 4).

[4] Compounds **DS1** *and* **DS2** *studied in Chapter 2 were provided by academic collaborators Dr. Raúl Losantos and Prof. Diego Sampedro at the University of La Rioja, Spain.*

[5] The characterisation of shinorine and porphyra-334 was carried out collaboratively and published in Whittock, A. L.; Auckloo, N.; **Cowden, A. M.**; Turner, M. A. P.; Woolley, J. M.; Wills, M.; Corre, C.; Stavros, V. G. Exploring the Blueprint of Photoprotection in Mycosporine-like Amino Acids. *J. Phys. Chem. Lett.* **2021**, *12* (14), 3641–3646. https://doi.org/10.1021/acs.jpclett.1c00728.

[6] Mycosporine glycine used in Chapter 5 was extracted and purified by Sopida Wongwas, PhD.

iv. Abstract

At present there are only a few UVA (315-400 nm) absorbers available for sunscreen formulations even though such compounds are essential for effective protection against the harms of solar radiation. The four major aims of this research are 1) to understand how the naturally occurring photoprotective motif (N/O=C-C=C-N-) can be scaffolded into synthetic molecules, 2) to propose new molecules for the global bank of UVA filters that is available to sunscreen manufacturers, 3) to characterise how a subset of molecules disperse excess energy after they are energetically excited by light, and 4) to investigate a natural product pathway in bacteria to produce new 'natural' and 'unnatural' sunscreens. These aims are achieved by a combination of experiment and theory, covering the natural product molecules, synthetic analogues and new hybrid sunscreens.

- In Chapter 1 an introduction is presented with reference to photochemical theory.
- In Chapter 2, the materials and methods used are in this work are detailed with reference to all relevant spectra in the Appendix.
- Both Chapters 3 and 5 refer to MAAs, a family of molecules characteristic of high UV marine environments. In Chapter 3 it is studied how sunscreen active ingredients absorb light and then relax from excited energetic states by dispersing excess energy in primarily non-radiative ways. In Chapter 5, the modification of a biosynthetic pathway of exemplar MAA, shinorine, is explored.
- In Chapter 4, it is shown how new hybrid molecules, designed by combining avobenzone and cinnamate motifs, match or exceed the photostability of industry standard avobenzone in polar, non-protic solvents.

A complete picture of sunscreening ability must consider the long- and short-term behaviour of molecules during and after interaction with light. The longer time studies in solar-like conditions track the fate of molecules on the minute to hour timescale; while ultrafast transient absorption spectroscopies on the femto- to nanosecond scale are used to track the energy flow shortly after photoexcitation, complemented by computational models.

In short, this work contributes to the understanding of sunscreening molecules and adds new compounds to our photoprotectant library. The techniques used to quantify photoprotection could be extended towards near-to-life conditions. The synthetic methods could be optimised to further improve the yields and scope. The molecular biology approach could be expanded to include a range of controls, an improved understanding of the limits of detection and other enzymes of interest.

v. List of Figures

1.1. ASTM G173-03 reference spectra derived from SMARTS v. 2.9.2. Presented as the total spectra and then with a 280-400 nm range in focus. The inset vertical line delineates UVA and UVB.

1.2. Qualitative Perrin-Jablonski diagram (or state-energy diagram) illustrating processes discussed in the text. Vibrational energy transfer occurs between the narrowly spaced (fainter) lines of the excited vibrational modes within each electronic state. Excited state absorption (ESA) shows that further absorption can occur within the excited state. Vertical transitions drawn as thicker blue arrows. IC is non-radiative and allows relaxation of the excited state by relaxing through vibrational levels.

1.3. Various de-excitation processes, from Valeur, B.; Berberan-Santos, M. N. *Molecular Fluorescence: Principles and Applications*, Second edition.; Wiley-VCH ; Wiley-VCH Verlag GmbH & Co. KGaA: Weinheim, Germany : [Chichester, England], 2012.

1.4. Diagram adapted from Singh, A et al. showing the penetration of UV radiation into the skin layers. Skin homeostasis is maintained by mesenchymal stem cells in inner layer dermis and epidermal stem cells in the outer layer dermis. This is a simplified model of the human skin and does not include any of the specialized cells, including melanocytes and sensory nerve endings of the skin; nor the more subtle delineation of the epidermis into the strata spinosum, granulosum and corneum…

1.5. An example of DNA base modification caused by UVR exposure. Overexposure can lead to irreversible modifications of genes, such as the p53 tumour suppressor gene30 and the onset or acceleration of disease as well as premature skin ageing. CPD: cyclobutene pyrimidine dimers. SSB: single strand breaks. ROS: Reactive oxygen species. 64PP: 6-4 PPs or pyrimidine (6-4) pyrimidone. The effect of ROS is driven primarily by UVA radiation exposure.

1.6. UVA absorbing compounds currently available in products in European markets and typical of the state-of-the-art UVA filters. Trade names: Mexoryl SX (Ecamsule), Mexoryl XL (Drometrizole trisiloxane), Tinosorb M (Bisoctrizole), Tinosorb S (Bemotrizinol).

1.7. Promising photoprotectant molecules from natural extracts (from top left to bottom right): usnic acid, hipposudoric acid, norhipposudoric acid, (-)-catechin, epicatechin, gyrophoric acid, resveratrol, scytonemin and shinorine.

1.8. Re-printed from Dunlap et al. UV-vis spectra in 20% THF/MeOH (v/v) from *Acropora formosa* tips collected at the indicated depths.

1.9. MAAs isolated in Dunlap et al. In order from top left to bottom right: Mycosporine glycine (containing the cyclohexanone scaffold, red), Palythine, Palythinol (stereochemistry undefined), Palythene and Usujirene (all containing the cyclohexenimine scaffold, purple and extended, green).

1.10. Shifting absorbance in the MAA motif due to increased functionalisation.

1.11. Aspects of the TEAS set-up. The beams interact with the sample in the window of the flow cell and optical density difference is recorded at different time points by the fibre-coupled spectrometer. A more complete experimental set-up, including ultrafast pump generation, can be found in Abiola et al.

1.12. Compounds shinorine and porphyra-334 from Whittock et al.

1.13. The enol and keto forms of oxybenzone.

1.14. (Top left) (trans) Sinapoyl malate and (right) the cis-isomer. (Bottom) Related cinnamic acids.

1.15. Dominant relaxation pathway proposed in Baker et al.

1.16. Illustration of the two major pathways followed by MAA or MAA-like molecules, demonstrated in a 3D model ball-and-stick model of usujirene/palythene without the C-5 substituents.

1.17. a) Scheme of the dominant relaxation pathway in usujirene from the study by Whittock et al. b) Optimised geometries in the S0 and at the S1/S0 CI.

2.1. The normalised spectrum obtained of the LCS-100 solar simulator used in the irradiation studies.

2.2 Critical wavelength determination of **DS1** (a) and **DS2** (b) from the corresponding steady-state UV-vis spectrum in ethanol. The integrated area of the spectrum on the right in each case is 90% of the spectrum to the left.

2.3 Determination of the extinction coefficients of **DS1** (left) and **DS2** (right) at the λ_{max} in ethanol.

2.4 Expression plasmids with annotations including the promotor region, gene of interest, resistance marker, lacI gene (which makes a protein that controls the promotor) highlighted.

2.5 Summary of the Mini-Prep plasmid DNA extraction scheme created in BioRender.com

2.6 Annotated agarose gel of the two constructs. The number of base pairs on the gel are in good agreement with the calculated values (9.8 kb bp).

3.1 (Left) Natural products (descending order: mycosporine glycine, shinorine, usujirene/palythene), (centre) Proposed molecules that can be considered structural analogues of the natural products, (right) Starting materials that can be bought commercially.

3.2 Reproduced final synthetic scheme of mycosporine glycine.

3.3 Synthesis from Cui et al. R = alkyl groups.

3.4 Synthesis from Andreguetti et al. AA = amino acid, here glutamic acid, histidine, and serine.

3.5 Synthesis of exocyclic β-enaminones using microwave irradiation in Bhattacherjee et al. (Left) Full scope displayed as a generic structure with undefined Rs. (Right) Selected compounds with reported yields.

3.6 Starting material and product for the synthesis in York et al.

3.7 Synthesis in Nguyen et al. A potential future avenue to explore would be larger conjugated, cyclised systems like those suggested in Figure E. In theory these could be prepared from previously reported 2-aryl-3-hydroxy-3-cyclohexenones (Chidipudi et al.) and are only included here for future reference.

3.8 Suggestions for a route to a cyclised structure incorporating the MAA scaffold.

3.9 Compounds proposed as protecting agents against UVR in patent 2013/181741

3.10 Vinamidinium salts prepared in Ostercamp et al. Addition of two different amines would be problematic.

3.11 Summary of key synthetic steps in patent WO 2013/181741 PCT/CA2013/000536

3.12 Summary of the synthetic details recorded in patent WO 02/39974A1.

3.13 Figure redrawn from Losantos et al. to illustrate the range of molecules synthesised.

3.14 Summary of key molecules discussed and made in the two series. Series 1: *single addition* products AC3, AC4, AC9, AC20. The biological substrates with glycine methyl ester or glycine side chains (AC23 ester and AC23 acid, respectively) used in Chapter 5 also can be considered single addition MAA analogues. Series 2: *double addition* products AC26 (amino alcohol) and AC33. Also included are molecules DS1 and DS2 provided by collaborators which can be considered double addition MAA analogues. Synthetic details can be found in the Materials and Methods.

3.15 Graph showing the shift to higher wavelength (bathochromic) by functionalising at the 2-position and by increasing conjugation through addition of a second amine. All molecules were synthesised using methods in the Materials and Methods section but not fully characterised. **1** was prepared following method in patent WO2013181741A1: 2013-12-12. Other single addition products were prepared using the same method as **AC34. 7** was prepared using the same method as **AC33**.

3.16 Unproductive route initially explored towards 2-functionalised enaminones.

3.17 Synthetic scheme from starting material pyrogallol to a functionalised enone. Percentage yields are reported in **bold**. RaNi – Raney nickel. $C_2H_6O_4S$ – dimethyl sulfate.

3.18 Proposed mechanism for enaminone formation.

3.19 Comparison of hemiacetal/acetal formation and hemiaminal/imine formation.

3.20 Summary of condensations leading to enaminones. $C_2H_4O_2$ – acetic acid. TEA – triethylamine. DCM- dichloromethane. **Δ** – heat/reflux.

3.21 Summary of double addition condensations. Further details are in Materials and Methods.

3.22 Natural product amino alcohol MAAs in the order listed in the text.

3.23 Structures and absorption spectra of the amino alcohol series in water. Note that the molecules are drawn without the tosylate counterion.

3.24 TAS presented as false colour heat maps of (a) **AC26**, (b) **AC27**, (c) **AC28**, (d) **AC30**, and (e) **AC35** in water photoexcited at their respective λ_{max}, 324, 305, 311, 305, and 325 nm. Time delays are plotted linearly until 1 ps and then as a logarithmic scale from 1 to 3000 ps. Inset are the 3D molecular structures of the molecules. The TAS are not chirp corrected.

3.25 Potential energy scheme for the amino alcohol compound **AC35**. Adapted from Woolley et al.

3.26 **DS1** and **DS2,** prepared by Losantos et al.

3.27 UV-visible spectra of **DS1** and **DS2** are displayed with the UVB (290-320 nm) and UVA (320-400 nm) regions highlighted. Absorption is normalised to the peak maximum (**1** λ_{max} = 341 nm and **2** λ_{max} = 329 nm).

3.28 Photostability as measured by change in UV-visible absorption (210-450 nm) of **DS1** (a) and **DS2** (b) in simulated solar conditions in ethanol across 2 hours irradiation. Absorbance is normalised to the peak maximum.

3.29 TEAS of **DS1** (a) and **DS2** (b) presented as false-colour heat maps. The time delay scale is linear to 1 ps and then logarithmic to 3000 ps in (a) while in (b) the scale is linear to 5 ps and logarithmic thereafter. The region between 340-349 nm and 320-334 nm has been omitted for all spectra for **1** and **2**, respectively, due to imperfect pump pulse subtraction. Selected time delays from the TEAS are plotted as lineouts in **1** (c) and **2** (d) beside the corresponding TEAS. The EADS of **1** (e) and **2** (f) produced by the fitting procedure (for details see Materials and Methods).

3.30 (Left) The difference spectrum of **DS1** after 2 hours of solar irradiation (right y-axis) overlayed with the longest trace in the TEAS experiment (3 ns, left y-axis) to evaluate whether the feature at ~380 nm is due to the formation of a photoproduct. (Right) Photostability of **DS1**

when irradiated for 1 hour at 341 nm in ethanol. A solution of ~10 μM concentration was irradiated at a single wavelength (λ_{max} = 341 nm) using a xenon arc lamp with the beam power adjusted to be comparable to the solar spectrum at that wavelength. The solution was irradiated continuously for one hour. In this case there was no significant change during the irradiation. Absorbance is normalised to the peak maximum.

3.31 (Top left) Transient vibrational absorption spectra (smoothed) of **DS1**. The most negative trace (black, dashed line) is the smoothed FTIR spectrum with the transmittance scale given on the right side of the plot. (Top right) Bi-exponential fit of the percentage recovery of the GSB feature in **DS1** . The integration region for the fit was 1504-1524 cm^{-1} and the two extracted time constants are τ_{v1} = 4.2 (±0.3) ps and τ_{v2} = >1 ns. The scale is linear up to 100 ps and logarithmic after 100 ps and up to 1 ns. (Bottom left) Transient vibrational absorption spectra (smoothed) of **DS2**. The most negative trace (black, dotted) is the smoothed FTIR spectrum with the transmittance scale given on the right side of the plot; (Bottom right) Bi-exponential fit of the percentage recovery of **DS2**. The integration region for the GSB feature fit is 1540-1560 cm^{-1} and the two extracted time constants are τ_{v1} = 2.4 (± 0.5) ps and τ_{v2} = 11.1 (± 7.6) ps. The scale is linear up to 100 ps and logarithmic after 100 ps and up to 1 ns.

3.32 (Left) Evidence that the ESA in the TAS of **DS2** extends out to ~30 ps. (Right) Photoproduct scan of **DS2** showing no significant photoproduct after 100 ps.

3.33 Power studies of **DS1.**

3.34 Power studies of **DS2**.

3.35 Solvent-only time-zero response of ethanol photoexcited at 341 nm. The black data points are the experimental signal at an average ~375 nm considering 3 wavelengths. The red-line is a frequency-dependent cross-correlation function (which takes into account any non-resonant contributions from the solvent and/or Harrick cell windows) and has been used previously to calculate the IRF in a related paper by our group using water as solvent.[31,32] The returned full width half maximum (FWHM) is 110 fs and corresponds to the FWHM of the instrument response function. The quoted errors in [accompanying] Table are 60 fs which are half the FWHM of the instrument response function rounded to the nearest 10 fs.

3.36 Heat map showing the residuals of the fit of **DS1** (left) and **DS2** (right). The residuals have not been chirp corrected.

3.37 Steady-state fluorescence detection of **1** and **2**, demonstrating weak fluorescence in both molecules. Abs = absorbance in arbitrary units derived from the UV-vis spectra.

4.1 (Left) Diketo form of avobenzone and (right) one representation of the chelated enol form.

4.2 Photodegradation scheme reproduced from ref.[5] Reading the final products in a clockwise direction: **1**. benzaldehyde, **2**. benzoic acid, **3**. phenylglyoxal, **4**. acetophenone. The recombination products from left to right are **5**. dibenzoylethane and **6**. benzils.

4.3 Mechanistic sequence based on Cantrell's findings

4.4 Formation of dibenzoylmethanes via reaction of a ketone and an ester.

4.5 Historical patents for dibenzoylmethanes

4.6 Molecules studied by Moi et al.

4.7 Differently α-substituted dibenzoylmethanes discussed in the text.

4.8 Reactive pathway identified for avobenzone fragments.

4.9 Octocrylene structure

4.10 Reaction occurring between octocrylene and a molecule containing a nucleophilic N atom.

4.11 Energies of the singlet and triplet states (of the two main forms) as summarised in the text. Energies* from Kikuchi et al. were converted to kJ/mol from cm^{-1} by multiplying by hcN_a. ND – *Not determined*.

4.12 Jablonski diagrams

4.13 Molecules studied by Kikuchi et al.

4.14 (Left) Cholic acid. (Right) Composition of the sunscreen molecule proposed in the patent cited in the text with the inert derivatized methyl ester of chenodeoxycholic acid in black, the UVB chromophore from octocrylene in red and the UVA chromophore from avobenzone in blue.

4.15 Generalised structure of AVOCTO compounds.

4.16 Retrosynthesis of **AVOCTO** compounds, illustrating the final esterification required.

4.17 Generalised mechanism of the ester coupling reaction.

4.18 Generalised complete synthetic scheme for the AVOCTOX series. Synthetic details are found in the Materials and Methods section. All reactions were carried out in an inert (N_2) atmosphere overnight. Percentage yields are in **bold**. 4-Hydroxyacetophenone is reacted with 3-bromoethanol in the presence of a base to afford the phenyl ether alcohol that was then reacted with a variously substituted ester in NaH/THF to afford the para-substituted 1,3-dicarbonyl compound with alcohol side chain. This compound was then reacted with the free carboxylic acid derived from octocrylene in the final ester coupling step. To synthesise AVOCTO3 a subsequent α-methylation was required, which was achieved with MeI/K_2CO_3 in diethyl ether. rt. = room temperature.

4.19 Unsuccessful reaction scheme. Compounds (a)-(c) were made in the same way as before. Compound (d) is the target molecule. Compound (e) is sinapinic acid. This was tested with two R^b groups, namely H and -OMe.

4.20 Reaction scheme for production of O-acyl protected AVOCINN. Synthetic details are found in the Materials and Methods section. All reactions were carried out in an inert (N_2) atmosphere at room temperature (rt.). Percentage yields are in **bold**. The synthesis of the top compound was described previously. Acetylation of the para-phenolic acid was achieved with acetic anhydride in pyridine. The condensation of the dicarbonyl and the protected acid was achieved in similar conditions to the final esterification step described for AVOCTO1-5, albeit with longer reaction times.

4.21 (Top Left) UV-vis spectrum of the compound (OAc-AVOCINN) produced by reaction scheme in Figure 4.20. This is an O-acyl protected composite molecule composed of an avobenzone derived part and a cinnamic acid derived part. (Top Right) UV-vis spectrum of the

partially deprotected product in an approximate 2:1 ratio with OAc-AVOCINN. Included below are the UV-vis spectra for AVOCTO1 and AVOCTO5. All spectra are in ethanol, demonstrating broad protection in one molecule.

4.22 UV-vis spectra of avobenzone in three solvents of varying polarity:

a) EtOH:Ethanol (λ_{max} = 358 nm); b) CHX: cyclohexane (λ_{max} = 352 nm); c) ACN: acetonitrile (λ_{max} = 357 nm). Concentration of avobenzone ~2 x 10^{-5} mol dm^{-3}.

4.23 A) Irradiation of avobenzone alone; B) Irradiation of an avobenzone and octocrylene mix (1:3 molar ratio); C) Simultaneous irradiation of avobenzone (black/purple trace) and an avobenzone and AC26 mixture (green trace); D) Simultaneous irradiation of avobenzone (black/purple trace), AC33 (yellow/orange trace) and an avobenzone and AC33 mixture (blue trace). All graphs are cropped in order to display the key points of interest. Inset are the loss of activity in percent (as defined in the previous section) where 'max' indicates that the measurement is taken at the λ_{max} and UVA indicates that the change across the entire UVA range is considered. NB: Octocrylene was irradiated alone separately and showed no degradation.

4.24 Avobenzone in binary mixtures in ethanol, degradation with best linear fits.

4.25 Set of graphs of binary mixtures in acetonitrile, room temperature. Graph A) Irradiation of avobenzone alone; B) Avobenzone incubated at ambient light (i.e., with no artificial irradiation); C) Irradiation of an avobenzone and octocrylene mixture; D) Irradiation of an avobenzone and AC26 mixture; E) Irradiation of an avobenzone and AC33 mixture. Displayed on the graphs are the stabiliser present and the loss of activity in percent where 'max' indicates that the measurement is taken at the λ_{max} and (inset) 'UVA' indicates that the change across the entire UVA range is considered.

4.26 Avobenzone in binary mixtures in acetonitrile, degradation with exponential fits.

4.27 Photostability results in acetonitrile of compounds discussed in the accompanying text.

4.28 Pump wavelengths selected for the TEAS experiment shown as vertical lines.

4.29.A1. AVOCTO1 (λ_{pump} = 290 nm) TEAS spectrum and 3000 ps scan in acetonitrile.

4.29.A2. AVOCTO3 (λ_{pump} = 280 nm) TEAS spectrum and 3000 ps scan in acetonitrile.

4.29.A3. AVOCTO5 (λ_{pump} = 285 nm) TEAS spectrum and 3000 ps scan in acetonitrile.

4.29.A4. AVOCTO1 (λ_{pump} = 350 nm) TEAS spectrum and 3000 ps scan in acetonitrile.

4.29.A5. AVOCTO5 (λ_{pump} = 355 nm) TEAS spectrum and 3000 ps scan in acetonitrile.

4.30 NMR spectra of AVOCTO5 before and after 60 minutes irradiation (same conditions as before in the longer pump wavelength scheme) in acetonitrile.

4.31.X1. AVOCTO1 - diketo form - optimised geometry transition with greatest oscillator strength. The centre orbital is the HOMO and the right-hand orbital is the LUMO.

4.31.X2. AVOCTO1 - chelated enol form - optimised geometry transition with greatest oscillator strength. The centre orbital is the HOMO and the right-hand orbital is the LUMO.

4.31.X3. AVOCTO5 - diketo form - optimised geometry transition with greatest oscillator strength. The centre orbital is the HOMO and the right-hand orbital is the LUMO.

4.31.X4. AVOCTO5 - chelated enol form - optimised geometry transition with greatest oscillator strength. The centre orbital is the HOMO and the right-hand orbital is the LUMO.

4.31.X5. AVOCTO3 - diketo form - optimised geometry transition with greatest oscillator strength. The centre orbital is the HOMO and the right-hand orbital is the LUMO.

4.31.X6. AVOCTO3 - chelated enol form - optimised geometry transition with greatest oscillator strength. The centre orbital is the HOMO and the right-hand orbital is the LUMO.

5.1 Gadusol (1,4,5-trihydroxy-5-hydroxymethyl-2-methyoxycyclohex-1-en-3-one). 4-Deoxygadusol.

5.2 Pathway in a species of cyanobacteria (*A. variabilis)* depicting a biosynthetic route to an oxy-type mycosporine, mycosporine-glycine. Sedoheptulose 7-phosphate (7-SHP) is a primary metabolite involved in the pentose phosphate pathway while deoxy-d-arabino-heptulosonate 7-phosphate (DAHP) is a primary metabolite involved in the shikimate pathway.

5.3 Postulated convergent pathways of MAA biosynthesis in cyanobacteria. EVS: 2-*epi*-5-*epi*-valiolone synthase. DAHP: deoxy-d-arabino-heptulosonate 7-phosphate. The EVS gene is typically absent in non-producers.

5.4 This simplified model demonstrates the ordered, modular mechanism of the NRPS enzyme. The thiol group of the 4'-phosphopantetheine arm tethered to the T domain captures an aminoacyl-AMP intermediate and C domain catalyses peptide bond formation between adjacent T domain-loaded thioester intermediates. The TE domain catalyses the release of the peptide from the NRPS.

5.5 One mechanism proposed by Balskus and Walsh. The radiolabelled-amino acid serine is activated as the thioester towards nucleophilic attack by the conjugated enaminone (MG) and a subsequent cyclisation process driven by a Michael addition of the free -NH_2 of the newly added amino sidechain leads to the final product.

5.6 Alternative mechanism proposed by Balskus and Walsh. Here the aminoacyl thioester enzyme complex acts directly as a nucleophile through the free -NH_2 group, while the oxo-MAA (MG) acts as the electrophile.

5.7 Comparative genetic analysis of domain organisation of NRPS-like proteins that are proposed to direct MAA biosynthesis in three species of cyanobacteria. The A group defines the specificity of the amino acid. PCP is a small domain with a thiol group that acts as nucleophile to towards a carbonyl (COOMP, anhydride, acyl chloride or SNAC etc.). The C domain is predicted to have a role in combining a substrate (e.g mycosporine glycine) and activated amino-acids. TE: thioesterase domain.

5.8 New plasmids. **P1**, *Chlorogloeopsis C domain only*. **P2**, *Moorea* C domain only.

5.9 Restriction digest. Gel Key: (left) Gel was prepared and run using Method 2. AMC1 and AMC2 are the original plasmids. P1D contains the desired plasmid derived from *Chlorogloeopsis* and P2A, P2C and P2D contain the desired plasmid derived from *Moorea*. (right) Virtual digest created in Benchling using PvuI.

5.10 Annotated agarose gel using Method 2 (Materials and Methods). Gel Key: **AMC1** and **AMC2** are the original plasmids. P1A, P1B, P1C and P1D were isolated from a culture of A1. P2A and P2B were isolated from a culture of A2. P2C and P2D were isolated from a culture of C2.

P1D (red) contains the desired plasmid derived from *Chlorogloeopsis* (C domain 1470 bp) and P2A, P2C and P2D (red) contain the desired plasmid derived from *Moorea* (C domain 1273 bp).

5.11 SDS-PAGE Gel of the protein produced by construct **P2C** containing the C-domain from the *Moorea* construct. The lane labelled 'concentrated protein' contains the protein of interest as confirmed by the theoretical base pair number.

5.12 A) .pdb file from Phyre2, visualised in EzMol. Phyre2 result based on template c5u89A_. 429 residues (98% of the sequence) were modelled with 100% confidence by the single highest scoring template. B) same file coloured by secondary structure.

5.13 .pdb file obtained from Alphafold 2.1.1 'best prediction', viewed in EzMol.

5.14 Overlay of the Alphafold 2.1.1 best prediction (purple) with the Phyre2 model prediction (red). Alignment RMSD: 2.175 Å. TM-score: 0.9166. Viewed using iCn3D Structure Viewer.

5.15 (Right) Desired products of the HPLC assay using the stated substrates (left). Enz = C domain.

5.16 Nanodrop assay confirming that substrates mycosporine glycine (MG), AC23 ester (AC23E) and AC23 acid (AC23A) absorb at 310 nm. These were prepared in prepared in 20 mL buffer (100 mM HEPES, 50 µM TCEP, pH 7.5) and diluted with distilled water until within the range of the Nanodrop.

5.17 **a)** HPLC chromatogram of mycosporine glycine (MG): 35 minute run, using standard gradient (H_2O/MeOH) and column. Blue traces show signal at 310 nm, purple traces show signal at 350 nm. λ_{max} (MG) ~310-320 nm. MG elutes at early times <5 mins. **b)** HPLC chromatogram of AC23 ester. 35 min gradient method *ut infra*. Dark blue traces show signal at 310 nm, light blue/green shows signal at 350 nm AC23 ester elutes between 8-9 mins. **c)** HPLC chromatogram of AC23 acid. 35 min gradient method *ut infra*. Trace colours as previous. This traces contains impurities at longer times, perhaps suggesting some decomposition during analysis. The analyte is assigned to one of the early peaks, i.e. <2 mins. **d)** HPLC chromatogram of SerSNAC*. 35 min gradient method *ut infra*. Trace colours as previous. Impurities at longer times are assigned to column debris and some decomposition during analysis. The analyte is assigned to one of the early peaks, i.e., <2 mins. **e)** HPLC chromatogram of ProSNAC. 35 min gradient method *ut infra*. Trace colours as previous. Impurities at longer times are assigned to

column debris and some decomposition during analysis. The analyte is assigned to one of the early peaks, i.e., <2 mins

5.18 Chromatograms obtained (top) for reaction (inset, above) when MG was incubated with SerSNAC* for 24 hours and analysed by HPLC (following standard method), (bottom) with enzyme added. 21 minute run using standard gradient method.

5.19 Chromatograms obtained (top) for reaction (inset, above) when MG was incubated with ProSNAC for 24 hours and analysed by HPLC (following standard method), (bottom) with enzyme added. 21 minute run using standard gradient method.

5.20 Chromatograms obtained (top) for reaction (inset, above) when AC23 ester was incubated with SerSNAC* for 24 hours and analysed by HPLC (following standard method), (bottom) with enzyme added. 21 minute run using standard gradient method.

5.21 Chromatograms obtained (top) for reaction (inset, above) when AC23 ester was incubated with ProSNAC for 24 hours and analysed by HPLC (following standard method), (bottom) with enzyme added. 21 minute run using standard gradient method.

5.22 Chromatograms obtained (top) for reaction (inset, above) when AC23 acid was incubated with SerSNAC* for 24 hours and analysed by HPLC (following standard method), (bottom) with enzyme added. 21 minute run using standard gradient method.

5.23 Chromatograms obtained (top) for reaction (inset, above) when AC23 acid was incubated with ProSNAC for 24 hours and analysed by HPLC (following standard method), (bottom) with enzyme added. 21 minute run using standard gradient method.

5.24 Reagents used in the bio-assay

vi. List of Tables

1.1 Examples of approximate molar absorption coefficients, ϵ.

1.2 Approximate lifetimes of the processes that lead to energy loss from the excited state.

1.3 Summary of λmax and $\boldsymbol{\varepsilon}$ for mycosporine glycine, palythine and palythene.

1.4 Processes that can be observed on a transient absorption spectrum.

1.5 Summary results for shinorine and porphyra-334 in water; and summary results for usujirene/palythene in water.

5.14 List of bacterial strains

5.15 List of vectors

5.16 List of primers

5.17 In total 12 samples were prepared, a set with enzyme added and a control set. Concentrations given are final concentrations in the sample.

3.1 Stability data for the amino alcohol series tested using the standard method.

3.2 Summary of time constants and associated errors of the dynamical processes extracted from the global sequential fit of all molecules photoexcited at their respective λ_{max}. The IRF derived error is ± 40 fs. VC – Vibrational cooling. TP – Trapped population.

3.3 Assignment of time constants to physical processes in **AC26**, **AC27**, **AC28**, **AC30**.

3.4 The time constants listed in the table were obtained through a global fit of the data with a sequential model and are quoted with associated errors which are half the instrument response estimated using solvent-only TAS. The final time constant for **DS1** is beyond the experimental time window of the TEAS experiment (3 ns). FC – evolution out of the Franck-Condon region; CI – conical intersection; VC – vibrational cooling; PP – long-lived population/photoproduct. Appended are the results from a previous study of **DS1.**

4.1 Solvent Properties of Common Liquids. p1 is a measure of the ability of the solvent to interact with various test solutes. p1 increases with solvent polarity.

4.2 Summary of the avobenzone in ethanol stabilisation results. NB: Avobenzone results are an average of three experiments.

4.3 Summary of the linear fits of avobenzone in ethanol stabilisation data.

4.4 Summary of the avobenzone in acetonitrile stabilisation results. Details of the conditions used are found in the Materials and Methods.

4.5 Data fits of avobenzone stabilisation studies in acetonitrile.

4.6 Summary of the UV-vis activity of **AVOCTO** compounds in acetonitrile after 40 minutes simulated solar irradiation using the 'ultraslow' set-up in the Materials and Methods. A generic chemical structure showing the identity of the AVOCTOX molecules is included below for reference.

4.7 Results from Holt et al. for avobenzone in ethanol.

4.8 Time constants obtained from fitting the TAS in acetonitrile at the longer pump wavelength. *Quoted errors here are from the fit in Glotaran. Experimental errors are half of the IRF.

4.9 Time constants obtained from fitting the TAS in acetonitrile at the shorter pump wavelength. *Quoted errors here are from the fit in Glotaran. Experimental errors are half of the IRF.

4.10 AVOCTO1 results summary

4.11 AVOCTO5 results summary

4.12. AVOCTO3 results summary

vii. Abbreviations

I - Intermediate (*used in equations*)

I_t - absorbance at time *t*

Δ - Change in (e.g., temperature) or difference in (e.g., $\Delta E_{1,2}$)

R – Chromophore (*used in equations*)

υ - inverse wavelength (i.e., 1/λ)

L - length (e.g., length of a box in the particle-in-a-box model)

h - Planck constant

I_{ref} - reference pulse

I_0 - unpumped absorbance or absorbance at time zero, t_0

R^*- Excited chromophore (*used in equations*)

I_{probe}- probe pulse

I_{pump} - pump pulse

(v/v) – volume to volume ratio

[M + Na]+ - Positively charged molecular ion containing sodium

~ approximately

< less than

> greater than

4-DG – 4-deoxygadusol

64PP - 6-4 PPs or pyrimidine (6-4) pyrimidone

7-SHP - Sedoheptulose-7-phosphate

A - Absorbance

ab initio – '[starting from the] *bottom up'*

Abs. arb. units – Absorbance in arbitrary units (i.e., 1 = maximum absorbance, 0.5 = 50% absorbance etc.)

ACN – Acetonitrile

AMP – Adenosine monophosphate

ASTM - American Society of Testing and Materials

ATCC 29133 - American Type Culture Collection number for *Nostoc punctiforme*

ATCC 29413 – American Type Culture Collection number for *Anabaena variabilis*

ATP – Adenosine triphosphate

AUC – area under curve (also. AUCI and AUCR: AUC index and ratio)

AVOCTO – portmanteau of **AVO**benzone and **OCTO**crylene, also AVOCTOX

B.C.E – Before common era

BER – Base excision repair

BGC – Biosynthetic gene cluster

BM-DBM - butyl methoxydibenzoylmethane i.e., avobenzone

c – speed of light (i.e. 3×10^8 m/s)

C domain – Condensation domain

C.E. – Common era

CAS number – Chemical Abstracts Service number

CASSCF/6-31G* - Complete active space self-consistent field with 6-31G* basis set

CD_3OD – deuterated methanol

$CDCl_3$ – Deuterated chloroform

CHX – Cyclohexane

CI – Conical intersection of two states (e.g., S_1/S_0 CI *or* $1^1\pi\pi^*/2^1\pi\pi^*$)

CPD(s) – Cyclobutene pyrimidine dimer(s)

CW – Critical wavelength

Cyclohexane-d_{12} – Fully deuterated cyclohexane

D_2O – deuterated H_2O

DAHP - Deoxy-d-arabino-heptulosonate 7-phosphate

DCC - Dicyclohexyl carbodiimide

DDG synthase - Desmethyl 4-deoxygadusol synthase

DHPG – Dihydropyrogallol

DMAP – Dimethylaminopyridine

DMSO – Dimethylsulfoxide

DNA - Deoxyribonucleic acid

DPH - 1,6-Diphenyl-1,3,5-hexatriene

DS1 – molecule 1 received from Diego Sampedro

DS2 – molecule 2 received from Diego Sampedro

E – Energy (e.g., E_n)

EADS – Evolution associated difference spectra

EDC - 1-Ethyl-3-(3-dimethylaminopropyl)carbodiimide

EDG – Electron donating group

EHMC - Ethylhexyl methoxycinnamate

E-isomer – geometric isomer where higher atomic weight priority groups on either end of a double bond are on the opposite sides (also known as a *trans* isomer)

EPS – Extracellular polymeric substances

ESA – Excited State Absorption

ESR spectroscopy – Electron spin resonance spectroscopy

EtOAc or EA – ethyl acetate

EU REACH – European Union Registration, Evaluation, Authorisation and Restriction of Chemicals Regulations

eV – electronvolts (equivalent to $1.602176634\times10^{-19}$ J)

EVS - 2-*epi*-5-*epi*-valiolone synthase

EWG – Electron withdrawing group

ε - Molar absorption coefficient (L mol^{-1} cm^{-1}) or ($M^{-1}cm^{-1}$)

FC – Franck-Condon

FDA – Food and Drug Administration

FWHM – Full-width half maximum

GC-MS – Gas chromatography mass spectrometry

GSB – Ground state bleach

HEPES - 4-(2-Hydroxyethyl)-1-piperazineethanesulfonic acid

HEPES - N-2-hydroxyethylpiperazine-N-2-ethane sulfonic acid

Hex – hexane

HOBt - 1-Hydroxybenzotriazole

hOGG1 - 8-oxoguanine DNA glycosylase

HOMO – Highest occupied molecular orbital

HPLC – High performance liquid chromatography

I_p – Ionisation potential

IR – Infrared (also FTIR – Fourier Transform Infrared)

IRF – Instrument response function

ISC – Intersystem crossing

J/m^2 – Joules per metre squared

LUMO – Lowest unoccupied molecular orbital

MAA(s) – Mycosporine-like amino acid(s)

-Me = $-CH_3$ – methyl group

MED – Minimum erythemal dose

$m_{electron}$ – Mass of electron

MeOH – Methanol

MG – Mycosporine glycine

MH+ (peak) – a single protonated molecular ion, M, typically observed on a mass spectrometer

MHz – Megahertz

Mmol – millimoles

Mol – moles

Mols – molecules

MP – Melting point

m_{proton} – Mass of proton

MS – Mass spectrometry

MYCAS - *a database on mycosporines and mycosporine-like amino acids*, presumably (MYC)osporine (A)mino acid(S)

n – an integer (i.e. 1, 2, 3, 4…) or n_f - final state or n_i – initial state

N – number of atoms

N_a – Avogadro's number (i.e., $6.02214076 \times 10^{23}$)

NCBI:txid1124 – Taxonomy identification for *Chlorogloeopsis fritschii*

NCBI:txid1155739 – Taxonomy identification for *Moorea producens*

NMR – Nuclear magnetic resonance (also ^{1}HNMR and ^{13}CNMR)

NP – Natural product

NRPS - Non-ribosomal peptide synthetase

OD – Optical density

-OMe = $-OCH_3$ – methoxy group

O-MT – O-methyl transferase

p (orbital) – Pi (orbital)

PCP - Peptidyl carrier protein

PMMA – Polymethylmethacrylate

PP – Photoproduct(s)

PPD – Persistent pigment darkening

Ppm – parts per million

PTFE – Polytetrafluoroethylene

QSAR – Quantitative structure activity relationship

ROS – Reactive oxygen species

rt. – room temperature (i.e., between 18°C and 21°C)

RVP – Red vet(inary) pet(rolatum)

s - Spin quantum number

S_0 – Ground [electronic] state

S_1 – First i.e., lowest energy [electronic] excited state

SDS-PAGE - Sodium dodecyl sulfate–polyacrylamide gel electrophoresis

SE – Stimulated emission

SED – Standard erythemal dose

$S_n \leftarrow S_0$ – Transition from the ground state to an undefined higher energy state during photoexcitation

$S_n \rightarrow S_m$ – Transition between excited energy states e.g., following photoexcitation

SNAC - N-acetylcysteamine thioesters

SPF – Sun protection factor

SSB – Single strand break

T_1 – Triplet state

TAS – Transient absorption spectrum/a

TCEP - Tris(2-carboxyethyl)phosphine

TCEP - *Tris*(2-carboxyethyl)phosphine

TE – Thioesterase

TEAS - Transient electron absorption spectroscopy *or* spectrum/a

THF – Tetrahydrofuran

TLC – Thin layer chromatography

TOF – Time of flight

TVAS – Transient vibrational absorbance spectroscopy

UNESCO - United Nations Educational, Scientific and Cultural Organization

UV-(vis) – Ultraviolet-(visible)

UVR – Ultraviolet radiation (incl. UVA, UVB, UVC etc.)

VC – Vibrational cooling

Z-isomer – geometric isomer where higher atomic weight priority groups on either end of a double bond are on the same side (also known as a *cis* isomer)

α (bond) – Bond formed from head-on overlap of atomic orbitals

α (orbital) – Sigma (orbital)

λ_{max} – wavelength where maximum absorption occurs (usually in nm)

π (bond) – Bond formed from lateral overlap of atomic orbitals

τ – Lifetime [of a physical or theoretical process]

Chapter 1. Introduction

In this chapter a background on the photochemistry of sunscreens is presented to contextualise the current understanding of a selection of organic molecules that act as ultraviolet filters in the natural world or in our cosmetic care industry and why such molecules are important for personal and public health. References are made to spectroscopic concepts that are important in understanding the experimental work in the body of this thesis, along with a general picture of energy flux in small molecular systems and an explanation of how sunscreen performance can be quantified and assessed in the laboratory. Particular emphasis is drawn to mycosporine-like amino acids (MAAs), the highly efficient natural product sunscreens that inspired some of the investigations that were undertaken during this research; and to avobenzone and octocrylene – two globally important sunscreen active ingredients.

1.1 Photochemistry, Sunscreens and Spectroscopy

Light has been a fundamental component of our Universe since the very beginning and the interaction of light with matter and the subsequent pathways for energy transformation and release are processes that are essential to life. The light from the sun provides the energy to sustain life on Earth by enabling photosynthetic organisms to produce carbohydrates, by creating the atmosphere, or for example by exciting an electron in a solar panel to generate electricity. Photochemistry (from "φως", from Greek for "light"; genitive case: "φοτος"→ photon) is, broadly speaking, the study of the fate of energetically excited molecules after they have gained energy by absorbing a photon. The excited state achieved when incident solar photons are absorbed by a chromophore in a molecule results from the resonant transfer of energy quanta that promote electrons to higher energy levels than the normal ground state. A chromophore can be thought of as a molecular blueprint or scaffold that absorbs particular wavelengths of light; and can range from individual bonds, e.g., C=O (carbonyl) and C=C (alkene) bonds, to long chains of -C=C- (polyenes), complex aromatic structures and heterogeneous collections of chromophores in e.g., eumelanin.[1] The ways in which a photoexcited molecule not in thermal equilibrium with its environment subsequently relaxes back to the ground state, or to other lower

energy states, by dissipation of heat can have functional applications - and an area where this is essential to understand is in sunscreen development or, in a more general framing, in molecular light-to-heat converters.[2]

'Sunscreen' is used throughout the text to refer both to the ultraviolet (UV) absorbing/blocking molecules themselves and the complex formulations that they are often present in. The natural world is a rich source of sunscreen compounds with optimised properties that have been selected through the environmental pressure of UV light, and therefore Nature's own pharmacy is an ideal starting point to search for promising molecules with photoprotective properties. By using spectroscopic methods, including modern ultrafast studies that have a resolution on the scale of important dynamic processes, and drawing insights from computational modelling, the molecular motions that take place femto- to nanoseconds after photoexcitation can be understood. We can go even further and provide a high level of understanding of the energy flux in specific small molecular systems under specific conditions; exemplified here in MAAs and in the dibenzoylmethane sunscreens that have been historically favoured by our personal care industries. In this research, the interaction of light is used with organic molecular sunscreens that were inspired by naturally occurring photoprotective compounds, namely MAAs; and other molecules that are hybrids of commercial UV filters. By using rational molecular design and interpreting the spectroscopic observables in our studies we are able to characterise molecules with potential applications as new sunscreens that can inspire confidence in consumers of the end-product formulations.

1.1.1 Historical perspective

In an article on the occasion of the UNESCO International Year of Light and Light-Based Technologies (2015) a history of optics was traced back to the thinking of Aristotle (384-322 B.C.E.). The ancient Greek philosopher characterised the nature of light as something that is 'active but transparent, something that isn't visible in itself but is made visible by the colour of some other thing' which, arguably, prefigures modern reflectance theories.[3] In *De anima* Book II, the ancient philosopher distinguished light absorption in the case of objects that have a colour during the day and a colour arising due to the emission of light, or luminescence, of some natural materials in the dark.[4] Later, Ibn-al-Haytham (Alhazen) (965-

1040 C.E.) demonstrated that light travels in straight lines through the Camera Obscura, or a pinhole camera where an exterior image is projected inside a box or tent structure; and argued that light is reflected from objects towards our eyes. This demonstration worked counter to an opposing theory that light was emitted from our eyes, or "the emission theory", that prevailed at the time.[5] Isaac Newton (1642-1727 C.E.), who famously characterised light as very tiny particles, considered how the internal properties of materials respond to interaction with light in *Optiks*: or, a Treatise of the Reflexions, Refractions, Inflexions and Colours of Light, where he asked "…all fixed bodies, when heated beyond a certain degree, emit Light and shine, and is not this emission perform'd by the vibrating motions of their parts?" and he adopted a corpuscular or particle view of light.[6] Newton is credited for conceiving of the first prism spectrometry and for that he invented the spectroscope – a scientific instrument consisting of a lens, prism and screen.[7] Later, Thomas Young (1733-1829 C.E.) demonstrated the interference of light in an 1807 lecture with an interference experiment which added to the understanding of the wave properties of light by demonstrating the inseparability of the wave and particle natures of light.[8] While these experiments helped to form the contemporary perception of light, other scientists showed the effect of light on observables such as on natural species or chemical compounds. In 1757, Iacopo Bartolomeo Beccari (1682-1766 C.E.) presented a paper to the Bologna Academy where he proposed that the fading of the colour of a flower was due to absorption of light and not the action of heat or air. Beccari demonstrated the relation between intensity, duration, and the colour of the absorbed light, comparing these to emitted light and linking specific chemical changes in the flower to interaction with light.
De Grotthuss, C.J.T. (1785-1822 C.E.) observed that alcoholic solutions of iron (III) chloride give a precipitate of iron hydroxide when exposed to light, demonstrating a cause-and-effect relationship. In the modern era, Thomas A. Edison (1847-1931 C.E.) was instrumental in taking us from an industrial world of candles and gas lamps to a new world illuminated by light bulbs. Further significant observations such as James Clerk Maxwell's (1831-1879 C.E.) definition of light as an electromagnetic spectrum in *Theory of Electromagnetic Field* (1865) with electric and magnetic fields that propagate at the speed of light, and De Broglie's (1892-1987 C.E.) postulation in his PhD thesis that light as a particle can be associated with a waveform contributed to the early 20th century concept of the duality of light (i.e. possessing both particle and wave-like qualities) and laid the foundation for the invention of coherent light, or laser technology, and the wide-ranging applications and opportunities of light response materials for modern civilisation. While in theory any part

of the light spectrum can be utilised, particular interest exists in materials that absorb either in the visible or ultraviolet ranges. All-visible light switches are one technology available for visible wavelengths;[9] while the focus of this research is on molecules that absorb in the UV range.

1.1.2 Ultraviolet radiation

Ultraviolet radiation (UVR) describes part of the non-visible part of the electromagnetic spectrum, consisting of wavelengths between 10-400 nm. This places UV light between X-rays (at shorter wavelengths) and at longer wavelengths to the highest energy violet light of the visible spectrum. UVR is sub-divided into UVA (320-400 nm, 3.88 – 3.1 eV), UVB (280-320 nm, 4.43 – 3.88 eV), UVC (100-280 nm, 12.4 eV – 4.43 eV) in order of increasing energy. Owing to the biological activity of certain wavelengths, UVA can also be sub-divided into UVAI (340-400-nm) and UVAII (320-340 nm).[10] An important band at lower energy is photosynthetically active radiation (PAR) or light between 400-700 nm and is the portion of the spectrum used by plants for photosynthesis.[11] While the divisions of the light spectrum mentioned here are useful in some contexts, a complicating factor in aligning the physical chemistry with the biology is the simple fact that action spectra for biological effects of UV do not fall neatly into definitions of UVA, B, and C wavelength regions.[12]

1.1.3 Solar radiation

Solar radiation extends from short, high-energy wavelengths with ionising radiation (<10 nm wavelengths) to UVR, visible light and infrared (IR). The solar spectrum that reaches the Earth's surface is a non-ionising radiation of wavelengths between 290-3000 nm comprising ~10% UVR, ~40% visible and ~50% IR. The terrestrial solar spectrum is affected by many atmospheric factors since Earth's atmosphere is a continuously changing filter that modifies the sunlight that travels through it.[13] One useful estimation to picture how UV propagates, is that UV increases by 4% for every 300 metre increase in altitude and at half metre depth under the sea UV is still 40% as intense as it is at the surface.[14] The American Society of Testing and Materials (ASTM) reference spectra (re-produced below from publicly available

data in Figure 1.1.) represent solar spectral irradiance under a set of specified atmospheric conditions. The three spectra displayed are the 2002 extra-terrestrial spectral irradiance, the global total spectral irradiance on the 37° sun-facing tilted surface for the atmospheric conditions known as U.S. Standard Atmosphere and the direct normal spectral irradiance.[15] The relevant international standard is ISO 9845-1: 1992. The difference between the extra-terrestrial spectrum (**black** trace) and the direct and tilted measurements shows the large degree of absorption of UVB within the atmosphere and the lesser degree of UVA absorption. UVC and high UVB is completely filtered out by stratospheric ozone (O_3) where it causes dissociation to molecular oxygen (O_2) and atomic oxygen (O). Longer UVB wavelengths are filtered out by air pollution, cloud cover and other environmental factors. As a consequence, the majority of UVR at surface level is UVA (90%+), which highlights the risk of personal exposure to these wavelengths.

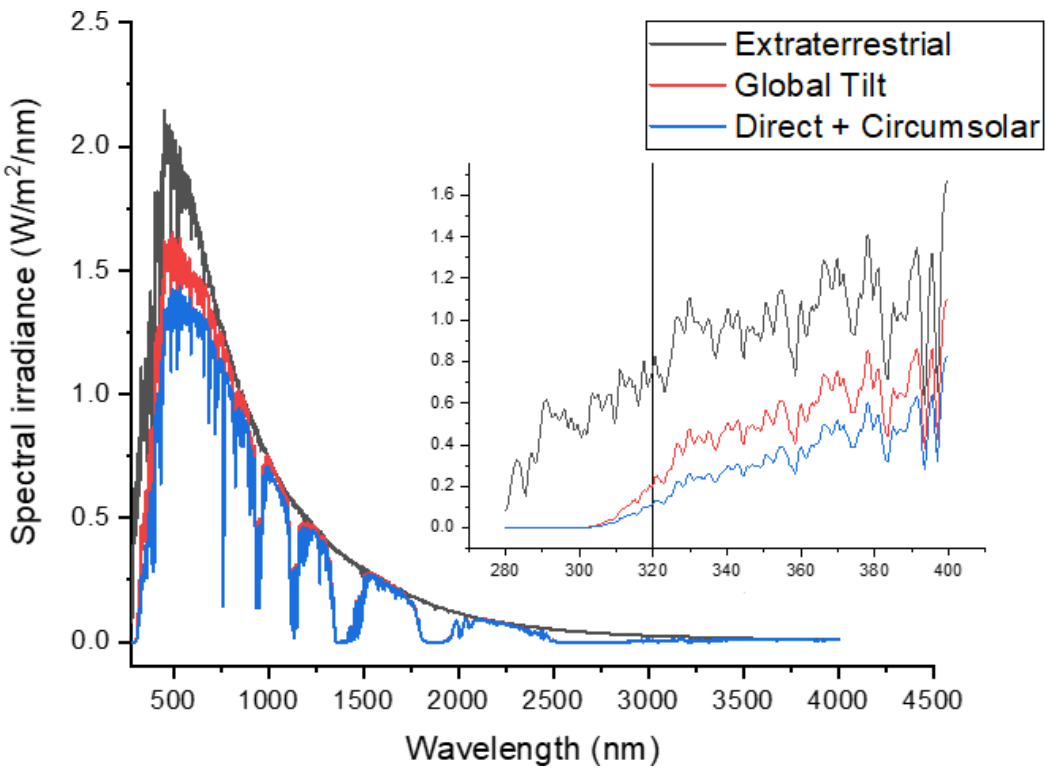

Figure 1.1. ASTM G173-03 reference spectra derived from SMARTS v. 2.9.2. Presented as the total spectra and then with a 280-400 nm range in focus. The inset vertical line delineates UVA and UVB.

1.1.4 Relationship between energy and wavelength

The interaction between light and matter is fundamental to the field of spectroscopy, which itself is made possible from the prediction of quantized energy levels derived from quantum mechanics. Electrons are restricted to a specific set of levels with discrete energies and a particular electron is said to occupy that energy level. Emission spectra or *line spectra* show that only certain wavelengths of light or in terms of the duality concept of light, photons of a particular energy, are emitted by excited atoms. For example, there is a highly characteristic emission line of sodium atoms at 589 nm.[16] If the energy levels were not quantized in this way in an atom or molecule then photons of any energy would be emitted following a change in energy of the electron configuration, and this is not the case. The wavelength of light, λ is related to its frequency, ν and the speed of light, c by:

$$\lambda \cdot \upsilon = \mathrm{c}$$

The Planck-Einstein relation encodes that light is composed of photons of energy, E, which is related to the frequency by the Planck constant, h:

$$E = h \cdot \upsilon$$

It follows that the energy of the photon is inversely related to the wavelength of light by:

$$E = h \cdot \frac{c}{\lambda}$$

Therefore, the light of a particular wavelength corresponds to photons of a particular energy which can be thought of as a particle-like “light-quanta”.

As is this case for all molecules, which are by definition multi-electronic systems, an electronic configuration is generated by virtue of how the atomic orbitals are occupied by

the electrons. The orbitals are populated from the lowest energy with the maximum occupancy of each orbital limited to two electrons of opposite spin. The intrinsic property of spin is what allows two negatively charged electrons to occupy the same orbital.

1.1.5 Laws of Photochemistry

The conditions for light and matter to interact are expressed in two laws of photochemistry. The first law states that light has to be absorbed to cause a photochemical reaction (the Grotthuss-Draper law). The second states that each molecule that takes part in a photochemical reaction initially absorbs one quantum of radiation (the Stark-Einstein law). For absorption to occur the energy gap between the initial state and the final state must match exactly, a requirement known as the 'resonance condition'.[17] Of course, after absorption of light and a consequent increase in the energy of the system, a number of processes can occur and these are best understood through the lens of electronic spectroscopy.

1.1.6 Selection Rules and Principles of Electronic Spectroscopy

The transfer of electrons within the orbitals of a molecule is subject to quantum selection rules and thus an understanding of quantum chemistry is essential to rationalise the photochemical behaviour of molecules. The strongest or most favourable absorption is for a fully allowed (both spatially and in terms of spin) process and any weaker absorption is due to selection rules that dictate how likely a certain process is to occur. There are also some additional principles that are applied to understand the molecular structures involved in photochemistry.

The Beer-Lambert Law states how the absorbance of a material is directly proportional to the pathlength (or thickness), the concentration (in solution phase) and a function of the material itself. It is expressed as:

$$A = \log(\frac{I_0}{I}) = \epsilon(\lambda) \cdot l \cdot C$$

where I_0 = intensity of the incident light, I = the intensity of the detected light, l = pathlength, C = concentration and $\epsilon(\lambda)$ is the wavelength dependent molar extinction coefficient, which additionally depends on solvent, pressure and temperature. A table of typical approximate values for the molar extinction coefficients of a number of compounds is given in Table 1.1.

Table 1.1. Examples of approximate molar absorption coefficients, ϵ from ref[18].

Compound	**ε (L mol^{-1}cm^{-1})**	**Compound**	**ε (L mol^{-1}cm^{-1})**
Benzene	200	**Acridine**	12000
Phenol	2000	**Biphenyl**	16000
Carbazole	4200	**Bianthryl**	24000
1-Naphtol	5400	**Acridine orange**	30000
Indole	5500	**Perylene**	34000
Fluorene	9000	**Eosin Y**	90000
Anthracene	10000	**Rhodamine B**	105000
Quinine sulfate	10000		

The Franck-Condon principle explains that when an electron is excited from the ground state, the positions of the atoms adapt to the new spatial electronic arrangement but that this process is delayed relative to the much faster electronic motion. Immediately following excitation, the molecule is in an electronically and vibrationally excited state. This initial excitation is referred to as a vertical transition which relates to the idea that the nuclei remain stationary on the timescale of an electronic transition, and therefore a line representing the transition drawn on a nuclear co-ordinates vs. energy diagram will be a

vertical line. Consequently, the region of the potential energy surface, i.e., an imaginary surface that relates nuclear/molecular co-ordinates and their relative energies, following excitation is sometimes referred to as the Franck-Condon region or geometry. The relative dexterity of the electron to the atoms is explained by the Born-Oppenheimer approximation, which relies on the idea that nuclear and electronic motion can be separated due to the large mass difference between them ($m_{proton}/m_{electron} \approx 1836$). The probability or intensity of the transition taking place is then proportional to the dipole moment for the vibronic (i.e., mixture of vibrational and electronic states) transition, which in turn is governed by the amount of overlap of the vibrational modes of the various states involved.

In molecular systems, the LaPorte symmetry selection rule states that the donor (i.e., source of the electron/s) and acceptor states (i.e., destination of the electrons) should have different symmetries. For example, a donor α orbital which is centrosymmetric would have an allowed transition to an acceptor α* orbital which is asymmetric with respect to the centre of inversion, and vice versa. While useful for estimating transition probabilities, distortions can occur through molecular vibrations that alter the symmetry elements of an orbital and thus symmetry rules can only provide a likelihood that a transition will occur.

The spin state of the acceptor and donor states also governs electronic emission and absorption intensity. A state with no unpaired electrons is a singlet state; 1 unpaired electron is a doublet state; 2 unpaired electrons is a triplet state; and 3 unpaired electrons is a quartet. In a transition, spin must be preserved and thus the number of unpaired electrons must be the same in both states; and this relates to the energy barrier of changing the spin state. To determine the multiplicity of a state the number of parallel spins is multiplied by two and one is added. For example, 2 parallel spins plus 1 is a triplet state (3). There is a selection rule that is simply stated as

$$\Delta s = 0$$

where the spin quantum number, s, is forbidden to change during a transition.

1.1.7 Relaxation from an Excited State

There are mechanisms by which a molecule can relax back to the ground state by transfer of energy within the molecule without re-emitting the absorbed energy. Internal conversion (IC) for example is radiationless. A molecule trapped in an energetically excited state with no pathway to relaxation will instead lose energy by emitting a photon radiatively. If the emission occurs from a singlet state this process is called fluorescence; and from a triplet state this is phosphorescence. The released radiation is lower in energy than the absorbed radiation which can be observed as a red shift (or Stokes shift) in fluorescence spectra, with the 'lost' energy having been dissipated as heat in molecular collisions and vibrational relaxation. Vibrational relaxation is thought of as an ensemble process in the solution-phase systems under consideration in this thesis with both intramolecular vibrational redistribution and intermolecular energy transfer components. Additionally, phosphorescence is a slower process compared to fluorescence due to the triplet excited to ground state being a spin forbidden transition. Approximate lifetimes for the processes discussed are presented in Table 1.2 and a schematic of the processes is presented in Figure 1.2.

Table 1.2. Approximate lifetimes of the processes that lead to energy loss from the excited state.

Relaxation process	**Approximate lifetime τ /s**	**Scale**
Fluorescence	10^{-7} – 10^{-1}	10^{-3} = millisecs/ms
Phosphorescence	10^{-6} - 1	10^{-6} = microsecs/µs
Internal Conversion (IC)	10^{-11} – 10^{-9}	10^{-9} = nanosecs/ns
Intersystem Crossing (ISC)	10^{-14} – 10^{-8}	10^{-12} = picosecs/ps
Vibrational Energy Transfer	10^{-12} – 10^{-8}	10^{-15} = femtosecs/fs

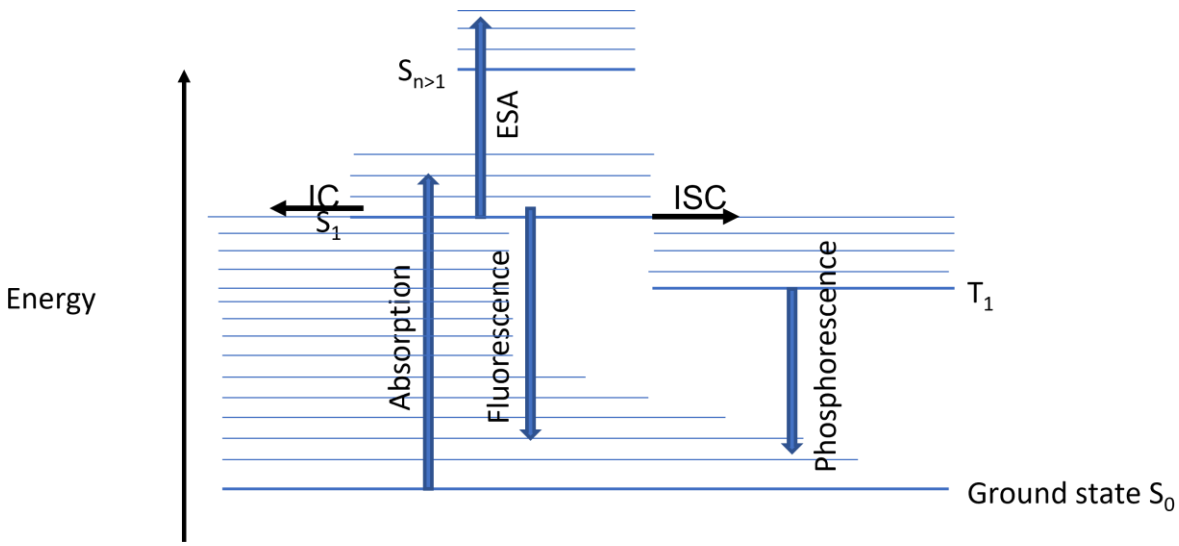

Figure 1.2. Qualitative Perrin-Jablonski diagram (or state-energy diagram) illustrating processes discussed in the text. Vibrational energy transfer occurs between the narrowly spaced (fainter) lines of the excited vibrational modes within each electronic state. Excited state absorption (ESA) shows that further absorption can occur within the excited state. Vertical transitions drawn as thicker blue arrows. IC is non-radiative and allows relaxation of the excited state by relaxing through vibrational levels. NB. Fluorescence always occurs from the lowest vibrational energy level in the S_n state.

Typical ways in which a molecule can relax efficiently without radiation is the distribution of energy into rotational and vibrational states during a cis-trans isomerisation, which is the way in which the sinapate or related cinnamate class of sunscreens relax efficiently to the ground state after UVB (and to some extent UVA) photoexcitation.[19,20] Energy transfer into vibrational modes means that the absorbed energy is converted into heat, which is then lost to the solvent bath or surrounding environment, and full relaxation of an excited state to the ground state can occur in this way efficiently if the vibrational modes of the states involved overlap and energy can move easily between them. In addition, the larger the molecule, the greater number of vibrational modes available for redistribution and the faster the vibrational cooling. A general rule is that the number of vibrational modes is equal to 3N-6 where N is the number of atoms in the molecule. A further consideration is that these processes are dependent on many factors not limited to solvent and temperature; with the ability of molecules to only fluorescence in certain environments having functional applications; e.g., 1,6-diphenyl-1,3,5-hexatriene (DPH) does not fluoresce in water but becomes highly fluorescent in organic solvents or lipid membranes and is used

as a fluorescence sensor for imaging membrane lipid domains.[21] In Chapter 1 of Valeur and Berberan's textbook on Molecular Fluorescence, a useful figure illustrates possible de-excitation pathways of excited molecules and is presented here as a summary and extension of the concepts discussed thus far (Figure 1.3.)

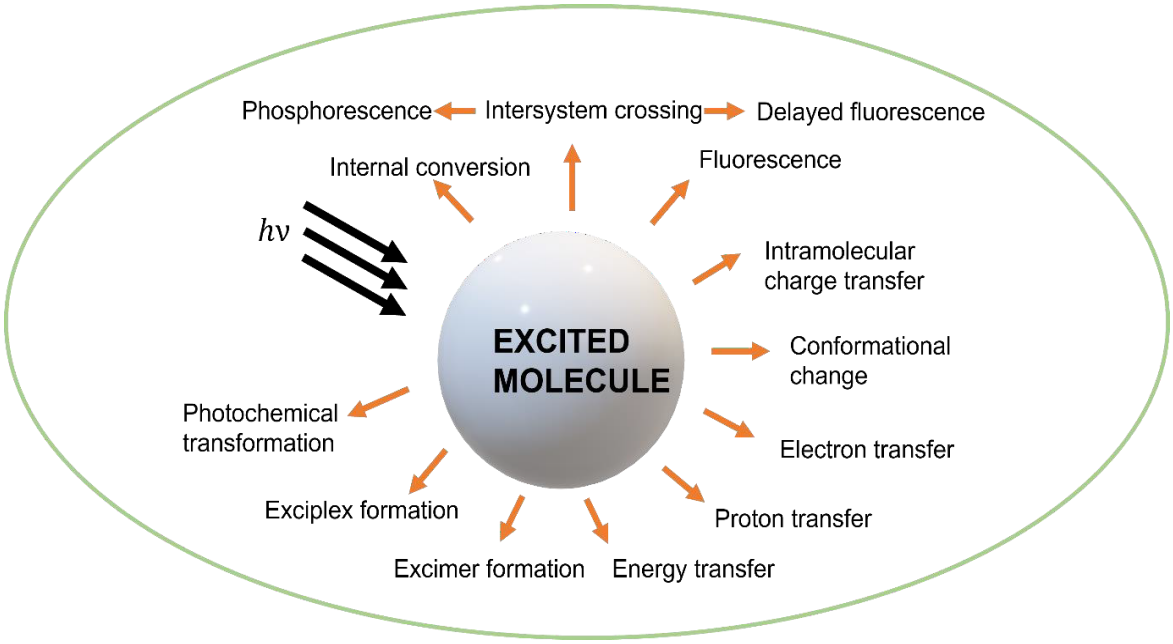

Figure 1.3. Various de-excitation processes, from ref[18].

1.1.8 Internal Conversion and Conical Intersections

Internal Conversion (IC) in photochemistry describes a radiationless de-excitation via a transition along an atomic reaction co-ordinate from a higher electronic state into a lower one. It relies on the coupling of the vibration modes of each state and is a function of the energy gap between states ($\Delta E_{1,2}$ for states 1 and 2) and the vibrational frequency υ, and is described by the following expression; highlighting that the smaller the energy gap the faster the rate of IC:

$$K_{IC} \propto e^{\left(\frac{-\Delta E_{1,2}}{h\upsilon}\right)}$$

A transition can occur through a conical intersection (CI) which is when two electronic states are iso-energetic, i.e., $\Delta E_{1,2} = 0$. It can be visualised as the meeting of the tips of two cones on an energy surface.[22] At the intersection, the Born-Oppenheimer approximation does not apply and the slightest perturbation leads to coupling between the electronic and nuclear motions. It is possible to conclude that molecules with accessible CIs are likely to dissipate energy efficiently. This key juncture in an energy flow and its relation to high performing sunscreens is exemplified by the accessible S_1/S_0 CI in gadusol/gadusolate and is referred to in many of the systems to be discussed.[23]

1.1.9 Intersystem Crossing and the Triplet state

It can be assumed that most organic molecules are singlets in the ground state and thus direct excitation to the triplet state is forbidden by the spin selection rule. However, the triplet state can be accessed instead by initial excitation to a higher singlet state followed by intersystem crossing. As the lowest excited triplet state is lower in energy than the lowest excited singlet state, electrons can relax from the singlet to the triplet state whereby the spins flip without releasing a photon. Intersystem crossing (ISC) is a radiationless transition between two electronic states with different multiplicities e.g., from the lowest singlet state to the triplet manifold. ISC is forbidden by the rule of conservation of angular momentum and thus occurs at long time scales. El-Sayed's rule states that the rate is relatively large if the transition involves a change of orbital type. For example, a ππ* singlet can transition to a nπ* triplet state. This rule aids understanding phosphorescence, vibrational relaxation, intersystem crossing, internal conversion and lifetimes of excited states in molecules.[24] Finally, as relaxation from a triplet state back to the singlet ground state is spin-forbidden the process is relatively slow (i.e. seconds to hours, see Table 1.2, above) and is termed phosphorescence. A chromophore in the triplet state behaves as a diradical, i.e. a species with two unpaired electrons, and is thus highly reactive and a starting point for many chemical reactions.[25] For the purpose of our sunscreen design, the presence of triplet states is thus seen as a liability.

1.1.10 Photostable process vs Bond-breaking/formation

Instead of relaxing to the ground state, a molecule in an excited state may undergo a bond-breaking or bond-forming reaction. If light is used in the initial excitation, then this is referred to as photolysis. Further if the sources provide coherent, monochromatic and direction light, then this is laser photolysis. The difference between a photostable situation where the energy is dissipated by radiative and non-radiative processes and a photolabile situation where new chemical products are formed can be illustrated by the two cases.
Firstly, the photostable situation:

$$R + hv \rightarrow R^{*} \rightarrow R$$

where R is the chromophore in the ground state, R* the same chromophore now in the excited state and the second arrow indicating a photophysical process with reformation of the starting chromophore. Secondly, the photolabile situation:

$$R + hv \rightarrow R^{*} \rightarrow I \rightarrow P$$

where I is a reactive intermediate and the final arrow is a thermal chemical process, and P is a chemical product.[17] Photoproducts can be identified in a number of ways, for example by comparing an NMR spectrum before and after irradiation, or by chromatography coupled with mass spectrometry to identify new masses in the reaction mixture. Often for our purpose the appearance or disappearance of absorption bands on a UV-vis spectrum is indicative of loss of starting materials or gain of new products. However, this method is not as robust as combined NMR/chromatography studies as it is possible that photoproducts have absorptions that are indistinguishable from the parent molecule and therefore go undetected by UV-vis spectroscopy. Even if the photoproducts in this case were non-toxic and still absorptive in the UVA/UVB, the photochemical characterisation would be somewhat incomplete. Photodissociation studies, not covered in this thesis, where the intention is to induce the loss of an atom can be used to elucidate photochemical

pathways; for example, in the photodissociation of aniline ($C_6H_5NH_2$) in the gas phase where photoexcitation (ca. 240 nm) to the $2^1\pi\pi^*$ state results in H-atom loss.[26]

1.1.11 Photosensitization

Photosensitization occurs when an excited state molecule collides with another molecule and transfers energy in a radiationless process. As this does not involve absorption or emission of a photon it is not governed by the selection rules above and can also lead to formation of a triplet state. This mechanism can be used to excite molecules that don't have strongly absorbing chromophores through excitation of a different molecule with a stronger chromophore followed by collision and energy transfer.

1.1.12 Effects of UVR in humans

Skin is the largest human organ and throughout a normal day is exposed to a variety of environmental stressors, including exposure to UVR. UV is a double edged sword for biological systems as, while essential to life, overexposure to the non-ionizing sections of the electromagnetic spectrum emitted by the sun is a known risk factor for acute and chronic diseases in humans.[27] Indeed, UVB light of 267 nm or 4.64 eV is able to directly ionise the DNA chain.[28] Disease pathways include photo dermatoses, inflammation, immunosuppression, premature skin ageing (photoaging) and cancer (particularly, basal cell carcinoma, squamous cell carcinoma and malignant melanoma).[12,29–32] The phenotype of extrinsically photoaged or prematurely aged skin can be distinguished from intrinsically aged skin by the presence of deep wrinkles, uneven pigmentation, rough texture and lack of hydration.[33] However, the physiological responses to UVR can also be beneficial, from enabling vitamin D and endorphin synthesis and modern light-based therapies.[34] A positive, life-sustaining effect of UVR is in the synthesis of vitamin D, which is essential to Ca regulation in the human body and prevention of osteoporosis and skeletal disease. Sunlight may also have a role in improving symptoms of mental health conditions by regulating mood and cognitive function.[35] While humans have presumably been aware of the need for some protection from the worst effects of overexposure throughout history, the particular role of UVA was in modern times underappreciated as its effects are not as obvious as

those of UVB. While UVB radiation causes burning of the skin – known as erythema, UVA's effects are cumulative and longer acting. Indeed, to produce the same erythemal response, approximately 1000 times more UVA dose is needed compared with UVB.[36] UVA radiation is able to penetrate deeper within the layers of the epidermis, and a small portion reaches sensitive subcutaneous tissue in a wavelength dependent manner, as illustrated in Figure 1.4.[37] When radiation reaches the basal layers responsible for the proliferation of epidermal cells, it contributes significantly to skin damage.[38] Indeed, 2-3 million non- melanoma skin cancers and over 100,000 melanoma skin cancers are diagnosed around the globe each year.[14] Our own physiological response to overexposure is an increase in melanin production but this is not fully effective in preventing damage; people with lighter skin have very low levels of melanin and it only absorbs about ¾ of the incident light in a slow response cycle that may take 3-5 days to provide sufficient photoprotection.[34,39,40] Melanin is actually at the centre of a paradox: energetically excited melanin fragments can transfer energy to DNA via a quantum triplet state, even in the dark and long after UVR exposure, causing delayed damage and mutations.[41] As public awareness has grown, thanks in part to public health campaigning, the importance of broadband sunscreens to efficiently block UV from reaching the skin is a topical issue in both popular media and scientific literature.

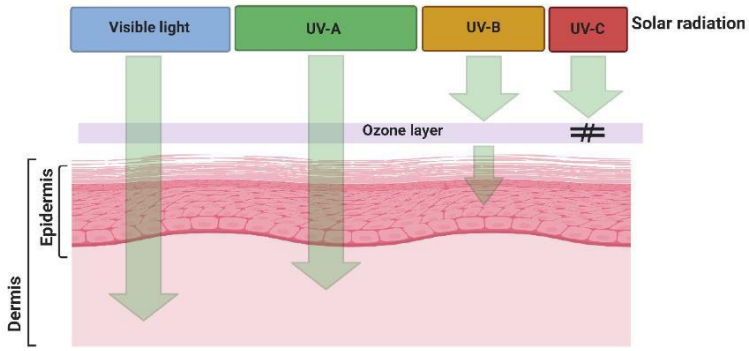

Figure 1.4. Diagram adapted from ref[42] showing the penetration of UV radiation into the skin layers. Skin homeostasis is maintained by mesenchymal stem cells in inner layer dermis and epidermal stem cells in the outer layer dermis. This is a simplified model of the human skin and does not include any of the specialized cells, including melanocytes and sensory nerve endings of the skin; nor the more subtle delineation of the epidermis into the strata spinosum, granulosum and corneum. For more information on the *burden of disease* refer to the review by Baker et al.[43] and for cell models for skin ageing through UVR exposure in the review by Panich et al.[32]

1.1.13 Effects of UV on DNA

The previously discussed "negative effects" of photoaging and carcinogenesis are mediated through UV's direct and indirect toxicity to DNA.[44] Direct effects of irradiation occur when DNA absorbs UVB photons resulting in structural rearrangements of nucleotides, manifesting as defects in the DNA strand.[32] A selection of deleterious outcomes for a strand of DNA affected by UV light is shown in Figure 1.5. A hallmark of UV damage is the formation of cyclobutene pyrimidine dimers (CPDs) or 6-4 photoproducts within picoseconds of irradiation; resulting in cytosine-to-thymine changes in DNA after replication.[41] The undesirable result of dimerization of adjacent pyrimidines (i.e., CC or TT) is a structural kink in the DNA strand that prevents pyrimidines from base pairing and prevents replication. Oxidative modifications to DNA is a less direct method of inducing mutations and proceeds via generation of reactive oxygen species or free radical that interacts with an oxidises DNA bases. Hallmarks of this process are single-stranded breaks and G to T transversion, where guanine is first oxidised to 8-oxoguanine and can no longer base pair to cytosine but can instead pair with adenine via two hydrogen bonds; when the second strand is synthesised the original guanine position is now occupied by thymine.

As may be expected, there are endogenous repair mechanisms or ways the body has evolved to reduce damage; including base excision repair (BER) of e.g. 8-oxo-dG, performed by enzymes, e.g. 8-oxoguanine DNA glycosylase (hOGG1); and subsequent restoration of DNA by DNA polymerases.[45] These mechanisms are unfortunately error-prone and deficiencies of any of the required proteins leads to diseases associated with DNA damage and premature skin ageing, including xeroderma pigmentosum, Cockayne syndrome and trichothiodystrophy.[46]

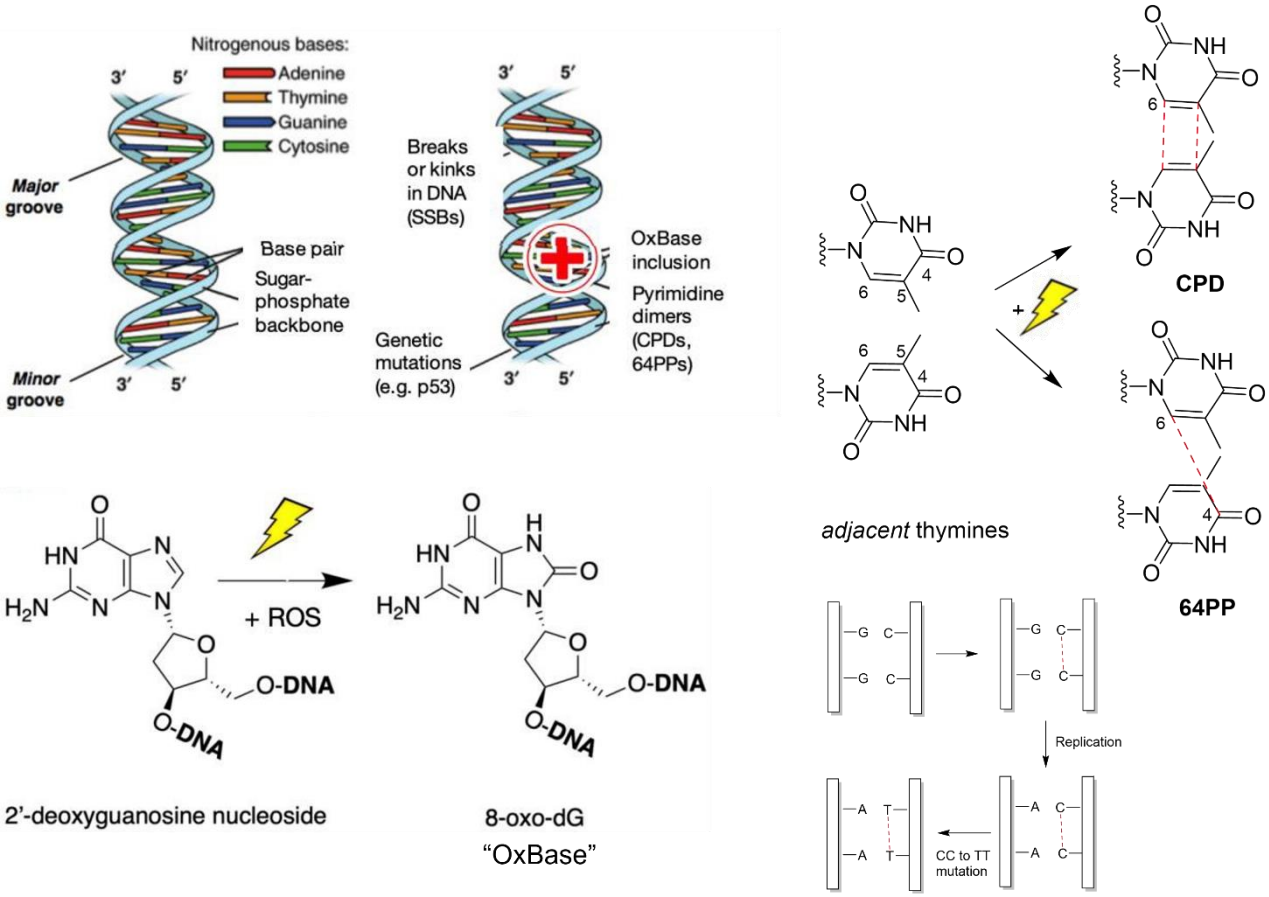

Figure 1.5. An example of DNA base modification caused by UVR exposure. Overexposure can lead to irreversible modifications of genes, such as the p53 tumour suppressor gene[30] and the onset or acceleration of disease as well as premature skin ageing. CPD: cyclobutene pyrimidine dimers. SSB: single strand breaks. ROS: Reactive oxygen species. 64PP: 6-4 PPs or pyrimidine (6-4) pyrimidone. The effect of ROS is driven primarily by UVA radiation exposure.

1.1.14 Notes on standards used in UV exposure

The total erythemal radiation received can be expressed in terms of standard erythema dose unit (SED) where 1 SED is defined as 100 J/m^2 erythemally effective radiation.[47] Strictly, the action spectrum is for erythema (sunburn), but it is also used as a proxy in quantifying UV for other UV effects.[48] The UV index, used globally in weather forecasting and for public health information, is simply erythemally effective UV scaled to give a dimensionless number between 1 and 12 (or more in extreme cases) that indicates the instantaneous sunburning potential of solar radiation. The minimum erythema dose (MED) is also based upon the erythema action spectrum, being the minimum dose of erythemal

radiation that produces a faint but perceptible reddening of the skin 24h after irradiation.[49] However, the MED is not a standardized term but a personal measure of susceptibility to sunburn; and indeed, there is such variation in the human response that the action spectrum can never be exact. In any case, the impact of increasing global temperatures, higher radiation flux at sea level and depletion of the stratospheric ozone layer, as well as societal trends and habits, is predicted to increase this form of exposure in the coming years.[50]

1.1.15 Sunscreens and Suncreams

At least since the chemistry student Franz Greiter suffered overexposure to solar radiation while climbing the mountain Piz Buin on the Swiss-Austrian border, modern sunscreen technology has sought to provide a topical, extracellular barrier to the penetration of UVR into the skin.[51,52] One earlier formulation "Ambre Solaire" was developed by L'Oréal founder, Eugène Schueller in 1935 and contained benzyl salicylate - a UVB absorber that was applied to the upper epidermis of the skin that helped to prevent sunburn, and is still used today in a range of products.[51] In 1944, Benjamin Green invented a sticky petroleum based sunscreen (RVP) to protect US troops against overexposure in the Pacific climates during World War II.[53] Despite progress in the range of products available (see Figure 1.6.), the cytotoxicity and environmental impact of current state-of-the-art sunscreens in global markets are a cause for concern to everyone from environmental campaigners to consumers and regulators; and such issues are subject to heated debate and competing interests. A particular focus since the 1990s has been to improve protection against UVA radiation. Indeed the sun protection factor (SPF) rating of sunscreens, as benchmarked by an erythemal response, only indicates UVB protection and there are now separate standardised tests for UVA protection, including the Persistent Pigment Darkening (PPD) test, the Critical Wavelength (CW) test and the Boots Star Rating system.[54] The Boots Star Rating system for instance takes chemical stability into consideration and the maximum rating (5 stars) is awarded only if the before and after UVA/UVB ratios are >0.89 and >0.86 respectively. European guidelines set a requirement for the minimum ratio of UVA protection alongside UVB protection, currently 1:3. When a sunscreen claims to be broad spectrum it is commonly understood that 10% of total protection is in excess of 370 nm, - the CW. As well as the organic filters discussed in this thesis, inorganic or mineral filters

(e.g., titanium dioxide or zinc oxide) are an alternative and work by a mixture of absorption and/or scattering of UVR light away from sensitive tissues, rather than absorption and dissipation as heat; and these are not discussed further.

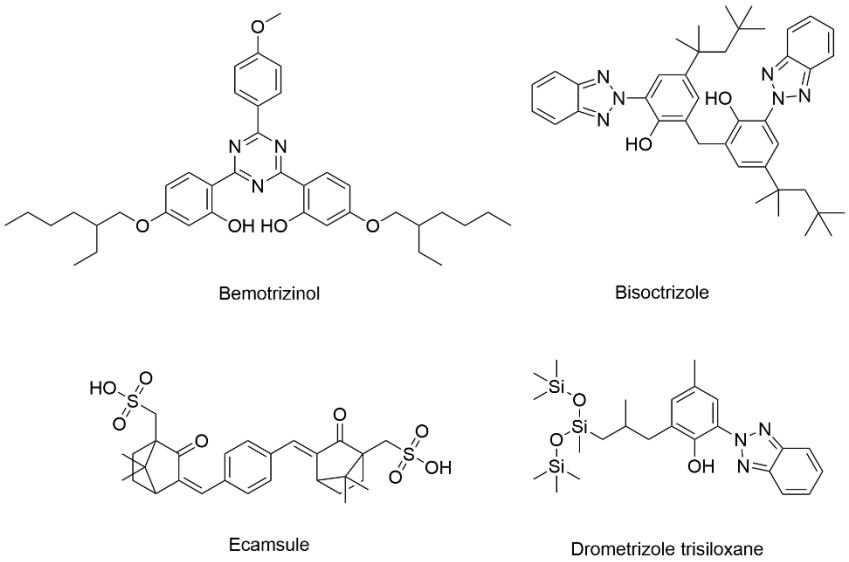

Figure 1.6**.** UVA absorbing compounds currently available in products in European markets and typical of the state-of-the-art UVA filters. Trade names: Mexoryl SX (Ecamsule), Mexoryl XL (Drometrizole trisiloxane), Tinosorb M (Bisoctrizole), Tinosorb S (Bemotrizinol).

1.1.16 Sunscreen safety

The safety of current sunscreens has been challenged and many legislators are moving to limit or ban certain sunscreen ingredients; and a number of existing challenges with current sunscreens are reviewed by Stavros et al.[23] Oxybenzone and benzophenones in general have been associated with reported allergenic responses, and the American Contact Dermatitis Group listed benzophenones as the allergen of the year in 2014. The amount of certain molecules allowed in a formulation is also limited, typically to around 5-10% but despite this, commonly used UV filters (oxybenzone, avobenzone, octocrylene, ecamsule,

octisalate, octinoxate and homosalate) were reported at concentration above the FDA safety threshold in various environments.[55] This latter conclusion has been picked up by popular media with a representative article in the New Scientist magazine (2019) highlighting that "only two of the original 16 "safe" ingredients [listed by the FDA] can actually be considered safe and effective" and calls for further research.[56] That article centres on the argument that while sunscreens do protect the skin, we seem to know less about their other effects on the body and beyond. One of the most controversial links with sunscreen molecules is the bleaching of corals. The colour of corals is due to the symbiotic relationship with micro-organisms within the single-celled microalgae and these are expelled when corals are placed under stress. While it is true that many tonnes of sunscreen are deposited in the oceans and may accumulate in the environment, the major direct cause of bleaching is more likely to be a rise in sea temperature.[57] However there is certainly no desire to contribute any further persistent or toxic pollutants to an already challenged marine eco-system.

1.1.17 Natural sunscreens and photoprotectants

Terrestrial and marine plants and animals are exposed to UVR and they have thus evolved resistance to potentially toxic UV rays on geological time scales.[58] Strategies for UVR damage mitigation can be sorted into avoidance, protection and repair.[10] In mammals for example a mixture of a red (hipposudoric acid) and orange pigment (norhipposudoric acid) in the sweat of the hippopotamus (*Hippopotamus amphibius*) provides UV protection across the UVA and UVB.[59] In plants in particular, to protect against overexposure, the internal environment is regulated by producing molecules via the phenylpropanoid pathway, which is analogous to melanogenesis in humans.[60] In plants, diverse secondary metabolites possessing UV photoprotective and antioxidant properties are produced in response to light, of which terpenoids, anthocyanins, flavonoids, carotenoids, and phenolic acids are typical examples.[61] Phenolic compounds, polyphenols, phenols and flavonoids encompass the many molecules that have been extracted and characterised from natural botanical sources, typically with an alcohol or aqueous solvent.[62–64] When extractions are carried out on samples of marine organisms, like cyanobacteria and macroalgae, MAAs are typically detected alongside other compounds.[65–67] In a 2022 review on the Challenges and Prospects of UV Filters, Jesus and co-workers concluded that among all compounds from

natural extracts reviewed, catechin, epicatechin, gyrophoric acid, and resveratrol seem to be the most promising compounds obtained from botanical extracts; considering their photostability, photoprotective, antioxidant potential, and non-cytotoxic profile at the concentrations studied. When considering marine-derived metabolites, MAAs (palythine, asterina-330, shinorine, porphyra-334), and scytonemin also have excellent protective ability against UVR.[68] In one study by Radice et al., usnic acid extracted from four Chilean lichens, i.e. a consortium of fungal and photosynthetic partners, contained within a natural extract had a comparable SPF (=4.2) to commercially available sunscreen products (SPF 6).[69,70] It is perhaps unsurprising that many of the molecules that appear to have been selected to protect against UV, contain π-electron systems, since π-electron containing molecules are also the primary targets of UV radiation damage; a long list of endogenous compounds such as unsaturated lipids, nucleic acids and aromatic and indolic amino acids, containing polypeptides.[71] A summary is provided in Figure 1.7.

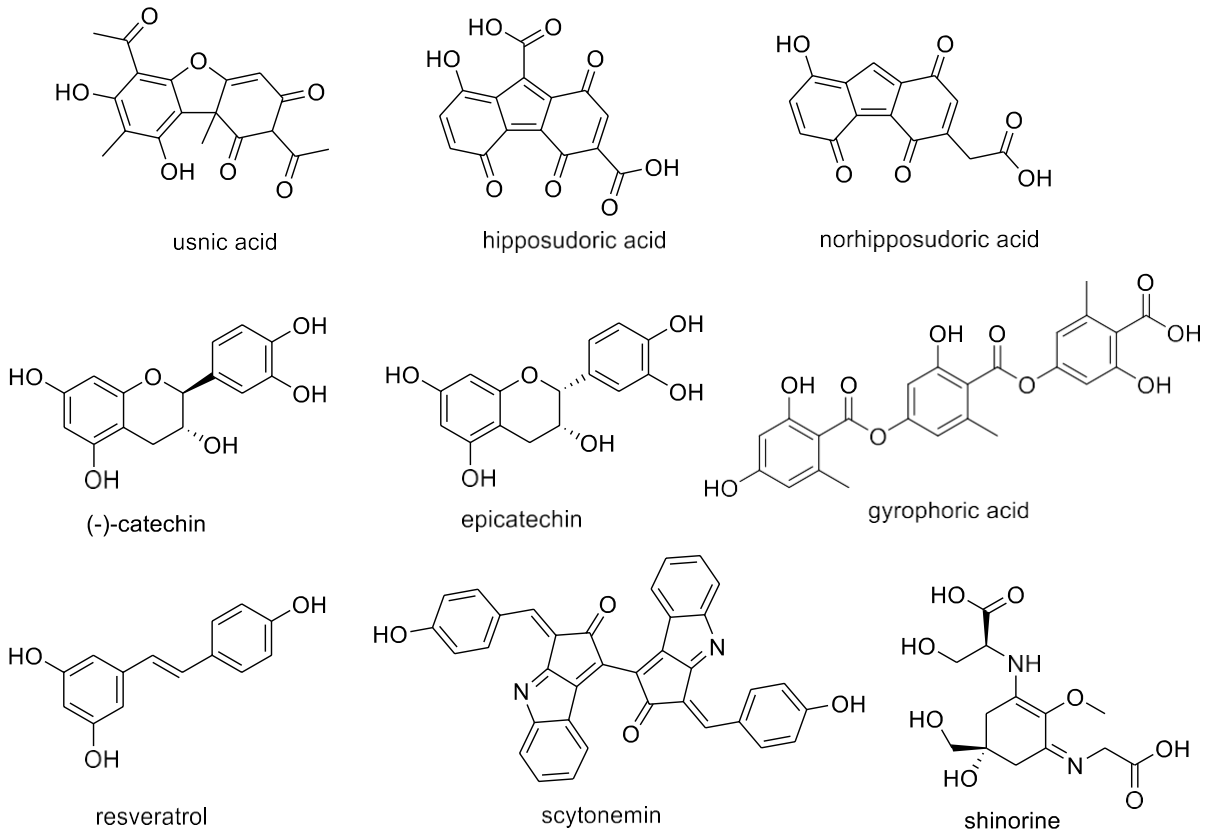

Figure 1.7. Promising photoprotectant molecules from natural extracts (from top left to bottom right): usnic acid, hipposudoric acid, norhipposudoric acid, (-)-catechin, epicatechin, gyrophoric acid, resveratrol, scytonemin and shinorine.

1.1.18 Mycosporine-like Amino Acids

Since they were first reported in the 1960s, mycosporines and their derivatives have been detected in a wide variety of fungi, bacteria and marine species including: cyanobacteria, marine algae, hermatypic coral, arthropod tissues, shrimp embryos, starfish, zoanthids and the lens tissue of fish up to maximum of 1% dry weight.[72–76] The name mycosporine is generally reserved for molecules that had been isolated from fungi and so the term mycosporine-like amino acids or MAAs is used in this thesis to refer to the complete family of related molecules.[58] In a study by Riegger and Robinson, the authors estimate that the presence of MAAs reduces the amount of harmful irradiation reaching cytoplasmic molecular targets in diatom cells by up to 50%, and even up to 72% in polar algae cultures (*Phaeocystis antarctica*).[77] However, their functions are thought to be manifold: they have putative roles as fungal sporulation inducing hormones, osmotic regulators, nitrogen reservoirs, antioxidants and/or microbial sunscreens.[78,79] It is worth nothing the fact that MAA molecules are transparent to visible light and are therefore not technically considered pigments; however a reference to a yellowish colour associated with mycosporine-like amino acids present in microalgae extracellular polymeric substances (EPS) suggests they are co-present with some pigments or may have a colour under some conditions.[80] Their low molecular weight and high water solubility are key features that allow them to be easily dispersed in the cytoplasm of microalgae and diatoms as well as the sun-exposed cells of marine invertebrates.[58] In general, MAAs are found in organisms that are routinely exposed to a high photon flux (namely intertidal, shallow-water and epipelagic species) and those that share, in a so-called 'symbiont hypothesis' of evolution, a genetic history with cyanobacteria. It is now accepted that hundreds of taxonomically diverse marine, freshwater and terrestrial organisms have the capacity to synthesize, accumulate and metabolize MAAs in order to address the direct and indirect damaging effects of UVR and the database will only increase as more researchers enter the field.[73]

MAA production varies with season and light exposure, and studies have shown that the quality and frequency of light can be used to induce the production of MAAs.[81] In a study by Bandaranayake and co-workers a clear depth dependence (i.e. MAA concentration vs. depth below sea level) was observed in Staghorn coral (*Acroposa formosa*) taken from between 1-15 m in the Great Barrier Reef (with a summary figure in Figure 1.8).[82] Other studies have concluded that microscale variations in the concentrations of MAAs along

algal thalli suggest that MAAs function as sunscreens as they respond to where light is incident on the organism; for example, young apical tips in *Palmaria palmata* (*P. palmata*) exhibit higher concentrations than older basal regions.[83]

A classic source of MAAs investigated is the edible red seaweed or dulse (*P. palmata*) found in northern Europe and along the Atlantic coast of North America. An aqueous methanol extraction and subsequent liquid chromatography isolated a mixture of mycosporines and MAAs with in vitro antioxidant activity and strong absorption of UVR; properties that were jointly attributed to a mix of MAAs. [84] A typical sample of MAAs were isolated by HPLC by Dunlap and co-workers (and is detailed in Figure 1.9).[85] Extraction procedures are required as the amino-acid nature of MAAs means that they have good water solubility and are therefore typically extracted from the cell cytoplasm.[58] Extracts yields are typically low; with one study by Sun et al. reporting an average of 1-2 mg/g seaweed (n = 323 different algae) using a unified extraction procedure of 40 °C for 2 hours in 3 cycles with a 1:25 g/mL solid–liquid ratio, but the current progress in the extraction, isolation and characterization of MAAs is far from sufficient in terms of effectiveness in application.[86] In one estimation the percentage of MAAs in the dry weight of MAA-producing organisms never exceeds 1%.[87]

A comprehensive database of known MAAs (MYCAS) is maintained online by Brazilian organisation, the *Centro de Energia Nuclear na Agricultura*. As of March 2022, there were 74 different MAAs in that resource.[88] A version that was accessed on 03/08/2022 is included in the Appendix. This database covers compounds that absorb light between 268-362 nm with high molecular absorption coefficients (ε=12,400-58,800 $M^{-1}cm^{-1}$). For comparison, the absorption coefficient of the leading sunscreen, avobenzone (ε=34 140 $M^{-1}cm^{-1}$) is in the same range.[89] The uniquely strong absorption in the UV range is the factor that has drawn attention to MAAs in recent years. However, to address the challenges of low extraction yields, complicated separations, and low natural abundance of MAAs, synthetic analogues have been proposed; and these are explored in Chapter 3 of this thesis.

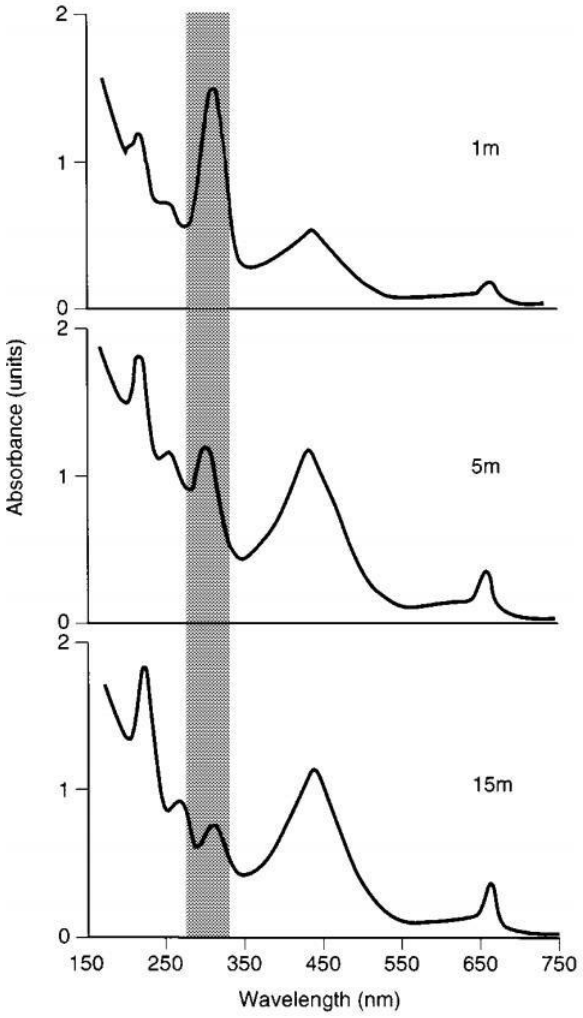

Figure 1.8. Re-printed from Ref.[82] UV-vis spectra in 20% THF/MeOH (v/v) from *Acropora formosa* tips collected at the indicated depths.

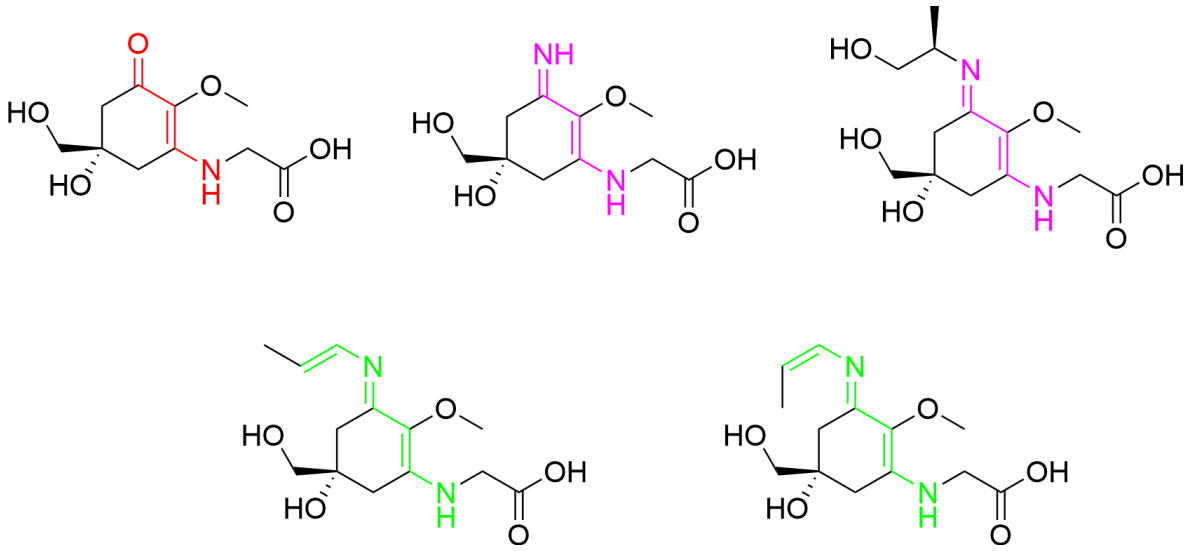

Figure 1.9. MAAs isolated in ref.[85] In order from top left to bottom right: Mycosporine glycine (containing the cyclohexanone scaffold, red), Palythine, Palythinol, Palythene and Usujirene (all containing the cyclohexenimine scaffold, purple and extended, green).

1.1.19 Natural synthetic pathways of MAAs

Gadusol (3,4,5-trihydroxy-5-(hydroxymethyl)-2-methoxycyclohex-2-en-1-one, see later Figure 5.1 for structure) is a molecular precursor to all MAAs and it was isolated from pre-spawning ovaries containing ripe eggs in cod (*Gadus morhua* L.) at a concentration of about 4 mg/g dry weight; with much lower concentrations in male and immature female cod.[90] In 2015 researchers found zebrafish could make gadusol which challenged the idea that MAAs are exclusively acquired by higher organisms through diet.[91,92] Following that discovery, the same gene cluster has been found in many species and may have originated from algae through horizontal gene transfer. Indeed, almost all vertebrates except for mammals have the genes to make gadusol. One theory to explain the loss of the gene cluster in humans is the so-called nocturnal bottleneck whereby the gene was not necessary, and therefore de-selected, during a primarily nocturnal period of our evolutionary history.[93] In any case many organisms within marine photosymbiotic systems, including the photo symbionts and the reef coral hosts themselves, are genetically capable of synthesizing MAAs and natural

routes to MAAs are many.[94,95] In Chapter 5, one natural pathway to shinorine and its associated biosynthetic gene cluster is discussed further and the heterologous expression of the C domain of a nonribosomal peptide synthetase (NRPS)-like enzyme from the cluster found in two species of cyanobacteria is investigated.

1.1.20 Identifying MAAs by HPLC-MS

Popular methods for identifying MAAs are a combination of HPLC and mass spectrometry. For example, mycosporine-glutaminol-glucoside and mycosporine glutamicol-glucoside were identified in microcolonial fungi by their UV absorption (310 nm) and by mass spectrometry (MS) via their molecular weights (465 m/z and 466 m/z, respectively, see Appendix for structures).[96] Where MS is unavailable it is possible to identify MAAs by retention time alone through the use of standards and retention time. In Chapter 5, HPLC is used in preliminary investigations to assess the activity, if any, of the C domain of a recombinant enzyme.

1.1.21 Bathochromic shifts in UV absorption spectra

Table 1.3 Summary of λ_{max} and ε for mycosporine glycine, palythine and palythene.

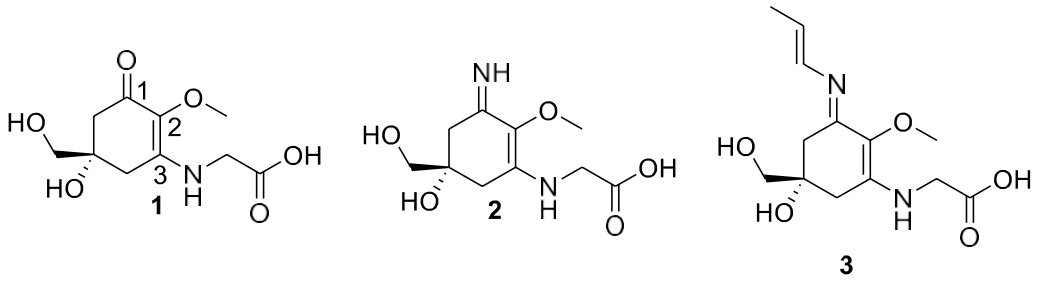

Compound	Name	λ_{max}	ε ($M^{-1}cm^{-1}$)
1	Mycosporine-glycine	310	28,800
2	Palythine	320	36,200
3	Palythene	360	60,000

The nature of the different substituents on the oxygen, or on the nitrogen atom in the 1-position has a significant effect on the λ_{max}. The greater the degree of electron

delocalisation or conjugation the longer the wavelength. This can be explained by a particle-in-a-box model as it is applied to conjugated polyene systems. In this simple model the energy difference between two energy levels is inversely proportional to the length of the 'box'. A general scheme, based on literature and results in Chapter 3, for the changing UV absorption of the MAA chromophore is summarised in Figure 1.10.

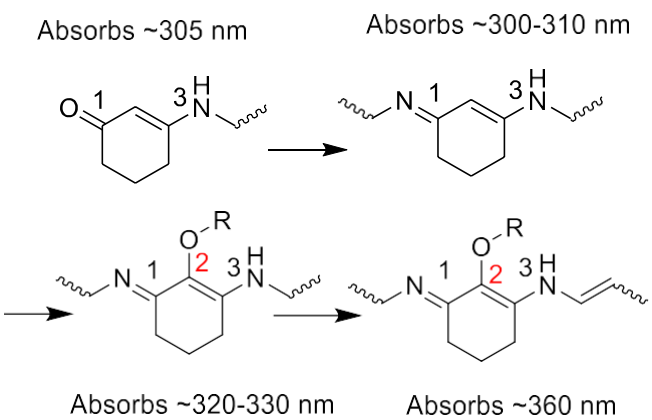

Figure 1.10. Shifting absorbance in the MAA motif due to increased functionalisation.

Energy levels are quantized (as discussed before) the energies corresponding to permitted wavenumbers, E_n can be expressed as:[97]

$$E_n = \frac{n^2h^2}{8mL^2}$$

where n is a positive integer, h is the Planck constant, m is the mass of the electron (i.e. 9.109×10^{-31} kg[98]) and L is the length of the box (corresponding to a total bond distance in a real molecule). A difference, ΔE between initial state, n_i and final state energy levels, n_f can therefore be expressed using the following equation; emphasising the inverse relationship between energy gap and total bond distance:

$$\Delta E = \frac{\left({n_f}^2 - {n_i}^2\right) \cdot h^2}{8mL^2}$$

1.1.22 The evolving definition of ultrafast

George Porter (Noble Prize 1966) developed flash photolysis, a technique that produces pulses of light on the µs timescale from a discharge lamp. However, given that the lifetime of an excited single state is on the ns timescale, only the initial and final products of bond-breaking and formation processes (so-called "productive pathways") could be determined but the other events occurring in between could not be resolved experimentally.[99] For an analysis of what happens thermally in a system on a second to minute timescale, a resolution of <100 ms enables monitoring of slow isomerization channels. However, for detail on anything shorter, i.e., on the scale of molecular motions, and for process that do not necessary produce a new, measurable product ("non-productive pathways"), much shorter pulses are required. The development of lasers with pulse lengths on the nanosecond or shorter scales allows us to interrogate experimentally the short-lived excited states of molecules that underlie molecular photochemistry. The work of Ahmed Zewail (Noble Prize in Chemistry, 1999) advanced the field of reaction dynamics to give unprecedented structural and dynamic information in the field of photochemistry and gave rise to femtochemistry and femtobiology. The concepts developed in these seminal pump-probe spectroscopy experiments are the basis for the transient absorption spectroscopy underpinning the experimental work of this thesis; with the desired outcome being the ability to interpret the ultrafast spectra in terms of the electronic and geometrical properties of the system.

1.1.23 Transient Electron Absorption Spectroscopy (TEAS) (Solution-Phase)

TEAS is a pump-probe, time-resolved technique that is widely used to monitor molecules after photoexcitation and the data are presented in this thesis as TAS (Transient Absorption Spectra). This technique allows direct study of photo-prepared molecules on the femto- to nano-second timescale, shining light on the fast processes that are not otherwise directly detectable in steady-state spectroscopies. A typical transient absorption dataset might contain between 30-500 absorption spectra at different pump-probe time-delays, and each

spectrum may contain features from multiple chemical species: ground and excited state reactants, reaction intermediates, solvent complexes, product species and isomers, etc.[100]

Experimentally, a pump laser beam (I_{pump}) causes absorption and leaves a fraction of sample molecules in an excited state in the solution phase within a flow-cell. A flow is used so the sample being irradiated is constantly replenished to ensure a fresh sample is irradiated each time. A second pulse (I_{probe}) which passes through the sample at a measured time delay (Δt) directly returns snapshots of the decay of the excited state with respect to time, acting as a sort of ultrafast camera with an adjustable time delay.
Additionally, the flow is not fast enough that a fresh sample is irradiated every pulse pair. To observe only the excited state dynamics, a baseline of the unpumped sample is recorded (I_0). The change in optical density (ΔOD) is recorded by a spectrometer as a function of wavelength and time as:[101]

$$\Delta OD\ (\lambda, t) = log_{10}(\ I_0(\ \lambda)) -\ log_{10}\ (\ I_t(\ \lambda_{probe}, t))$$

By sampling absorption spectra at set time delays, a motion picture of the excited state photodynamics is obtained on very short timescales.

For further details on the experimental set-up, see Materials and Methods. An illustration of the key components once the beam has reached the laser table is included below (Figure 1.11.)

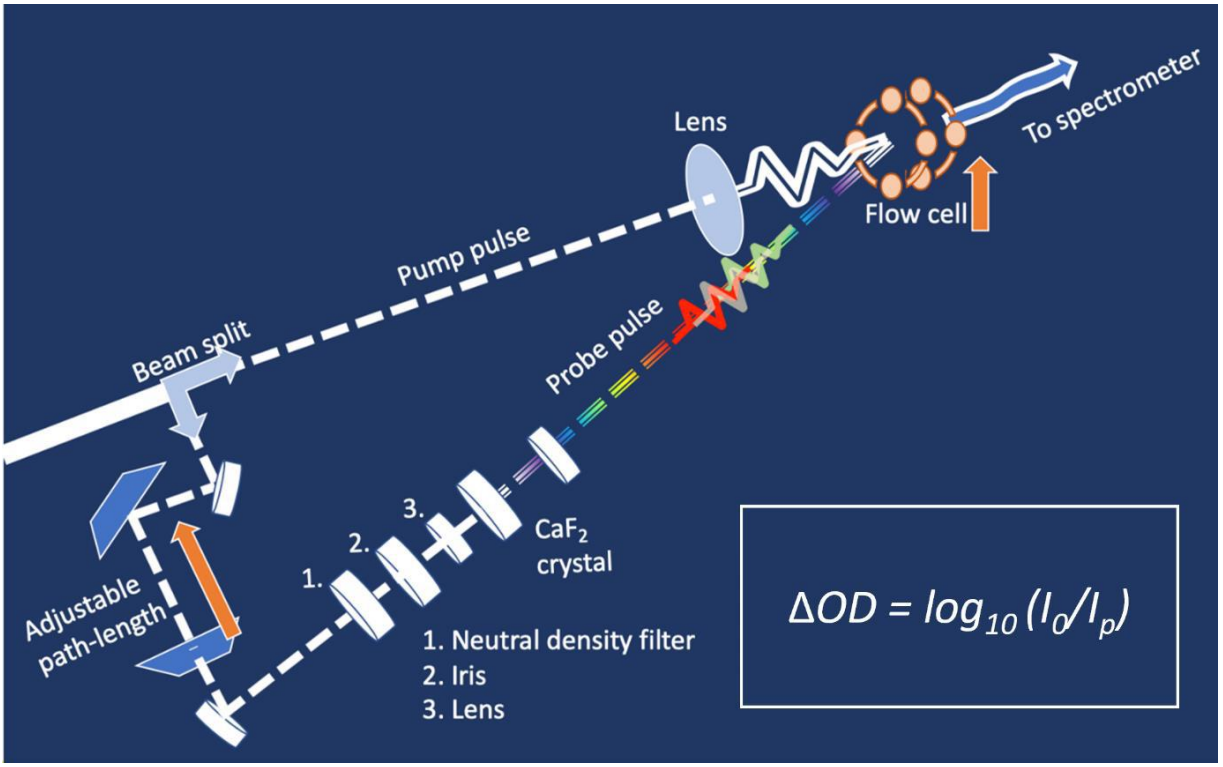

Figure 1.11. Aspects of the TEAS set-up. The beams interact with the sample in the window of the flow cell and optical density difference is recorded at different time points by the fibre-coupled spectrometer. A more complete experimental set-up, including ultrafast pump generation, can be found in ref.[23]

1.1.24 Photochemical Processes as Signals on Electronic Transient Absorption Spectra

The transient absorption spectra (TAS) obtained are a convolution of signals that appear as differences in absorbance between the ground and excited states (ΔOD). Generally, the absorption signals from multiple different species will often be heavily overlapped and must first be separated from the combined total spectrum before the full story of the chemical process can be discerned.[100] When the measured absorption is substituted into the equation above either a positive signal (i.e. when $I_0 > I_t$) or a negative signal (i.e. when

$I_0 < I_t$) is obtained. A negative signal arises because more of the probe light reaches the detector for the excited analyte than would have done if all the molecules were in the ground state. The opposite is true for processes that generate a positive signal. A comparison of the major processes occurring at this time scale and the nature of the resultant signal is contained in the table (Table 1.3.) below:

Table 1.4. Processes that can be observed on a transient absorption spectrum.

Process	Positive or negative signal	Description
Ground-state bleach (GSB)	Negative	Fraction of molecules excited by pump pulse no longer absorb in the ground state
Stimulated emission (SE)	Negative	Interaction of photon from the probe pulse with excited state molecules causes emission of an additional photon (fluorescence)
Excited state absorption (ESA)/ Triplet state of e.g., the parent molecule and/or a photoproduct	Positive	New electronic transitions in the excited state take place by absorbing the probe pulse at different wavelengths to the ground state

A fitting procedure is required to extract dynamic lifetimes for these processes from the experimental data. A 'user's guide' to fitting transient electronic spectra was published by Beckwith and co-workers in 2020 and is covered in more detail in the Materials and Methods section of this thesis.[102] There are multitude factors that influence the productive and non-productive pathways in any molecular system but key considerations are the influence of through-space interactions, i.e. solvent (or no solvent if in the gas-phase), and the influence of through-bond interactions, i.e. the effect of sterics (i.e. molecular bulk and shape of the molecule) or the electronic effects of electron donating or withdrawing

substituents. It is key to bear in mind that even small changes in relative energy pathways may lead to different outcomes and so judicious consideration of the experimental parameters in which photochemical experiments are carried out is necessary. Indeed, the outcome of any photochemical processes is determined by the form of the potential energy surfaces involved.

1.1.25 Transient Vibrational Absorption Spectroscopy (TVAS)

The mid-infrared contains the fingerprint region, where molecules can be identified by their vibrations. In TVAS the pump pulse chosen is the same as used in the TEAS, but the probe pulse is in the IR. It is possible to also use an IR pump in TVAS studies but this approach was not used here. The set-up used for the TVAS of two molecules (**DS1** and **DS2,** see Chapter 3 for structures) is described in the Materials and Methods.

1.1.26 Defining an ideal and promising sunscreen molecule

With no constraints on the design of an ideal sunscreen molecule in the lab, one could imagine an easily synthesizable molecule (perhaps one or two steps from precursors with a renewable source) with a well-defined chromophore that absorbs across the entire UV region; shows no significant photoluminescence (i.e. does not fluorescence or phosphoresce); has photodynamics that we can quantify and resolve reliably; remains stable for the duration of application on the surface of the skin in human tests and shows no environmental or human toxicity. For an idea of how nature has optimised energy dissipation, DNA bases can be considered as the photoprotective properties of these compounds are likely to have played a critical role as early life evolved in the absence of an ozone layer. Kohler et al. showed that DNA bases (adenosine, cytidine, guanosine and thymidine) relax from a singlet excited state to the ground state in hundreds of femtoseconds in neutral pH aqueous solution.[103] Molecules that can dissipate energy in this range should thus be considered very promising as the faster the relaxation the higher the constraint on excited singlet states to participate in bimolecular reactions. The ideal mechanism for excess energy dissipation is as heat to the environment or surrounding solvent bath; and ultrafast

internal conversion routes and their implications for sunscreens are explored more fully in Karsili et al.[104]

Any chemical or physical modification to a molecule or formulation strategy that increases the efficiency of conversion to the ground state can confer additional advantages. To highlight a couple of cases: microsolvation within reverse micelles is used to improve performance by removing an energetic bottleneck, and in another, organic molecules are chemically bonded to the surface of silicon dioxide microspheres within a nanocomposite in an attempt to improve scavenging of reactive species and completely negate absorption into the skin.[105,106] Ultimately a typical sunscreen formulation will contain tens of components with considerations to the efficient absorption or scattering of UVR as well as blending and aesthetic qualities that make the mixture attractive to consumers.

1.1.27 *In silico* toxicology

In the present study cell-based assays were not investigated as a way of testing the in vitro/in vivo safety of the molecules extracted or synthesised. However, in silico methods for predicting safety are available, which have the benefit of reducing time and cost as well as minimising animal testing. These models can predict toxicity based on the similarity principle; whereby similar compounds tend to have similar safety profiles. A read-across approach predicts unknown toxicity using chemical analogues of a compound using a quantitative structure-activity relationship (QSAR) model. For this approach to be valid there need to be experimental data for at least some of the compounds in a related group. Another approach is to look for toxicophores or toxic fragments within molecules, and a potential hit or safety concern will be raised if any of the common toxic motifs are present. Platforms used for such analysis are the VEGA platform (for ecotoxicology), the open-source T.E.S.T. (v4.2.1) and LASAR (Lazy, Structure-Activity Relationship) for mutagenicity or carcinogenicity. All of these tools work in a similar way with the input of a chemical structure (e.g., SMILES string), processing the data through database (e.g., known factors for skin sensitization) and then assigning a score value. None of the compounds synthesised in this thesis had any hits on any of the platforms investigated. If we do wish to extend our studies to near-to-life systems, a synthetic skin mimic (VITRO-CORNEUM®) can be used to model human skin; and is investigated by colleagues at the University of Warwick.[19,107,108]

1.2 Case studies on photochemistry of sunscreens

1.2.1 Photoprotection in Natural Product Mycosporine-like Amino Acids

In the paper 'Exploring the Blueprint of Photoprotection in Mycosporine-like Amino Acids',[32] it was demonstrated that, in aqueous solution, MAAs relax along an S_1 coordinate toward a S_1/S_0 conical intersection (CI) within a few hundred femtoseconds after photoexcitation. At this point, as discussed above in **1.1.8**, the energy surfaces are at the same energy and population can be efficiently transferred between them. In addition, we observe that MAAs then traverse the CI and vibrationally cool in approximately 1 ps through heat transfer to the solvent.[109] The two MAAs, shinorine and porphyra-334, were extracted and purified from Helioguard 365© (Mibelle Biochemistry), a commercial product that contains an extract (from the red algae *Porphyra umbilicalis*) that consists of about 0.1% MAAs (dry weight). The conclusions are presented as in Figure 1.12 and Table 1.4 below. The conclusion of the paper is that nonradiative decay is the dominant relaxation mechanism for excited shinorine and porphyra-334. Relaxation to the ground state in these molecules and the consequent vibrational cooling occur within ~2 ps with at most 5% GSB not recovering within 1.9 ns. This study provides an important benchmark for comparison with any future studies on synthetic MAA analogues and is to our knowledge the first time TEAS has been used to track the nonradiative energy flow in two MAAs shinorine and porphyra- 334 where their ultrafast relaxation dynamics is explicitly linked with their long-term photostability.

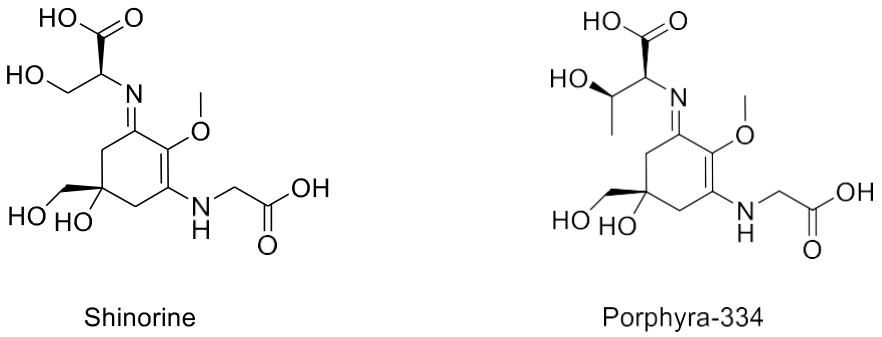

Figure 1.12 . Compounds shinorine and porphyra-334 from ref.[109]

In a complementary study by Conde et al., isomeric pair usujirene and palythene (*cis* and *trans* respectively) were irradiated at 366 nm in aqueous solution and analysed by quantitative HPLC. The *cis*-isomer usujirene was depleted over 10 hours while palythene was formed with an approximately linear dependence with irradiation time.[110] The *trans* isomer absorbs at a slighter longer wavelength (360 nm) vs the *cis*-isomer (357 nm) and thus there was an overall red-shift in the absorbance profile during the irradiation. A blank sample was used to verify that thermolysis and thermal isomerization of the compounds during the irradiation was negligible. An initial ratio of usujirene:palythene of ~21:1 led to a photostationary mixture of 1:11. The preferential accumulation of palythene over usujirene in several dinoflagellate species seems to be supported by this conclusion; however, usujirene is the preferential isomer in several species of red algae. The diverse responses suggest that there is enzymatic photochemical control and not just environmental control of MAA synthesis. Researchers Whittock et al. subsequently studied the ultrafast dynamics of usujirene and palythene in aqueous solution after extraction from dried flakes of *P. palmata*. The results are appended to Table 1.4. for comparison, bearing in mind some experimental differences.[111] The second time constant, τ_2 in the latter study has been resolved into a component that describes the population traversing the conical intersection ($\tau_{2,\ CI}$) and a component that describes the vibrational cooling ($\tau_{2,\ VC}$). Within the experimental window (3 ns) ~85% recovery was observed.

Table 1.5. Summary results for shinorine and porphyra-334 in water;[109] and summary results for usujirene/palythene in water.[111]

Time constant (τ_n)	**Shinorine**	**Porphyra**	**Description**	τ_n	**Usujirene/ palythene**	**Description**
τ_1	190 ± 90 fs	310 ± 90 fs	fast geometry relaxation along the S_1 reaction co-ordinate towards the S_1/S_0 CI	τ_1	110 ± 70 fs	geometry rearrangement of solute and solvent traversing out of FC region towards the S_1/S_0 CI
τ_2	1.17 ± 0.09 ps	1.11 ± 0.09 ps	population traversing through the S_1/S_0 CI and vibrational cooling along the S_0 coordinate	$\tau_{2,CI}$	390 ± 70 fs	population traversing through the S_1/S_0 CI
				$\tau_{3,VC}$	1.46 ± 0.07 ps	vibrational cooling along the S_0 coordinate via vibrational energy transfer
τ_3	>1.9 ns	>1.9 ns	Long-lived species trapped in their excited state.	τ_4	>3 ns	Long-lived components including in the GSB and associated ESA at around 360 and 390 nm respectively.

1.2.2 Photoprotection in oxybenzone

In the paper 'Probing the Ultrafast Energy Dissipation Mechanism of the Sunscreens Oxybenzone after UVA irradiation', Baker et al. studied the active ingredient oxybenzone (Figure 1.13.).[112]

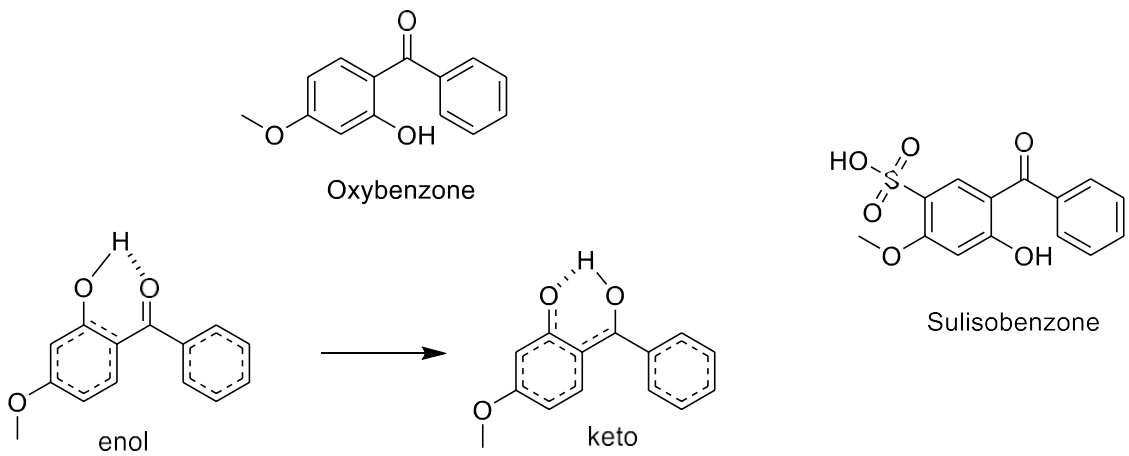

Figure 1.13. The enol and keto forms of oxybenzone

The study concluded that the full mechanism of energy dissipation was excitation (325 nm) from the enol-oxybenzone ground state, S_0 to S_2 ($S_2 \leftarrow S_0$, ($1^1\pi\pi^*$)), followed by excited state hydrogen transfer, resulting in enol ➔ keto isomerisation and relaxation to S_1 in around 100 fs; aliphatic C-C bond rotation in around 400 fs; and then internal conversion from the S_1 to S_0 (S_1 ($1^1n\pi^*$) ➔ S_0) through a CI and vibrational energy transfer back the ground state, S_0 within 5 ps. A ground-state hydrogen transfer and vibrational energy transfer to the solvent allows reformation of the enol isomer on the timescale of around 5-8 ps. Through *ab initio* calculations a small probability of long lived photoproducts was identified and the most likely photoproduct (~10% on ultrafast timescales) was thought to be the trans-keto isomer or less likely formation of a phenoxyl radical by monophotonic O-H cleavage. Additionally in this study the pump pulse was varied from the UVA to the UVB and no difference was found in the observed mechanism of energy dissipation, emphasising that this molecule displays broadband protection. Sulisobenzone (Figure 1.13., above) was studied separately by Ignasiak at al. and was found to have relaxation components of around 700 fs and around 3-4 ps, similar to the pathway determined for oxybenzone.[113]

1.2.3 Photoprotection in sinapoyl malate

In the paper 'Ultrafast Photoprotecting Sunscreens in Natural Plants', Baker et al. studied the natural sunscreening molecule, sinapoyl malate; which is found on the upper epidermis of terrestrial plant leaves, e.g. in thale cress (*Arabidopsis thaliana*) (Figure 1.14.).[20,114] The dominant relaxation mechanism via a trans-cis isomerisation that repopulates the ground-state after UVB photoexcitation is presented in Figure 1.15. The authors proposed that following excitation (~ 330 nm) to the first singlet excited state ($1^1\pi\pi^*$), sinapoyl malate undergoes multiple processes that are convoluted together and defined by time constants, τ_1 and τ_2, thereby making the distinct assignment of any one process to these lifetimes difficult. The authors proposed that τ_1 corresponds to the instrument response function and evolution out of the initially excited geometry; and τ_2 was suggested to be the result of the solvent rearrangement and internal conversion via a $1^1\pi\pi^*/2^1\pi\pi^*$ conical intersection.
Finally, τ_3 was assigned to isomerization along the $2^1\pi\pi^*$ state to generate the *cis*-isomer in the S_0 through a (second) $2^1\pi\pi^*/S_0$ CI with the remaining population returning to the original ground state *trans*-isomer. This behaviour is similar to that found in structurally related ferulic and caffeic acids, which are also members of the cinnamate class of sunscreens (Figure 1.14.).[115]

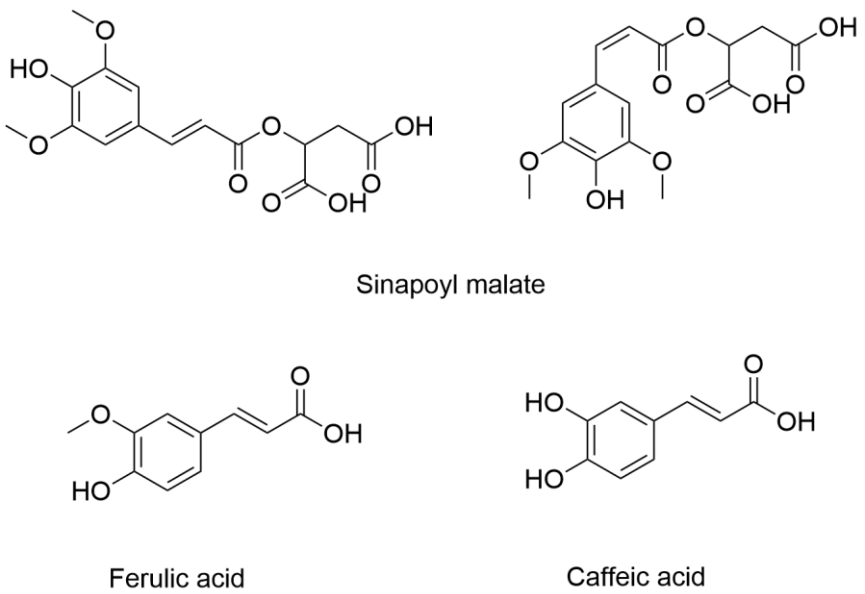

Figure 1.14. (Top left) *trans* sinapoyl malate and (right) the *cis*-isomer. NB: absolute stereochemistry not shown. (Bottom) Related cinnamic acids.

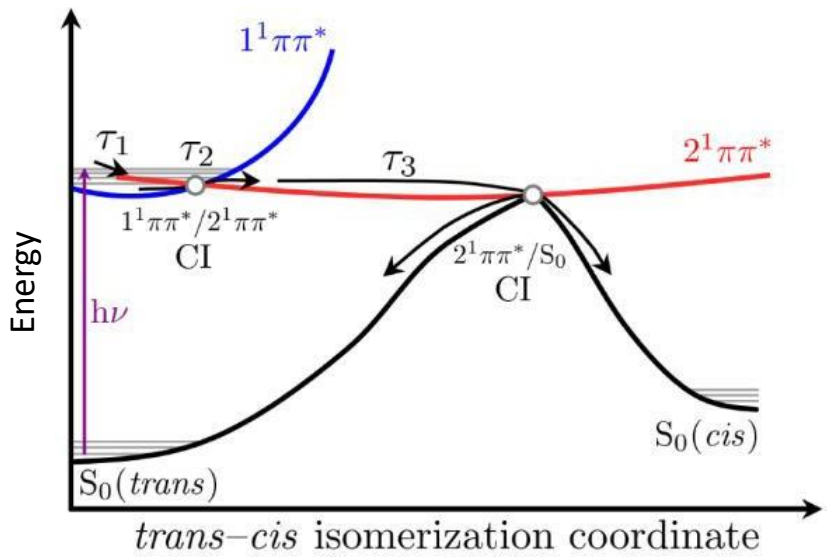

Figure 1.15. Dominant relaxation pathway proposed in ref[20].

Building on this work, a study by Horbury et al. investigated the effect of solvent viscosity on the proposed photodynamics of sinapoyl malate.[116] Using TEAS measurements the study revealed that the time constant assigned to the relaxation of the excited state population along the *trans-cis* photoisomerization coordinate increases considerably with increasing viscosity, namely from 47 ps in ethanol to 560 ps in glycerol. The authors concluded that photoisomerization of sinapoyl malate is likely facilitated by the out-of-plane rotation about the C=C bond and consequently is the reason for the large solvent viscosity effect on its photodynamics. This study underlines the importance of considering the surrounding environment in which the energy dissipation is taking place. Further studies have extended this line of work to include symmetrically functionalized sinapate esters to circumvent the concerns surrounding the potential genotoxicity of the *cis*-isomers[19,117] and in a range of solvents and emollients, and on skin mimics; and are reviewed elsewhere.[118]

1.2.4 Visualising photoprotection in 3 dimensions

Based on the experimental and theoretical work by the Stavros group at the University of Warwick, Hatekayama et al., and Sampedro et al., two main molecular motions following photoexcitation are evoked when talking about mycosporine-like amino acids and their

synthetic analogues.[109,119–121] The first major pathway is rotation around the C-N bond (shown in Figure 1.16. below for a 3-D model of usujirene/palythene by a green arrow). This involves a rotation of one the C-N bonds as one arm spins out of plane with the ring. This pathway seems to be favoured by aromatic substituents and therefore is present only in the synthetic analogues. The second pathway (also illustrated in the Figure below with orange arrows) is a ring-buckling mechanism whereby the 6-membered ring flexes relative to its starting position. This latter mechanism is the pathway that has been found in the natural MAAs and is theoretically proposed for synthetic analogues with amino alcohol or alkyl substituents. This hypothesis is taken forward into Chapter 3 of this thesis.

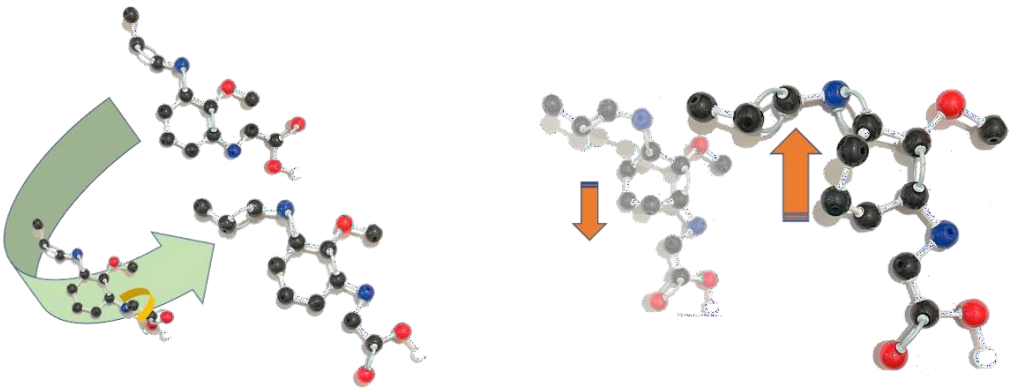

Rotation around a C-N bond
(here in truncated model of usujirene/palythene)

Ring buckling
(here in truncated model of usujirene/palythene)

Figure 1.16. Illustration of the two major pathways followed by MAA or MAA-like molecules, demonstrated in a 3D model ball-and-stick model of usujirene/palythene without the C-5 substituents.

A mixed experimental and computational study that examines the pathways in usujirene was conducted by Whittock et al.[111] In that study state-averaged CASSCF/6-31G* optimised geometries for the S_0 and S_1/S_0 CI were used. The overall photodynamics appear to be relaxation from an initial planar geometry after vertical excitation towards a non-planar geometry at the S_1/S_0 CI to planar in the S_0 ring flexing pathway (also called ring-buckling). Note that the authors did not find any energetically feasible geometries along an isomerisation pathway between usujirene/palythene, which may explain the low quantum yields observed for the isomerisation process.

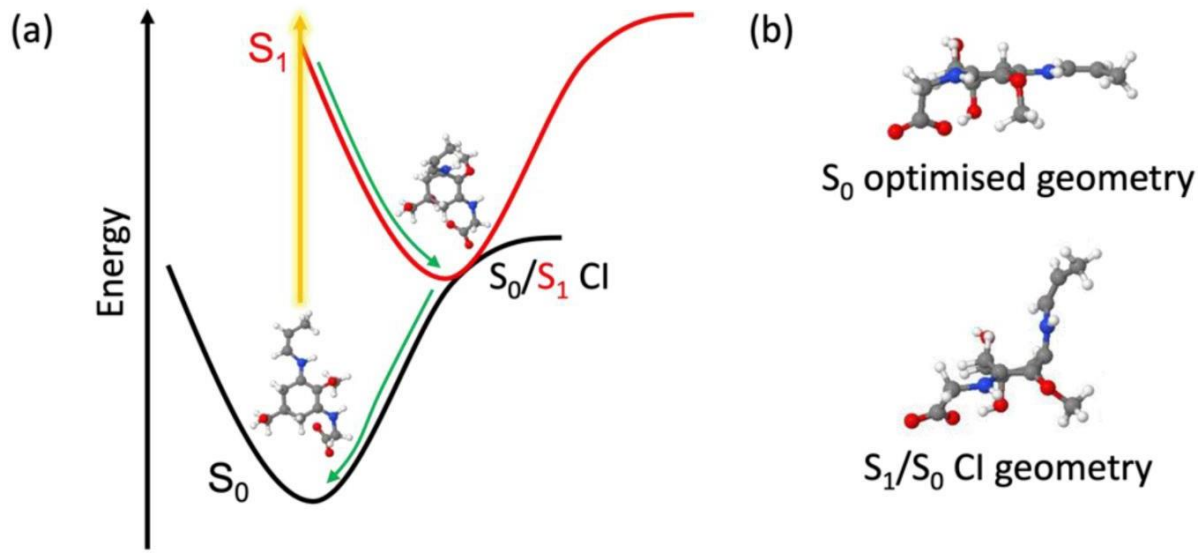

Figure 1.17. a) Scheme of the dominant relaxation pathway in usujirene from the study by Whittock et al. b) Optimised geometries in the S_0 and at the S_1/S_0 CI.

1.3 Chapter summary

In this chapter, a background of some key fundamentals of photochemistry and a brief history of sunscreens were presented with examples of previous work on characterising energy flux in small molecular systems. This background sets the scene for discussions in the remainder of this thesis, where molecular analogues of the organic molecules that act as ultraviolet filters in the natural world and/or in our cosmetic care industry are further explored. Spectroscopic concepts, particularly those that can explain ultrafast spectral signatures are important in understanding the experimental work in the remainder of this thesis. The above mentioned case studies show how time-resolved spectroscopy and good chemical sense have been applied before to rationalise the most effective sunscreens. The study of amino alcohol imino-mycosporine-like molecules and **DS1** and **DS2** in Chapter 3 brings together how sunscreen performance can be assessed and quantified in the lab as well as beginning to unravel their ultrafast photodynamics. It should be noted that the photoprotective mechanisms of MAAs and MAA-inspired molecules are different to those of commercial sunscreens which typically involve a double bond isomerisation (cinnamates) or excited state proton transfer (avobenzone and oxybenzone), therefore truly representing a new class of sunscreen to be studied. Additionally, the study of the **AVOCTO** molecules in Chapter 4 shows how composite molecules can retain the photodynamic properties of their parent molecules, at least in an experimental setting.

When considering the rest of this work it is worth bearing in mind that de-excitation pathways are influenced by many factors and they cannot be considered in isolation; rather they play out in a complicated energy landscape involving solvent, light, temperature amongst others. As many future technologies could be interfaced with light, this line of research will surely continue into the future and inform design proposals.

Chapter 2. Materials and Methods (Synthesis)

2.1 General Synthesis Notes

All solvents and reagents used were used as received by the chemical supplier without further purification. Where the supplier of a substance is not indicated, it can be assumed to be 95%+ pure and from Sigma Aldrich. Dry solvents were used without additional drying in oven-dried glassware. Room temperature (rt) refers to ambient temperature between 20-22 °C. Overnight implies at least 12 hours. Reactants are used in 1 equivalent unless otherwise stated. “In ice” or “in an ice bath” indicates an ice bath with some added brine at a temperature <0 °C. Experiments that involve heating at a specific temperature were thermostatically controlled (±2 °C) using a hot-plate and thermostat. Reactions were monitored by thin layer chromatography (TLC) with aluminium backed silica gel 60 (F254) plates using a solvent system of equal volumes ethyl acetate and hexane (i.e., EtOAc:Hexane (1:1)). Where the solvent system used for TLC was different, it is stated. TLC spots were visualised under a short-range UV lamp (254 nm) and in most cases stained with potassium permanganate dip dye for visualisation. Flash column chromatography was conducted on a packed silica column using 60 Å silica gel (Merck) in standard laboratory glassware. Low resolution mass spectra were obtained using an Agilent 6130B single Quad (Electrospray Ionisation, EI) mass spectrometer in either positive (+) or negative mode (-). High resolution mass spectra (HRMS) were obtained using the Mass Spectrometry service at Warwick University and are presented as a calculated and experimental mass. Melting points (MP) were determined using a Stuart Scientific SMP 1 instrument. NMR spectra (^{1}H, ^{13}C) were recorded on an in-house open-access Bruker Avance III HD (300, 400 or 500 MHz for ^{1}HNMR) spectrometer. Chemical shifts are reported in δ units, ppm relative to a solvent signal (deuterated chloroform, $CDCl_3$, deuterated water, D_2O or deuterated methanol, MeOD). *J* values are given in Hz. Spectra were processed using the MestReNova software package from MestreLab Research S.L. In the annotation of CNMR spectra, Cipso refers to a carbon that is not bonded to a hydrogen atom. IR spectra were obtained on a Bruker IR spectrometer in the Warwick Teaching Laboratories, Chemistry Department.
NMR and IR spectra are included for reference in the Appendix. Some compounds are given an AC number or AVOCTO number for ease of comparison with the main text.

2.2 Synthesis of singly substituted MAA derivatives based on oxo-mycosporines

Preparation of 2,3-dihydroxycyclohex-2-en-1-one ("dihydropyrogallol", DHPG) [1]

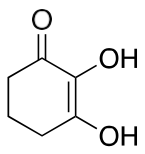

This compound has been reported and fully characterised in Pecherer, B.; Jampolsky, L. M.; Wuest, H. M. *J. Am. Chem. Soc*. **1948***, 70,* 2587–2589.[1] Pyrogallol (6.3 g, 50 mmol) was added to a basic solution (2.0 g NaOH in 12.6 cm^3 H_2O) in the glass insert of a Parr high pressure reactor with a stirrer bar at rt. Raney Nickel (~2.1 g, ~12.8 mmol, 0.26 eq.) was added and the reactor was pressurised to 69 bar H_2 and the temperature was increased to 60 °C for 5 hours with stirring. The reactor was allowed to cool to rt overnight before depressurising. The mixture was filtered, the filtrate cooled in an ice bath and acidified dropwise with 37% HCl. On standing for 30 mins a greyish precipitate formed and was filtered. On further acidification an off-white product (2.7 g, 21.1 mmol, 42%) was obtained. The precipitate was filtered and redissolved in minimal hot EtOAc and dried in vacuo. A further portion of product mixed with starting material as a brown oil can be recovered by extracting the mother liquor with EtOAc (3 x 10 cm^3), drying the combined organic layers with anhydrous sodium sulphate, and drying under vacuum. Note: if the reaction is incomplete then the product may not crystallise, and the starting material/product mixture can be isolated through extraction with EtOAc in this case. The aqueous solution should not be diluted as this will reduce the yield due to the water solubility of the reagent and product. Too long a reaction time will result in over-reduction. The data matched that reported.

TLC: R_f ~0.2-0.3 (*broad);*

LRMS (ESI) m/z: Found 151.0 $[M + Na]^+$;

δ_H (400 MHz, CD_3OD): 2.43 (4H, t, *J* = 6.4 Hz, $C\underline{H}_2CH_2C\underline{H}_2$), 1.98-1.92 (2H, m, $CH_2C\underline{H}_2CH_2$) ppm.

Preparation of 3-hydroxy-2-methoxycyclohex-2-en-1-one[2]

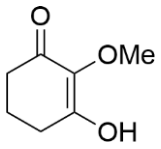

This compound has been reported and fully characterised in Mayer, W.; Bachmann, R.; Kraus, F. *Chem. Ber.* **1955**, *88*, 316–329.[2] Dihydropyrogallol (2.40 g, 18.8 mmol) was dissolved in aqueous NaOH (4M, 10 cm^3, 40 mmol) and stirred under nitrogen in an iced water bath (<5 °C) for 10 mins. Dimethyl sulphate (5.0 g, 3.8 cm^3, 40.1 mmol, 2.1 eq.) was added by dropping funnel over 10 mins and the mixture was stirred for 30 mins. A second portion of NaOH (4M, 10 cm^3, 40 mmol) was added by syringe and the flask was removed from the bath and gradually allowed to warm to rt over 18 hours with stirring. The resulting solution was cooled to rt by placing in an iced water bath and acidified to pH ~4-5 dropwise with concentrated HCl (~2 cm^3) and extracted with diethyl ether (3 x 25 cm^3) with vigorous stirring. The combined ether extracts were dried over anhydrous sodium sulphate and the solvent was removed in vacuo to leave the product (560 mg, 3.94 mmol, 21%) as a lightly yellow coloured solid. The data matched that reported.

TLC: in 10% MeOH in EtOAc, R_f ~0.8;

LRMS (ESI) m/z: Found 143.1 $[M + H]^+$;

δ_H (300 MHz, $CDCl_3$): 6.20 (1H, *broad*, OH), 3.73 (3H, s, OCH_3), 2.49-2.45 (4H, m, $C\underline{H}_2CH_2C\underline{H}_2$), 1.97-1.93 (2H, m, $CH_2C\underline{H}_2CH_2$) ppm.

Preparation of 3-(phenylamino)cyclohex-2-en-1-one, AC3[3]

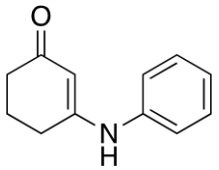

This compound has been reported and fully characterised in Wang, T.; Chen, G.; Lu, Y.; Chen, Q.; Huo, Y.; Li, X. Intermolecular Multiple Dehydrogenative Cross-Couplings of Ketones with Boronic Acids and Amines via Copper Catalysis. *Adv. Synth. Catal.* **2019**, *361* (16), 3886–3892.[3] 1,3-Cyclohexanedione (500 mg, 4.45 mmol) was added to 20% (v/v) acetic acid in water with stirring. Aniline (414 mg, 0.40 cm^3, 4.5 mmol, 1.01 eqs.) was added at rt and the mixture. The solution was heated to reflux (~100 °C) for 5 hours and stirred overnight. After cooling to rt, a solid was formed by adding small amounts of chilled distilled water to the solution. Once a precipitate had formed the product was isolated by filtration and dried under vacuum. The product was purified by washing a few times with minimal amounts of ice-cold EtOAc or by flash chromatography on a silica-gel column using a 1:99 to 10:90 methanol:DCM gradient. The product (365 mg, 1.95 mmol, 44%*)* was obtained as a yellowish solid via the chromatography method. The data matched that reported.

MP: 175 °C;

TLC: in EtOAc, R_f ~0.15;

LRMS (ESI) m/z: Found 188.1 $[M+H]^+$;

δ_H (400 MHz, $CDCl_3$): 7.34-7.29 (2H, m, ArH), 7.26-7.15 (3H, m, ArH), 6.56 (1H, *broad*, NH), 5.57 (1H, s, =CH), 2.52-2.48 (2H, m, CH_2), 2.37-2.32 (2H, m, CH_2), 2.04-2.00 (2H, m, CH_2) ppm;

δ_C (101 MHz, $CDCl_3$) 129.4 (ArC), 125.6 (ArC), 124.0 (ArC), 100.3 (=CH), 36.5 (CH_2), 29.2 (CH_2), 21.9 (CH_2) ppm (C=O and Cipsos do not show clearly).

ν_{max}/cm^{-1} 3258 (NH), 3061 (CH), 2942 (CH)

Preparation of 2-methyl-3-(phenylamino)cyclohex-2-enone, AC4[4]

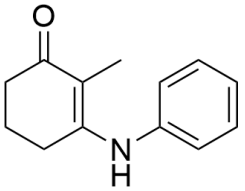

This compound has been reported but was not fully characterised previously in Gramain, J.-C.; Husson, H.-P.; Troin, Y. Synthèse Stéréospecifique Par Voie Photochimique de Trans Hexahydro-1,2,3,4,4a,9a Carbazolones-4 Substituées en 4a1. *Tetrahedron Letters* **1985**, *26* (19), 2323–2326.[4] 2-Methyl-1,3-cyclohexanedione (400 mg, 3.17 mmol) and aniline hydrochloride (450 mg, 3.47 mmol) were added to an oven-dried round bottom flask at rt. Toluene (20 cm^3) was added, and the solution was heated to 120 °C for 2 days. After cooling to rt, the solution was transferred to a separating funnel. Equal volumes of EtOAc (10 cm^3) and saturated NH_4Cl solution (10 cm^3) were added. The organic layer was separated and washed with half of that volume of NH_4Cl solution and brine consecutively. The organic layer was concentrated under reduced pressure. The concentrated residue was triturated with cool EtOAc until a pinkish-grey solid formed. The solid was dried and recrystallised from diethyl ether to yield the product (186 mg, 0.925 mmol, 29%). This procedure was chosen to avoid column chromatography as this compound appeared to degrade on silica. NB: aniline hydrochloride was prepared by dissolving aniline and diethyl ether in an ice bath and adding conc. HCl slowly with stirring until the reaction stops. The diethyl ether is decanted and the white solid dried thoroughly.

MP: 140 °C; TLC: in EtOAc, R_f ~0.15;

LRMS (ESI) m/z: Found 202.1 $[M+H]^+$;

HRMS (ESI-TOF): Calc'd for $C_{13}H_{16}NO+$ 202.1226. Found 202.1228;

δ_H (400 MHz, $CDCl_3$): 7.36 (2H, t, J = 7.8 Hz, ArH), 7.20 (1H, t, J = 7.4 Hz, ArH), 7.08 (2H, d, J = 7.8 Hz, ArH), 6.23 (1H, *broad*, NH), 2.48-2.45 (2H, m, CH_2), 2.41-2.38 (2H, m, CH_2), 1.94-1.90 (2H, m, CH_2), 1.86 (3H, s, CH_3) ppm;
δ_C (101 MHz, $CDCl_3$) 129.3 (ArC), 125.5 (ArC), 124.8 (ArC), 77.0, 36.2 (CH_2), 27.0 (CH_2), 22.0 (CH_2), 8.1 (CH_3) ppm. (C=O and C ipsos do not show clearly).

ν_{max}/cm^{-1} 3287 (NH), 3233 (CH), 2942 (CH)

Preparation of 2-hydroxy-3-(phenylamino)cyclohex-2-enone, AC9[2]

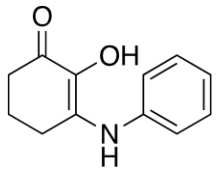

This compound has been reported but not fully characterised in Mayer, W., Bachmann, R.; Kraus, F. *Chem. Ber.* **1955***, 88,* 316–329.[2] Dihydropyrogallol (400 mg, 3.13 mmol), and freshly prepared aniline hydrochloride (420 mg, 3.24 mmol) were mixed well in a round bottom flask. Minimum distilled water (~2 cm^3) was added with stirring until all had dissolved and the solution was then stirred at rt while being purged with nitrogen for 30 mins, or until a solid formed. The flask was then sealed and transferred to the fridge overnight. The solid product thus formed was filtered, washed with minimal cold toluene, and dried under vacuum and not purified further (112 mg, 0.55 mmol, 18% yield).

MP: 120 °C;

LRMS (ESI) m/z: Found 204.1 $[M+H]^+$;

HRMS (ESI-TOF) Calc'd for $C_{12}H_{14}NO_2$+ 204.1019. Found 204.1016;

δ_H (400 MHz, $CDCl_3$): 7.36-7.32 (2H, m, ArH), 7.17-7.14 (1H, m, ArH), 7.08-7.06 (2H, m, ArH), 6.80 (1H, broad, NH), 5.65 (1H, s, =CH), 2.64-2.61 (2H, m, CH_2), 2.49-2.47 (2H, m, CH_2)), 2.00-1.95 (2H, m, CH_2) ppm;

δ_C (101 MHz, $CDCl_3$): 188.3 (C=O), 142.3 (C), 138.6 (C), 129.7 (C), 129.3 (ArCH), 124.7 (ArCH), 123.3 (ArCH), 34.4 (CH_2), 25.4 (CH2), 21.8 (CH_2).

ν_{max}/cm^{-1} ~3200 (br, OH), 2920 (CH)

Preparation of 2-methoxy-3-(phenylamino)cyclohex-2-enone, AC20

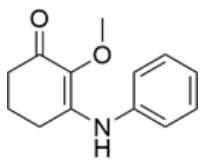

This compound is novel. 3-Hydroxy-2-methoxycyclohex-2-enone (100 mg, 0.70 mmol) was added, with aniline hydrochloride (130 mg, 1.0 mmol) to a round bottom flask. Toluene (5 cm^3), and molecular sieves were added. The solution was heated to reflux (~120 °C) for 5 hours and then stirred overnight at rt. The solvent was decanted off and a 1:1 (v/v) mixture of EtOAc and saturated NH_4Cl solution (10 cm^3 total) was added to the remaining residue. The mixture was filtered into a separating funnel. The organic layer was separated, and the remaining aqueous solution was extracted further with EtOAc (2 x 10 cm^3). The organic layers were combined, dried over sodium sulphate and concentrated under reduced pressure to yield a solid after drying (101 mg, 0.47 mmol, 66% yield). No further purification was needed.

LRMS (ESI) m/z: Found 218.1 $[M+H]^+$;

HRMS (ESI-TOF): Calc'd for $C_{13}H_{16}NO_2^+$ 218.1176. Found 218.1179;

δ_H (400 MHz, $CDCl_3$) 7.35-7.33 (2H, m, ArH), 7.17-7.14 (1H, m, ArH), 7.08-7.06 (2H, m, ArH), 3.77 (3H, s, OCH_3), 2.60-2.57 (2H, m, CH_2), 2.42-2.40 (2H, m, CH_2)), 1.92-1.90 (2H, m, CH_2) ppm;

δ_C (101 MHz, $CDCl_3$) 189.4 (C=O), 152.0 (Cipso), 138.2 (Cipso), 133.2 (Cipso), 129.3 (ArCH), 125.2 (ArCH), 124.0 (ArCH), 59.6 (CH), 37.0 (CH_2), 26.0 (CH_2), 21.8 (CH_2) ppm.

ν_{max}/cm^{-1} 3208 (NH), 3071 (CH), 2929 (CH), 1727 (C=C)

Preparation of 2-methoxy-3-((4-methoxyphenyl)amino)cyclohex-2-en-1-one, AC34

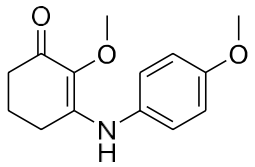

This compound is novel. 3-Hydroxy-2-methoxycyclohex-2-enone (150 mg, 1.1 mmol) was added, with 4-methoxybenzenaminium chloride (185 mg, 1.2 mmol, 1.1 eqs.) to a round bottom flask. Toluene (5 cm^3), and molecular sieves were added. The solution was heated to reflux (~120 °C) for 5 hours and then stirred overnight at rt. The solvent was decanted off and a 1:1 (v/v) mixture of EtOAc and saturated NH_4Cl solution (10 cm^3 total) was added to the remaining residue. The mixture was filtered into a separating funnel. The organic layer was separated, and the remaining aqueous solution was extracted further with EtOAc (2 x 10 cm^3). The organic layers were combined, dried over sodium sulfate and concentrated under reduced pressure to yield a solid after drying (110 mg, 0.45 mmol, 41% yield). No further purification was carried out.

δ_H (400 MHz, $CDCl_3$): 7.03 (2H, *J* = 8.8 Hz, d, ArH), 6.88 (2H, *J* = 8.8, d, ArH), 3.81 (3H, s, CH_3), 3.76 (3H, s, CH_3), 2.47-2.35 (4H, *m*, 2 x CH_2), 1.91-1.90 (2H, m, CH_2).

δ_C (101 MHz, $CDCl_3$) 126.6 (ArC), 114.5 (ArC), 59.6 (CH_3), 55.5 (CH_3), 36.8 (CH_2), 25.8 (CH_2), 21.5 (CH_2) ppm (C=O and C ipsos do not show clearly).

2.3 Synthesis of substrates for biological assays

2.3.1 MAA-derivatives

Preparation of methyl (2-methoxy-3-oxocyclohex-1-en-1-yl)glycinate, AC23 ester

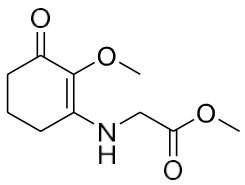

This compound has been previously made in patent US-2017119641-A1. 3-Hydroxy-2-methoxycyclohex-2-en-1-one (1 g, 4.69 mmol) was dissolved in a round bottom flask in DCM (5 cm^3) at rt. Methyl glycinate hydrochloride (1.10 g, 8.76 mmol, 1.2 eqs.) was added with 4A° molecular sieves (3 g). Triethylamine (0.97 mL, 0.71 g, 7.01 mmol, 1.5 eq.) was added, and the mixture was stirred under nitrogen for 16 hours. The pH was maintained between 5.7-6.6. The mixture was filtered and the filter paper was washed through with DCM. Excess solvent was removed to leave the crude product. The crude product was separated using a Biotage® Selekt set-up with a 5-100% MeOH in H_2O gradient and a C18 column. Combining all the fractions containing UV peaks corresponding to the product absorption (~310 nm) and removing solvent under high vacuum yielded the product as a lightly coloured oil (180 mg, 0.84 mmol, 12%) contaminated with some residual triethylamine. Performing the reaction without triethylamine did produce some product but in much reduced yield.

Alternative work-up without using Biotage: Redissolve crude extract in DCM and wash with saturated $NaHCO_3$, dry with sodium sulphate and remove solvent in vacuo. Substantial product is lost in the wash, but it is required to separate product from triethylamine.HCl salt. The product can be recrystallised from light petroleum.

LRMS (ESI) m/z: Found 214.1 $[M+H]^+$; 449.2 $[2M+Na]^+$;

δ_H (400 MHz, MeOH): 3.58 (3H, s, CH_3), 3.36 (3H, s, CH_3), 3.32 (~2H, s, CH_2), 2.54-2.51 (2H, t, *J* = 6.2 Hz, CH_2), 2.35-2.32 (2H, t, *J* = 6.4 Hz, CH_2), 1.95-1.89 (2H, m, CH_2).

δ_H (300 MHz, $CDCl_3$): 3.98 (2H, J = 6.0 Hz, d, CH_2), 3.76 (3H, s, CH_3), 3.65 (3H, s, CH_3), 2.42-2.38 (2H, t, *J* = 6.0 Hz, CH_2), 2.35-2.31 (2H, t, *J* = 6.0 Hz, CH_2), 1.95-1.89 (2H, m, CH_2). [*$CDCl_3$ spectrum provided by Martin Wills*]

Preparation of (2-methoxy-3-oxocyclohex-1-en-1-yl)glycine (AC23 acid) via hydrolysis of methyl (2-methoxy-3-oxocyclohex-1-en-1-yl)glycinate

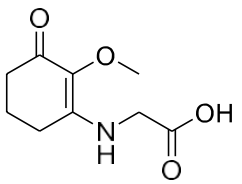

This compound is novel. Methyl (2-methoxy-3-oxocyclohex-1-en-1-yl)glycinate (100 mg, 0.47 mmol) was dissolved in a 1:1 solution of distilled water (or THF) and methanol (2 mL total). LiOH (17 mg, 0.71 mmol, 1.5 eqs.) was added in one portion. The flask was sealed and the solution was stirred overnight at rt. The solvent was removed under vacuum. Hydrolysis was confirmed by NMR.

δ_H (400 MHz, MeOD): 5.15 (s, OH exchange, MeOH, H_2O, COOH), 3.80 (2H, s, CH_2), 3.59 (3H, s, OCH_3), 2.57 (2H, t, J = 6.2 Hz, CH_2), 2.31 (2H, t, J = 6.4 Hz, CH_2), 1.94-1.88 (2H, m, CH_2).

Preparation of methyl (3-oxocyclohex-1-en-1-yl)glycinate, AC36[5]

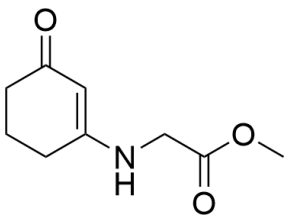

This known compound[5] was prepared using the same method as **AC23 ester**, infra, in 20% yield.

δ_H (400 MHz, $CDCl_3$): 5.00 (enol H, s), 3.83-3.82 (2H, m, CH_2 amide), 3.81 (3H, s, CH_3), 2.40 (2H, t, *J* = 6.2 Hz, CH_2), 2.32 (2H, t, *J* = 6.5 Hz, CH_2), 2.02-1.96 (2H, m, CH_2).

2.3.2 Preparation of aminoacyl-SNACs (aminoacyl-N-acetylcysteamine thioesters)[6]

The procedure for making the amino acid-derived substrates for the C domain was taken with some minor differences from Ehmann, D. E.; Trauger, J. W.; Stachelhaus, T.; Walsh, C. T. Aminoacyl-SNACs as Small-Molecule Substrates for the Condensation Domains of Nonribosomal Peptide Synthetases. *Chemistry & Biology* **2000**, *7* (10), 765–772.[6] Butyloxycarbonyl (Boc-) protected amino acids were purchased from ABCR (UK) LTD. Coupling of N-acetylcysteamine (NAC) to a Boc-protected amino acid was effected with DCC/HOBt and K_2CO_3. Deprotection of the resulting Boc-aminoacyl-SNAC afforded the product aminoacyl-SNAC as the trifluoroacetic acid (TFA) salt. Characterisation was performed by LRMS.

Preparation of a mixture of S-(2-acetamidoethyl) (S)-2-amino-3-hydroxypropanethioate and S-(2-acetamidoethyl) (S)-2-amino-3-tertbutoxypropanethioate (SerSNAC*)

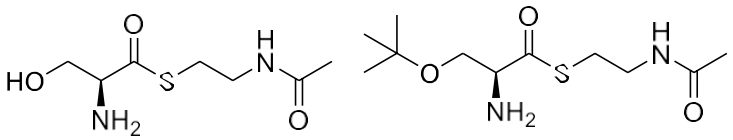

Ser-SNAC (O^{t}Bu)-Ser-SNAC

NB: A mixture of the O^{t}Bu-protected Ser-SNAC and fully deprotected Ser-SNAC was obtained. Boc-protected O^{t}Bu-serine (400 mg, 1.53 mmol, 1 eq.) was dissolved in 5 mL THF under nitrogen at RT. DCC (316 mg, 1.53 mmol, 1 eq.), HOBt (413 mg, 1.53 mmol, 1 eq.) and NAC (182 mg, 1.53 mmol, 1 eq.) were added and stirred for 45 mins. K_2CO_3 (106 mg, 0.77 mmol, 0.5 eqs.) was added and mixture stirred for 3 hours. The mixture was filtered and concentrated. The residue was redissolved in ethyl acetate and washed with 1 vol 10% $NaHCO_3$ (aq.). The organic layer was separated and dried to give 380 mg of crude Boc-(O^{t}Bu -)Ser-SNAC (crude NMR is included in the Appendix but not assigned). The SNAC was partially deprotected using a 1:1 mixture of TFA and stirred for 1 hour at RT. The solvents were removed on rota, DCM was added and removed again twice to remove all TFA. The resulting slightly orange oil (~100 mg) contained partially deprotected Ser-SNAC because it still contained (O^{t}Bu -Ser). The oil was thoroughly dried under vacuum and stored in the fridge. LRMS (calc'd): 207.3 (MH^+) and 263.4 (O^{t}Bu -MH^+); observed 207.2 ($[MH]^+$) and 263.2 (O^{t}Bu, $[MH]^+$). Assuming 1:1 ratio of the two products, yield of SerSNAC **~16%**.

Preparation of S-(2-acetamidoethyl) (S)-pyrrolidine-2-carbothioate

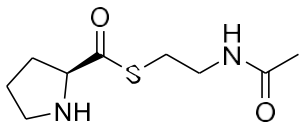

Pro-SNAC

The same method as above was applied with Boc-protected proline (200 mg) to produce ~200 mg of the crude product as a yellowish oil. Crude NMR of Boc-protected proline-SNAC is included in the Appendix but is not assigned. LRMS (calc'd): 217.3 ($[MH]^+$); observed 217.2 ($[MH]^+$). Assuming crude ~ 70% product, yield **~70%**.

2.4 Synthesis of doubly substituted MAA derivatives based on imino-mycosporines

2.4.1 General procedure and amino alcohols

The ketone (1 equiv.), amino alcohol (4 equiv.) and tosic acid monohydrate (1 equiv.) were combined in a dry round-bottom flask using enough toluene to cover the reactants. The reaction was heated at reflux (>120 °C) with stirring for at least 24 hours (monitoring by LRMS to judge if the reaction has gone to completion). Shorter reaction times typically lead to a mixture of single addition and double addition products. Use of a Dean-Stark apparatus is recommended for small scale reactions but is not essential. When complete, excess toluene was decanted off at rt, and the residue was washed with minimal hexane to remove residual toluene and the product was dried under vacuum to obtain the crude product as a highly hygroscopic solid or oil at rt. Characterisation by LRMS and ^{1}HNMR is possible at this stage but generally reveals a crude mixture containing excess amino alcohol starting material and sometimes the product formed by addition of only 1 equivalent of amine. Reverse-phase chromatography (e.g., Biotage® Selekt) using e.g., a MeOH:H_2O mobile phase with gradient is recommended to purify the salt but the high polarity of the product often means it has very short retention times; particularly with the molecules formed from ethanolamine. Amberlite IRA-900 Cl ion-exchange resin (ACROS Organics) can be used to exchange the tosylate counterion for a chloride but exchange can also take place on a C18 resin where the counterion is most likely exchanged for a hydroxide or chloride ion.

Preparation of 2-hydroxy-N-(3-((2-hydroxyethyl)amino)-2-methoxycyclohex-2-en-1-ylidene)ethan-1-aminium 4-methylbenzenesulfonate, AC26

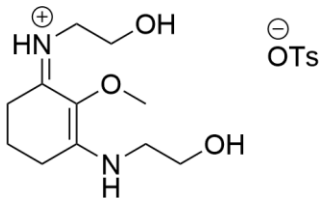

This compound is novel. 2-Methoxycyclohexane-1,3-dione (200 mg, 1.41 mmol) and tosic acid monohydrate (268 mg, 1.41 mmol, 1 eq.) were added in toluene (20 cm^3).
Ethanolamine (340 mg, 0.34 cm^3, 0.56 mmol, 4 eqs.) was added last. The mixture was stirred and heated under reflux (>120 °C) for 18 hours. At rt, the supernatant toluene was decanted off to leave a dark residue (1.01 g). By NMR this is the product contaminated with ethanolamine. Washing with cold EtOAc and cold methanol in turn mostly removes the ethanolamine but with substantial loss of product too and an approximate yield of 100 mg (31%). A number of solvent washes were tried to recrystallise a solid from the residue but were unsuccessful. The residue is soluble in water and methanol, but insoluble in EtOAc, dichloromethane, and toluene.

UV (λ_{max}, EtOH): 326 nm;

LRMS (ESI) m/z: Found 229.1 $[M+H]^+$;

HRMS (ESI-TOF) m/z: [M+H]+ Calc'd for $C_{11}H_{21}N_2O_3$ 229.1547; Found 229.1543 (error 1.5 ppm);

δ_H (400 MHz, D_2O) 7.70 (2H, d, *J* = 8 Hz, ArH), 7.38 (2H, d, *J* = 8 Hz, ArH), 3.77-3.74 (4H, m, $NCH_2C\underline{H}_2OH$), 3.57-3.55 (4H, m, $NC\underline{H}_2CH_2OH$), 3.56 (3H, s, $-OCH_3$), 2.71-2.68 (4H, m, 2 x CH_2), 2.40 (3H, s, counterion), 1.92 (2H, m, CH_2) ppm.

Preparation of 2-hydroxy-N-(3-((2-hydroxyethyl)amino)cyclohex-2-en-1-ylidene)ethan-1-aminium 4-methylbenzenesulfonate, AC27

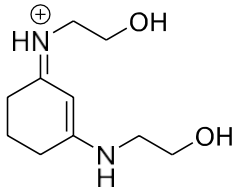

This compound is novel. Cyclohexane-1,3-dione (200 mg, 1.79 mmol) and tosic acid monohydrate (339 mg, 1.79 mmol, 1 eq.) were added in 5 cm^3 toluene. Ethanolamine (0.43 cm^3, 437 mg, 4 eqs.) was added last. The mixture was stirred and heated under reflux (>120 °C) for 18 hours. When cool, supernatant toluene was decanted off to leave a dark oily residue (690 mg). By NMR this was the product contaminated with around one equivalent ethanolamine. A mixture of keto-enol tautomers is observed by NMR. To improve the purity, a portion was passed through a column packed with reverse phase silica using 1% MeOH in DCM as eluent. UV active fractions were collated and a proton NMR of the concentrated residue showed that the ethanolamine had been removed along with the counter-ion with an approximate yield of 50 mg (10%). It appears that the tosylate ion was exchanged with chloride or hydroxide on the column.

UV (λ_{max}, EtOH): 209 nm;

LRMS m/z: Found 199.1 $[M+H]^+$;

HRMS (ESI-TOF) m/z: [M+H]+ Calc'd for $C_{10}H_{19}N_2O_2$+ 199.1441; Found 199.1440 (error 0.1 ppm);

δ_H (400 MHz, $CDCl_3$): 5.36 (C=C-H en-imine, integrates ~0.7H), 3.77 (4H, t, *J* = 5.3 Hz, NC*H*$_2$C*H*$_2$OH), 3.46 (4H, t, *J* = 5.3 Hz, NC*H*$_2$C*H*$_2$OH), 3.10-3.00 (s, C-CH_2 di-imine, integrates ~1.4H), 2.53 (4H, t, *J* = 6.3 Hz, 2 x CH_2), 1.90-1.86 (2H, m, CH_2) ppm; NB: ethanolamine contaminant (1 eq.) centred on 3.61 (t) , 2.75 (t) ppm.

Preparation of 2-hydroxy-N-(3-((2-hydroxyethyl)amino)cyclohex-2-en-1-ylidene)ethan-1-aminium, AC28

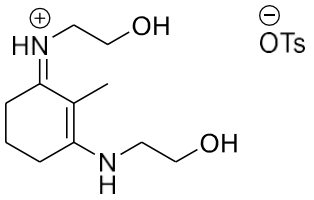

This compound is novel. 2-Methylcyclohexane-1,3-dione (226 mg, 1.79 mmol) and tosic acid monohydrate (339 mg, 1.76 mmol, 1 eq.) were added in toluene (5 cm^3). Ethanolamine (0.43 g, 0.43 cm^3, 7.11 mmol, 4 eqs.) was added last. The mixture was stirred and heated under reflux (>120 °C) for 24 hours. When cool, supernatant toluene was decanted off and this left a yellow residue when solvent was removed in vacuo. By NMR this is the product contaminated with ~1 eq. ethanolamine. Washing with excess DCM and/or EtOAc did not seem to selectively remove any ethanolamine. There was no improvement when the reaction was repeated with fewer equivalents of ethanolamine (2.2 instead of 4) were used, which led to contamination with ethanolamine and the single addition product. To improve the purity a portion was passed through a column packed with reverse phase silica using 10% MeOH in acetonitrile as eluent. UV active fractions were collated to produce the product (36 mg, 0.18 mmol, 10%). The residue analysed by NMR showed much improved purity and retention of the tosylate counterion.

UV (λ_{max}, EtOH): 302 nm;

LRMS (ESI) m/z: Found 213.1 $[M+H]^+$;

HRMS (ESI-TOF) m/z: [M+H]+ Calc'd for $C_{11}H_{21}N_2O_2$ 213.1598; Found 213.1597 (error 0.3 ppm);

δ_H (400 MHz, $CDCl_3$): 7.67-7.65 (2H, d, ArH, J = 8 Hz), 7.34-7.32 (2H, d, ArH, J = 8 Hz), 3.72-3.71 (4H, m, NC*H*$_2$C*H*$_2$OH), 3.54-3.53 (4H, m, NC*H*$_2$C*H*$_2$OH), 2.58-2.50 (4H, m, 2 x CH_2), 2.40 (3H, s, counterion), 1.81 (2H, m, CH_2), 1.70 (3H, s, CH_3) ppm.

Preparation of (S)-2-Amino-3-phenylpropan-1-ol[7]

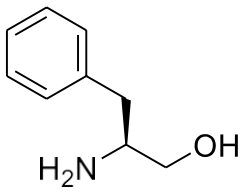

This compound was previously reported and characterised in Reddy, R. B.; Dudhe, P.; Chauhan, P.; Sengupta, S.; Chelvam, V. Synthesis of Tubuphenylalanine and *Epi*-Tubuphenylalanine via Regioselective Aziridine Ring Opening with Carbon Nucleophiles Followed by Hydroboration-Oxidation of 1,1-Substituted Amino Alkenes. *Tetrahedron* **2018**, *74* (48), 6946–6953.[7] L-phenylalanine (500 mg, 3.02 mmol) was added in dry THF (5 cm^3) under nitrogen in an RBF. The flask was cooled in an ice bath. $NaBH_4$ (287 mg, 7.9 mmol, 2.6 eq.) was added in one portion. Iodine (660 mg, 2.6 mmol, 0.9 eq.) was dissolved in dry THF (3 cm^3) and added dropwise to the first solution. The rate of addition was adjusted so that a drop was added once the yellow colour began to fade. When addition was complete the mixture was refluxed overnight. The mixture was cooled to rt and methanol was added dropwise until the solution was colourless. The clear solution was transferred to a dry flask and the solvent was removed under vacuum to leave a white paste. 2M NaOH (5 cm^3) was added and the mixture was stirred for 1 hour at rt and then extracted with DCM (3 x 10 cm^3). The organic layers were combined and reduced under vacuum to yield the product as a white solid (483 mg, 3.20 mmol, 92%). The data matched that reported.

MP: 90-94 °C;

LRMS m/z: Found 152.1 $[M+H]^+$;

δ_H (400 MHz, $CDCl_3$) 7.31-7.18 (5H, m, ArH), 3.64 (1H, dd, *J* = 10.6, 3.9 Hz, CH_2), 3.38 (1H, dd, *J* = 10.6,7.2 Hz, CH_2), 3.15-3.09 (1H, *broad* m, CH), 2.79 (1H, dd, *J* = 13.5, 5.2 Hz, CH_2), 2.52 (1H, dd, *J* = 13.5, 8.7 Hz, CH_2), 2.10-1.58 (3H, *broad* m, OH and NH_2) ppm;

Preparation of 1-hydroxy-N-(3-((1-hydroxy-3-phenylpropan-2-yl)amino)-2-methoxycyclohex-2-en-1-ylidene)-3-phenylpropan-2-aminium 4-methylbenzenesulfonate, AC33

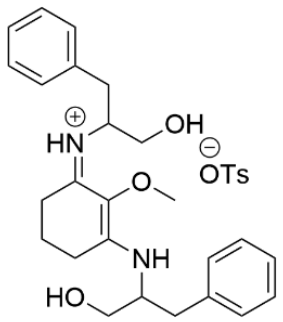

This compound is novel. 2-Methoxycyclohexane-1,3-dione (100 mg, 0.70 mmol) and tosic acid monohydrate (134 mg, 0.70 mmol, 1 eq.) were added in toluene (10 cm^3). (S)-2-Amino-3-phenylpropan-1-ol (426 mg, 2.82 mmol, 4 eqs.) was added last. Mixture was stirred and heated under reflux (>120 °C) for 48 hours. When cool, supernatant toluene was decanted. Residue was dissolved in DCM and filtered. Washing with cold DCM and hexane gradually removes the excess amino alcohol starting material at the cost of reduced yield (~20 mg, 0.05 mmol, 7%). The filtrate was dried to a light orange oil. *Due to lack of well-resolved NMR spectrum, stereochemical information is not shown.*

UV (λ_{max}, EtOH): 332 nm;

LRMS m/z: Found 409.3 $[M+H]^+$;

δ_H (400 MHz, MeOD): 7.80 (2H, d, J = 10.0 Hz, ArH), 7.21-7.17 (10H, m, ArH), 7.10-7.08 (2H, m, ArH), 3.95-3.60 (4H, m, OCH_2), 2.85-2.80 (2H, m, NCH), 3.27 (3H, s, OCH_3), 2.15 (3H, s, CH_3), 1.80-1.60 (4H, m, NH and OH), 1.30-1.25 (4H, m, CH_2), 0.80-0.70 (2H, m, CH_2).

Preparation of 5-hydroxy-N-(3-((5-hydroxypentyl)amino)cyclohex-2-en-1-ylidene)pentan-1-aminium tosylate, AC30

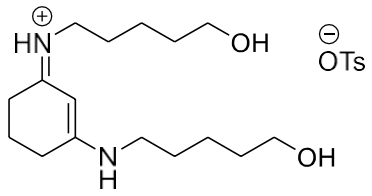

This compound is novel. Cyclohexane-1,3-dione (100 mg, 0.89 mmol, 1 eq.) and tosic acid monohydrate (169 mg, 0.89 mmol, 1 eq.) were added in 5 cm^3 toluene. 5-Aminopentanol (368 mg, 0.41 mL, 4 eqs.) was added last. Mixture was stirred and heated under reflux (>120 °C) for 18 hours. When cooled to rt, supernatant toluene was decanted off to leave a gel-like residue. Washing with acetone (3x 10 cm^3) produced an amber oil (~400 mg). The product was directly purified from this oil by Biotage Selekt with UV detection using a gradient: 5-100 % methanol in water in 45 mins, 100 % methanol for 20 minutes. Pure AC30 (15 mg, 0.05 mmol, 6%) was isolated as a pale oil in fractions 9-12 (~20% methanol in water) illustrated by the chromatogram:

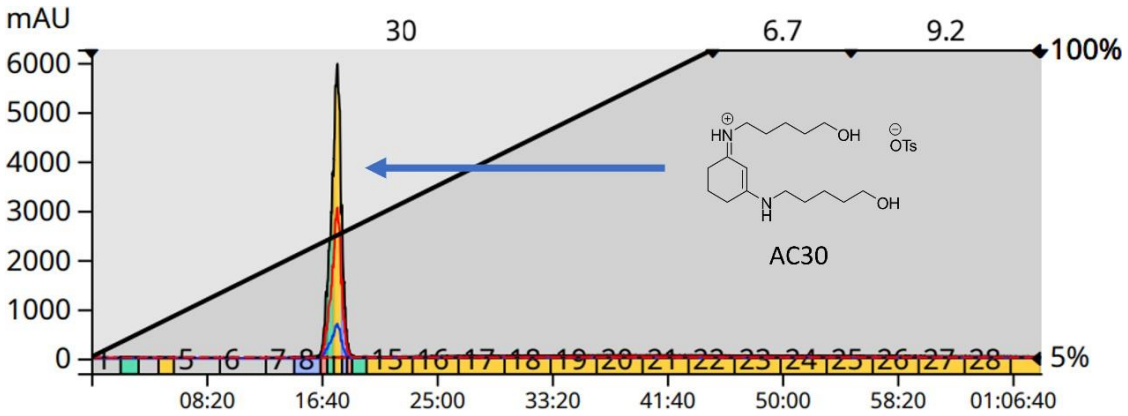

Elution time (mm:ss)

UV (λ_{max}, EtOH): 308 nm;

LRMS m/z: Found 283.2 $[M+H]^+$;

HRMS (ESI-TOF) m/z: $[M+H]^+$ Calc'd for $C_{16}H_{31}N_2O_2$ 283.2380; Found 283.2379 (error 0.3 ppm);

δ_H (400 MHz, D_2O): 7.69 (3H, d, *J* = 8.2, ArH counterion), 7.37 (3H, d, *J* = 8.0 Hz, ArH counterion), 5.28 (1H, s, integrates to ~0.6, enol), 3.61 (4H, t, J = 6.5, 2 x OCH_2), 3.33 (4H, t, J = 7.0. 2 x NCH_2), 2.52 (4H, t, J = 6.2, 2 x CH_2), 2.4 (~4H, s, 2 x CH_2), 1.89 (2H, m, CH_2), 1.67 (4H, m, 2 x CH_2), 1.58 (4H, m, 2 x CH_2), 1.41 (4H, m, 2 x CH_2).

Preparation of 5-hydroxy-N-(3-((5-hydroxypentyl)amino)-2-methoxycyclohex-2-en-1-ylidene)pentan-1-aminium tosylate, AC35

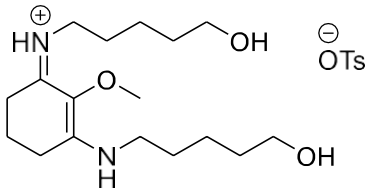

This compound is novel. 2-Methoxycyclohexane-1,3-dione (100 mg, 0.70 mmol, 1 eq.) and tosic acid monohydrate (133 mg, 0.70 mmol, 1 eq.) were added in 5 cm^3 toluene. 5-Aminopentanol (289 mg, 2.8 mmol, 4 eqs.) was added last. The mixture was stirred and heated under reflux (>120 °C) for 18 hours. When cooled to rt, supernatant toluene was decanted off to leave a gel-like residue. Washing with acetone (3x 10 cm^3) produced a dark oil (300 mg). This produced a crude product (~100 mg, ~46%) contaminated with 5-aminopentanol.

UV (λ_{max}, EtOH): 326 nm;

LRMS m/z: Found 313.2 $[M+H]^+$;

δ_H (400 MHz, D_2O): 7.69 (3H, d, *J* = 8.2, ArH, counterion), 7.37 (3H, d, *J* = 8.0 Hz, ArH, counterion), 3.61 (4H, t, J = 6.5, 2 x CH_2), 3.52 (3H, s, $-OCH_3$), 3.33 (4H, t, J = 7.0. 2 x CH_2), 2.62 (4H, t, J = 6.2, 2 x CH_2), 2.38 (~4H, s, 2 x CH_2), 1.91-1.85 (2H, m, CH_2), 1.70-1.53 (4H, m, 2 x 2 x CH_2) + 5-aminopentanol, 1.43-1.34 (4H, m, 2 x CH_2) + 5-aminopentanol.

Confirmation of counter-ion exchange (general)

From the disappearance of the three NMR signals derived from the tosylate counterion (~7.6, ~7.3, ~2.4 ppm) with the retention of all other signals corresponding to the cation, we can ascertain that the counterion is fully exchanged. There are no new proton NMR signals when the exchange is between tosylate and chloride.

2.4.2 NMR and LRMS characterisation of DS1 and DS2

DS1 (4-methoxy-N-(3-((4-methoxyphenyl)amino)-2-methylcyclohex-2-en-1-ylidene)benzenaminium chloride) and **DS2** (N-(3-(cyclohexylamino)-2-methylcyclohex-2-en-1-ylidene)cyclohexanaminium chloride) were prepared by colleagues at the Universidad de La Rioja, Spain. NMRs were recorded by us to ensure integrity of the molecule on arrival.

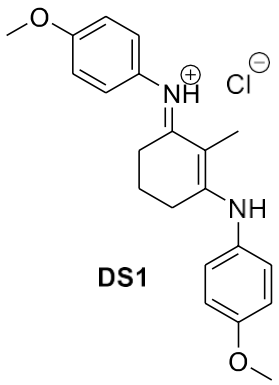

DS1

δ_H (400 MHz, MeOD): 7.22 (4H, d, J = 8.7 Hz, ArH), 7.03 (4H, d, J = 8.7, ArH), 3.84 (6H, s, 2 x -OCH_3), 2.53 (4H, t, 2 x CH_2), 2.07 (3H, s, CH_3), 1.82-1.75 (2H, m, CH_2).

LRMS m/z: Found 337.2 $[M+H]^+$;

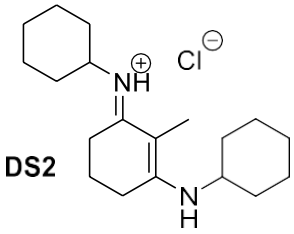

δ_H (400 MHz,): 3.67-3.60 (1H, m), 2.67 (2H, t, J = 6.3 Hz, NCH), 1.94-1.85 (4H, m, CH_2), 1.80-1.70 (8H, m, CH_2), 1.68 (3H, s, CH_3), 1.70-1.60 (~2H, m, CH_2), 1.52-1.35 (10H, m, CH_2), 1.27-1.15 (2H, m, CH_2).

LRMS m/z: Found 289.2 $[M+H]^+$;

2.4.3 Characterisation of shinorine and porphyra-334

[This was previously published in Whittock, A. L.; Auckloo, N.; Cowden, A. M.; Turner, M. A. P.; Woolley, J. M.; Wills, M.; Corre, C.; Stavros, V. G. Exploring the Blueprint of Photoprotection in Mycosporine-like Amino Acids. *J. Phys. Chem. Lett.* **2021**, *12* (14), 3641–3646. https://doi.org/10.1021/acs.jpclett.1c00728.]

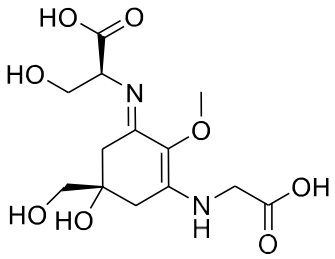

Shinorine

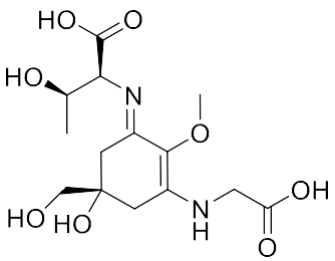

Porphyra-334

Commercially available Helioguard™ 365 samples (Mibelle Biochemistry) were received as an aqueous preparation containing 0.1 % mycosporine-like amino acids (MAAs) according to the manufacturer's report. The product is described as 80% *Porphyra umbilicalis* extract with 0.1% mycosporine-like amino acids, 3% phospholipids, 15% absolute ethanol, 0.16% sodium lactate and deionized water. Ethanol co-solvent and most of the water was removed under vacuum on a rotary evaporator and the residue was resuspended in HPLC-grade water and filtered through 0.25 µm filters in preparation for Ultra High Performance

Liquid Chromatography - High Resolution Mass Spectrometry (UHPLC-HRMS) analysis. The analysis was performed with a 2 µL sample injection through a reverse phase column (Zorbax Eclipse Plus C18, size 2.1 x 100 mm, particle size 1.8 µm) connected to a Dionex 3000RS UHPLC coupled to Bruker Ultra High Resolution (UHR) Q-TOP MS MaXis II mass spectrometer using ESI (Electrospray Ionization in positive mode) with 10 mM sodium formate through loop injection. A m/z range of 50-2500 was used. Column elution was done with the following gradient: 0 min: 2 % B, 5 min: 10 % B, 25 min: 20 % B, 30 min: 100 % B, 35 min: 100 % B (solvent A = 0.1 % (v/v) formic acid in water and solvent B = acetonitrile with 0.1 % formic acid)

Shinorine: HRMS (ESI-TOF) m/z: $[M+H]^+$ calc'd for $C_{13}H_{21}N_2O_4^+$ 333.1292; Found 333.1291 (error 0.3 ppm).

Porphyra-334: HRMS (ESI-TOF) m/z: $[M+H]^+$ calc'd for $C_{14}H_{23}N_2O_3^+$ 347.1449; Found 347.1448 ; (error 0.3 ppm).

To obtain purer samples for analysis and further study Reverse-phase High Performance Liquid Chromatography (HPLC) was performed using a PrepHT XDB-C18 column (21.2 x 100 mm, particle size 5 µm) connected to an Agilent 1260 HPLC equipped with a binary pump and diode-array detection detector. Injection volumes of 200 µL were used with the following conditions: 5 % B for 15 min; 10 % B for 10 min; then increasing to 100 % B over 5 min; and 100 % B for 10 min (solvent A = 0.1 % formic acid in water; solvent B = 0.1 % formic acid in methanol) with a flow rate of 5 mL/min. Fractions were collected based on absorbance at 333 nm using an automated fraction collector. The retention time of shinorine was 4.35 min while the retention time of porphyra-334 was 6.15 min. The fractions containing each compound were combined and the solvent was evaporated using a centrifugal evaporator.

Each compound was confirmed by UHPLC-HRMS analysis following the same conditions given above. A UV-vis spectrum centred at 333 nm for each sample shows a single peak with the retention time correlating to the correct mass spectra. In addition, an NMR of a sample of porphyra-334 was recorded on a Bruker Avance III 400 MHz spectrometer and agreed with a previously reported spectrum in Klisch, M.; Richter, P.; Puchta, R.; Häder, D.-P.; Bauer, W. The Stereostructure of Porphyra-334: An Experimental and Calculational NMR

Investigation. Evidence for an Efficient 'Proton Sponge.' HCA 2007, 90 (3), 488–511. https://doi.org/10.1002/hlca.200790052.[8]

Literature NMR: δ_H (400 MHz, D_2O): δH 1.18 (3H, d, J = 6.4 Hz); 2.68 (1H, d, J = 17.6 Hz); 2.70 (1H, d, J = 17.8 Hz); 2.80 (1H, d, J = 17.8 Hz); 2.83 (1H, d, J = 17.6 Hz); 3.49 (2H, s); 3.61 (3H, s); 4.11 (2H, *br*, s); 4.19 (1H, d, J = 4.0 Hz).[9]

δ_H (400 MHz, D_2O): 4.28 (1H, d, *J* = 4.1 Hz), 4.20 (2H, s), 3.70 (3H, s), 3.58 (2H, s), 2.95-2.75 (~4H, m), 1.27 (3H, d, *J* = 6.5 Hz). OH, NH, CO_2H protons exchange with the solvent. The large impurity (peak-picked at 4.45-4.35 and 1.43-1.41 ppm but not integrated) is thought to be lactic acid, which is present in the original formulation according to the manufacturer.

NB: An ^{1}H-NMR of shinorine was obtained but was of poor quality and MS and UV characterisation were sufficient for this compound.

2.5 Synthesis of precursors to avobenzone/ octocrylene ("AVOCTOX") compounds

2.5.1 Precursors

Preparation of 4-(3-hydroxypropoxy)phenylethan-1-one[10]

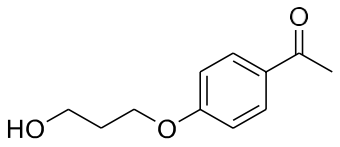

This compound was reported previously in J. L Besombes, G. Cheminat, G. Mousset, C. Mousty, Bull. Soc. Chem. Fr. 1992, 129, 513–522.[10] 4-Hydroxyacetophenone (544 mg, 4.0 mmol), 3-bromoethanol (0.84 g, 6.0 mmol, 1.5 eqs.) were added to acetonitrile (ca. 10 cm^3) and K_2CO_3 (1.12 g, 8.0 mmol, 2.0 eqs.) was added. The resulting mixture was stirred at 80 °C under a N_2 atmosphere overnight. At the end of this time the reaction was allowed to cool to rt and the K_2CO_3 was filtered off using gravity filtration. The filter paper was rinsed with DCM (~20-30 cm^3) to wash the product into the flask. The liquid phase was dried ($MgSO_4$), filtered and the solvent removed by high vacuum pump for 2-3 hours minimum after rota has removed the solvent to yield the product as a yellow oil (543 mg, 2.80 mmol, 70%). The product used in the next step without further purification. The data matched that reported.

TLC: R_f ~0.2; in EtOAc:Hexane (1:1), visualised by UV.

ν_{max} : 3400 (*br*, O-H stretch), 2941 and 2880 (intramolecular C=O---H-OH bond or C-H stretching), 1665 (C=O stretch) cm^{-1};

LRMS (ESI): m/z: Found [M+H]+ 195.0, $[M+Na]^+$ 217.1;

HRMS (ESI) m/z: [M + H]+ Calc'd for $C_{11}H_{15}O_3$ 195.1016; Found 195.1018 (error 1.0 ppm);

δ_H (400 MHz, $CDCl_3$): 7.94 (2H, d, J = 9.0 Hz, ArH), 6.96 (2H, d, J = 9.0, ArH), 4.21 (2H, t, J = 6.0 Hz, OCH_2), 3.90 (2H, t, J = 6.0 Hz, OCH_2), 2.58 (3H, s, CH_3), 2.10 (2H, pent, J = 6.0 Hz, CH_2), 1.76 (1H, *broad*, OH) ppm.

Preparation of 4-(3-hydroxypropoxy)phenyl-3-phenylpropane-1,3-dione[11]

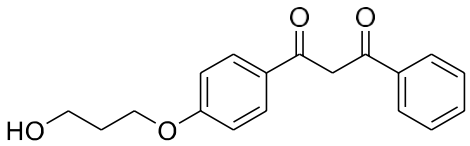

This compound was reported previously in Jin, H.; Zhang, W.; Wang, D.; Chu, Z.; Shen, Z.; Zou, D.; Fan, X.; Zhou, Q. Dendron-Jacketed Electrophosphorescent Copolymers: Improved Efficiency and Tunable Emission Color by Partial Energy Transfer. *Macromolecules* **2011**, *44* (24), 9556–9564.[11] Sodium hydride (60% suspension in oil, 1.2 g, 30.0 mmol, 3 eq.) was dissolved in dry THF (10 cm^3) in a dry round bottom flask under nitrogen. The suspension was stirred for 10 mins at rt. 1-(4-(3-Hydroxypropoxy)phenyl)ethan-1-one (2.00 g, 10.3 mmol) was added by syringe and the mixture was stirred for 15 mins. Methyl benzoate (2.52 cm^3, 2.72 g, 20.0 mmol, 2 eq.) was added dropwise with stirring along with dry THF (10 cm^3). The solution was heated to 66 °C overnight under reflux. After cooling to rt, distilled water (ca. 5 cm^3) was added, and the solution was extracted with EtOAc (3 x 20 cm^3). The combined organic layers were washed with brine (~10 cm^3) and reduced on rotary evaporator to a crude residue. The product was isolated as a white solid (0.57 g, 1.91 mmol, 19%) using a silica column with EtOAc:Hexane (1:1) as the mobile phase. The data matched that reported.

TLC: R_f ~0.5; in EtOAc:Hexane (1:1); visualisation by UV, $KMnO_4$;

ν_{max} 3311 (O-H stretch), 3058, 2957, 2924, 2877 (C-H stretches), 1714 (C=O stretch), 1600 (enol C=C) cm^{-1};

LRMS (ESI) m/z: Found $[M+H]^+$ 299.1;

HRMS (ESI) m/z: $[M+H]^+$ Calc'd for $C_{18}H_{19}O_4$ 299.1278; Found 299.1279 (error 0.4 ppm);

δ_H (400 MHz, $CDCl_3$): 7.97 (4H, d, *J* = 7.9 Hz, ArH), 7.54-7.52 (1H, m, ArH), 7.50-7.46 (2H, m, ArH), 6.98 (2H, d, *J* = 8.6 Hz, ArH), 6.79 (1H, s, CH enol), 4.25 (2H, t, *J* = 6.0 Hz, CH_2), 3.88 (2H, t, *J* = 6.0 Hz, CH_2), 2.11-2.05 (2H, m, CH_2) ppm. OH was not observed;

δ_C (101 MHz, $CDCl_3$): 186.2 (C=O), 184.0 (C=O), 162.61 (ArC), 135.5 (ArC), 132.2 (ArC), 129.4 (ArCH), 128.7 (ArCH), 127.0 (ArCH), 114.5 (ArCH), 92.4 (CH, enol), 65.7 (CH_2), 60.0 (CH_2), 32.0 (CH_2).

Preparation of 1-(4-(*tert*-butyl)phenyl)-3-(4-(3-hydroxypropoxy)phenyl)propane-1,3-dione

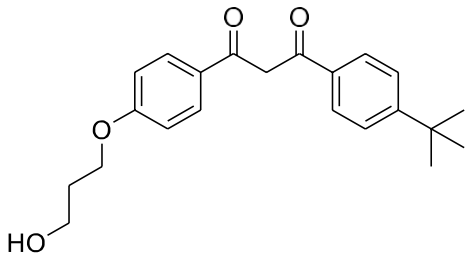

This compound is novel**.** Sodium hydride (60% dispersion in oil, 247 mg, 6.19 mmol, 3 eq.) was added to dry THF (3 cm^3) under nitrogen in a round bottom flask. A solution of (4-(3-Hydroxypropoxy)phenyl)ethanone (400 mg, 2.06 mmol) in dry THF (5 cm^3) was added to this suspension. The suspension was stirred for 30 mins at rt. Methyl 4-(*tert*-butyl)benzoate (793 mg, 0.80 cm3, 4.1 mmol, 2 eq.) was added slowly via syringe. The mixture thickens and so further portions of THF were added until stirring returned. The reaction was stirred at rt overnight. Distilled water (3 cm^3) was added and the product was extracted with EtOAc (3 x 10 cm^3). The combined extracts were dried under vacuum to a crude that was observed by NMR to be mostly the product contaminated with mineral oil. The product was purified by flash chromatography on silica column with a 1:1 EtOAc:Hexane mobile phase to isolate the product as an oil (220 mg, 0.62 mmol, 30%, *eluted as the second spot of two visible spots*).

TLC: R_f ~ 0.85; (visualisation by UV, $KMnO_4$);

ν_{max} 2955 and 2871 (intramolecular C=O---H-OH bond or C-H stretching), 1699 (C=O stretch), 1592 (C=C-C=O of enol form) cm^{-1};

LRMS (ESI) m/z: Found $[M]^-$ 353.2 m/z;

HRMS (ESI) m/z: $[M+H]^+$ Calc'd for $C_{22}H_{27}O_4$ 355.1904; Found 355.1901 (error 0.9 ppm);

δ_H (400 MHz, $CDCl_3$): 7.96 (2H, d, *J* = 8.6 Hz, ArH), 7.91 (2H, d, *J* = 8.1 Hz, ArH), 7.50 (2H, d, , *J* = 8.6 Hz, ArH), 6.98 (2H, d, *J* = 8.2 Hz, ArH), 6.77 (1H, s, CH enol), 4.20 (2H, t, *J* = 8.6 Hz, CH_2), 3.88 (2H, t, *J* = 8.6 Hz, CH_3), 2.10-2.04 (2H, m, CH_2), 1.36 (9H, s, *t*Bu) ppm;

δ_C (101 MHz, $CDCl_3$): 185.8 (C=O), 184.3 (C=O), 162.4 (ArC), 156.0 (ArC), 132.8 (ArC), 129.3 (2 x ArCH), 128.4 (ArC), 114.4 (ArCH), 92.1 (CH, enol), 65.6 (CH_2), 60.0 (CH_2), 31.9 (CH_2), 31.2 (3 x CH_3) ppm.

Preparation of 1-(4-(3-hydroxypropoxy)phenyl)-3-(4-methoxyphenyl)propane-1,3-dione

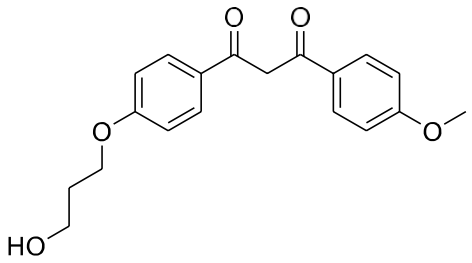

This compound is novel. Sodium hydride (60% suspension in oil, 234 mg, 5.85 mmol, 3 eq.) was dissolved in dry THF (5 cm^3) in a dry round bottom flask and placed under nitrogen. The suspension was stirred for 10 mins at rt. 1-(4-(3-Hydroxypropoxy)phenyl)ethan-1-one (380 mg, 1.95 mmol, 1 eq.) was added by syringe and the mixture was stirred for 15 mins. Methyl 4-methoxybenzoate (650 mg, 3.91 mmol, 2 eq.) was added dropwise with stirring along with dry THF (5 cm^3). The solution was stirred at rt overnight. Distilled water (~5 cm^3) was added, and the solution was extracted with EtOAc (2 x 15 cm^3). The combined organic layers were washed with brine (~15 cm^3) and reduced on rota to a crude orange residue with a complex TLC (>4 spots). The product was isolated as an oil (70 mg, 0.21 mmol, 11%) using a silica column with 1:1 EtOAc:Hexane as the mobile phase.

TLC: R_f ~0.75; (visualisation by UV, $KMnO_4$);

ν_{max} 2926 and 2854 (intramolecular C=O---H-OH bond or C-H stretching), 1667 (C=O stretch);

LRMS m/z: $[M+H]^+$ Found 329.1;

HRMS (ESI) m/z: $[M+H]^+$ Calc'd for C19H20NaO5 351.1203; Found 351.1197 (error 1.8 ppm);

δ_H (400 MHz, $CDCl_3$): 7.96-7.92 (4H, m, ArH), 6.96 (4H, d, *J* = 8.8 Hz, ArH), 6.71 (1H, s, CH enol), 4.18 (2H, t, *J* = 6.0 Hz, CH_2), 3.88-3.85 (5H, m, CH_2 + OCH_3), 2.07 (2H, pent, J= 6.0 Hz, CH_2) ppm;

δ_C (101 MHz, $CDCl_3$): 184.7 (C=O), 163.1 (ArC), 162.4 (ArC), 131.4 (ArC), 129.1 (ArCH x2), 128.2 (ArC), 114.43 (ArCH), 114.0 (ArCH), 91.5 (CH, enol), 65.6 (CH_2), 60.0 (CH_2), 55.5 (CH_3), 31.9 (CH_2) ppm.

Preparation of 1-(4-Chlorophenyl)-3-(4-(3-hydroxypropoxy)phenyl)propane-1,3-dione

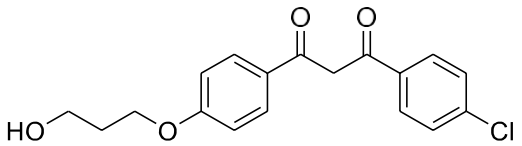

This compound is novel. Sodium hydride (60% suspension in oil, 698 mg, 17.5 mmol, 3 eq.) was suspended in dry THF (10 cm^3) in a dry round bottom flask and placed under nitrogen. The suspension was stirred for 10 mins at rt. 1-(4-(3-Hydroxypropoxy)phenyl)ethan-1-one (1.13 g, 5.81 mmol, 1 eq.) was added by syringe and the mixture was stirred for 15 mins. Ethyl 4-chlorobenzoate (3.98 cm^3, 3.95 g, 21.4 mmol, 3.7 eqs.) was added dropwise with stirring along with dry THF (5 cm^3). The solution was stirred at RT overnight. Then distilled water (~5 cm^3) was added and the solution was extracted with EtOAc (2 x 20 cm^3). The combined organic layers were washed with brine (10 cm^3) and reduced under vacuum to give a crude residue. The product was isolated as a white solid (620 mg, 1.86 mmol, 32%) using a silica gel column with 1:1 EtOAc:Pet. ether as the mobile phase.

TLC: R_f ~0.8; (visualisation by UV, $KMnO_4$);

ν_{max} 3258 (O-H stretch), 2951, 2865 (C-H stretches), 1624 (C=O stretch), 1586 (enol C=C-C=O stretch) cm^{-1};

LRMS (ESI) m/z: $[M]^-$ 331;

HRMS (ESI) m/z: $[M+H]^+$ Calc'd for $C_{18}H_{18}{}^{35}ClO_4$ 333.0888; Found 333.0884 (error 1.2 ppm);

δ_H (400 MHz, $CDCl_3$): 7.98 (2H, d, *J* = 8.4 Hz, ArH), 7.90 (2H, d, *J* = 8.4 Hz, ArH), 7.45 (2H, d, *J* = 8.3 Hz, ArH), 6.98 (2H, d, *J* = 8.6 Hz, ArH), 6.74 (1H, s, enol), 4.20 (2H, t, *J* = 6.0 Hz, CH_2), 3.88 (2H, t, *J* = 6.0 Hz, CH_2), 2.11-2.05 (2H, m, CH_2) ppm;

δ_C (101 MHz, $CDCl_3$): 186.2 (C=O), 182.9 (C=O), 162.7 (ArC), 129.4 (ArC), 129.0 (ArCH x2), 128.4 (ArC), 114.4 (ArCH), 92.3 (CH, enol), 65.6 (CH_2), 60.0 (CH_2), 31.9 (CH_2) ppm.

Preparation of 2-Cyano-3,3-diphenylacrylic acid[12]

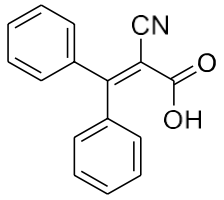

This compound was previously reported in Li, J.; Chen, H.; Zhang-Negrerie, D.; Du, Y.; Zhao, K. Synthesis of Coumarins via PIDA/I_2-Mediated Oxidative Cyclization of Substituted Phenylacrylic Acids. RSC Adv. 2013, 3 (13), 4311.[12] Octocrylene (5.72 g, 16.4 mmol) was suspended in MeOH (20 cm^3) and LiOH (923 mg, 33 mmol, 2 eq.) was added at rt. The solution was stirred overnight at rt, after which the MeOH was removed under vacuum and water (30 cm^3) was added. The aqueous solution was extracted with EtOAc (3 x 30 cm^3), then 37% HCl was added until the aqueous solution was at pH <1. This solution was then extracted with DCM (3 x 30 cm^3), the combined extracts were dried over $MgSO_4$, filtered and the solvent removed under vacuum to give the product (2.26 g, 9.08 mmol, 55%) as a white solid. The data matched that reported.

LRMS (ESI) m/z: Found $[M]^-$ 248.25;

δ_H (500 MHz, $CDCl_3$) 7.56-7.39 (8H, m, ArH), 7.19 (2H, d, J = 7.5 Hz, ArH), acid OH was not observed;

δ_C (126 MHz, $CDCl_3$) 172.27 (CO or CN), 166.18 (CO or CN), 138.4 (ipso), 138.2 (ipso), 132.0 (ArCH), 139.9 (ArCH), 130.5 (ArCH), 129.6 (ArCH), 128.6 (ArCH), 128.2 (ArCH), 116.7 (C=C), 102.4 (C=C).

Preparation of methyl 4-methoxybenzoate[13]

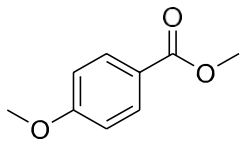

This compound was previously reported in Subramanian, K.; Yedage, S. L.; Bhanage, B. M. An Electrochemical Method for Carboxylic Ester Synthesis from *N* -Alkoxyamides. *J. Org. Chem.* **2017**, *82* (19), 10025–10032.[13] 4-Methoxybenzoic acid (1.00 g, 8.20 mmol) was added to dry DMF (5 cm^3). K_2CO_3 (1.37 g, 10.0 mmol, 1.2 eq.) was added and mixture was stirred at rt for 5 mins under nitrogen. Methyl iodide (0.62 cm^3, 1.41 g, 10.0 mmol 1.2 eq.) was added dropwise by syringe and the mixture was stirred overnight at RT. Distilled water (5 cm^3) was then added and the solution was extracted with EtOAc (3 x 15 cm^3). The combined organic extracts were washed with distilled water (3 x 15 cm^3) and then with brine (15 cm^3). The organic layer was dried to yield the product (650 mg, 3.61 mmol, 48%). The data matched that reported.

TLC: R_f ~0.7; (visualisation by UV, $KMnO_4$);

δ_H (400 MHz, $CDCl_3$): 7.98-7.96 (2H, d, *J* = 8.8 Hz, ArH), 6.90-6.88 (2H, d, *J* = 8.8 Hz, ArH), 3.86 (3H, s, CH_3), 3.83 (3H, s, CH_3) ppm.

Preparation of ethyl 4-chlorobenzoate

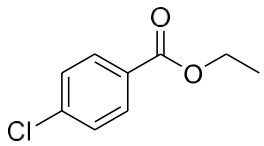

This is a known compound. 4-Chlorobenzoyl chloride (0.59 mL, 0.8 g, 1 eq.) and DMAP (56 mg, 0.1 eqs.) were added in 5 ml DCM in a round bottom flask resting in an ice bath. Ethanol (0.27 mL, 0.21 g, 1 eq.) and TEA (1.27 mL, 0.92g, 2 eqs.) were added by syringe. The emulsion was then warmed slowly to RT and stirred for 1 hour. The contents of the flask were added directly to a short silica column and eluted using DCM to yield the product as a clear liquid (500 mg, 59%) when dried under vacuum.

TLC: R_f ~ 0.75 (in 100% DCM on aluminium-backed silica gel, visualised by UV)

LRMS m/z: Calc $[M+H]^+$ C9H10ClO2+ 185.4. Found 391.3 $[2M+Na]^+$.

δ_H (400 MHz, $CDCl_3$): 7.95-7.93 (2H, d, ArH), 7.37-7.35 (2H, d, ArH), 4.37-4.31 (2H, q, CH_2), 1.37-1.34 (3H, t, CH_3)

δ_C (101 MHz, $CDCl_3$): 165.6 (C=O), 139.2 (ArC), 139.9 (ArCH), 128.9 (ArC), 128.6 (ArCH), 61.2 (CH_2), 14.3 (CH_3).

2.5.2 DCC coupling in the synthesis of avobenzone/octocrylene ("AVOCTOX") compounds

One equivalent of 2-cyano-3,3-diphenylacrylic acid is added in DCM (1 g/10 cm^3 solvent) under a nitrogen atmosphere in dry glassware with stirring. DCC (1.1 eq.) and DMAP (0.1 eq.) are added. The mixture is stirred at rt for 10 mins. One equivalent of the relevant alcohol is dissolved in DCM (100 mg/3 cm^3) and is added in one portion. The resulting mixture is stirred overnight at rt. The mixture is filtered into a clean flask using DCM and the organic solvent is removed under vacuum. Flash chromatography is used to isolate the product from the crude residue.

Preparation of 3-(4-(3-Oxo-3-phenylpropanoyl)phenoxy)propyl 2-cyano-3,3-diphenylacrylate, "AVOCTO1"

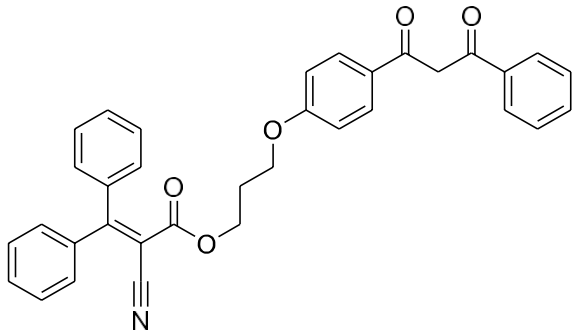

This compound is novel. 2-Cyano-3,3-diphenylacrylic acid (0.33 g, 1.32 mmol) was added to DCM (5 cm^3) under nitrogen. DCC (0.30 g, 1.46 mmol, 1.1 eq.) and DMAP (16 mg, 0.13 mmol, 0.1 eq.) were added and the mixture was stirred for 10 mins at rt. 1-(4-(3-Hydroxypropoxy)phenyl)-3-phenylpropane-1,3-dione (0.40 g, 1.34 mmol) was dissolved in DCM (5 cm^3) and added to the mixture. The mixture was stirred overnight at rt. The mixture was then passed through filter paper, and the filtrate was reduced under vacuum. A silica column with 1:1 EtOAc:Hexane as mobile phase was used to isolate the product (350 mg, 0.662 mmol, 50%) as an off-white gum. *Product elutes quickly as the 2nd spot observed on the TLC.*

TLC: R_f ~0.8. in EtOAc:Hex (1:1) on aluminium-backed silica gel; visualisation by UV, *stains brightly with $KMnO_4$*;

ν_{max} 3055 and 2928 (intramolecular C=O---H-OH bond or C-H stretching), 1715 (C=O stretch), 1592 (C=C-C=O of enol form) cm^{-1};

LRMS (ESI) m/z: Found $[M+Na]^+$ 552.2; HRMS (ESI-TOF) m/z: $[M+Na]^+$ Calc'd for $C_{34}H_{27}NO_5Na$ 552.1781; Found 552.1787 (error 1 ppm);

δ_H (400 MHz, $CDCl_3$): 7.98 (4H, d, *J* = 8.0 Hz, ArH), 7.54-7.16 (11H, m, ArH), 7.15 (2H, d, *J* = 7.3 Hz, ArH), 6.93 (2H, d, *J* = 8.6 Hz, ArH), 6.81 (1H, s, CH enol), 4.32 (2H, t, *J* = 6.0 Hz, CH_2), 3.94-3.91 (2H, t, *J* = 6.0 Hz, CH_2), 2.07-2.02 (2H, m ,CH_2). Singlet at 4.59 ppm is likely to be the diketo form.

δ_C (101 MHz, $CDCl_3$): 186.1 (CO or CN), 184.1 (CO or CN), 169.6 (CO or CN), 162.7 (CO or CN or Cipso or C=C), 162.3 (CO or CN or Cipso or C=C), 138.6 (Cipso or C=C), 138.2 (Cipso or C=C), 135.6 (Cipso or C=C), 132.2 (ArCH), 131.6 (ArCH), 130.6 (ArCH), 130.3 (ArCH), 129.3 (ArCH), 128.7 (ArCH), 128.6 (ArCH), 128.3 (Cipso or C=C), 127.0 (ArCH), 116.9 (Cipso or C=C), 114.5 (ArCH), 103.7 (Cipso or C=C), 92.4 (CH enol), 64.1 (CH_2), 62.6 (CH_2), 28.2 (CH_2).

Preparation of 3-(4-(3-(4-(*tert*-butyl)phenyl)-3-oxopropanoyl)phenoxy)propyl 2-cyano-3,3-diphenylacrylate, "AVOCTO2"

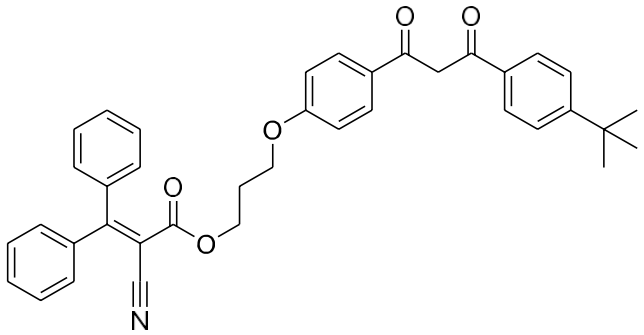

This compound is novel. 2-Cyano-3,3-diphenylacrylic acid (154 mg, 0.618 mmol, 1 eq.) was added to DCM (5 cm^3) under nitrogen. DCC (141 mg, 0.684 mmol, 1.1 eq.) and DMAP (~7 mg, 0.057 mmol, 0.1 eq.) were added and the mixture was stirred for 10 mins at rt. 1-(4-(*Tert*-butyl)phenyl)-3-(4-(3-hydroxypropoxy)phenyl)propane-1,3-dione (220 mg, 0.621 mmol, 1 eq.) was dissolved in DCM (5 cm^3) and added to the mixture. The mixture was stirred over a weekend at rt. The mixture was then passed through filter paper, and the solvent was removed under reduced pressure. A silica column with 25:75 EtOAc:Pet. ether as mobile phase was used to isolate the product in low yield (~30 mg, 0.051 mmol, 8%) as a yellow oil which on further drying formed a sticky solid residue.

TLC: R_f ~0.6; in EtOAc:Hex (1:1) on aluminium-backed silica gel; visualisation by UV, $KMnO_4$;

ν_{max} 3059, 2957 and 2865 (intramolecular C=O---H-OH bond or C-H stretching), 2215 (CN stretch), 1717 (C=O stretch), 1593 (C=C-C=O of enol form) cm^{-1};

LRMS (ESI) m/z: Found $[M+Na]^+$ 608.26; HRMS (ESI-TOF) m/z: $[M+Na]^+$ Calc'd for $C_{38}H_{35}NO_5Na$ 608.2407; Found 608.2406 (error 0.3 ppm);

δ_H (400 MHz, $CDCl_3$): 7.98 (2H, d, *J* = 8.1 Hz, ArH), 7.94 (2H, d, *J* = 8.1 Hz, ArH), 7.52-7.33 (10H, m, ArH), 7.15 (2H, d, *J* = 7.1 Hz, ArH), 6.94 (2H, d, *J* = 8.3 Hz, ArH), 6.81 (1H, s, enol CH), 4.32 (2H, t, *J* = 5.8 Hz, CH_2), 3.90 (2H, t, *J* = 5.8 Hz, CH_2), 2.05-2.01 (2H, m, CH_2), 1.36 (s, tBu, 9H) ppm;

δ_C (101 MHz, $CDCl_3$): 185.8 (CO or CN), 184.3 (CO or CN), 169.5 (CO or CN), 162.7 (CO or CN or Cipso or C=C), 162.3 (CO or CN or Cipso or C=C), 138.6 (Cipso or C=C), 138.3 (Cipso or C=C), 132.8 (Cipso or C=C), 131.6 (ArCH), 130.6 (ArCH), 129.4 (ArCH), 129.3 (ArCH), 128.6 (ArCH), 128.5 (ArCH), 128.3 (Cipso or C=C), 127.0 (ArCH), 125.7 (ArCH), 116.9 (Cipso or C=C), 114.5 (ArCH), 103.7 (Cipso or C=C), 92.2 (CH enol), 64.1 (CH_2), 62.7 (CH_2), 31.2 (3xCH_3), 28.2 (CH_2).

Preparation of 3-(4-(2-Methyl-3-oxo-3-phenylpropanoyl)phenoxy)propyl 2-cyano-3,3-diphenylacrylate, "AVOCTO3"

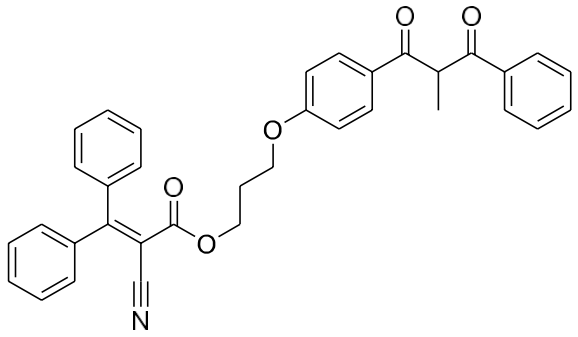

This compound is novel. 3-(4-(3-Oxo-3-phenylpropanoyl)phenoxy)propyl 2-cyano-3,3-diphenylacrylate (AVOCTO1) (30 mg, 0.057 mmol) was added to a suspension of K_2CO_3 (8 mg, 0.058 mmol, 1 eq.) in dry acetone (2 cm^3) and stirred for 5 mins at rt. Methyl iodide (9.6 mg, 4.2 µL, 0.068 mmol, 1.2 eqs.) was added dropwise and the mixture was stirred overnight at rt. Diethyl ether (5 cm^3) was added, and the mixture was filtered and reduced under vacuum. The product (30 mg, 0.055 mmol, 97%) was isolated as an oil by silica column using EtOAc:Hexane (1:1) as the mobile phase.

TLC: in EtOAc:Hex (1:1) on aluminium-backed silica gel: R_f of the product is slightly less than the R_f of the starting material in EtOAc:Hex (1:1), R_f ~ 0.8 (visualisation by UV/$KMnO_4$).

ν_{max} 3061, 2927 and 2856 (intramolecular C=O---H-OH bond or C-H stretching), 2216 (CN stretch), 1700 (C=O stretch), 1600, 1555 (C=C-C=O of enol form) cm^{-1};

LRMS (ESI) m/z: Found $[M+Na]^+$ 566.2; HRMS (ESI-TOF) m/z: $[M+Na]^+$ Calc'd for $C_{35}H_{29}NO_5Na$ 566.1938; Found 566.1938 (error 0.1 ppm);

δ_H (400 MHz, $CDCl_3$) 7.95 (4H, d, *J* = 7.3 Hz, ArH), 7.56-7.30 (~10H, m, ArH), 7.13 (2H, d, *J* = 7.4 Hz, ArH), 6.88 (2H, d, *J* = 8.6 Hz, ArH), 5.21 (1H, q, *J* =7.0 Hz, C*H*CH_3), 4.30 (2H, t, *J* = 5.9 Hz, CH_2), 3.90 (2H, t, *J* = 5.9 Hz, CH_2), 2.05-1.99 (2H, m, CH_2), 1.60 (3H, d, *J* = 7.0 Hz, CH_3);

δ_C (101 MHz, $CDCl_3$): 197.3 (CO or CN), 195.8 (CO or CN), 169.6 (CO or CN), 162.9 (CO or CN or Cipso or C=C), 162.6 (CO or CN or Cipso or C=C), 138.6 (Cipso or C=C), 138.2 (Cipso or C=C), 135.8 (Cipso or C=C), 133.4 (ArCH), 131.6 (ArCH), 130.9 (ArCH), 130.5 (ArCH), 130.3 (ArCH), 129.3 (ArCH), 128.9 (ArCH), 128.6 (ArCH), 128.5 (Cipso or C=C), 128.3 (ArCH), 127.0 (ArCH), 116.8 (Cipso or C=C), 114.6 (ArCH), 103.6 (Cipso or C=C), 64.2 (CH_2), 62.5 (CH_2), 28.1 (CH_2), 14.5 (CH_3).

Preparation of 3-(4-(3-(4-Methoxyphenyl)-3-oxopropanoyl)phenoxy)propyl 2-cyano-3,3-diphenylacrylate, "AVOCTO4"

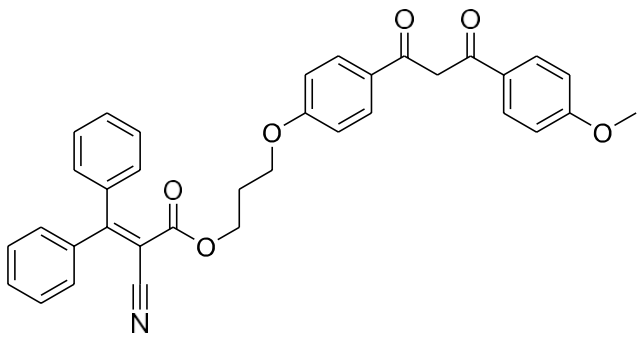

This compound is novel. 2-Cyano-3,3-diphenylacrylic acid (75 mg, 0.301 mmol, 1 eq.) was added to DCM (2 cm^3) under nitrogen. DCC (68 mg, 0.33 mmol, 1.1 eq.) and DMAP (4 mg, 0.032 mmol, 0.1 eq.) were added and the mixture was stirred for 15 mins. 1-(4-Methoxyphenyl)-3-(4-(3-hydroxypropoxy)phenyl)propane-1,3-dione (100 mg, 0.305 mmol, 1 eq.) was dissolved in DCM (2 cm^3) and added to the mixture. The mixture was stirred overnight at rt under nitrogen. The mixture was then passed through filter paper, and the filtrate was reduced under vacuum to yield the crude product. A silica column with 1:1 EtOAc:Hexane as mobile phase was used to isolate the product (~15 mg, 0.027 mmol, 9%) as an oil.

TLC: R_f ~ 0.85; in EtOAc:Hex (1:1) on aluminium-backed silica gel; visualisation by UV, $KMnO_4$;

ν_{max} 3057, 2940 and 2935 (intramolecular C=O---H-OH bond or C-H stretching), 2217 (CN stretch), 1717 (C=O stretch), 1591 (C=C-C=O of enol form) cm^{-1};

LRMS (ESI) m/z: Found $[M+Na]^+$ 582.2; HRMS (ESI-TOF) m/z: $[M+Na]^+$ Calc'd for $C_{35}H_{29}NO_6Na$ 582.1887; Found 582.1884 (error 0.6 ppm);

δ_H (400 MHz, $CDCl_3$): 7.96 (4H, 2 x d, *J* = 3.9 Hz, ArH), 7.49-7.32 (~9H, m, ArH), 7.14 (2H, d, *J* = 7.0 Hz, ArH), 6.98 (2H, d, *J* = 8.9 Hz, ArH), 6.92 (2H, d, *J* = 8.8 Hz, ArH), 6.94 (1H, s, enol), 4.32 (2H, t, *J* = 6.1 Hz, CH_2), 3.93 (2H, t, *J* = 12.1 Hz, CH_2), 3.89 (3H, s, CH_3), 2.04-2.00 (2H, m CH_2) ppm.

δ_C (101 MHz, $CDCl_3$): 186.7 (CO or CN), 184.5 (CO or CN), 163.1 (CO or CN), 162.1 (CO or CN or Cipso or C=C), 138.6 (Cipso or C=C), 131.6 (Cipso or C=C), 130.5 (Cipso or C=C), 130.3 (ArCH), 129.3 (ArCH), 129.1 (ArCH), 129.1 (ArCH), 128.6 (ArCH), 128.4 (ArCH), 128.3 (Cipso or C=C), 114.5 (Cipso), 114.0 (Cipso or C=C), 102 (C=C), 91.5 (CH enol), 64.1 (CH_2), 62.6 (CH_2), 55.5 (CH_3), 28.2 (CH_2). NB: 5 C signals are undetected.

Preparation of 3-(4-(3-(4-Chlorophenyl)-3-oxopropanoyl)phenoxy)propyl 2-cyano-3,3-diphenylacrylate, "AVOCTO5"

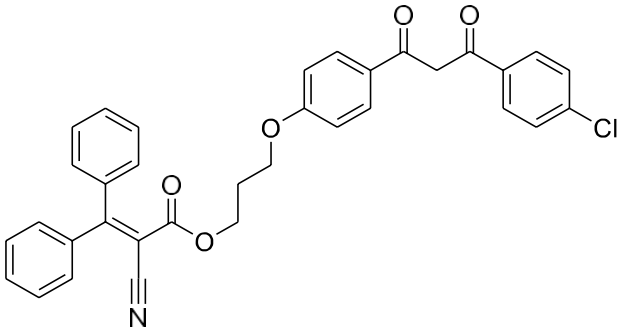

This compound is novel. 2-Cyano-3,3-diphenylacrylic acid (284 mg, 1.14 mmol, 1 eq.) was added to DCM (2 cm^3) under nitrogen. DCC (258 mg, 1.25 mmol, 1.1 eq.) and DMAP (14 mg, 0.115 mmol, 0.1 eq.) were added and the mixture was stirred for 15 mins at rt. 1-(4-Chlorophenyl)-3-(4-(3-hydroxypropoxy)phenyl)propane-1,3-dione (380 mg, 1.14 mmol, 1 eq.) was dissolved in DCM (2 cm^3) and added to the mixture. The mixture was stirred overnight at rt under nitrogen. The mixture was then passed through filter paper, and the filtrate was reduced under vacuum to yield the crude product. A silica column with EtOAc:Pet. ether (25:75) as mobile phase was used to isolate the product (230 mg, 0.41 mmol, 36%) as a solid.

TLC: R_f ~0.7; in EtOAc:Hex (1:1) on aluminium-backed silica gel; visualisation by UV, $KMnO_4$;

ν_{max} 2945 and 2864 (intramolecular C=O---H-OH bond or C-H stretching), 1587 (C=C-C=O of enol form) cm^{-1};

LRMS (ESI) m/z: $[M+Na]^+$ 586.1; HRMS (ESI-TOF) m/z: $[M+Na]^+$ Calc'd for $C_{35}H_{22}N_5OClNa$ 586.1405; Found 586.1397 (error 1.3 ppm);

δ_H (400 MHz, $CDCl_3$): 7.97 (2H, d, *J* = 8.6 Hz, ArH), 7.92 (2H, d, *J* = 8.4 Hz, ArH), 7.50-7.32 (10H, m, ArH), 7.15 (2H, d, *J* = 7.4 Hz, ArH), 6.93 (2H, d, *J* = 8.7 Hz, ArH), 6.75 (1H, s, enol), 4.31 (2H, t, *J* = 6.1 Hz, CH_2), 3.94 (2H, t, *J* = 6.0 Hz, CH_2), 2.07-2.01 (2H, m, CH_2), 1.56 (1H, s, *possibly H_2O*);

δ_C (101 MHz, $CDCl_3$): 186.1 (CO or CN), 182.9 (CO or CN), 169.7 (CO or CN), 162.6 (CO or CN or Cipso or C=C), 162.5 (CO or CN or Cipso or C=C), 131.6 (Cipso or C=C), 130.5 (Cipso or C=C), 130.3 (Cipso or C=C), 129.4 (ArCH), 129.3 (ArCH), 129.0 (ArCH), 128.6 (ArCH), 128.4 (ArCH), 128.3 (ArCH), 128.1 (ArCH), 116.9 (Cipso or C=C), 114.6 (ArCH), 92.3 (CH enol), 64.1 (CH_2), 62.6 (CH_2), 28.2 (CH_2).

2.5.3 Preparation of 1-(4-Chlorophenyl)-3-(4-methoxyphenyl)propane-1,3-dione[14]

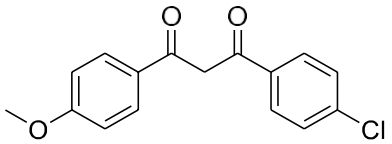

This compound has been previously characterised in He, Z.; Qi, X.; Li, S.; Zhao, Y.; Gao, G.; Lan, Y.; Wu, Y.; Lan, J.; You, J. Transition-Metal-Free Formal Decarboxylative Coupling of α-Oxocarboxylates with α-Bromoketones under Neutral Conditions: A Simple Access to 1,3-Diketones. *Angew. Chem. Int. Ed.* **2015**, *54* (3), 855–859.[14] 4-Hydroxyacetophenone (1.00 g, 7.34 mmol) was added with K_2CO_3 (1.52 g, 11.0 mmol, 1.5 eqs.) in acetone (10 cm^3) with stirring at rt in a sealed RBF. Methyl iodide (0.68 cm^3, 1.56 g, 11.0 mmol, 1.5 eq.) was added via syringe. After 19 hours, the reaction mixture was filtered and the filtrate was concentrated under reduced pressure to yield the intermediate 1-(4-methoxyphenyl)ethan-1-one (800 mg, 5.3 mmol, 73%). A portion of the dried solid (100 mg, 0.67 mmol) was added to NaH (60% suspension in mineral oil, 72 mg, 1.8 mmol, 3 eqs.) in dry THF (4 cm^3) at rt and stirred for 10 minutes. Previously prepared ethyl 4-chlorobenzoate (222 mg, 1.2 mmol, 2 eqs.) was dissolved in dry THF (~3 cm^3) and added. The mixture was heated under a findenser to 66 °C overnight. The mixture was cooled to rt and a few mLs of distilled water were added. The resulting suspension was extracted with excess ethyl acetate (15 cm^3), washed once with brine and dried to a crude residue under reduced pressure. The product (60 mg, 0.21 mmol, 31%, off-white, slightly pink solid) was isolated on a packed silica column using 1:1 EtOAc:Hex as eluent.

TLC: R_f ~0.7; in EtOAc:Hex (1:1) on aluminium-backed silica gel; visualisation by UV, $KMnO_4$;

ν_{max} 3258 (O-H stretch), 2951, 2865 (C-H stretches), 1624 (C=O stretch), 1586 (enol C=C-C=O stretch) cm^{-1};

LRMS m/z: $[M+H]^+$ Not detected;

δ_H (400 MHz, $CDCl_3$) 7.97 (2H, d, J = 8.6 Hz, ArH), 7.90 (2H, d, J= 8.4 Hz, ArH), 7.45 (2H, J = 8.3 Hz, ArH), 6.98 (2H, d, J = 8.6 Hz, ArH), 6.74 (1H, s, CH enol), 3.88 (3H, s, CH_3), ppm. Peak at 1.26 is attributed to H_2O;

δ_C (101 MHz, $CDCl_3$) (*literature*.[14]) 186.3 (CO), 183.0 (CO), 163.5 (C), 138.5 (C), 134.2 (C), 129.5 (CH), 129.1 (CH), 128.5 (CH), 128.1 (CH), 114.2 (CH), 92.4, 55.7 (CH_3).

2.5.4 Preparation of 1-(4-(Tert-butyl)phenyl)-3-(4-methoxyphenyl)-2-methylpropane-1,3-dione[15]

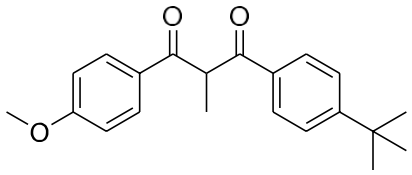

This compound was previously reported and fully characterised in Paris, C.; Lhiaubet-Vallet, V.; Jiménez, O.; Trullas, C.; Miranda, M. Á. A Blocked Diketo Form of Avobenzone: Photostability, Photosensitizing Properties and Triplet Quenching by a Triazine-Derived UVB-Filter. *Photochemistry and Photobiology* **2009**, *85* (1), 178–184.[15] Avobenzone (200 mg, 0.64 mmol) was added with K_2CO_3 (177 mg, 1.28 mmol, 2 eq.) in acetone (10 cm^3) under nitrogen. Methyl iodide (364 mg, 165 µL, 2.56 mmol, 4 eq.) was added dropwise at room temperature. The solution was heated to 45 °C overnight. When cooled the solution was filtered through filter paper and the organic layer was concentrated under reduced pressure. A packed silica column with Hex:EtOAc (60:40) was used as eluent to isolate the product (30 mg, 0.09 mol, 14% yield) as a colourless oil. Stereochemistry undefined.

LRMS m/z: $[M+H]^+$ Found 325.1

δ_H (400 MHz, $CDCl_3$) 7.95 (2H, d, J = 8.7 Hz, ArH), 7.90 (2H, d, J= 8.3 Hz, ArH), 7.44 (2H, J = 8.3 Hz, ArH), 6.92 (2H, d, J = 8.7 Hz, ArH), 5.22-5.16 (1H, m, CH), 3.84 (3H, s, OCH_3), 1.57 (3H, d, J = 7.0 Hz), 1.31 (9H, s, ^{t}Bu) ppm;

δ_C (101 MHz, $CDCl_3$) 196.9 (CO), 195.9 (CO), 163.8 (C), 157.2 (C), 133.1 (C), 130.9 (CH), 128.7 (C), 128.5 (CH), 125.8 (CH), 114.1 (CH), 55.5 (CH_3), 51.0 (CH), 35.1 (C), 31.0 (CH_3), 14.5 (CH_3).

2.5.5 Preparation of (E)-3-(4-acetoxy-3,5-dimethoxyphenyl)acrylic acid[16]

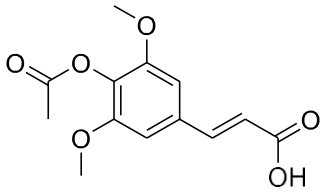

This compound was previously characterised in Allais, F.; Martinet, S.; Ducrot, P.-H. Straightforward Total Synthesis of 2-O-Feruloyl-l-Malate, 2-O-Sinapoyl-l-Malate and 2-O-5-Hydroxyferuloyl-l-Malate. *Synthesis* **2009**, *2009* (21), 3571–3578.[16] Sinapinic acid (1.00 g, 4.46 mmol) was added to pyridine (1.0 mL, 0.98 g, 12.4 mmol, 2.8 eqs.) and acetic anhydride (0.99 mL, 1.07 g, 10.47 mmol, 2.3 eqs.) at rt in an RBF. The mixture was stirred at rt for 3 hours and then poured onto an ice/water mixture (10 mL) in a beaker. The resultant white precipitate was filtered and washed with H_2O (10 mL) and dried to give the product as a white solid (1.12 g, 4.21 mmol, 94%). This product, confirmed by NMR, was used in the following steps without further purification.

δ_H (400 MHz, $CDCl_3$): 7.71 (1H, d, J= 15.9 Hz, =CH), 6.79 (2H, s, ArH), 6.40 (1H, d, J=15.9 Hz,=CH), 3.86 (6H, s, OCH_3), 2.35 (3H, s, CH_3);

2.5.6 Preparation of 3-(4-(3-oxo-3-phenylpropanoyl)phenoxy)propyl (E)-3-(4-acetoxy-3,5-dimethoxyphenyl)acrylate (OAc-AVOCINN)

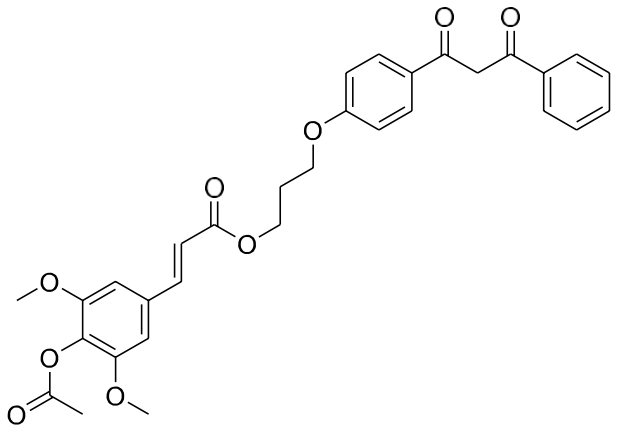

This compound is novel. 1-(4-(3-Hydroxypropoxy)phenyl)-3-phenylpropane-1,3-dione (50 mg, 0.17 mmol, 1 eq.) and (E)-3-(4-acetoxy-3,5-dimethoxyphenyl)acrylic acid (45 mg, 0.17 mmol, 1 eq.) were combined in a mixture of DCC (39 mg, 0.91 mmol, 1.1 eqs.), DMAP (2 mg, 0.017 mmol, 0.1 eqs.) and DCM (5 cm^3), sealed and stirred for 3 days at rt. The solution was passed through filter paper using excess DCM and concentrated under reduced pressure. The product (<10 mg) was isolated in reasonable purity from the complex mixture as the 3rd spot on the TLC using a packed silica column with EtOAc:Hex (1:1) as eluent.

TLC: R_f ~0.6; in EtOAc:Hex (1:1) on aluminium-backed silica gel; visualisation by UV, $KMnO_4$;

LRMS m/z: $[M+H]^+$ Found 547.1, $[M+Na]^+$ Found 569.1;

δ_H (400 MHz, $CDCl_3$): 7.99 (4H, m, ArH), 7.62 (1H, d, J = 15.9 Hz, =CH), 7.56-7.47 (3H, m, ArH), 7.01-6.98 (2H, m, ArH), 6.80 (1H, s, =CH), 6.76-6.73 (2H, m, ArH), 6.39 (1H, d, J= 15.9 Hz, =CH, 4.44 (2H, t, J=6.2 Hz, CH_2), 4.19 (2H, t, J = 6.2 Hz, CH_2), 3.85 (6H, s, OCH_3), 2.34 (3H, s, CH_3), 2.28-2.22 (2H, m, CH_2).

2.5.7 Deprotection (Deacetylation) of 3-(4-(3-oxo-3-phenylpropanoyl)phenoxy)propyl (E)-3-(4-acetoxy-3,5-dimethoxyphenyl)acrylate (AVOCINN)

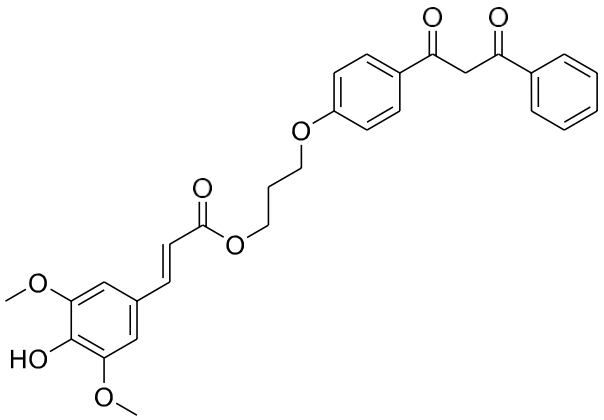

A procedure for an analogous compound was previously reported in Allais, F.; Martinet, S.; Ducrot, P.-H. Straightforward Total Synthesis of 2-O-Feruloyl-l-Malate, 2-O-Sinapoyl-l-Malate and 2-O-5-Hydroxyferuloyl-l-Malate. *Synthesis* **2009**, *2009* (21), 3571–3578.[16] A sample of 3-(4-(3-oxo-3-phenylpropanoyl)phenoxy)propyl (E)-3-(4-acetoxy-3,5-dimethoxyphenyl)acrylate (~ 20 mg) was refluxed under a findenser and positive nitrogen pressure first for 3 hours and then overnight in a 1:1 solution of 3M HCl:acetone. The progress of the reaction was monitored by the relative integrals of the peaks on the NMR spectrum corresponding to the acetyl group and the neighbouring multiplet (i.e., 2.34 (s, 3H), 2.28-2.22 (m, 2H), see above). At both time points the deprotection had produced a ratio of approximately 2 parts product to 1 part protected starting material.

2.6 Materials and Methods (Spectroscopy/Spectrometry)

2.6.1 'Ultraslow' Spectroscopies

Long term (5 mins< t <2 hours) and steady-state i.e., static photostability measurements (UV-vis) were obtained using samples of ~µM concentrations in HPLC grade solvent (i.e., acetonitrile or absolute ethanol (VMR chemicals)). Samples were prepared in High Precision quartz cuvettes (Hellma Analytics) of 10 x 10 mm pathlength containing 2 mLs of each solution. For photostability studies, concentrations were adjusted in the relevant solvent to give a stable absorption between 0.6-0.8 (arbitrary units) before irradiation. Spectra were recorded on a UV-vis spectrometer (Cary 60 UV-vis, Agilent Technologies) at specified intervals up to 2 hours at a scan rate of 600 nm/min at 1 nm intervals with baseline correction (i.e. the solvent alone is run as baseline). To simulate the response under near-to-life conditions, solar simulator irradiations were carried out using a solar simulator (LCS-100, Newport) with an AM1.5G spectral correction filter. The filter generates the solar spectrum and then the cuvette is placed at a working distance to mimic 1 SUN irradiance i.e. the distance of the cuvette from the lamp was adjusted to equate to 1,000 W/m^2 (100

mW/cm^2) sustained over 2 hours which is equivalent to the Sun's energy at Earth's surface.[1] The normalised irradiance spectrum is presented in Figure 2.1.

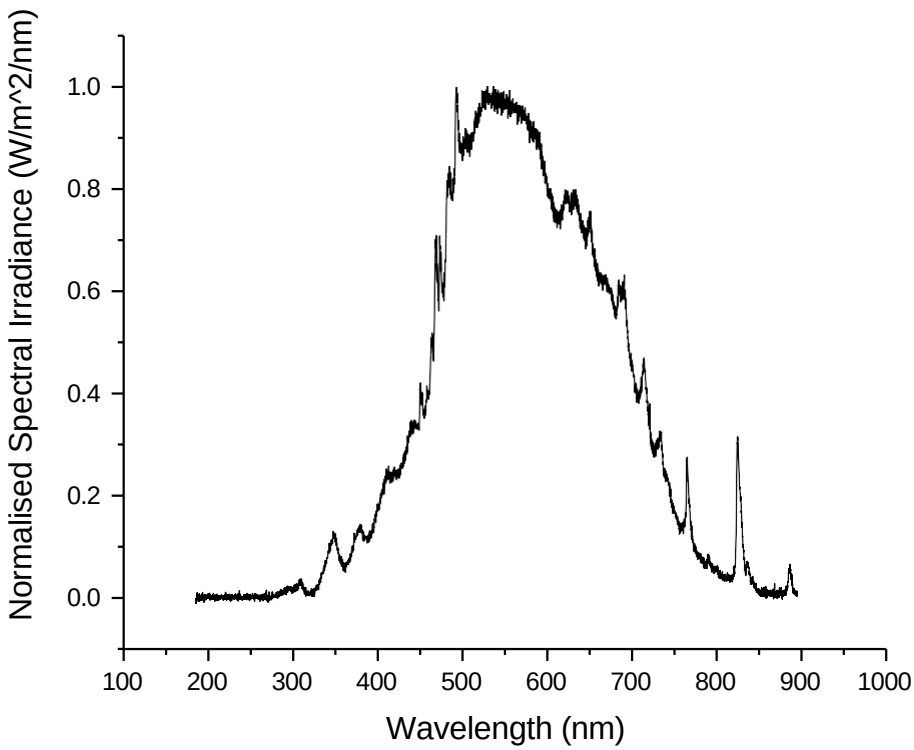

Figure 2.1. The normalised spectrum obtained of the LCS-100 solar simulator used in the irradiation studies.

2.6.2 Quantifying photostability

A key measurement of photostability is the percentage degradation of a molecule under the action of UV or solar light, and this can be quantified by the ratio of the difference between initial and final concentrations to the initial concentration as a percentage, i.e.:

$$\frac{C(I) - C(F)}{C(I)} \times 100$$

Another measure of stability is percentage recovery, which is defined as

$$\frac{(C(I) - C(F)) - (C(I) - C(R))}{C(I)} \times 100$$

where $C(I)$ is the initial concentration before irradiation, $C(F)$ is the concentration after irradiation and $C(R)$ is the recovered concentration after the sample has been removed from the source of irradiation for a set time (e.g., typically 1 hour). The concentration can be directly converted into absorption by Beer's law (see Introduction) and therefore the difference in concentration is a direct measure of the change in absorbance. In terms of sunscreens, a low percentage degradation (e.g., <10% change in activity) is preferred and ideally complete photostability is approached in all solvents. In one study with photoprotective lipsticks by Maier et al, over 5% loss of activity for a UV exposure of 12.5 standard erythema doses (SED) was determined to be a threshold below which a sunscreen can be considered photostable.[2] For information, one SED is equivalent to an erythemally effective radiant exposure of 100 J/m^2 when the radiation is weighted by the erythema action spectrum normalized to its maximum. Percentage recovery, i.e., once the sample is returned to the dark, in the case of avobenzone would indicate re-appearance of the enol form after irradiation has ceased and the sample had been moved to the dark. Recovery of the UV absorption could indicate that the molecular integrity of the chemical filter has recovered by re-formation of the original molecule; while incomplete recovery indicates that irreversible processes have taken place that have led to permanent loss of the parent molecule. An area-under-curve index (AUC_I), which is a ratio of the final area (AUC_F) and the initial area (AUC_I) over a given wavelength range for the irradiation can be calculated by the equation:

$$AUCI = \frac{AUC_F}{AUC_I}$$

An $AUCI$ > 0.80 has previously been used as a criterion for a photostable molecule.[3,4]

2.6.3 Ultrafast/Transient Absorption Spectroscopies

Here an additional overview (supplementary to the description in the Introduction) of the experimental photochemistry techniques of TEAS is given and more detailed descriptions can be found in Turner, M. A. P., *Examining Solvent Effect in Theoretical and Ultrafast Spectroscopy*, PhD thesis (2020) and Holt, E. L. H, *Towards a deeper understanding of the photodynamics of UV filters for sunscreen applications, using ultrafast spectroscopy and complementary analytical techniques,* PhD thesis (2022) as well as the additional information available on Warwick Centre for Ultrafast Spectroscopy (WCUS) website (https://warwick.ac.uk/fac/sci/wcus/). The focus herein is on the key aspects of the laser set-up that allow us to analyse the excited state of the studied molecules as well as any photoproducts that could be generated: these include the generation of the pump pulse, the white light probe continuum, the laser table itself and the data acquisition system.

2.6.4 Transient Electronic Absorption Spectroscopy (TEAS)

A commercial Newport Spectra Physics laser system is used to generate the fundamental beam of the experiment. The final output of this system is an 800 nm Gaussian-profiled pulse train with an approximately 40 fs duration and 1 kHz repetition rate and ~10 μJ/ pulse. The spectral bandwidth of the pulses is ~60 nm. A supercontinuum of white light (320 – 720 nm) is produced by focussing the laser on a 1 mm thick CaF_2 window and precautions are taken to minimise damage by vertical translating the window on a motorised delay stage. Prior to generation of the white light, the beam is passed through a half-wave plate (λ/2) to polarize the light to 54.7° to ensure that rotational anisotropy effects are not detected and reduce spectral noise. The white light probe should be as wide (in terms of wavelength) as needed to resolve all the spectral signatures within a given relaxation mechanism and, in the current experiments, this is generally covered by 320-720 nm. A typical spectral profile of the continuum can be found in M. Turner's thesis, cited above. To produce the exact wavelength needed for our experiments the remaining 1 W beam is directed into a TOPAS optical parametric amplifier and is set to the maximum absorption of the molecule under study in the relevant solvent. The TOPAS allows

generation of pump wavelengths ~235-1600 nm which is achieved through wavelength specific non-linear processes and supercontinuum generation.

A motorised delay stage with a travel range of 500 mm and resolution 5 ± 0.5 µm extends the length of the white light path to create a delay between the pump and probe pulses. In the set-up used in this thesis a maximum delay of ~3 ns is achieved by accurately aligning the seed beam (i.e. the initial output of the laser) to be parallel to the direction of motion. The delay stage includes a precision motorised translation stage, a motor controller and a hollow gold retroreflector. The delay stage has a minimum step of 7 fs, which is faster than the instrument response (~ 80 fs). An arrangement of choppers is used to obtain 'pump on' and 'pump off' readings and to block sequential pump pulses to reduce irradiation of the sample when data are not being acquired. As the laser has a 1 kHz repetition rate and the optical chopper spins at 500 Hz, half the pump pulses are detected during the experiment, allowing for a "probe alone" spectrum that can then be input into the ΔOD equation. As the laser samples the analyte at 1 kHz it is important that the analyte is cycled quickly away in a continuous flow from the interaction region with the pump pulse. This ensures that as fresh a sample as possible is irradiated between each pump-probe pair and therefore that the molecule of interest is being probed and less likely a degradation product. Each pulse pair is every 2 ms and flow is approximately 20 mL/min. A Harrick cell is used to contain the sample which is a steel cell with CaF_2 windows (1 mm at the front, 2 mm at the back) and polytetrafluoroethylene (PTFE) spacers. The pathlength of the beam can be tuned with the size of the spacers. If the continuous flow speed is too low an increase in probe noise is observed while if it is too fast turbulence can affect the flow. Other sample delivery methods can be used e.g., a liquid jet or even a simple static cell. After the white light continuum leaves the sample, it is detected by the spectrometer (Avantes) with a 900 nm spectral range; and resolution of 1.2 nm, with an integration time of 0.85 ms, allowing a maximum sample rate of 1.1 kHz, and thus fully sampling the 1 kHz laser. The data are processed by a custom made LabVIEW virtual instrument that fully automates the data acquisition.

Due to group velocity dispersion artefacts, the TAS are *chirped*, i.e., $\Delta t = 0$ is different for each probe wavelength (λ_{pr}). For visual purposes in TAS figures, the spectra have been chirp corrected (i.e. pre-processed) using the software package KOALA.[5,6] Global fitting analysis across all λ_{pr} of the TAS is achieved using the software package Glotaran.[7,8] A third order polynomial is included in the fitting algorithm to account for the chirp in the TAS. Glotaran models a data matrix for each λ_{pr} and Δt as a superposition of n_{comp} components. For typical

TAS within this thesis, three or four step (n_{comp} = 3 or 4) sequential kinetic models (where A → B is defined by constant τ_1 and B → by τ_2 etc.) are employed which can be viewed mathematically as:

$$\Psi(\lambda, t) = \sum_{l=1}^{n_{comp}} c_l^{EADS}(t, \Theta) EADS_l(\lambda)$$

where $c_l^{EADS}(t, \Theta)$ is the exponentially decaying concentration of component l convoluted with the Gaussian instrument response function and $EADS_l(\lambda)$ is the evolution associated difference spectrum for each component l. For each set of initial parameters, the fit is allowed to iterate until converged. From this, lifetimes (τ_l) for each component l can be obtained. A residual matrix is then calculated as the difference between the converged fit Ψ and the inputted raw data and can be used as a visual guide to the appropriateness of the fit. The instrument response function (IRF), mentioned several times, takes into account any non-resonant contributions from the solvent and/or the Harrick cell window; and is fitted with a frequency-dependent cross correlation function. The function used is:

$$f(t) = A \,.\, \exp\left(-\frac{(t - t_0)^2}{2\sigma^2}\right) + s$$

where A denotes the amplitude of the fitted curve; t_0 is the time zero of the fit, indicating the centre of the curve at the peak amplitude; σ is the standard deviation of the curve and s is a variable that allows for any signal offset. In practice, t_0 is the exact time where the pump and probe meet the sample at the same time. The value of σ is converted to the full width at half maximum (FWHM) value to extract the IRF, by multiplying by the scaling factor $2\sqrt{2ln2}$.

Pump power dependency studies can be performed to ensure that optical density (OD) is linearly dependent on photon flux, and this was carried out for **DS1** and **DS2** (see Chapter 3). In these technically optional but complementary experiments, the Topas-Prime output power is varied to several powers around the power used for the transient scans. At a specified pump-probe time delay, the signal is integrated over 10 nm windows. The

integration window and pump-probe time delays are chosen to cover a region of the TAS with a positive or negative feature. A gradient of ~1 in a log (Power) vs log (Signal) plot indicates that the observed dynamics are one-photon initiated dynamics and not multi-photon processes.

2.6.5 Transient Vibrational Absorption Spectroscopy (TVAS)

For the TVAS set-up used in the analysis of **DS1** and **DS2**, 10 mM solutions of **DS1** and **DS2** were circulated through a demountable liquid cell the same way as for the TEAS. The method used previously reported by our group is adapted to this experiment.[9] The pump beam wavelengths and power were the same for the TEAS experiment (341 nm for **DS1** and 329 nm for **DS2** at 500 µW) but a mirror was flipped to re-direct the beam onto the TVAS table. The IR probe beam was generated by seeding a second optical parametric amplifier (Topas-C, Spectra-Physics) with a second fraction of the fundamental 800 nm beam. The generated probe beam allows for a tuneable IR wavelength that includes 6,288 and 6,536 nm which were the central wavelengths used for **DS1** and 6,456 nm which was used for **DS2**. Two probe wavelengths were used for **DS1** due to oversaturation of the detector and were stitched together to produce the final spectrum. The path length of the probe beam was varied in a similar way to the TEAS set-up to give time delays (Δt) of up to 1 ns. Like in the TEAS experiment, the pump beam passes through an optical chopper operating at the same repetition rate. Atmospheric absorption lines (H_2O and CO_2) were excluded by purging the probe line with nitrogen gas. The probe pulse passed through the sample where it was partially absorbed before entering an imaging spectrometer (iHR320, HORIBA Scientific). Once in the spectrometer, the probe was dispersed by a diffraction grating (6 µm blaze, 100 lines mm^{-1} resolution) onto a mercury cadmium telluride (MCT) detector 64-pixel array (FPAS-0144, Infrared Systems Development). The MCT detector was cooled using liquid nitrogen to reduce thermal contributions to the signal. Pixel number was converted to wavenumber using a mid-IR polystyrene calibration card (Perkin Elmer) as reference. Bi-exponential fits of the GSB features were employed to extract lifetimes associated with the dynamical processes following photoexcitation.

2.6.6 FTIR Spectroscopy

Fourier-transform infrared spectra (FTIR) for **DS1** and **DS2** were recorded on a FTIR spectrometer (VERTEX 70v, Bruker) between 500-4000 cm^{-1} with 1 cm^{-1} resolution. A nitrogen environment was used to remove vibrational modes associated with atmospheric gases. 10 mM solutions were contained within a demountable liquid cell (Harrick Scientific Products Inc.) with a path length of 100 µm. This was achieved by inserting 100 µm PTFE spacers between two CaF_2 windows (front window 1 mm and back window 2 mm thickness).

2.6.7 Open-access LRMS and HRMS [Mass Spectrometry]

Lower resolution mass spectra were recorded on a time of flight (TOF) mass spectrometer (Agilent 6130B single Quad) by the electrospray ionisation (ESI) method with a potential mass range of 50 - 3,000 m/z. This is coupled with an isocratic Agilent 1100 HPLC (without column) as an automatic sample delivery system. Higher resolution mass spectra were submitted for analysis via the Mass Spec Service and recorded on a Bruker Compact Q-TOF mass spectrometer.

Current information on the facility is available here:

https://warwick.ac.uk/fac/sci/chemistry/research/facilities/massspec

Briefly, the mass spectrometer consists of three basic parts: an ion source, a mass analyser, and a detector system. The stages within a mass spectrometer are 1) production of ions from the sample (**ionisation stage**), 2) separation of ions with different masses (**ions analysis**), 3) detection of the number of ions of each mass produced (**detecting ions**), 4) collection of data to generate the mass spectrum (**multiplier**).

2.6.8 Open-access NMR Spectrometry

^1H nuclear magnetic resonance (NMR) spectra were recorded using $CDCl_3$ (δ_H = 7.26 ppm) or CD_3OD (δ_H = 4.87 ppm) as the solvent at ambient temperature on the 300 or 400 MHz spectrometer (Bruker Avance III HD) in the NMR facility at Warwick. Data are presented as follows: chemical shift (in ppm), integration, multiplicity (s = singlet, d = doublet, t = triplet

and m = multiplet), coupling constant (J/Hz) and interpretation. ^{13}C NMR spectra were recorded by broadband spin decoupling for $CDCl_3$ (δ_C = 77.2 ppm) at ambient temperature at 101 MHz. Chemical shift values are reported in ppm. Current information on the facility can be found at:

https://warwick.ac.uk/fac/sci/chemistry/chemintra/research/facilities/nmr/

2.6.9 Critical wavelength determination

A critical wavelength (λ_C), defined as the wavelength at which the sunscreen allows 10% of solar rays to penetrate can be formulated as:

$$\int_{\lambda_l}^{\lambda_c} A(\lambda)d\lambda = 0.9\int_{\lambda_l}^{400} A(\lambda)d\lambda$$

i.e. the wavelength up to which 90% of the UVA + UVB (290-400 nm, i.e. λ_l = 290 or UVA (320-400 nm, i.e. λ_l = 320) occurs. This measurement is offered with the caveat that in the present studies this is only an estimate of a 'true' critical wavelength based on the steady state UV absorption spectrum of a compound. The 'true' critical wavelength in the spirit of the Code of Federal Regulations guidance (21 CFR 201.327(j)) requires pre-equilibration of 0.75 mg/cm^2 on roughened optical-grade polymethylmethacrylate (PMMA) plates with an irradiation dose of 4 minimal erythemal doses (MEDs) which is equivalent to an erythemal effective dose of 800 J/m^2 (i.e., 800 J/m^2-eff). Erythema-effective dose (E) is expressed as effective Joules per square meter (J/m^2-eff).

Figure 2.2 demonstrates how by integrating 90% under the area of a curve in the UVA + UVB region, a critical wavelength can be determined. The area-under-curve (AUC) function in OriginPro was used for this purpose.

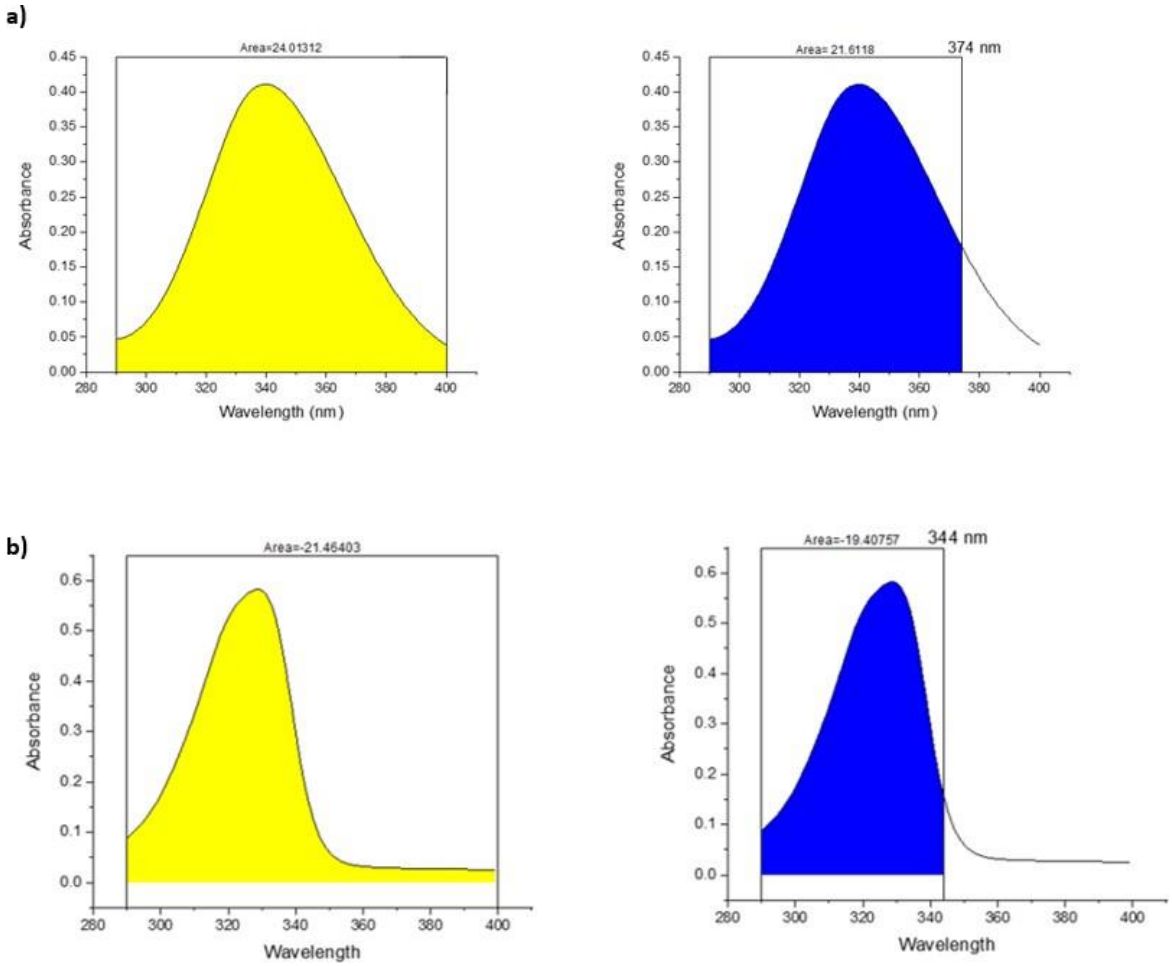

Figure 2.2. Critical wavelength determination of **DS1** (a) and **DS2** (b) from the corresponding steady-state UV-vis spectrum in ethanol. The integrated area of the spectrum on the right in each case is 90% of the spectrum to the left.

2.6.10 Determination of extinction coefficients

Samples were prepared for 5 concentrations of **DS1** and **DS2** in ethanol and the absorbance was measured using the standard steady-state set-up described above. A linear interpolation of the resultant graph of Abs vs. Concentration gave the quoted values with units (ε ($M^{-1}cm^{-1}$)) (see Figure 2.3.)

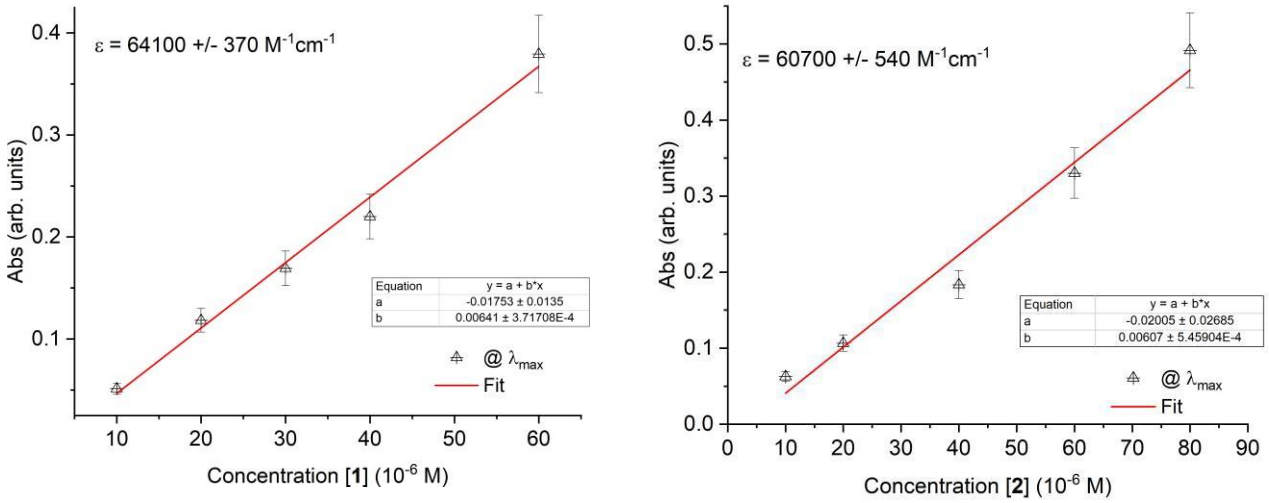

Figure 2.3. Determination of the extinction coefficients of **DS1** (left) and **DS2** (right) at the λ_{max} in ethanol.

2.7 Materials and Methods (Molecular Biology): Cloning, Expression and Purification of Moorea and Chlorogloeopsis C domain

2.7.1 Cloning summary

Two bacterial expression plasmids (pET151 vectors) containing genes-of-interest from two species of Cyanobacteria, *Chlorogloeopsis fritschii* (NCBI:txid1124), **AMC1**, and *Moorea producens* (NCBI:txid1155739), **AMC2**, were used as received in the lab group plasmid inventory. The full gene cluster for MAA synthesis was contained in plasmids ordered by Dr. Nazia Auckloo (Figure 2.4.). These plasmids were modified by deletion PCR to make new constructs that only contained the C domain gene and these were then used to express an encoded protein in *E. coli*. Plasmids were checked with PCR, sequencing and restriction digest.

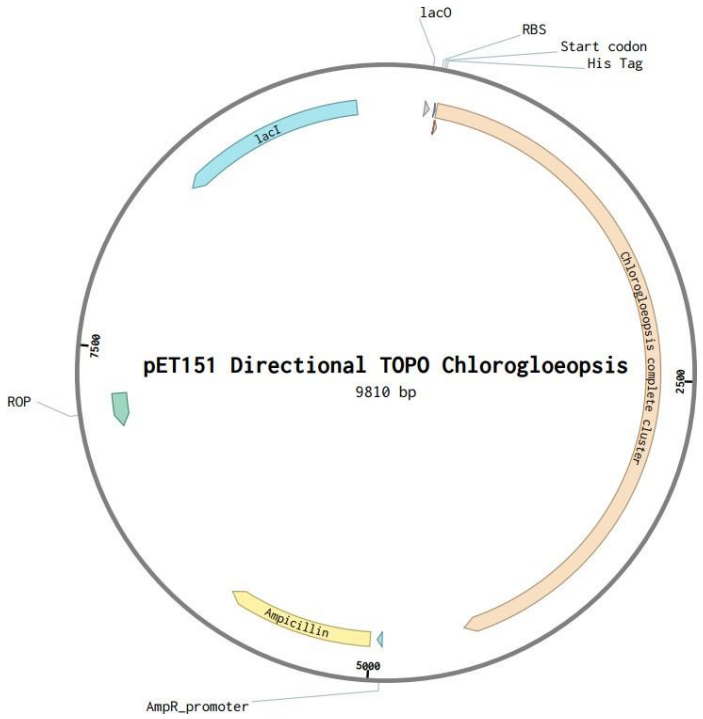

AMC1

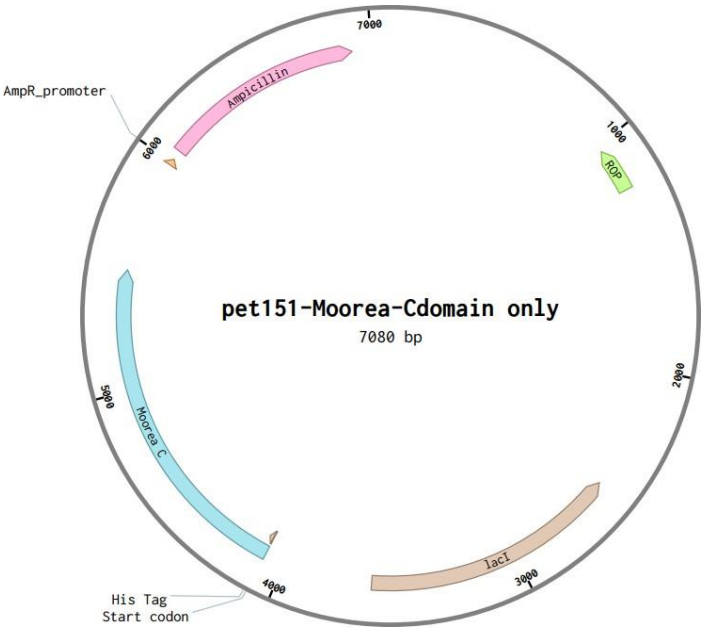

AMC2

Figure 2.4. Expression plasmids with annotations including the promotor region, gene of interest, resistance marker, lacI gene (which makes a protein that controls the promotor) highlighted.

2.7.2 DNA Manipulation and Cloning Techniques

Table 2.1. List of bacterial strains

Name	Genotype
Escherichia coli (*E. coli*) TOP10	F- mcrA Δ(mrr-hsdRMS-mcrBC) φ80lacZΔM15 ΔlacX74 nupG recA1 araD139 Δ(ara-leu)7697 galE15 galK16 rpsL(Str^R) endA1 λ^-
E. coli BL21(DE3)	B F^- *ompT gal dcm lon* $hsdS_B(r_B^- m_B^-)$ λ(DE3 [*lacI lacUV5-T7p07 ind1 sam7 nin5*]) $[malB^+]_{K-12}(\lambda^S)$

Table 2.2. List of vectors

Name	**Description**
pET151 *Chlorogloeopsis* (**AMC1**)	'Complete coding sequence of nrps-like gene' (C, A, PCP, T domain)
pET151 *Moorea* (**AMC2**)	'Complete coding sequence of nrps-like gene' ' (C, A, PCP, T domain)
pET151 *Chlorogloeopsis* C domain only (**P1**)	Stand-alone C domain (as opposed to the C-domain as part of the complete NRPS-like protein) from *Chlorogloeopsis*
pET151 *Moorea* C domain only (**P2**)	Stand-alone C domain (as opposed to the C-domain as part of the complete NRPS-like protein) from *Moorea*

The amino acid sequence of the C domains can be found in the Appendix 8.3.

2.7.3 Preparation of Plasmid DNA

Plasmid DNA was extracted by Mini-Prep (ThermoFisher Scientific GeneJET Plasmid Miniprep kit) according to the manufacturer's instructions. The steps are illustrated in Figure 2.5 below.

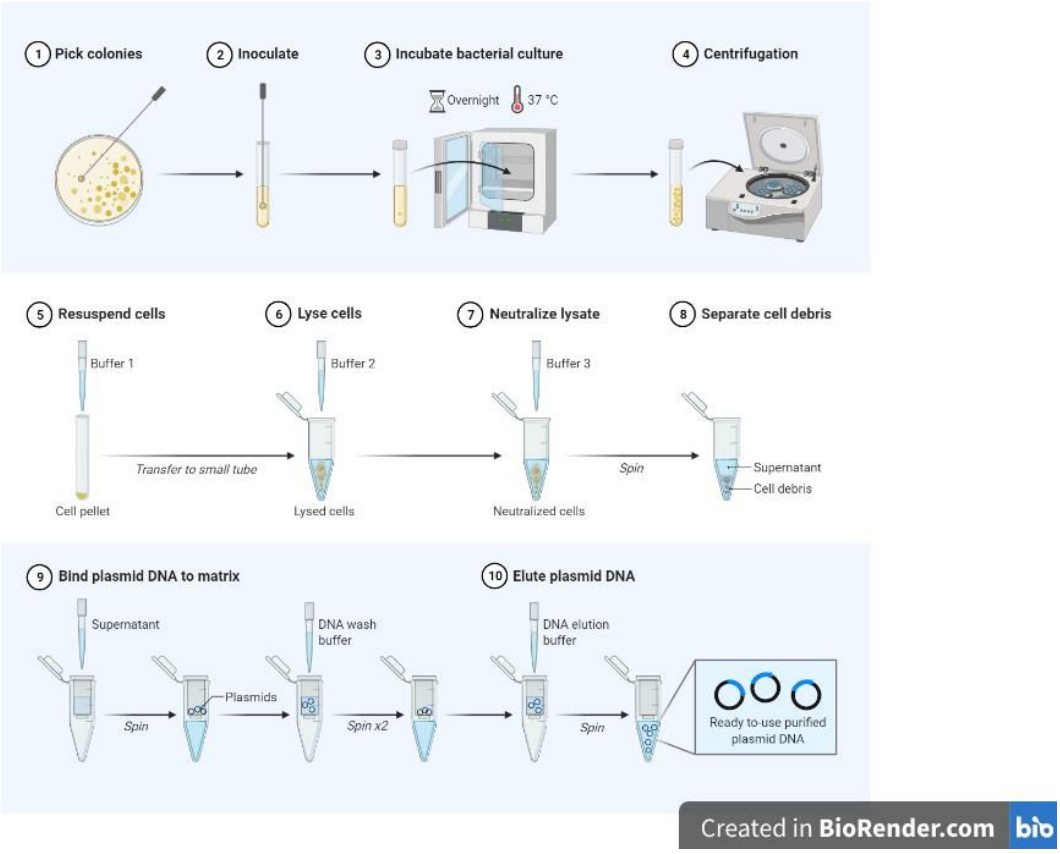

Figure 2.5. Summary of the Mini-Prep plasmid DNA extraction scheme created in BioRender.com

2.7.4 DNA quantification

After Mini-Prep the concentration of DNA was determined using a NanoDrop ND-1000 spectrophotometer (Thermo Scientific) using 1.5 µL samples.

Sample (plasmid)	DNA concentration (ng/µL)
A1 (AMC1)	55.9
C1 (AMC1)	55.7
A2 (AMC2)	78.9
C2 (AMC2)	102.1

Table 2.3. List of primers

Primer Name	Sequence 5' to 3'
Moorea_forward	/5Phos/GCTCGCCATCACTCAGCATCG
Chloro_forward	/5Phos/TTCGCGGTCACTCAGCAGCGG
_reverse	/5Phos/TGATAAAGCTCAGATCCGGCTGCTAAC
T7_forward	TAATACGACTCACTATAGGG
T7_reverse	GCTAGTTATTGCTCAGCGG

Primers used in this study were designed to amplify the C domain of each gene cluster and were ordered from Integrated DNA Technologies (UK).

2.7.5 Polymerase Chain Reaction

PCR was conducted in duplicate for each construct. A standard solution was prepared using 2.5 µL forward primer, 2.5 µL reverse primer, 2 µL plasmid template DNA (100 µM), 25 µL NEB Q5 High-Fidelity 2X Master Mix DNA polymerase and 18 µL sterile water. Dividing this solution in half gave a total volume of 25 µL for each sample.

PCR reactions were performed on an Eppendorf Mastercycler Gradient Thermocycler using the following programme:

Pre-denaturation	98 °C for 30 seconds
Denaturation, annealing, extension	25 cycles of 98 °C for 10 seconds, 67 °C for 30 seconds, 72 °C for 5.5 minutes
Post-extension	72 °C for 2 minutes

2.7.6 Agarose Gel Electrophoresis (Method 1)

An agarose gel was prepared by dissolving 1% (w/v) agarose in sterile water. The gel was placed in a gel tank and submerged in TAE buffer (40 mM Tris acetate, 1 mM EDTA). Samples were loaded along with 5 µL of Quick-Load Purple 1 kb DNA Ladder (BioLabs) and Gel Loading Dye, Purple (6X) (BioLabs). Electrophoresis was performed at 100 V for 40 min and the gel was visualised with UV light. The product was observed at ~7000 bp in both cases (Figure 2.6).

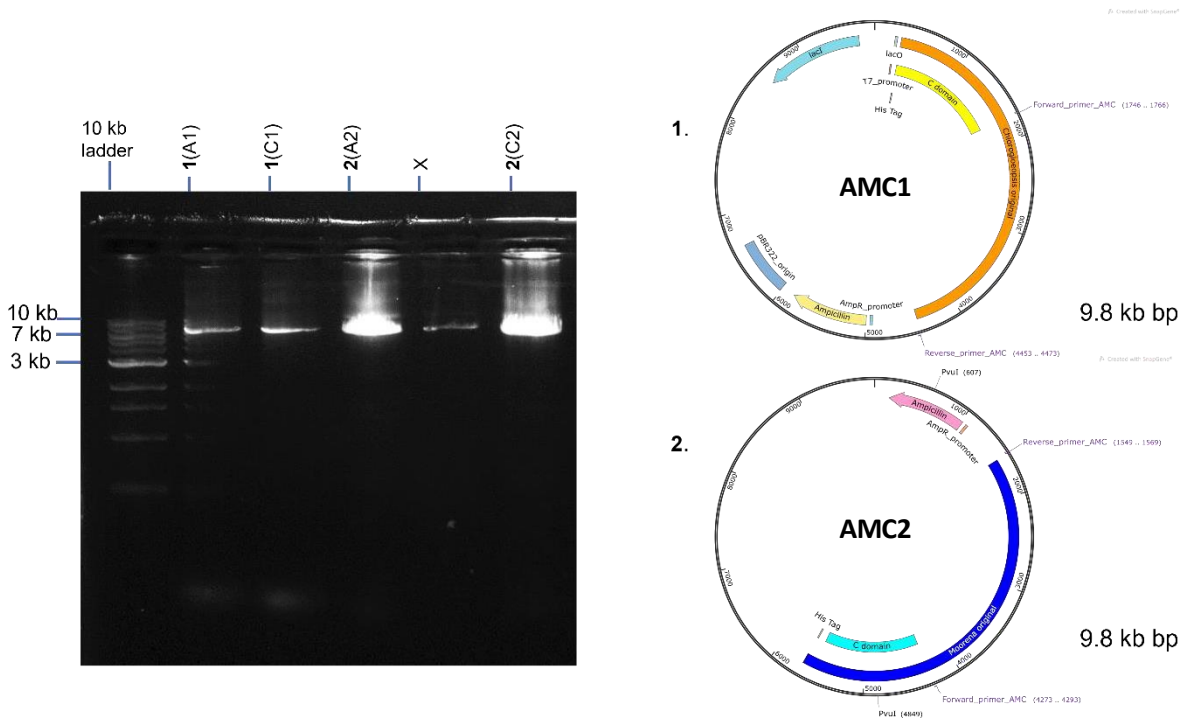

Figure 2.6. Annotated agarose gel of the two constructs. The number of base pairs on the gel are in good agreement with the calculated values (9.8 kb bp).

2.7.7 Dpn1 digest

The original (methylated) plasmid was removed from the PCR product by performing a digest. For each digest DNA (20 µL), rCutSmart (5 µL, BioLabs) and dpn1 enzyme (1 µL) were used.

2.7.8 Purification of DNA from PCR reaction and restriction digests

DNA clean-up was performed with a kit (Monarch PCR & DNA Clean-up Kit, New England BioLabs) according to the manufacturer's instructions.

2.7.9 Ligations

T4 ligase was used to re-ligate the plasmid in a mixture (total volume 20 µL) consisting of T4 ligase buffer (2 µL), T4 ligase (5 µL), sterile water (1 µL). The mixture was incubated at 30 mins at room temperature and heat inactivated at 65 °C for 10 mins.

2.7.10 Preparation of plasmid DNA

The plasmids were chemically transformed into competent cells by mixing with *E. coli* BL21 and incubating on ice for 30 mins. The transformed cells were plated onto LB* agar with ampicillin and incubated overnight at 37 °C. Cultures that grew were selected, spun down and plasmid DNA was prepared as before. The concentration of DNA was determined using the same method as above:

Sample	DNA concentration (ng/µL)
P1A [from A1 culture]	176.4
P1B [from A1 culture]	213.6
P1C [from A1 culture]	139.0
P1D [from A1 culture]	137.3
P2A [from A2 culture]	98.5
P2B [from A2 culture]	417.5
P2C [from C2 culture]	239.1
P2D [from C2 culture]	147.2

*LB (Luria-Bertani medium) was prepared from 1 g Bacto-tryptone, 0.5 g Bacto-yeast extract, 1 g NaCl, H_2O added to 100 mL; pH adjusted to 7.2 and autoclaved.

2.7.11 Agarose Gel Electrophoresis (Method 2)

An agarose gel was prepared by dissolving 0.9% (w/v) agarose in sterile water. Gels were placed in a gel tank and submerged in TBE buffer (50 mL). Samples (10 µL) were loaded along with 2 µL of Quick-Load Purple 1 kb DNA Ladder (BioLabs) and Gel Loading Dye, Purple (6X) (BioLabs). Electrophoresis was performed at 100 V for 45 min and the gel was visualised with UV light.

2.7.12 Restriction Digest

A restriction digest was performed to check the length of the new sequences using the original plasmids (AMC1 and AMC2), and selected samples from the transformation (P1D, P2A, P2C and P2D). 0.5 µL PvuI restriction endonuclease, 1 µL CutSmart buffer, 1 µL plasmid and 7.5 µL H_2O were used to give a total volume of 10 µL for each sample. The mixture was incubated for 1 hour at 37 °C. The digest was checked by running a gel using Method 2.

2.7.13 Sequencing

For sequencing, 5 µL primer (either forward or backward) was added with 4 µL H_2O and 1 µL plasmid DNA for a total volume of 10 µL. The samples were submitted for Sanger Sequencing by supplier GATC through the Genomics Facility at Warwick University for confirmation of correct constructs or sequence. The sequencing data were then uploaded to Benchling analysed by sequence alignment between the template and the sequencing data.

2.7.14 Transformation of plasmid into bacteria

To generate producer strains for the protein, each plasmid (0.5 µL) was added separately to competent cells (30 µL) and incubated on ice for 30 minutes. The cells were heat shocked (42 °C) for 45 seconds and then placed on ice for 5 minutes. LB (1 mL) was added and the mixtures were incubated with shaking at 37 °C for 1 hour. Cells were centrifuged at 13,000 rpm for 1 minute and 100 µL of each was spread onto a plate.

2.7.15 Growing cells

One colony was selected from the LB plate and was added to LB (10 mL) with ampicillin (100 µg/mL). The colonies were incubated at 37 °C for 4 hours. 1 mL was taken and added to LB (100 mL) containing ampicillin (100 µL/mL). Cells were incubated overnight at 37 °C.

2.7.16 Induction

15 mL of each culture was added to LB (1.5 L) with ampicillin (1.5 mL) and incubated at 37 °C. When the $OD_{600} \approx 0.6$-0.8, the temperature was reduced to 24 °C and IPTG (1M, 375 µL, 0.25 mM) was added with a small scoop of riboflavin. The mixtures were incubated overnight at 15 °C. Cells were centrifuged at 4000 rpm at 4 °C for 20 minutes and then stored at -80 °C before purification.

2.7.17 Protein purification

Cells were resuspended in 200 mL phosphate buffer (100 mM phosphate, 150 mM NaCl, 20 mM imidazole, pH 7.4) sonicated for 5 minutes (5 s on, 15 s off, 80% amplitude) and then centrifuged (4°C, 60 minutes, 25000 rpm). The supernatant was loaded into a Ni-NTA column, washed with 300 mL buffer containing 20 mM, 50 mM imidazole, and eluted with 50 mL buffer containing 250 mM imidazole. The protein was concentrated using a Vivaspin 20 centricon (10000 MWCO), aliquoted and stored at -80°C. The identity (by weight proxy) of the produced protein was checked with an SDS-PAGE gel prepared using standard methods.

The C domain from the *Moorea* construct was successfully purified and aliquoted into 12 Eppendorf vials each containing 0.2 mg protein/ 100 µL (total volume 100 µL, total amount of protein 2.4 mg) in this way while the *Chlorogloeopsis* construct did not produce the protein of interest, perhaps due to the protein not folding successfully. The C domain from the *Chlorogloeopsis* construct was insoluble and was not purified successfully.

2.7.18 Preparation of substrates for HPLC assay

Activated amino acids (SerSNAC and ProSNAC) were prepared using the methods described above in the Synthetic Materials and Methods. Mycosporine glycine (MG) was isolated by Sopida Wongwas, PhD using a methanol/water gradient on a Biotage (automated flash chromatography setup) from a supernatant following an extraction from lab-cultured *Streptomyces albus* with *mysABC* genes. The identity of MG was confirmed by MS and UV-vis.

2.7.19 Preparation of samples for HPLC assay

A mixture containing 100 mM HEPES (pH 7.5) and 50 µM TCEP was prepared by dissolving 477 mg HEPES and 0.3 mg TCEP.HCl in 20 mL distilled water. 50 µL of this mixture was then added to an Eppendorf vial for each sample. In the samples with enzyme, the purified protein was added for a final concentration of 600 nM by taking 1.52 µL from each protein stock (0.2 mg/ 100 µL = 0.04 mM, MW = 50515.07 Da) and adding to the Eppendorf. The ketone substrate was then added for a final concentration of 50 µM by preparing a 200 µM solution of the ketone in water i.e., 0.42 mg of AC23-ester in 10 mL water or 0.39 mg of AC23-acid in 10 mL water and adding 25 µL to the Eppendorf. In the case of the extracted mycosporine glycine 50 µL of the 100 µM stock were added. The amino acid substrate was added for a final concentration of 50 µM by preparing a stock of 200 µM and adding 25 µL to each Eppendorf. Stock SerSNAC* was prepared by dissolved 0.41 mg in 10 mL water and stock ProSNAC was prepared by dissolved 0.43 mg in 10 mL. A matrix of the prepared sample combinations (final volume 100 µL) is included below with final concentrations (see Table 2.4). The in-lab Nanodrop apparatus was used to check approximate concentrations. Samples were gently inverted and briefly vortexed and then incubated at room temperature for 24 hours before being immediately prepared for analysis by HPLC

Table 2.4. In total 12 samples were prepared, a set with enzyme added and a control set. Concentrations given are final concentrations in the sample.

Activated amino acid / Ketone/oxo-mycosporine substrate		
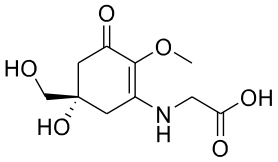 Mycosporine glycine	50 µM Ser-SNAC* 50 µM Myc-Gly HEPES 50 mM TCEP 25 µM (Enzyme** 600 nM)	50 µM Pro-SNAC 50 µM Myc-Gly HEPES 50 mM TCEP 25 µM (Enzyme 600 nM)
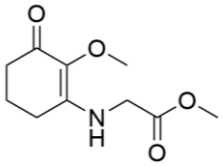	50 µM Ser-SNAC 50 µM AC23-ester HEPES 50 mM TCEP 25 µM (Enzyme 600 nM)	50 µM Pro-SNAC 50 µM AC23-ester HEPES 50 mM TCEP 25 µM (Enzyme 600 nM)
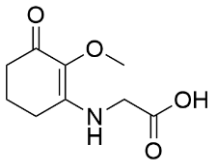	50 µM Ser-SNAC 50 µM AC23-acid HEPES 50 mM TCEP 25 µM (Enzyme 600 nM)	50 µM Pro-SNAC 50 µM AC23-acid HEPES 50 mM TCEP 25 µM (Enzyme 600 nM)

Notes:

[*]Ser-SNAC was used as a mixture of O^tBu protected and deprotected

[**]Enzyme here is the purified C domain from the *Moorea* gene cluster

2.7.20 HPLC assay for detection of potential products

An Agilent Polaris 180A amide-C18 – 150 mm, 4.6 mm, 5 µm – Analytical Reverse-Phase C18 column, max pressure 3600 psi/250 bar, max loading capacity 100 µL was used to analyse the samples on the Agilent 1260 HPLC set-up in WISB (Warwick Integrative Synthetic Biology centre). This column was chosen as a good general purpose column for polar analytes on an analytical scale. A standard gradient method of HPLC grade methanol and water was used:

Method 1 (35 minute runs): Methanol:water mobile phase (HPLC grade) with a 5-100% gradient over 34 minutes then returning to 5% in the last minute. 6 minute equilibration time. Flow 1mL/min using a C18-Polaris amide column.

Method 2 (21 minute runs): Methanol:water mobile phase (HPLC grade) with a 3-100% gradient over 20 minutes then moving to 5% in the last minute. 6 minute equilibration time. Flow 1mL/min using a C18-Polaris amide column.

2.8 Materials and Methods (Computational Techniques)

2.8.1 Density Functional Theory

Density functional theory (DFT) approximates a solution to the Schrödinger equation for an N-body system by estimating the repulsion between electrons or exchange correlation energy term as an average density while treating the dynamic correlation between electrons exactly. In DFT an approximation to the experimental geometry of a molecule is obtained by iterating over a theoretical potential energy surface so as to minimise the total electronic energy as a function of the geometry. A set of wavefunctions that describe the atomic orbitals forms the basis set for the calculation. A functional (a function of the wavefunction) is then applied to the basis set in order to map the optimised electronic structure onto energy. The ground electronic state is typically singlet (S=0), consisting of paired electrons and is the 'simplest' to model. Higher energy singlet (S≠0) and triplet (T≥1, two unpaired electrons with parallel spins) states that can be accessed by photoexcitation with light of a matching energy require modified functionals for their study using time-dependent DFT. This latter technique attempts to model the response of the system to time dependent potentials and is essential for predicting UV-vis results.

The probability of a particular transition occurring is related to its transition dipole moment. This parameter is seen as the strength with which an external field interacts with the molecule to induce a transition, as well as the Franck-Condon factors which describe the overlap between the vibrational states in the two electronic states. The complexity of the model is increased by the presence of a manifold of vibrationally excited states within each electronic state and the superimposing of electronic transitions:- a set of phenomena that explains the Gaussian-like shaped peaks seen in a typical UV-vis spectrum. As the model is constructed in a bottom-up type approach without any experimental input initially it is termed ab initio and can output values for the wavelength at maximum absorption and transition energies independently of experiment. The values output by the model are then compared to experiment to assess the quality of the model. A simple functional with an average size basis set can be useful to identify trends in certain properties but absolute inaccuracies in the output values are usually due to limitations inherent in the model. It is not usually possible to expand the basis set indefinitely by adding more functions due to

the exponential scaling of computation time with N where N is the number of atoms in the basis set. In practice, the assumptions made by the model are often made for convenience and ease of computation. The methods chosen in this thesis effectively model the molecules with a polarisation continuum by treating the presence of solvent implicitly; though unfortunately by consequence also becoming one step farther removed from real systems.[1] A possible extension of any model is to include interactions with a solvent (explicit solvent modelling), which considers the effect of solvent surrounding the active molecule- something which is not generally included as the computational cost is increased with N - and this is perhaps at the penalty of missing an important mechanism or alternative pathway.[2]

2.8.2 AVOCTO calculations

All calculations were performed using the NWChem software package.[3] Due to the large number of atoms and single bonds in the full avobenzone-octocrylene molecules, it was not possible to achieve convergence at the lower level of theory, hence only the truncated forms were studied. DFT geometry optimisations for the chelated *enol* and *diketo* structures of the avobenzone section of each molecule were studied only (see Fig. 4.31 for optimised structures). These geometry optimisations were carried out to determine the most stable, lowest energy conformations in the ground state. These calculations were conducted in implicitly modelled acetonitrile, using the conductor-like screening model (COSMO, with SMD) built into NWChem.[4,5] The relaxation of the initial *enol* and *diketo* structures of each truncated molecule was initially carried out using DFT at the PBE0/6-31g* level of theory. This initial structure was then further optimized by increasing the basis set to 6-311++g**, before arriving at the final structure, which was calculated at the PBE0/6-311++g** level of theory.

Once the six optimised structures were attained, time-dependent DFT (TD-DFT) was carried out to attain the vertical excitation energies of the singlet (S_{1-5}) states of each species in acetonitrile using the same COSMO model, using TD-DFT at the PBE0/6-311++g** level of theory. The state characters were also calculated during these TD-DFT calculations and assigned manually.

For the reported T_1 state energies, a ΔSCF methodology was used.[6] The triplet single point energy for the ΔSCF method was calculated at the PBE0/6-311++g** level of theory. For this, the multiplicity was set to three on each of the optimised ground state structures; the single point energy (T_1) was then compared to the ground state (S_0) single point energy.

2.8.3 Submission to Alphafold via SCRTP and Phyre2

AlphaFold is an AI system developed by DeepMind (https://www.deepmind.com/about) that predicts a protein's 3D structure from its amino acid sequence. The submission to Alphafold was run locally using the Avon HPC cluster, available via the Scientific Computing RTP at the University of Warwick. Briefly, a FASTA file for the amino acid sequence for the protein of interest was downloaded from Benchling and prepared with a SLURM submission script. The following modules were loaded:

```
module load GCC/10.2.0 CUDA/11.1.1 OpenMPI/4.0.5
module load AlphaFold/2.1.1
```

*.pdb (Protein Data Bank) files were viewed in EzMol (a web server for molecular modelling[7]), accessed at:

http://www.sbg.bio.ic.ac.uk/ezmol/

More information on Alphafold can be found:

https://warwick.ac.uk/research/rtp/bioinformatics/software/alphafold/

Phyre2 (**P**rotein **H**omology/analog**Y** **R**ecognition **E**ngine V 2.0) , a web-based service for protein structure prediction, that uses remote homology detection methods was used to predict a 3D model in Chapter 5[8]:

http://www.sbg.bio.ic.ac.uk/phyre2

Chapter 3. Synthetic Derivatives with MAA motifs

3.1 Background

The chemical synthesis of analogues of mycosporine-like amino acids (MAAs) is necessary due to the low extraction yield of MAAs from natural sources. Molecular analogues of MAAs are useful to understand the properties of the natural products they resemble by helping to define which molecular motifs are essential for photoprotection and which are less important. In terms of application, we may speculate that these MAA-like molecules could prove to be promising sunscreens in their own right. Several structures that have explicitly based their design on MAAs have been published in the chemical literature and in commercial patents, while the general molecular scaffolds have been synthesised for other purposes in general synthetic chemistry literature. For the structures of natural MAAs the reader is referred to Chapter 1. Figure 3.1 contains a sketch of possible analogues of natural products that can be synthesised from standard starting materials.

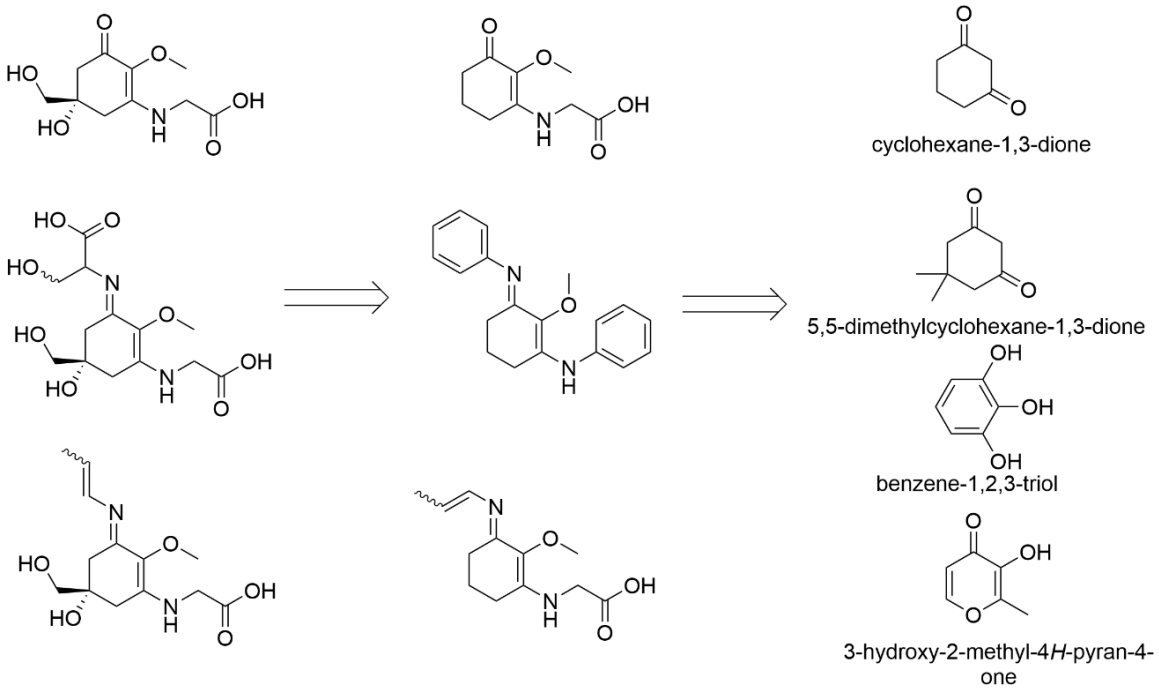

Figure 3.1. (Left) Natural products (descending order: mycosporine glycine, shinorine, usujirene/palythene), (centre) Proposed molecules that can be considered structural analogues of the natural products, (right) Starting materials that can be bought commercially.

3.1.1 Total synthesis

The only total synthesis of mycosporine-glycine, an oxo-mycosporine with a glycine substituent, to date was published by J.D. White and co-workers in 1995.[1] This synthesis was conceived to identify conclusively the absolute stereochemistry of the chiral centres in mycosporine-glycine and apparently without the sunscreen industry in mind. With the synthesis running to 15 steps overall, it is an impractical route for the purpose of producing sunscreen compounds on a realistically useful scale. The final working route arrived upon in the paper is redrawn below using their numbering of the intermediates (Figure 3.2).

The stereochemistry was carefully considered at each step, and reaction conditions that might lead to oxidation and re-aromatization were avoided. Oxo-mycosporines (i.e., the structure of the final product of this synthesis) are known to be unstable to hydrolysis, where they can transform to a meso-cyclohexane-1,3-dione structure. Furthermore, the authors note that molecules of this type containing a 6-membered ring with heteroatoms can undergo a facile transformation to a benzenoid system (i.e., they aromatize and lose stereospecificity). It is interesting to note that the amino acid chain was installed via an aza-Wittig/Staudinger reaction by making an iminophosphorane from the vinylogous acyl azide (reaction 63➔68). It is clear that the group wished to extend the synthesis to imino-mycosporines but they noted that any attempts to introduce a second amino acid, presumably via a condensation with the ketone, were unsuccessful. This final conclusion discouraged us from choosing a route that relied on an intermediate oxo-mycosporine that had to be isolated.

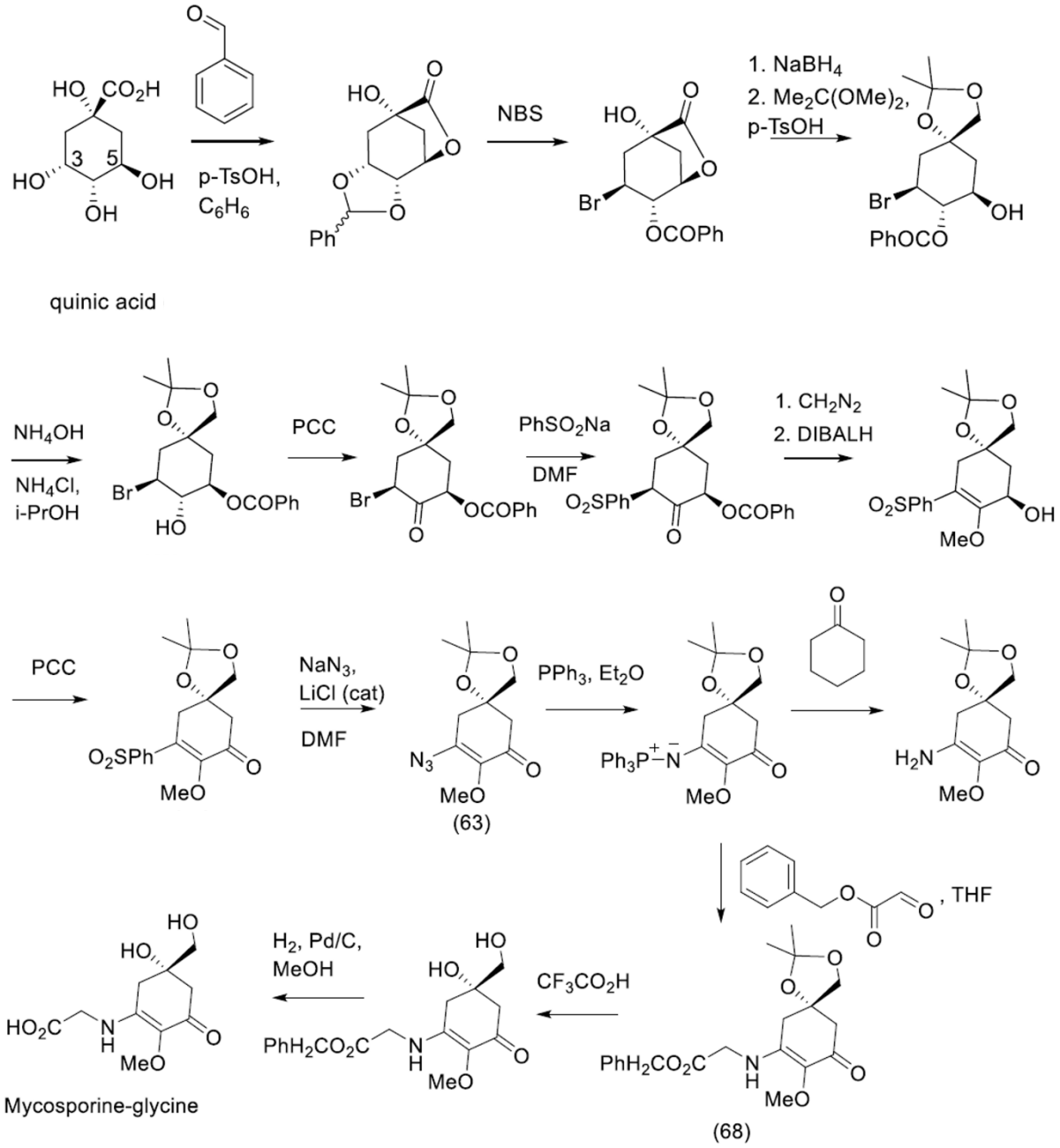

Figure 3.2. Reproduced final synthetic scheme of mycosporine glycine.[1]

3.1.2 Bottom-up Approach

The core structure of the MAA motifs is an enaminone (O=C-C=C-NH-) or en-di-imine (R-N=C-C=C-NH). The following discussion begins with a background on the synthesis of enaminones as the key basic building block and then is extended to include the synthesis of the more complex en-di-imine scaffolds, using literature examples.

3.1.3 Exocyclic enaminones

1,3-Cyclohexanedione is the simplest starting cyclic diketone for many of the reported cyclic enaminone syntheses. It can be obtained naturally or through hydrogenation of resorcinol.[2] Dimedone, which is the 5,5-dimethyl cousin of 1,3-cyclohexanedione can be prepared by the reacting mesityl oxide and diethyl malonate.[3]

Various methods have been reported for the reaction of diones with amines to produce β-enaminones. The conventional method for the synthesis of enaminones is the azeotropic removal of water by refluxing an amine with 1,3-diketone in an aromatic solvent. A typical solvent for this purpose is toluene which is then heated above 100 °C. Milder conditions are possible for this transformation and Cui and co-workers published a simple procedure for the synthesis of β-enaminones from 5-substituted-1,3-cyclohexanedione and excess molar equivalents of aromatic amines using dilute hydrochloric acid (30 mmol/L) at 70-80 °C (Figure 3.3).[4] Despite the excess equivalents of amine used, no double addition products were reported.

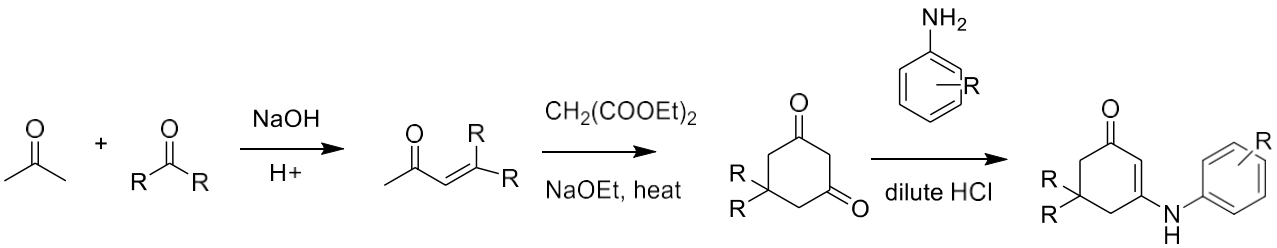

Figure 3.3. Synthesis from ref[4]. R = alkyl groups.

It is also typical to catalyse this transformation with a Lewis acid or other catalyst. Examples include SiO_2, $NaAuClO_4$, montmorillonite K-10, $Zn(ClO_4)2.6H_2O$, $CeCl_3.H_2O$, $Bi(TFA)_3$, iodine, $HClO_4.SiO_2$ and ionic liquids.[5]

Andreguetti and co-workers published a microwave-promoted synthesis of oxo-mycosporine analogues in the liquid and solid phases (see Figure 3.4).[6] The products were obtained by substitution of one oxygen of 1,3-cyclohexanedione with the nitrogen of an amino acid. In the liquid phase, either glutamic acid, histidine or serine was irradiated in a microwave for 10 minutes with the 1,3-cyclohexanedione under a cold reflux system and the crude products were purified by HPLC in good (>70%) yield. These molecules had shorter maximum absorbance wavelengths than MAAs due to the absence of the methoxy (-OMe) at the 2-position of the substituted 1,3-diketone.

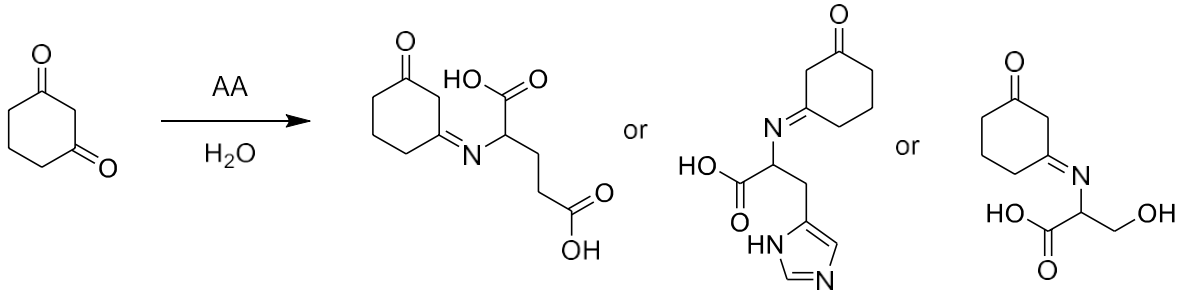

Figure 3.4. Synthesis from ref[6]. AA = amino acid, here glutamic acid, histidine, and serine.

Finally, Bhattacharjee et al. described a synthesis for a large range of exocyclic β-enaminones.[7] A 1:1 mixture of the cyclic-1,3-dione and corresponding amine were mixed with 20 mol% acetic acid and placed in a microwave reactor at 110-130 °C for 10-20 minutes. The crude was dissolved in ethyl acetate and passed over anhydrous Na_2SO_4 before column chromatography (EtOAc:Hex) over silica. The full scope of the reactions and the yields for a few selected relevant compounds is shown in Figure 3.5.

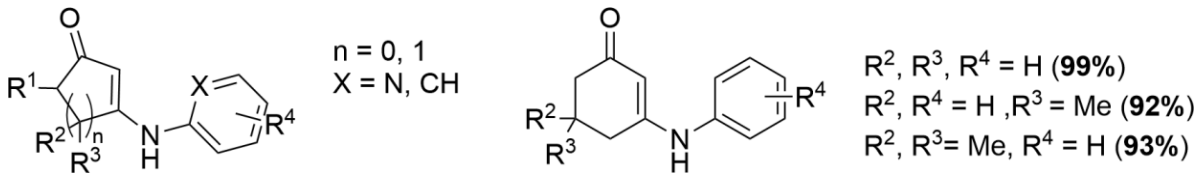

Figure 3.5. Synthesis of exocyclic β-enaminones using microwave irradiation in ref.[7] (Left) Full scope displayed as a generic structure with undefined Rs. (Right) Selected compounds with reported yields.

3.1.4 Endocyclic enaminones

It is also possible to contain the enaminone structure within a ring, where the N of the amino substituent is now *endo* to the ring rather than *exo* as in the preceding examples. This *endo* scaffold can be considered a step further away from the natural product structure but nonetheless leads to molecules with comparable properties and perhaps greater resistance to hydrolysis.

York and co-workers published a synthesis of a "bio-inspired" UVB absorber, taking inspiration from mycosporine-glycine, with the structure of an endocyclic enamineone.[8] They began with commercially available 3,3-dimethylglutaric acid and arrived at the product in 5 steps using continuous-flow chemistry and an overall yield of 55%. The product is a UVB absorber with a λ_{max}(methanol) = 307 nm and $\varepsilon = 29{,}300\ M^{-1}cm^{-1}$ (Figure 3.6).

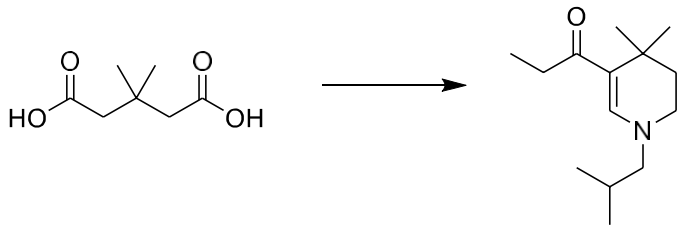

Figure 3.6. Starting material and product for the synthesis in ref[8].

The endocyclic motif can also be synthesised in other ways. For example, Nguyen and co-workers published a gold-mediated synthesis and functionalization of chiral 5-halopyridones from β-amino-ynone intermediates via a halodeauration process. The MAA motif is now fixed within a heterocyclic ring and the halogen atom (X in Figure 3.7) could be modified in various ways, particularly through Pd-catalysis, with a range of substitutions.[9]

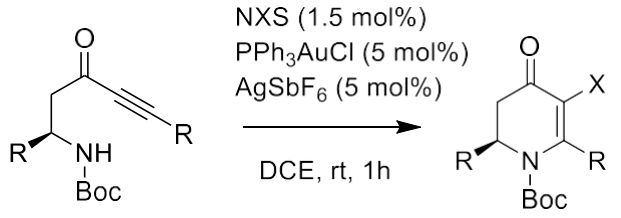

Figure 3.7. Synthesis in ref[9].

A potential future avenue to explore would be larger conjugated, cyclised systems like those suggested in Figure 3.8. In theory these could be prepared from previously reported 2-aryl-3-hydroxy-3-cyclohexenones[10] and are only included here for future reference.

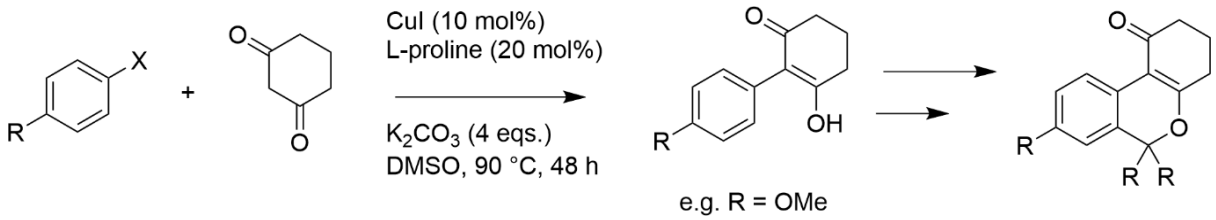

Figure 3.8. Suggestions for a route to a cyclised structure incorporating the MAA scaffold.

Finally, a patent (EP288441B1, WO 2013/181741) covers “Imino compounds as protecting agents against ultraviolet radiations” and contains the synthetic sequence in Figure 3.9.

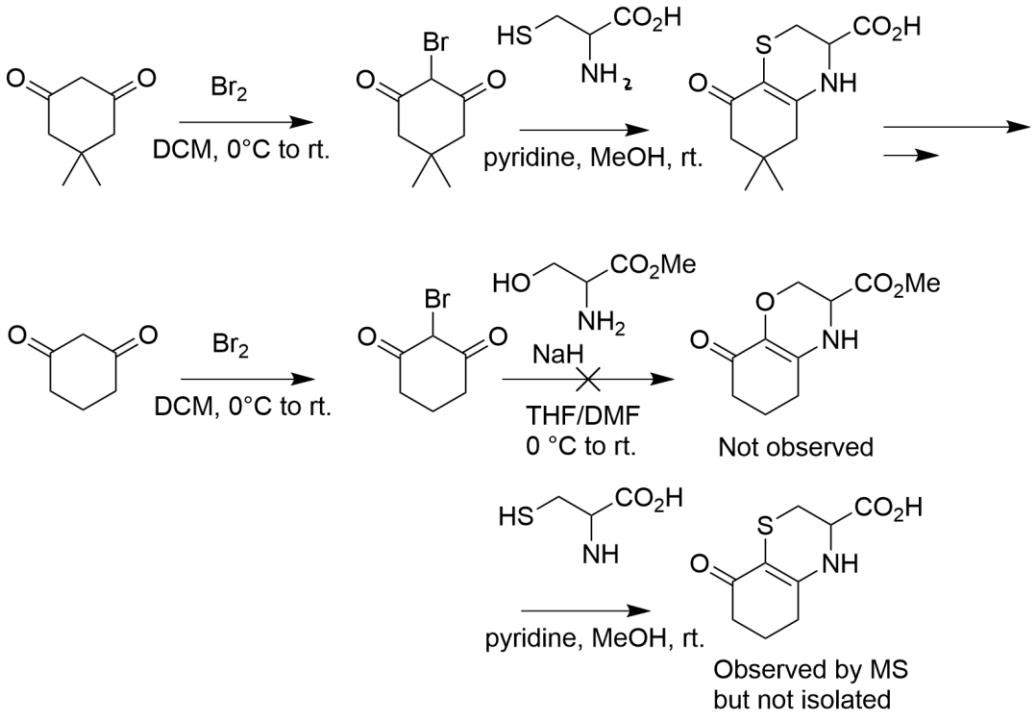

Figure 3.9. Compounds proposed as protecting agents against UVR in patent 2013/181741

3.1.5 Amino-cyclohexenimine unit

To extend the conjugation of the system further and create a chromophore that absorbs into the UVA region it is essential to condense a second group with the enaminone core. In the natural products, it is true that the second group is typically not the same as the first (which is in turn typically glycine), leading to an asymmetrically substituted molecule. In the laboratory this sort of transformation is more difficult to achieve selectively, with the potential for multiple side-products increasing via amine/imine exchange mechanisms.

The cyclohexenimine motif was explored in a study to understand the rotameric behaviour of vinamidinium salts, wherein compounds in Figure 3.10 were prepared.[9] The target molecules contain the key π-donor and π-acceptor groups of the MAA core in the form of a saturated nitrogen ($-NR_2$) and an imino group ($C=NR_2$) respectively. The product was isolated as a mixture of C=N bond rotamers which were characterised by NMR. A conclusion of the study is that anchoring the heteroatoms to a cyclohexene core has a stabilising effect which is referred to in the paper as a “rigid core”. This study indicates that for the purpose of our MAA analogue design, it is possible to prepare the imino-

mycosporine chromophore as an isolable salt. This may be a method to avoid the instability issues discussed above and to reduce the number of potential ionisation states of the molecule, thereby simplifying any photochemical characterisation.

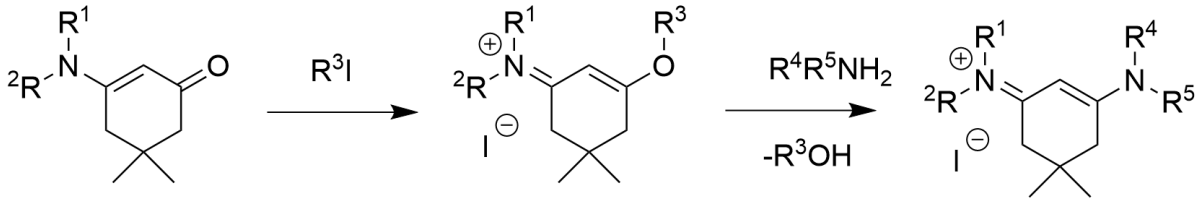

Figure 3.10. Vinamidinium salts prepared in ref[11]. Addition of two different amines would be problematic.

In the same patent that was referred to previously (WO2013/181741) Abou-Khalil et al. reported the synthesis of compounds with the structures in Figure 3.11.

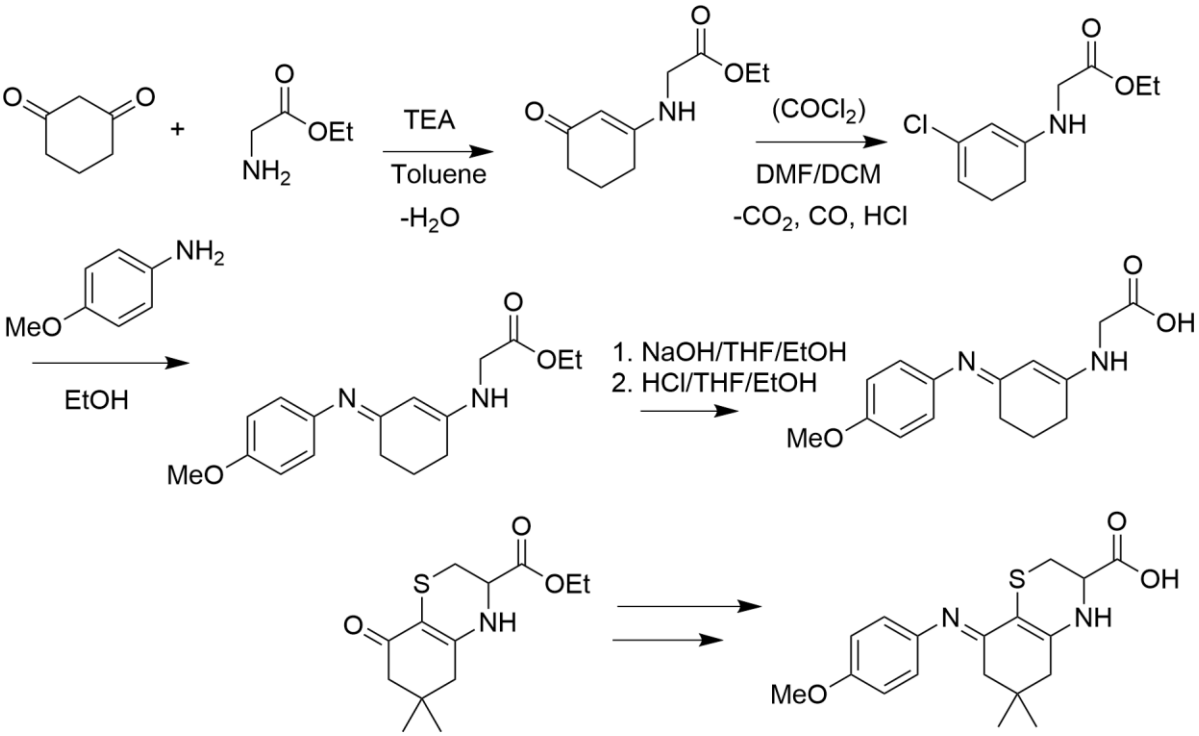

Figure 3.11. Summary of key synthetic steps in patent WO 2013/181741 PCT/CA2013/000536

In patent WO 02/39974A1 Llewellyn et al. patent 'Personal Care Compositions' where MAAs are purported to be chemically synthesised with the scheme in Figure 3.12.; however due to the lack of chemical or characterisation details it is unclear whether these reactions were carried out by the inventors or they are simply proposed.

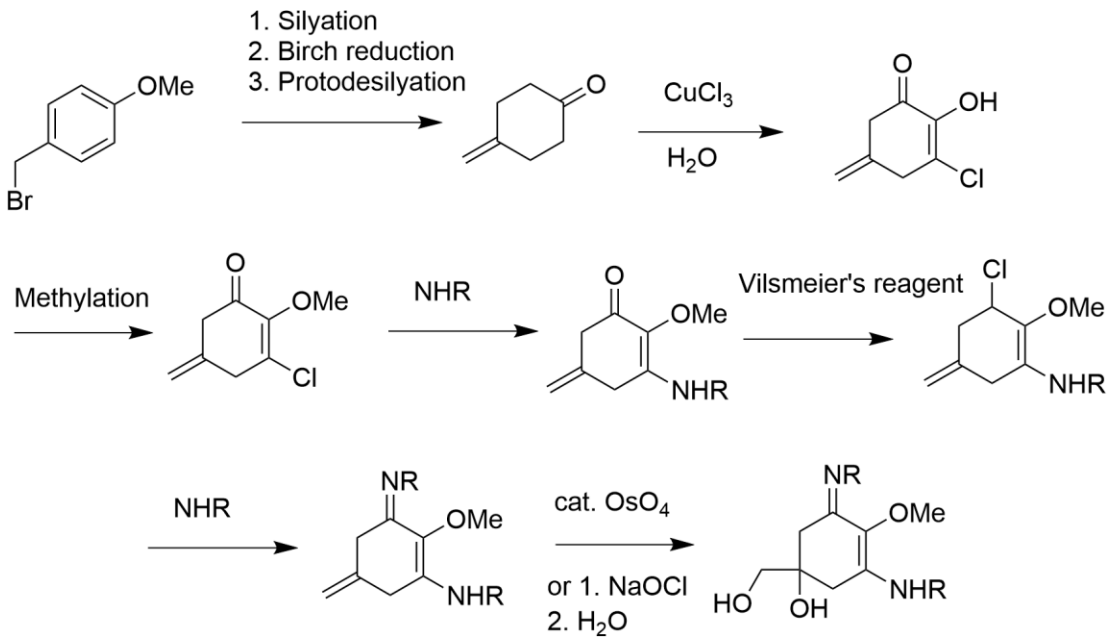

Figure 3.12. Summary of the synthetic details recorded in patent WO 02/39974A1.

Losantos et al. prepared a range of molecules, combining "scaffolds" with "decorating substituents" for the purpose of reproducing the cyclohexenimine scaffold of MAAs (Figure 3.13).[12] The naturally occurring amino acid substituent is replaced by *N*-phenyl groups or other cyclic and non-cyclic alkyl groups. Functionalisation with heteroatoms at the 2-position of the 1,3-enimine motif was also investigated by introducing alkyl, alkoxy and sulphur containing groups as this position is recognised as having an influence on the chromophore UV absorption activity.[13] The synthetic procedure involved suspension of the starting enaminone in toluene with one equivalent of p-toluene sulphonic acid monohydrate, followed by addition of the amine and reflux. The authors reported that with a mixture of 10% of molecule **16**, 10% of molecule **17**, 10% octinoxate and 5% avobenzone an SPF of 73 and UVA-PF of 23 was obtained, although this may not be clinically relevant.

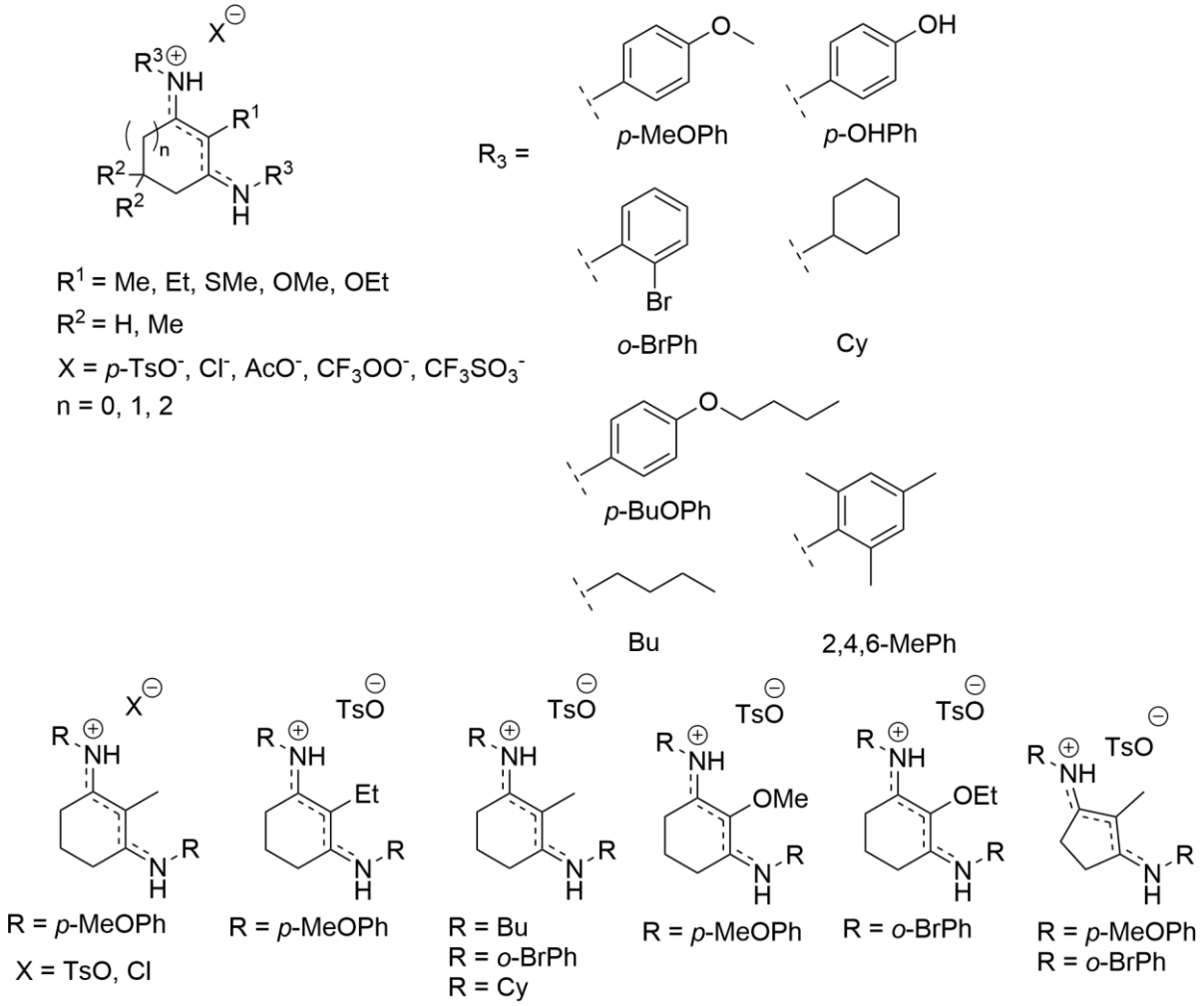

Figure 3.13. Figure redrawn from Losantos et al. to illustrate the range of molecules synthesised.

A computational study of one of the four synthetic molecules evidenced that inclusion of the *N*-phenyl groups favours a C=N isomerization channel over the out-of-plane ring deformation that had previously been characterized for the *N*-methyl molecules (see Chapter 1). This channel is similar to the geometrical C=N isomerization proposed in by Conde et al. for the natural MAA palythine.[14] This indicates that although the photodynamic pathway following photoexcitation is altered by swapping phenyl groups for methyl groups, the di-substituted imines still retain high UV absorptivity and stability. More generally this study shows that informed design of nature-inspired chromophores is a valid approach and, in this thesis, new compounds are added to the already growing library of promising UV filters and an increased understanding of this important motif is achieved.

3.2 This work

In this chapter, the synthesis of two series of molecules containing MAA motifs is reported. As a reference to the stepwise natural biosynthetic pathway for these molecules the series are referred to as “single addition” and “double addition” (see Figure 3.14.). Access to a common precursor for both series is achieved in two steps from pyrogallol. In both series the variable features are the identity of the *N*-substituents and the presence, or not, of functionalisation at the 2-position. As will be shown, the identity of the *N*-substituents has an effect on the photodynamics of the system while functionalisation at the 2-position with an electron-rich oxygen-containing moiety causes a shift in the absorbance to longer wavelength (see Figure 3.15).

The first series of “single addition” MAAs, where a single amine substituent is condensed with a 1,3-diketone, absorb at shorter wavelengths than the second series and resemble the core unit of mycosporine-glycine and other fungal oxo-mycosporines. These were used in studies by research collaborators at the University of Warwick in order to understand how a sub-unit of mycosporines affects the photodynamics. The manuscript for this work was recently published as Whittock, A. L.; Cowden, A. M.; Wills, M.; Stavros, V. Examining the Substituent Effect on Mycosporine-Inspired Ultraviolet Filters. Phys. Chem. Chem. Phys. 2023, 10.1039.D2CP05934G. https://doi.org/10.1039/D2CP05934G.

Molecules in the second series resemble the final biosynthetic product MAAs. Of this series, two were tested as potential photostabilisers for avobenzone and tested in solution (see Chapter 4). In collaboration with other researchers at the University of Warwick, five molecules were tested for their ultraslow and ultrafast spectroscopic abilities.

Finally, two molecules (**DS1** and **DS2**) which were synthesised by collaborators at the University of La Rioja, and sent to us for analysis, are examined in detail and are closely related to the double addition series.

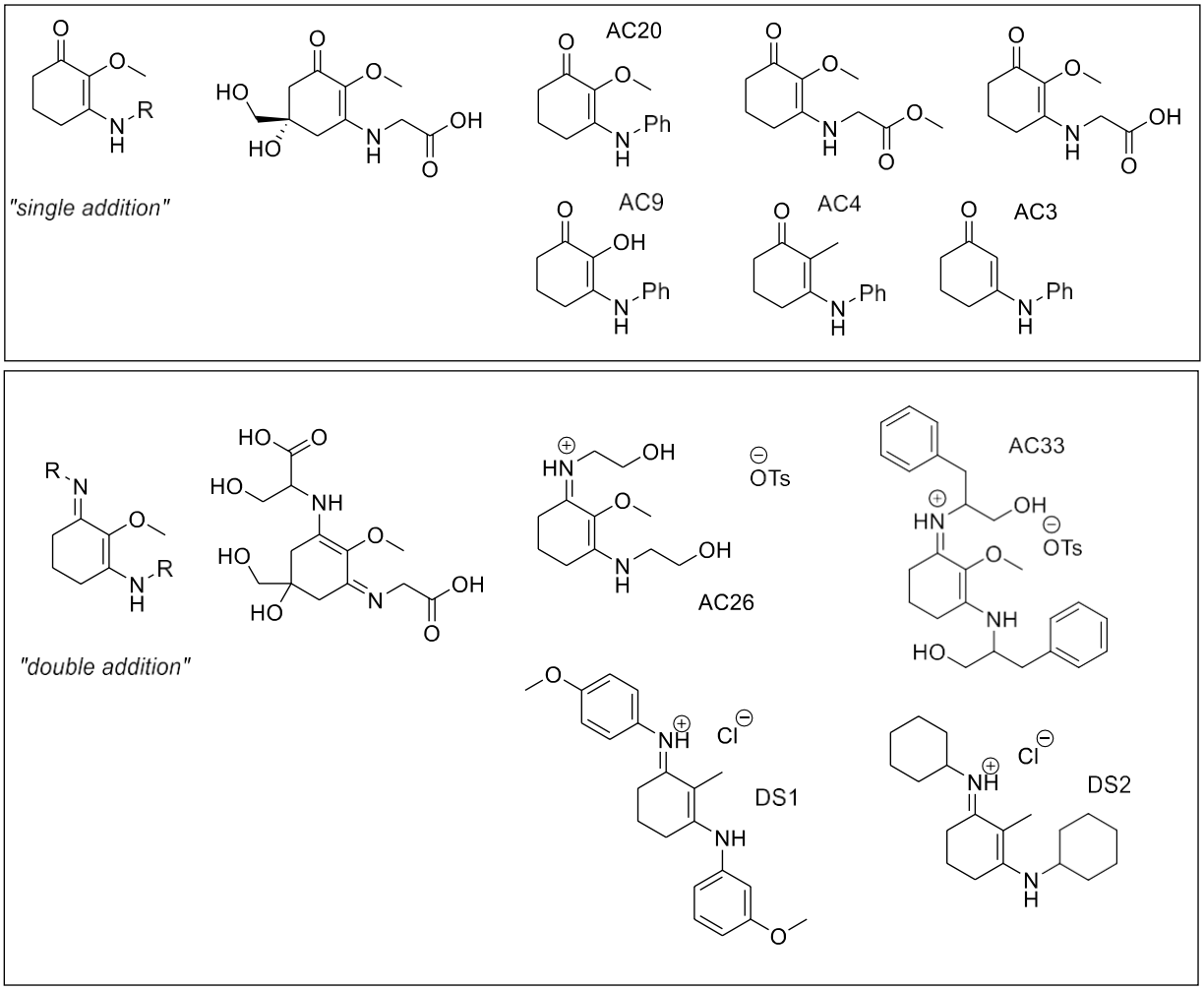

Figure 3.14. Summary of key molecules discussed and made in the two series. Series 1: *single addition* products AC3, AC4, AC9, AC20. The biological substrates with glycine methyl ester or glycine side chains (AC23 ester and AC23 acid, respectively) used in Chapter 5 also can be considered single addition MAA analogues. Series 2: *double addition* products AC26 (amino alcohol) and AC33. Also included are molecules DS1 and DS2 provided by collaborators which can be considered double addition MAA analogues. Synthetic details can be found in the Materials and Methods.

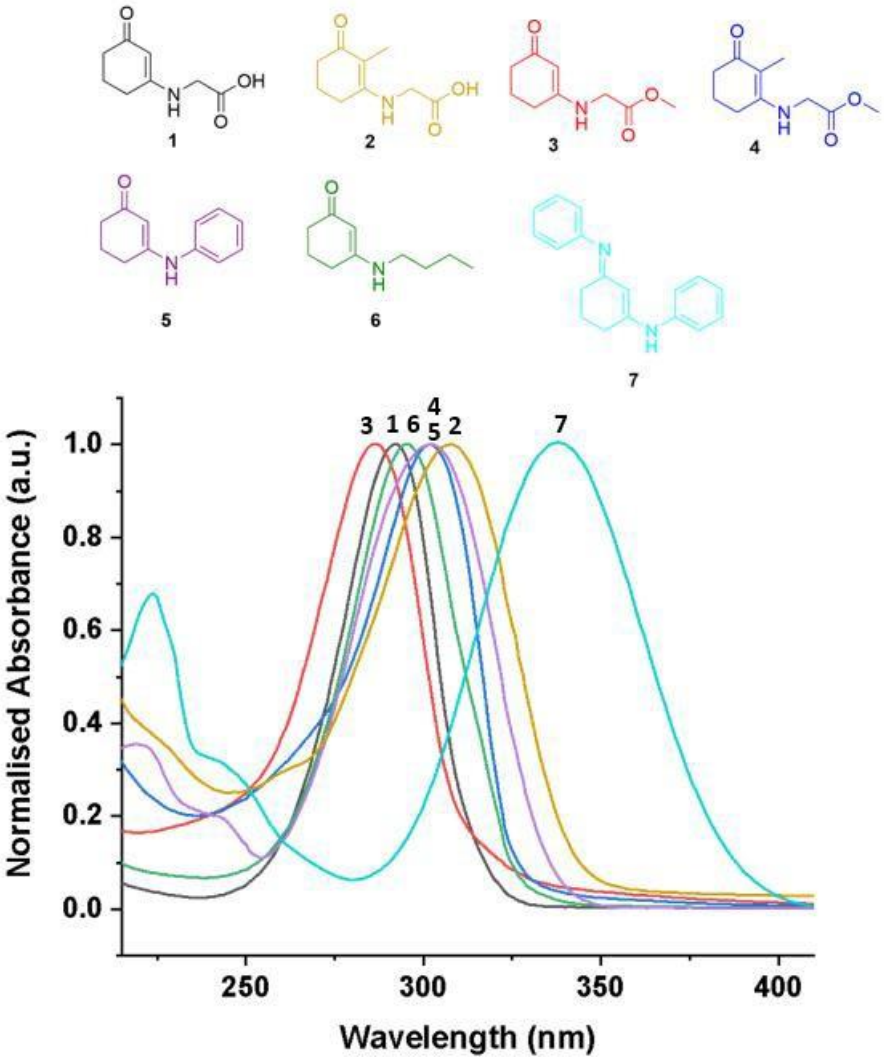

Figure 3.15. Graph showing the shift to higher wavelength (bathochromic) by functionalising at the 2-position and by increasing conjugation through addition of a second amine. All molecules were synthesised using methods in the Materials and Methods section. **1** was prepared following method in patent WO2013181741A1: 2013-12-12. Other single addition products were prepared using the same method as **AC34. 7** was prepared using the same method as **AC33**.

3.2.1 Functionalisation of cyclic 1,3-diketones

The influence on the UV-vis absorption profiles of substituents at the 2-position is clear from Figure 3.15 (above) and therefore substituents such as methyl or methoxy can be considered auxochromes – a term borrowed from dye chemistry to refer to groups of atoms attached to a chromophore that modify its ability to absorb light.[15] Comparing the red and blue traces where the molecule only differs by a 2-methyl group shows that adding an electron-donating substituent causes a shift to longer wavelength. This can be reconciled as the energy gap between the highest occupied molecular orbital (HOMO) and the lowest unoccupied molecular orbital (LUMO); corresponding to the initial and final energy states for a simple absorption/emission process (see Section 1.1.21). Notably, not all transitions in the UV-vis spectra of organic molecules are HOMO-LUMO as this may also be a dark transition. A bathochromic shift corresponds to a smaller energy gap; and in electron-donating substituents this is typically attributed to a decrease in HOMO energy and/or an increase in LUMO energy;[16] the relative degrees of which determine the overall effect. Exploration of functionalisation of the 2-position of 1,3-cyclohexanedione began with a route that was compiled from a number of patents (Figure 3.16).[17–19]

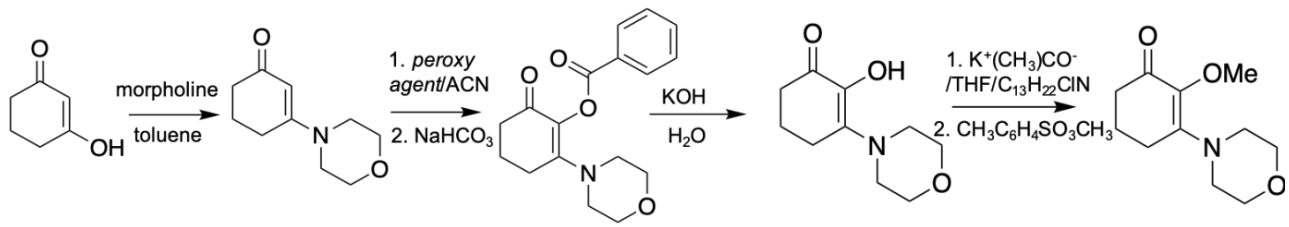

Figure 3.16. Unproductive route initially explored towards 2-functionalised enaminones.

The proposed route involved condensation with morpholine to give a morpholino adduct that could then be oxidised with benzoyl peroxide and then hydrolysed to the 2-hydroxy compound. While this proved initially promising due to stability of the morpholine adduct, the subsequent hydrolysis and methylation steps were unproductive and the route was abandoned in favour of the final route adopted further below.

A photochemical approach was also considered following a report that showed that irradiating cyclic 1,3-diketones with a mercury lamp in methanol at room temperature introduced oxygen functionalisation.[20] This methodology proved difficult to handle in the lab and was also abandoned in favour of a simple two-step reduction and methylation procedure starting from pyrogallol (Figure 3.17.):

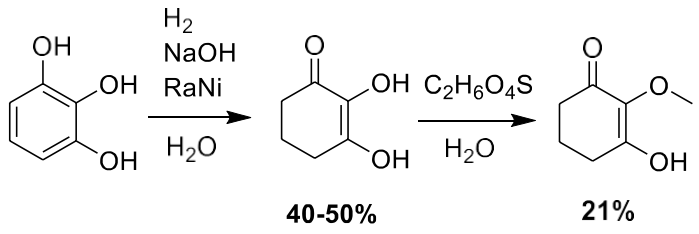

Figure 3.17. Synthetic scheme from starting material pyrogallol to a functionalised enone. Percentage yields are reported in **bold**. RaNi – Raney nickel. $C_2H_6O_4S$ – dimethyl sulfate.

The first step in the final synthesis is a Raney nickel catalysed pressure hydrogenation of pyrogallol carried out at 60 °C in sodium hydroxide solution which then proceeds for 5 hours before cooling slowly overnight. Stoichiometrically the reduction uses 2 molar equivalents hydrogen and produces the hydrogenated product as the sodium salt. The Ni catalyst is then recovered by filtration, while acidification of the filtrate and re-crystallisation yields dihydropyrogallol with a maximum experimental yield of ~50%. The second step is carried out in basic solution with two equivalents of sodium hydroxide and two equivalents of the methylating agent, dimethyl sulphate. The two equivalents of hydroxide are assumed to be used due to a facile initial deprotonation which produces a resonance-stabilised anion. The second equivalent of base then deprotonates at the 2-hydroxyl group which can act as nucleophile towards the methylating agent. The excess equivalents of the methylating agent do not lead to over-methylation but compensate for any *in situ* hydrolysis. The work up involves extraction with organic solvent which yields the product in about 20% yield. For further details see Materials and Methods.

3.2.2 Condensation of functionalised cyclic 1,3-diketones with amines

The formation of the enaminone structure that is the basis for further substitution is via the solution-phase condensation of a ketone and an amine. Mechanistically, the formation of the imine is reversible (i.e. forward is transimination, reverse is hydrolysis) but is promoted by acid catalysis and/or removal of water by heating or dehydrating agent.[21] Therefore, the hydrochloride salt of the primary amine aniline and the hydrochloride salt of the methyl ester of glycine were the preferred reagents for the conversion along with a 1,3-diketone. Deliberate removal of water may not be necessary, as the formation of **AC9** does show that the reaction can also take place in aqueous solution, although this proved to be an unreliable reaction compared to the others in the series.

The mechanism for the condensations (Figure 3.18) and imine formations (Figure 3.19) carried out (summarised in Figure 3.20.) are proposed below. The former is thought to proceed via acid-catalysed nucleophilic addition of the amine to the carbonyl bond to form a tetrahedral hemiaminal intermediate. Removal of water at this stage by heating in organic solvent (typically toluene) means that the step is rendered irreversible and an imine (also known as Schiff base) is formed, which here has a resonance form as an enaminone. The α-proton (of the methylene group) is acidic and can be exchanged to form the beta-enaminone structure of the product. The rate determining step of the reaction in water is reported to be pH-dependent: decomposition of the tetrahedral intermediate at alkaline pH and nucleophilic attack at acidic pH.[22] The loss of water is also thought to be acid-catalysed and is proposed to be a rate limiting step in this type of reaction. As most of the condensations in this thesis are in organic solvents, the formation of charged species is strongly disfavoured. Indeed, a kinetic study showed that equilibrium in $CDCl_3$ for the condensation between benzaldehyde and butylamine was reached 37 times more slowly than in CD_3CN, indicating that increasing polarity in the solvent favours the polar nature of the rate determining step.[23] However loss of the water by heating in organic solvent appears to drive this reaction forward. This mechanism is comparable to acetal formation, wherein the electrophile is also a carbonyl (i.e., aldehyde or ketone) but the nucleophile is O-centred (i.e., an alcohol) rather than on N (i.e., a primary amine). In Figure 3.19, a standard mechanism for acetal formation is shown. Notably the main difference is in how the intermediate cation is resolved; as there is no additional proton available as in imine formation, the oxonium cation becomes a target for a second nucleophilic addition.

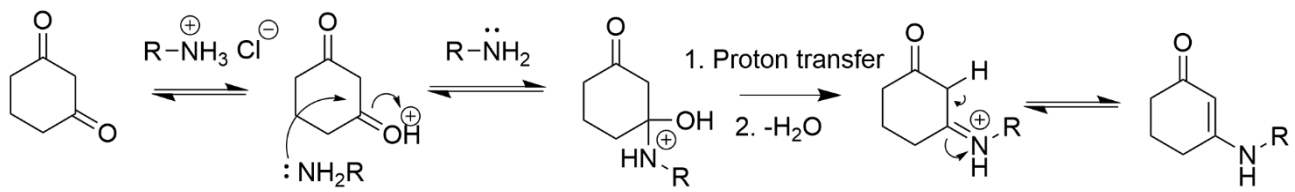

Figure 3.18. Proposed mechanism for enaminone formation.

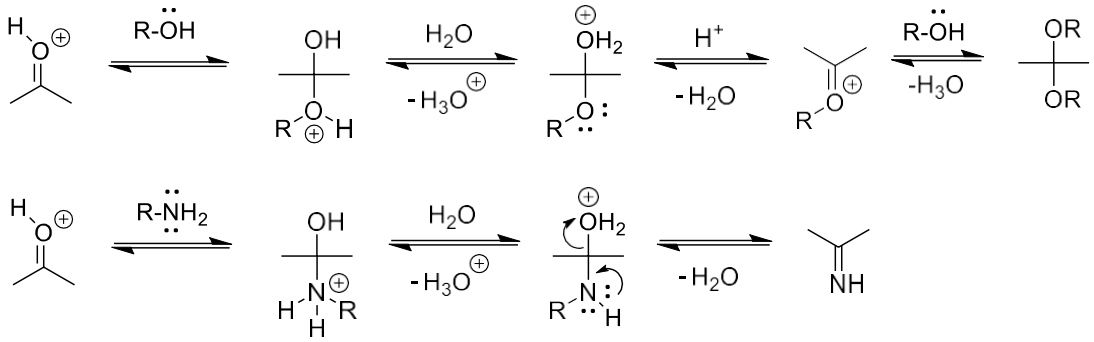

Figure 3.19. Comparison of hemiacetal/acetal formation and hemiaminal/imine formation.

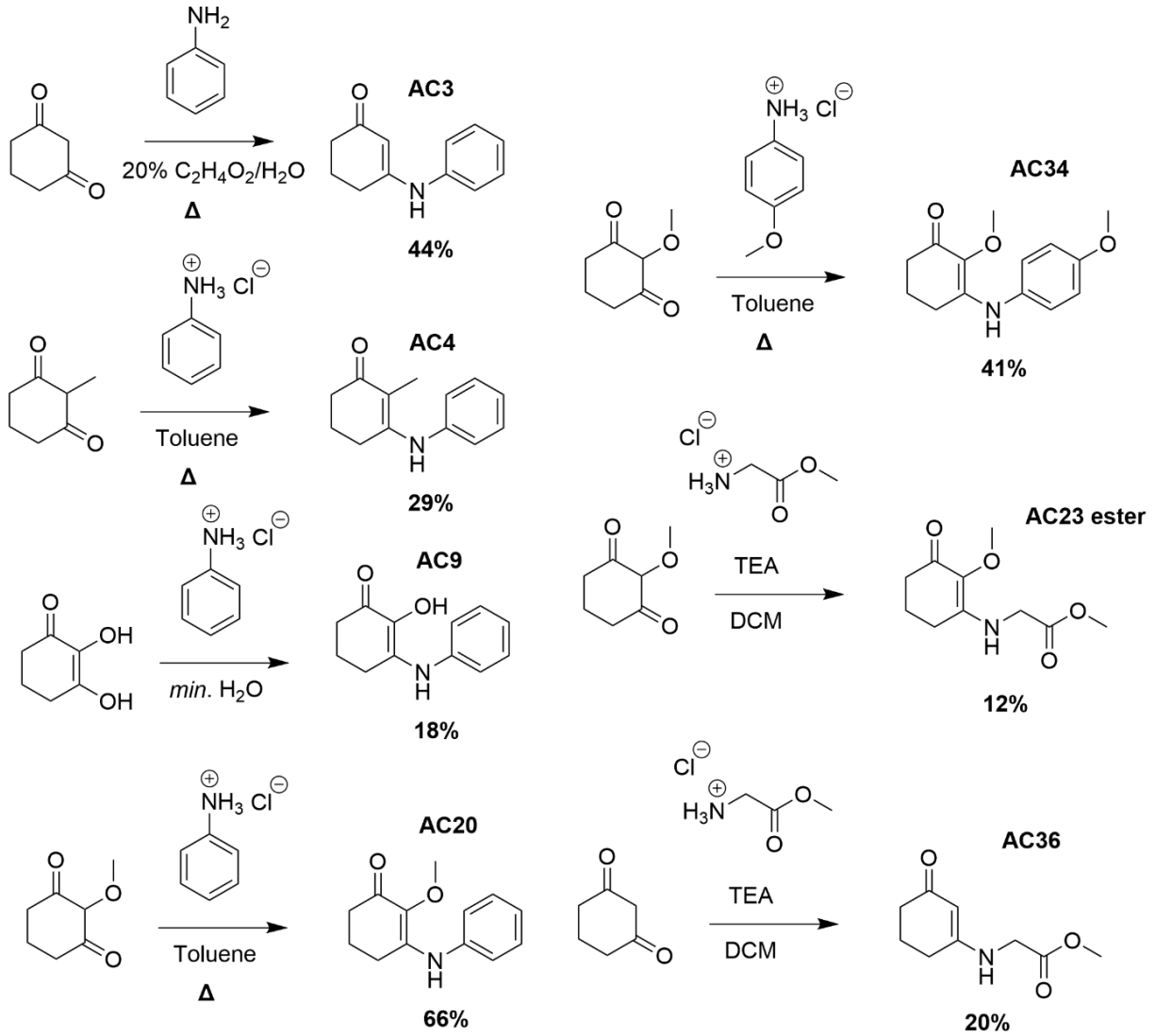

Figure 3.20. Summary of condensations leading to enaminones. $C_2H_4O_2$ – acetic acid. TEA – triethylamine. DCM- dichloromethane. **Δ** – heat/reflux.

3.2.3 Condensation of enaminones with second equivalent of amine

In the double addition series, a second equivalent amine is reacted, either in the same pot as the first addition or in a separate step. The mechanism by which this proceeds is presumably analogous to the condensation of the first equivalent amine. Elimination of water leads to formation of the final product as a salt. However, metathesis reactions are also possible, whereby the amine reacts with a preformed imine; and in literature these are reported to only occur in the presence of a catalyst.[21] A summary of the double addition products covered in this thesis is given in Figure 3.21. Characterisation of the final product

by mass spectrometry (MS) techniques is recommended at this stage as the compound exists as a positively charged ion and is observed clearly as the MH+ peak.

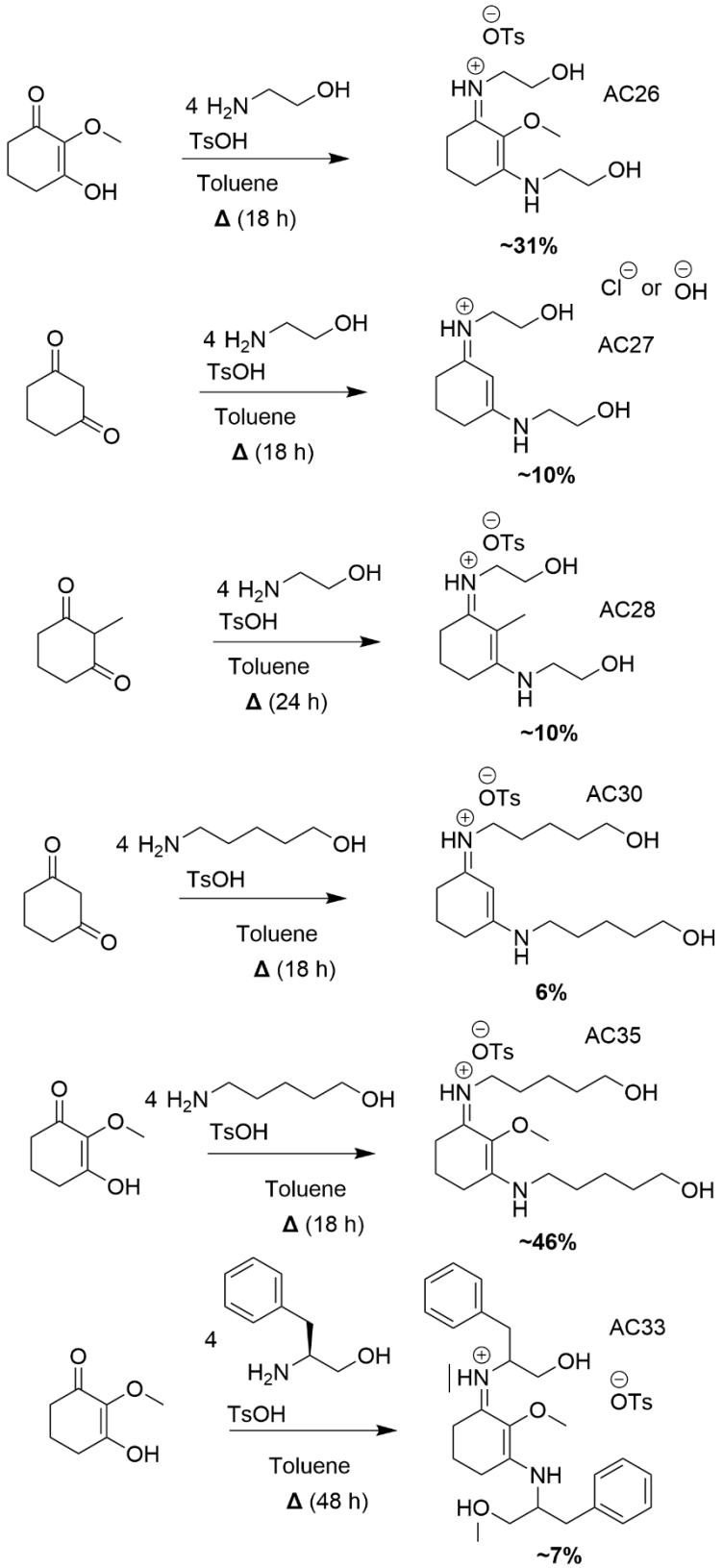

Figure 3.21. Summary of double addition condensations. Further details are in Materials and Methods.

The five molecules prepared where the amine attached is an amino alcohol were prepared as synthetic analogues of natural products. The basic motif is also present in mycosporine serinol from *Collema cristatum*, mycosporine glutamicol from *Gnomonia leptostyla* and mycosporine hydroxy-glutamicol from *Nephroma laevigatum* (structures in Figure 3.22.).[24–26] Amino alcohols were either by prepared in one step from diketones and amino alcohols or by first reducing an amino acid to an amino alcohol and then condensing. Synthetic details are found in Materials and Methods.

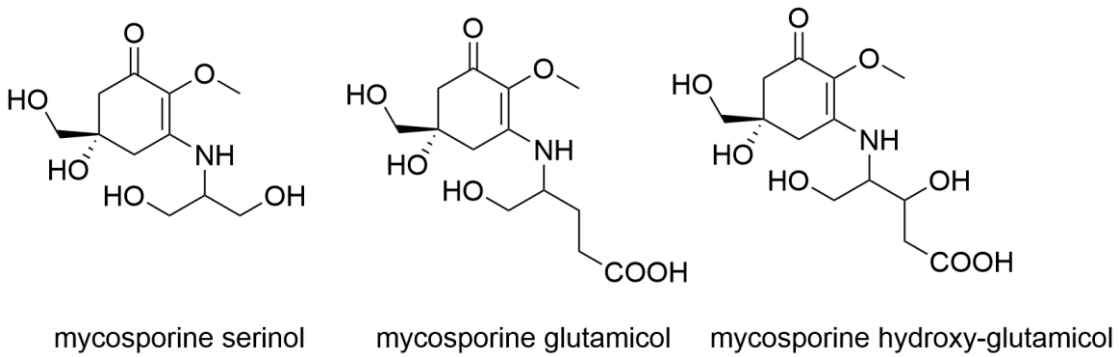

Figure 3.22. Natural product amino alcohol MAAs in the order listed in the text.

3.2.4 Spectroscopy of the amino alcohol series

A series of amino alcohols, of which **AC26** was the first chronologically, was made as double addition products with amino alcohol side chains and had not to our knowledge been characterised or studied before. The more polar amino alcohol side chains of this series means that the products are more soluble in water than **DS1** and **DS2** which are explored in greater depth in later sections. The structures and absorption spectra in water of amino alcohols **AC26**, **27**, **28**, **30** and **35** are presented below in Figure 3.23. Synthetic procedures and characterisation for each molecule are found in Materials and Methods.

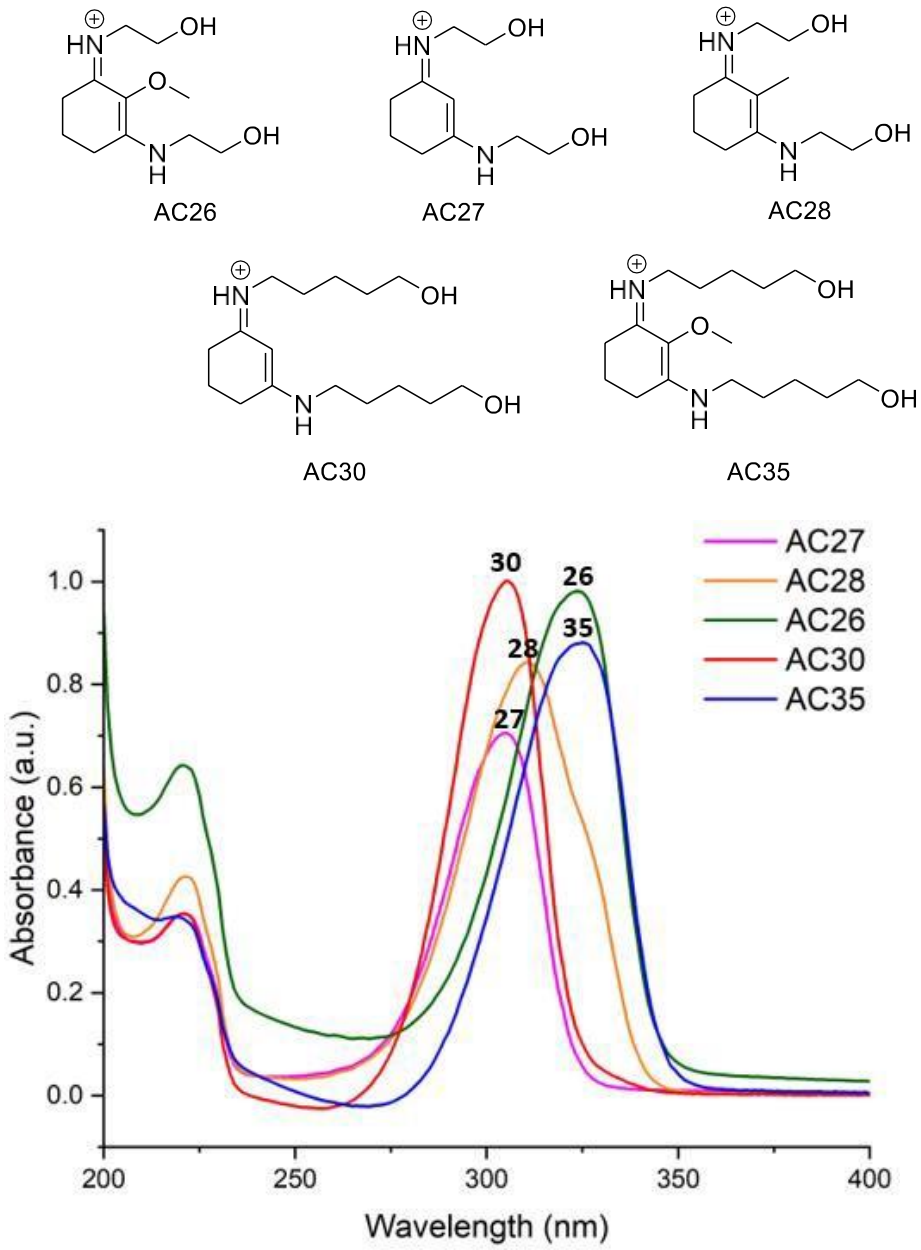

Figure 3.23. Structures and absorption spectra of the amino alcohol series in laboratory-grade distilled water. Note that the molecules are drawn without the tosylate counterion.

Comments on the synthesis of the amino alcohol series

There were a number of considerations when choosing the best reaction conditions for this 'double' condensation. Generally, the reaction is carried out in a dry round-bottom flask

using sufficient toluene to cover the reactants using 1 equivalent of ketone with 4 equivalents of an amino alcohol, and 1 equivalent tosic acid monohydrate. Reflux (>120 °C) conditions were used with stirring for at least 24 hours (monitoring by LRMS to judge if the reaction has gone to completion) and presumably most of the water had been driven off. A common result of shorter reaction times or when the temperature does not reach the set level is a mixture of single addition and double addition products, which is detectable by MS and may explain shoulder peaks in UV-vis spectra for example. After excess toluene has been decanted, the crude product is obtained as a highly hygroscopic solid or oil at room temperature. Washing with minimal hexane to remove any remaining toluene, minimal ethyl acetate to remove some amino alcohol, and drying under vacuum usually produces a product that is sufficient for UV-vis studies. A number of solvent washes were trialled in order to improve the purity of the crude and a best guess was that a polar organic solvent such as ethyl acetate would remove excess amino alcohol while leaving the product salt in the flask; however, this does require optimisation, perhaps by chromatographic methods such as Biotage. Furthermore, a simple characterisation by LRMS and ^{1}H NMR is possible to determine whether the purity is sufficient at for spectroscopy experiments. Additionally, it is not believed that any of the impurities with the possible exception of the single addition side-product would absorb in the same UV-vis region as the product and thus interfere with the pump-probe experiments.

3.2.5 Photostability of the amino alcohol series

The data for the photostability of this series of molecules were obtained by MSc student Nurbolat Toktamys at Warwick and are presented as in Table 3.1 below. The loss of activity over 2 hours in water was measured using our standard method as described in Materials and Methods. The AUCI method was also used as a measure of photostability and is presented here as a ratio of the area under the curve of the UVA region after and before irradiation. All five molecules meet the criteria for photostable UV absorbers as defined previously; i.e., less than 5% loss of activity after a prolonged irradiation. There is good agreement between the percentage loss and the AUC R value apart from in **AC28**, which is attributed to a potential impurity and experimental error.

Table 3.1. Stability data for the amino alcohol series tested using the standard method.

Molecule (Abs. max/nm)	**Loss of activity in 2 hours at peak absorbance in ethanol (%)**	**Loss of activity in 2 hours using AUC R (UVA)**
AC26 (324)	2.5	0.98
AC27 (305)	2.1	0.97
AC28 (311)	2.3	0.86
AC30 (305)	1.8	0.99
AC35 (325)	2.4	0.98

3.2.6 Ultrafast Spectroscopy of the amino alcohol series

[The ultrafast experiments and the resultant spectra were prepared by Nurbolat Toktamys as part of an MSc research project.]

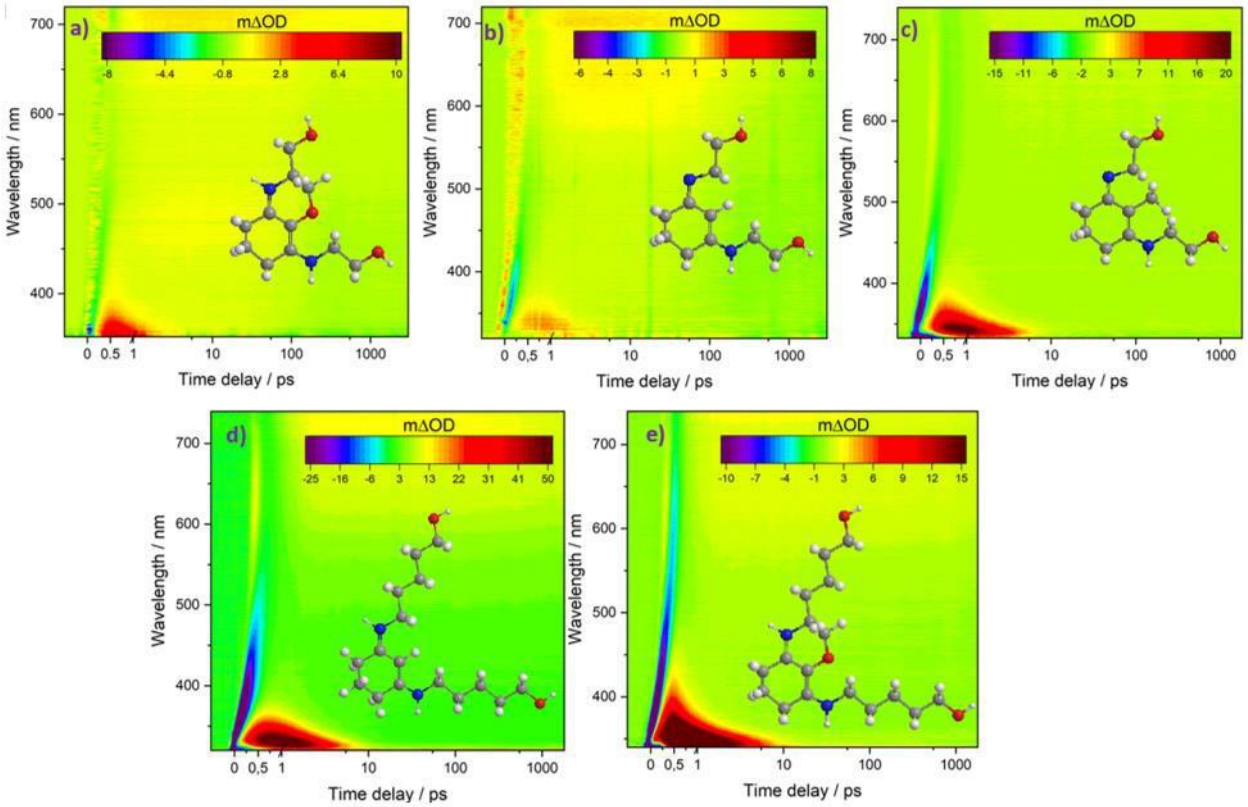

Figure 3.24. TAS presented as false colour heat maps of (a) **AC26**, (b) **AC27**, (c) **AC28**, (d) **AC30**, and (e) **AC35** in water photoexcited at their respective λ_{max}, 324, 305, 311, 305, and 325 nm. Time delays are plotted linearly until 1 ps and then as a logarithmic scale from 1 to 3000 ps. Inset are the 3D molecular structures of the molecules. The TAS are not chirp corrected.

As the results presented in Figure 3.24 show, TAS of all molecules are characterised by three main features, with associated lifetimes, $\tau_{1\text{-}3}$ (see Table 3.2). Firstly (τ_1), there is a ground state bleach (GSB) present from time zero (Δt = 0) and 310-350 nm where the probe and pump beams are temporally overlapped). This is to be expected as the UV-vis absorption profiles of **AC28**, **AC30**, and **AC35** extend to ~350 nm. The GSB of **AC26** and **AC27** (in Fig. Q a) and b)) is almost invisible, while it was centred around ~350 nm for the rest molecules in Fig. Q c), d), and e). Additionally, stimulated emission (SE) is observed in all molecules spanning ~380–550 nm at early times, Δt, which spectrally red-shifts over time. The third feature is an excited state absorption (ESA) that grows at after time zero around 330-400 nm, indicating sequential kinetics. In **AC26**, **AC27**, **AC28, AC30** and **AC35,**

the ESAs are centred at ~350, 335, 350, 350 and 375 nm respectively. The SE is present from time zero while the ESA grows in shifted from time-zero and then decay in a few ps almost for all molecules. The differences between the signals, including their phases, are explained in the Chapter 1. A summary of the photochemical characterisation of this series is presented as a scheme in Figure 3.25; where energy dissipation is thought to proceed through a S_1/S_0 conical intersection. A summary of the putative physical processes is presented in Table 3.3.

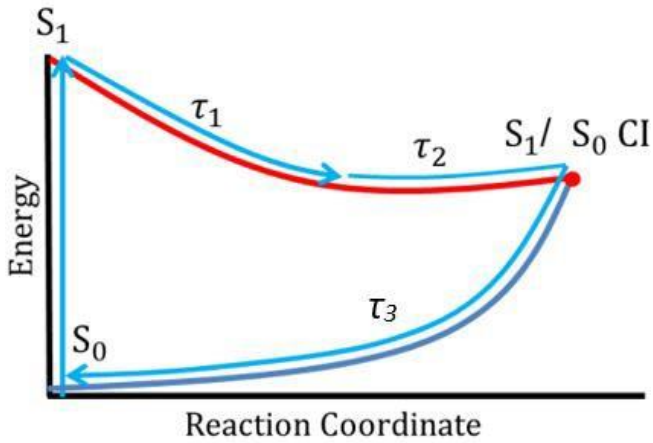

Figure 3.25. Potential energy scheme for the amino alcohol compound **AC35**. Adapted from ref[27].

Table 3.2. Summary of time constants and associated errors of the dynamical processes extracted from the global sequential fit of all molecules photoexcited at their respective λ_{max}. The IRF derived error is ± 40 fs. VC – Vibrational cooling. TP – Trapped population.

Time constants/ Samples	**τ_1(fs)**	**τ_2(fs)**	**τ_3(ps)**	
AC26	330 ±40	940 ±40	294 ±155	-
AC27	210 ±40	630 ±40	196 ±6.82	-
AC28	540 ±40	890 ±40	2483 ±322	-
AC30	200 ±40	2.28 ±0.04 **(ps)**	>3x10^3	-
	τ_1(fs)	**τ_2(fs)**	**τ_3(ps) VC**	**τ_4(ps) TP**
AC35	230 ±40	260 ±40	1.667 ±40	>3x10^3

Table 3.3. Assignment of time constants to physical processes in **AC26**, **AC27**, **AC28**, **AC30**.

Time constant	**Range of values**	**Description**
τ_1	200-540 fs	fast geometry relaxation along the S_1 reaction coordinate toward the S_1/S_0 conical intersection (CI).
τ_2	260 fs – 2.28 ps	population traversing through the S_1/S_0 CI and subsequent vibrational cooling along the S_0 coordinate via vibrational energy transfer
τ_3 etc.	~ 2 ps - >$3x10^3$ ps	any remaining species trapped in their excited state or recovery of signal due to solvated electron/s

In conclusion, all molecules show very good photostability and ultrafast dynamics which are comparable to the MAAs, shinorine, porphyra-334 and usujirene/palythene as summarised in the Introduction.

3.2.7 Full experimental characterisation of DS1 and DS2

The two molecules chosen for a more in-depth study - **4-methoxy-N-(3-((4-methoxyphenyl)amino)-2-methylcyclohex-2-en-1-ylidene)benzenaminium chloride** and **N-(3-(cyclohexylamino)-2-methylcyclohex-2-en-1-ylidene)cyclohexanaminium chloride** - (called hereafter **DS1** and **DS2**, respectively, Figure 3.26) are modelled on the MAA structure (exemplified by shinorine) but differ in their *N*-substituents. The *N*-substituents were rationally chosen as a computational study by Losantos et al. had identified a new reaction channel warranting further investigation that is available to compounds with phenyl substituents compared to other related compounds with non-aromatic substituents (e.g., methyl or cyclohexyl substituents).[13] For the first time, to our knowledge, a direct comparison can be made between the two proposed mechanisms; as here both the cyclic hexenimine previously studied (**DS1**) and new molecule **DS2** are studied under the same experimental conditions.

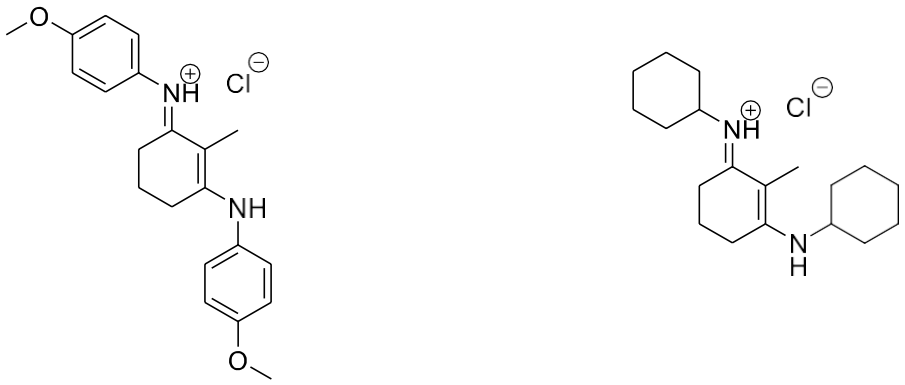

Figure 3.26. **DS1** and **DS2,** prepared by Losantos et al.

The compounds were prepared in a single reaction with good yield and simple purification process, which are ideal features for their use in sunscreens. The chloride counterion is a standard counterion used in many approved drugs.[28] The UV-visible absorption profiles as illustrated in Figure 3.27. are in the UVA-UVB region and confirm that they are absorbers of solar UV radiation. The extinction coefficients (ε ($M^{-1}cm^{-1}$)) were determined (see Materials and Methods) at the respective absorption maxima as ~64100 (**DS1**) and ~60700 (**DS2**) $M^{-1}cm^{-1}$ in ethanol; and these values in comparison with the extinction coefficient table (Table 1.1) in the Introduction suggest that they are very strong absorbers of light.

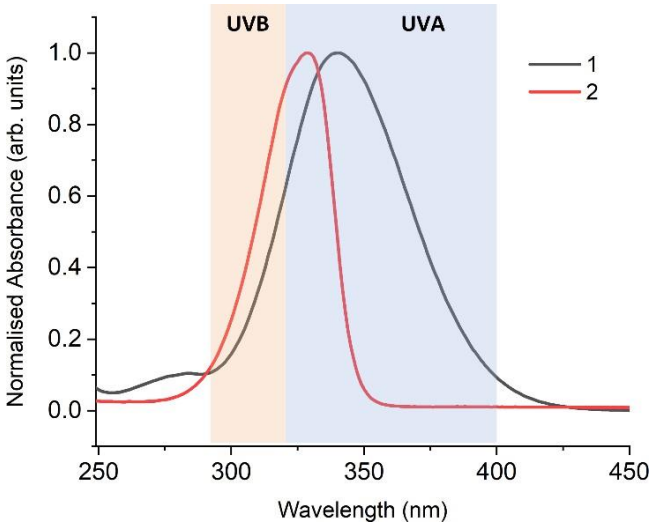

Figure 3.27. UV-visible spectra of **DS1** and **DS2** are displayed with the UVB (290-320 nm) and UVA (320-400 nm) regions highlighted. Absorption is normalised to the peak maximum (**1** λ_{max} = 341 nm and **2** λ_{max} = 329 nm).

The steady-state irradiation data using the solar simulator are presented in Figure 3.28. Over 2 hours continuous irradiation (using the standard method in Materials and Methods), the profile of **DS2** did not change significantly (<1%) whereas irradiation of **DS1** was accompanied by a 12.3% decrease at the peak absorbance. The AUCI (320-400 nm) for **DS1** was calculated as 0.88 and the AUCI for **DS2** was >0.99. An AUCI > 0.80 has previously been used as a quantitative criterion for a photostable molecule and by this AUC method, both molecules can be considered photostable. [29,30]

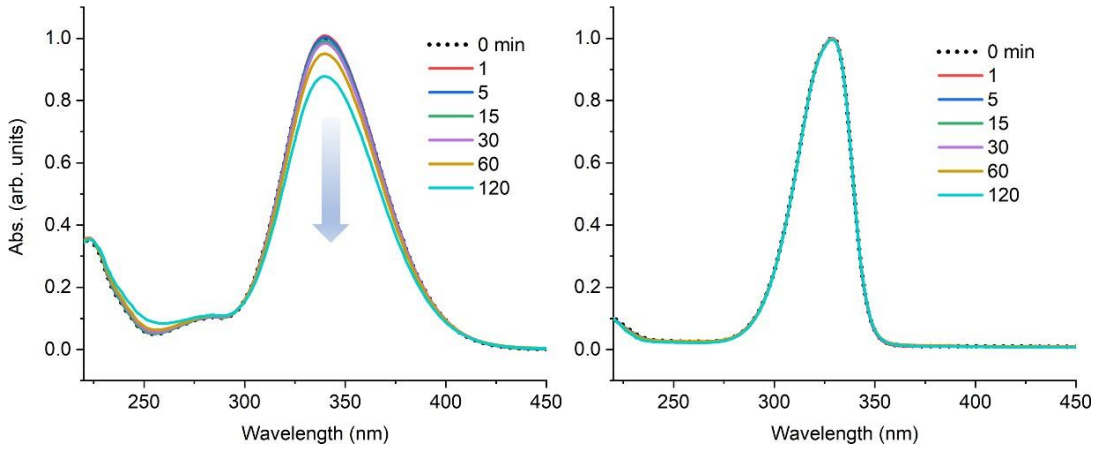

Figure 3.28. Photostability as measured by change in UV-visible absorption (210-450 nm) of **DS1** (a) and **DS2** (b) in simulated solar conditions in ethanol across 2 hours irradiation. Absorbance is normalised to the peak maximum.

To investigate the femtosecond (10^{-15} s) to nanosecond (10^{-9} s) behaviour of **DS1** and **DS2**, ultrafast TEAS measurements were performed and the data are displayed in Figure 3.29. Firstly **DS1** will be discussed and then the results for **DS2** will be discussed subsequently. In the TAS of **DS1**, from time-zero a ground-state bleach (GSB) feature is observed that is centred at the blue-edge of the spectrum (~340 nm). In the GSB, light that was previously absorbed in that spectral region by molecules in the ground-state now reaches the detector and the feature is thus characterised by a negative absorption (i.e., $I > I_0$ where the ΔOD = $\log_{10}(I_0/I)$). There is also a broad stimulated emission (SE) feature which is immediately evident on the fs timescale after excitation and spans the red-edge of the spectrum (500-700 nm region) and is detected with a negative ΔOD. There is a broad excited state absorption (ESA) feature that appears across 380-550 nm and which lasts on the sub-ps to ps timescale, characterised by a positive absorption due to the opposite reasoning to the GSB and SE. The ESA in the spectral region 375-450 nm occurs immediately following photoexcitation and the broadening out to 550 nm occurs shifted from time-zero possibly due to competing stimulated emission at early time which is stronger in intensity. Finally, after ~10 ps, the ESA has mostly decayed but there is a long-lived component which persists beyond the time-window of the experiment, appearing as a GSB at ~340 nm and an ESA at ~380 nm. The TAS look similar to that reported in previous literature and the following time constant assignments were guided for **DS1** by Losantos et al.[13] and for **DS2** by that of J. Woolley et al..[27]

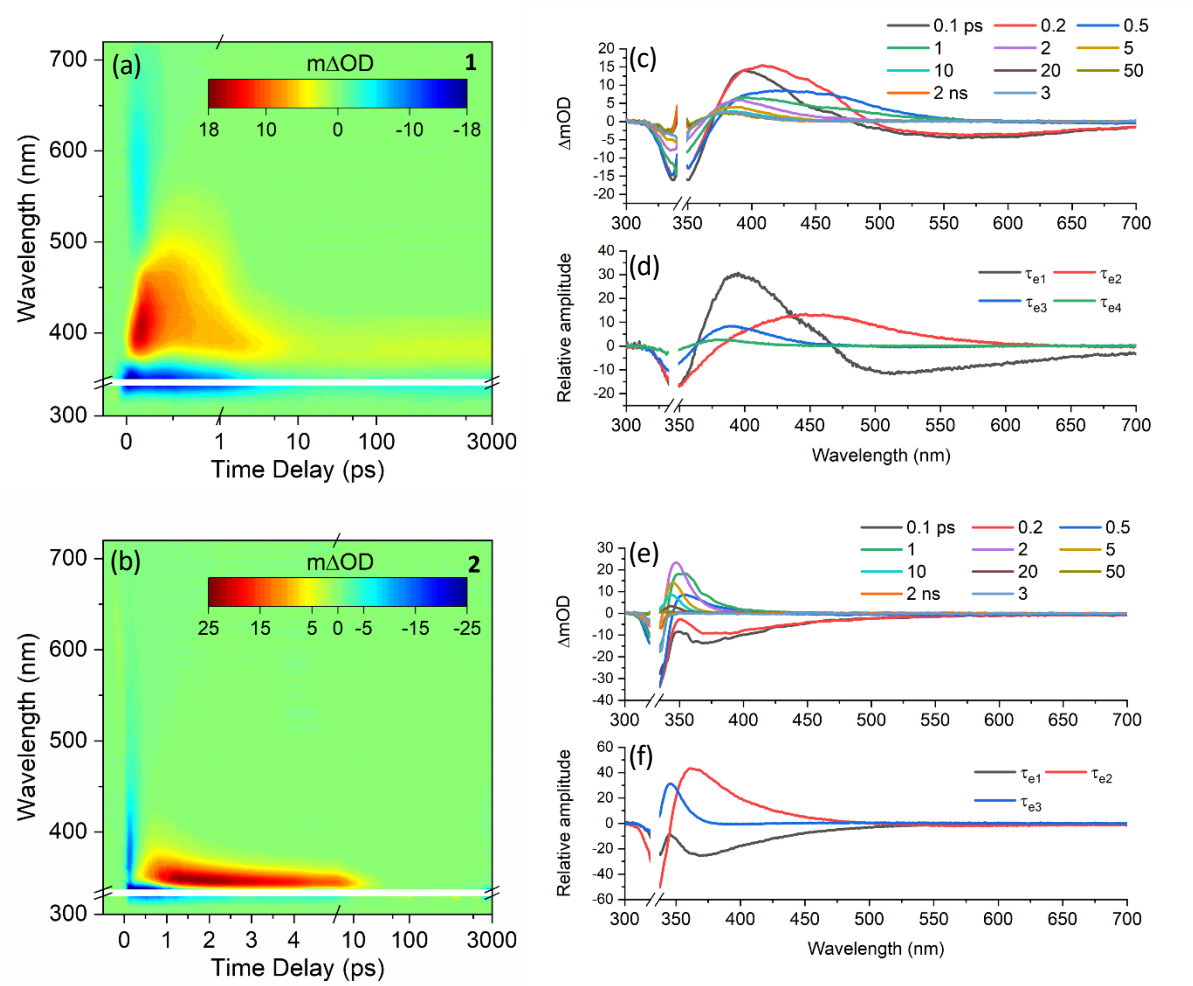

Figure 3.29. TEAS of **DS1** (a) and **DS2** (b) presented as false-colour heat maps. The time delay scale is linear to 1 ps and then logarithmic to 3000 ps in (a) while in (b) the scale is linear to 5 ps and logarithmic thereafter. The region between 340-349 nm and 320-334 nm has been omitted for all spectra for **1** and **2**, respectively, due to imperfect pump pulse subtraction. Selected time delays from the TEAS are plotted as lineouts in **1** (c) and **2** (d) beside the corresponding TEAS. The EADS of **1** (e) and **2** (f) produced by the fitting procedure (for details see Materials and Methods).

The photodynamic processes that produce the signals and their temporal evolution are defined by time constants that are extracted from the data by our fitting procedure (see Materials and Methods). The evolution associated difference spectra (EADS) produced from the fit are included along with the TAS to support the assignments (Fig. T.). The whole spectral region of the probe was used for the sequential model minus the 340-355 nm

region due to imperfect pump beam subtraction. In the case of **DS1**, the sequential kinetic fit extracted four time constants (see Table 3.4). The process with a lifetime of ~150 fs (τ_{e1}) is the first extracted time constant and is attributed to evolution out of the Frank-Condon region of the initially prepared first electronically excited state (S_1) as evidenced by the decay of the SE. This assignment is in accordance with the previous study.[13] The second time constant, ~620 fs (τ_{e2}), is assigned to the population of **DS1** as it progresses towards the S_1/S_0 conical intersection on the S_1 potential energy surface and passes through the conical intersection to populate the vibrationally hot electronic ground-state; much like in other previously discussed systems. The third time constant of ~3 ps (τ_{e3}) is attributed to the slower process of vibrational cooling in the vibrationally hot ground-state, via vibrational energy transfer, both intramolecular and intermolecular (i.e., to the solvent). A blue-shift, observed by a tailing off, of the ESA in the TAS ~380-400 nm is also indicative of ground-state vibrational cooling and this is reflected in the blue-shift between the EADS of τ_{e2} and τ_{e3}. The final time constant is >3 ns (τ_{e4}) and this is assigned to a persistent long-lived feature that is present after ~10 ps with no spectral changes out to the final time delay of our experiment (Δt = 3 ns). The difference spectrum after 2 hours of solar irradiation can be used to evaluate whether the feature at ~380 nm is due to the formation of a stable photoproduct (see Figure 3.30.). As the long-lived feature is not present in the difference spectrum at longer times, this indicates that it is likely due to a minor portion of population trapped in either the singlet or triplet state rather than a distinct photoproduct although metastable isomer is possible. Further experiments were carried out to probe this feature. We did not observe any degradation after irradiating **DS1** with monochromatic light for 1 hour, which more closely mimics the TEAS experiment compared to the solar simulator experiment, we believe that the trapped population eventually returns to the ground-state. We propose that the trapped population mostly finds its way to the S_1/S_0 CI beyond 3 ns as only weak fluorescence was observed (see later); implying that the trapped population only in part recovers via this decay mechanism. However, the persistent ground-state bleach in the 2 hour solar-simulated irradiation study does indicate that the parent molecule could be sensitive to some photodegradation in a more real-life environment.

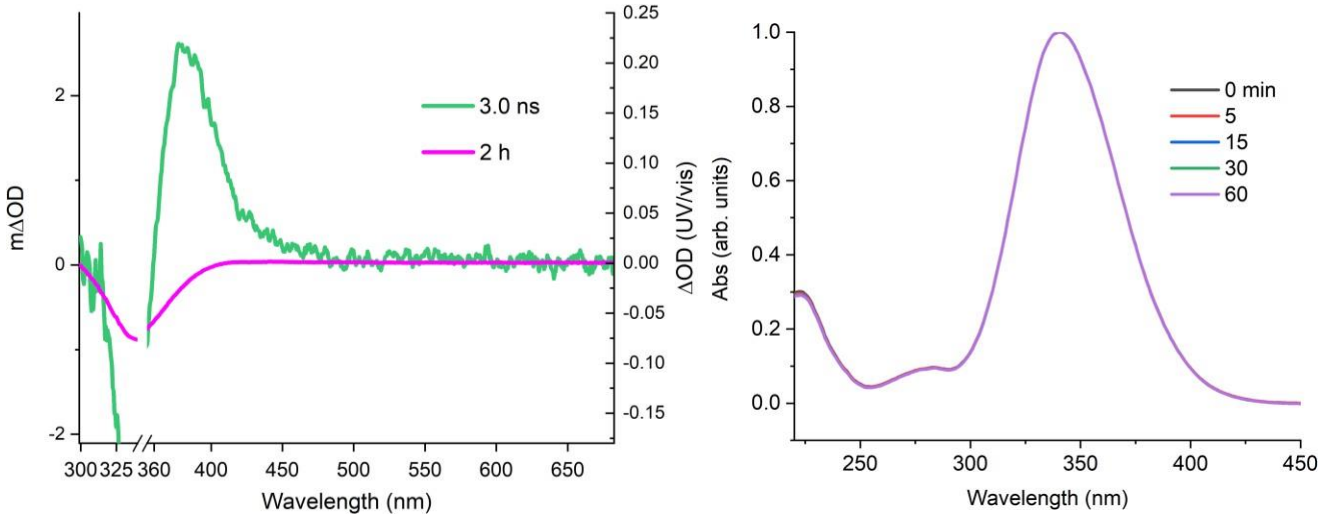

Figure 3.30. (Left) The difference spectrum of **DS1** after 2 hours of solar irradiation (right y-axis) overlayed with the longest trace in the TEAS experiment (3 ns, left y-axis) to evaluate whether the feature at ~380 nm is due to the formation of a photoproduct. (Right) Photostability of **DS1** when irradiated for 1 hour at 341 nm in ethanol. A solution of ~10 μM concentration was irradiated at a single wavelength (λ_{max} = 341 nm) using a xenon arc lamp with the beam power adjusted to be comparable to the solar spectrum at that wavelength. The solution was irradiated continuously for one hour. In this case there was no significant change during the irradiation. Absorbance is normalised to the peak maximum.

TVAS data were obtained for further insight into the photoprotective mechanism, specifically into the nature of the vibrational relaxation in the S_0 and to support our time constant assignment for the TEAS data. To cover the regions 1480-1660 cm^{-1} two probe beams were used and the data was stitched together by matching the signal intensity at 1535 cm^{-1}. The resulting spectra (Fig. Ha) contains three negative features; these being a sharp and intense feature at ~1510 cm^{-1}, a broad and weaker feature at ~1535 cm^{-1} and a third weak feature at ~1610 cm^{-1}. These features correspond to the GSB of **DS1**'s S_0 vibrational modes in this region evidenced by their spectral match with the FTIR spectrum. We have chosen to fit a bi-exponential decay to the most prominent feature (by integrating across 1504-1524 cm^{-1}) to model the GSB recovery in the first 1 ns after photoexcitation (Fig. 5b). The first time constant of the fit, 4.2 ps (τ_{v1}), is attributed to vibrational cooling

and is on the same timescale as the component of vibrational cooling seen on the TEAS (~3 ps) which supports our assignment. The second time constant, >1 ns (τ_{v2}), extends beyond the experiment time-window and describes the incomplete GSB recovery; indeed, there is only ~83% recovery overall within 1 ns for this feature. This is in accordance with the TEAS measurements as there was the presence of a remnant GSB beyond 3 ns. The remaining ~17% that hasn't recovered is believed to be trapped population in the excited state or a metastable isomer as described above.

Table 3.4. The time constants listed in the table were obtained through a global fit of the data with a sequential model and are quoted with associated errors which are half the instrument response estimated using solvent-only TAS. The final time constant for **DS1** is beyond the experimental time window of the TEAS experiment (3 ns). FC – evolution out of the Franck-Condon region; CI – conical intersection; VC – vibrational cooling; PP – long-lived population/photoproduct. Appended are the results from a previous study of **DS1.**

	Time constant (molecule DS1)	**Time constant (molecule DS2)**	**Process**	**DS1 from previous study[13] (341 nm)**
TEAS				
τ_{e1} (fs)	150 ± 60	470 ± 60	FC	320 ± 110
τ_{e2} (fs)	620 ± 60	450 ± 60	CI	1.7 ± 0.48
τ_{e3} (ps)	2.99 ± 0.06	5.74 ± 0.06	VC	9.7 ± 1.04
τ_{e4} (ns)	>3		PP	
TVAS				
τ_{v1} (ps)	4.2 (±0.3)	2.4 (± 0.5)	VC	
τ_{v2} (ps)	>1000	11.1 (± 7.6)	VC	

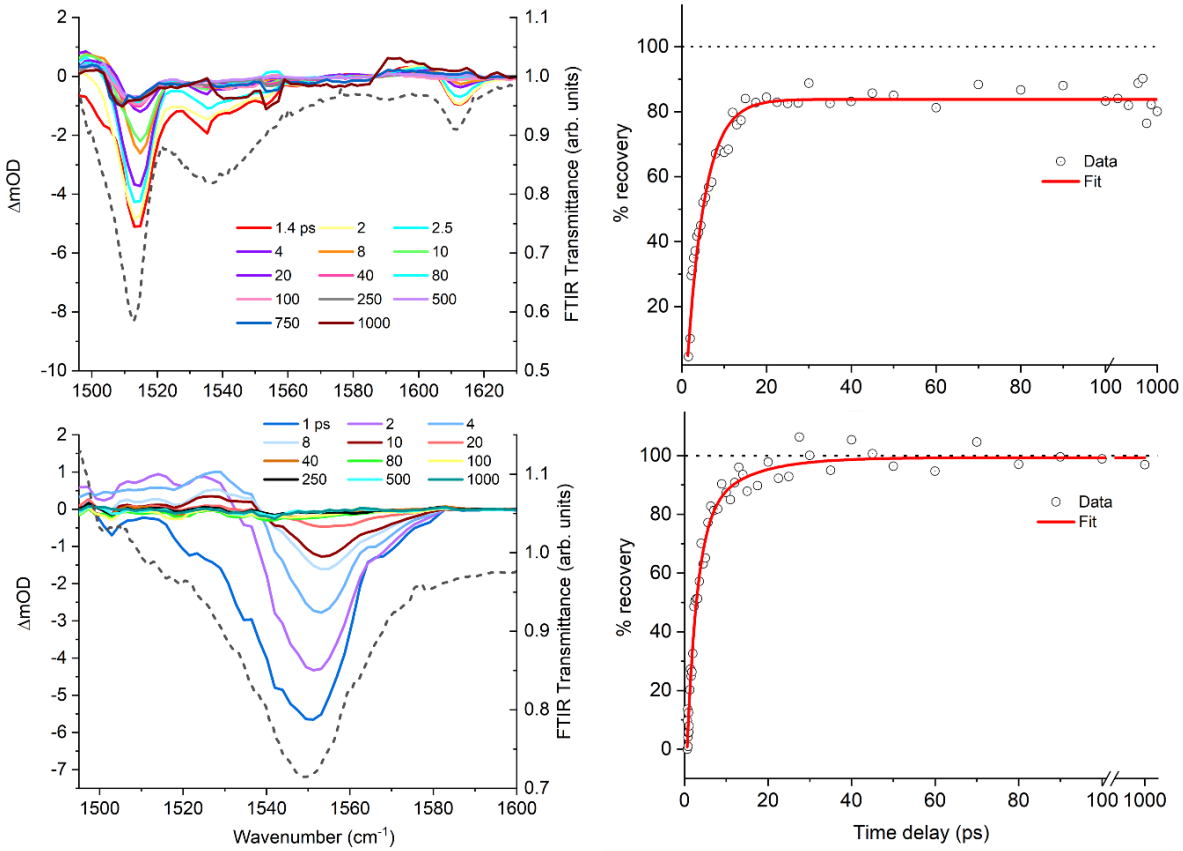

Figure 3.31. (Top left) Transient vibrational absorption spectra (smoothed) of **DS1**. The most negative trace (black, dashed line) is the smoothed FTIR spectrum with the transmittance scale given on the right side of the plot. (Top right) Bi-exponential fit of the percentage recovery of the GSB feature in **DS1** . The integration region for the fit was 1504-1524 cm^{-1} and the two extracted time constants are τ_{v1} = 4.2 (±0.3) ps and τ_{v2} = >1 ns. The scale is linear up to 100 ps and logarithmic after 100 ps and up to 1 ns. (Bottom left) Transient vibrational absorption spectra (smoothed) of **DS2**. The most negative trace (black, dotted) is the smoothed FTIR spectrum with the transmittance scale given on the right side of the plot; (Bottom right) Bi-exponential fit of the percentage recovery of **DS2**. The integration region for the GSB feature fit is 1540-1560 cm^{-1} and the two extracted time constants are τ_{v1} = 2.4 (± 0.5) ps and τ_{v2} = 11.1 (± 7.6) ps. The scale is linear up to 100 ps and logarithmic after 100 ps and up to 1 ns.

The discussion now turns to the TEAS of **DS2**, which is also presented in Figure 3.29. Similar to **DS1**, there is a GSB feature from time-zero centred at the blue-edge of the spectrum (~340 nm). There is also a broad stimulated emission (SE) feature which is immediately

evident on the fs timescale after excitation and spans the red-edge of the spectrum (500-700 nm region). There is an excited state absorption feature (ESA) that appears across 340-370 nm and which lasts on the sub-ps to ps scale. A slight shift from time-zero may indicate that the absorption is the result of a relaxation process.

In the case of **DS2**, the whole spectral region of the probe was used for the fit minus the 320-334 nm region due to imperfect pump subtraction. The sequential, global kinetic fit extracted only 3 time constants (see Table 3.4)**.** The process with a lifetime of ~470 fs (τ_{e1}) is the first extracted time constant and is attributed to evolution out of the Franck-Condon region of the initially prepared first electronically excited state (S_1) as evidenced by the decay of the stimulated emission. The second time constant, ~450 fs (τ_{e2}), is assigned to the population of **DS2** as it progresses towards the S_1/S_0 conical intersection on the electronic excited state potential energy surface and passes through the conical intersection to populate a vibrationally hot electronic ground state. Low levels of stimulated emission at the red-edge of the probe window in the EADS for τ_{e2} support this assignment. The third time constant of ~5.7 ps (τ_{e3}) is attributed to the slower process of vibrational cooling from the vibrationally hot ground state, via vibrational energy transfer, both intramolecular and intermolecular. A blue-shift of the ESA in the TAS in this region is also indicative of ground-state spectrum cooling. A negative artefact that appears at longer times (~3 ns) was investigated in a separate photoproduct scan and was found not to be a significant feature.

We also acquired TVAS data for **DS2** using a single probe to cover the regions 1480-1660 cm^{-1}. The obtained spectrum (Fig. 5c) has a prominent feature at ~1550 cm^{-1}. A bi-exponential decay fit was used across the feature (1540-1560 cm^{-1}) to model the recovery in the first 1 ns (Fig 5d.). The first time constant of this fit, 2.4 ps (τ_{v1}), is attributed to vibrational cooling of the S_0. The second time constant, ~11 ps (τ_{v2}) with a large associated error, was found to be a minor contribution that could indicate a slower component of vibrational cooling in the ground electronic state, for example, $\nu_0 \leftarrow \nu_1$ or remnant population that funnels through the S_1/S_0 CI at a slower rate. The time constant attributed to vibrational cooling in the TEAS is an intermediate value of the two time constants extracted from the TVAS, indicating that of the two methods only the TVAS has been able to resolve the vibrational cooling into two parts. Although there is evidence that the ESA extends out to ~30 ps in the TEAS (see Figure 3.32.), our fitting model was unable to extract a longer lifetime; perhaps due to a drop-off in signal. In accordance with the TEAS results, 100% GSB recovery of **DS2** was observed. Weak fluorescence was also observed in **DS2** when irradiated at the peak maximum (see later).

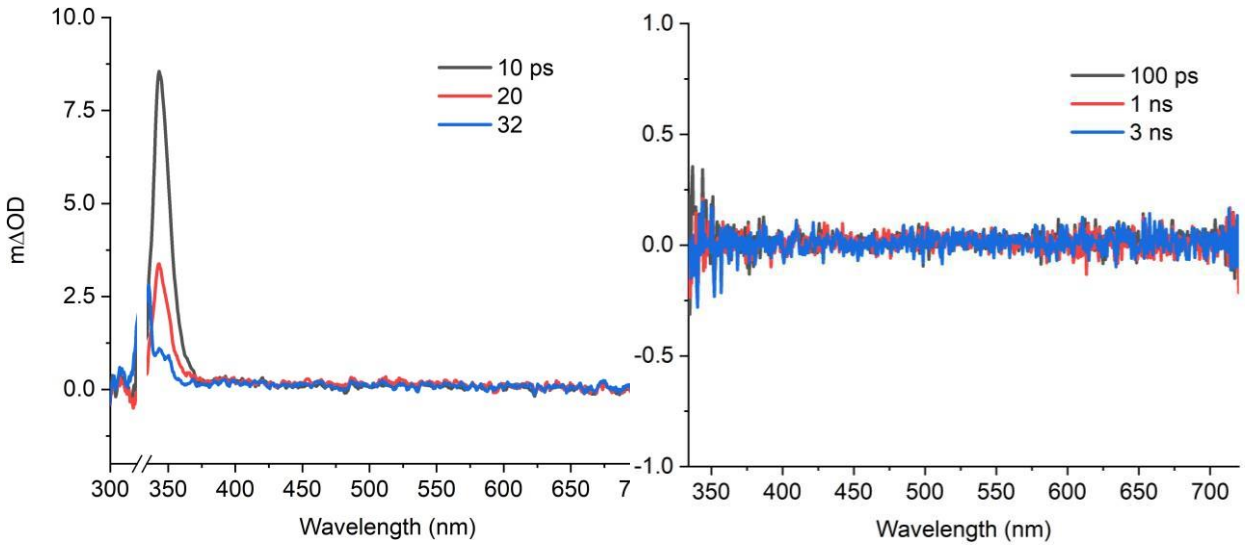

Figure 3.32. (Left) Evidence that the ESA in the TAS of **DS2** extends out to ~30 ps. (Right) Photoproduct scan of **DS2** showing no significant photoproduct after 100 ps.

To compare directly, the relaxation dynamics in both have sub ps excited state lifetimes followed by a few picoseconds of cooling, demonstrating a quick and efficient relaxation mechanism. On irradiating both samples in a closer-to-real-life irradiation environment such as a solar simulator, **DS2** is the more stable of the two molecules in this study. The persistent GSB in both the TEAS and TVAS studies of **DS1** could be linked to this degradation. The ~17 % population trapped in the excited state for **DS1**, while we believe it recovers at longer timescales based on how the monochromatic irradiation experiment showed no degradation, may have repercussions in a more complex environment; such as in a sunscreen formulation in the real world where it could react with other molecules and lose its UV protection.

3.2.8 Power studies of DS1 and DS2

As described in the Materials and Methods, power studies were also carried out on the samples of **DS1** and **DS2** used in the main study. These additional studies are included to show that the features in the TAS are due to single photon processes and not the result of multi-photon induced dynamics. Features are chosen on the TAS to cover the main assignments and a linear fit of gradient ~1 confirms a linear relationship between the beam power and the optical density. The data are presented in Figures 3.33. and 3.34.

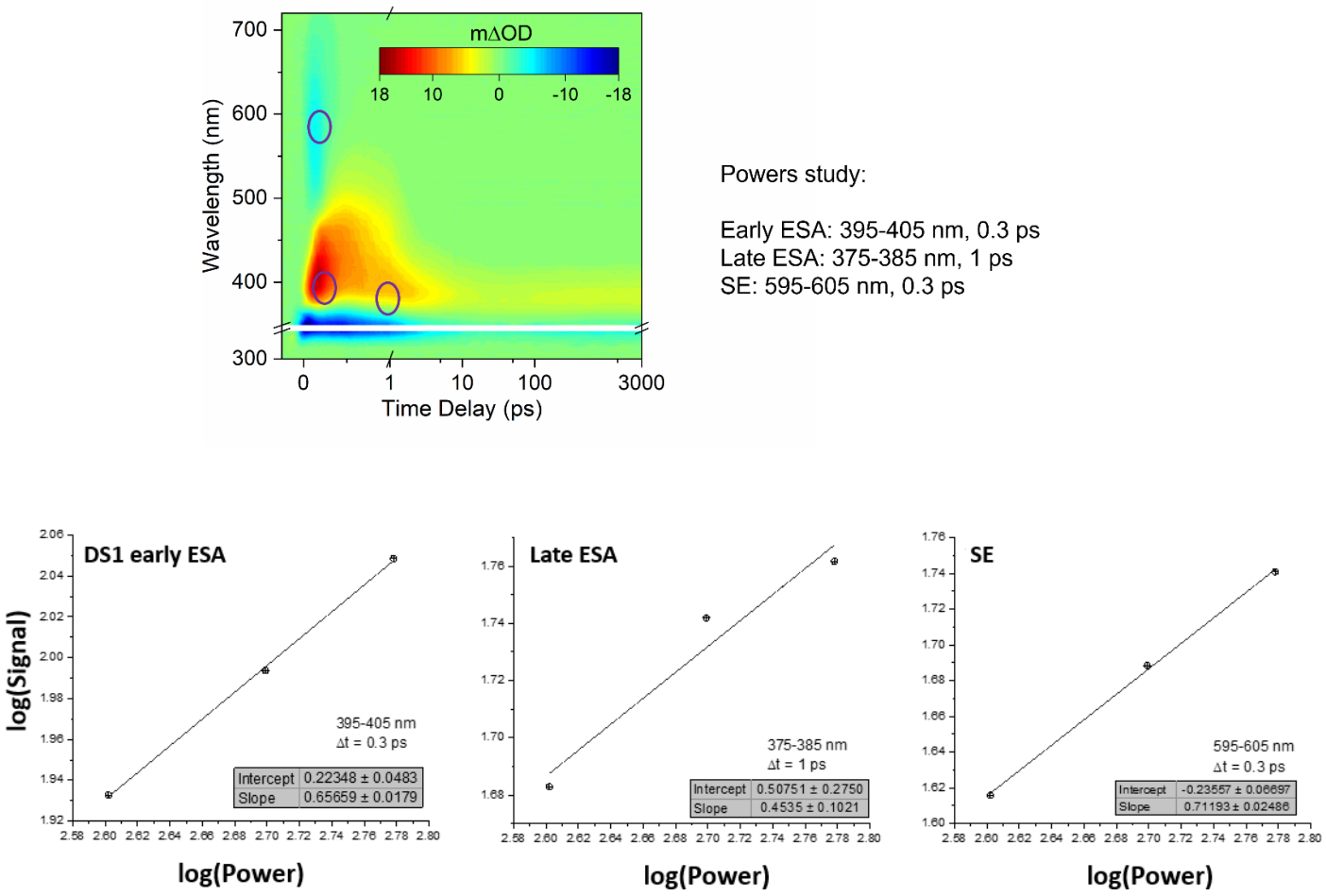

Figure 3.33. Power studies of **DS1.**

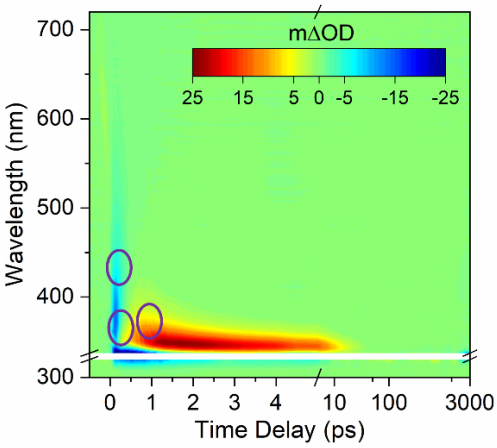

Powers study:

Early ESA: 360-370 nm, 0.3 ps
Late ESA: 375-385 nm, 1 ps
SE: 430-440 nm, 0.3 ps

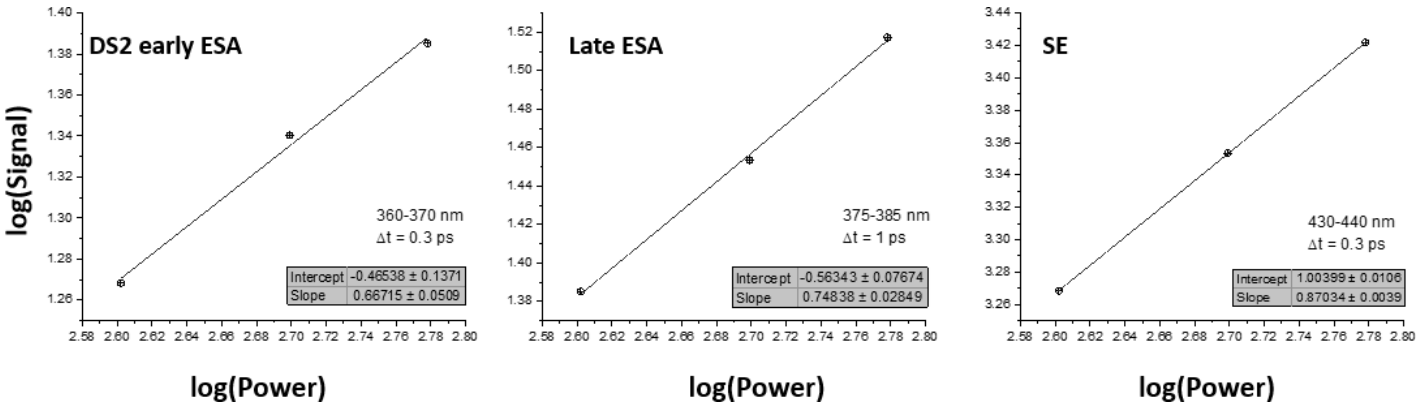

Figure 3.34. Power studies of **DS2**.

3.2.9 Investigating the response of the solvent to irradiation

It is also important to observe what occurs when the solvent alone (i.e., in the absence of any analyte) is irradiated under the stated conditions and it is standard to measure a solvent response or instrument response function (IRF) which defines the temporal resolution of the experiment. The solvent response from pure ethanol is shown in Figure 3.35, fitted with a Gaussian curve as described in the Fcc function in Chapter 1. This response curve is used to assign errors to the results; if the error from our fit is less than 50% of the IRF, 50% of the IRF is quoted as the final error.

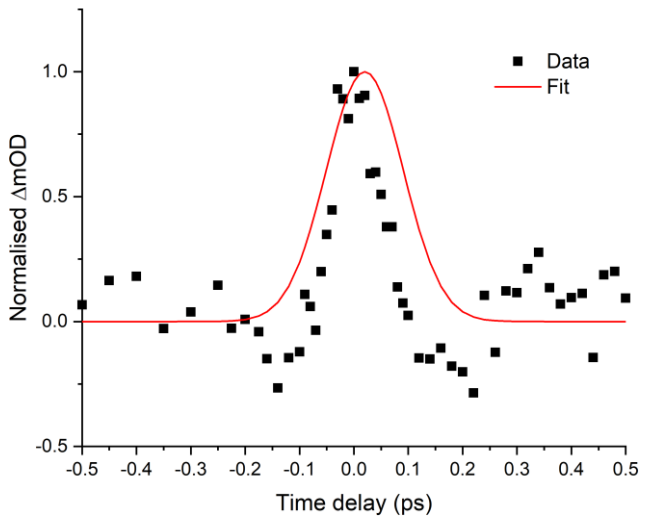

Figure 3.35. Solvent-only time-zero response of ethanol photoexcited at 341 nm. The black data points are the experimental signal at an average ~375 nm considering 3 wavelengths. The red-line is a frequency-dependent cross-correlation function (which takes into account any non-resonant contributions from the solvent and/or Harrick cell windows) and has been used previously to calculate the IRF in a related paper by our group using water as solvent.[31,32] The returned full width half maximum (FWHM) is 110 fs and corresponds to the FWHM of the instrument response function. The quoted errors in Table 3.4 are 60 fs which are half the FWHM of the instrument response function rounded to the nearest 10 fs.

3.2.10 Residuals

The residuals produced by the fit can be displayed in their own heat map (Figure 3.36) and they are a way of visualising how well the fit matches the experimental data. These are difference spectra and show the points that have been less well covered by our final fit. The residual values for **DS2** are relatively large around 4 ps and 350 nm (-2 mΔOD). Glotaran extracts lifetimes for a fixed EAD and the ESA in **DS2** blueshifts with time which is not captured by the τ_3 EAD. Including a shift within a fit is not possible within Glotaran.

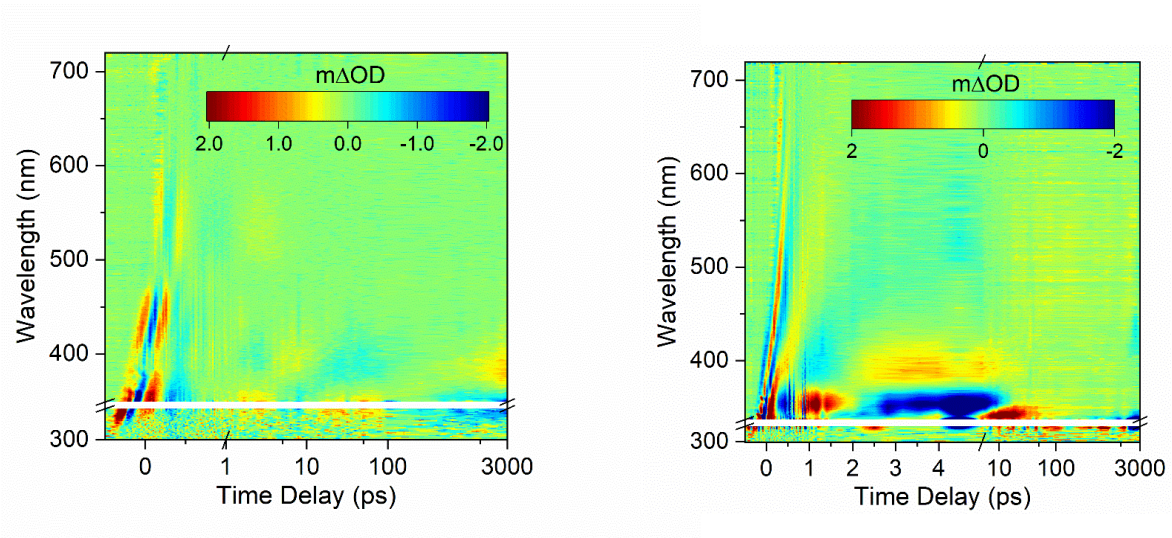

Figure 3.36. Heat map showing the residuals of the fit of **DS1** (left) and **DS2** (right). The residuals have not been chirp corrected.

3.2.11 Fluorescence of DS1 and DS2

Preliminary fluorescence results are displayed in Figure 3.37. The quantum yields are not quantified as they represent less than 1%. Our conclusion is that low levels of fluorescence are displayed by both molecules, suggesting that there are no significant trapped population or excited states that could present a barrier to sunscreen development.

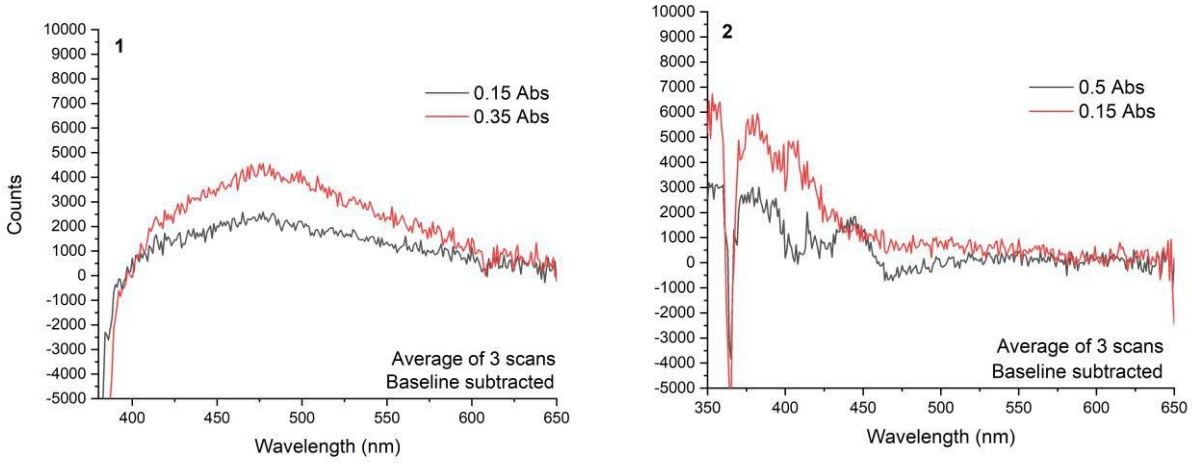

Figure 3.37. Steady-state fluorescence detection of **1** and **2**, demonstrating weak fluorescence in both molecules. Abs = absorbance in arbitrary units derived from the UV-vis spectra.

3.3 Chapter summary

In this chapter the essential cyclohexenone motif of the mycosporine family and the cyclohexenimine motif of the MAA family was explored by understanding the key scaffold structure of the MAAs natural products and trimming away the parts that are superficially non-essential for their application as sunscreens. Some ways in which the key enaminone and en-imine motifs can be synthesised are explored and this lays the ground for future work. Functionalisation of the motif (particularly with electron-rich oxygen) is then shown to redshift the absorbance profile, being practically essential to their function as UVA absorbers. The nature of the side-chain substituents (attached via N to the ring) is explored through a series of amino alcohol derived compounds with an MAA-like scaffold; and these were shown to be photostable through steady-state and ultrafast studies and there is now an opportunity to improve their purification and refine their synthetic protocols. Once those issues have been resolved, further studies into their safety profile could be conducted as their photostability is promising and resembles natural product MAAs. Two synthetic molecules, based on the cyclohexenimine scaffold, are explored in depth (**DS1** and **DS2**). At the beginning of the study, the photodynamics of both were expected to be slightly different despite sharing the same core structure; as suggested by previous studies. As we wait for the results of high-level computational studies to confirm (these are ongoing with our collaborators from the University of La Rioja, Spain), we hypothesise that the phenyl substituted **DS1** undergoes a C-N bond rotation as its predominant internal conversion mechanism after photoexcitation as previously defined by Losantos et al. due to how the phenyl substituents critically alter the potential energy surface; while **DS2** undergoes a ring-buckling (i.e. non-planar to planar relaxation) mechanism that is typical of all the natural product MAAs studied so far and discussed in the Introduction. As our photostability studies show, **DS2** is the more stable of the two molecules, perhaps confirming nature's choice of side-chain amino acids and aminols. Further studies could be conducted to ascertain whether the amino alcohol series follows the C-N bond rotation or ring-buckling mechanism; and whether this can also be linked to their photostability.

Chapter 4. Stabilisation of Avobenzone and Octocrylene in Composite Sunscreens (AVOCTOX and AVOCINN)

In this chapter a background is provided on avobenzone and octocrylene as sunscreen active ingredients. Experiments that probe the stability of avobenzone in binary mixtures with octocrylene and with synthetic mycosporine-inspired molecules are presented. Then the synthesis of a class of composite sunscreens designed by linking avobenzone and octocrylene derived moieties is discussed. Spectroscopy of the fused molecules is presented to show their stability and potential function as ultraviolet filters. Finally, computational results are presented for truncated versions of a subset of the molecules studied.

4.1.1 Background of avobenzone as a sunscreen ingredient

Avobenzone is a sunscreen active ingredient that is included in the Federal Drug Administration's (FDA) 1999 monograph of Sunscreen Drug Products for Over-the-Counter Human Use and in the European Chemical Agency's Allowed UV Filters under the Cosmetics Products Regulation.[1,2] In INCI (International Nomenclature of Cosmetic Ingredients) terms the compound is referred to as butyl methoxydibenzoylmethane (BM-DBM) but it is also found under a number of commercial names e.g., Parsol 1789, Eusolex 9020, Neo Heliopan 357 etc. To avoid confusion, its CAS number is 70356-09-1 (a unique number assigned by the Chemical Abstracts Service) and its structure is reproduced below in Figure 4.1. At the time of writing, avobenzone is approved under EU REACH (Registration, Evaluation, Authorisation and Restriction of Chemicals Regulations) but is under assessment as persistent, bio-accumulative and toxic. In 2010 apart from TiO_2 and oxybenzone, avobenzone was the only approved UVA filter world-wide.[3]

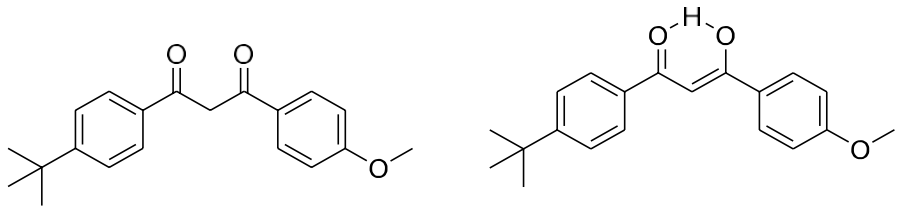

Figure 4.1. (Left) Diketo form of avobenzone and (right) one representation of the chelated enol form.

In a review of the evolution of sunscreen products in the United States, Wang and co-workers report how protection against UVA I irradiation (340-400 nm) was specifically emphasised with the introduction of dibenzoylmethane derivatives in 1979, with avobenzone as the most prominent member of this class.[4] In the same review the authors note how FDA approval of avobenzone (and zinc oxide) in 1997 led to an effective narrowing of the discrepancy between what is claimed on the packaging of a "broadband protection" sunscreen product and its actual protection. Indeed, the number of products containing a known UVA filter such as avobenzone (using sample sizes between 60 (in 1997) and 330 (2009)) increased from 5% to 70% in 12 years while UVA protection claims have remained relatively constant. This suggests that manufacturers had over-promised on UVA protection before the technology had been widely adopted.

4.1.2 Photofragmentation patterns of avobenzone

The photochemistry of dibenzoylmethane UVA filters was studied by Schwack and co-workers.[5] They reported that while UVA photodegradation was low in polar solvents (in their study: isopropanol and methanol), avobenzone was sensitive to UVA light in non-polar solvents (cyclohexane and isooctane). This finding is significant to sunscreens as high screening efficiency cannot be guaranteed if there are photochemical pathways that are in competition with non-radiative relaxation and that ultimately can lead to loss of UV absorbing activity and the production of side-products. In the aforementioned study, a total of about a dozen photoproducts were identified by HPLC and GC-MS during an 8 hour solar-simulated irradiation in cyclohexane and some of these are summarised in the photodegradation scheme in Figure 4.2.

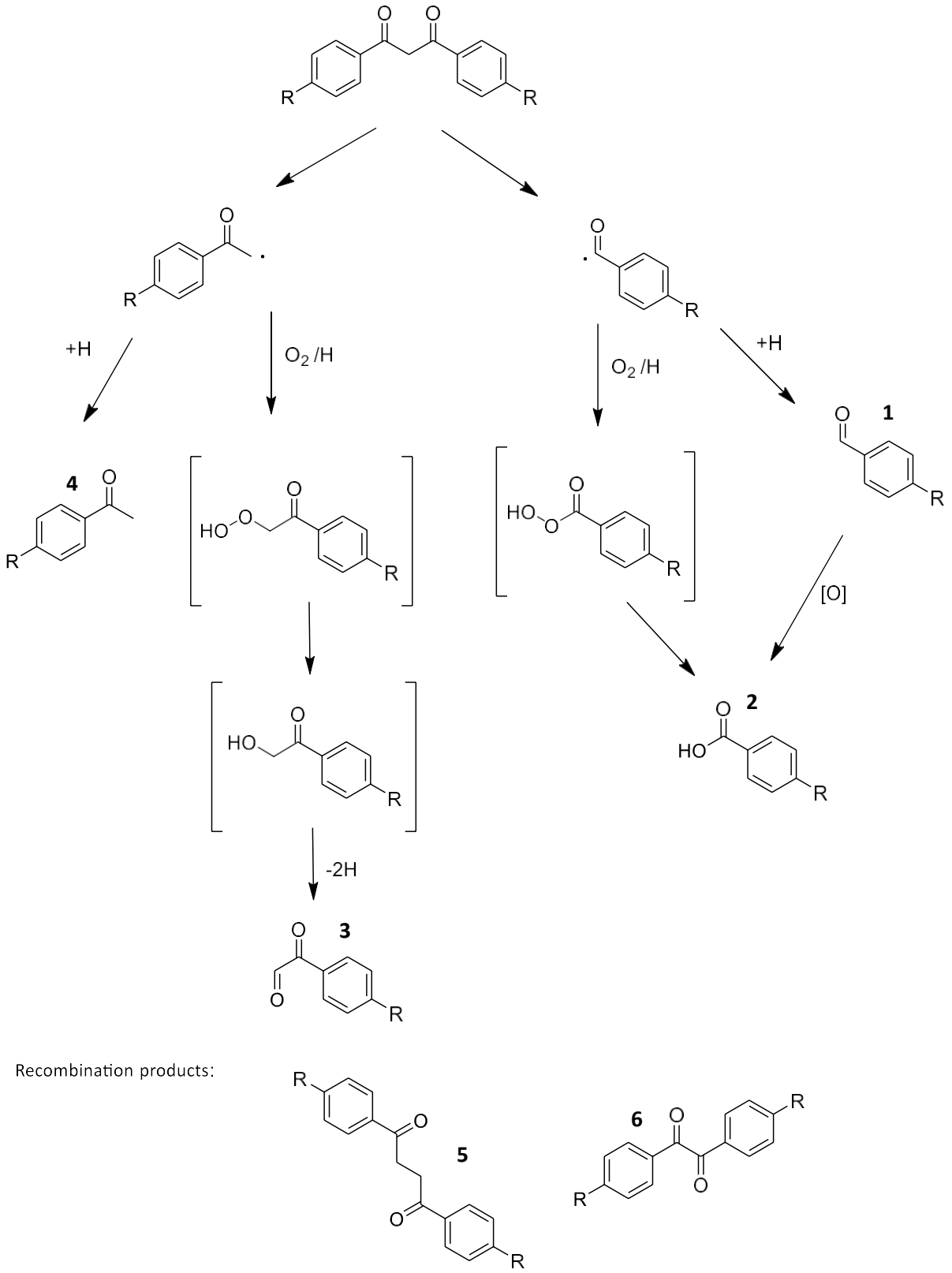

Figure 4.2. Photodegradation scheme reproduced from ref.[5] Reading the final products in a clockwise direction: **1**. benzaldehyde, **2**. benzoic acid, **3**. phenylglyoxal, **4**. acetophenone. The recombination products from left to right are **5**. dibenzoylethane and **6**. benzils.

In all cases of photodegradation, it is suggested that tautomerisation to the diketo form of avobenzone precedes fragmentation in non-polar solvents. Evidence for this can be found in complementary NMR studies that demonstrated that while the tautomerisation equilibrium always lies towards the enol form, around 3.5% was detected in the diketo form in cyclohexane-d_{12} while none was observed in deuterated polar solvent; and significant fragmentation was only observed in the deuterated cyclohexane solvent. A contemporary study by Roscher and co-workers identified only *p-tert*-butylbenzoic acid and *p*-methoxybenzoic acid as products from an extended irradiation. The fewer products in this latter study can be attributed to the higher irradiance and longer irradiation times used. In addition, that study suggests that the benzoic acids are the most stable photoproducts observed.[6] The carbon-centred free radicals (benzoyl and phenacyl radicals) proposed by Schwack as the key intermediate in the fragmentation pathway were additionally observed experimentally by electron-spin resonance (ESR) spectroscopy signals that persist for several minutes after cessation of irradiation.[7]

4.1.3 Conformers present in avobenzone solutions

In a standard ethanolic solution of avobenzone, a UV absorption band around 356 nm with ππ* character is assigned to the convolution of two practically degenerate *cis* enols that are stabilised by an intramolecular hydrogen bond between the 1,3-dicarbonyl moieties.

Steady-state irradiation of solution phase avobenzone leads to the appearance of the tautomeric keto form with an absorption of nπ* character at 265 nm; a wavelength that has been implicated in avobenzone photoinstability; and supportive of the previous inference that the diketo form is a key intermediate in degradation.[8,9] A full characterisation of the chemistry of avobenzone is complicated by the presence of various tautomers and conformers. Laser (nanosecond) flash photolysis studies by Cantrell and co-workers revealed that the ground-state chelated enol form is in equilibrium with the diketo form (as discussed above) as well as two non-chelated enols that can be accessed by 355 nm laser light and rotation of the C-C bond to form the Z-isomer or the C=C bond to form the E-isomer, possibly involving an excited state intramolecular proton transfer.[10] The decay rates of the two non-chelated enols demonstrates a strong solvent dependence which is reflected in the variation in recovery time of the ground-state in different solvents.

Generally, the experimental recovery rate of the chelated enol is slowest in acetonitrile, intermediate for cyclohexane and fastest in polar, protic solvents methanol and ethanol.

An excited state of the diketo form can also be accessed directly by 266 nm light. A change in absorption of the system is attributed to how the internal conjugation is perturbed as the molecule tends away from linearity. Indeed, during photochemical ketonization the molecule tends away from planarity, which is generally true of β-dicarbonyl compounds.[11] A proposed wavelength-dependent mechanistic sequence based on Cantrell's findings is reproduced in Figure 4.3, beginning with the chelated enol form (top left). Note that the triplet excited state of the diketo form is symbolised by a superscript *.

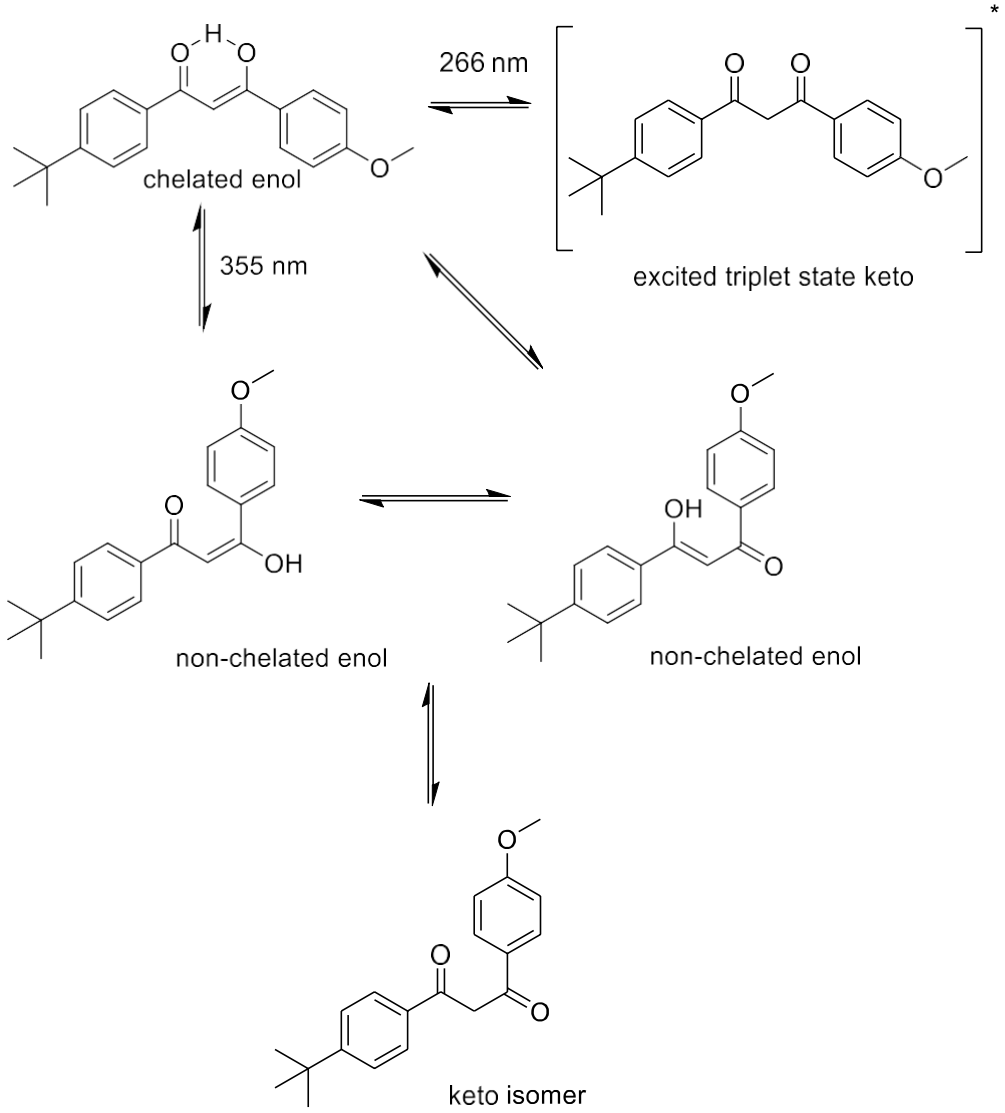

Figure 4.3. Mechanistic sequence based on Cantrell's findings in ref[10].

From this scheme, it may be concluded that any way to stabilise the ground-state chelated enol form and avoid formation of the excited triplet state keto will also stabilise the molecule against photodegradation. This could include by means of formulation in emollients of appropriate stabilising polarity, encapsulation, by including antioxidant additives such as glutathione or, as will be explained below, by modifying the structure of the molecule itself to shift the equilibrium towards the enol form; supported by a number of studies.[12–16]

4.1.4 Ultrafast Photoprotective Properties of Avobenzone

Holt and co-workers extended the work of previous researchers by investigating the ultrafast dynamics of avobenzone in ethanol, cyclohexane and two common emollients (di-isopropyl adipate and lauryl lactate). In all cases, after laser pulse excitation at 350 nm, evolution of the chelated enol form out of the Franck-Condon region was described by an initial time constant, τ_1 on the order of 100s.[17] While it is possible that there are additional ultrafast processes occurring within this time for a portion of the excited molecules, such as excited-state intramolecular proton transfer, or rotation around the C–O single bond of the hydroxyl group to form non-chelated enol avobenzone species, the closeness of τ_1 to the instrument response function meant that other branching pathways could not be confirmed in this experiment. Decay of the initially excited S_1 state by stimulated emission then occurred with second time constant, τ_2; with a faster decay in the non-polar solvent compared to the polar solvent. It is noted that that the 1-2 ps duration of this SE is probably too short to describe fluorescence (i.e., natural release of a photon), as the latter typically occurs on a nanosecond or greater timescale (see Introduction); but is rather a photon-catalysed SE process. However, measurements conducted by Bonda and co-workers proposed a fluorescence lifetime of the enol form to be 13 ps.[18] An offset that persisted beyond the window of the experiment was attributed to the formation of a triplet state of enolic avobenzone (i.e., $^1\pi\pi^* \rightarrow {}^3n\pi^*$) which agreed with TD-DFT calculations by Holt et al. The relaxation of vibrationally hot chelated enol form to the ground state was described by a third time constant, τ_3 (~8 ps); and incomplete ground-state recovery is described by a final fourth constant, τ_4 (> 2.5 ns). The observed incomplete ground state recovery is attributed to the formation of triplet states, or an excited state that undergoes ISC to form the triplet state; and the formation of photoproducts. A final significant

observation in the cited paper was that changes in concentration (between 1 mM and 10 mM) and changes in temperature (room vs. skin temperature) had no significant impact on the observed photoprotection mechanism. Avobenzone's strong absorption in the UVA recommends its use as a sunscreen but the possibility of side-reactions evidenced by incomplete ground-state recovery suggests that there is opportunity for improvement.

4.1.5 Previous work on substituted dibenzoylmethane derivatives

Substituted dibenzoylmethane derivatives may be prepared by condensation of a ketone with an ester in the presence of a strong base as recorded in several patents. As well as avobenzone, isopropyldibenzoylmethane (tradename Eusolex® 8020) and butylmethoxydibenzoylmethane (PARSOL®) are typical commercial dibenzoylmethane derivatives. Patent WO2012084770 protects the formation of the potassium salt of dibenzoylmethanes via the reaction in high-boiling point organic solvent (Figure 4.4):

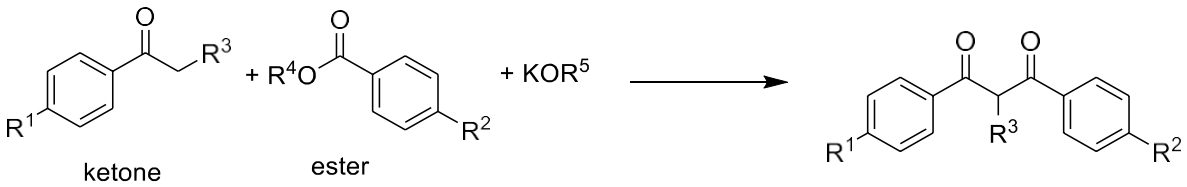

R^1 and R^2 chosen from H, alkyl, alkoxy, alkenyl and alkenyloxy
R^3 is H
R^4 and R^5 are alkyl

Figure 4.4. Formation of dibenzoylmethanes via reaction of a ketone and an ester.

In situ formation of side-product alcohols arising from the -OR group of the ester is solved by distillation of the alcohols and subsequent hydrolysis of the salt yields the desired compound.

In the patent literature the formulae depicted in Figure 4.5. were protected by Hopp et al. US Pat., 4,562,067, 1985 (left) and Raspanti et al. US Pat., 5,776,439, 1998 (right):

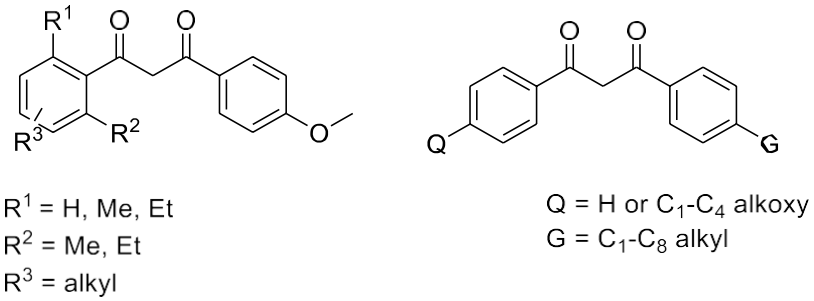

Figure 4.5. Historical patents for dibenzoylmethanes

In a synthetic study by Moi *et al.* the -OMe group of avobenzone (Figure 4.6) is replaced with an acid in 4-(3-(4-(tert-butyl)phenyl)-3-oxopropanoyl)benzoic acid (POBA) and an ester moiety in methyl 4-(3-(4-(tert-butyl)phenyl)-3-oxopropanoyl)benzoate (POBE) via condensation of 4-*tert*- butyl acetophenone and 4-formyl benzoic acid to form an intermediary chalcone.[19] The chalcone was submitted to bromination and then hydrolysis to yield POBA.

Esterification of the acid using methanolic thionyl chloride yielded the ester. These modifications are sensibly chosen if UV activity is to be retained relative to the parent avobenzone molecule as they are distant to the essential 1,3-dicarbonyl unit that absorbs in the UVA in the enol form.

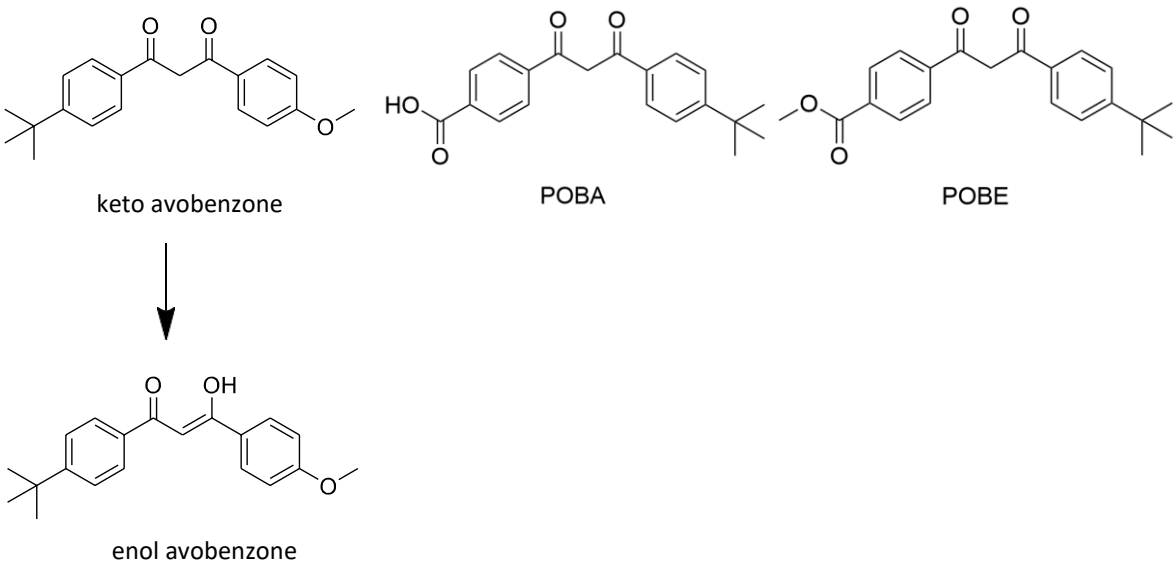

Figure 4.6. Molecules studied by Moi et al.[19]

The experimental UV activity of POBA and POBE in the steady state are broadly similar to avobenzone, allowing for a shift in the enol maximum absorbance peak slightly to 352 nm and the keto form to 255 nm. An increase in the keto forms during extended irradiation of

both (2) and (3) were observed in acetonitrile which is consistent with the behaviour of avobenzone.

In the cited paper by Moi and co-workers, photodegradation in all molecules (using the concentration of the enol form as the initial concentration with natural sunlight as source) was observed and attributed to Norrish Type 1 cleavage (CO-C) products, i.e., producing carbon-based radicals after ketonization; also consistent with other avobenzone studies cited above. After a total of 6 hours' irradiation, avobenzone and POBE had degraded completely (i.e., half-life ~ 3 hours) but POBA had not yet reached 50% degradation; indicating that POBA has a half-life longer than 6 hours. Further analysis indicated that in all solvents tested (ethanol, acetonitrile, DMSO and ethyl acetate) the POBA was more stable than avobenzone, and apart from in ethanol, the POBE was also more stable than avobenzone. While a detailed mechanism is not proposed in the paper, computational evidence that the bonds next to the carbonyls are strengthened in the excited state by both substitutions, and therefore experience increased stability to α-cleavage, would support the increased stability overall.

The results of this study were promising and showed that apparent photostability can be improved with simple modifications to the structure of avobenzone. Moreover, this study indicated that replacing the electron-donating -OMe group with an electron withdrawing group such as -COOH/-$COOCH_3$ has beneficial effects, including improved photostability, greater percentage recovery and better photostabilisation by glutathione. This opens the possibility of investigating a whole range of different modifications to the benzophenone unit that could explore the electronic and steric effects of different substituents.

Other studies have investigated how blocking the keto-enol tautomerisation can facilitate the study of the pure diketo form.[20] In one study, Wang and co-workers chose four molecules with different substituents on the C2-position of the 1,3-dicarbonyl (the α-carbonyl position in Figure 4.7.). In all cases the keto-enol tautomerisation was blocked efficiently.

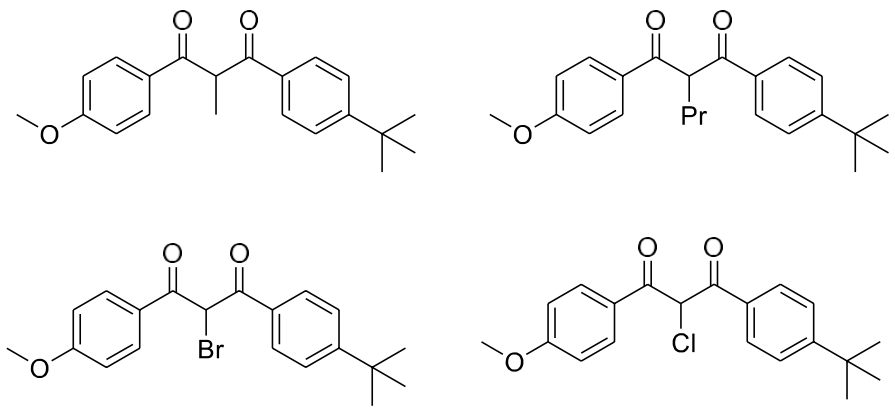

Figure 4.7. Differently α-substituted dibenzoylmethanes discussed in the text.

4.1.6 Interaction of avobenzone with other molecules

The diketo form of avobenzone that can be excited to form a triplet and/or the carbon-based radicals discussed above are potentially reactive towards biological substrates and indeed the photosensitizing ability of avobenzone has been illustrated in a number of studies where it is observed in increased cytotoxicity in human keratinocytes;[21] lipid peroxidation;[22] and direct strand breaks in plasmid DNA.[23]

Avobenzone is thought to have synergistic effects with other sunscreen additives, and it could potentially react with any of the other components in a complex formulation. In one article, the photo-generated fragments from avobenzone led to DNA-toxic photoproducts when irradiated with cinnamate filters such as octinoxate or EHMC, as well as the concurrent loss of UV activity.[24] The identified mechanism followed a [2+2] cycloaddition of the enolic form of the diketone to the electrophilic alkene, followed by ring-opening in the well-known De Mayo reaction (Figure 4.8).[25]

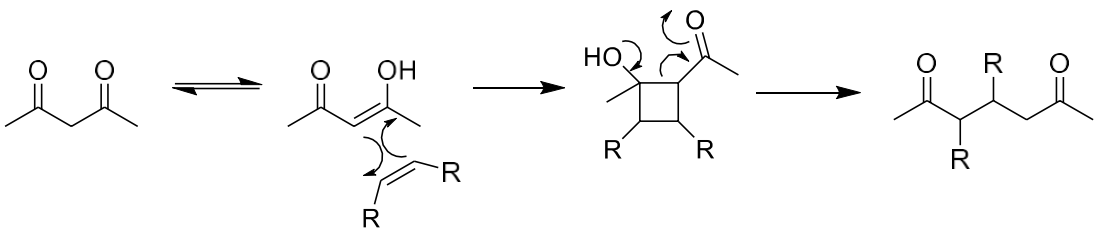

Figure 4.8. Reactive pathway identified for avobenzone fragments.

4.1.7 Background of octocrylene as a sunscreen ingredient

The UVB/short-UVA absorber octocrylene (Figure 4.9) is an ester formed by the condensation of diphenylcyanoacrylic acid with 2-ethylhexanol, and in sunscreen taxonomy belongs to the cinnamate family.[26] In INCI terms it is also known as 2-cyano-3,3-diphenyl acrylic acid or 2-ethylhexyl ester. Its CAS number is 6197-30-4. It is currently allowed up to 10% by weight in a formulation under the same Cosmetics Products Regulation.

Octocrylene has excellent photostability and thus it is included in sunscreens to increase the overall stability of the formulation.[27] The combination of avobenzone and octocrylene has seen a rapid increase in popularity in recent years. One study from the United States noted how the avobenzone/octocrylene combination was not present at all in 48 chosen products in 1999; increasing to 12% in 118 products in 2003; then further to 54% of 141 products in 2009.[4] In the United Kingdom in 2010, 91% of 337 commercial sunscreens contained octocrylene, a 2.5-fold increase from 2005.[28,29]

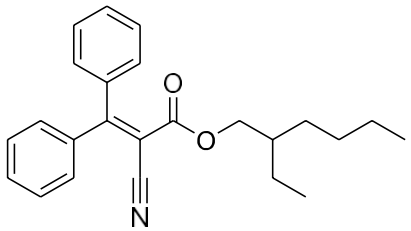

Figure 4.9. Octocrylene structure. NB: undefined stereocenter.

4.1.8 Photoprotective properties of octocrylene

As octocrylene shows no significant fluorescence or phosphorescence, this suggests that ultrafast processes outcompete spontaneous emission.[30] In other cinnamates, the dominant relaxation pathway has been shown to be isomerisation around the C=C double bond.[31] Baker and co-workers identified a minor relaxation pathway that suggested the presence of a long-lived triplet state in the ultrafast transient electronic absorption spectra of octocrylene in both methanol and cyclohexane.[32] It is thought that this triplet state, which can be prepared through collision with avobenzone in the excited state, can thus improve avobenzone stability.[33] Baker et al. also do not rule out the possibility of a long-

lived charge transfer state due to the -CN substituent. Their working hypothesis for a description of the excited state dynamics in the pump-probe experiment is a $\pi\pi^* \leftarrow S_0$ transition caused by the pump pulse. Then an ensemble of close-in-energy $n^1\pi\pi^*$ states decay to a lower excited state in τ_1. Another excited state $^1\pi\pi^*$ is in turn populated in τ_2. A third time constant, τ_3 describes relaxation of the population in the $^1\pi\pi^*$ state. Finally, almost full recovery of octocrylene ground-state is described by τ_4 in a process mediated by a combination of intramolecular vibrational energy redistribution and vibrational energy transfer to the surrounding solvent molecules and/or isomerisation around the C=C double bond. While there are complexities around the assigning of absolute values for τ_n, a clear overall picture of the relaxation dynamics in octocrylene emerged:- UV-B photoexcited octocrylene undergoes ultrafast non-radiative relaxation which repopulates the ground state with high efficiency. The excited state dynamics are over in the first ~5 ps after photoexcitation, with most of the processes over within the first 2 ps of photoexcitation.

4.1.9 Reactivity of octocrylene

Octocrylene has been implicated in contact and photo-contact allergies.[34,35] Karlsson and co-workers have shown that octocrylene reacts in the dark with benzylamine via a retro-aldol condensation reaction to form benzophenone-*N*-benzylimine (see Figure 4.10).[36] In the excited state (in the presence of light) a new reaction pathway outcompetes the former to form *N*-benzyl-2-cyano-3,3-diphenylacrylamide.[27] The increased reactivity in the excited state as well as different hapten-protein interactions arising from the different products could explain the higher incidence of photo-contact allergy compared to contact allergy in octocrylene studies. In real settings the interaction between octocrylene and amino acid lysine, or indeed other nucleophilic amino acids, could lead to analogous products to those in the study.

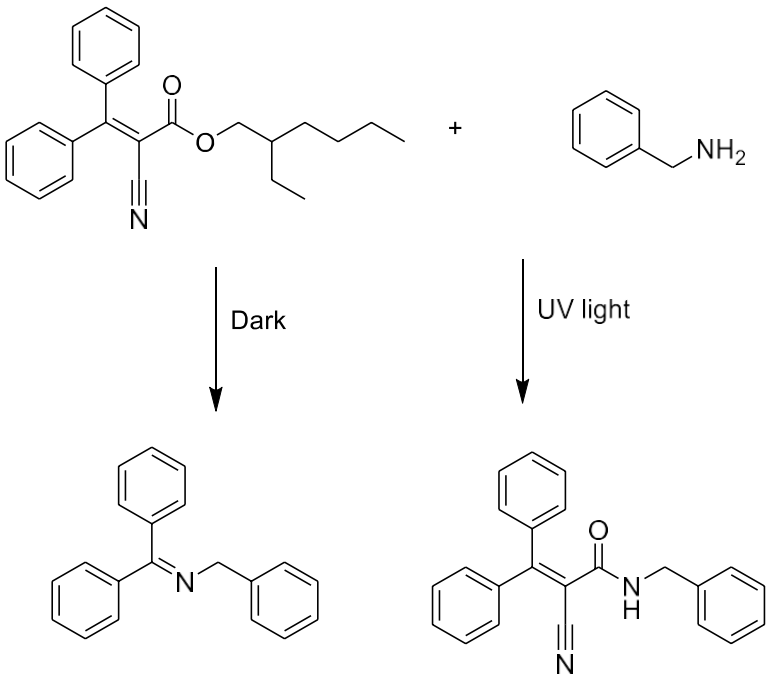

Figure 4.10. Reaction occurring between octocrylene and a molecule containing a nucleophilic N atom.

Other studies have shown that octocrylene is capable of forming deposits inside the lipid phase of the stratum corneum.[37] This is attributed to octocrylene's lipophilicity and is a significant parameter that has to be taken into account in formulating sunscreens.

Sunscreen active ingredients must remain on the skin surface (i.e., on top of the stratum corneum), creating a barrier against UV radiation without epidermal penetration. One synthetic study confirmed that the lipophilicity can be reduced by making a series of octocrylene analogues in two steps from cyanoacetic acid starting material.[38] Esterification of the acid with an alcohol and a niobium pentachloride catalyst in toluene gave the cyanoacetate. Knoevenagel condensation between the cyanoacetate and an aldehyde with catalytic piperidine base in dry toluene under Dean-Stark conditions gave the acrylate, analogous to octocrylene. Simply removing one of the phenyl rings adjacent to the double bond and functionalising the remaining ring produced a series of promising UVA and UVB filters.

4.1.10 Triplet energy transfer

It is thought that the majority of photostabilisers on the market function act as quenchers of avobenzone's diketo triplet state.[39] Energy can transfer efficiently between a triplet donor and acceptor when the respective energies are within 1-2 kcal (i.e. 4.18-8.37 kJ) of eachother.[40] Triplet state energies can be directly measured using oxygen perturbation, which involves measurement of the absorption spectrum under 2000 psi oxygen to allow for direct absorption from the ground state to the first triplet state.[41,42] The result can be compared with phosphorescence data to obtain a good estimate of the triplet state energy (E_T). Gonzenbach and co-workers determined an E_T of 62 kcal/mol (260 kJ/mol) from phosphorescence data and an E_T of 59.5 kcal/mol (248.7 kJ/mol) with the oxygen enhanced spectrum for the enolic form of avobenzone. While these are in good comparison, the value of 248.7 kJ/mol is thought to be more precise. For comparison, a literature search revealed the lowest singlet excited state (E_S) of avobenzone (enol form) to be 73.2 kcal/mol (306.2 kJ/mol);[30] and the lowest excited triplet state of avobenzone (diketo form) to be 72 kcal/mol (301 kJ/mol).[6] The energy level of the T_1 state of the keto form is much higher than that of the T_1 state of the enol form, implying that the active triplet is the diketo (see Figure 4.11 below for a summary).

In a different study by Kikuchi and co-workers, the excited states of avobenzone and a bis-alkylated analogues were reported. The single state energy (E_S) was obtained from the intersection point of the UV absorption and fluorescence spectra and the triplet state energy (E_T) was obtained from the first peak of phosphorescence in ethanol at 77 K.[43]

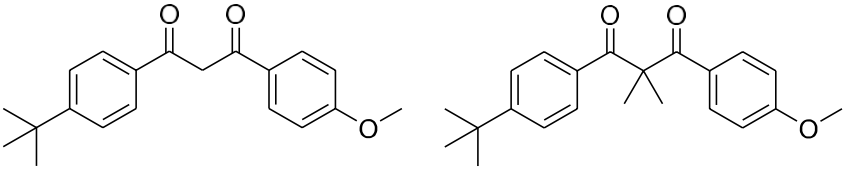

E_S(enol) 306.2 kJ/mol	-
E_S(keto) ND	E_S(keto) 322.0 kJ/mol*
E_T(enol) 248.7 or 244.0* kJ/mol	-
E_T(keto) 301.0 or 291.9* kJ/mol	E_T(keto) 293.1 kJ/mol*

Figure 4.11. Energies of the singlet and triplet states (of the two main forms) as summarised in the text. Energies* from Kikuchi et al. were converted to kJ/mol from cm^{-1} by multiplying by hcN_a. ND – *Not determined*.

The key process is the interaction of the singlet and triplet states. The S_1 state of the keto form of avobenzone possesses mainly a $^1n\pi^*$ character, whereas that of the enol form possesses a $^1\pi\pi^*$ character. The intersystem crossing (ISC) between [the singlet] $^1n\pi^*$ and [the triplet] $^3\pi\pi^*$ states should be much faster than that between $^1\pi\pi^*$ and $^3\pi\pi^*$ states, as suggested by El-Sayed's selection rule.[44]

A further prerequisite for a transfer process to occur is a limit of intermolecular distance between a donor and acceptor molecule. For triplet-triplet interaction this distance is about 1 nm, compared with the longer distance of ~10 nm for singlet-singlet processes.[45] To assess whether the mean free path (*p*) of the molecules in a given solution is on the order where such processes can occur, the equation:

$$p = \frac{1}{\pi \cdot n \cdot d^2}$$

can be used, where n is the number of molecules per volume (mols/L) and d is the molecular diameter (nm).[46] If an approximate diameter of a typical sunscreen molecule is 1 nm then a lower limit on the concentration for a triplet-triplet process could be approximated by:

$$n = \frac{1}{\pi} = 0.3183\ mols/L$$

Note here that this concentration is much higher than the concentration used in our steady-state irradiation studies. In contrast the concentrations used in real formulations exceed this lower limit by many orders of magnitude. Using the maximum concentration threshold from the 'Cosmetic Products Regulation, Annex VI - Allowed UV Filters' for avobenzone (=5%, molecular weight = 310.39 g/mol) and octocrylene (=10%, molecular weight = 361.48 g/mol), using an estimate for the average body surface area of an adult (=1.79 m^2)[47], applying the NHS recommended two tablespoons (~30 g) gives approximate concentrations of avobenzone and octocrylene, respectively, as:

$$n = 5\% \ \times \frac{30\ g}{179\ L\ x\ 310.39\ g/mol} \times \frac{6.022\ x\ 10^{23}}{mol} = 1.63\ \times\ 10^{19}\ mols/L$$

$$n = 10\ \% \ \times \frac{30\ g}{179\ L\ x\ 361.48\ g/mol} \times \frac{6.022\ x\ 10^{23}}{mol} = 2.79\ \times\ 10^{19}\ mols/L$$

4.1.11 Octocrylene as quencher (via triplet-triplet energy transfer)

Herzog and co-workers studied the photostabilisation of octocrylene on avobenzone.[46] The Jablonski diagrams for the systems studied are reproduced below (Figure 4.12) from the above reference:

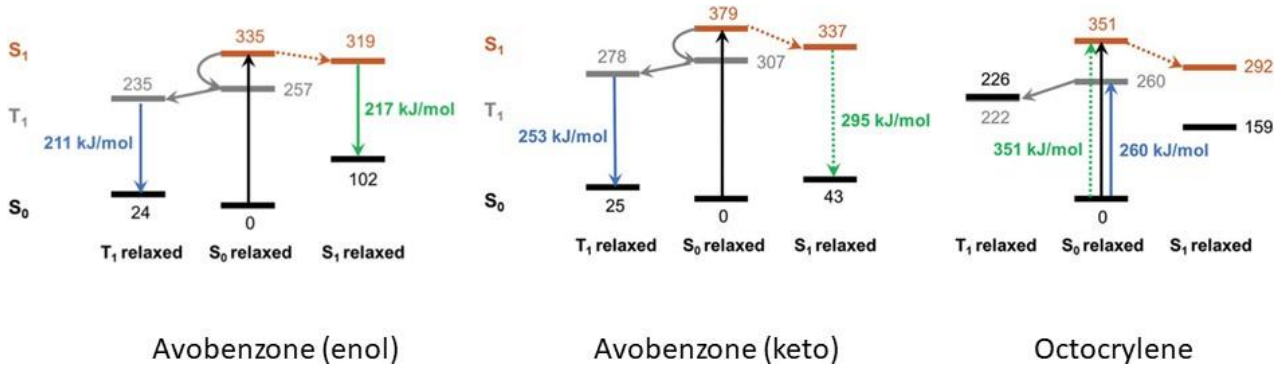

Figure 4.12. Jablonski diagrams from ref.[46]

In their quantum chemical computational analysis, singlet-singlet energy transfer between the relaxed singlet excited state of the keto form of avobenzone and ground-state octocrylene is shown not to be likely due to the large energy difference (295 kJ/mol vs 351 kJ/mol). In contrast, triplet-to-triplet energy transfer is more likely between the relaxed triplet state of the keto form and the ground-state of octocrylene (253 kJ/mol vs 260 kJ/mol). To support their hypothesis of a quenching effect between avobenzone and octocrylene, experimental data were obtained. All emulsions in which the molecules were combined showed a significant increase in photostability; even when the background effect of spectral overlap was considered.

4.1.12 Role of the *tert*-butyl and methoxy groups in para-substitution to the carbonyl

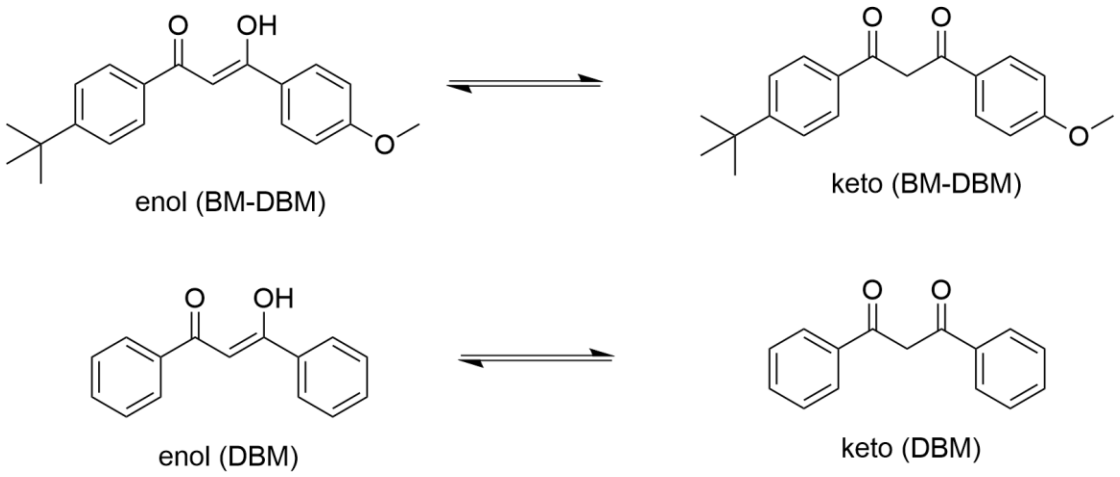

Figure 4.13. Molecules studied by Kikuchi et al.[43]

As a starting point for any discussion for the difference in stabilities between the variously substituted **AVOCTO** compounds in the following sections, reference can be made to the effect of para-substitution with electron donating groups (EDGs) on aromatic carbonyls (Figure 4.13) as studied by phosphorescence, optically detected magnetic resonance, and other optical techniques by Kikuchi et al.[43] There is near degeneracy between the T_1 and T_2 states in many studied aromatic carbonyls which may be explained by the large spin-orbit coupling constant of the carbonyl oxygen and its important role in the mixing between the T_1 $^3\pi\pi^*$and T_2 $^3n\pi^*$ states and singlet states. The S_1 state of the keto form of BM-DBM possesses mainly $^1n\pi^*$ character, whereas that of the enol form possesses mainly $^1\pi\pi^*$ character. The intersystem crossing (ISC) between [keto] $^1n\pi^*$ and $^3\pi\pi^*$ states should be much faster than that between [enol] $^1\pi\pi^*$ and $^3\pi\pi^*$ states, as suggested by El-Sayed's rule. The energy of the T_1 state (mostly $^3\pi\pi^*$) is reduced by the effect of para-substitution with an electron donating group while the energy of the T_2 state (mostly $^3n\pi^*$) is increased; as observed experimentally when benzaldehyde is compared to p-methylbenzaldehyde and p-methoxybenzaldehyde.[48] Kikuchi and co-workers observed an increase in the T_1 lifetime with avobenzone-like molecules substituted with *tert*-butyl and methoxy groups (i.e. BM-DBM vs. DBM) and offered an explanation for the effect of para-substitution in lengthening the triplet state lifetimes: the purity of the T_1 state is recovered by an electron-donating substituent because the $^3\pi\pi^*$ excitation energy decreases. A longer triplet lifetime means

that the excited state molecule remains in a high energetic state for longer and thus has a greater probability of reacting further, a property that is unfavourable to its use as a sunscreen. In this thesis, the effect of an electron-withdrawing group (EWG, i.e. -Cl) is studied along with EDGs (-OMe,-*t*Bu).

4.2 Design of AVOCTO molecules

The name **AVOCTO** is used for ease of reference and is a portmanteau, coined from joining the names of the two main chromophore units; one of which is derived from avobenzone and the other from octocrylene. The idea of covalently bonding known sunscreens together was explored in a US patent (U.S. Pat. No. 10143642B2, 2018)[49] where avobenzone and octocrylene were attached to inert cholic acid. Cholic acid is a steroid acid that naturally occurs in human bile with the structure in Figure 4.14 below. In the same figure is the structure of the proposed sunscreen.

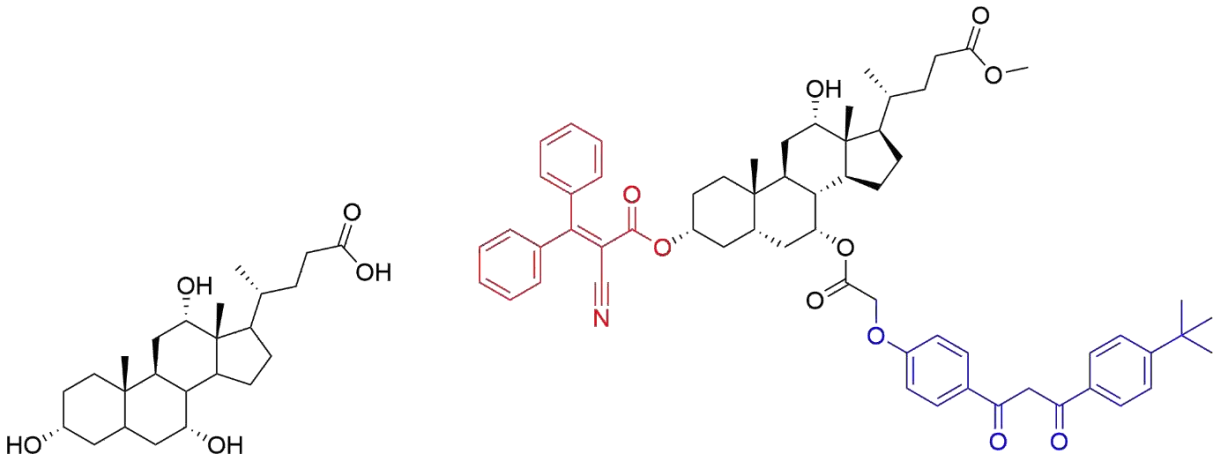

Figure 4.14. (Left) Cholic acid. (Right) Composition of the sunscreen molecule proposed in the patent cited in the text with the inert derivatized methyl ester of chenodeoxycholic acid in black, the UVB chromophore from octocrylene in red and the UVA chromophore from avobenzone in blue.

The photostability of the sunscreen was measured in the presence of UV radiation (5.5 mW/cm^3), irradiated on plates and quantified by ultraviolet absorption densitometry analysis; and showed a significant improvement in stability versus the avobenzone and octocrylene controls. This study gave confidence that a simpler inert linker could produce a similar improvement in stability. It is additionally worth noting that there is no significant change to the peak maxima of each chromophore compared to the parent molecules; indeed, in the patent the peak maxima of the composite molecule are reported as 358 nm and 290 nm.

Given the above, a series of five molecules (AVOCTO1-5 or AVOCTOX) was designed to investigate the effects of electronegativity and the effects of linking chromophores; summarised by the generalised structure below (Figure 4.15.):

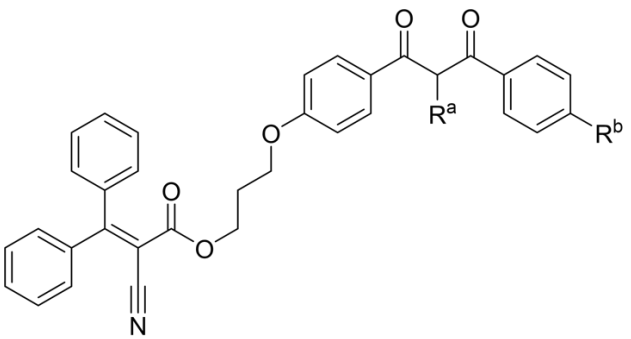

AVOCTO **1** R^a = H, R^b = H
2 R^a = H, R^b = *t*-Bu
3 R^a = CH_3, R^b = H
4 R^a = H, R^b = OCH_3
5 R^a = H, R^b = Cl

Figure 4.15. Generalised structure of AVOCTO compounds.

Synthetic details of the forward synthesis are reported in the Materials and Methods. The final step in the forward synthesis is an ester synthesis, which was achieved by a Steglich esterification (an ester coupling reaction). A simple retrosynthesis (Figure 4.16) suggests an alcohol and a carboxylic acid that could be synthesised from known starting materials and then coupled. Typical reactants for this transformation are coupling agent dicyclohexyl carbodiimide (DCC), base/catalyst 4-dimethylaminopyridine (DMAP) and coupling additive 1-hydroxybenzotriazole (HOBt).[50]

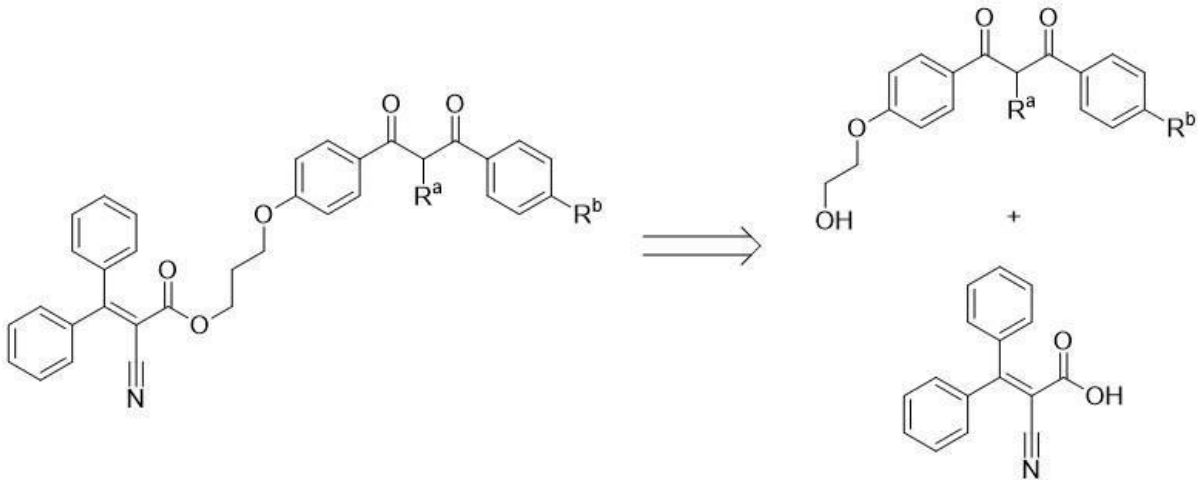

Figure 4.16. Retrosynthesis of **AVOCTO** compounds, illustrating the final esterification required.

A literature search uncovered a synthetic study by Lutjen and co-workers where cinnamic acid derivatives were coupled with ethanol using modified Steglich conditions using EDC as the carbodiimide and acetonitrile as the solvent.[51] This methodology was developed in preference to the use of the Fischer esterification or use of acyl chloride intermediates and we found that the Steglich conditions of DCC/DMAP/HOBt worked well for our purposes

4.2.1 Mechanism of the Steglich esterification

Mechanistically the reaction uses the carbodiimide (e.g., DCC) with DMAP to activate the acid and enable formation of the ester. The first activation step forms an O-acylisourea intermediate which is then attacked by the nucleophilic amino group of DMAP to minimise formation of an acyl migration by product, which is a competitive, non-productive pathway. The alcohol can then approach the acyl pyridinium intermediate and reacts to regenerate DMAP and for the ester product. A generalised mechanism is re-produced below (Figure 4.17).

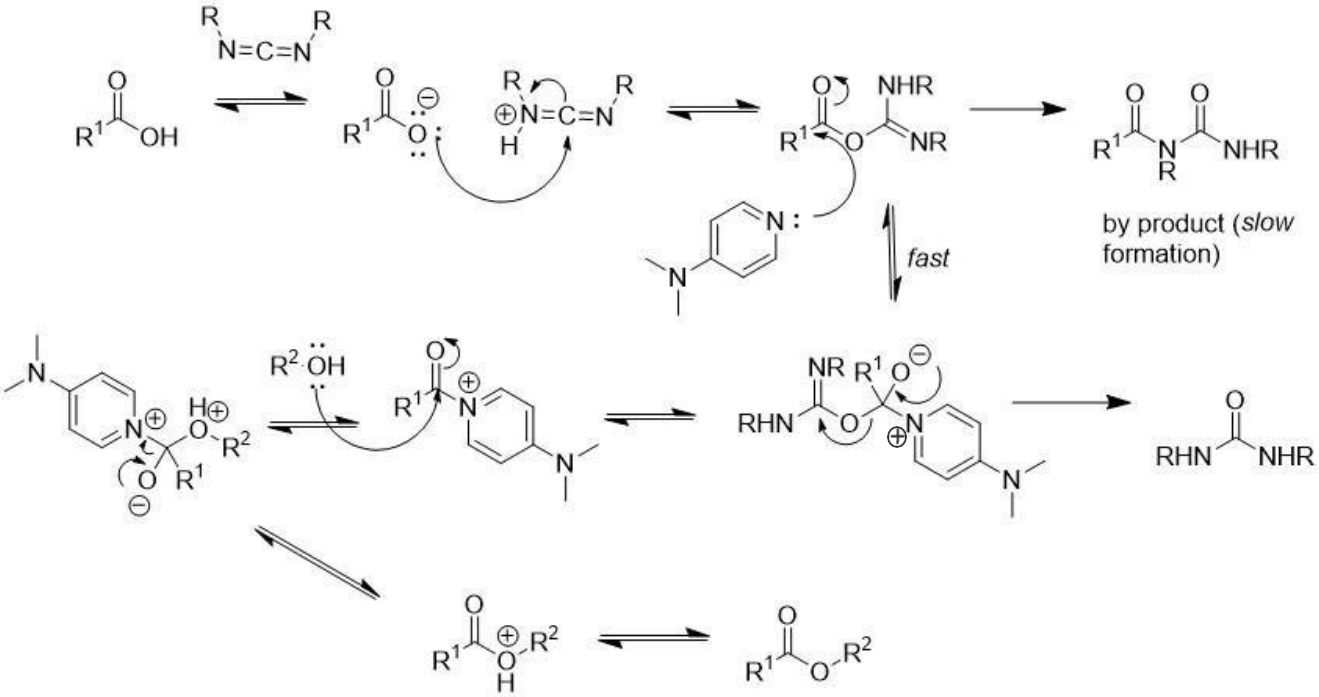

Figure 4.17. Generalised mechanism of the ester coupling reaction.

The synthetic details of the other steps, leading to the alcohol and carboxylic acid intermediates are found in Materials and Methods. A full synthetic scheme, generalised to include all five molecules of the series is included below (Figure 4.18):

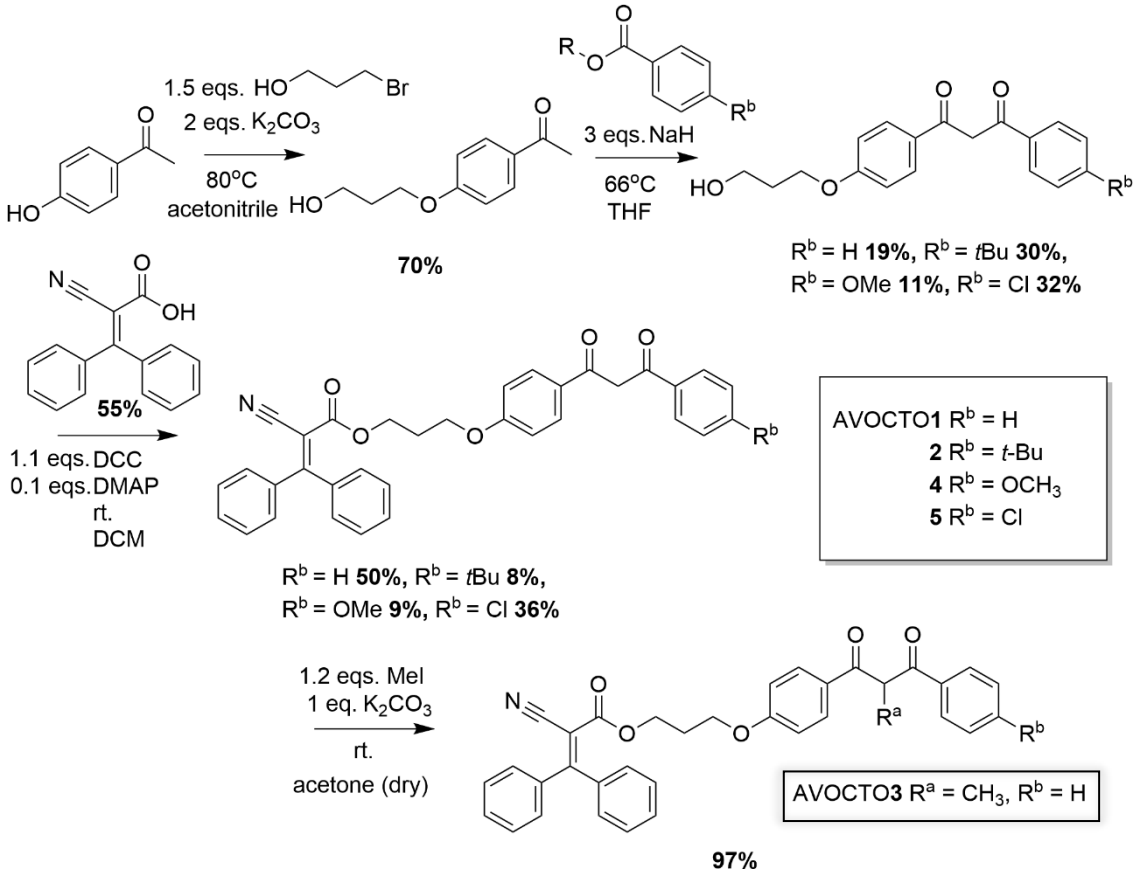

Figure 4.18. Generalised complete synthetic scheme for the AVOCTOX series. Synthetic details are found in the Materials and Methods section. All reactions were carried out in an inert (N_2) atmosphere overnight. Percentage yields are in **bold**. 4-Hydroxyacetophenone is reacted with 3-bromoethanol in the presence of a base to afford the phenyl ether alcohol that was then reacted with a variously substituted ester in NaH/THF to afford the para-substituted 1,3-dicarbonyl compound with alcohol side chain. This compound was then reacted with the free carboxylic acid derived from octocrylene in the final ester coupling step. To synthesise AVOCTO3 a subsequent α-methylation was required, which was achieved with MeI/K_2CO_3 in diethyl ether. rt. = room temperature.

4.2.2 Expanding the Synthetic Scope

In an extension of the synthetic scheme above it was proposed that other acids could be used in place of deprotected octocrylene in the final step to produce a new series of esters with a cinnamic acid derived part, referred to as AVOCINN. Sinapate ester derivatives are a class of plant-derived UV filters and are reviewed elsewhere.[52] Direct condensation of sinapinic acid (a substituted cinnamic acid shown as compound (e) in Figure 4.19.) did not produce the desired product. This was most likely due to the free phenol group in the *para*-position to the double bond.

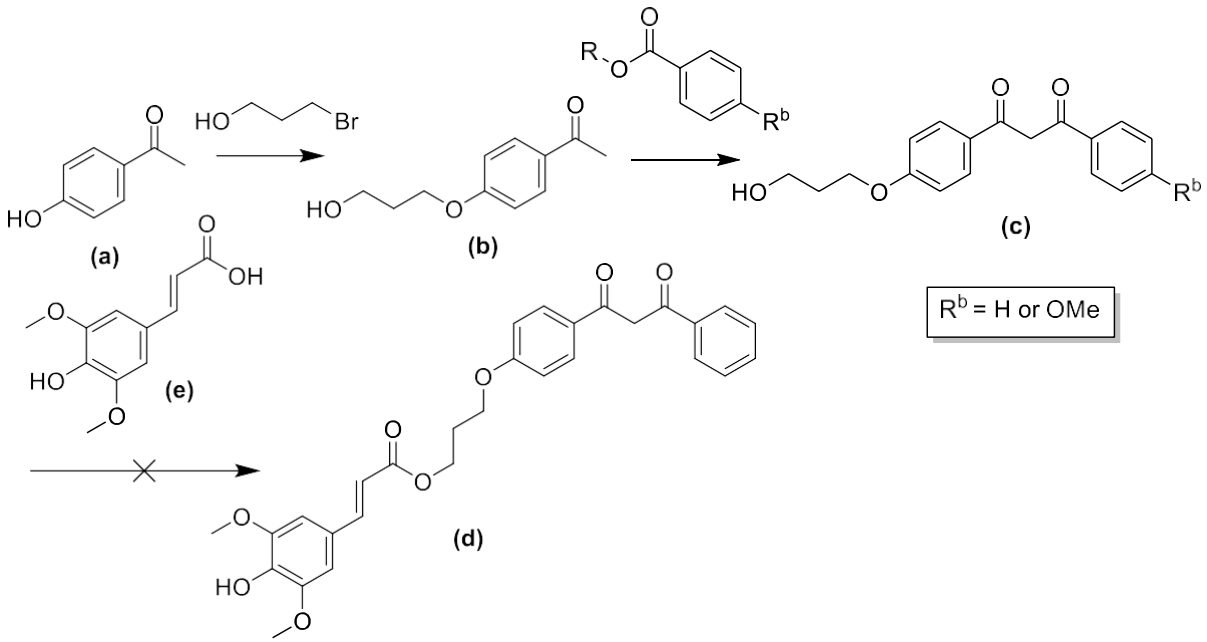

Figure 4.19. Unsuccessful reaction scheme. Compounds (a)-(c) were made in the same way as before. Compound (d) is the target molecule. Compound (e) is sinapinic acid. This was tested with two R^b groups, namely H and -OMe.

To overcome the unproductive final step, an alternative route involving acylation, condensation and deprotection to yield the final compound, inspired by a total synthesis by Allais et al. where they used an analogous method to make 2-O-sinapoyl-l-malate, was proposed.[53] Full synthetic details are found in the Materials and Methods and a summary reaction scheme is found below (Figure 4.20.):

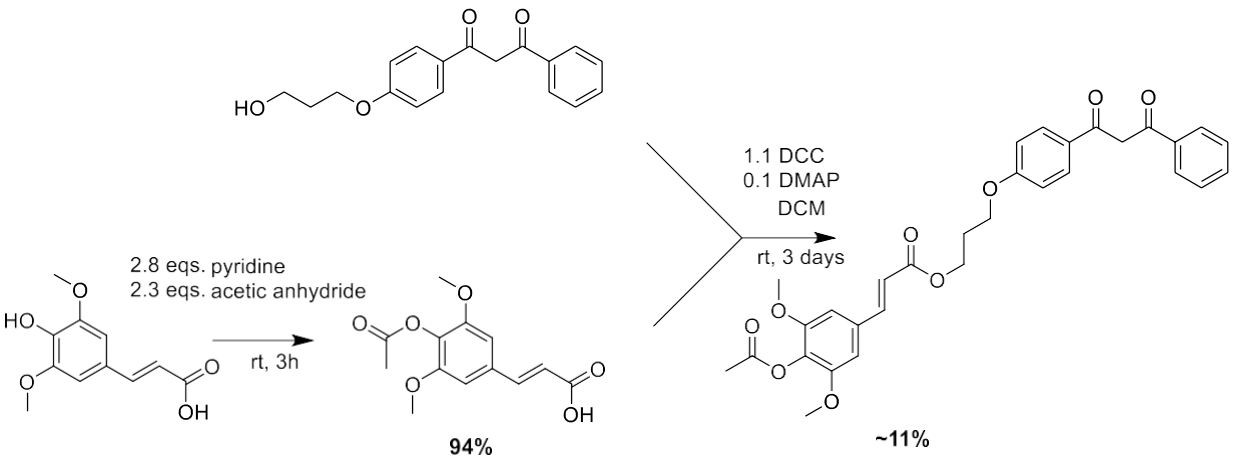

Figure 4.20. Reaction scheme for production of O-acyl protected AVOCINN. Synthetic details are found in the Materials and Methods section. All reactions were carried out in an inert (N_2) atmosphere at room temperature (rt.). Percentage yields are in **bold**. The synthesis of the top compound was described previously. Acetylation of the para-phenolic acid was achieved with acetic anhydride in pyridine. The condensation of the dicarbonyl and the protected acid was achieved in similar conditions to the final esterification step described for AVOCTO1-5, albeit with longer reaction times.

The resultant compound AVOCINN had two distinct peaks in its UV-vis spectrum, presumably due to the presence of two chromophores (Figure 4.21). A notable difference is that the shorter wavelength peak (<300 nm) is closer in intensity to the longer wavelength peak (>350 nm) than is the case for the **AVOCTO** molecules. This suggests that the extinction coefficient (ε) for sinapinic acid is greater than octocrylene and closer in value to that of avobenzone. However no study has measured all three under the same conditions and a literature value[54] for ε(sinapinic acid, λ_{max}, methanol/water (1:1)) = 5894 ± 365 $dm^3mol^{-1}cm^{-1}$ cannot reasonably be compared to that reported by Shaath et al.[3] for ε(octocrylene) = 12290 $dm^3mol^{-1}cm^{-1}$ and for ε(avobenzone) = 34140 $dm^3mol^{-1}cm^{-1}$ as the conditions in the latter are not specified. Finally, the O-acyl deprotected product was partially deprotected in acidic solution but in insufficient yield to conduct further tests.

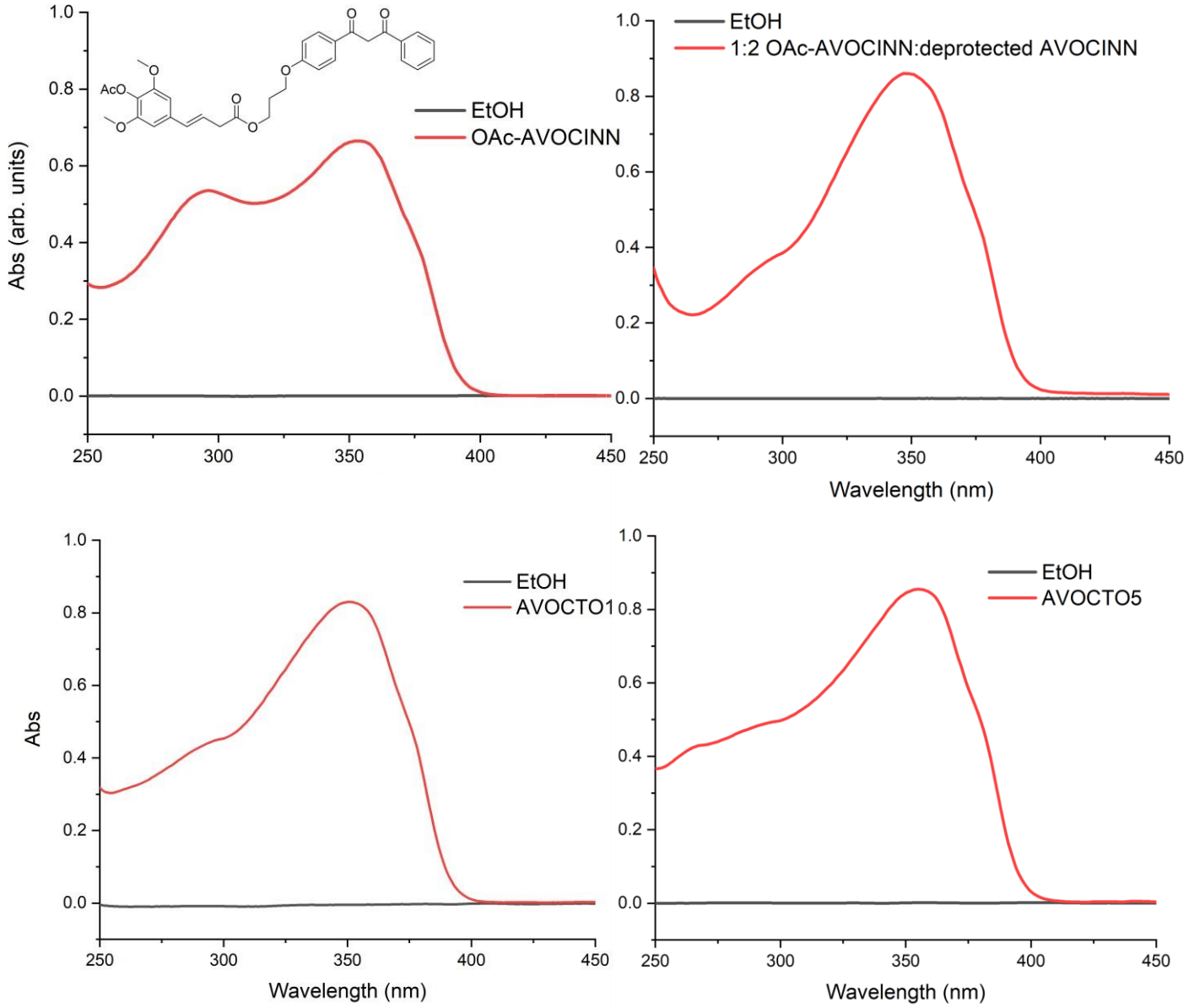

Figure 4.21. (Top Left) UV-vis spectrum of the compound (OAc-AVOCINN) produced by reaction scheme in Figure 4.20. This is an O-acyl protected composite molecule composed of an avobenzone derived part and a cinnamic acid derived part. (Top Right) UV-vis spectrum of the partially deprotected product in an approximate 2:1 ratio with OAc-

AVOCINN. Included below are the UV-vis spectra for AVOCTO1 and AVOCTO5. All spectra are in ethanol, demonstrating broad protection in one molecule.

4.3 Avobenzone stabilisation results

Avobenzone (Eusolex® 9020 from Merck) was tested for stability in ethanol, acetonitrile, cyclohexane and DMSO at µM concentrations using UV-vis spectroscopy as described in the Materials and Methods. A range of solvents was chosen to reflect the complex environment in which sunscreen active ingredients are found. Ethanol was chosen as it is a typical solvent in the cosmetics industry; where it is used to solubilise ingredients with aqueous solubility and is protic due to the labile H^+ of the OH bond. Acetonitrile is a polar solvent and in contrast to ethanol is non-protic and therefore does not readily donate H^+ to solute molecules. DMSO is the most polar solvent chosen and is also non-protic.
Cyclohexane is chosen as it is nonpolar and can reflect the environment of the oil-phase of a sunscreen formulation in terms of polarity. The key solvent properties can be referred to in Table 4.1.

Table 4.1. Solvent Properties of Common Liquids.[55] p1 is a measure of the ability of the solvent to interact with various test solutes. p1 increases with solvent polarity.

Solvent	Polarity Index (p1)	Boiling Point (°C)	Density at 20°C (g/mL)
Acetonitrile	5.8	81.6	0.781
Cyclohexane	0.2	80.7	0.778
Ethanol	4.3	78	0.789
DMSO	7.2	189	1.1
Water	10.2	100	1.0

4.3.1 UV-visible properties of avobenzone in solution

The UV-vis properties of avobenzone in the absence of any other additives are shown in Figure 4.22. Two major absorption bands are visible in the spectrum. The higher energy band centred around 275 nm is due to the keto form, as in other open-chain 1,3-diketones. The lower energy band centred around 355 nm is due to the chelated enol forms that are in a rapid thermal equilibrium.

There is a small shift to shorter wavelengths in the less polar solvents as can be observed in cyclohexane versus acetonitrile and ethanol but this is presumably due to a solvation effect rather than a shift in the keto-enol equilibrium. The lower energy absorbance of the enol form relative to the diketo form can be explained by the increased conjugation, the stabilising effect of the intramolecular hydrogen bond and π delocalisation in the enol form. The enol absorption has a noticeable shoulder occurring at longer wavelengths in all solvents but the reason for this is unknown. As well as a concentration dependence, the relative absorbance intensity of the two bands can be justified by considering the orbital nature of the transitions. The more intense absorption of the enol band is due to a symmetry allowed transition – a bonding electron in a π-orbital is excited to an anti-bonding π*-orbital giving rise to the high intensity (π -π*) band. The less intense diketo band is attributed to excitation of the lone pair of electrons on the carbonyl oxygen (n) to a π* orbital, giving rise to a localised, symmetry forbidden transition.

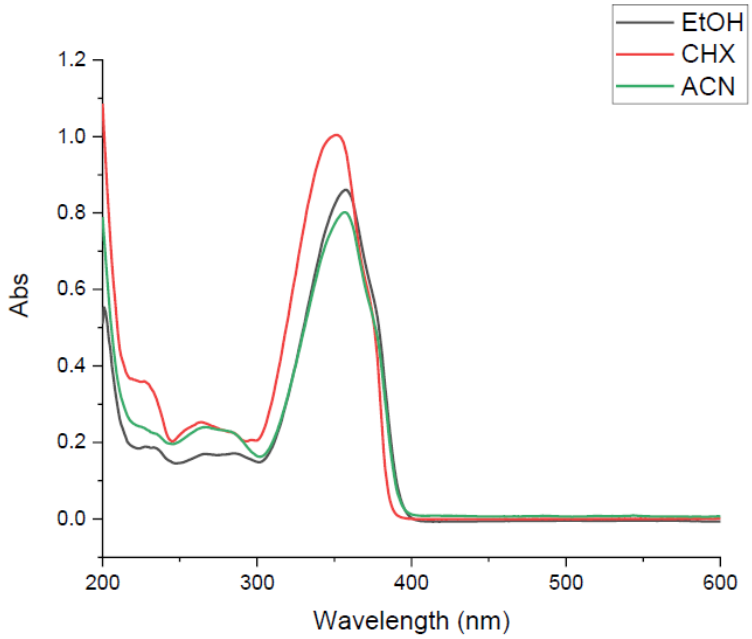

Figure 4.22. UV-vis spectra of avobenzone in three solvents of varying polarity:
a) EtOH:Ethanol (λ_{max} = 358 nm); b) CHX: cyclohexane (λ_{max} = 352 nm); c) ACN: acetonitrile (λ_{max} = 357 nm). Concentration of avobenzone ~2 x 10^{-5} mol dm^{-3}.

4.3.2 Assessing stabilisation effects in binary mixtures in ethanol

To assess stabilisation effects in binary (i.e., two-component) mixtures of avobenzone and one other molecule, avobenzone was combined in ethanol and in acetonitrile with potential stabilisers to observe any synergistic effects between the compounds. Details of the method used are found in Materials and Methods. The stabilisers were commercially available octocrylene (Merck) and synthesised molecules AC26 and AC33 (see Chapters 2 and 3). Octocrylene is often found in formulations with avobenzone (see Chapter 1) and is therefore a good point of comparison. The absorbance change in the system was measured both at the absorbance peak and across the entire UVA range.

In the binary mixtures in ethanol there was a reduced loss of activity at the UVA peak absorbance when avobenzone was combined with AC26 and with AC33 (-0.6% and -0.4%) than when combined with octocrylene (-3%). This is also the case across the entire UVA range. A stoichiometric ratio of 1:3 (avobenzone: octocrylene) was used as this is typical of a sunscreen product and results in an approximately equal absorbance at both peak maxima.

From these data alone, it is difficult to distinguish the effect of spectral overlap and photon shielding from that of a true stabilising effect, especially when the overall loss of activity is low. When modelled with linear rates of photodegradation (**y = a + b*x)** the rate constants (**b**) are within error of each other. These data do not appear to show any significant stabilisation at these concentrations in ethanol. There is in any case a larger degree of spectral overlap between AC26 and avobenzone, and AC33 and avobenzone, than in octocrylene and avobenzone, which could explain the less photodegradation measured overall. Experimental data are recorded in Table 4.2, displayed in Figure 4.23 and the fits are presented in Figure 4.24 and Table 4.3.

Table 4.2. Summary of the avobenzone in ethanol stabilisation results. NB: Avobenzone results are an average of three experiments.

Molecule/mixture	**Average degradation per hour at peak absorbance in ethanol**	**Degradation per hour using AUC R (UVA)**
Avobenzone	1.5 %	1.1 %
Avobenzone/Octocrylene	3.0 %	2.6 %
Avobenzone/AC26	0.6 %	0.5 %
Avobenzone/ AC33	0.4 %	0.2 %

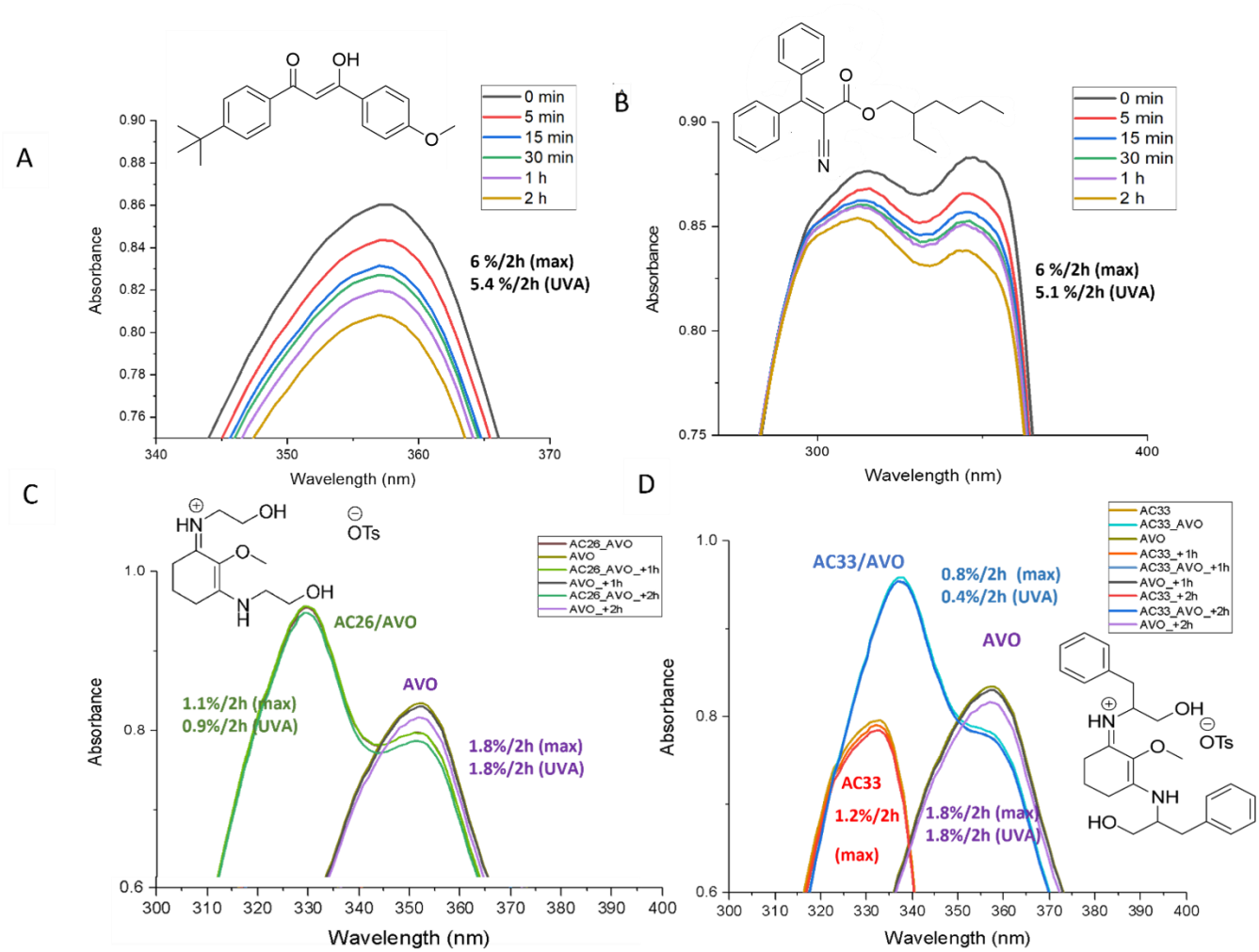

Figure 4.23. A) Irradiation of avobenzone alone in ethanol; B) Irradiation of an avobenzone and octocrylene mix (1:3 molar ratio); C) Simultaneous irradiation of avobenzone (black/purple trace) and an avobenzone and AC26 mixture (green trace); D) Simultaneous irradiation of avobenzone (black/purple trace), AC33 (yellow/orange trace) and an avobenzone and AC33 mixture (blue trace). All graphs are cropped in order to display the key points of interest. Inset are the loss of activity in percent (as defined in the previous section) where 'max' indicates that the measurement is taken at the λ_{max} and UVA indicates that the change across the entire UVA range is considered. NB: Octocrylene was irradiated alone separately and showed no degradation.

Table 4.3. Summary of the linear fits of avobenzone in ethanol stabilisation data.

Equation	**y = a + b*x**			
Experiment	**AVO in EtOH**	**AVO/OCTO**	**AVO/AC26**	**AVO/AC33**
a	0.86 ± 0.011	0.86 ± 0.010	0.82 ± 0.014	0.81 ± 0.012
b	-4.46 ± 1.405E-4	-4.42 ± 1.277E-4	-3.31 ± 1.861E-4	-3.48 ± 1.492E-4

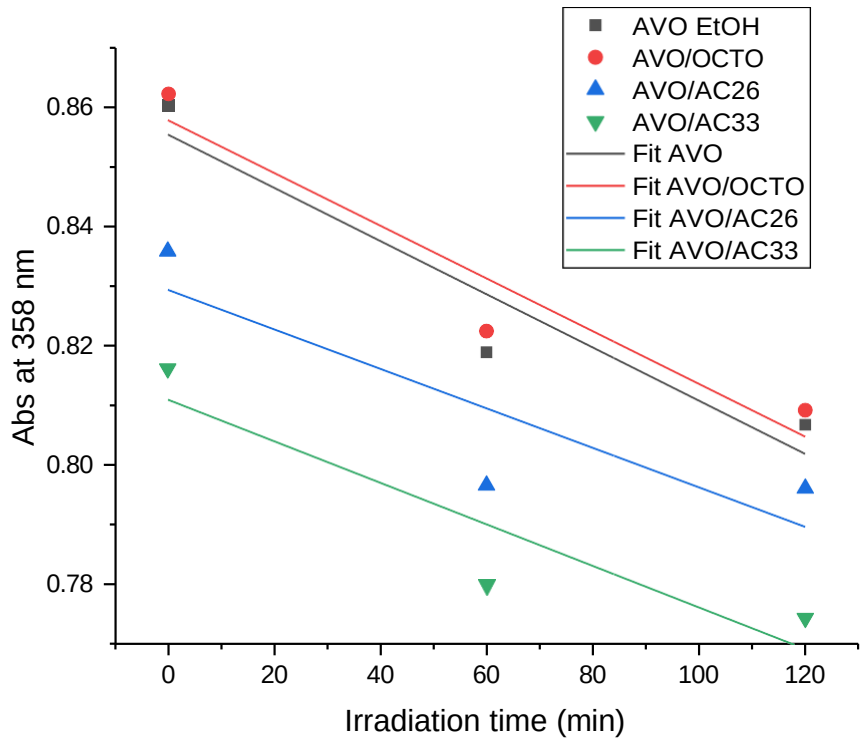

Figure 4.24. Avobenzone in binary mixtures in ethanol, degradation with best linear fits.

4.3.3 Assessing stabilisation effects in binary mixtures in acetonitrile

When assessed for stability under the same conditions used in the ethanol experiments, the results for acetonitrile (data in Table 4.4, fits in Table 4.5) show that the avobenzone UVA activity loss is significantly greater in the polar, non-protic solvent than in polar protic, with an increase to ~70% loss of activity during an hour of irradiation. In acetonitrile, the loss of activity is best modelled as an exponential decay (**y = A*exp(-x/t) + y**) and the data show significant difference between avobenzone in the two-component mixtures versus avobenzone alone. The most stable mixture of avobenzone and AC26 lost only 47% of the maximum absorbance while AC33 and avobenzone decreased by 60%, which is still less than the -73% of avobenzone alone. As a control, one cuvette containing only avobenzone was not irradiated and the loss of activity was considerably less (~7% vs. ~70%). This indicates that the major factor in driving the loss of the UVA activity is a light-driven process and there may be a minor effect of tautomerization that occurs without irradiation and is due to the solvent environment alone. As with the results for ethanol, it is beyond the scope of this experiment to distinguish the effects of spectral overlap and photon shielding. In any case the decrease in the UVA absorbance activity is reduced in line with the average degradation at peak absorbance but whether there is a direct stabilisation mechanism or this is simply a result of spectral overlap remains an unresolved question. Details of each experimental result are presented in Figure 4.25 and a summary in Figure 4.26.

Table 4.4. Summary of the avobenzone in acetonitrile stabilisation results. Details of the conditions used are found in the Materials and Methods.

Molecule/mixture	**Average loss of activity per hour at peak absorbance in acetonitrile**	**Degradation per hour using AUC R (UVA)**
Avobenzone	-73 %	-71 %
Avobenzone in ambient light	-6.8 %	~-4.5%[*unstable baseline*]
Avobenzone + Octocrylene	-72 %	-58 %
Avobenzone + AC26	-47 %	-39 %
Avobenzone + AC33	-60 %	-51 %

A

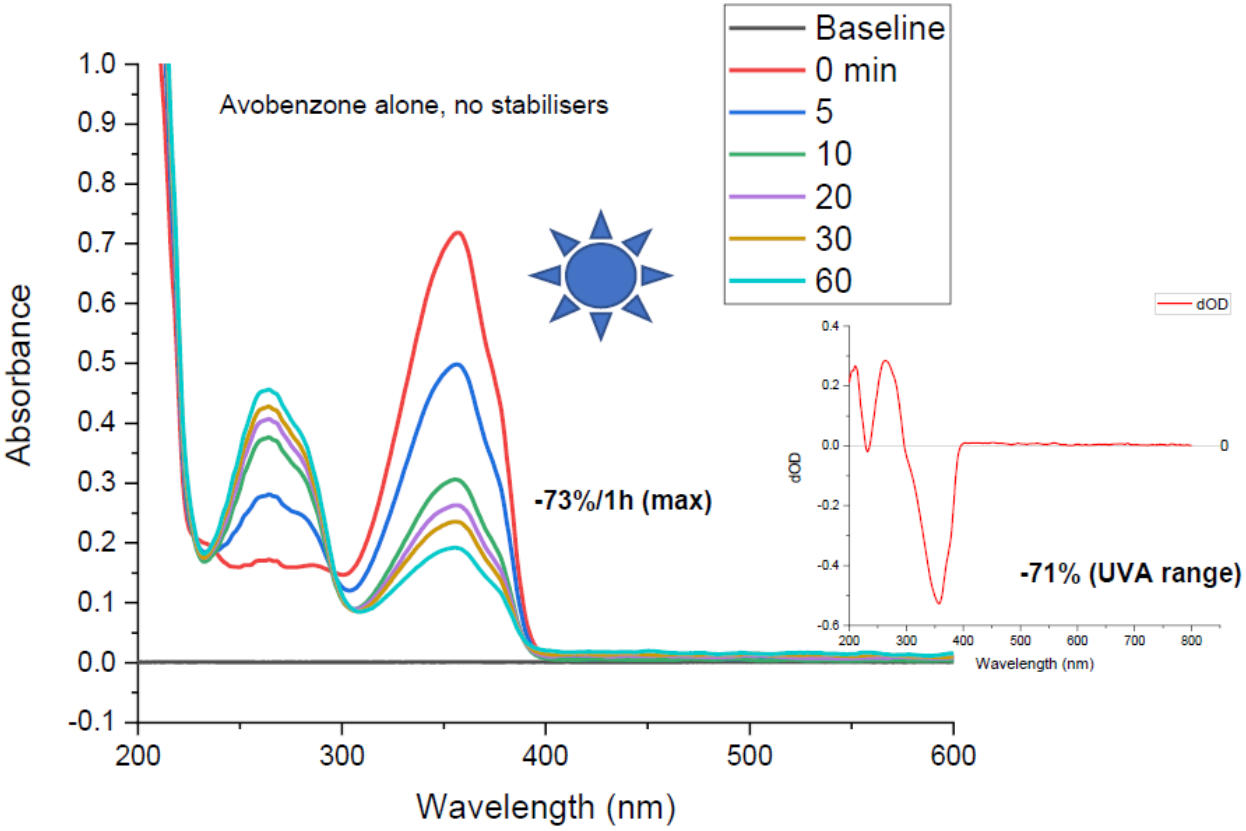
Avobenzone alone, no stabilisers
Baseline
0 min
5
10
20
30
60
-73%/1h (max)
-71% (UVA range)
dOD
Absorbance
Wavelength (nm)

B

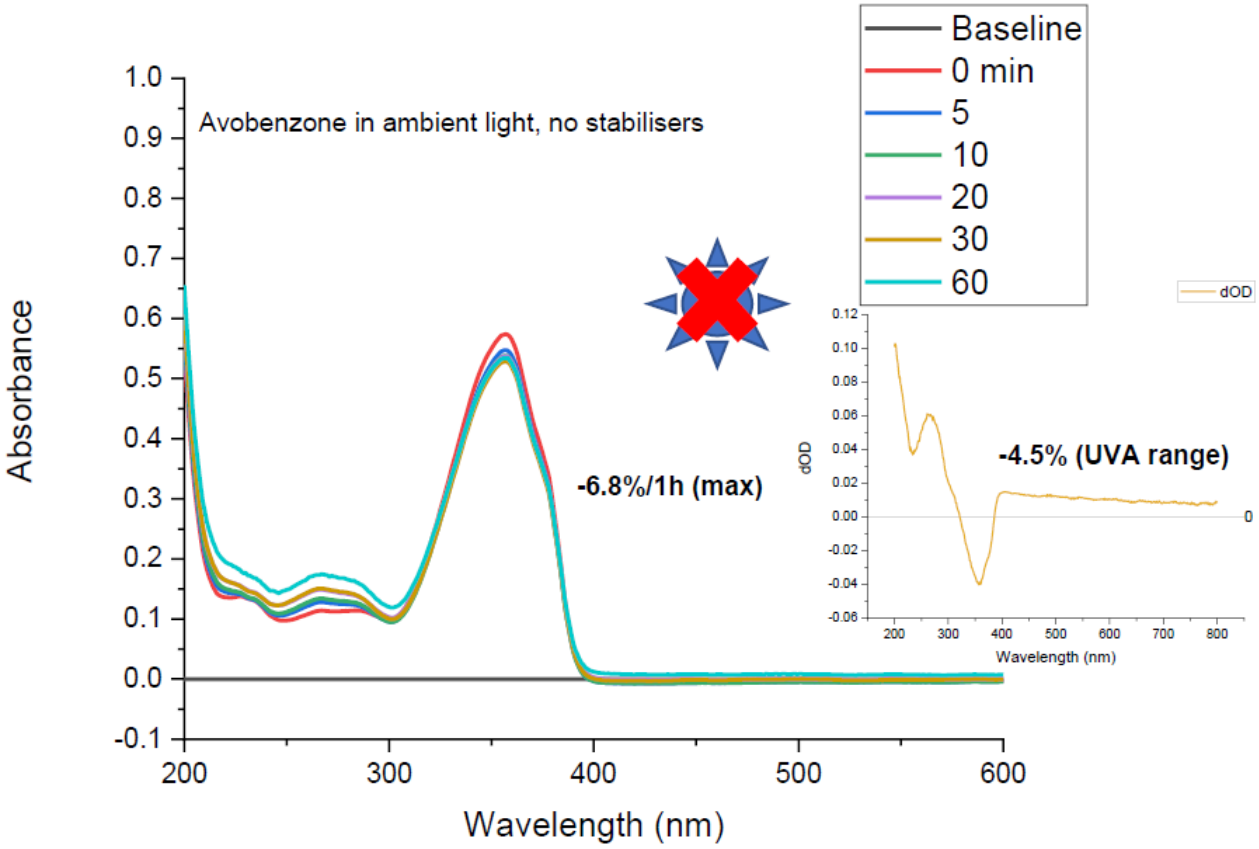
Avobenzone in ambient light, no stabilisers
Baseline
0 min
5
10
20
30
60
-6.8%/1h (max)
-4.5% (UVA range)
dOD
Absorbance
Wavelength (nm)

C

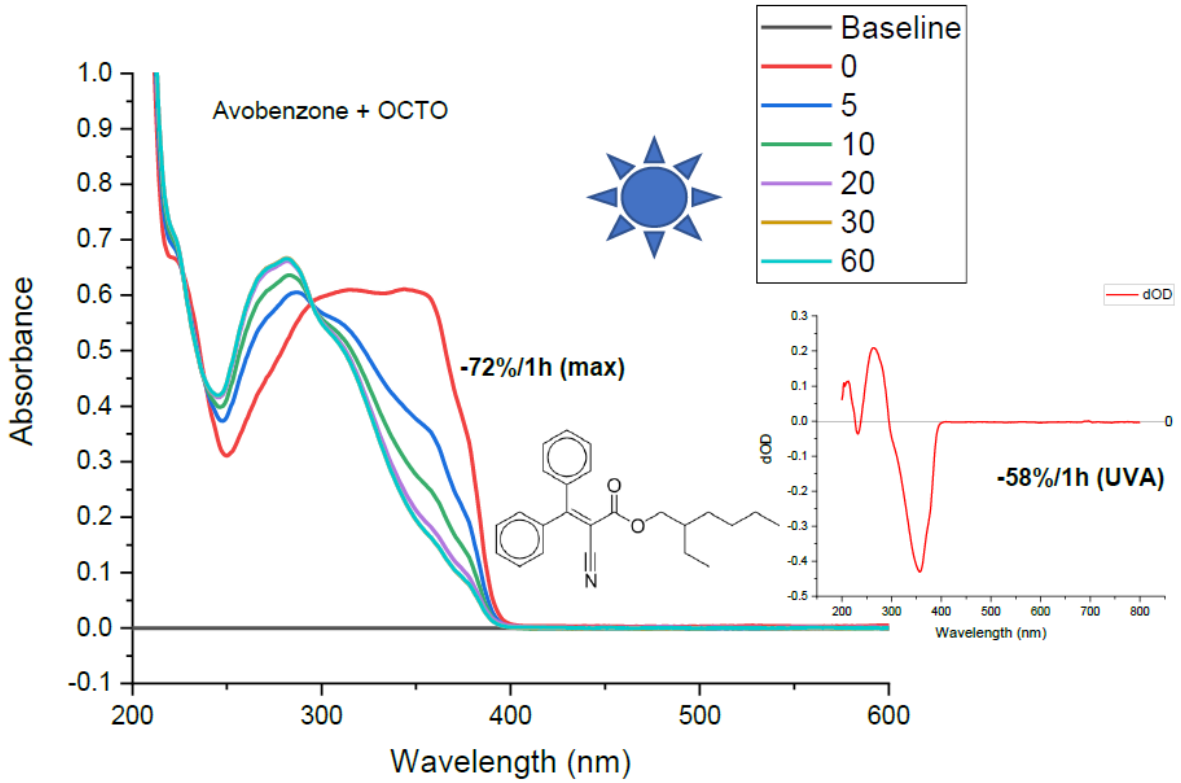
Avobenzone + OCTO
Baseline
0
5
10
20
30
60
-72%/1h (max)
-58%/1h (UVA)
dOD
Absorbance
Wavelength (nm)

D

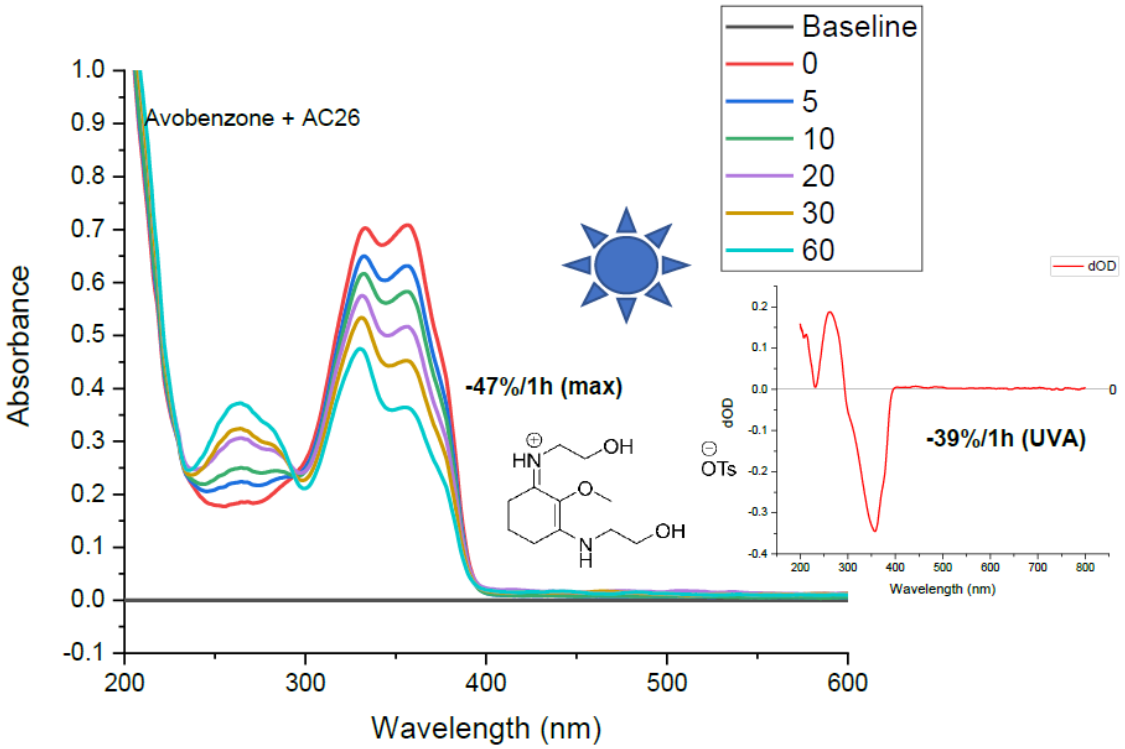
Avobenzone + AC26
Baseline
0
5
10
20
30
60
-47%/1h (max)
-39%/1h (UVA)
dOD
Absorbance
Wavelength (nm)

E

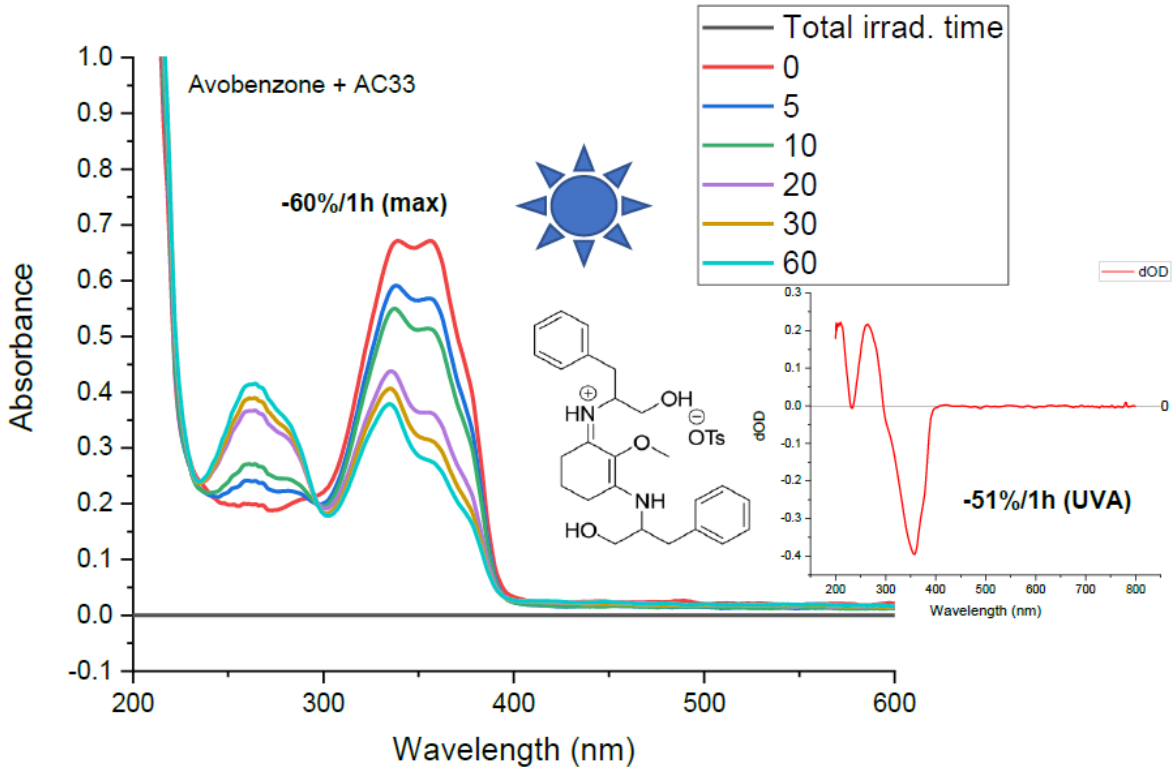

Figure 4.25. Set of graphs of binary mixtures in acetonitrile, room temperature. Graph A) Irradiation of avobenzone alone; B) Avobenzone incubated at ambient light (i.e., with no artificial irradiation); C) Irradiation of an avobenzone and octocrylene mixture; D) Irradiation of an avobenzone and AC26 mixture; E) Irradiation of an avobenzone and AC33 mixture. Displayed on the graphs are the stabiliser present and the loss of activity in percent where 'max' indicates that the measurement is taken at the λ_{max} and (inset) 'UVA' indicates that the change across the entire UVA range is considered.

Table 4.5. Data fits of avobenzone stabilisation studies in acetonitrile.

Equation	$y = A*\exp(-x/t) + y_0$			
Data set	**AVO ACN**	**AVO/OCTO**	**AVO/AC26**	**AVO/AC33**
y_0	0.21 ± 0.023	0.16 ± 0.002	0.340 ± 0.020	0.25 ± 0.025
A	0.51 ± 0.037	0.43 ± 0.003	0.38 ± 0.018	0.42 ± 0.027
t	7.46 ± 1.301	6.16 ± 0.098	28.44 ± 3.26	16.53 ± 2.773

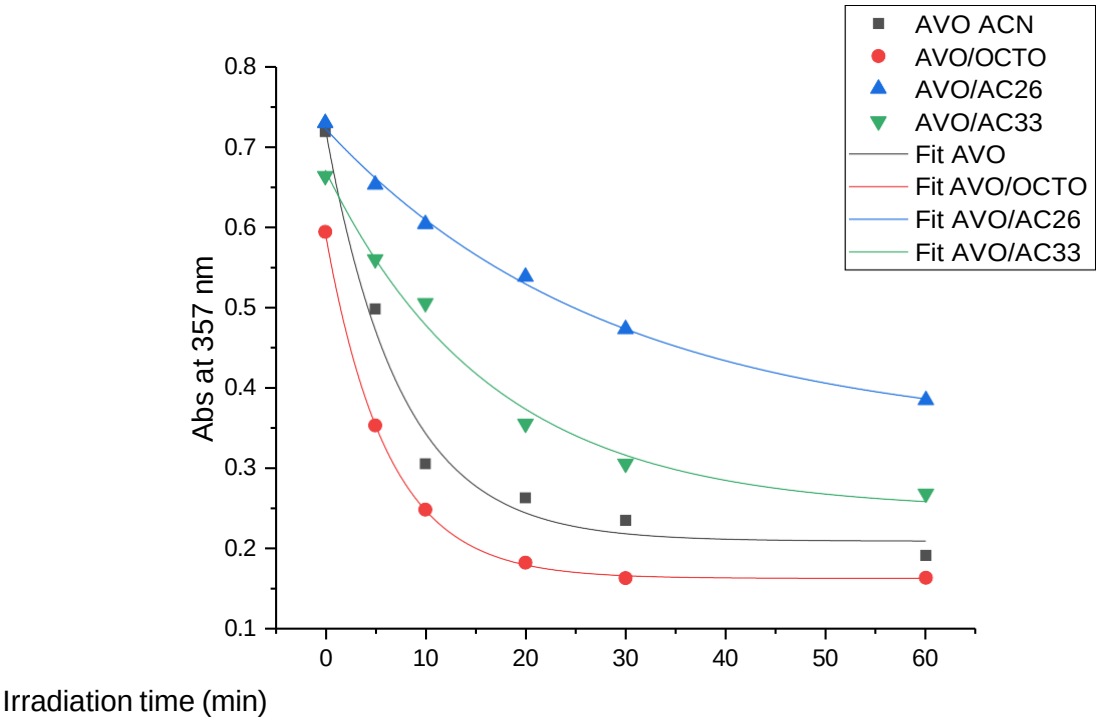

Figure 4.26. Avobenzone in binary mixtures in acetonitrile, degradation with exponential fits.

4.4 Covalently linked dibenzoylmethane and cinnamate chromophores

The **AVOCTO** compounds were designed as potential new broadband sunscreen molecules and as a way to stabilise avobenzone to photodegradation. This new series of molecules contains two chromophores in a single molecule; a cinnamate-derived chromophore related to octocrylene and a chromophore related to avobenzone. As the two chromophores are covalently linked via an *inert* alkane ($-C_3H_6-$) linker, any reaction (presumably bimolecular) that occurs between octocrylene and avobenzone in a complex mixture will not occur; although arguably this may occur between the different parts of two separate molecules. Inert in this instance means unreactive but also that electronic conjugation is not present between the two chromophores. This can be concluded from the fact that the UV-vis absorption of **AVOCTO** compounds is directly comparable to the absorption profiles of the parent molecules. The broadband profile of **AVOCTO** compounds is due to the combined effect of the octocrylene or cinnamate chromophore of the molecule, covering the shorter wavelength UVB range while the avobenzone chromophore absorbs in the UVA. Electronic modifications to the avobenzone chromophore by para-substitution of the phenyl ring (i.e., relative to the carbonyl) can then be used to tune the stability of the dicarbonyl under irradiation. As discussed previously, by stabilising the enol form of avobenzone, photodegradation and fragmentation can be significantly reduced. **AVOCTO** compounds were made in 3-5 steps from commercially available reagents.

4.4.1 Assessing the photostability of AVOCTO compounds

The photostability of the synthesised molecules was assessed by steady-state irradiation in ethanol and acetonitrile, using the same methodology as in the preceding avobenzone photostabilisation studies. The results are summarised in Table 4.6. All molecules were stable, or did not significantly degrade, in ethanol over the time of the experiment, which is consistent with the stability of both parent molecules in ethanol. However, there was a significant drop in UVA absorption in some molecules in acetonitrile. AVOCTO2, which has the closest structural similarity to avobenzone, degraded the most with almost 50% loss of activity at the peak maximum in 40 minutes. AVOCTO4 which is identical to AVOCTO2 except for para-substitution with a different electron donating group ($-OCH_3$ vs. *t*-Bu)

demonstrated the second highest loss of activity. AVOCTO1 has a hydrogen atom in para-substitution to the carbonyl with a neutral electronic effect on the ring system and the loss of activity at the peak maximum is significantly less (-34% instead of -41/-49%). Finally, para-substitution with a chlorine atom which acts as an electron-withdrawing group by induction in the AVOCTO5 molecule, results in significantly smaller loss of activity at the peak maximum. Over 40 minutes there is only a 5% loss of activity which is almost a tenth of the photodegradation observed in the least photostable molecule of the series. As the absorption peak maximum of AVOCTO3 is shifted completely to the diketo form (see earlier discussion) it is an outlier in the series and is not included in the current discussion. Interestingly a similar trend is seen when comparing avobenzone and chloro-avobenzone, which suggests that it is the substitution with the chlorine atom that confers the extra stability. All relevant spectra are included in Figure 4.27.

Table 4.6. Summary of the UV-vis activity of **AVOCTO** compounds in acetonitrile after 40 minutes simulated solar irradiation using the 'ultraslow' set-up in the Materials and Methods. A generic chemical structure showing the identity of the AVOCTOX molecules is included below for reference.

Compound	Change in absorbance at (λ_{max})	Para-substituent (R^b)
AVOCTO1	-34% (350 nm)	H
AVOCTO2	-49% (356 nm)	*t*-Bu
AVOCTO3	Peak max shifted	H
AVOCTO4	-41% (361 nm)	OCH_3
AVOCTO5	-5% (354 nm)	Cl

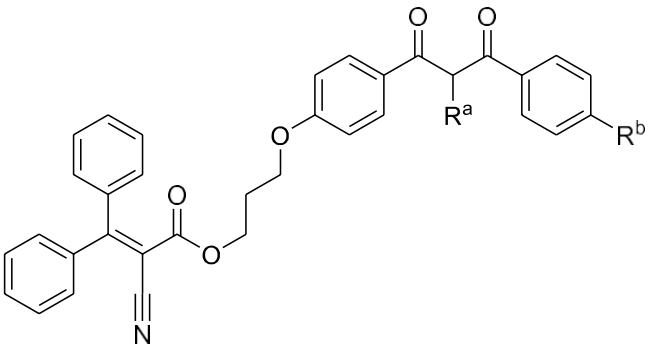

AVOCTO **1** R^a = H, R^b = H
2 R^a = H, R^b = *t*-Bu
3 R^a = CH_3, R^b = H
4 R^a = H, R^b = OCH_3
5 R^a = H, R^b = Cl

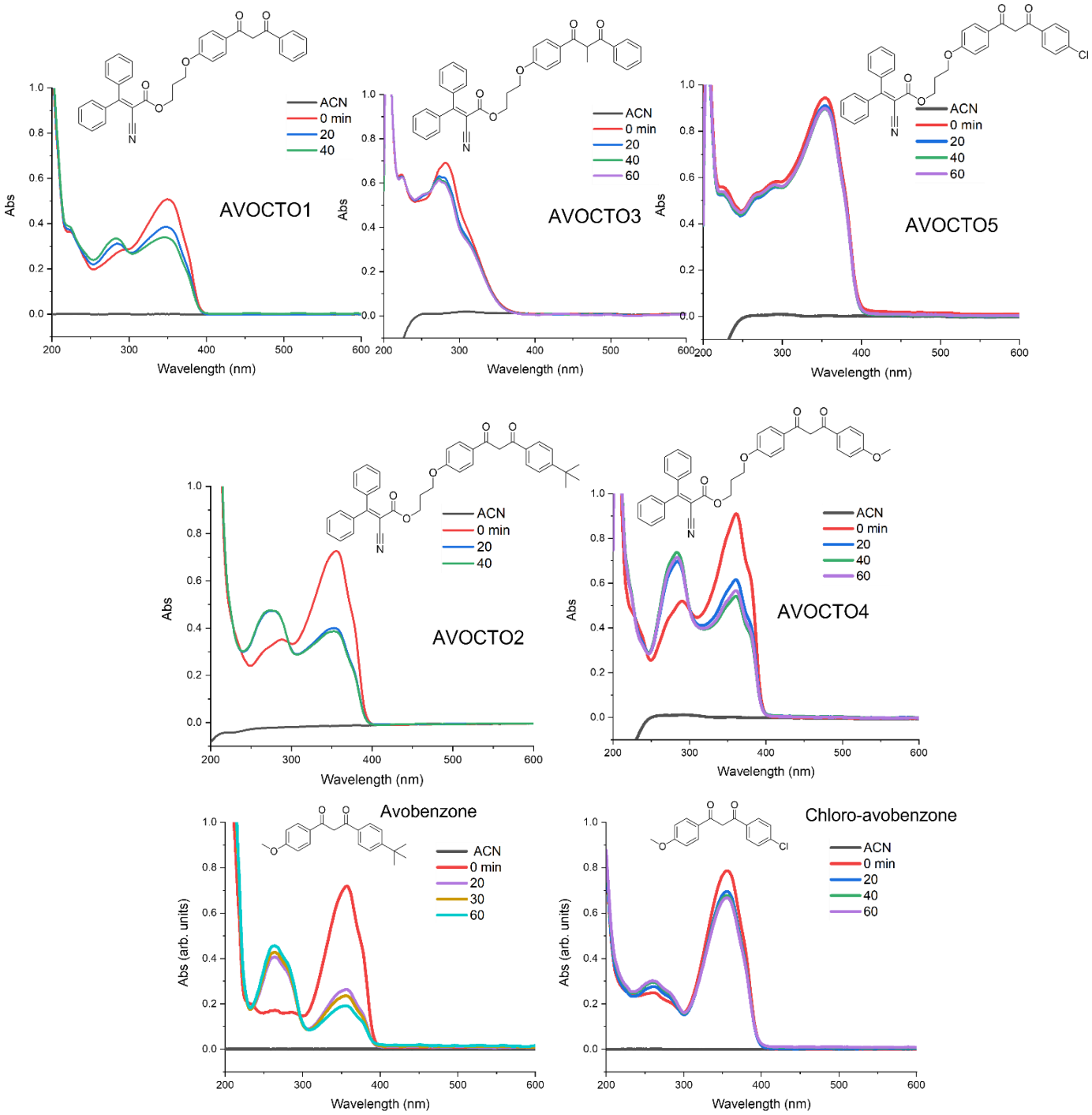

Figure 4.27. Photostability results in acetonitrile of compounds discussed in the accompanying text. Briefly the greatest improvement in stability at the UVA wavelength is achieved by substituting a chlorine atom in place of the *tert*-butyl group while covalently linking to reduced octocrylene allows for broadband protection through one molecule.

4.4.2 Ultrafast Spectroscopy of AVOCTO compounds

Molecules AVOCTO1, AVOCTO3 and AVOCTO5 were submitted for ultrafast spectroscopy studies in the WCUS facility. Excitation (i.e. pump) wavelengths were chosen based on the absorption maxima of the spectra as displayed in Figure 4.28.

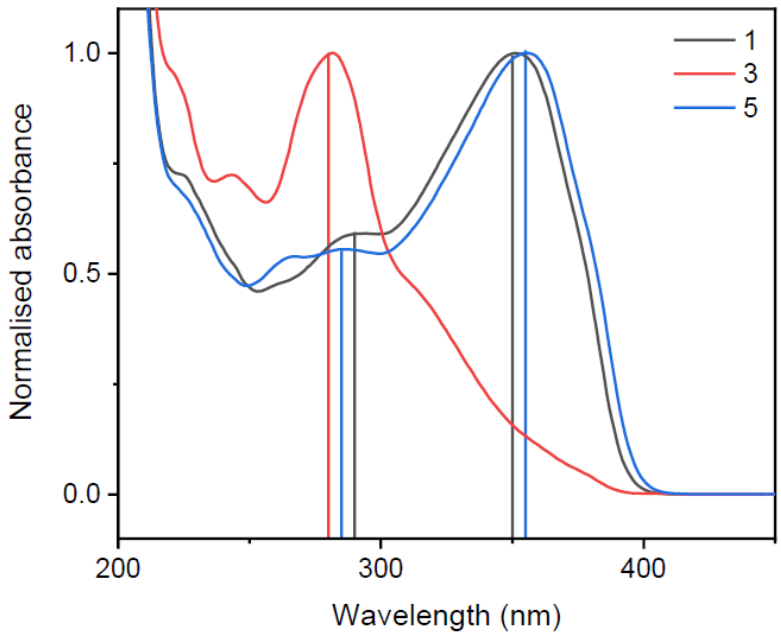

Figure 4.28. Pump wavelengths selected for the TEAS experiment shown as vertical lines.

As seen in Figure 4.28, two wavelengths were chosen for AVOCTO1 and for AVOCTO5 while only one was chosen for AVOCTO3. The resultant TAS are displayed below (Figures 4.29.A1-A5):

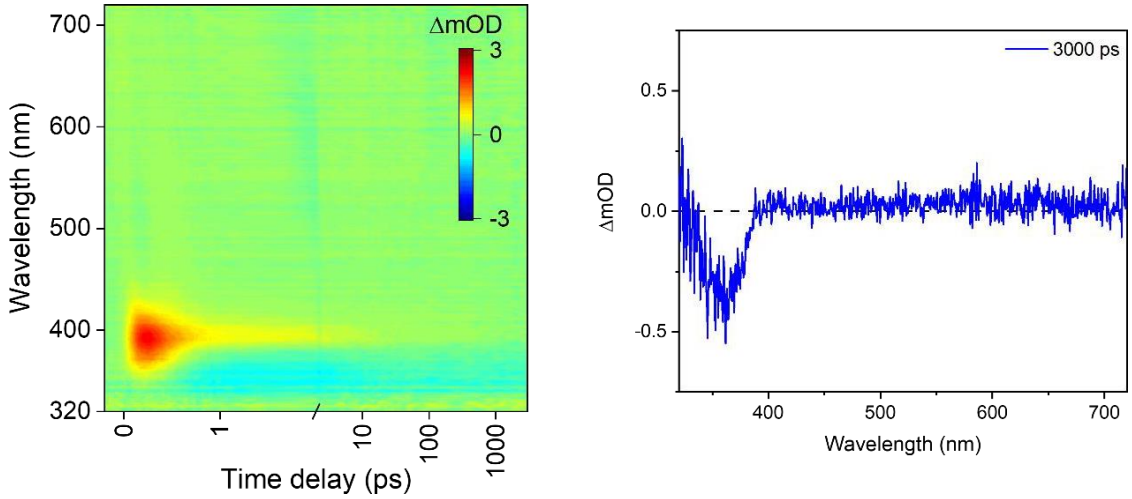

Figure 4.29.A1. AVOCTO1 (λ_{pump} = 290 nm) TEAS spectrum and 3000 ps scan in acetonitrile.

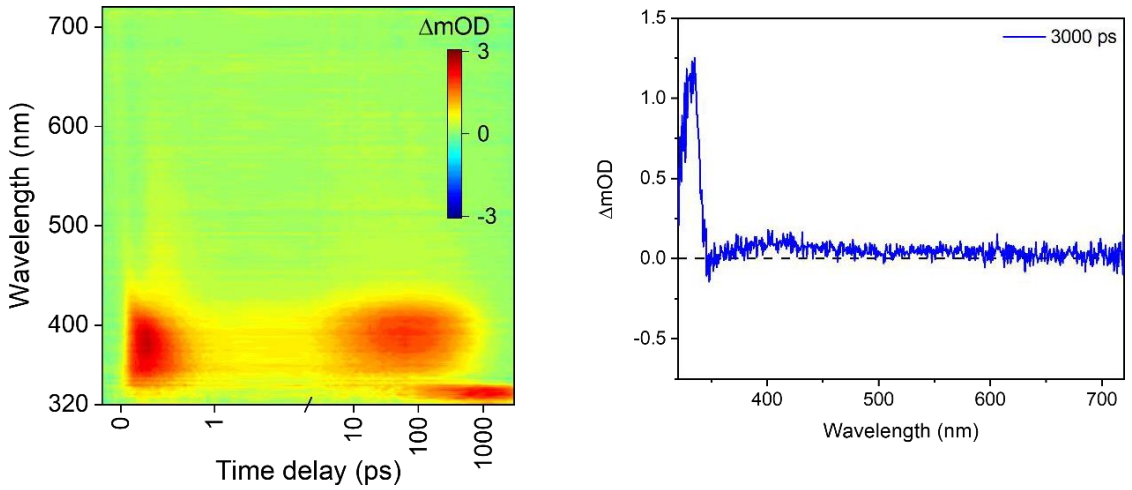

Figure 4.29.A2. AVOCTO3 (λ_{pump} = 280 nm) TEAS spectrum and 3000 ps scan in acetonitrile.

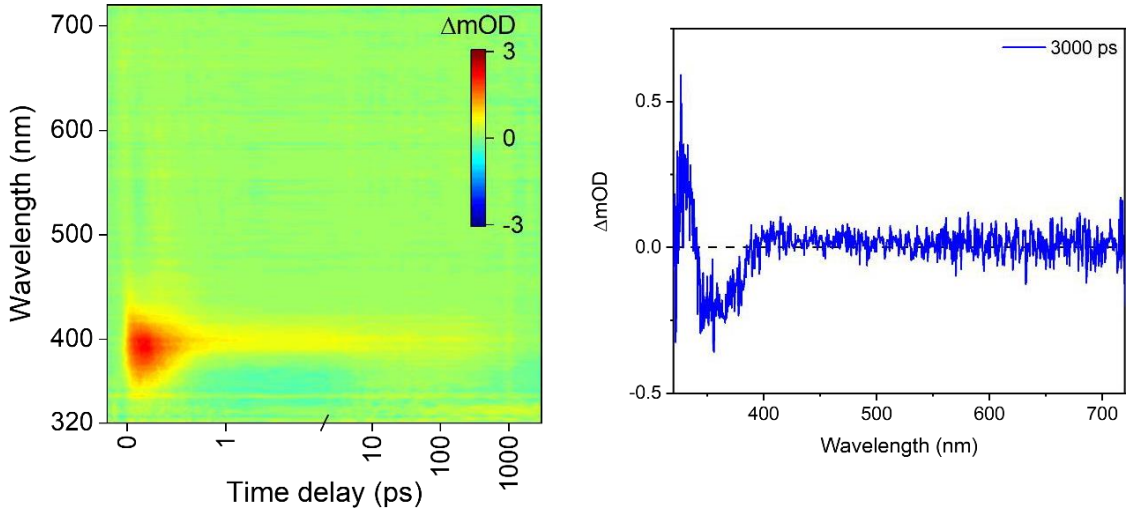

Figure 4.29.A3. AVOCTO5 (λ_{pump} = 285 nm) TEAS spectrum and 3000 ps scan in acetonitrile.

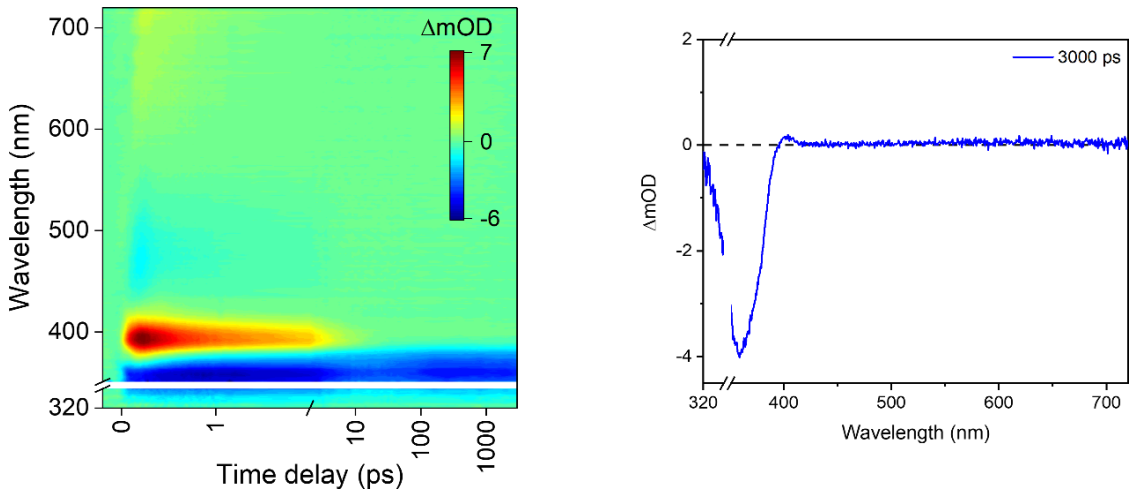

Figure 4.29.A4. AVOCTO1 (λ_{pump} = 350 nm) TEAS spectrum and 3000 ps scan in acetonitrile.

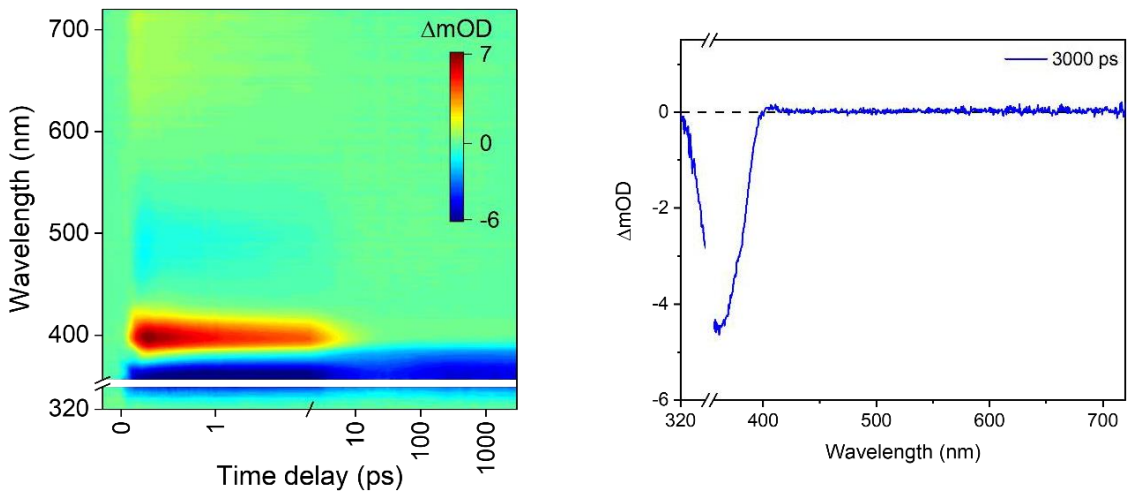

Figure 4.29.A5. AVOCTO5 (λ_{pump} = 355 nm) TEAS spectrum and 3000 ps scan in acetonitrile.

As can be seen qualitatively the Figures 4.29.A4 and A5, AVOCTO1 and AVOCTO5 are practically indistinguishable at both pump wavelengths with the same ESA, SE and GSB features. AVOCTO3 however exhibits remarkably different spectroscopy with the shorter wavelength pump. In AVOCTO3, an initial ESA grows out within 1 ps and then a second ESA with similar absorption grows in between ~8-500 ps. The second ESA feature is then replaced by a higher energy positive absorption feature that could perhaps indicate formation of a radical species, perhaps an oxygen-centred radical. The sharp and narrow nature of this feature would support this justification.

4.4.3 Assigning the features in the TAS at pump wavelength >350 nm

Previous ultrafast work on avobenzone conducted in our lab by E. Holt can be used to interpret the features present in the spectra above.[17] In that report, avobenzone is studied in ethanol and cyclohexane, and a summary of the results in presented in Table 4.7. Due to the similarity of the results, only the results in ethanol will be recounted. An intense GSB is seen between 330-380 nm which is the result of the overlap of probe wavelengths with the ground-state absorption region of avobenzone. An ESA between 380-430 nm and a short-lived SE between 450-550 nm are also present in the TAS. A global fit kinetics parallel

model was used to assign four time constants (τ_n) to the spectral features. A summary is given below:

Table 4.7. Results from ref[17] for avobenzone in ethanol.

Time constant	Lifetime	Description
τ_1	150 ± 140 fs	the evolution of the chelated enol form of avobenzone from the Franck Condon region.*
τ_2	1.2 ± 0.1 ps	the decay of the initially excited S1 state of the chelated enol form of avobenzone via SE**
τ_3	8.2 ± 0.1 ps	the vibrationally hot chelated enol form of avobenzone in the ground electronic state (S0).
τ_4	>2.5 ns	incomplete GSB recovery due to perhaps formation of long-lived photoisomers e.g., the diketo form

***** It is possible that there are additional ultrafast processes occurring within this time on a proportion of the excited molecules, such as excited-state intramolecular proton transfer, or rotation around the C–O single bond of the hydroxyl group to form non-chelated avobenzone species.

****** The timescale of the SE is very short compared to the much longer timescales that would be expected for fluorescence. This indicates that long-lived radiative decay (4 ns), which would be of concern for sunscreen applications, does not occur in avobenzone.

The spectra obtained for AVOCTO1 and AVOCTO5 excited at 350 nm and 355 nm respectively in acetonitrile (Figures 4.29.A4 and A5) were fitted (Table 4.8). Avobenzone was also studied in the same conditions for comparison.

Table 4.8. Time constants obtained from fitting the TAS in acetonitrile at the longer pump wavelength. *Quoted errors here are from the fit in Glotaran. Experimental errors are half of the IRF.

Time constant	**AVOCTO1**	**AVOCTO5**	**Avobenzone**
τ_1	453 ± 3.7 fs*	513 ± 5.3 fs	450 ± 7.2 fs
τ_2	3.03 ± 0.027 ps	4.05 ± 0.024 ps	2.7 ± 0.03 ps
τ_3	48.3 ± 1.17 ps	73.7 ± 1.9 ps	60.9 ± 1.70 ps
τ_4	>3 ns	>3 ns	>3 ns

The results for avobenzone in these experiments produce lifetimes that are longer than those of the main comparison work above but the results for avobenzone are closely comparable to the results for AVOCTO1 and AVOCTO5. Thus, it is believed that in AVOCTO compounds (with the exception of AVOCTO3), excitation ~350 nm and the subsequent photodynamics are due to excitation of the avobenzone-derived chromophore. The lifetimes do not seem to be affected by the other parts of the molecule. In keeping with the conclusion of Holt, E. the lifetimes are assigned to the same processes with the discrepancy due to solvent and instrumental effects.

4.4.4 Assigning the features in the TAS at pump wavelength <290 nm

When attempting to fit the shorter pump wavelength TAS, there was no fit that converged for AVOCTO3. AVOCTO1 and AVOCTO5 did return fits (Table 4.9) but there was less similarity between them than in the longer wavelength studies. The second time constant for AVOCTO5 is much longer than AVOCTO1 while the first time constant is very similar in length. The difficulty in obtaining a fit for AVOCTO3 is due to the more complex spectral features and the software is unable to unravel the different processes taking places. As the

primary interest in the UVA band, detailed analysis of the features in this part are not within the scope of this thesis.

Table 4.9. Time constants obtained from fitting the TAS in acetonitrile at the shorter pump wavelength. *Quoted errors here are from the fit in Glotaran. Experimental errors are half of the IRF.

Time constant	**AVOCTO1**	**AVOCTO3**	**AVOCTO5**
τ_1	261 ± 3.3 fs*	NA	217 ± 2.8 fs
τ_2	13.4 ± 0.49 ps	NA	426.3 ± 20 ps
τ_3	>3 ns	NA	>3 ns

4.4.5 NMR study of AVOCTO5 photostability

A complementary study that was carried out to confirm the stability of AVOCTO5 involved taking an NMR spectrum before and then immediately after irradiation in acetonitrile. The two spectra produced are displayed below (Figure 4.30.). There was no significant change in the ratio of the peaks that correspond to the relative amount of the enol and keto forms (marked with dashed blue lines on the spectra). This study suggests that the same molecular entity is present before and after irradiation but does not preclude that other molecules are formed that were not detected. Combined with the ultrafast studies this seems to confirm that the processes that produce a loss of activity in the UV are ultrafast and then, at longer times, the parent molecule is recovered.

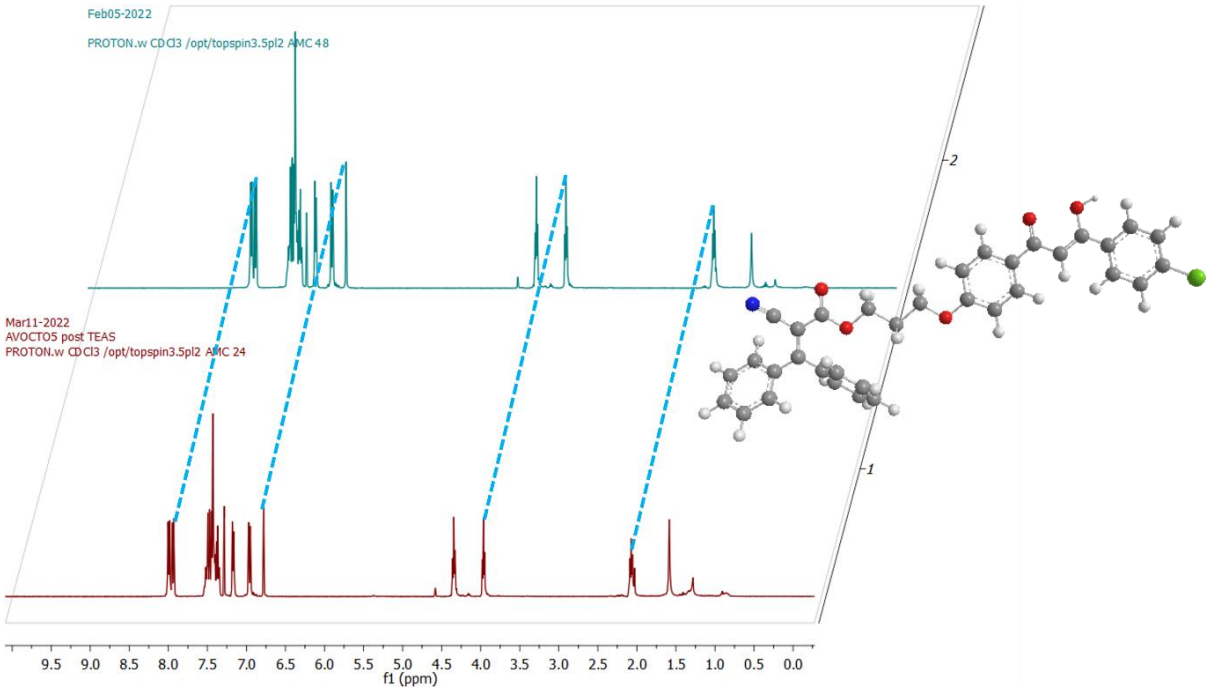

Figure 4.30. NMR spectra of AVOCTO5 before and after 60 minutes irradiation (same conditions as before in the longer pump wavelength scheme) in acetonitrile.

4.4.6 Computational results (AVOCTO1, AVOCTO3 and AVOCTO5)

Truncated models for AVOCTO1, AVOCTO3 and AVOCTO5 were investigated computationally as it was not possible to achieve convergence for the complete structures. Our assertion above that photodynamics following UVA excitation are predominately due to the avobenzone-derived moiety allows us to truncate the molecule to only include the avobenzone-derived part in our initial geometry optimisation. Results are displayed as figures (Figures 4.31.X1-X6) with accompanying summaries (Table 4.10-12). For computational details including basis set and functional, see Materials and Methods.

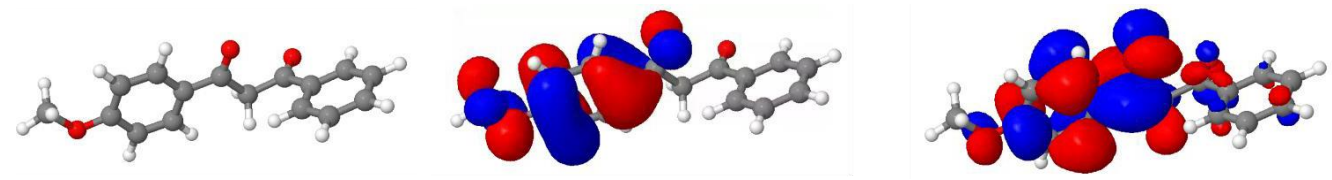

Figure 4.31.X1. AVOCTO1 - diketo form - optimised geometry transition with greatest oscillator strength. The centre orbital is the HOMO and the right-hand orbital is the LUMO.

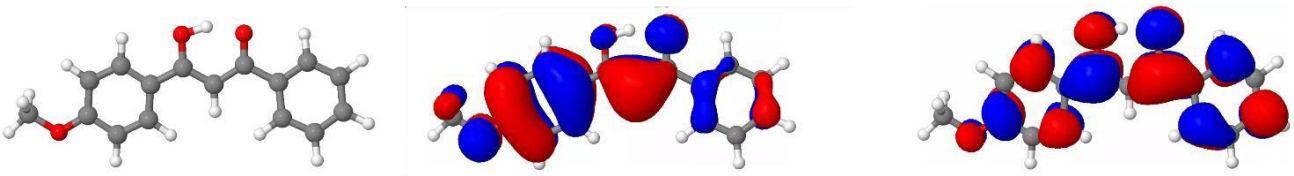

Figure 4.31.X2. AVOCTO1 - chelated enol form - optimised geometry transition with greatest oscillator strength.

Table 4.10. AVOCTO1 results summary

AVOCTO1 form	**S_n**	**E (eV)**	**E (nm)**	**State character**	**Total oscillator strength**
Diketo	S_1	3.84	322	nπ*	0.0003
	S_2	4.06	306	nπ*	0.0001
	S_3	4.34	285	ππ*	0.0142
	S_4	4.60	269	ππ*	0.4963
	S_5	4.74	262	nπ*	0.0143
Enol	S_1	3.62	342	ππ*	0.8873
	S_2	3.97	312	nπ*	0.0002
	S_3	4.46	278	ππ*	0.0229
	S_4	4.50	275	ππ*	0.0227
	S_5	4.63	267	ππ*	0.0633

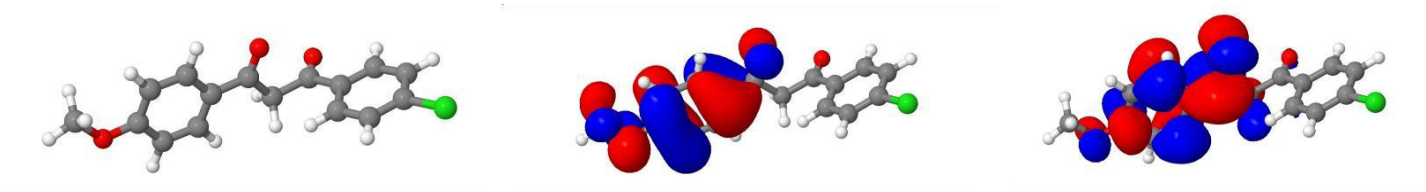

Figure 4.31.X3. AVOCTO5 - diketo form - optimised geometry transition with greatest oscillator strength. The centre orbital is the HOMO and the right-hand orbital is the LUMO.

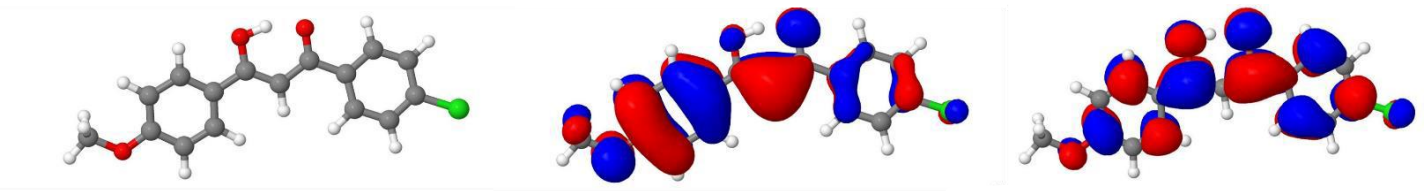

Figure 4.31.X4. AVOCTO5 - chelated enol form - optimised geometry transition with greatest oscillator strength.

Table 4.11. AVOCTO5 results summary

AVOCTO5 form	**S_n**	**E (eV)**	**E (nm)**	**State character**	**Total oscillator strength**
Diketo	S_1	3.83	324	ππ*	0.0004
	S_2	4.09	303	ππ*	(3.0802E-5)
	S_3	4.26	291	ππ*	0.0028
	S_4	4.60	270	ππ*	0.5655
	S_5	4.67	266	nπ*	0.0033
Enol	S_1	3.57	347	ππ*	0.9422
	S_2	3.97	312	nπ*	0.0004
	S_3	4.40	281	ππ*	0.0732
	S_4	4.56	272	ππ*	0.0804
	S_5	4.62	268	ππ*	0.0080

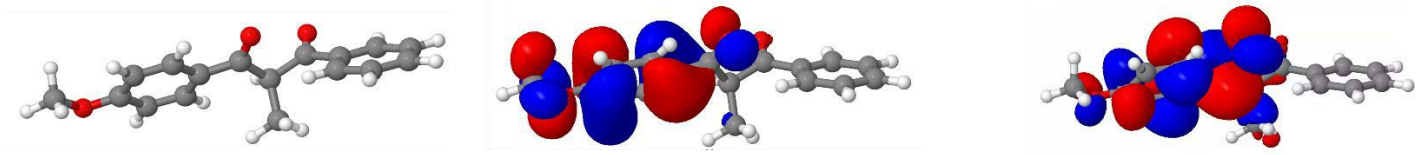

Figure 4.31.X5. AVOCTO3 - diketo form - optimised geometry transition with greatest oscillator strength. The centre orbital is the HOMO and the right-hand orbital is the LUMO.

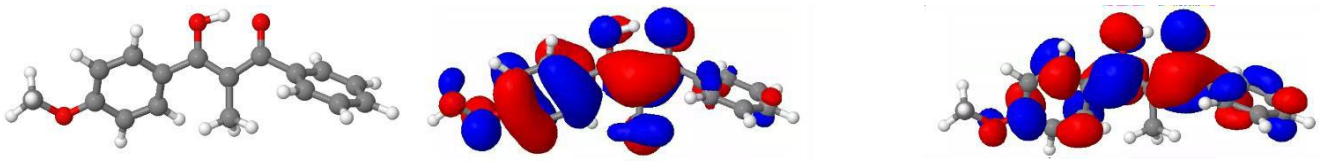

Figure 4.31.X6. AVOCTO3 - chelated enol form - optimised geometry transition with greatest oscillator strength.

Table 4.12. AVOCTO3 results summary

AVOCTO3 form	**State**	**E (eV)**	**E (nm)**	**State character**	**Total oscillator strength**
Diketo	S_1	3.89	324	nπ*	0.0013
	S_2	4.00	310	nπ*	0.0018
	S_3	4.46	278	ππ*	0.0022
	S_4	4.59	270	ππ*	0.5159
	S_5	4.75	261	ππ*	0.0176
Enol	S_1	3.81	326	ππ*	0.6110
	S_2	4.07	305	ππ*	0.1109
	S_3	4.57	271	nπ*	0.0203
	S_4	4.70	263	ππ*	(1E-5)
	S_5	4.76	260	ππ*	0.0069

The highest oscillator strength corresponds to the predicted brightest transition, and a higher degree of vibronic coupling. The values obtained for AVOCTO1 (enol, 342 nm) agrees well with experiment (350 nm). For AVOCTO5 (enol, 347 nm) the value is also in agreement

with our experimental value (354 nm) and also accounts for the slight redshift in the absorbance. This is attributed to an allowed transition (S_1 <- S_0) with ππ* character. The brightest transitions for the diketo forms of AVOCTO1, 5 and 3 respectively are 269 nm, 270 nm and 270 nm and these are in reasonable agreement with our experimental values of 290 nm, 285 nm and 280 nm. This is also attributed to an allowed transition to a higher lying energy state (S_4 <- S_0) with ππ* character.

4.5 Chapter summary

While avobenzone is one of the most widely used sunscreen active ingredients it is known to degrade over time and to have a particularly efficient degradation pathway in polar aprotic environments. Experiments using binary mixtures are interesting in order to gain an initial idea of whether there is an interaction between both molecules in solution at low concentration; but it is an unresolved question whether there is a direct stabilisation effect or not despite empirical evidence that degradation or loss of activity is reduced when mixing avobenzone with synthetic MAA analogues or with octocrylene under some conditions.

A composite sunscreen that is a hybrid of known efficient sunscreening molecules may provide a number of advantages. It is shown here that the new composite sunscreen molecules (AVOCTOX) are stable to UV light and this innovation addresses the main degradation pathway of avobenzone in acetonitrile. It is also shown that the esterification reaction that forms the final ester bond can be expanded, with some modifications, to other acids and this can allow adjustment of properties that could confer further benefits. It is also believed that the body of literature already published on avobenzone can be drawn on to understand the photodynamics of the new molecules given that our ultrafast spectra and computational results demonstrate that the behaviour is highly comparable to avobenzone itself; a result that suggests that hybrid sunscreen molecules could be created from other state-of-the-art sunscreens that are already seen as effective from a photochemical perspective. Further research could explore the effect of modifying the linker atoms, with the possibility of introducing other chromophores.

More studies would have to be conducted in order to ascertain the exact mechanism of the photostability as a ground state bleach in our ultrafast spectra suggests that the full recovery of the parent molecule AVOCTO5 occurs at longer timescales than the ultrafast experiments but at shorter times than can be observed reliably using UV-vis spectroscopy. Additionally, the larger molecular weight of the composite sunscreen may also be useful in formulations as higher molecular weights are less likely to be absorbed through the skin and enter systemic circulation.

Chapter 5. Exploiting Genomics for Natural Product Synthesis

"I want to replace all the chemists with bacteria, and the bacteria will use carbon dioxide and sugar and will be able to genetically program all the chemical factories of the future…they make one product and not a lot of waste products – human chemists haven't learned how to do that."

Frances Arnold

(speaking on *The Life Scientific*, BBC Radio 4 - 06/09/2022)

5.1.1 Background

Enzymes are a product of millions of years of evolution and in recent times researchers have investigated the potential of engineering the biological world with applications in fields ranging from pharmaceuticals to renewable fuels. Broadly speaking, bioengineering is the study of how to make compounds of interest based on Nature's tools, biosynthesis is the study of how to make natural products and biocatalysis investigates how to deploy enzymes that can be used at scale. Developing a scalable and versatile synthesis of bulk and fine chemicals using the tools already present in Nature and through bioengineering are key ambitions of a future global biorefinery, which could allow us to meet our chemical needs in the future. One pioneer in this field is 2018 Noble laureate Frances Arnold, who uses directed evolution to optimise chemistry through molecular biology. In one definition, molecular biology means using the cellular machinery available within a cell and combining it with synthetic (i.e., laboratory-made) substrates. The naturally occurring compounds gadusol and 4-deoxygadusol (Figure 5.1) contain the key building block cyclohexenone motif with 4-deoxygadusol an intermediate in the biosynthetic pathway of mycosporine-like amino acids (MAAs) in Cyanobacteria. In Nature, these precursors are then transformed by a series of enzymes into a wide range of MAAs; and understanding the steps in this process could allow us to adapt an important secondary metabolite synthetic pathway from Cyanobacteria to our needs.

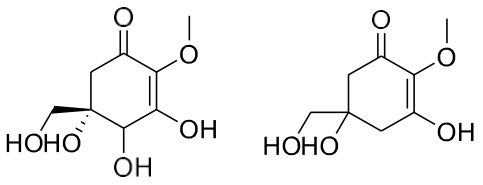

Figure 5.1. (left) Gadusol (1,4,5-trihydroxy-5-hydroxymethyl-2-methyoxycyclohex-1-en-3-one). (right) 4-Deoxygadusol.[1]

5.1.2 Convergent pathways in Cyanobacteria

Cyanobacteria are phototropic prokaryotes that live in shallow water habitats i.e., they obtain their energy from sunlight and are exposed to high levels of UVR. As well as their primary metabolism, they also prolific producers of bioactive secondary metabolites.[2] In 2010, a 6.5 kb, four gene biosynthetic cluster was identified for the conversion of natural primary metabolite sedoheptulose-7-phosphate (7-SHP) to the MAA, shinorine in the filamentous diazotrophic, nitrogen-fixing cyanobacteria *Anabaena variabilis* (ATCC 29413) and *Nostoc punctiforme* (ATCC 29133) via the pentose phosphate pathway (Figure 5.2).[3] Genes *ava_3858* and *ava_3857* encode the enzymes desmethyl 4-deoxygadusol (DDG) synthase and *O*-methyltransferase (O-MT), respectively in *A. variabilis*. The stepwise action of these enzymes produces 4-deoxygadusol (4-DG). The product of the gene *ava_3856* catalyses the addition of glycine to 4-DG to form mycosporine-glycine – a well-known MAA (See Figure 5.2.)

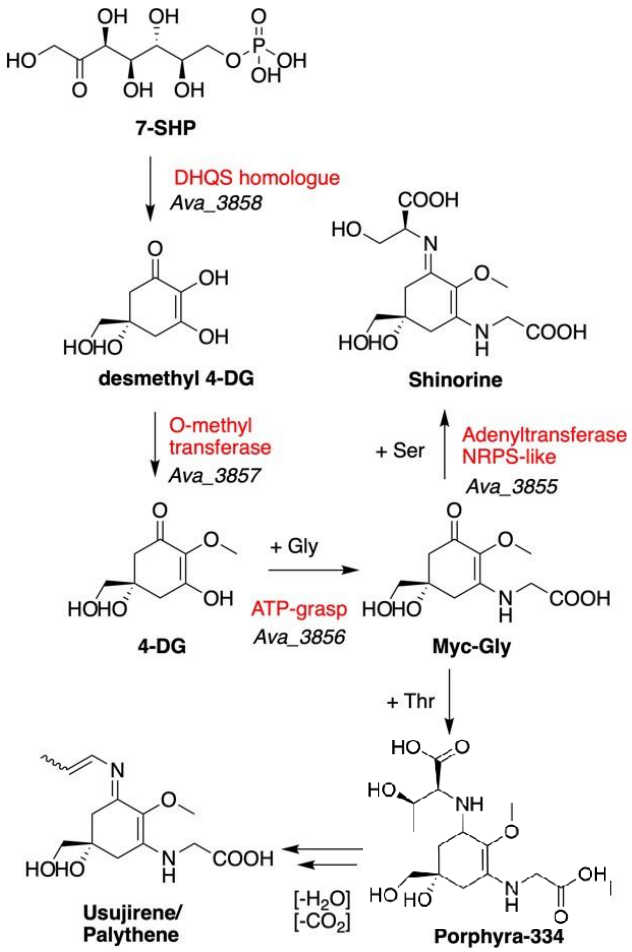

Figure 5.2. Pathway in a species of cyanobacteria (*A. variabilis)* depicting a biosynthetic route to an oxy-type mycosporine, mycosporine-glycine. Sedoheptulose 7-phosphate (7-SHP) is a primary metabolite involved in the pentose phosphate pathway while deoxy-d-arabino-heptulosonate 7-phosphate (DAHP) is a primary metabolite involved in the shikimate pathway.

Previous studies had exclusively assigned biosynthesis of MAAs to the shikimate pathway.[4–6] Despite the more recent discovery of the role of the pentose phosphate pathway, the shikimate pathway still appears to be the predominant pathway in *A. variabilis* in terms of amount produced as confirmed by a gene knockout experiment (Figure 5.3).[7] Both "functionally duplicate yet distinct" convergent pathways have a common intermediate in 4- deoxygadusol and after the pathways converge at the shared intermediate, addition of a glycine residue produces mycosporine-glycine (MG). MG is then the common intermediate for di-substituted (iminocyclohexenimine-type) MAAs which are the key end-product UVA absorbers and promising sunscreens of this thesis.

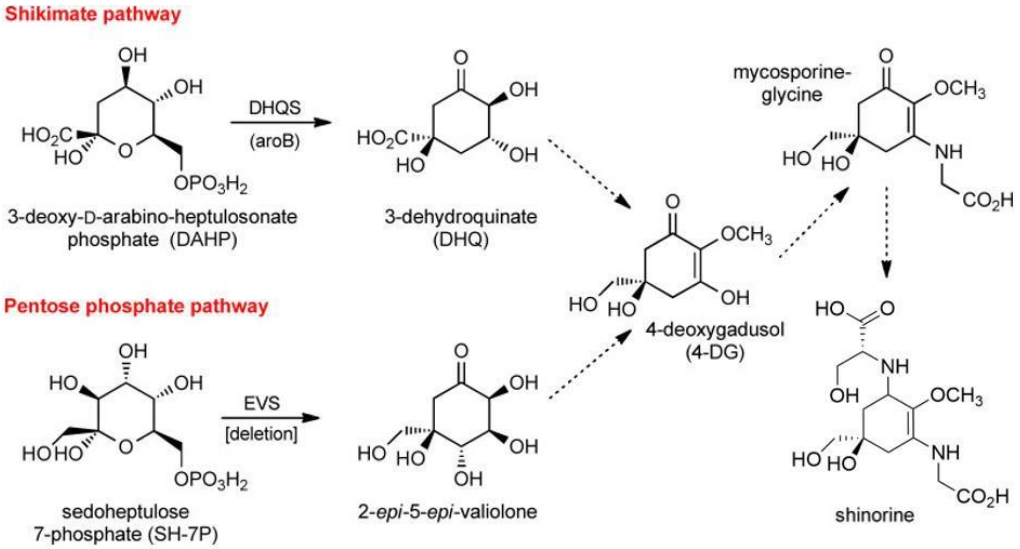

Figure 5.3. Postulated convergent pathways of MAA biosynthesis in cyanobacteria re-printed from ref[8]I. EVS: 2-*epi*-5-*epi*-valiolone synthase. DAHP: deoxy-d-arabino-heptulosonate 7-phosphate. The EVS gene is typically absent in non-producers.[9]

5.1.3 Mycosporine glycine synthesis in *A. variabilis*

In *A. variabilis*, the second amino acid residue is condensed with mycosporine-glycine in a step that is encoded by a nonribosomal peptide synthetase (NRPS)-like enzyme (the product of *ava_3855*, see Figure 5.2, above). It is this final enzyme in the cluster that will be explored in more detail.

5.1.4 NRPS enzymes

Non-ribosomal peptide synthetases (NRPSs) are multi-modular enzymes that are involved in the synthesis of a diverse range of secondary metabolites and, in particular, peptides. Vancomycin, a heptapeptide glycopeptide antibiotic is produced primarily by three NRPSs.[10] It is the sequential arrangement of the modules within each NRPS that determines

the structure of the final product. In general, NRPSs activate specific amino acids by converting them into the aminoacyl thioester complexes, leading to peptide bond formation between the activated amino acids and/or a nucleophilic substrate (see Figure 5.4). Both proteinogenic as well as nonproteinogenic amino acids can be activated and incorporated into natural products in this way by NRPS enzymes.[11] The A domain is effectively a gatekeeper domain that defines the specificity of the amino acid. The C domain is predicted to be less selective and to be able to activate a wider range of amino acids as the corresponding thioesters and to have a role in the condensation reaction. Indeed, the A and PCP domains are always present in NRPS modules whereas the condensation (C) is normally present in chain extension modules. Additionally, NRPS are energy intensive and use the conversion of ATP to AMP as an energy source. Finally, the NRPS method of making proteins stands in contrast to how peptides are synthesised in the ribosome, where anticodons (tRNA) are used to assemble proteins.

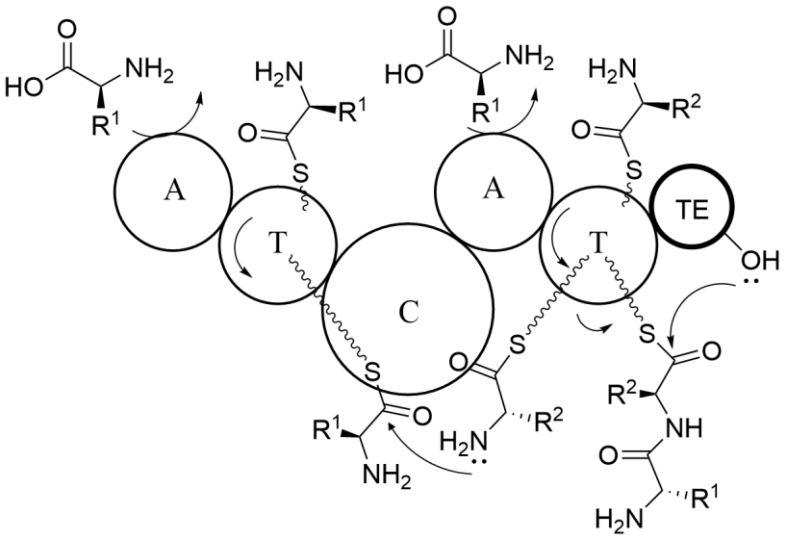

Figure 5.4 Adapted from ref.[15] This simplified model demonstrates the ordered, modular mechanism of the NRPS enzyme. The thiol group of the 4'-phosphopantetheine arm tethered to the T domain captures an aminoacyl-AMP intermediate and C domain catalyses peptide bond formation between adjacent T domain-loaded thioester intermediates. The TE domain catalyses the release of the peptide from the NRPS.

5.1.5 Mechanism of mycosporine glycine synthesis in *A. variabilis*

One understanding of the reaction mechanism is the activation of the serine carboxylate by adenylation, activating the amino acid as aminoacyl-AMP. Subsequently, the activated amino acid is transferred to the 4'-phosphopantetheine moiety of the thiolation domain (T-domain) or peptidyl carrier protein (PCP) domain with the release of AMP (see Figure 5.5).[12]

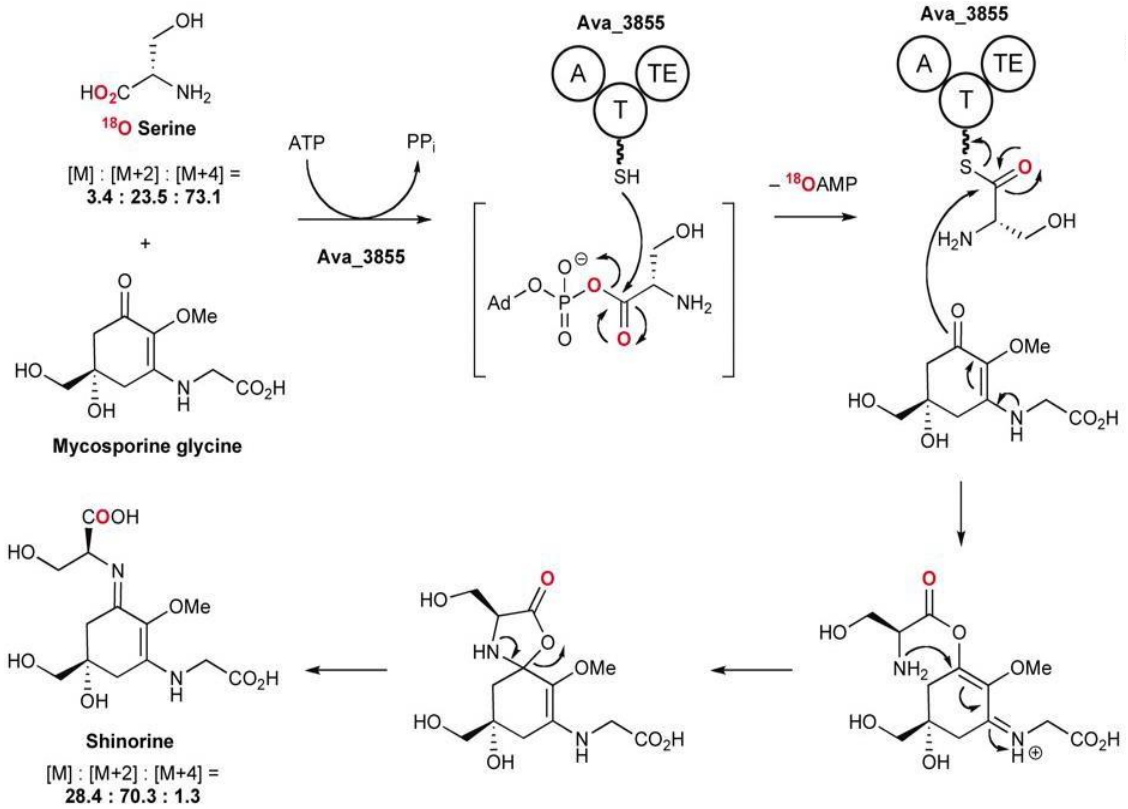

Figure 5.5. One mechanism proposed by Balskus and Walsh.[3] The radiolabelled-amino acid serine is activated as the thioester towards nucleophilic attack by the conjugated enaminone (MG) and a subsequent cyclisation process driven by a Michael addition of the free -NH_2 of the newly added amino sidechain leads to the final product.

An alternative mechanism for conversion of mycosporine-glycine to shinorine is proposed by the same authors and is re-drawn in Figure 5.6.

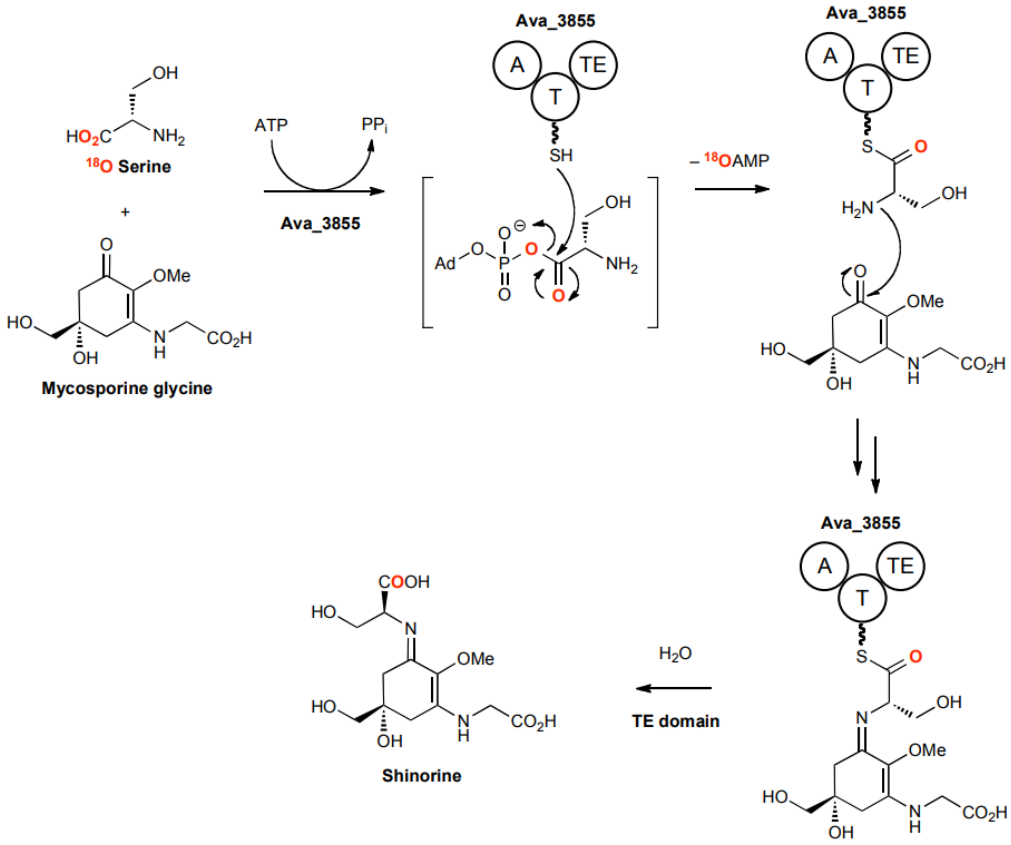

Figure 5.6. Alternative mechanism proposed by Balskus and Walsh. Here the aminoacyl thioester enzyme complex acts directly as a nucleophile through the free -NH_2 group, while the oxo-MAA (MG) acts as the electrophile. NB: This mechanism has greater similarity to the biosynthetic mechanism with the bound amino acid acting as a nucleophile.

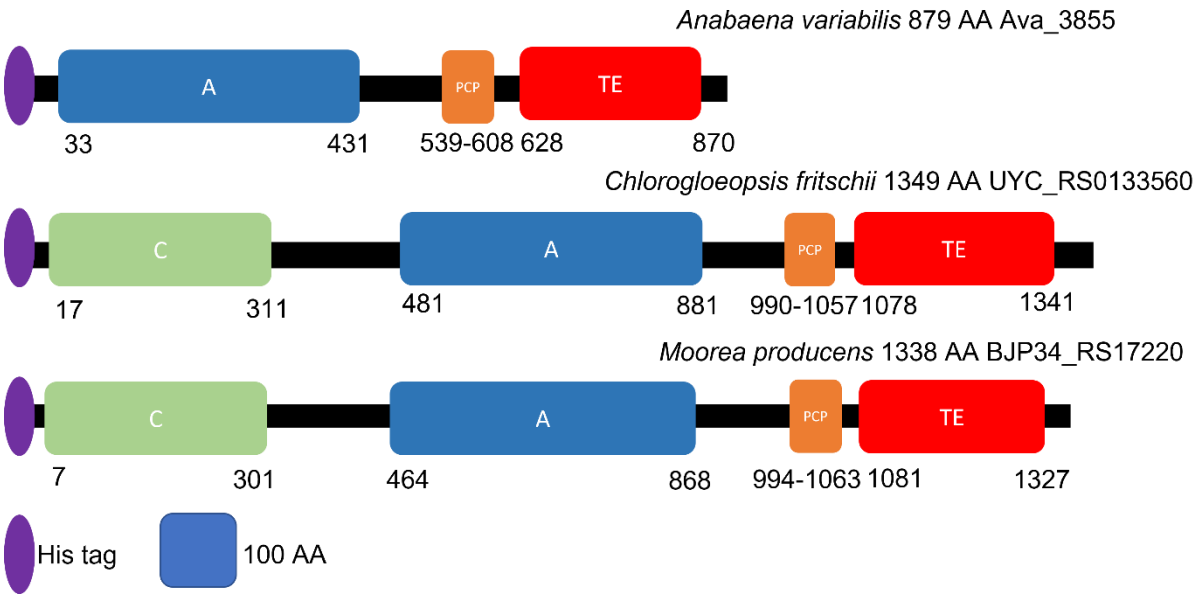

Figure 5.7. Comparative genetic analysis of domain organisation of NRPS-like amino acid sequences that direct MAA biosynthesis in three species of cyanobacteria. The A group defines the specificity of the amino acid. PCP (orange) is a small domain with a thiol group that acts as nucleophile to towards a carbonyl. The C domain may have a role in combining a substrate and activated amino-acid, although it may also not be essential at all in this case and merely an evolutionary relic in the latter two sequences. TE: thioesterase domain. Details of the analysis (and full sequences) can be found in the thesis of Dr. Nazia Auckloo. Briefly, Clustal Omega (https://www.ebi.ac.uk/Tools/msa/clustalo/) was used to carry out sequence alignment. AntiSMASH bacterial version (https://antismash.secondarymetabolites.org/#!/start) was used to delineate the specific domains. AA = amino acids. Domain annotation was confirmed by Conserved Domain Search (https://www.ncbi.nlm.nih.gov/Structure/cdd/wrpsb.cgi).

From genome mining similar clusters have been found in other species and these are explored in Dr. Nazia Auckloo's thesis *Investigation and Exploitation of Mycosporine-like amino acids from Rhodophytes and Bacteria* (University of Warwick). A cryptic biosynthetic cluster that, based on sequence analysis, should produce a novel MAA where proline is activated and reacted with mycosporine-glycine was found in another cyanobacterium, *Moorea producens*. Other organisms including *C. fritschii*, are predicted to contain similar (but not cryptic) clusters (a comparative analysis is displayed Figure 5.7., above) but with different amino-acid selectivities.[13] For example in the *C. fritschii* case, shinorine is produced where selectivity is for threonine, as in the Balskus and Walsh paper above. BLAST searches or the more modern biosynthetic gene cluster-mining tool, AntiSMASH can be used to identify biosynthetic pathways.[14]

5.1.6 Metabolic potential of the genus *Moorea*

Preliminary genomic analysis has suggested that genome-guided approaches can enable the discovery of novel compounds (i.e., natural products (NPs)) from even well-studied *Moorea* strains, highlighting the importance of obtaining complete genomes.[13] There is, to our knowledge, no experimental record of a *Moorea* strain producing an MAA. Inspecting the complete genome of the filamentous tropical marine cyanobacterium, *Moorea producens* PAL, reveals that about one fifth of its genome is devoted to production of secondary metabolites - four times the cyanobacterial average and a higher than average number of biosynthetic gene clusters (BGCs). [PAL refers to the geographical source of the strain: Palmyra Atoll in the Northern Pacific Ocean, USA]. On top of that, as of 2017, the genus *Moorea* has yielded more than 40% of all reported marine cyanobacterial NPs with an average of 18% of their genome dedicated to secondary metabolism. Thus, our main motivation is choosing *Moorea* for further investigation was the specificity of the A domain and the recognised potential of the strain to produce NPs.

5.1.7 Aims and Objectives

- To re-engineer a complete coding sequence of nrps-like gene (containing a C, A, PCP, T domain) that has not previously expressed a fully functional protein, to express only the C domain.

- To purify and characterise the protein/s to enable study of the particular role of that domain within MAA biosynthesis.

- To detect whether incubating the proteins with substrates (either extracted from natural sources or made synthetically) leads to production to predicted products

5.2 Results

5.2.1 Cloning/purification

The Materials and Methods section records in detail the strategy used for the cloning and purification steps and it is summarised here. Two bacterial expression plasmids containing the full gene cluster identified in the genomic analysis from two species of cyanobacteria, *Chlorogloeopsis fritschii* (NCBI:txid1124), **AMC1**, and *Moorea producens* (NCBI:txid1155739), i.e., containing a codon with a condensation domain, an adenylation domain, a PCP domain, were re-engineered to only express the condensation domain (C domain, see Figure 5.8). The identity of the new vectors was checked by restriction digest (Figure 5.9), agarose gel (Figure 5.10) and the purified protein was analysed by SDS-PAGE gel (Figure 5.11). Expressing and purifying the condensation domain (hereafter referred to variably as the C domain or enzyme) avoids the need for substrate uptake into the cell and simplifies a search for compatible substrates through in vitro assays. The C domain from the *Moorea* cluster was expressed and purified successfully. However, as the *Chlorogloeopsis* C domain-only gene product was insoluble and therefore not possible to study further, the remainder of this chapter will focus only the *Moorea* C domain-only gene product.

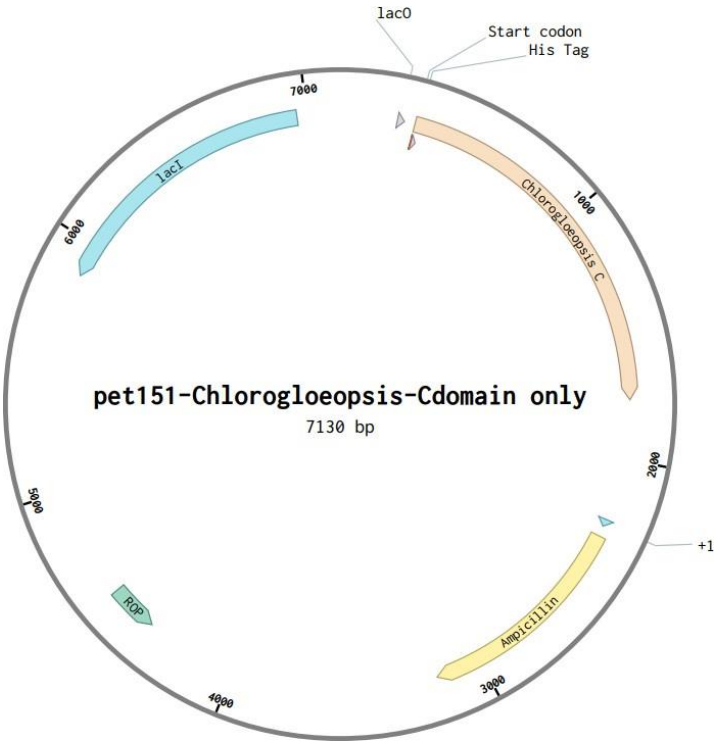

P1

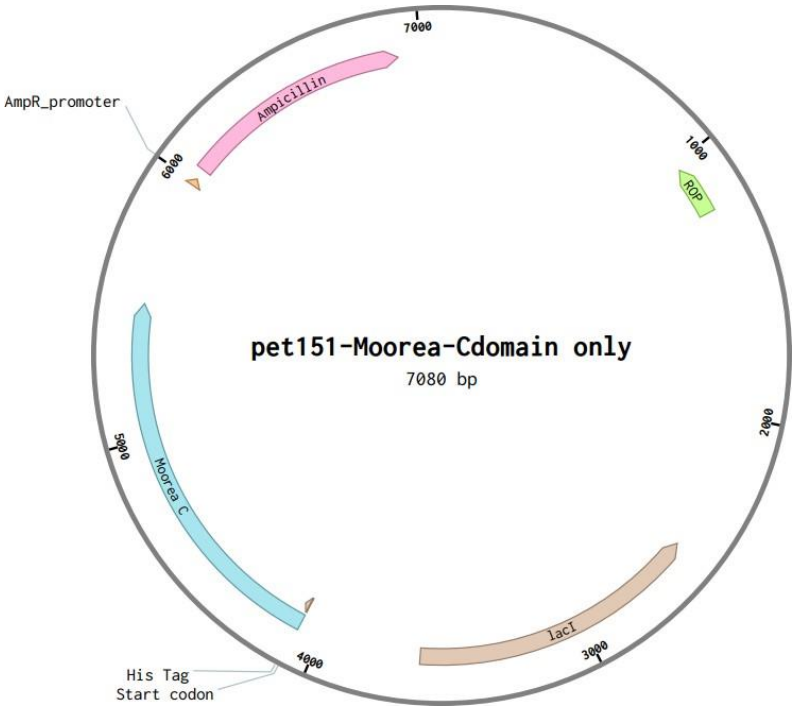

P2

Figure 5.8. New plasmids. **P1**, *Chlorogloeopsis C domain only*. **P2**, *Moorea* C domain only.

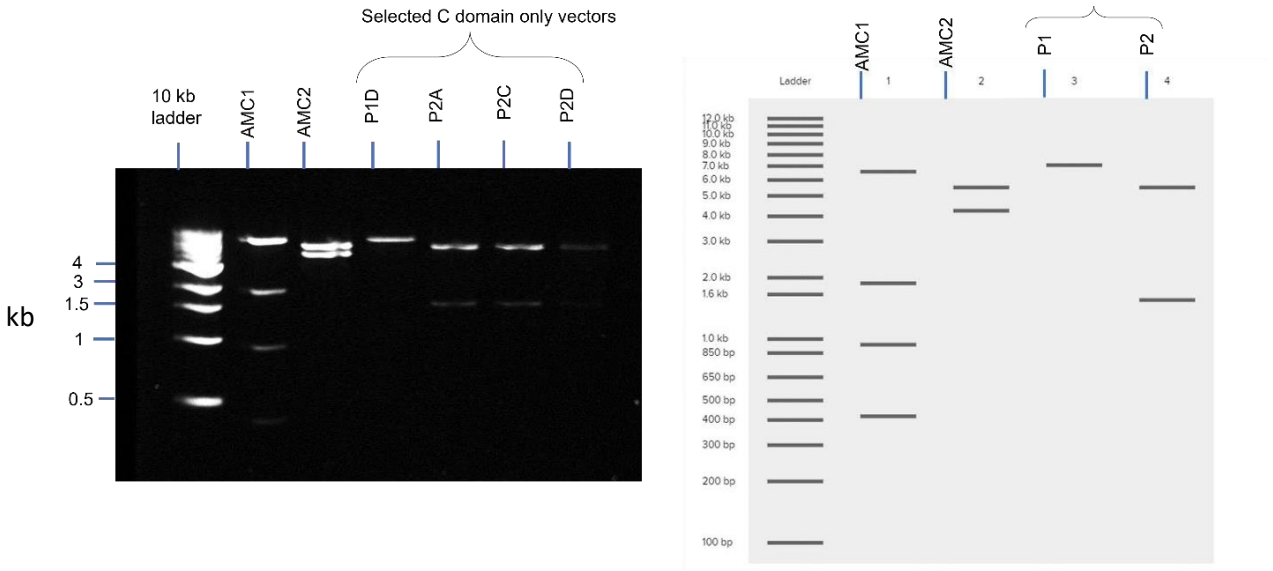

Figure 5.9. Restriction digest. Gel Key: (left) Gel was prepared and run using Method 2. AMC1 and AMC2 are the original plasmids. P1D contains the desired plasmid derived from *Chlorogloeopsis* and P2A, P2C and P2D contain the desired plasmid derived from *Moorea*. (right) Virtual digest created in Benchling using PvuI.

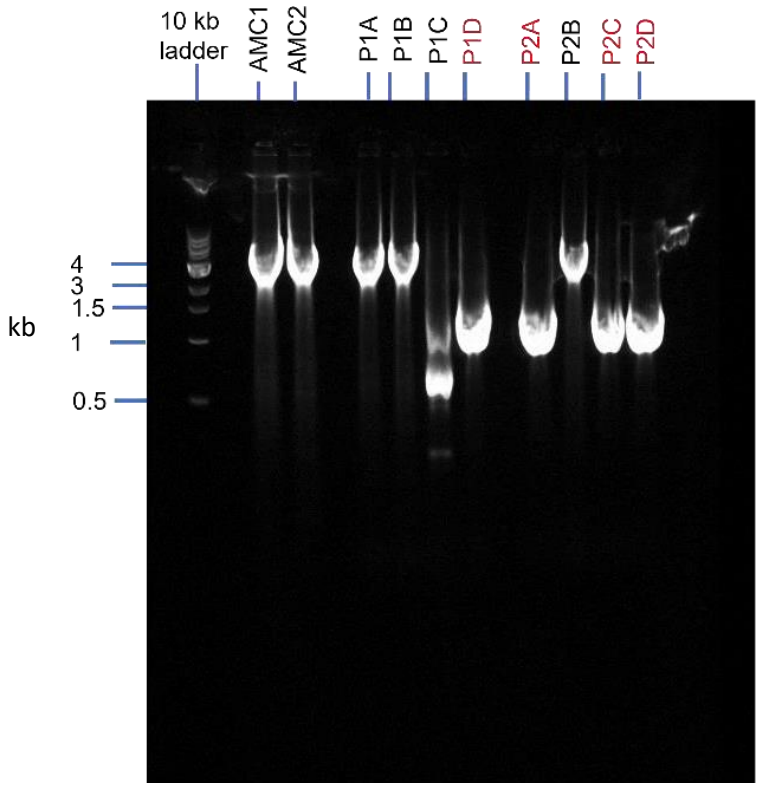

Figure 5.10. Annotated agarose gel using Method 2 (Materials and Methods). Gel Key: **AMC1** and **AMC2** are the original plasmids. P1A, P1B, P1C and P1D were isolated from a culture of A1. P2A and P2B were isolated from a culture of A2. P2C and P2D were isolated from a culture of C2. P1D (red) contains the desired plasmid derived from *Chlorogloeopsis* (C domain 1470 bp) and P2A, P2C and P2D (red) contain the desired plasmid derived from *Moorea* (C domain 1273 bp).

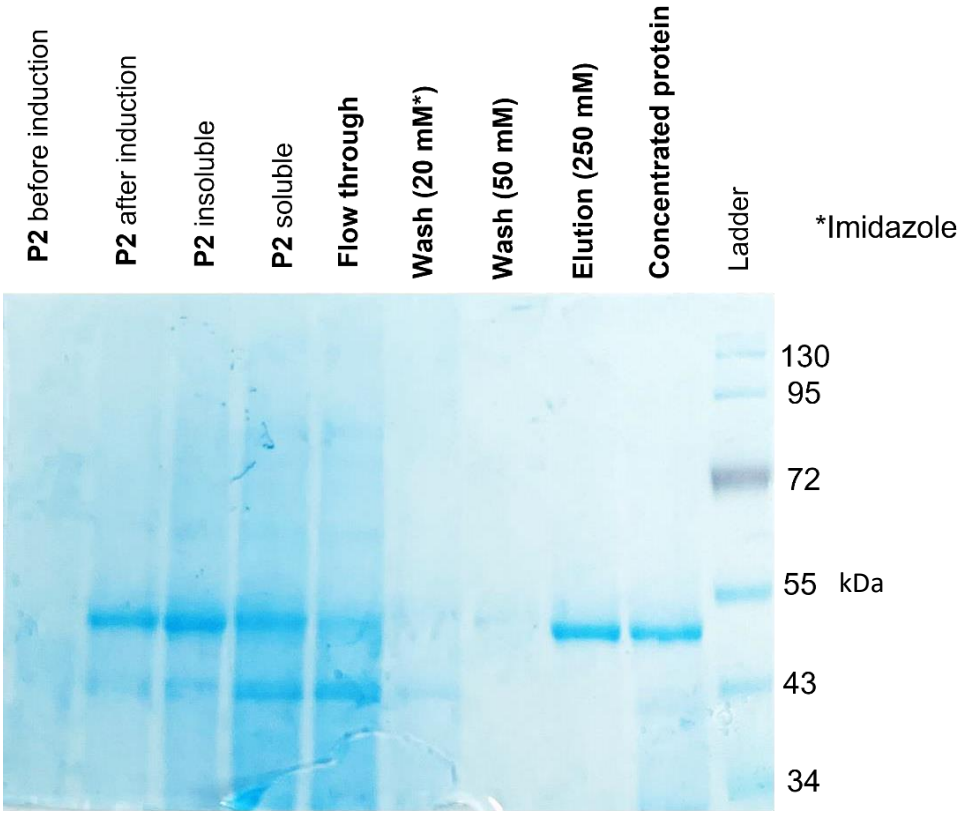

Figure 5.11. SDS-PAGE Gel of the protein produced by construct **P2C** containing the C-domain from the *Moorea* construct. The lane labelled 'concentrated protein' contains the protein of interest as confirmed by the theoretical base pair number.

5.2.2 Computational modelling results for the *Moorea* C domain

Using *in silico* tools, a best guess model for the structure of the *Moorea* C domain was obtained. Firstly Phyre2 (Figure 5.12.) was used to compare across known structures with sequence homology. Secondly Alphafold (Figure 5.13.) was used, drawing on state-of-the-art machine learning, to obtain a best prediction structure for the C domain. There is very good agreement between the structures obtained via the two methods (~92%), demonstrated by the overlay in Figure 5.14.

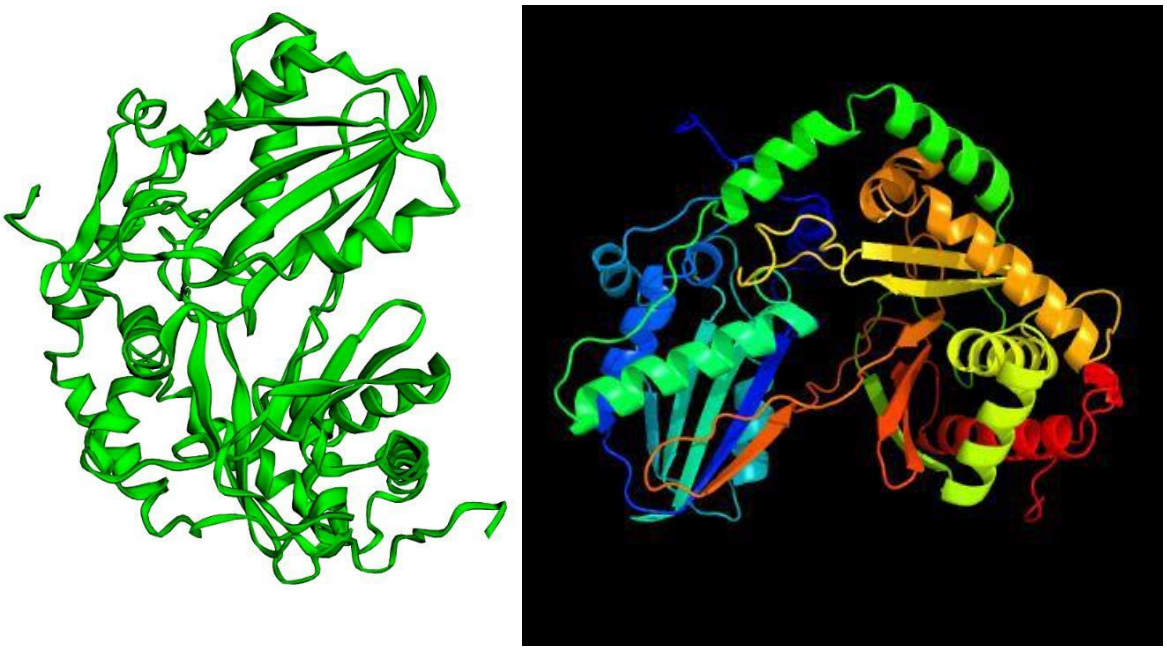

Figure 5.12. A) pdb file from Phyre2, visualised in EzMol. Phyre2 result based on template c5u89A . 429 residues (98% of the sequence) were modelled with 100% confidence by the single highest scoring template. B) same file coloured by secondary structure.

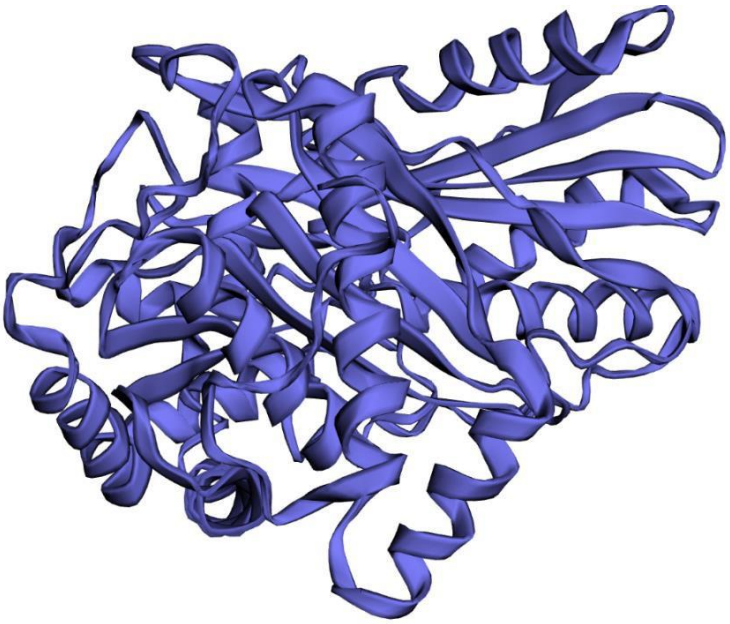

Figure 5.13. .pdb file obtained from Alphafold 2.1.1 'best prediction', viewed in EzMol.

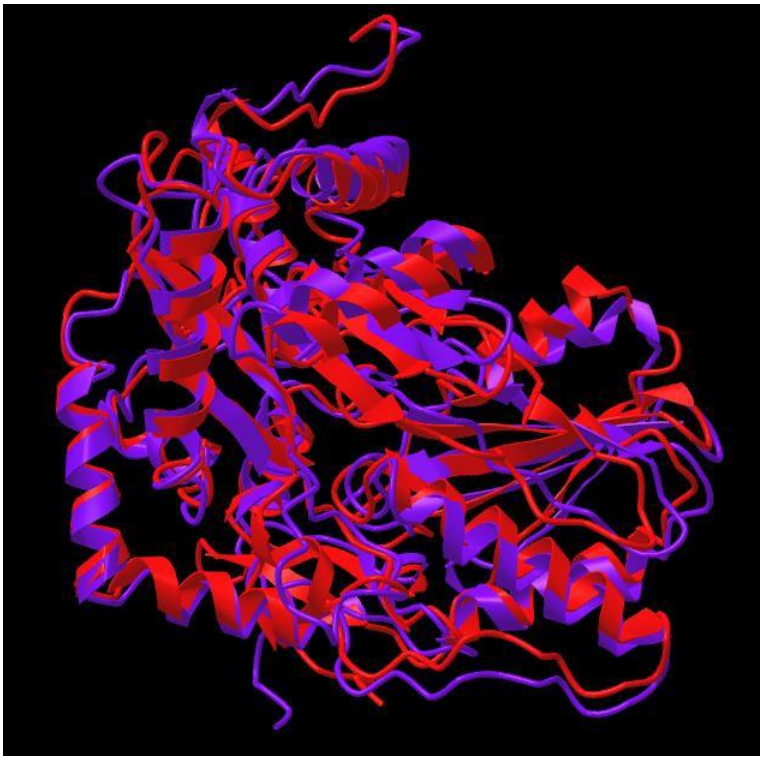

Figure 5.14. Overlay of the Alphafold 2.1.1 best prediction (purple) with the Phyre2 model prediction (red). Alignment RMSD: 2.175 Å. TM-score: 0.9166. Viewed using iCn3D Structure Viewer.

5.2.3 Detection of potential products with an HPLC assay

An HPLC assay was carried out as described in the Materials and Methods section in order to observe any reactions between any of the substrates and the activated (i.e., thioesterified) amino-acids, and whether adding enzyme had any effect. The SNAC thioester is a reasonable mimic of the biosynthetic pathway owing to its similarity to the enzyme-bound thioester. The reactions under consideration with proposed products are detailed in Figure 5.15. If a product were to be detected, the desired products based on the mechanisms introduced above would all appear at longer wavelengths, as predicted by their more conjugated structures.

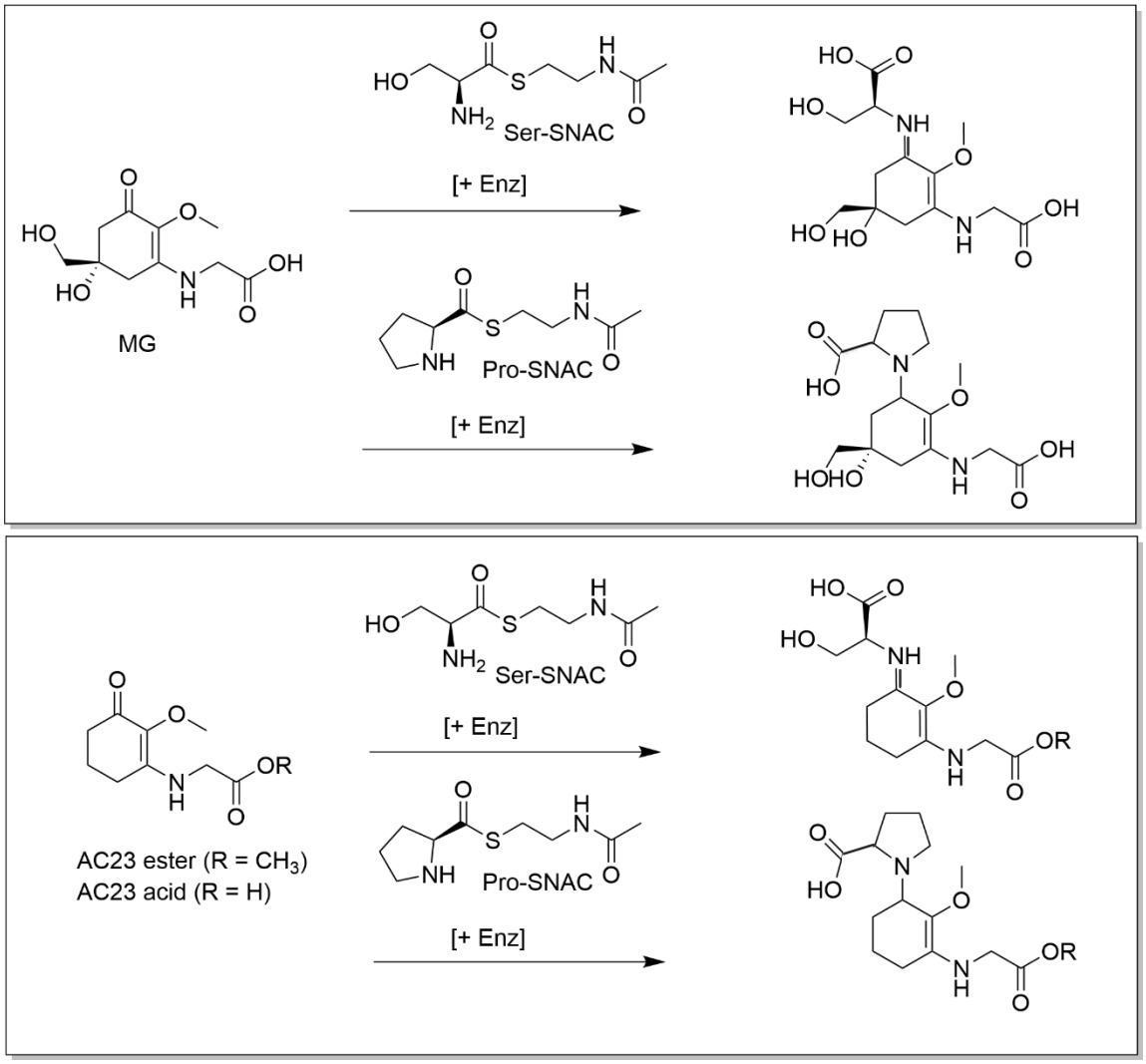

Figure 5.15. (Right) Desired products of the HPLC assay using the stated substrates (left). Enz = C domain.

Images of the HPLC chromatograms, firstly the substrates individually and then the incubations with and without enzyme at room temperature, obtained are included below. A Nanodrop 'check' of the UV-vis absorption of the three key MAA-like substrates is included for reference in Figure 5.16. From an inspection of these results (Figure 5.17-5.23), incubation with the *Moorea* C domain enzyme did not affect any of the chromatograms and no new significant peaks were observed when substrates were incubated for 24 hours, although there is evidence of decomposition in some samples Additional mass spectrometry experiments and testing of the solutions on the in-lab Nanodrop failed to show any emerging new peaks in the UV-vis region also. The reasons for this could be that the amount produced was below the threshold of detection for any of the methods used; the concentrations of substrates could be too low in the mixture to react; the enzyme concentration could be insufficient to catalyse the reaction; the reactants could undergo other reaction pathways that do not lead to the expected products.

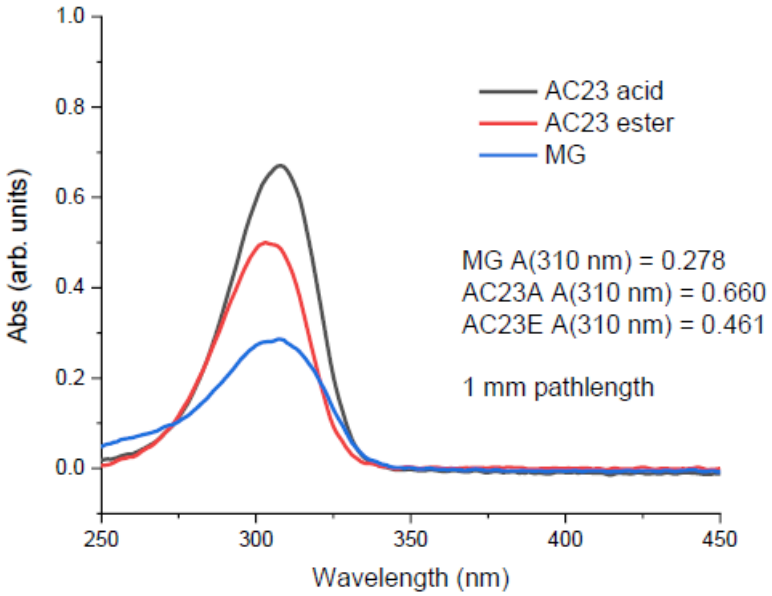

Figure 5.16. Nanodrop assay confirming that substrates mycosporine glycine (MG), AC23 ester (AC23E) and AC23 acid (AC23A) absorb at 310 nm. These were prepared in prepared in 20 mL buffer (100 mM HEPES, 50 µM TCEP, pH 7.5) and diluted with distilled water until within the range of the Nanodrop.

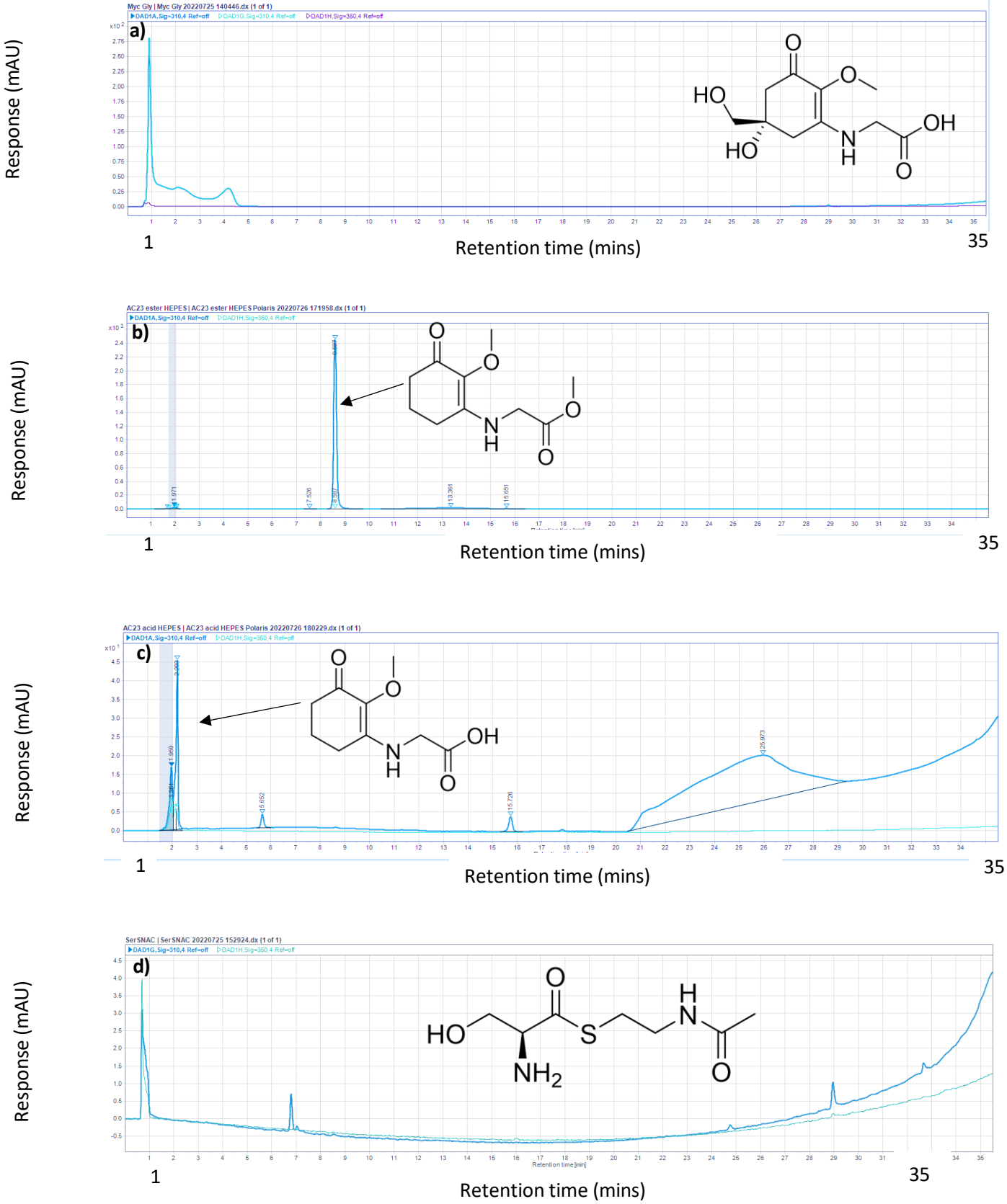
a)
Response (mAU)
1
Retention time (mins)
35
b)
Response (mAU)
1
Retention time (mins)
35
c)
Response (mAU)
1
Retention time (mins)
35
d)
Response (mAU)
1
Retention time (mins)
35

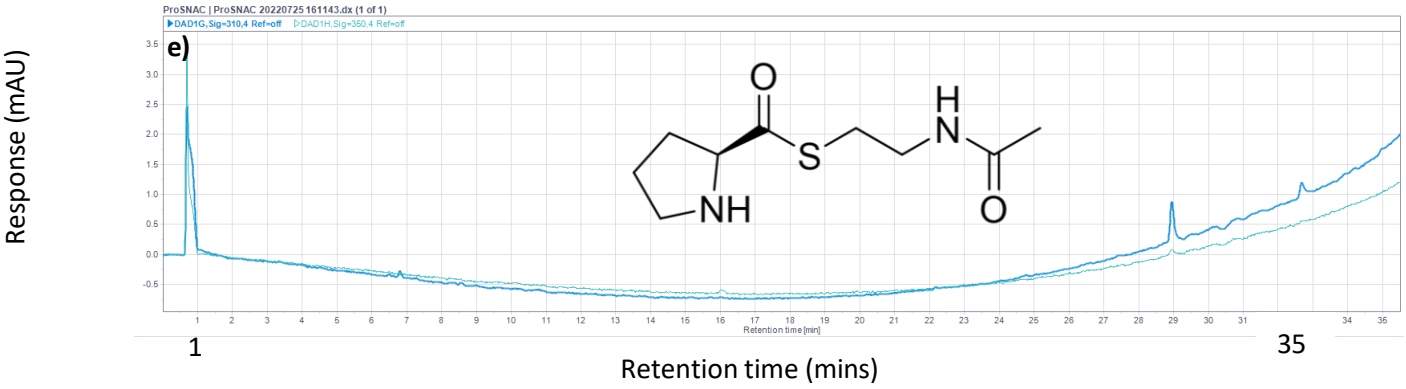

Figure 5.17. **a)** HPLC chromatogram of mycosporine glycine (MG): 35 minute run, using standard gradient (H_2O/MeOH) and column. Blue traces show signal at 310 nm, purple traces show signal at 350 nm. λ_{max} (MG) ~310-320 nm. MG elutes at early times <5 mins. **b)** HPLC chromatogram of AC23 ester. 35 min gradient method *ut infra*. Dark blue traces show signal at 310 nm, light blue/green shows signal at 350 nm AC23 ester elutes between 8-9 mins. **c)** HPLC chromatogram of AC23 acid. 35 min gradient method *ut infra*. Trace colours as previous. This traces contains impurities at longer times, perhaps suggesting some decomposition during analysis. The analyte is assigned to one of the early peaks, i.e. <2 mins. **d)** HPLC chromatogram of SerSNAC*. 35 min gradient method *ut infra*. Trace colours as previous. Impurities at longer times are assigned to column debris and some decomposition during analysis. The analyte is assigned to one of the early peaks, i.e., <2 mins. **e)** HPLC chromatogram of ProSNAC. 35 min gradient method *ut infra*. Trace colours as previous. Impurities at longer times are assigned to column debris and some decomposition during analysis. The analyte is assigned to one of the early peaks, i.e., <2 mins

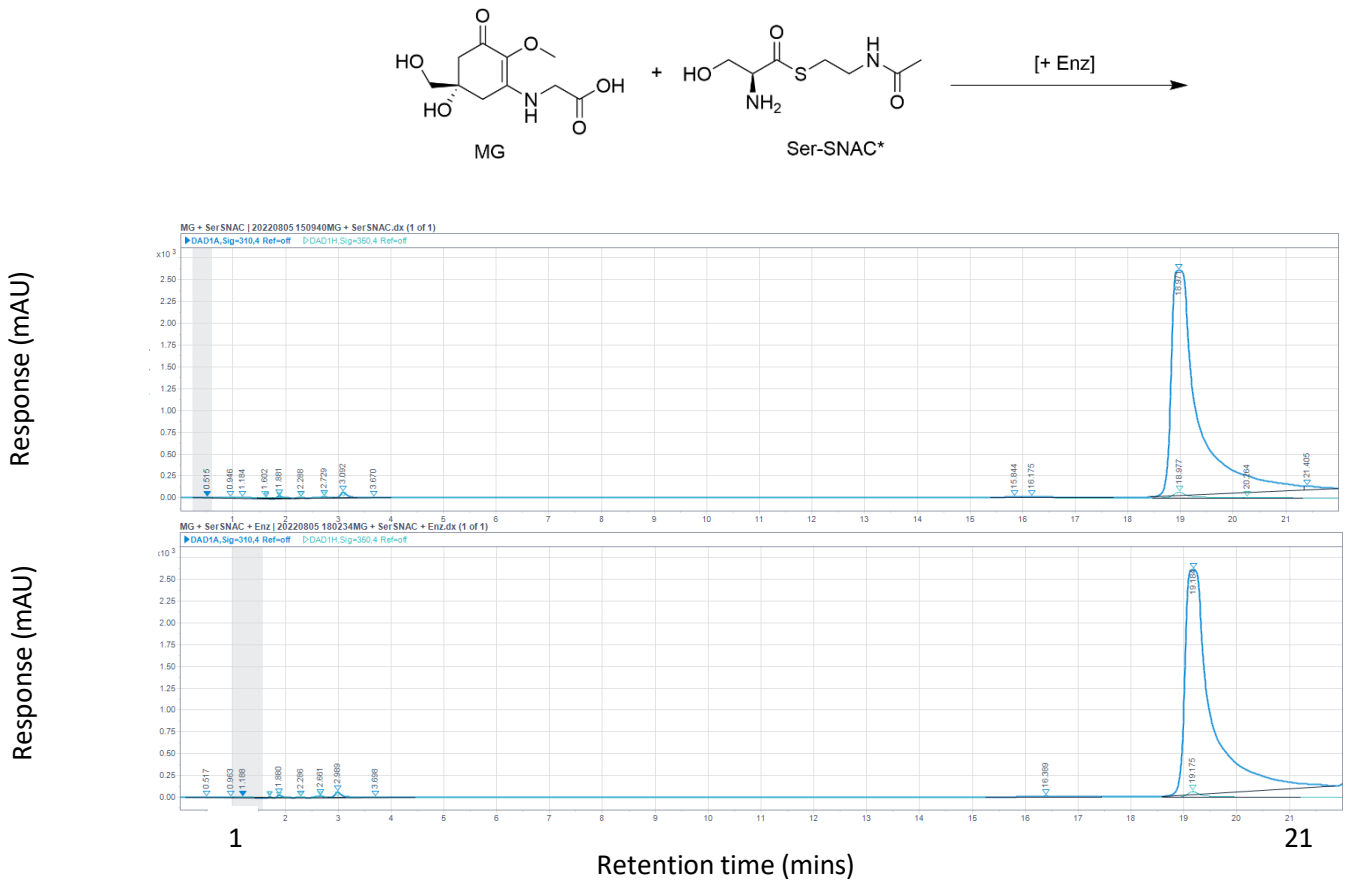

Figure 5.18. Chromatograms obtained (top) for reaction (inset, above) when MG was incubated with SerSNAC* for 24 hours and analysed by HPLC (following standard method), (bottom) with enzyme added. 21 minute run using standard gradient method.

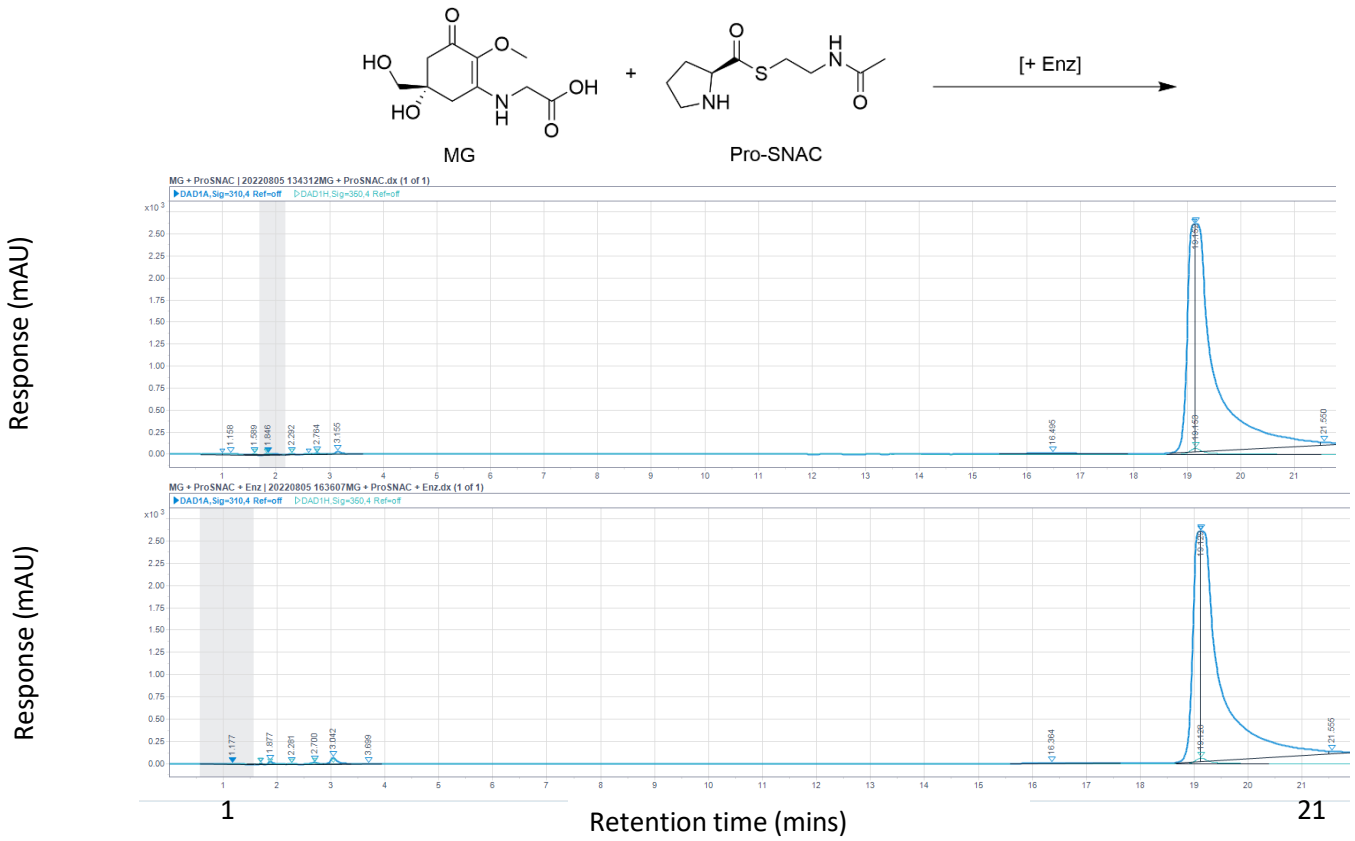

Figure 5.19. Chromatograms obtained (top) for reaction (inset, above) when MG was incubated with ProSNAC for 24 hours and analysed by HPLC (following standard method), (bottom) with enzyme added. 21 minute run using standard gradient method.

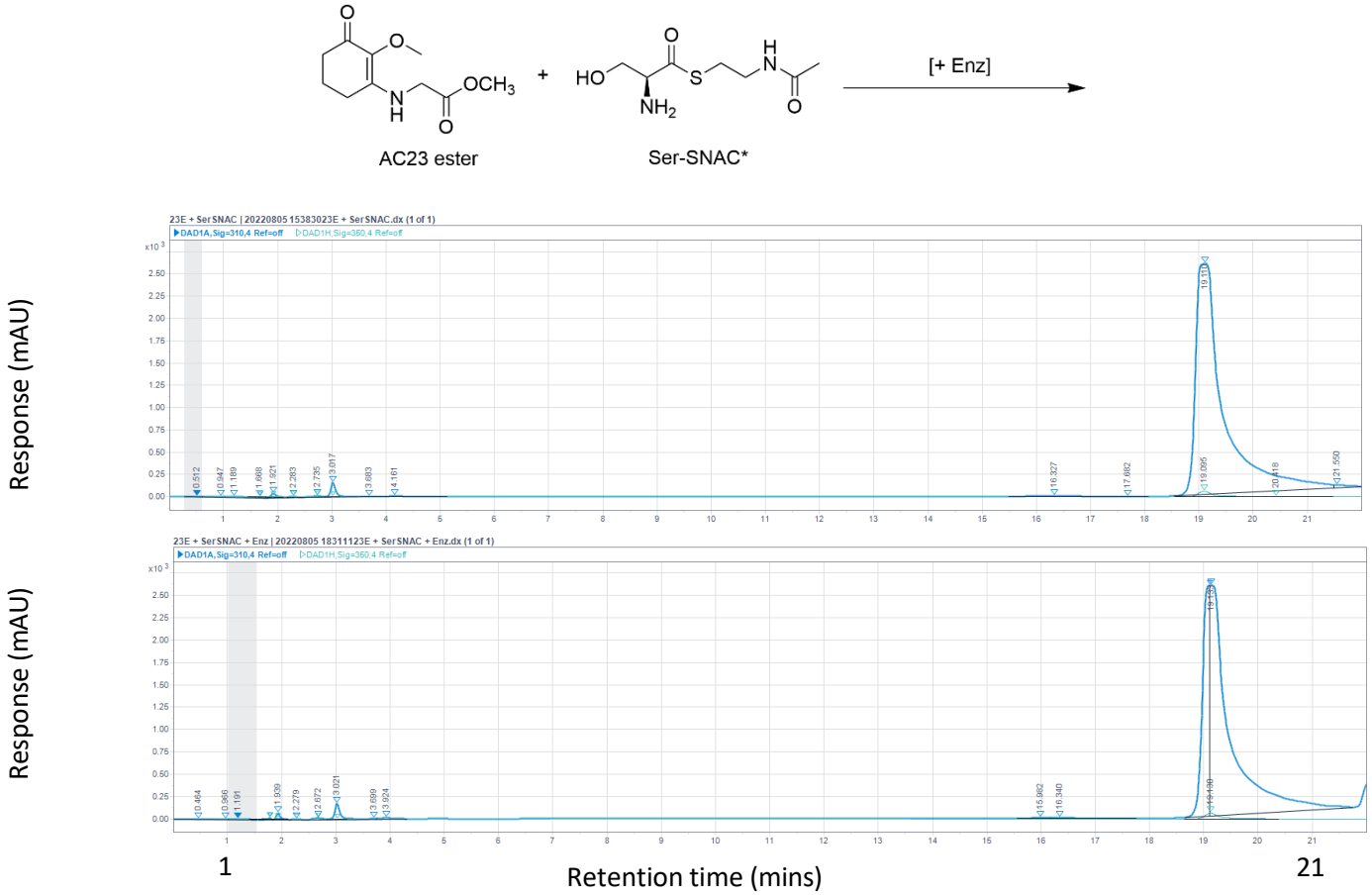

Figure 5.20. Chromatograms obtained (top) for reaction (inset, above) when AC23 ester was incubated with SerSNAC* for 24 hours and analysed by HPLC (following standard method), (bottom) with enzyme added. 21 minute run using standard gradient method.

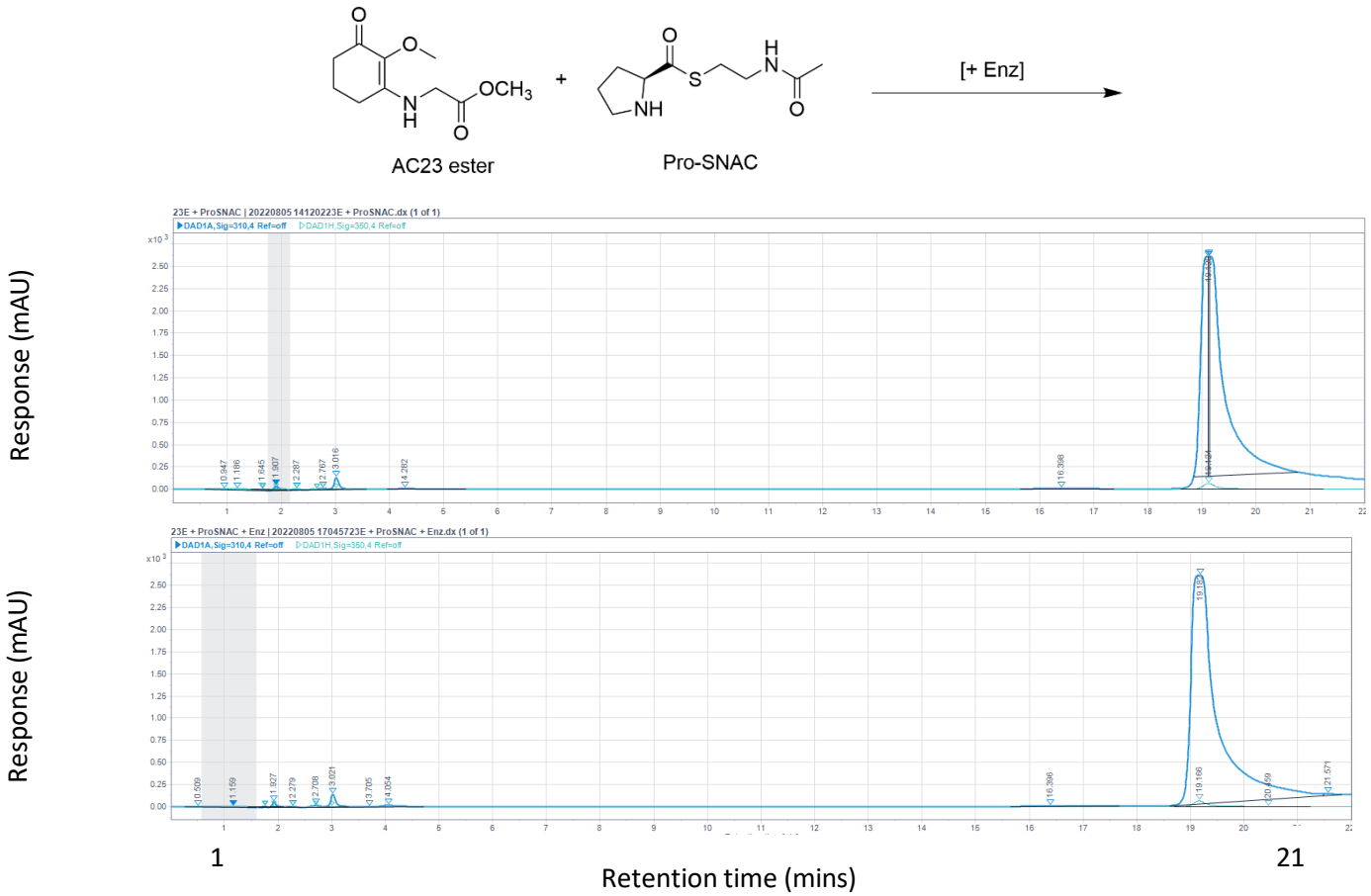

Figure 5.21. Chromatograms obtained (top) for reaction (inset, above) when AC23 ester was incubated with ProSNAC for 24 hours and analysed by HPLC (following standard method), (bottom) with enzyme added. 21 minute run using standard gradient method.

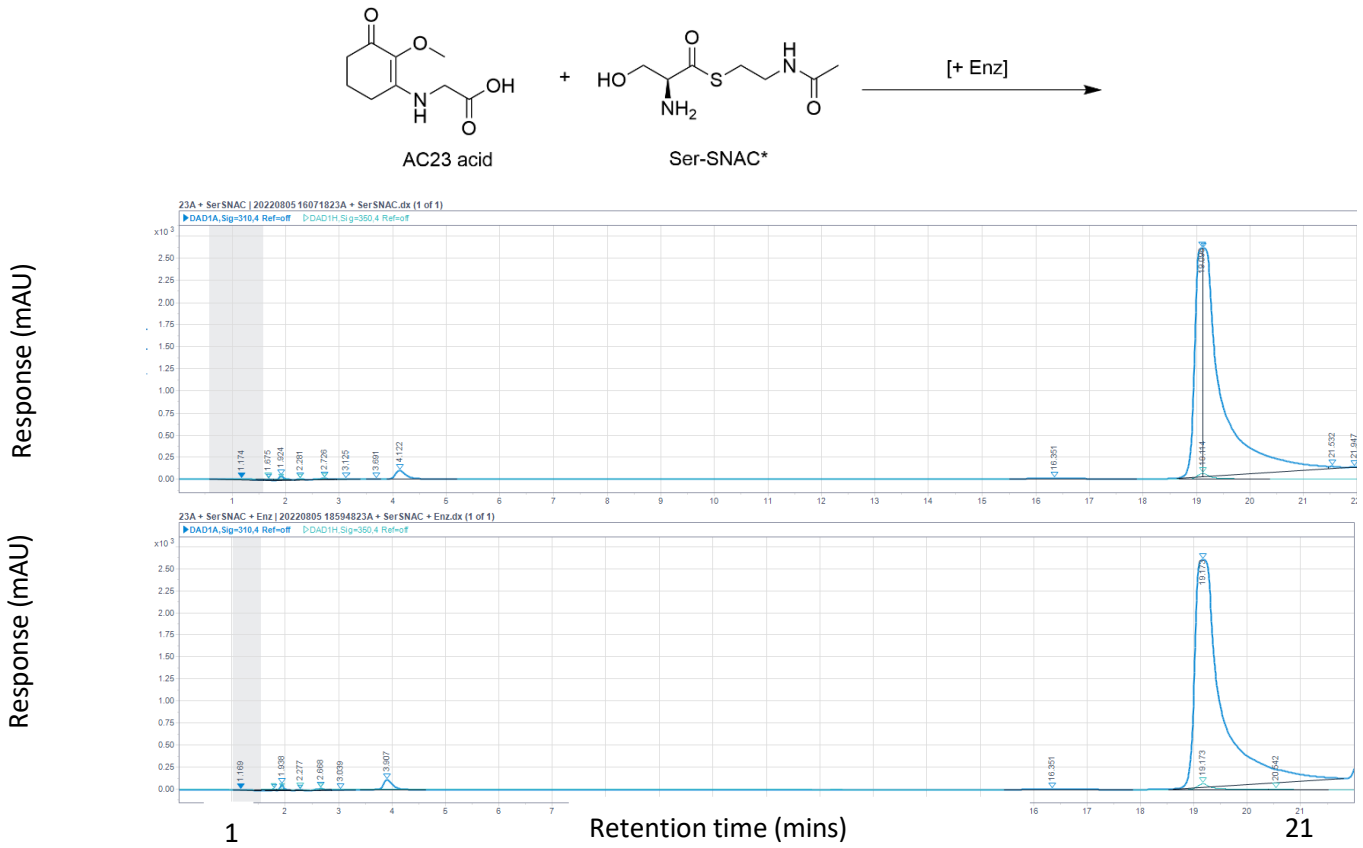

Figure 5.22. Chromatograms obtained (top) for reaction (inset, above) when AC23 acid was incubated with SerSNAC* for 24 hours and analysed by HPLC (following standard method), (bottom) with enzyme added. 21 minute run using standard gradient method.

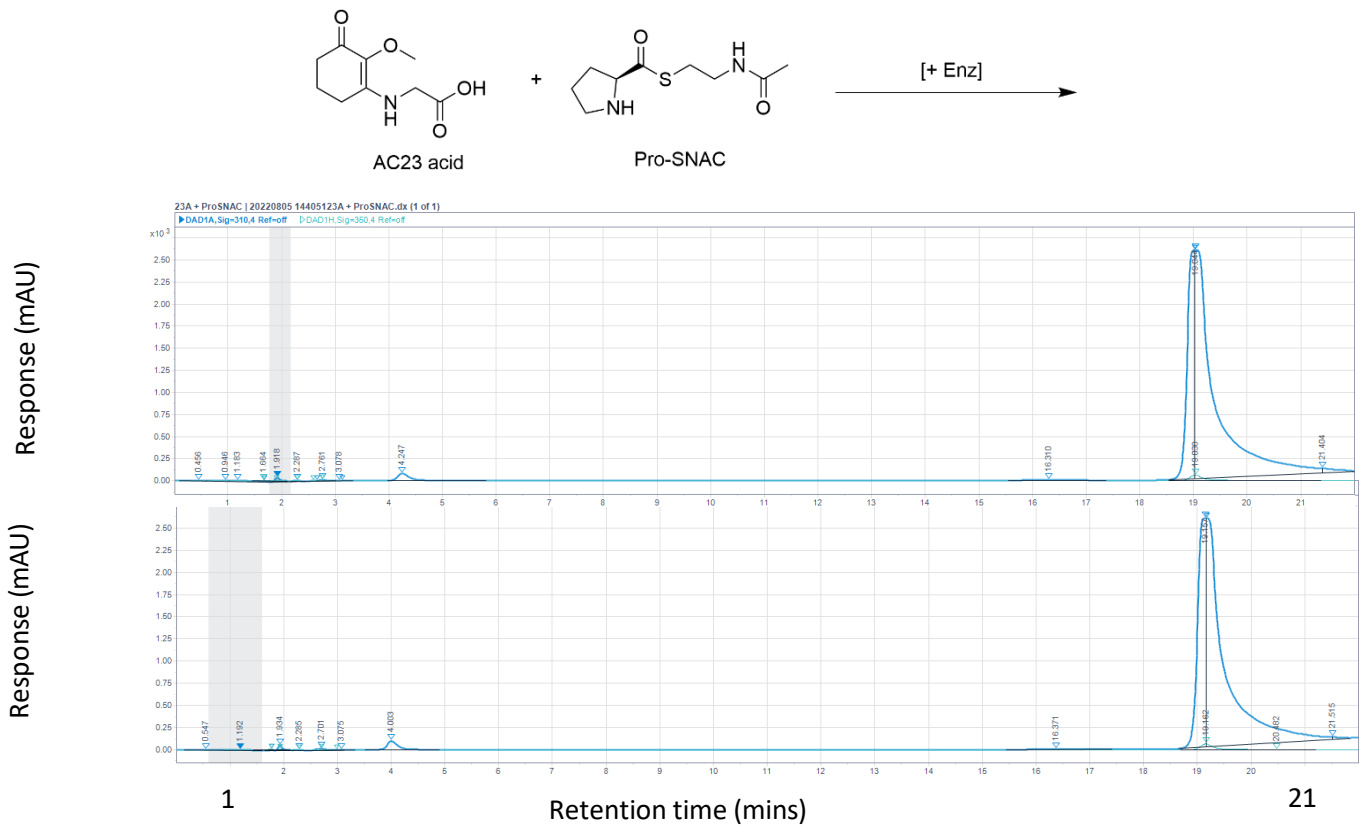

Figure 5.23. Chromatograms obtained (top) for reaction (inset, above) when AC23 acid was incubated with ProSNAC for 24 hours and analysed by HPLC (following standard method), (bottom) with enzyme added. 21 minute run using standard gradient method.

The agents used in the buffer (TCEP and HEPES, structures included in Figure 5.24) are both predicted to have very low or no UV absorption. However, imidazole, used in the elution and storage buffers for the enzyme does have a UV absorption (λ_{max} = 280 nm) and would be detected at 310 nm. Other possible identities for assigned peaks include reduced forms of the substrates, in particularly a reduced form of mycosporine glycine; a transformation that should increase retention time without a large change in the UV absorption maximum.

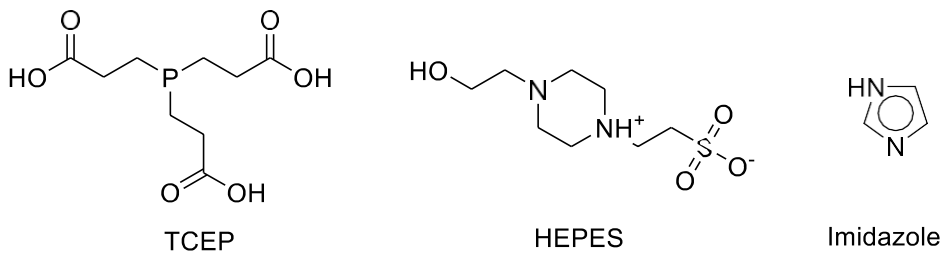

5.24. Reagents used in the bio-assay

5.3 Chapter conclusions

The C domain from the *Moorea* gene cluster was successfully engineered and expressed from a plasmid containing the full gene cluster as described above and in the Materials and Methods section. The enzyme identity was confirmed by SDS-PAGE gel and its structure was predicted with two computational methods. The total amount of protein produced was 2.4 mg.

Preliminary experiments (using HPLC analysis of room temperature incubated mixtures of two substrates) did not show any activity between either the natural substrate (mycosporine-glycine) or two synthetic analogues and activated amino acids, with or without enzyme. This could be due to low concentrations but the lack of any change in the UV-vis absorption profile suggests that the reaction conditions do not produce the desired products, as the products would have a significantly red-shifted UV absorption profile. Given more time, a limit of detection could have been calculated for the experiment. Interestingly, the absorption coefficient for shinorine is about twice that of mycosporine glycine (~40000 vs ~20000) and this should aid detection of the product in the assay. Future work could explore a wider range of conditions, including expanding the number of controls, and we encourage further attempts to express the whole protein as encoded by the full gene cluster. At this stage it appears likely that the C domain does not catalyse the condensation reaction directly (as the *ava* cluster is able to produce shinorine without a C domain), however we cannot rule out some, perhaps structural, role.

Amino acids activated as thioesters were synthesised (SerSNAC ~ 16% yield, ProSNAC ~ 70% yield) in the lab and used as analogues for the activated enzyme complex. Other SNACs could be synthesised in the same way from other amino acids.

Future work could refine the HPLC assay and try different conditions, including higher concentrations of the substrates and of the enzyme. At high enough concentrations Nanodrop (UV-vis) should be sufficient to detect any new products, while HPLC should be able to isolate any product formed due to predicted large difference (~30 nm in UV-vis max absorption). High resolution mass spectrometry would be a useful complementary tool to identify all peaks in the chromatogram.

6. General discussion and Conclusion

There is a large body of evidence that regular sunscreen use in conjunction with other precautions has a major role in personal, preventative UV protection. There are many commercial options available when choosing a sunscreen but recently natural sunscreen motifs have inspired researchers to propose a new class of sunscreen molecules that hasn't been widely used before in commercial applications. Thus far however, the widespread use of mycosporines and related compounds has been limited by the difficulty in extracting these structurally diverse natural products at scale from their plant and animal sources. Given that many MAAs have now been characterized and a handful of biosynthetic pathways detected, rational design can take into account known chemistry and computational predictions to allow researchers to develop the key chromophores from this type of molecule into viable sunscreens, either by chemical or biochemical means. The studies in Chapters 3 and 5 can be used to guide future development. The photoprotective mechanism of MAAs and MAA-like molecules is different to that of state-of-the-start commercial sunscreens, truly representing a new potential class of sunscreen.

Additionally, the **AVOCTO** molecules in Chapter 4 can considered as promising sunscreens, given their photostability in the lab and their potential use to supplement or replace avobenzone as they do not degrade to the same extent in polar non-protic solvents as that widely used sunscreen ingredient. To this end, their synthesis would need to be refined and be shown to be competitive on an industrial scale. In the future, the scope of this scheme could be extended to include acids derived from more environmentally attractive sources in place of octocrylene; as demonstrated by the AVOCINN product.

This research is also of interest to the physics community as ultrafast spectroscopy is able to unravel fundamental photodynamics at play when small organic molecules absorb light; and of course, to the health community, as solutions to growing numbers of preventable skin cancers are sought where customer trust is essential. It also hoped that consumer compliance and awareness will be improved by more complete studies and better molecular characterisation, as well allaying concerns about the side effects and environmental implications of sunscreen use.

This work is an interdisciplinary area of research between chemistry, physics, medicine, biology, environmental policy and industry, and continued collaboration between these areas is key to ensure progress. Designing a good sunscreen product in the lab should thus involve time-resolved studies (to determine the most effective components) as well as thin-film studies with the active ingredients formulated in the creams, pastes and oils which are closer to commercial products and could be brought forward to clinical trials.

7. Bibliography

Chapter 1

(1) Kohl, F. R.; Grieco, C.; Kohler, B. Ultrafast Spectral Hole Burning Reveals the Distinct Chromophores in Eumelanin and Their Common Photoresponse. *Chem. Sci.* **2020**, *11* (5), 1248–1259. https://doi.org/10.1039/C9SC04527A.

(2) Abiola, T. T.; Rioux, B.; Toldo, J. M.; Alarcan, J.; Woolley, J. M.; Turner, M. A. P.; Coxon, D. J. L.; Telles do Casal, M.; Peyrot, C.; Mention, M. M.; Buma, W. J.; Ashfold, M. N. R.; Braeuning, A.; Barbatti, M.; Stavros, V. G.; Allais, F. Towards Developing Novel and Sustainable Molecular Light-to-Heat Converters. *Chem. Sci.* **2021**, *12* (46), 15239–15252. https://doi.org/10.1039/D1SC05077J.

(3) Kalderon, M. E. *Form without Matter: Empedocles and Aristotle on Color Perception*, First edition.; Oxford University Press: Oxford, 2015.

(4) Albini, A. Some Remarks on the First Law of Photochemistry. *Photochem. Photobiol. Sci.* **2016**, *15* (3), 319–324. https://doi.org/10.1039/C5PP00445D.

(5) Smith, A. M. *From Sight to Light: The Passage from Ancient to Modern Optics*, Paperback edition.; University of Chicago Press: Chicago, 2017.

(6) Newton, I.; Hemming, G. W.; Burndy Library. *Opticks: Or, A Treatise of the Reflections, Refractions, Inflexions and Colours of Light : Also, Two Treatises of the Species and Magnitude of Curvilinear Figures*; Printed for Sam. Smith, and Benj. Walford: London, 1704. https://doi.org/10.5479/sil.302475.39088000644674.

(7) Duarte, F. J. Spectrometry and Interferometry. In *Tunable Laser Optics*; Elsevier, 2003; pp 227–248. https://doi.org/10.1016/B978-012222696-0/50058-2.

(8) Heavens, O. S.; Ditchburn, R. W. *Insight into Optics*; Wiley: Chichester ; New York, 1991.

(9) Bléger, D.; Hecht, S. Visible-Light-Activated Molecular Switches. *Angew. Chem. Int. Ed.* **2015**, *54* (39), 11338–11349. https://doi.org/10.1002/anie.201500628.

(10) Cockell, C. S.; Knowland, J. Ultraviolet Radiation Screening Compounds. *Biol. Rev.* **1999**, *74* (3), 311–345. https://doi.org/10.1017/S0006323199005356.

(11) Carruthers, T. J. B.; Longstaff, B. J.; Dennison, W. C.; Abal, E. G.; Aioi, K. Measurement of Light Penetration in Relation to Seagrass. In *Global Seagrass Research Methods*; Elsevier, 2001; pp 369–392. https://doi.org/10.1016/B978-044450891-1/50020-7.

(12) Kripke, M. L. The ABCs Of Sunscreen Protection Factors. *Journal of Investigative Dermatology* **2003**, *121* (1), vii–viii. https://doi.org/10.1046/j.1523-1747.2003.12337.x.

(13) Holzle, E.; Honigsmann, H. Ultraviolette Strahlung - Quellen, Spektren, Umwelteinflusse. UV-Radiation - Sources, Wavelength, Environment. *J Deut Dermatol Gesell* **2005**, *3* (s2), S3–S10. https://doi.org/10.1111/j.1610-0387.2005.04392.x.

(14) World Health Organization; World Meteorological Organization; United Nations Environment Programme; International Commission on Non-Ionizing Radiation Protection. Global solar UV index : a practical guide. **2002**, No. WHO/SDE/OEH/02.2.

(15) Gueymard, C. A.; Myers, D.; Emery, K. Proposed Reference Irradiance Spectra for Solar Energy Systems Testing. *Solar Energy* **2002**, *73* (6), 443–467. https://doi.org/10.1016/S0038-092X(03)00005-7.

(16) Brown, R. A.; Chaffee, F. H., Jr. High-Resolution Spectra of Sodium Emission from IO. *ApJ* **1974**, *187*, L125. https://doi.org/10.1086/181413.

(17) Turro, N. J.; Ramamurthy, V.; Scaiano, J. C. Modern Molecular Photochemistry of Organic Molecules. *Photochemistry and Photobiology* **2012**, *88* (4), 1033–1033. https://doi.org/10.1111/j.1751-1097.2012.01178.x.

(18) Valeur, B.; Berberan-Santos, M. N. *Molecular Fluorescence: Principles and Applications*, Second edition.; Wiley-VCH ; Wiley-VCH Verlag GmbH & Co. KGaA: Weinheim, Germany : [Chichester, England], 2012.

(19) Horbury, M. D.; Holt, E. L.; Mouterde, L. M. M.; Balaguer, P.; Cebrián, J.; Blasco, L.; Allais, F.; Stavros, V. G. Towards Symmetry Driven and Nature Inspired UV Filter Design. *Nat Commun* **2019**, *10* (1), 4748. https://doi.org/10.1038/s41467-019-12719-z.

(20) Baker, L. A.; Horbury, M. D.; Greenough, S. E.; Allais, F.; Walsh, P. S.; Habershon, S.; Stavros, V. G. Ultrafast Photoprotecting Sunscreens in Natural Plants. *J. Phys. Chem. Lett.* **2016**, *7* (1), 56–61. https://doi.org/10.1021/acs.jpclett.5b02474.

(21) Barrantes, F. J. Fluorescence Sensors for Imaging Membrane Lipid Domains and Cholesterol. In *Current Topics in Membranes*; Elsevier, 2021; Vol. 88, pp 257–314. https://doi.org/10.1016/bs.ctm.2021.09.004.

(22) Srinivasan, R. Dark Structures in Molecular Radiationless Transitions Determined by Ultrafast Diffraction. *Science* **2005**, *307* (5709), 558–563. https://doi.org/10.1126/science.1107291.

(23) Abiola, T. T.; Whittock, A. L.; Stavros, V. G. Unravelling the Photoprotective Mechanisms of Nature-Inspired Ultraviolet Filters Using Ultrafast Spectroscopy. *Molecules* **2020**, *25* (17), 3945. https://doi.org/10.3390/molecules25173945.

(24) El-Sayed, M. A. Double Resonance and the Properties of the Lowest Excited Triplet State of Organic Molecules. *Annu. Rev. Phys. Chem.* **1975**, *26* (1), 235–258. https://doi.org/10.1146/annurev.pc.26.100175.001315.

(25) Bonda, C. A.; Lott, D. Sunscreen Photostability. In *Principles and Practice of Photoprotection*; Wang, S. Q., Lim, H. W., Eds.; Springer International Publishing: Cham, 2016; pp 247–273. https://doi.org/10.1007/978-3-319-29382-0_14.

(26) Cole-Filipiak, N. C.; Stavros, V. G. New Insights into the Dissociation Dynamics of Methylated Anilines. *Phys. Chem. Chem. Phys.* **2019**, *21* (26), 14394–14406. https://doi.org/10.1039/C8CP07061J.

(27) Gallagher, R. P.; Lee, T. K.; Bajdik, C. D.; Borugian, M. Ultraviolet Radiation. *Chronic Dis Can* **2010**, *29 Suppl 1*, 51–68.

(28) Kuimova, M. K.; Cowan, A. J.; Matousek, P.; Parker, A. W.; Sun, X. Z.; Towrie, M.; George, M. W. Monitoring the Direct and Indirect Damage of DNA Bases and Polynucleotides by Using Time-Resolved Infrared Spectroscopy. *Proc. Natl. Acad. Sci. U.S.A.* **2006**, *103* (7), 2150–2153. https://doi.org/10.1073/pnas.0506860103.

(29) Fourtanier, A.; Moyal, D.; Seite, S. UVA Filters in Sun-Protection Products: Regulatory and Biological Aspects. *Photochem. Photobiol. Sci.* **2012**, *11* (1), 81–89. https://doi.org/10.1039/C1PP05152K.

(30) Ananthaswamy, H. N.; Loughlin, S. M.; Cox, P.; Evans, R. L.; Ullrich, S. E.; Kripke, M. L. Sunlight and Skin Cancer: Inhibition of P53 Mutations in UV-Irradiated Mouse Skin by Sunscreens. *Nat Med* **1997**, *3* (5), 510–514. https://doi.org/10.1038/nm0597-510.

(31) Nghiem, D. X.; Kazimi, N.; Clydesdale, G.; Ananthaswamy, H. N.; Kripke, M. L.; Ullrich, S. E. Ultraviolet A Radiation Suppresses an Established Immune Response: Implications for Sunscreen Design. *Journal of Investigative Dermatology* **2001**, *117* (5), 1193–1199. https://doi.org/10.1046/j.0022-202x.2001.01503.x.

(32) Panich, U.; Sittithumcharee, G.; Rathviboon, N.; Jirawatnotai, S. Ultraviolet Radiation-Induced Skin Aging: The Role of DNA Damage and Oxidative Stress in Epidermal Stem Cell Damage Mediated Skin Aging. *Stem Cells International* **2016**, *2016*, 1–14. https://doi.org/10.1155/2016/7370642.

(33) Farage, M. A.; Miller, K. W.; Elsner, P.; Maibach, H. I. Intrinsic and Extrinsic Factors in Skin Ageing: A Review. *Int J Cosmet Sci* **2008**, *30* (2), 87–95. https://doi.org/10.1111/j.1468-2494.2007.00415.x.

(34) Brenner, M.; Hearing, V. J. The Protective Role of Melanin Against UV Damage in Human Skin†. *Photochemistry and Photobiology* **2008**, *84* (3), 539–549. https://doi.org/10.1111/j.1751-1097.2007.00226.x.

(35) Kent, S. T.; McClure, L. A.; Crosson, W. L.; Arnett, D. K.; Wadley, V. G.; Sathiakumar, N. Effect of Sunlight Exposure on Cognitive Function among Depressed and Non-Depressed Participants: A REGARDS Cross-Sectional Study. *Environ Health* **2009**, *8* (1), 34. https://doi.org/10.1186/1476-069X-8-34.

(36) de Gruij, F. R. Action Spectrum for Photocarcinogenesis. In *Skin Cancer: Basic Science, Clinical Research and Treatment*; Garbe, C., Schmitz, S., Orfanos, C. E., Eds.; Springer Berlin Heidelberg: Berlin, Heidelberg, 1995; pp 21–30.

(37) Meinhardt, M.; Krebs, R.; Anders, A.; Heinrich, U.; Tronnier, H. Wavelength-Dependent Penetration Depths of Ultraviolet Radiation in Human Skin. *J. Biomed. Opt.* **2008**, *13* (4), 044030. https://doi.org/10.1117/1.2957970.

(38) Lorenzo, A.; Delgado, J.; Montaño, L.; Quesada, I. Safety of UV Radiation for Autofluorescence Diagnosis of Skin Cancer. *Revista Mexicana de Física* **2006**, *52*.

(39) Jablonski, N. G.; Chaplin, G. The Evolution of Human Skin Coloration. *Journal of Human Evolution* **2000**, *39* (1), 57–106. https://doi.org/10.1006/jhev.2000.0403.

(40) Eller, M. S.; Gilchrest, B. A. Tanning as Part of the Eukaryotic SOS Response: DNA Damage and Melanogenesis. *Pigment Cell Research* **2000**, *13*, 94–97. https://doi.org/10.1034/j.1600-0749.13.s8.17.x.

(41) Premi, S.; Wallisch, S.; Mano, C. M.; Weiner, A. B.; Bacchiocchi, A.; Wakamatsu, K.; Bechara, E. J. H.; Halaban, R.; Douki, T.; Brash, D. E. Chemiexcitation of Melanin Derivatives Induces DNA Photoproducts Long after UV Exposure. *Science* **2015**, *347* (6224), 842–847. https://doi.org/10.1126/science.1256022.

(42) Singh, A.; Čížková, M.; Bišová, K.; Vítová, M. Exploring Mycosporine-Like Amino Acids (MAAs) as Safe and Natural Protective Agents against UV-Induced Skin Damage. *Antioxidants* **2021**, *10* (5), 683. https://doi.org/10.3390/antiox10050683.

(43) Baker, L. A.; Greenough, S. E.; Stavros, V. G. A Perspective on the Ultrafast Photochemistry of Solution-Phase Sunscreen Molecules. *J. Phys. Chem. Lett.* **2016**, *7* (22), 4655–4665. https://doi.org/10.1021/acs.jpclett.6b02104.

(44) Ravanat, J.-L.; Douki, T.; Cadet, J. Direct and Indirect Effects of UV Radiation on DNA and Its Components. *Journal of Photochemistry and Photobiology B: Biology* **2001**, *63* (1–3), 88–102. https://doi.org/10.1016/S1011-1344(01)00206-8.

(45) Javeri, A.; Guy Lyons, J.; Huang, X. X.; Halliday, G. M. Downregulation of Cockayne Syndrome B Protein Reduces Human 8-Oxoguanine DNA Glycosylase-1 Expression and Repair of UV Radiation-Induced 8-Oxo-7,8-Dihydro-2'-Deoxyguanine. *Cancer Science* **2011**, *102* (9), 1651–1658. https://doi.org/10.1111/j.1349-7006.2011.02005.x.

(46) Kamenisch, Y.; Berneburg, M. Progeroid Syndromes and UV-Induced Oxidative DNA Damage. *Journal of Investigative Dermatology Symposium Proceedings* **2009**, *14* (1), 8–14. https://doi.org/10.1038/jidsymp.2009.6.

(47) *Standard Erythema Dose: A Review*; Internationale Beleuchtungskommission, Ed.; Technical report / CIE; CIE Central Bureau: Vienna, 1997.

(48) Webb, A. R.; Slaper, H.; Koepke, P.; Schmalwieser, A. W. Know Your Standard: Clarifying the CIE Erythema Action Spectrum. *Photochemistry and Photobiology* **2011**, *87* (2), 483–486. https://doi.org/10.1111/j.1751-1097.2010.00871.x.

(49) Epstein, J. H. Polymorphous Light Eruptions: Wavelength Dependency and Energy Studies. *Arch Dermatol* **1962**, *85* (1), 82. https://doi.org/10.1001/archderm.1962.01590010088010.

(50) Bharath, A.; Turner, R. Impact of Climate Change on Skin Cancer. *J R Soc Med* **2009**, *102* (6), 215–218. https://doi.org/10.1258/jrsm.2009.080261.

(51) Urbach, F. The Historical Aspects of Sunscreens. *Journal of Photochemistry and Photobiology B: Biology* **2001**, *64* (2–3), 99–104. https://doi.org/10.1016/S1011-1344(01)00202-0.

(52) Urbach, F. Franz Greiter — The Man and His Work. In *Photobiology*; Riklis, E., Ed.; Springer US: Boston, MA, 1991; pp 761–761. https://doi.org/10.1007/978-1-4615-3732-8_82.

(53) Svarc, F. A Brief Illustrated History on Sunscreens and Sun Protection. *Pure and Applied Chemistry* **2015**, *87* (9–10), 929–936. https://doi.org/10.1515/pac-2015-0303.

(54) Hojerová, J.; Medovcíková, A.; Mikula, M. Photoprotective Efficacy and Photostability of Fifteen Sunscreen Products Having the Same Label SPF Subjected to Natural Sunlight. *International Journal of Pharmaceutics* **2011**, *408* (1–2), 27–38. https://doi.org/10.1016/j.ijpharm.2011.01.040.

(55) Matta, M. K.; Zusterzeel, R.; Pilli, N. R.; Patel, V.; Volpe, D. A.; Florian, J.; Oh, L.; Bashaw, E.; Zineh, I.; Sanabria, C.; Kemp, S.; Godfrey, A.; Adah, S.; Coelho, S.; Wang, J.; Furlong, L.-A.; Ganley, C.; Michele, T.; Strauss, D. G. Effect of Sunscreen Application Under Maximal Use Conditions on Plasma Concentration of Sunscreen Active Ingredients: A Randomized Clinical Trial. *JAMA* **2019**, *321* (21), 2082. https://doi.org/10.1001/jama.2019.5586.

(56) Hamzelou, J. Sunscreen Safety Fears. *New Scientist* **2019**, *243* (3240), 20–21. https://doi.org/10.1016/S0262-4079(19)31373-9.

(57) Hoegh-Guldberg, O. Climate Change, Coral Bleaching and the Future of the World's Coral Reefs. *Mar. Freshwater Res.* **1999**. https://doi.org/10.1071/MF99078.

(58) La Barre, S.; Roullier, C.; Boustie, J. Mycosporine-Like Amino Acids (MAAs) in Biological Photosystems. In *Outstanding Marine Molecules*; La Barre, S., Kornprobst, J.-M., Eds.; Wiley-VCH Verlag GmbH & Co. KGaA: Weinheim, Germany, 2014; pp 333–360. https://doi.org/10.1002/9783527681501.ch15.

(59) Galasso, V.; Pichierri, F. Probing the Molecular and Electronic Structure of Norhipposudoric and Hipposudoric Acids from the Red Sweat of *Hippopotamus Amphibius* : A DFT Investigation. *J. Phys. Chem. A* **2009**, *113* (11), 2534–2543. https://doi.org/10.1021/jp809138s.

(60) Fraser, C. M.; Chapple, C. The Phenylpropanoid Pathway in Arabidopsis. *The Arabidopsis Book* **2011**, *9*, e0152. https://doi.org/10.1199/tab.0152.

(61) Vega, J.; Bonomi-Barufi, J.; Gómez-Pinchetti, J. L.; Figueroa, F. L. Cyanobacteria and Red Macroalgae as Potential Sources of Antioxidants and UV Radiation-Absorbing Compounds for Cosmeceutical Applications. *Marine Drugs* **2020**, *18* (12), 659. https://doi.org/10.3390/md18120659.

(62) Alves, G. de A. D.; de Souza, R. O.; Rogez, H.; Masaki, H.; Fonseca, M. J. V. Cecropia Obtusa, an Amazonian Ethanolic Extract, Exhibits Photochemoprotective Effect in Vitro and Balances the Redox Cellular State in Response to UV Radiation. *Industrial Crops and Products* **2016**, *94*, 893–902. https://doi.org/10.1016/j.indcrop.2016.09.064.

(63) Wróblewska, K. B.; Baby, A. R.; Grombone Guaratini, M. T.; Moreno, P. R. H. In Vitro Antioxidant and Photoprotective Activity of Five Native Brazilian Bamboo Species. *Industrial Crops and Products* **2019**, *130*, 208–215. https://doi.org/10.1016/j.indcrop.2018.12.081.

(64) Rasheed, A.; Shama, S. N.; Mohanalakshmi, S.; Ravichandran, V. Formulation, Characterization and in Vitro Evaluation of Herbal Sunscreen Lotion. *Orient Pharm Exp Med* **2012**, *12* (4), 241–246. https://doi.org/10.1007/s13596-012-0069-z.

(65) Rangel, K. C.; Villela, L. Z.; Pereira, K. de C.; Colepicolo, P.; Debonsi, H. M.; Gaspar, L. R. Assessment of the Photoprotective Potential and Toxicity of Antarctic Red Macroalgae Extracts from Curdiea Racovitzae and Iridaea Cordata for Cosmetic Use. *Algal Research* **2020**, *50*, 101984. https://doi.org/10.1016/j.algal.2020.101984.

(66) Prasedya; Syafitri; Geraldine; Hamdin; Frediansyah; Miyake; Kobayashi; Hazama; Sunarpi. UVA Photoprotective Activity of Brown Macroalgae Sargassum Cristafolium. *Biomedicines* **2019**, *7* (4), 77. https://doi.org/10.3390/biomedicines7040077.

(67) Liu, Z. Occurrence of Mycosporine-like Amino Acids (MAAs) in the Bloom-Forming Cyanobacterium Microcystis Aeruginosa. *Journal of Plankton Research* **2004**, *26* (8), 963–966. https://doi.org/10.1093/plankt/fbh083.

(68) Jesus, A.; Sousa, E.; Cruz, M. T.; Cidade, H.; Lobo, J. M. S.; Almeida, I. F. UV Filters: Challenges and Prospects. *Pharmaceuticals* **2022**, *15* (3), 263. https://doi.org/10.3390/ph15030263.

(69) Cocchietto, M.; Skert, N.; Nimis, P.; Sava, G. A Review on Usnic Acid, an Interesting Natural Compound. *Naturwissenschaften* **2002**, *89* (4), 137–146. https://doi.org/10.1007/s00114-002-0305-3.

(70) Radice, M.; Manfredini, S.; Ziosi, P.; Dissette, V.; Buso, P.; Fallacara, A.; Vertuani, S. Herbal Extracts, Lichens and Biomolecules as Natural Photo-Protection Alternatives to Synthetic UV Filters. A Systematic Review. *Fitoterapia* **2016**, *114*, 144–162. https://doi.org/10.1016/j.fitote.2016.09.003.

(71) COCKELL, C. S. Ultraviolet Radiation, Evolution and the π-Electron System. *Biological Journal of the Linnean Society* **1998**, *63* (3), 449–457. https://doi.org/10.1006/bijl.1997.0201.

(72) Cardozo, K. H. M.; Guaratini, T.; Barros, M. P.; Falcão, V. R.; Tonon, A. P.; Lopes, N. P.; Campos, S.; Torres, M. A.; Souza, A. O.; Colepicolo, P.; Pinto, E. Metabolites from Algae with Economical Impact. *Comparative Biochemistry and Physiology Part C: Toxicology & Pharmacology* **2007**, *146* (1–2), 60–78. https://doi.org/10.1016/j.cbpc.2006.05.007.

(73) Carreto, J. I.; Carignan, M. O. Mycosporine-Like Amino Acids: Relevant Secondary Metabolites. Chemical and Ecological Aspects. *Marine Drugs* **2011**, *9* (3), 387–446. https://doi.org/10.3390/md9030387.

(74) Nakamura, H.; Kobayashi, J.; Hirata, Y. Separation of Mycosporine-like Amino Acids in Marine Organisms Using Reversed-Phase High-Performance Liquid Chromatography. *Journal of Chromatography A* **1982**, *250*, 113–118. https://doi.org/10.1016/S0021-9673(00)95219-1.

(75) Nakamura, H.; Kobayashi, J.; Hirata, Y. Isolation and Structure of a 330 Nm UV-Absorbing Substance, Asterina-330 From the Starfish *Asterina Pectinifera*. *Chem. Lett.* **1981**, *10* (10), 1413–1414. https://doi.org/10.1246/cl.1981.1413.

(76) Ito, S.; Hirata, Y. Isolation and Structure of a Mycosporine from the Zoanthid. *Tetrahedron Letters* **1977**, *18* (28), 2429–2430. https://doi.org/10.1016/S0040-4039(01)83784-9.

(77) Riegger, L.; Robinson, D. Photoinduction of UV-Absorbing Compounds in Antarctic Diatoms and Phaeocystis Antarctica. *Mar. Ecol. Prog. Ser.* **1997**, *160*, 13–25. https://doi.org/10.3354/meps160013.

(78) Kageyama, H.; Waditee-Sirisattha, R. Mycosporine-Like Amino Acids as Multifunctional Secondary Metabolites in Cyanobacteria: From Biochemical to Application Aspects. In *Studies in Natural Products Chemistry*; Elsevier, 2018; Vol. 59, pp 153–194. https://doi.org/10.1016/B978-0-444-64179-3.00005-0.

(79) Gunde-Cimerman, N.; Plemenitaš, A.; Oren, A. Strategies of Adaptation of Microorganisms of the Three Domains of Life to High Salt Concentrations. *FEMS Microbiology Reviews* **2018**, *42* (3), 353–375. https://doi.org/10.1093/femsre/fuy009.

(80) Gongi, W.; Pinchetti, J. L. G.; Cordeiro, N.; Sadok, S.; Ouada, H. B. Characterization of Biodegradable Films Based on Extracellular Polymeric Substances Extracted from the Thermophilic Microalga Graesiella Sp. *Algal Research* **2022**, *61*, 102565. https://doi.org/10.1016/j.algal.2021.102565.

(81) Korbee, N.; Figueroa, F. L.; Aguilera, J. Effect of Light Quality on the Accumulation of Photosynthetic Pigments, Proteins and Mycosporine-like Amino Acids in the Red Alga Porphyra Leucosticta (Bangiales, Rhodophyta). *Journal of Photochemistry and Photobiology B: Biology* **2005**, *80* (2), 71–78. https://doi.org/10.1016/j.jphotobiol.2005.03.002.

(82) Dunlap, W. C.; Chalker, B. E.; Bandaranayake, W. M.; Wu Won, J. J. Nature's Sunscreen from the Great Barrier Reef, Australia. *Int J Cosmet Sci* **1998**, *20* (1), 41–51. https://doi.org/10.1046/j.1467-2494.1998.171734.x.

(83) Karsten, U.; Wiencke, C. Factors Controlling the Formation of UV-Absorbing Mycosporine-like Amino Acids in the Marine Red Alga Palmaria Palmata from Spitsbergen (Norway). *Journal of Plant Physiology* **1999**, *155* (3), 407–415. https://doi.org/10.1016/S0176-1617(99)80124-2.

(84) Yuan, Y. V.; Westcott, N. D.; Hu, C.; Kitts, D. D. Mycosporine-like Amino Acid Composition of the Edible Red Alga, Palmaria Palmata (Dulse) Harvested from the West and East Coasts of Grand Manan Island, New Brunswick. *Food Chemistry* **2009**, *112* (2), 321–328. https://doi.org/10.1016/j.foodchem.2008.05.066.

(85) Dunlap, W. C.; Chalker, B. E. Identification and Quantitation of Near-UV Absorbing Compounds (S-320) in a Hermatypic Scleractinian. *Coral Reefs* **1986**, *5* (3), 155–159. https://doi.org/10.1007/BF00298182.

(86) Sun, Y.; Han, X.; Hu, Z.; Cheng, T.; Tang, Q.; Wang, H.; Deng, X.; Han, X. Extraction, Isolation and Characterization of Mycosporine-like Amino Acids from Four Species of Red Macroalgae. *Marine Drugs* **2021**, *19* (11), 615. https://doi.org/10.3390/md19110615.

(87) Garcia-Pichel, F.; Castenholz, R. W. Occurrence of UV-Absorbing, Mycosporine-Like Compounds among Cyanobacterial Isolates and an Estimate of Their Screening Capacity. *Appl Environ Microbiol* **1993**, *59* (1), 163–169. https://doi.org/10.1128/aem.59.1.163-169.1993.

(88) Geraldes, V.; Pinto, E. Mycosporine-Like Amino Acids (MAAs): Biology, Chemistry and Identification Features. *Pharmaceuticals* **2021**, *14* (1), 63. https://doi.org/10.3390/ph14010063.

(89) Shaath, N. A. Ultraviolet Filters. *Photochem. Photobiol. Sci.* **2010**, *9* (4), 464. https://doi.org/10.1039/b9pp00174c.

(90) Plack, P. A.; Fraser, N. W.; Grant, P. T.; Middleton, C.; Mitchell, A. I.; Thomson, R. H. Gadusol, an Enolic Derivative of Cyclohexane-1,3-Dione Present in the Roes of Cod and Other Marine Fish. Isolation, Properties and Occurrence Compared with Ascorbic Acid. *Biochemical Journal* **1981**, *199* (3), 741–747. https://doi.org/10.1042/bj1990741.

(91) Osborn, A. R.; Almabruk, K. H.; Holzwarth, G.; Asamizu, S.; LaDu, J.; Kean, K. M.; Karplus, P. A.; Tanguay, R. L.; Bakalinsky, A. T.; Mahmud, T. De Novo Synthesis of a Sunscreen Compound in Vertebrates. *eLife* **2015**, *4*, e05919. https://doi.org/10.7554/eLife.05919.

(92) Brotherton, C. A.; Balskus, E. P. Shedding Light on Sunscreen Biosynthesis in Zebrafish. *eLife* **2015**, *4*, e07961. https://doi.org/10.7554/eLife.07961.

(93) Gerkema, M. P.; Davies, W. I. L.; Foster, R. G.; Menaker, M.; Hut, R. A. The Nocturnal Bottleneck and the Evolution of Activity Patterns in Mammals. *Proc. R. Soc. B.* **2013**, *280* (1765), 20130508. https://doi.org/10.1098/rspb.2013.0508.

(94) Shinzato, C.; Shoguchi, E.; Kawashima, T.; Hamada, M.; Hisata, K.; Tanaka, M.; Fujie, M.; Fujiwara, M.; Koyanagi, R.; Ikuta, T.; Fujiyama, A.; Miller, D. J.; Satoh, N. Using the Acropora Digitifera Genome to Understand Coral Responses to Environmental Change. *Nature* **2011**, *476* (7360), 320–323. https://doi.org/10.1038/nature10249.

(95) Balskus, E. P.; Walsh, C. T. The Genetic and Molecular Basis for Sunscreen Biosynthesis in Cyanobacteria. *Science* **2010**, *329* (5999), 1653–1656. https://doi.org/10.1126/science.1193637.

(96) Volkmann, M.; Gorbushina, A. A. A Broadly Applicable Method for Extraction and Characterization of Mycosporines and Mycosporine-like Amino Acids of Terrestrial, Marine and Freshwater Origin. *FEMS Microbiology Letters* **2006**, *255* (2), 286–295. https://doi.org/10.1111/j.1574-6968.2006.00088.x.

(97) Davies, J. H. *The Physics of Low-Dimensional Semiconductors: An Introduction*; Cambridge university press, 1998.

(98) Cohen, E. R. The Rydberg Constant and the Atomic Mass of the Electron. *Phys. Rev.* **1952**, *88* (2), 353–360. https://doi.org/10.1103/PhysRev.88.353.

(99) Zewail, A. H. Laser Femtochemistry. *Science* **1988**, *242* (4886), 1645–1653. https://doi.org/10.1126/science.242.4886.1645.

(100) Grubb, M. P.; Orr-Ewing, A. J.; Ashfold, M. N. R. KOALA: A Program for the Processing and Decomposition of Transient Spectra. *Review of Scientific Instruments* **2014**, *85* (6), 064104. https://doi.org/10.1063/1.4884516.

(101) Berera, R.; van Grondelle, R.; Kennis, J. T. M. Ultrafast Transient Absorption Spectroscopy: Principles and Application to Photosynthetic Systems. *Photosynth Res* **2009**, *101* (2–3), 105–118. https://doi.org/10.1007/s11120-009-9454-y.

(102) Beckwith, J. S.; Rumble, C. A.; Vauthey, E. Data Analysis in Transient Electronic Spectroscopy – an Experimentalist's View. *International Reviews in Physical Chemistry* **2020**, *39* (2), 135–216. https://doi.org/10.1080/0144235X.2020.1757942.

(103) Crespo-Hernández, C. E.; Cohen, B.; Hare, P. M.; Kohler, B. Ultrafast Excited-State Dynamics in Nucleic Acids. *Chem. Rev.* **2004**, *104* (4), 1977–2020. https://doi.org/10.1021/cr0206770.

(104) Karsili, T. N. V.; Marchetti, B.; Ashfold, M. N. R.; Domcke, W. *Ab Initio* Study of Potential Ultrafast Internal Conversion Routes in Oxybenzone, Caffeic Acid, and Ferulic Acid: Implications for Sunscreens. *J. Phys. Chem. A* **2014**, *118* (51), 11999–12010. https://doi.org/10.1021/jp507282d.

(105) Tan, E. M. M.; Hilbers, M.; Buma, W. J. Excited-State Dynamics of Isolated and Microsolvated Cinnamate-Based UV-B Sunscreens. *J. Phys. Chem. Lett.* **2014**, *5* (14), 2464–2468. https://doi.org/10.1021/jz501140b.

(106) Qiao, Y.; Dong, H.; Zhang, X. A Versatile Sunscreen with Minimal ROS Damage and Low Permeability. *ACS Appl. Mater. Interfaces* **2020**, *12* (5), 6217–6225. https://doi.org/10.1021/acsami.9b18996.

(107) Abiola, T. T.; Rioux, B.; Johal, S.; Mention, M. M.; Brunissen, F.; Woolley, J. M.; Allais, F.; Stavros, V. G. Insight into the Photodynamics of Photostabilizer Molecules. *The Journal of Physical Chemistry A* 2022, 126 (45), 8388-8397. https://doi.org/10.1021/acs.jpca.2c05580

(108) Abiola, T. T.; Rodrigues, N. d N.; Ho, C.; Coxon, D. J.; Horbury, M. D.; Toldo, J. M.; do Casal, M. T.; Rioux, B.; Peyrot, C.; Mention, M. M. New Generation UV-A Filters: Understanding Their Photodynamics on a Human Skin Mimic. *The Journal of Physical Chemistry Letters* **2020**, *12* (1), 337–344.

(109) Whittock, A. L.; Auckloo, N.; Cowden, A. M.; Turner, M. A. P.; Woolley, J. M.; Wills, M.; Corre, C.; Stavros, V. G. Exploring the Blueprint of Photoprotection in Mycosporine-like Amino Acids. *J. Phys. Chem. Lett.* **2021**, *12* (14), 3641–3646. https://doi.org/10.1021/acs.jpclett.1c00728.

(110) Conde, F. R.; Carignan, M. O.; Churio, M. S.; Carreto, J. I. In Vitro Cis-Trans Photoisomerization of Palythene and Usujirene. Implications on the in Vivo Transformation of Mycosporine-like Amino Acids. *Photochem. Photobiol.* **2003**, *77* (2), 146–150. https://doi.org/10.1562/0031-8655

(111) Whittock, A. L.; Woolley, J. M.; Auckloo, N.; Corre, C.; Stavros, V. G. Investigating the Ultrafast Dynamics and Long-Term Photostability of an Isomer Pair, Usujirene and Palythene, from the Mycosporine-like Amino Acid Family. *Molecules* **2022**, *27* (7), 2272. https://doi.org/10.3390/molecules27072272.

(112) Baker, L. A.; Horbury, M. D.; Greenough, S. E.; Coulter, P. M.; Karsili, T. N. V.; Roberts, G. M.; Orr-Ewing, A. J.; Ashfold, M. N. R.; Stavros, V. G. Probing the Ultrafast Energy Dissipation Mechanism of the Sunscreen Oxybenzone after UVA Irradiation. *J. Phys. Chem. Lett.* **2015**, *6* (8), 1363–1368. https://doi.org/10.1021/acs.jpclett.5b00417.

(113) Ignasiak, M. T.; Houée-Levin, C.; Kciuk, G.; Marciniak, B.; Pedzinski, T. A Reevaluation of the Photolytic Properties of 2-Hydroxybenzophenone-Based UV Sunscreens: Are Chemical Sunscreens Inoffensive? *ChemPhysChem* **2015**, *16* (3), 628–633. https://doi.org/10.1002/cphc.201402703.

(114) Chapple, C. C.; Vogt, T.; Ellis, B. E.; Somerville, C. R. An Arabidopsis Mutant Defective in the General Phenylpropanoid Pathway. *Plant Cell* **1992**, *4* (11), 1413–1424. https://doi.org/10.1105/tpc.4.11.1413.

(115) Horbury, M. D.; Baker, L. A.; Quan, W.-D.; Greenough, S. E.; Stavros, V. G. Photodynamics of Potent Antioxidants: Ferulic and Caffeic Acids. *Phys. Chem. Chem. Phys.* **2016**, *18* (26), 17691–17697. https://doi.org/10.1039/C6CP01595F.

(116) Horbury, M. D.; Quan, W.-D.; Flourat, A. L.; Allais, F.; Stavros, V. G. Elucidating Nuclear Motions in a Plant Sunscreen during Photoisomerization through Solvent Viscosity Effects. *Phys. Chem. Chem. Phys.* **2017**, *19* (31), 21127–21131. https://doi.org/10.1039/C7CP04070A.

(117) Sharma, A.; Bányiová, K.; Babica, P.; El Yamani, N.; Collins, A. R.; Čupr, P. Different DNA Damage Response of Cis and Trans Isomers of Commonly Used UV Filter after the Exposure on Adult Human Liver Stem Cells and Human Lymphoblastoid Cells. *Science of The Total Environment* **2017**, *593–594*, 18–26. https://doi.org/10.1016/j.scitotenv.2017.03.043.

(118) Whittock, A. L.; Abiola, T. T.; Stavros, V. G. A Perspective on Femtosecond Pump–Probe Spectroscopy in the Development of Future Sunscreens. *J. Phys. Chem. A* **2022**, *126* (15), 2299–2308. https://doi.org/10.1021/acs.jpca.2c01000.

(119) Sampedro, D. Computational Exploration of Natural Sunscreens. *Phys. Chem. Chem. Phys.* **2011**, *13* (13), 5584. https://doi.org/10.1039/c0cp02901g.

(120) Losantos, R.; Funes-Ardoiz, I.; Aguilera, J.; Herrera-Ceballos, E.; García-Iriepa, C.; Campos, P. J.; Sampedro, D. Rational Design and Synthesis of Efficient Sunscreens To Boost the Solar Protection Factor. *Angew. Chem. Int. Ed. Engl.* **2017**, *56* (10), 2632–2635. https://doi.org/10.1002/anie.201611627.

(121) Hatakeyama, M.; Koizumi, K.; Boero, M.; Nobusada, K.; Hori, H.; Misonou, T.; Kobayashi, T.; Nakamura, S. Unique Structural Relaxations and Molecular Conformations of Porphyra-334 at the Excited State. *J. Phys. Chem. B* **2019**, *123* (36), 7649–7656. https://doi.org/10.1021/acs.jpcb.9b03744.

Chapter 2

Synthesis

(1) Pecherer, B.; Jampolsky, L. M.; Wuest, H. M. Dihydropyrogallol, A New Ene-Diol and Its Oxidation Product. 1,2,3-Cyclohexanetrione Dihydrate—A Ketonic Isomer of Pyrogallol. *J. Am. Chem. Soc.* **1948**, *70* (7), 2587–2589. https://doi.org/10.1021/ja01187a087.

(2) Mayer, W.; Bachmann, R.; Kraus, F. Über carbocyclische Reduktone. Dihydropyrogallol und Dihydrogallussäure. *Chem. Ber.* **1955**, *88* (3), 316–329. https://doi.org/10.1002/cber.19550880303.

(3) Wang, T.; Chen, G.; Lu, Y.; Chen, Q.; Huo, Y.; Li, X. Intermolecular Multiple Dehydrogenative Cross-Couplings of Ketones with Boronic Acids and Amines via Copper Catalysis. *Adv. Synth. Catal.* **2019**, *361* (16), 3886–3892. https://doi.org/10.1002/adsc.201900419.

(4) Gramain, J.-C.; Husson, H.-P.; Troin, Y. Synthese Stereospecifique Par Voie Photochimique de Trans Hexahydro-1,2,3,4,4a,9a Carbazolones-4 Substituees En 4a1. *Tetrahedron Letters* **1985**, *26* (19), 2323–2326. https://doi.org/10.1016/S0040-4039(00)95087-1.

(5) Hemmerling, H.-J.; Reiss, G. Partially Saturated Indeno[1,2- *b*]Indole Derivatives via Deoxygenationof Heterocyclic α-Hydroxy- *N* , *O* -Hemiaminals. *Synthesis* **2009**, *2009* (06), 985–999. https://doi.org/10.1055/s-0028-1087983.

(6) Ehmann, D. E.; Trauger, J. W.; Stachelhaus, T.; Walsh, C. T. Aminoacyl-SNACs as Small-Molecule Substrates for the Condensation Domains of Nonribosomal Peptide Synthetases. *Chemistry & Biology* **2000**, *7* (10), 765–772. https://doi.org/10.1016/S1074-5521(00)00022-3.

(7) Reddy, R. B.; Dudhe, P.; Chauhan, P.; Sengupta, S.; Chelvam, V. Synthesis of Tubuphenylalanine and Epi-Tubuphenylalanine via Regioselective Aziridine Ring Opening with Carbon Nucleophiles Followed by Hydroboration-Oxidation of 1,1-Substituted Amino Alkenes. *Tetrahedron* **2018**, *74* (48), 6946–6953. https://doi.org/10.1016/j.tet.2018.10.024.

(8) Klisch, M.; Richter, P.; Puchta, R.; Häder, D.-P.; Bauer, W. The Stereostructure of Porphyra-334: An Experimental and Calculational NMR Investigation. Evidence for an Efficient 'Proton Sponge.' *HCA* **2007**, *90* (3), 488–511. https://doi.org/10.1002/hlca.200790052.

(9) Orfanoudaki, M.; Hartmann, A.; Karsten, U.; Ganzera, M. Chemical Profiling of Mycosporine-like Amino Acids in Twenty-three Red Algal Species. *J. Phycol.* **2019**, *55* (2), 393–403. https://doi.org/10.1111/jpy.12827.

(10) J. L Besombes, G. Cheminat, G. Mousset, C. Mousty. *Bull. Soc. Chem. Fr.* **1992**, *129*, 513–522. *DOI is unavailable.*

(11) Jin, H.; Zhang, W.; Wang, D.; Chu, Z.; Shen, Z.; Zou, D.; Fan, X.; Zhou, Q. Dendron-Jacketed Electrophosphorescent Copolymers: Improved Efficiency and Tunable Emission Color by Partial Energy Transfer. *Macromolecules* **2011**, *44* (24), 9556–9564. https://doi.org/10.1021/ma2018556.

(12) Li, J.; Chen, H.; Zhang-Negrerie, D.; Du, Y.; Zhao, K. Synthesis of Coumarins via PIDA/I2-Mediated Oxidative Cyclization of Substituted Phenylacrylic Acids. *RSC Adv.* **2013**, *3* (13), 4311. https://doi.org/10.1039/c3ra23188g.

(13) Subramanian, K.; Yedage, S. L.; Bhanage, B. M. An Electrochemical Method for Carboxylic Ester Synthesis from *N* -Alkoxyamides. *J. Org. Chem.* **2017**, *82* (19), 10025–10032. https://doi.org/10.1021/acs.joc.7b01473.

(14) He, Z.; Qi, X.; Li, S.; Zhao, Y.; Gao, G.; Lan, Y.; Wu, Y.; Lan, J.; You, J. Transition-Metal-Free Formal Decarboxylative Coupling of α-Oxocarboxylates with α-Bromoketones under Neutral Conditions: A Simple Access to 1,3-Diketones. *Angew. Chem. Int. Ed.* **2015**, *54* (3), 855–859. https://doi.org/10.1002/anie.201409361.

(15) Paris, C.; Lhiaubet-Vallet, V.; Jiménez, O.; Trullas, C.; Miranda, M. Á. A Blocked Diketo Form of Avobenzone: Photostability, Photosensitizing Properties and Triplet Quenching by a Triazine-Derived UVB-Filter. *Photochemistry and Photobiology* **2009**, *85* (1), 178–184. https://doi.org/10.1111/j.1751-1097.2008.00414.x.

(16) Allais, F.; Martinet, S.; Ducrot, P.-H. Straightforward Total Synthesis of 2-O-Feruloyl-l-Malate, 2-O-Sinapoyl-l-Malate and 2-O-5-Hydroxyferuloyl-l-Malate. *Synthesis* **2009**, *2009* (21), 3571–3578. https://doi.org/10.1055/s-0029-1216983.

Spectroscopy

(1) Ni, G.; Li, G.; Boriskina, S. V.; Li, H.; Yang, W.; Zhang, T.; Chen, G. Steam Generation under One Sun Enabled by a Floating Structure with Thermal Concentration. *Nat Energy* **2016**, *1* (9), 16126. https://doi.org/10.1038/nenergy.2016.126.

(2) Maier, H.; Schauberger, G.; Martincigh, B. S.; Brunnhofer, K.; Honigsmann, H. Ultraviolet Protective Performance of Photoprotective Lipsticks: Change of Spectral Transmittance Because of Ultraviolet Exposure. *Photoderm Photoimm Photomed* **2005**, *21* (2), 84–92. https://doi.org/10.1111/j.1600-0781.2005.00143.x.

(3) Gonzalez, H.; Tarras-Wahlberg, N.; Strömdahl, B.; Juzeniene, A.; Moan, J.; Larkö, O.; Rosén, A.; Wennberg, A.-M. Photostability of Commercial Sunscreens upon Sun Exposure and Irradiation by Ultraviolet Lamps. *BMC Dermatol* **2007**, *7* (1), 1. https://doi.org/10.1186/1471-5945-7-1.

(4) Hojerová, J.; Medovcíková, A.; Mikula, M. Photoprotective Efficacy and Photostability of Fifteen Sunscreen Products Having the Same Label SPF Subjected to Natural Sunlight. *International Journal of Pharmaceutics* **2011**, *408* (1–2), 27–38. https://doi.org/10.1016/j.ijpharm.2011.01.040.

(5) Walmsley, I.; Waxer, L.; Dorrer, C. The Role of Dispersion in Ultrafast Optics. *Review of Scientific Instruments* **2001**, *72* (1), 1–29. https://doi.org/10.1063/1.1330575.

(6) Grubb, M. P.; Orr-Ewing, A. J.; Ashfold, M. N. R. KOALA: A Program for the Processing and Decomposition of Transient Spectra. *Review of Scientific Instruments* **2014**, *85* (6), 064104. https://doi.org/10.1063/1.4884516.

(7) Mullen, K. M.; Stokkum, I. H. M. van. **TIMP** : An *R* Package for Modeling Multi-Way Spectroscopic Measurements. *J. Stat. Soft.* **2007**, *18* (3). https://doi.org/10.18637/jss.v018.i03.

(8) Snellenburg, J. J.; Laptenok, S. P.; Seger, R.; Mullen, K. M.; Stokkum, I. H. M. van. **Glotaran** : A *Java* -Based Graphical User Interface for the *R* Package **TIMP**. *J. Stat. Soft.* **2012**, *49* (3). https://doi.org/10.18637/jss.v049.i03.

(9) Whittock, A. L.; Turner, M. A. P.; Coxon, D. J. L.; Woolley, J. M.; Horbury, M. D.; Stavros, V. G. Reinvestigating the Photoprotection Properties of a Mycosporine Amino Acid Motif. *Front. Chem.* **2020**, *8*, 574038. https://doi.org/10.3389/fchem.2020.574038.

Computational

(1) Zhang, J.; Zhang, H.; Wu, T.; Wang, Q.; van der Spoel, D. Comparison of Implicit and Explicit Solvent Models for the Calculation of Solvation Free Energy in Organic Solvents. *J. Chem. Theory Comput.* **2017**, *13* (3), 1034–1043. https://doi.org/10.1021/acs.jctc.7b00169.

(2) Turner, M. A. P.; Turner, R. J.; Horbury, M. D.; Hine, N. D. M.; Stavros, V. G. Examining Solvent Effects on the Ultrafast Dynamics of Catechol. *J. Chem. Phys.* **2019**, *151* (8), 084305. https://doi.org/10.1063/1.5116312.

(3) Valiev, M.; Bylaska, E. J.; Govind, N.; Kowalski, K.; Straatsma, T. P.; Van Dam, H. J. J.; Wang, D.; Nieplocha, J.; Apra, E.; Windus, T. L.; de Jong, W. A. NWChem: A Comprehensive and Scalable Open-Source Solution for Large Scale Molecular Simulations. *Computer Physics Communications* **2010**, *181* (9), 1477–1489. https://doi.org/10.1016/j.cpc.2010.04.018.

(4) Klamt, A.; Schüürmann, G. COSMO: A New Approach to Dielectric Screening in Solvents with Explicit Expressions for the Screening Energy and Its Gradient. *J. Chem. Soc., Perkin Trans. 2* **1993**, No. 5, 799–805. https://doi.org/10.1039/P29930000799.

(5) Marenich, A. V.; Cramer, C. J.; Truhlar, D. G. Universal Solvation Model Based on Solute Electron Density and on a Continuum Model of the Solvent Defined by the Bulk Dielectric Constant and Atomic Surface Tensions. *J. Phys. Chem. B* **2009**, *113* (18), 6378–6396. https://doi.org/10.1021/jp810292n.

(6) Charlton, R. J.; Fogarty, R. M.; Bogatko, S.; Zuehlsdorff, T. J.; Hine, N. D. M.; Heeney, M.; Horsfield, A. P.; Haynes, P. D. Implicit and Explicit Host Effects on Excitons in Pentacene Derivatives. *The Journal of Chemical Physics* **2018**, *148* (10), 104108. https://doi.org/10.1063/1.5017285.

(7) Reynolds, C. R.; Islam, S. A.; Sternberg, M. J. E. EzMol: A Web Server Wizard for the Rapid Visualization and Image Production of Protein and Nucleic Acid Structures. *Journal of Molecular Biology* **2018**, *430* (15), 2244–2248. https://doi.org/10.1016/j.jmb.2018.01.013.

(8) Kelley, L. A.; Mezulis, S.; Yates, C. M.; Wass, M. N.; Sternberg, M. J. E. The Phyre2 Web Portal for Protein Modeling, Prediction and Analysis. *Nat Protoc* **2015**, *10* (6), 845–858. https://doi.org/10.1038/nprot.2015.053.

Chapter 3

(1) White, J. D.; Cammack, J. H.; Sakuma, K.; Rewcastle, G. W.; Widener, R. K. Transformations of Quinic Acid. Asymmetric Synthesis and Absolute Configuration of Mycosporin I and Mycosporin-Gly. *J. Org. Chem.* **1995**, *60* (12), 3600–3611. https://doi.org/10.1021/jo00117a008.

(2) Mekler, A. B.; Ramachandran, S.; Swaminathan, S.; Newman, M. S. 2-Methyl-1,3-Cyclohexanedione: 1,3-Cyclohexanedione, 2-Methyl-. In *Organic Syntheses*; John Wiley & Sons, Inc., Ed.; John Wiley & Sons, Inc.: Hoboken, NJ, USA, 2003; pp 56–56. https://doi.org/10.1002/0471264180.os041.15.

(3) Shriner, R. L.; Todd, H. R. 5,5-Dimethyl-1,3-Cyclohexanedione: 1,3-Cyclohexanedione, 5,5-Dimethyl-. In *Organic Syntheses*; John Wiley & Sons, Inc., Ed.; John Wiley & Sons, Inc.: Hoboken, NJ, USA, 2003; pp 14–14. https://doi.org/10.1002/0471264180.os015.06.

(4) Cui, B.; Wang, R.-H.; Chen, L.-Z.; Jin, Y.; Han, G.-F. Synthesis of Enaminones in Aqueous Media Using Catalytic Dilute HCl. *Synthetic Communications* **2011**, *41* (7), 1064–1070. https://doi.org/10.1080/00397911003797775.

(5) Rajitha, B.; Penthala Narsimha Reddy; Buridapad Sunil Kumar; Srinivasulu, N.; Yerram Reddy Thirupathi Reddy. VCl3 Catalysed Efficient Synthesis of β-Enamine Esters and Ketones from β-Keto Esters. *j. chem. res. (s)* **2005**, *2005* (8), 535–536. https://doi.org/10.3184/030823405774663237.

(6) Andreguetti, D.; Stein, E. M.; Pereira, C. M. P.; Pinto, E.; Colepicolo, P. Antioxidant Properties and UV Absorbance Pattern of Mycosporine-Like Amino Acids Analogs Synthesized in an Environmentally Friendly Manner: Synthesis And Antioxidant Activity Of Maas Analogues. *J Biochem Mol Toxicol* **2013**, *27* (6), 305–312. https://doi.org/10.1002/jbt.21489.

(7) Bhattacherjee, D.; Thakur, V.; Sharma, S.; Kumar, S.; Bharti, R.; Reddy, C. B.; Das, P. Iodine(III)-Promoted Ring Contractive Cyanation of Exocyclic β-Enaminones for the Synthesis of Cyanocyclopentanones. *Adv. Synth. Catal.* **2017**, *359* (13), 2209–2214. https://doi.org/10.1002/adsc.201601208.

(8) York, M.; Jarvis, K. E.; Freemont, J. A.; Ryan, J. H.; Savage, G. P.; Logan, S. A.; Bright, L. A Scalable, Combined-Batch, and Continuous-Flow Synthesis of a Bio-Inspired UV-B Absorber. *Aust. J. Chem.* **2019**, *72* (11), 860. https://doi.org/10.1071/CH19252.

(9) Nguyen, K. H.; Tomasi, S.; Le Roch, M.; Toupet, L.; Renault, J.; Uriac, P.; Gouault, N. Gold-Mediated Synthesis and Functionalization of Chiral Halopyridones. *J. Org. Chem.* **2013**, *78* (16), 7809–7815. https://doi.org/10.1021/jo400827b.

(10) Reddy Chidipudi, S.; Khan, I.; Lam, H. W. Functionalization of C Sp 3 H and C Sp 2 H Bonds: Synthesis of Spiroindenes by Enolate-Directed Ruthenium-Catalyzed Oxidative Annulation of Alkynes with 2-Aryl-1,3-Dicarbonyl Compounds. *Angew. Chem. Int. Ed.* **2012**, *51* (48), 12115–12119. https://doi.org/10.1002/anie.201207170.

(11) Ostercamp, D. L.; Dinh, Y.; Graff, D.; Wiles, S. Rigid Core Vinamidinium Salts and Their N,N'-Rotamers. *J. Org. Chem.* **2003**, *68* (8), 3099–3105. https://doi.org/10.1021/jo020654l.

(12) Losantos, R.; Funes-Ardoiz, I.; Aguilera, J.; Herrera-Ceballos, E.; García-Iriepa, C.; Campos, P. J.; Sampedro, D. Rational Design and Synthesis of Efficient Sunscreens To Boost the Solar Protection Factor. *Angew. Chem. Int. Ed. Engl.* **2017**, *56* (10), 2632–2635. https://doi.org/10.1002/anie.201611627.

(13) Losantos, R.; Lamas, I.; Montero, R.; Longarte, A.; Sampedro, D. Photophysical Characterization of New and Efficient Synthetic Sunscreens. *Phys. Chem. Chem. Phys.* **2019**, *21* (21), 11376–11384. https://doi.org/10.1039/C9CP01267B.

(14) Conde, F. R.; Churio, M. S.; Previtali, C. M. Experimental Study of the Excited-State Properties and Photostability of the Mycosporine-like Amino Acid Palythine in Aqueous Solution. *Photochem. Photobiol. Sci.* **2007**, *6* (6), 669. https://doi.org/10.1039/b618314j.

(15) Franco, J. H.; da Silva, B. F.; Dias, E. F. G.; de Castro, A. A.; Ramalho, T. C.; Zanoni, M. V. B. Influence of Auxochrome Group in Disperse Dyes Bearing Azo Groups as Chromophore Center in the Biotransformation and Molecular Docking Prediction by Reductase Enzyme: Implications and Assessment for Environmental Toxicity of Xenobiotics.

Ecotoxicology and Environmental Safety **2018**, *160*, 114–126. https://doi.org/10.1016/j.ecoenv.2018.04.066.

(16) Carey, F. A.; Sundberg, R. J. *Advanced Organic Chemistry*, 5th ed.; Springer: New York, 2007.

(17) Adler, M.; Schank, K.; Schmidt, V. Einführung von Sauerstoff-Funktionen in die α-Stellung von β-Diketonen, 1. Acyloxylierungen von 3-sek.-Amino-2-cyclohexen-1-onen mit Diacylperoxiden. *Chem. Ber.* **1979**, *112* (6), 2314–2323. https://doi.org/10.1002/cber.19791120638.

(18) Adler, M.; Schank, K.; Schmidt, V. Einführung von Sauerstoff-Funktionen in die α-Stellung von β-Diketonen, 2. Umfunktionalisierungen von 2-Acyloxy-3-sek.-amino-2-cyclohexen-1-onen. *Chem. Ber.* **1979**, *112* (6), 2324–2331. https://doi.org/10.1002/cber.19791120639.

(19) Schank, K.; Lieder, R.; Lick, C.; Glock, R. Chemie Freier Cyclischer Vicinaler Tricarbonyl-Verbindungen ('1,2,3-Trione'). Teil 3. *Helvetica Chimica Acta* **2004**, *87*, 869–924. https://doi.org/10.1002/hlca.200490085.

(20) Ji, S.-J.; Lu, J.; Lang, J.-P.; Horiuchi, C. A. Synthesis of Camphoric Anhydride via Unsensitized Photo-Oxidation Of Camphorquinone. *Synthetic Communications* **2002**, *32* (11), 1659–1663. https://doi.org/10.1081/SCC-120004256.

(21) Ciaccia, M.; Di Stefano, S. Mechanisms of Imine Exchange Reactions in Organic Solvents. *Org. Biomol. Chem.* **2015**, *13* (3), 646–654. https://doi.org/10.1039/C4OB02110J.

(22) Jones, R. A. Y. *Physical and Mechanistic Organic Chemistry*; Cambridge texts in chemistry and biochemistry; Cambridge University Press: Cambridge ; New York, 1979.

(23) Ciaccia, M.; Cacciapaglia, R.; Mencarelli, P.; Mandolini, L.; Di Stefano, S. Fast Transimination in Organic Solvents in the Absence of Proton and Metal Catalysts. A Key to Imine Metathesis Catalyzed by Primary Amines under Mild Conditions. *Chem. Sci.* **2013**, *4* (5), 2253. https://doi.org/10.1039/c3sc50277e.

(24) Torres, A.; Hochberg, M.; Pergament, I.; Smoum, R.; Niddam, V.; Dembitsky, V. M.; Temina, M.; Dor, I.; Lev, O.; Srebnik, M.; Enk, C. D. A New UV-B Absorbing Mycosporine with Photo Protective Activity from the Lichenized Ascomycete Collema Cristatum: Photo Protective Mycosporine from Collema Cristatum. *European Journal of Biochemistry* **2004**, *271* (4), 780–784. https://doi.org/10.1111/j.1432-1033.2004.03981.x.

(25) Fayret, J.; Bernillon, J.; Bouillant, M.-L.; Favre-Bonvin, J.; Arpin, N. Open and Ring Forms of Mycosporin-2 from the Ascomycete Gnomonia Leptostyla. *Phytochemistry* **1981**, *20* (12), 2709–2710. https://doi.org/10.1016/0031-9422(81)85273-9.

(26) Roullier, C.; Chollet-Krugler, M.; Pferschy-Wenzig, E.-M.; Maillard, A.; Rechberger, G. N.; Legouin-Gargadennec, B.; Bauer, R.; Boustie, J. Characterization and Identification of Mycosporines-like Compounds in Cyanolichens. Isolation of Mycosporine Hydroxyglutamicol from Nephroma Laevigatum Ach. *Phytochemistry* **2011**, *72* (11–12), 1348–1357. https://doi.org/10.1016/j.phytochem.2011.04.002.

(27) Woolley, J. M.; Staniforth, M.; Horbury, M. D.; Richings, G. W.; Wills, M.; Stavros, V. G. Unravelling the Photoprotection Properties of Mycosporine Amino Acid Motifs. *J. Phys. Chem. Lett.* **2018**, *9* (11), 3043–3048. https://doi.org/10.1021/acs.jpclett.8b00921.

(28) Di, L.; Kerns, E. H. Solubility. In *Drug-Like Properties*; Elsevier, 2016; pp 61–93. https://doi.org/10.1016/B978-0-12-801076-1.00007-1.

(29) Gonzalez, H.; Tarras-Wahlberg, N.; Strömdahl, B.; Juzeniene, A.; Moan, J.; Larkö, O.; Rosén, A.; Wennberg, A.-M. Photostability of Commercial Sunscreens upon Sun Exposure and Irradiation by Ultraviolet Lamps. *BMC Dermatol* **2007**, *7* (1), 1. https://doi.org/10.1186/1471-5945-7-1.

(30) Hojerová, J.; Medovcíková, A.; Mikula, M. Photoprotective Efficacy and Photostability of Fifteen Sunscreen Products Having the Same Label SPF Subjected to Natural Sunlight. *International Journal of Pharmaceutics* **2011**, *408* (1–2), 27–38. https://doi.org/10.1016/j.ijpharm.2011.01.040.

(31) Kovalenko, S. A.; Dobryakov, A. L.; Ruthmann, J.; Ernsting, N. P. Femtosecond Spectroscopy of Condensed Phases with Chirped Supercontinuum Probing. *Phys. Rev. A* **1999**, *59* (3), 2369–2384. https://doi.org/10.1103/PhysRevA.59.2369.

(32) Whittock, A. L.; Auckloo, N.; Cowden, A. M.; Turner, M. A. P.; Woolley, J. M.; Wills, M.; Corre, C.; Stavros, V. G. Exploring the Blueprint of Photoprotection in Mycosporine-like Amino Acids. *J. Phys. Chem. Lett.* **2021**, *12* (14), 3641–3646. https://doi.org/10.1021/acs.jpclett.1c00728.

Chapter 4

(1) Sunscreen Drug Products for Over-the-Counter Human Use; Final Monograph. Food and Drug Administration, HHS. Final Rule. *Fed Regist* **1999**, *64* (98), 27666–27693.

(2) *Cosmetic Products Regulation, Annex VI - Allowed UV Filters*; Regulation 1223/2009/EC on Cosmetic Products, as corrected by Corrigendum to Commission Regulation (EU) 2021/850, 17 June 2021; European Chemicals Agency, 2021. https://echa.europa.eu/cosmetics-uv-filters (accessed 2022-02-07).

(3) Shaath, N. A. Ultraviolet Filters. *Photochem. Photobiol. Sci.* **2010**, *9* (4), 464. https://doi.org/10.1039/b9pp00174c.

(4) Wang, S. Q.; Tanner, P. R.; Lim, H. W.; Nash, J. F. The Evolution of Sunscreen Products in the United States – a 12-Year Cross Sectional Study. *Photochem. Photobiol. Sci.* **2013**, *12* (1), 197–202. https://doi.org/10.1039/C2PP25112D.

(5) Schwack, W.; Rudolph, T. Photochemistry of Dibenzoyl Methane UVA Filters Part 1. *Journal of Photochemistry and Photobiology B: Biology* **1995**, *28* (3), 229–234. https://doi.org/10.1016/1011-1344(95)07118-L.

(6) Roscher, N. M.; Lindemann, M. K. O.; Bin Kong, S.; Cho, C. G.; Jiang, P. Photodecomposition of Several Compounds Commonly Used as Sunscreen Agents. *Journal of Photochemistry and Photobiology A: Chemistry* **1994**, *80* (1–3), 417–421. https://doi.org/10.1016/1010-6030(94)01043-9.

(7) Sayre, R. M.; Dowdy, J. C.; Gerwig, A. J.; Shlelds, W. J.; Lioyd, R. V. Unexpected Photolysis of the Sunscreen Octinoxate in the Presence of the Sunscreen Avobenzone¶. *Photochemistry and Photobiology* **2007**, *81* (2), 452–456. https://doi.org/10.1111/j.1751-1097.2005.tb00207.x.

(8) Yamaji, M.; Kida, M. Photothermal Tautomerization of a UV Sunscreen (4- *Tert* -Butyl-4'-Methoxydibenzoylmethane) in Acetonitrile Studied by Steady-State and Laser Flash Photolysis. *J. Phys. Chem. A* **2013**, *117* (9), 1946–1951. https://doi.org/10.1021/jp312774e.

(9) Dubois, M.; Gilard, P.; Tiercet, P.; Deflandre, A.; Lefebvre, M. A. Photoisomerisation of the Sunscreen Filter PARSOL © 1789. *J. Chim. Phys.* **1998**, *95* (2), 388–394. https://doi.org/10.1051/jcp:1998149.

(10) Cantrell, A.; McGarvey, D. J. Photochemical Studies of 4-Tert-Butyl-4'-Methoxydibenzoylmethane (BM-DBM). *Journal of Photochemistry and Photobiology B: Biology* **2001**, *64* (2–3), 117–122. https://doi.org/10.1016/S1011-1344(01)00226-3.

(11) St. Nikolov, G.; Markov, P. Photochemical Hydrogen Abstraction as a Radiationless Transition in the Photoketonization of β-Dicarbonyl Compounds. *Journal of Photochemistry* **1981**, *16* (2), 93–104. https://doi.org/10.1016/0047-2670(81)80023-8.

(12) Hanson, K. M.; Cutuli, M.; Rivas, T.; Antuna, M.; Saoub, J.; Tierce, N. T.; Bardeen, C. J. Effects of Solvent and Micellar Encapsulation on the Photostability of Avobenzone. *Photochem. Photobiol. Sci.* **2020**, *19* (3), 390–398. https://doi.org/10.1039/C9PP00483A.

(13) Burnett, M. E.; Wang, S. Q. Current Sunscreen Controversies: A Critical Review: Sunscreen Controversies. *Photodermatology, Photoimmunology & Photomedicine* **2011**, *27* (2), 58–67. https://doi.org/10.1111/j.1600-0781.2011.00557.x.

(14) Scalia, S.; Mezzena, M.; Ramaccini, D. Encapsulation of the UV Filters Ethylhexyl Methoxycinnamate and Butyl Methoxydibenzoylmethane in Lipid Microparticles: Effect on in Vivo Human Skin Permeation. *Skin Pharmacol Physiol* **2011**, *24* (4), 182–189. https://doi.org/10.1159/000324054.

(15) Niculae, G.; Lacatusu, I.; Bors, A.; Stan, R. Photostability Enhancement by Encapsulation of α-Tocopherol into Lipid-Based Nanoparticles Loaded with a UV Filter. *Comptes Rendus Chimie* **2014**, *17* (10), 1028–1033. https://doi.org/10.1016/j.crci.2013.12.007.

(16) Govindu, P. C. V.; Hosamani, B.; Moi, S.; Venkatachalam, D.; Asha, S.; John, V. N.; Sandeep, V.; Gowd, K. H. Glutathione as a Photo-Stabilizer of Avobenzone: An Evaluation under Glass-Filtered Sunlight Using UV-Spectroscopy. *Photochem. Photobiol. Sci.* **2019**, *18* (1), 198–207. https://doi.org/10.1039/C8PP00343B.

(17) Holt, E. L.; Rodrigues, N. d. N.; Cebrián, J.; Stavros, V. G. Determining the Photostability of Avobenzone in Sunscreen Formulation Models Using Ultrafast Spectroscopy. *Phys. Chem. Chem. Phys.* **2021**, *23* (42), 24439–24448. https://doi.org/10.1039/D1CP03610F.

(18) Bonda, C.; Pavlovic, A.; Hanson, K.; Bardeen, C. Singlet Quenching Proves Faster Is Better for Photostability. *Cosmet. Toiletries* **2010**, *125*, 40–48.

(19) Moi, S.; Hosamani, B.; Kumar, K.; Gunaga, S.; Raghothama, S.; Gowd, K. H. Photochemical Studies of New Synthetic Derivatives of Avobenzone under Sunlight Using UV-Spectroscopy. *Journal of Photochemistry and Photobiology A: Chemistry* **2021**, *420*, 113488. https://doi.org/10.1016/j.jphotochem.2021.113488.

(20) Wang, J.; Lei, Y.; Guo, Y.; Wang, J.; Ma, J. Investigation of Different Photochemical Reactions of Avobenzone Derivatives by Ultrafast Transient Absorption Spectroscopy. *Photochem. Photobiol. Sci.* **2019**, *18* (12), 3000–3007. https://doi.org/10.1039/C9PP00333A.

(21) Armeni, T.; Damiani, E.; Battino, M.; Greci, L.; Principato, G. Lack of in Vitro Protection by a Common Sunscreen Ingredient on UVA-Induced Cytotoxicity in Keratinocytes. *Toxicology* **2004**, *203* (1–3), 165–178. https://doi.org/10.1016/j.tox.2004.06.008.

(22) Damiani, E.; Baschong, W.; Greci, L. UV-Filter Combinations under UV-A Exposure: Concomitant Quantification of over-All Spectral Stability and Molecular Integrity. *J Photochem Photobiol B* **2007**, *87* (2), 95–104. https://doi.org/10.1016/j.jphotobiol.2007.03.003.

(23) Damiani, E.; Greci, L.; Parsons, R.; Knowland, J. Nitroxide Radicals Protect DNA from Damage When Illuminated in Vitro in the Presence of Dibenzoylmethane and a Common Sunscreen Ingredient. *Free Radical Biology and Medicine* **1999**, *26* (7–8), 809–816. https://doi.org/10.1016/S0891-5849(98)00292-5.

(24) Dondi, D.; Albini, A.; Serpone, N. Interactions between Different Solar UVB/UVA Filters Contained in Commercial Suncreams and Consequent Loss of UV Protection. *Photochem. Photobiol. Sci.* **2006**, *5* (9), 835. https://doi.org/10.1039/b606768a.

(25) Kornis, G.; Mayo, P. D. Photochemical Syntheses: 9. The Conversion of Dibenzoylmethane to Tribenzoylethane. *Can. J. Chem.* **1964**, *42* (12), 2822–2827. https://doi.org/10.1139/v64-417.

(26) de Groot, A. C.; Roberts, D. W. Contact and Photocontact Allergy to Octocrylene: A Review: Contact and Photocontact Allergy to Octocrylene. *Contact Dermatitis* **2014**, *70* (4), 193–204. https://doi.org/10.1111/cod.12205.

(27) Karlsson, I.; Persson, E.; Mårtensson, J.; Börje, A. Investigation of the Sunscreen Octocrylene's Interaction with Amino Acid Analogs in the Presence of UV Radiation.

Photochemistry and Photobiology **2012**, *88* (4), 904–912. https://doi.org/10.1111/j.1751-1097.2012.01142.x.

(28) Kerr, A. C. A Survey of the Availability of Sunscreen Filters in the UK: A Survey of the Availability of Sunscreen Filters in the UK. *Clinical and Experimental Dermatology* **2011**, *36* (5), 541–543. https://doi.org/10.1111/j.1365-2230.2010.04007.x.

(29) Wahie, S.; Lloyd, J. J.; Farr, P. M. Sunscreen Ingredients and Labelling: A Survey of Products Available in the UK. *Clin Exp Dermatol* **2007**, *32* (4), 359–364. https://doi.org/10.1111/j.1365-2230.2007.02404.x.

(30) Kikuchi, A.; Hata, Y.; Kumasaka, R.; Nanbu, Y.; Yagi, M. Photoexcited Singlet and Triplet States of a UV Absorber Ethylhexyl Methoxycrylene. *Photochem Photobiol* **2013**, *89* (3), 523–528. https://doi.org/10.1111/php.12017.

(31) Pattanaargson, S.; Munhapol, T.; Hirunsupachot, P.; Luangthongaram, P. Photoisomerization of Octyl Methoxycinnamate. *Journal of Photochemistry and Photobiology A: Chemistry* **2004**, *161* (2–3), 269–274. https://doi.org/10.1016/S1010-6030(03)00282-X.

(32) Baker, L. A.; Horbury, M. D.; Stavros, V. G. Ultrafast Photoprotective Properties of the Sunscreening Agent Octocrylene. *Opt. Express* **2016**, *24* (10), 10700. https://doi.org/10.1364/OE.24.010700.

(33) Forestier, S. Rationale for Sunscreen Development. *J Am Acad Dermatol* **2008**, *58* (5 Suppl 2), S133-138. https://doi.org/10.1016/j.jaad.2007.05.047.

(34) Carrotte-Lefebvre, I.; Bonnevalle, A.; Segard, M.; Delaporte, E.; Thomas, P. Contact Allergy to Octocrylene: First 2 Cases. *Contact Dermatitis* **2003**, *48* (1), 45–55. https://doi.org/10.1034/j.1600-0536.2003.480108_2.x.

(35) Pigatto, P. D.; Guzzi, G.; Schena, D.; Guarrera, M.; Foti, C.; Francalanci, S.; Cristaudo, A.; Ayala, F.; Vincenzi, C. Photopatch Tests: An Italian Multicentre Study from 2004 to 2006. *Contact Dermatitis* **2008**, *59* (2), 103–108. https://doi.org/10.1111/j.1600-0536.2008.01374.x.

(36) Karlsson, I.; Vanden Broecke, K.; Mårtensson, J.; Goossens, A.; Börje, A. Clinical and Experimental Studies of Octocrylene's Allergenic Potency. *Contact Dermatitis* **2011**, *64* (6), 343–352. https://doi.org/10.1111/j.1600-0536.2011.01899.x.

(37) Fonseca, M. J. V.; Vilela, F. M. P.; Vicentini, F. T. M. C.; et al. Sunscreen Protection against Ultraviolet-Induced Oxidative Stress: Evaluation of Reduced Glutathione Levels, Metalloproteinase Secretion, and Myeloperoxidase Activity. *Pharmazie* **2013**, No. 11, 872–876. https://doi.org/10.1691/ph.2013.3045.

(38) Polonini, H. C.; Lopes, R. S.; Beatriz, A.; Gomes, R. S.; Silva, A. O.; Lima, R. V. de; Nunes, Gláucia. A.; Brandão, M. A. F.; Raposo, N. R. B.; Lima, D. P. de. Synthesis and Evaluation of Octocrylene-Inspired Compounds for UV-Filter Activity. *Química Nova* **2014**. https://doi.org/10.5935/0100-4042.20140160.

(39) Bonda, C. A.; Lott, D. Sunscreen Photostability. In *Principles and Practice of Photoprotection*; Wang, S. Q., Lim, H. W., Eds.; Springer International Publishing: Cham, 2016; pp 247–273. https://doi.org/10.1007/978-3-319-29382-0_14.

(40) Sandros, K.; Haglid, F.; Ryhage, R.; Ryhage, R.; Stevens, R. Transfer of Triplet State Energy in Fluid Solutions. III. Reversible Energy Transfer. *Acta Chem. Scand.* **1964**, *18*, 2355–2374. https://doi.org/10.3891/acta.chem.scand.18-2355.

(41) Evans, D. F. 257. Perturbation of Singlet–Triplet Transitions of Aromatic Molecules by Oxygen under Pressure. *J. Chem. Soc.* **1957**, *0* (0), 1351–1357. https://doi.org/10.1039/JR9570001351.

(42) Gonzenbach, H.; Hill, T. J.; Truscott, T. G. The Triplet Energy Levels of UVA and UVB Sunscreens. *Journal of Photochemistry and Photobiology B: Biology* **1992**, *16* (3–4), 377–379. https://doi.org/10.1016/1011-1344(92)80025-Q.

(43) Kikuchi, A.; Oguchi, N.; Yagi, M. Optical and Electron Paramagnetic Resonance Studies of the Excited States of 4- *Tert* -Butyl-4'-Methoxydibenzoylmethane and 4- *Tert* -Butyl-4'-Methoxydibenzoylpropane. *J. Phys. Chem. A* **2009**, *113* (48), 13492–13497. https://doi.org/10.1021/jp905236m.

(44) El-Sayed, M. A. Double Resonance and the Properties of the Lowest Excited Triplet State of Organic Molecules. *Annu. Rev. Phys. Chem.* **1975**, *26* (1), 235–258. https://doi.org/10.1146/annurev.pc.26.100175.001315.

(45) Wardle, B. *Principles and Applications of Photochemistry*; 2009.

(46) Herzog, B.; Giesinger, J.; Settels, V. Insights into the Stabilization of Photolabile UV-Absorbers in Sunscreens. *Photochem. Photobiol. Sci.* **2020**, *19* (12), 1636–1649. https://doi.org/10.1039/D0PP00335B.

(47) Sacco, J. J.; Botten, J.; Macbeth, F.; Bagust, A.; Clark, P. The Average Body Surface Area of Adult Cancer Patients in the UK: A Multicentre Retrospective Study. *PLoS ONE* **2010**, *5* (1), e8933. https://doi.org/10.1371/journal.pone.0008933.

(48) Hayashi, H.; Nagakura, S. The Lowest Nπ* and Ππ* Triplet Levels of Benzaldehydes and Their Correlation with the Zero-Field Splittings. *null* **1974**, *27* (4), 969–979. https://doi.org/10.1080/00268977400100891.

(49) Mohan Vijaykumar Chavan, Vijay Ramchandra Gadgil, Balu Kunjupillai, Ashish Anant Vaidya. Sunscreen Molecule and Compositions Thereof. US10143642B2, December 4, 2018.

(50) 87. Steglich Esterification. In *Organic Chemistry: 100 Must-Know Mechanisms*; De Gruyter, 2020; pp 194–195. https://doi.org/10.1515/9783110608373-087.

(51) Lutjen, A. B.; Quirk, M. A.; Barbera, A. M.; Kolonko, E. M. Synthesis of (E)-Cinnamyl Ester Derivatives via a Greener Steglich Esterification. *Bioorganic & Medicinal Chemistry* **2018**, *26* (19), 5291–5298. https://doi.org/10.1016/j.bmc.2018.04.007.

(52) Abiola, T. T.; Whittock, A. L.; Stavros, V. G. Unravelling the Photoprotective Mechanisms of Nature-Inspired Ultraviolet Filters Using Ultrafast Spectroscopy. *Molecules* **2020**, *25* (17), 3945. https://doi.org/10.3390/molecules25173945.

(53) Allais, F.; Martinet, S.; Ducrot, P.-H. Straightforward Total Synthesis of 2-O-Feruloyl-l-Malate, 2-O-Sinapoyl-l-Malate and 2-O-5-Hydroxyferuloyl-l-Malate. *Synthesis* **2009**, *2009* (21), 3571–3578. https://doi.org/10.1055/s-0029-1216983.

(54) Kaeswurm, J. A. H.; Scharinger, A.; Teipel, J.; Buchweitz, M. Absorption Coefficients of Phenolic Structures in Different Solvents Routinely Used for Experiments. *Molecules* **2021**, *26* (15), 4656. https://doi.org/10.3390/molecules26154656.

(55) Snyder, L. R. Classification of the Solvent Properties of Common Liquids. *Journal of Chromatography A* **1974**, *92* (2), 223–230. https://doi.org/10.1016/S0021-9673(00)85732-5.

Chapter 5

(1) Arbeloa, E. M.; Uez, M. J.; Bertolotti, S. G.; Churio, M. S. Antioxidant Activity of Gadusol and Occurrence in Fish Roes from Argentine Sea. *Food Chemistry* **2010**, *119* (2), 586–591. https://doi.org/10.1016/j.foodchem.2009.06.061.

(2) Dittmann, E.; Gugger, M.; Sivonen, K.; Fewer, D. P. Natural Product Biosynthetic Diversity and Comparative Genomics of the Cyanobacteria. *Trends in Microbiology* **2015**, *23* (10), 642–652. https://doi.org/10.1016/j.tim.2015.07.008.

(3) Balskus, E. P.; Walsh, C. T. The Genetic and Molecular Basis for Sunscreen Biosynthesis in Cyanobacteria. *Science* **2010**, *329* (5999), 1653–1656. https://doi.org/10.1126/science.1193637.

(4) Favre-Bonvin, J.; Arpin, N.; Brevard, C. Structure de La Mycosporine (P 310). *Can. J. Chem.* **1976**, *54* (7), 1105–1113. https://doi.org/10.1139/v76-158.

(5) Portwich, A.; Garcia-Pichel, F. Ultraviolet and Osmotic Stresses Induce and Regulate the Synthesis of Mycosporines in the Cyanobacterium Chlorogloeopsis PCC 6912. *Archives of Microbiology* **1999**, *172* (4), 187–192. https://doi.org/10.1007/s002030050759.

(6) Sinha, R. P.; Ambasht, N. K.; Sinha, J. P.; Klisch, M.; Häder, D.-P. UV-B-Induced Synthesis of Mycosporine-like Amino Acids in Three Strains of Nodularia (Cyanobacteria). *Journal of Photochemistry and Photobiology B: Biology* **2003**, *71* (1–3), 51–58. https://doi.org/10.1016/j.jphotobiol.2003.07.003.

(7) Spence, E.; Dunlap, W. C.; Shick, J. M.; Long, P. F. Redundant Pathways of Sunscreen Biosynthesis in a Cyanobacterium. *ChemBioChem* **2012**, *13* (4), 531–533. https://doi.org/10.1002/cbic.201100737.

(8) Spence, E.; Dunlap, W. C.; Shick, J. M.; Long, P. F. Corrigendum: Redundant Pathways of Sunscreen Biosynthesis in a Cyanobacterium. *ChemBioChem* **2012**, *13* (4), 497–497. https://doi.org/10.1002/cbic.201200076.

(9) Singh, S. P.; Klisch, M.; Sinha, R. P.; Häder, D.-P. Genome Mining of Mycosporine-like Amino Acid (MAA) Synthesizing and Non-Synthesizing Cyanobacteria: A Bioinformatics Study. *Genomics* **2010**, *95* (2), 120–128.

(10) Samel, S. A.; Marahiel, M. A.; Essen, L.-O. How to Tailor Non-Ribosomal Peptide Products—New Clues about the Structures and Mechanisms of Modifying Enzymes. *Mol. BioSyst.* **2008**, *4* (5), 387. https://doi.org/10.1039/b717538h.

(11) Mander, L. N.; Liu, H. *Comprehensive Natural Products II: Chemistry and Biology*; Elsevier Science: Oxford, 2010.

(12) Gao, Q.; Garcia-Pichel, F. An ATP-Grasp Ligase Involved in the Last Biosynthetic Step of the Iminomycosporine Shinorine in Nostoc Punctiforme ATCC 29133. *J Bacteriol* **2011**, *193* (21), 5923–5928. https://doi.org/10.1128/JB.05730-11.

(13) Leao, T.; Castelão, G.; Korobeynikov, A.; Monroe, E. A.; Podell, S.; Glukhov, E.; Allen, E. E.; Gerwick, W. H.; Gerwick, L. Comparative Genomics Uncovers the Prolific and Distinctive Metabolic Potential of the Cyanobacterial Genus *Moorea*. *Proc Natl Acad Sci USA* **2017**, *114* (12), 3198–3203. https://doi.org/10.1073/pnas.1618556114.

(14) Weber, T.; Blin, K.; Duddela, S.; Krug, D.; Kim, H. U.; Bruccoleri, R.; Lee, S. Y.; Fischbach, M. A.; Müller, R.; Wohlleben, W.; Breitling, R.; Takano, E.; Medema, M. H. AntiSMASH 3.0—a Comprehensive Resource for the Genome Mining of Biosynthetic Gene Clusters. *Nucleic Acids Res* **2015**, *43* (W1), W237–W243. https://doi.org/10.1093/nar/gkv437.

(15) Winn, M.; Fyans, J. K.; Zhuo, Y.; Micklefield, J. Recent Advances in Engineering Nonribosomal Peptide Assembly Lines. Nat. Prod. Rep. 2016, 33 (2), 317–347. https://doi.org/10.1039/C5NP00099H.

8. Appendix

8.1 Spectra

NMR spectra are displayed here in the order in which the compound is reported in the Materials and Methods section. IR spectra are also included for some compounds.

1H NMR of **2,3-dihydroxycyclohex-2-en-1-one ("dihydropyrogallol", DHPG)**

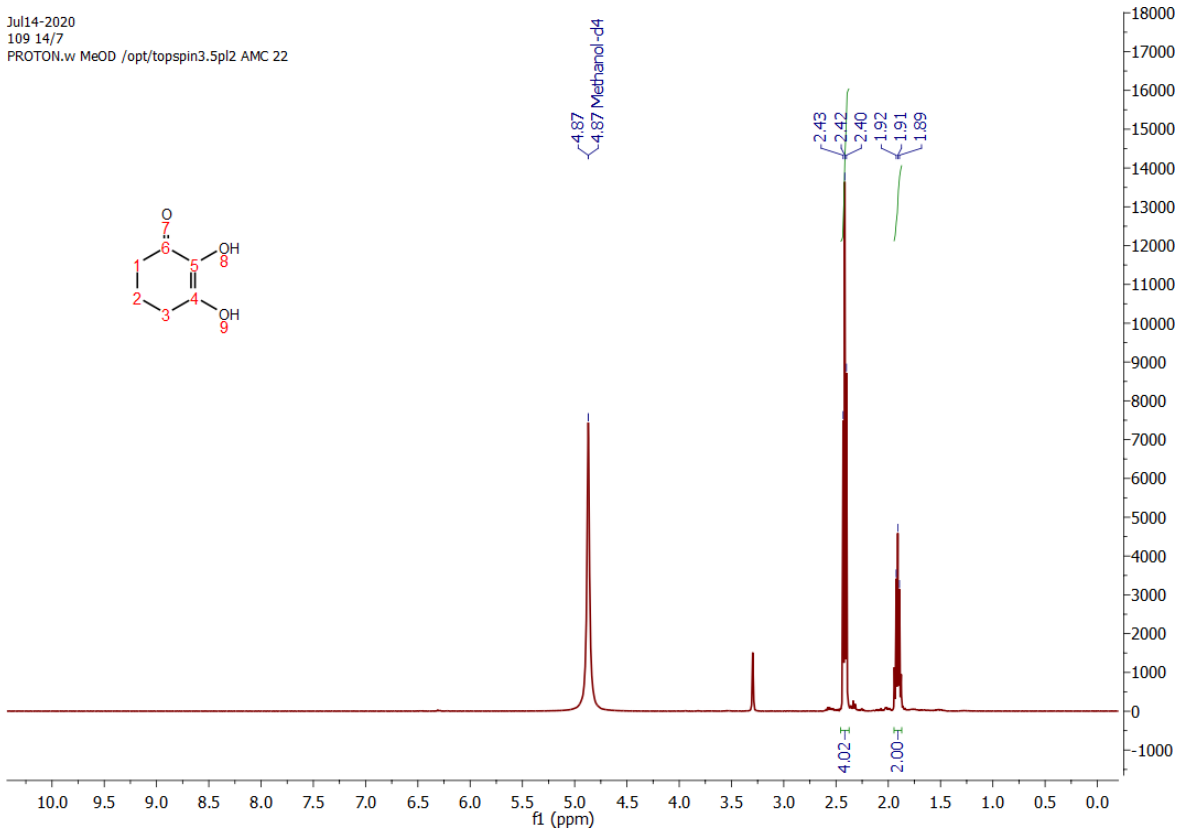

1H NMR of **3-hydroxy-2-methoxycyclohex-2-en-1-one**

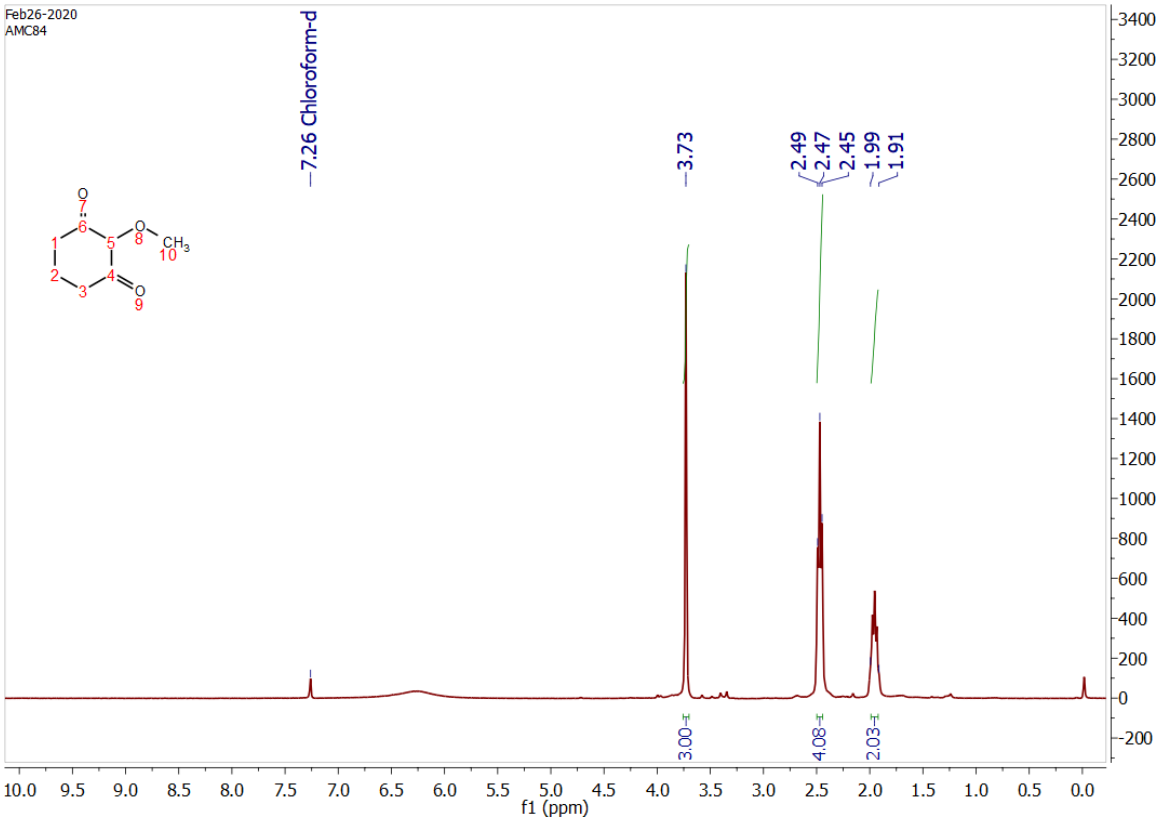

1H NMR of **3-(phenylamino)cyclohex-2-en-1-one, AC3**

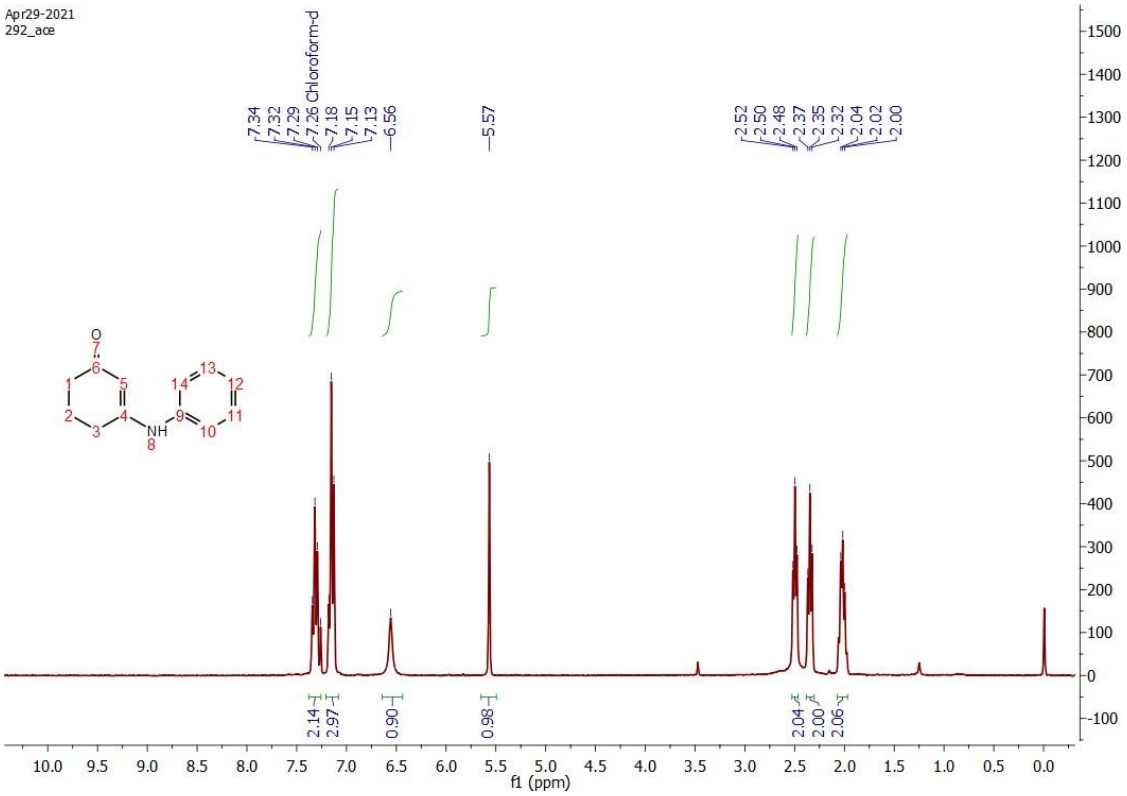

1H NMR of **2-methyl-3-(phenylamino)cyclohex-2-enone, AC4**

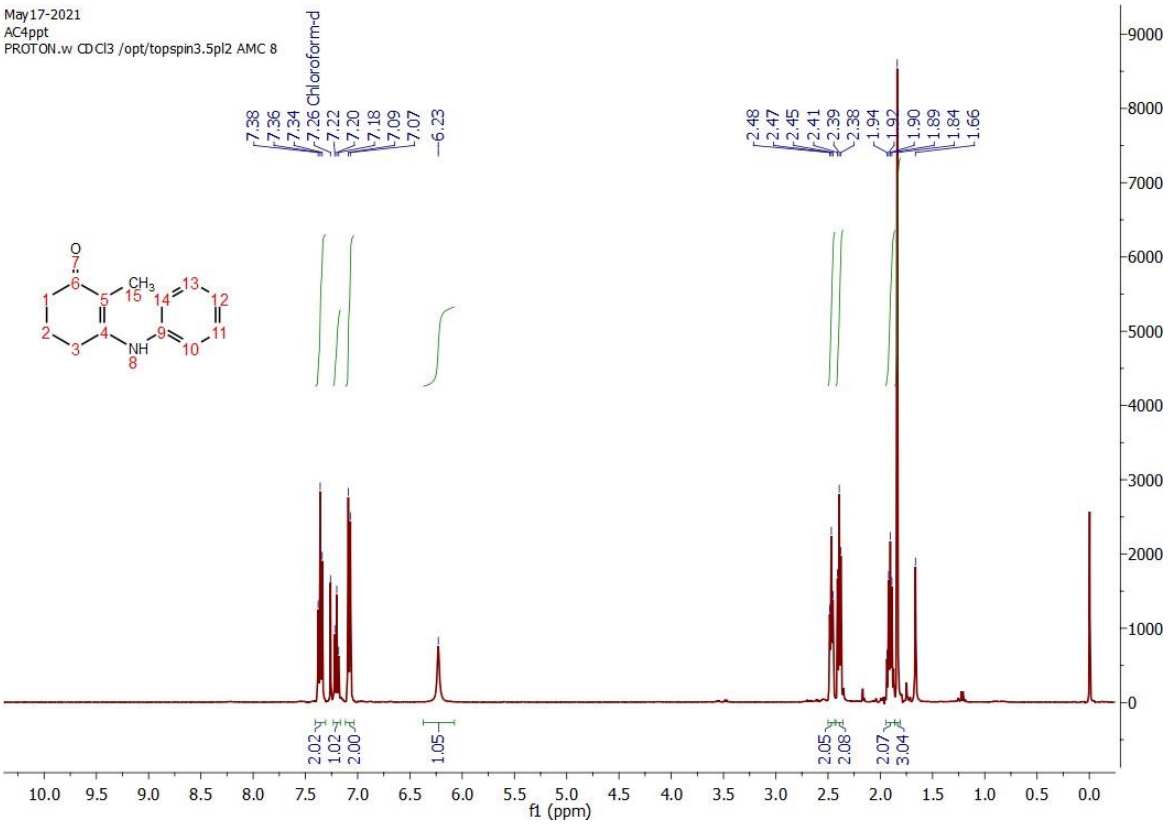

1H NMR of **2-hydroxy-3-(phenylamino)cyclohex-2-enone, AC9**

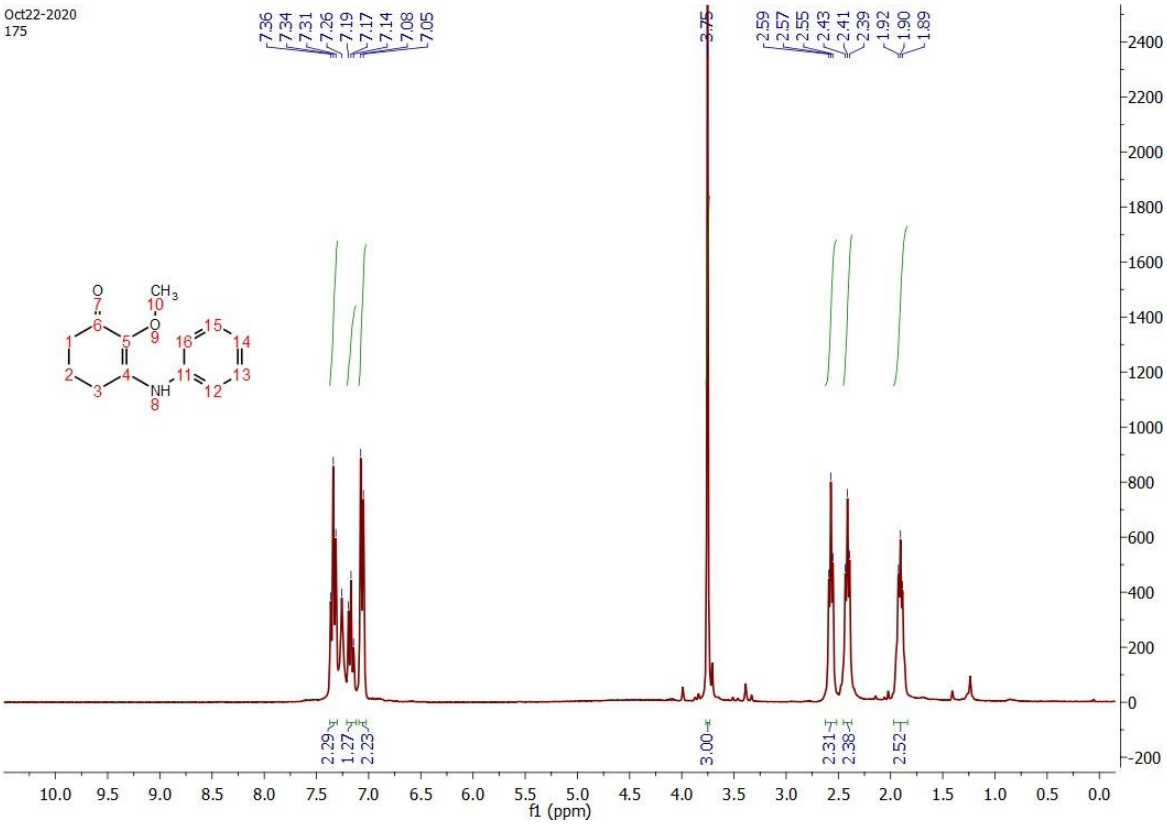

1H NMR of **2-methoxy-3-(phenylamino)cyclohex-2-enone, AC20**

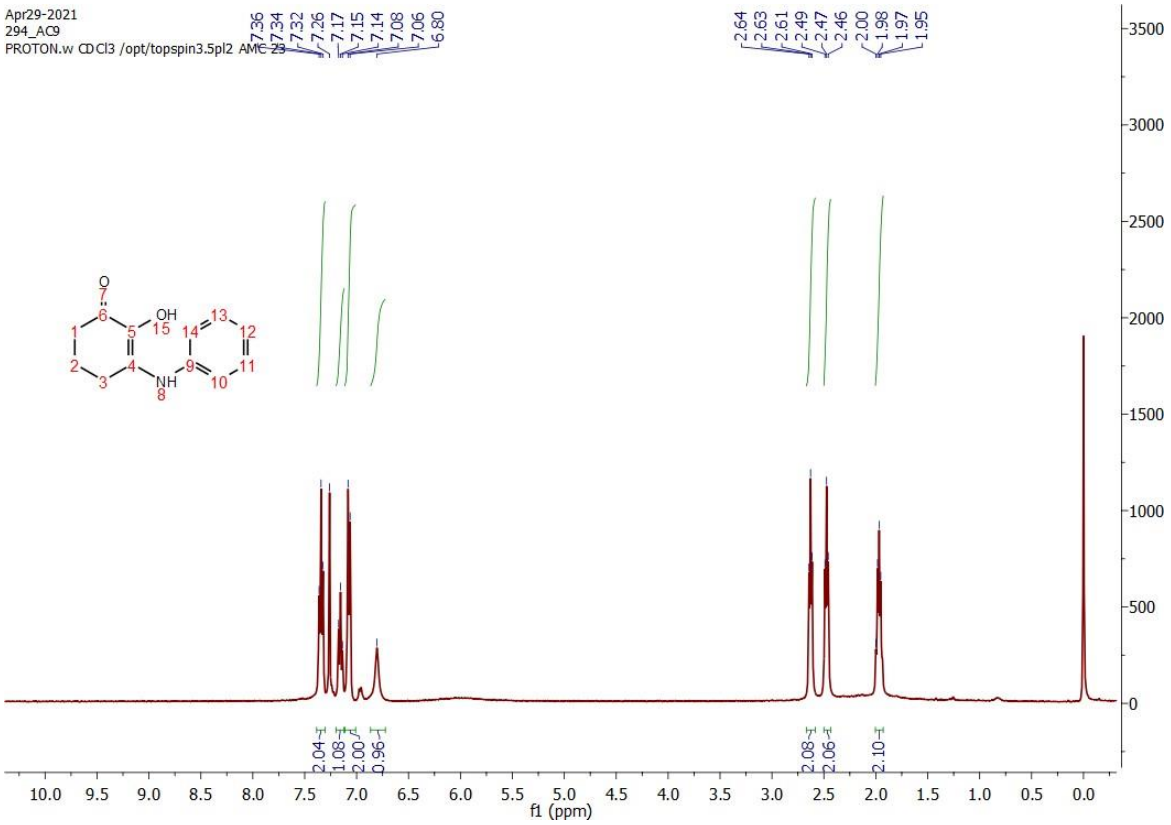

1H NMR of **2-methoxy-3-((4-methoxyphenyl)amino)cyclohex-2-en-1-one, AC34**

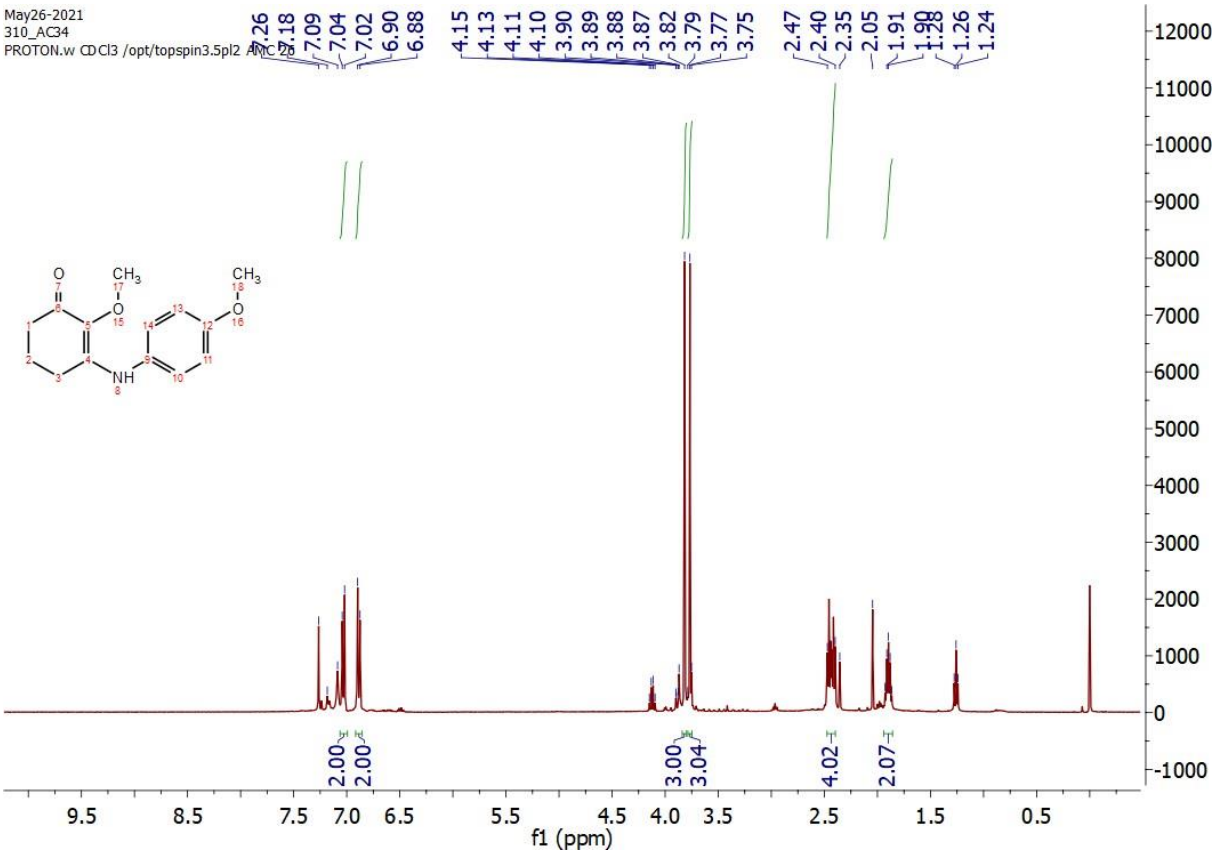

13C NMR of **2-methoxy-3-((4-methoxyphenyl)amino)cyclohex-2-en-1-one, AC34**

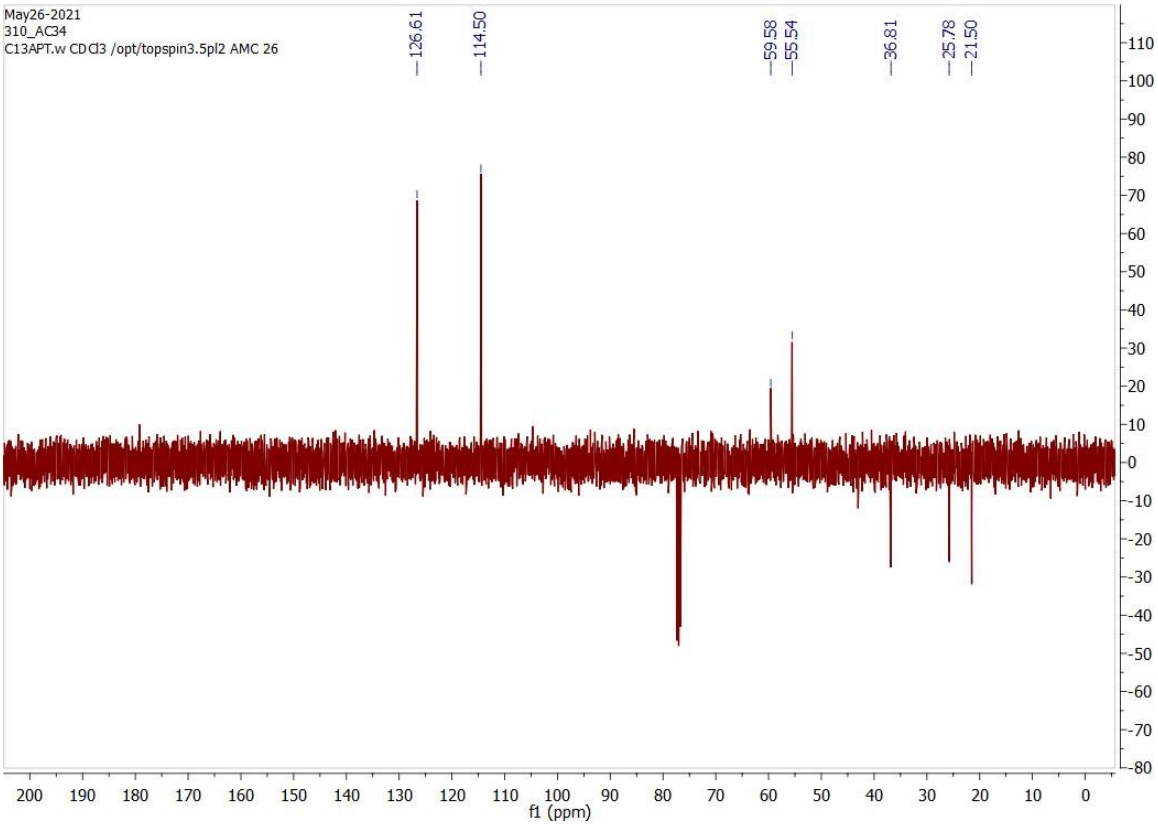

1H NMRs of **methyl (2-methoxy-3-oxocyclohex-1-en-1-yl)glycinate, AC23 ester**

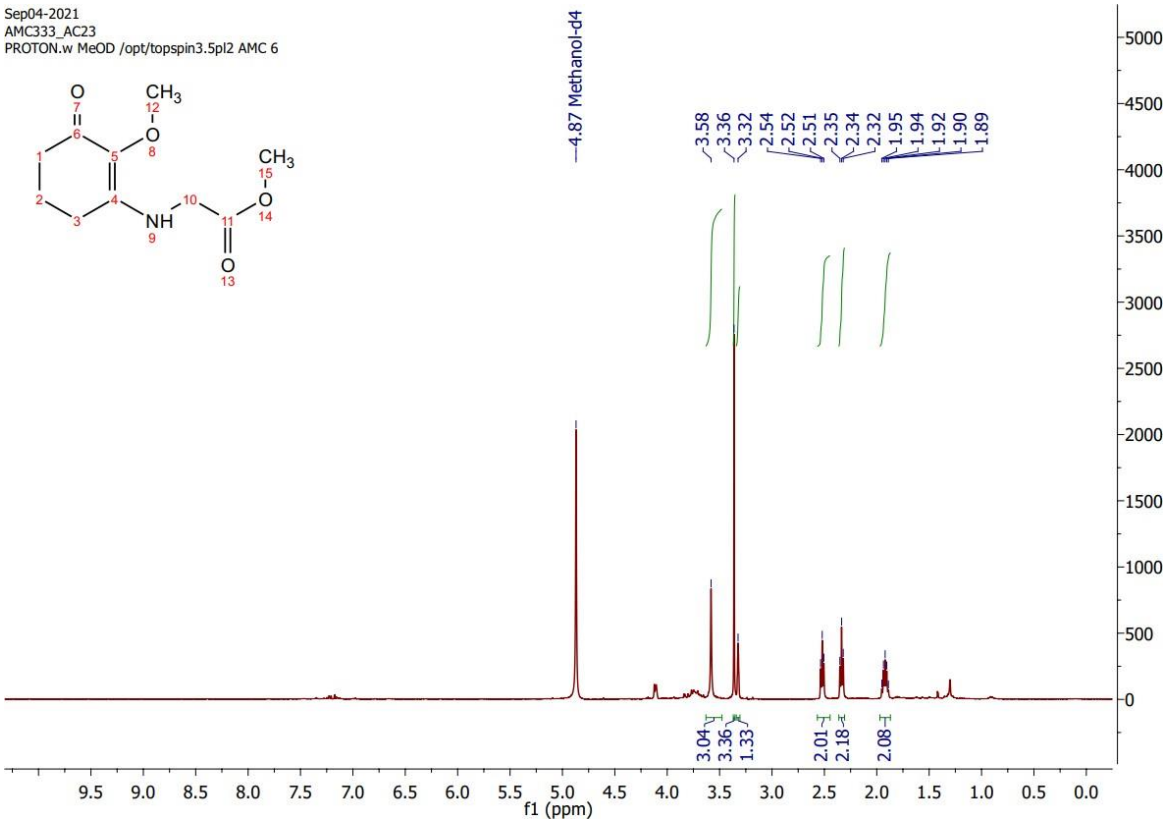

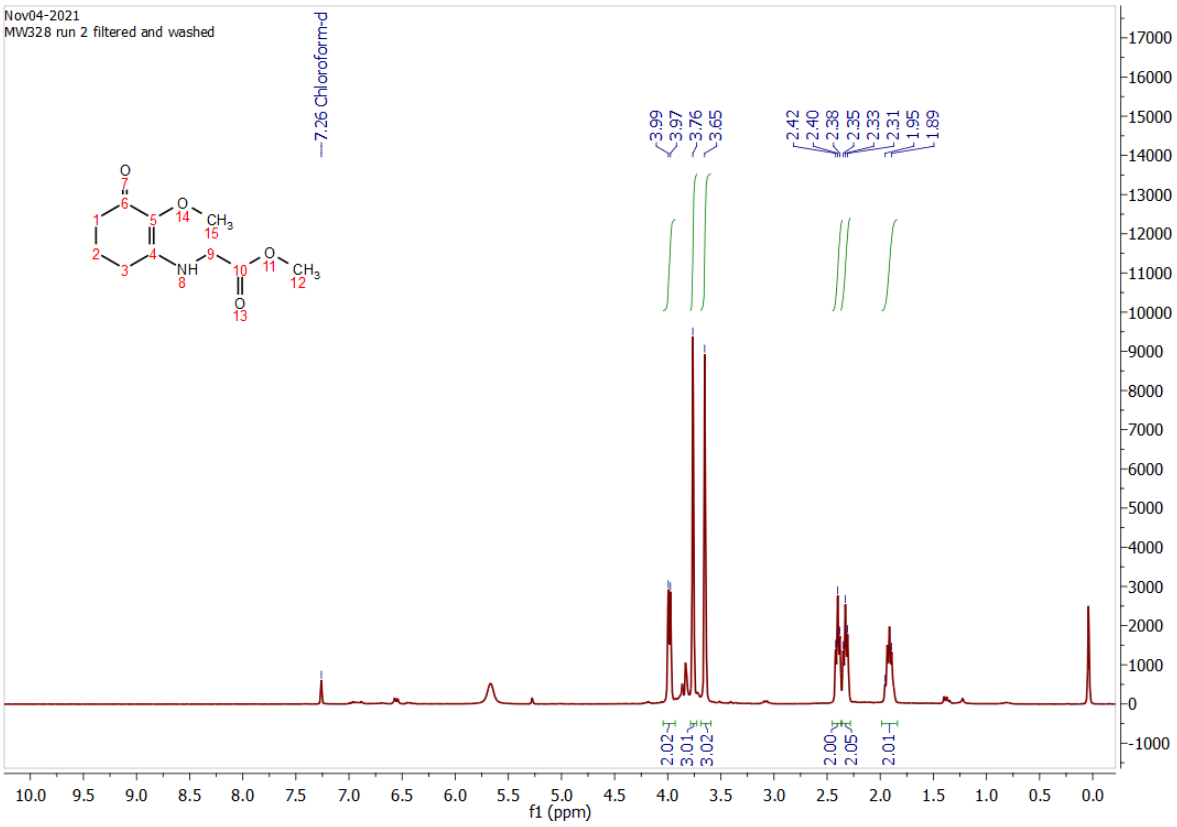

1H NMR of **(2-methoxy-3-oxocyclohex-1-en-1-yl)glycine, AC23 acid**

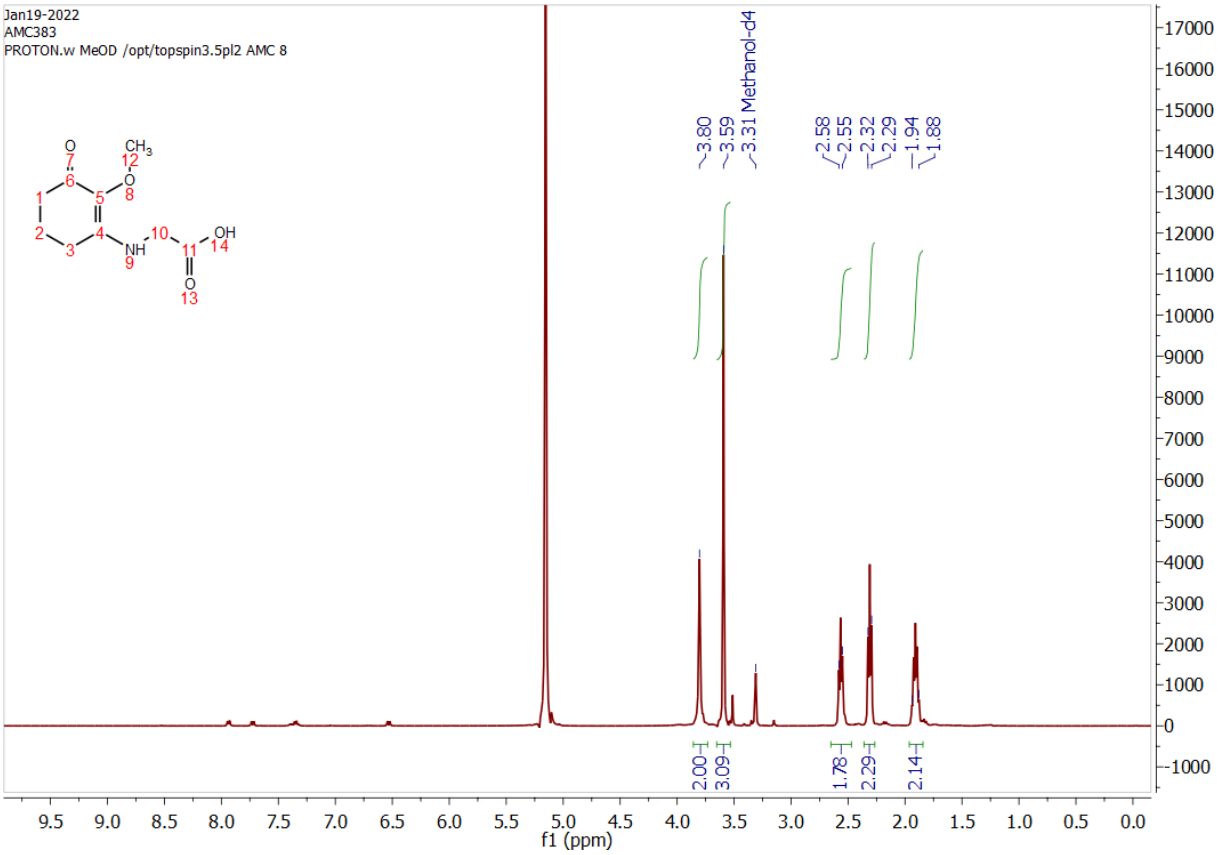

1HNMR of **methyl (3-oxocyclohex-1-en-1-yl)glycinate, AC36**

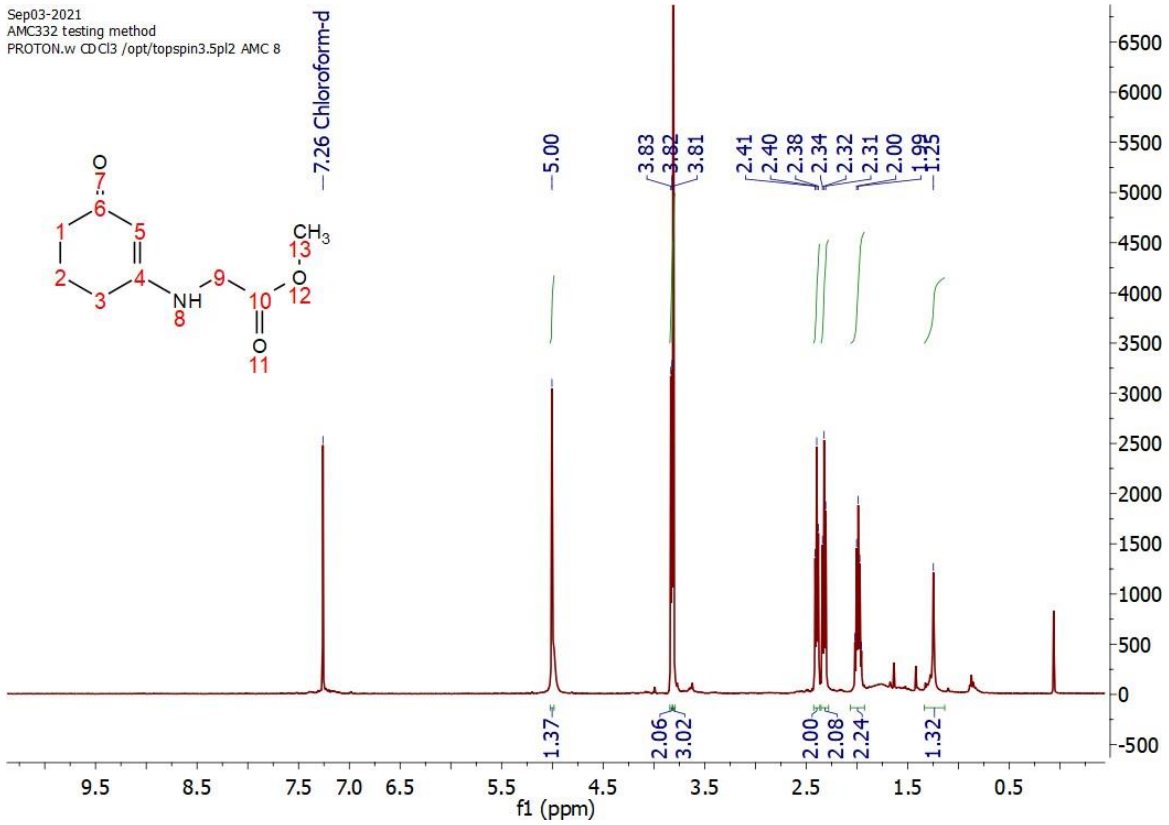

1H NMRs of **SNACs**

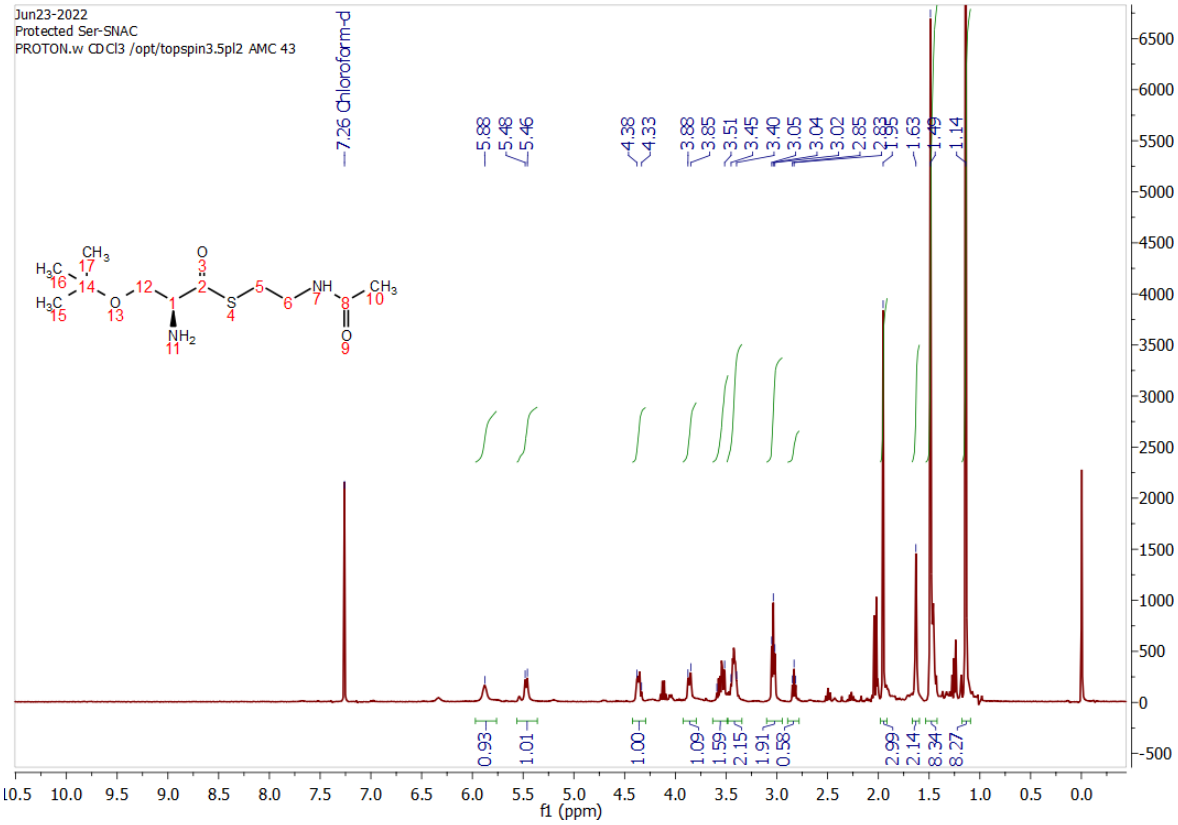

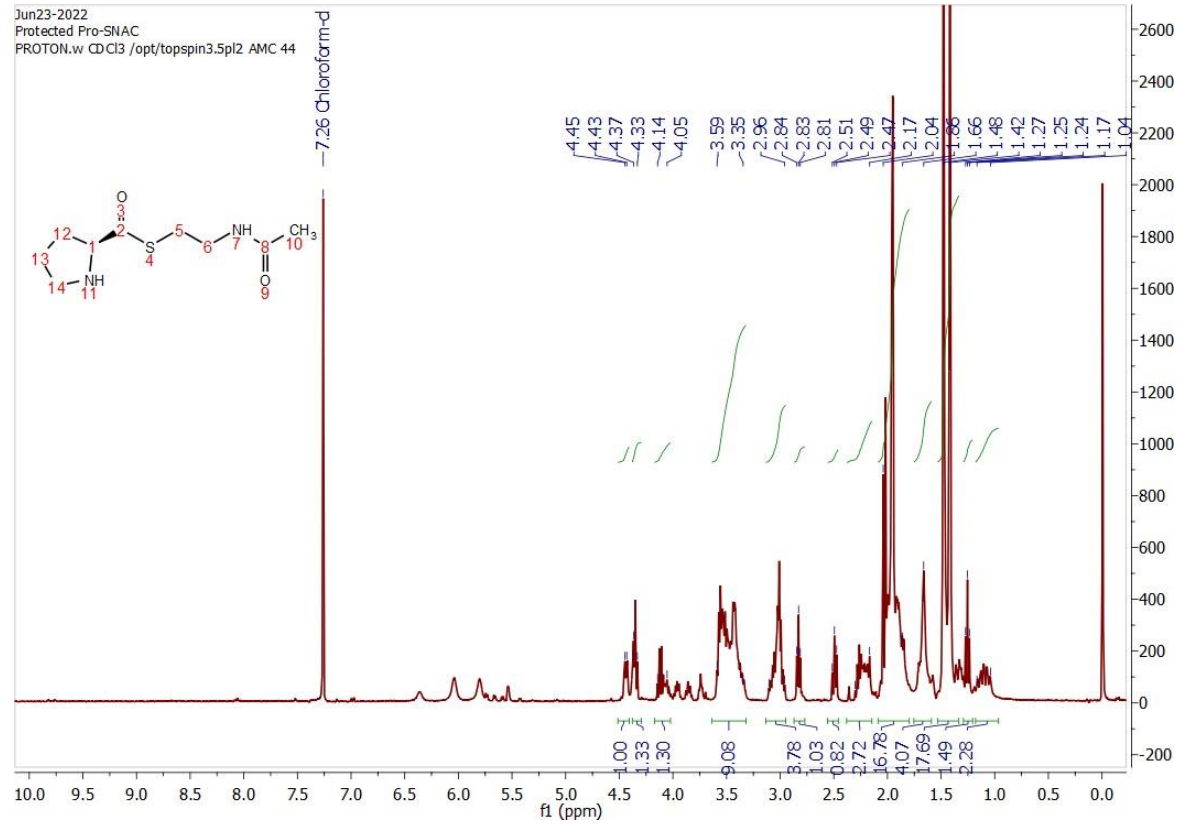

1H NMR of **2-hydroxy-N-(3-((2-hydroxyethyl)amino)-2-methoxycyclohex-2-en-1-ylidene)ethan-1-aminium 4-methylbenzenesulfonate, AC26**

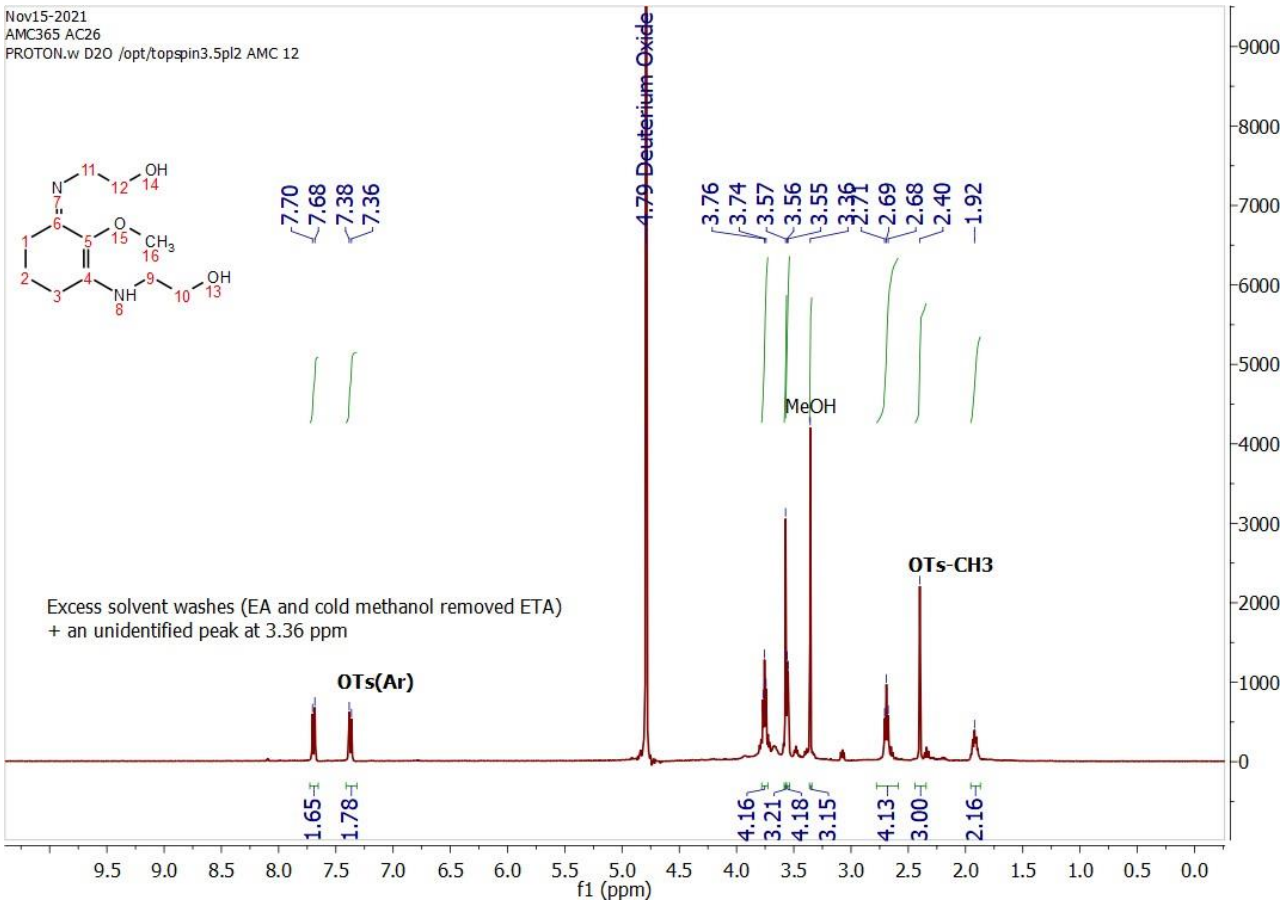

1H NMR of **2-hydroxy-N-(3-((2-hydroxyethyl)amino)cyclohex-2-en-1-ylidene)ethan-1-aminium 4-methylbenzenesulfonate, AC27**

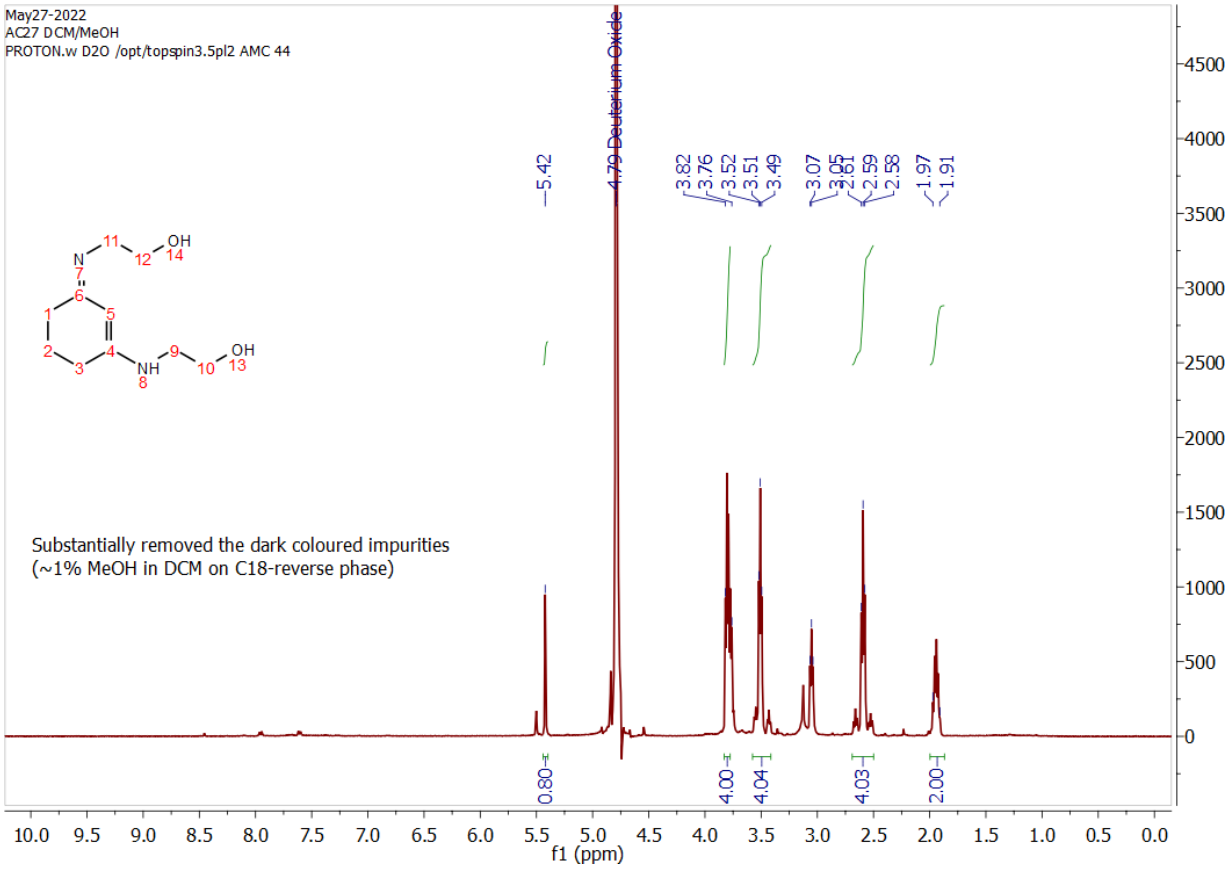

1H NMR of **2-hydroxy-N-(3-((2-hydroxyethyl)amino)cyclohex-2-en-1-ylidene)ethan-1-aminium, AC28**

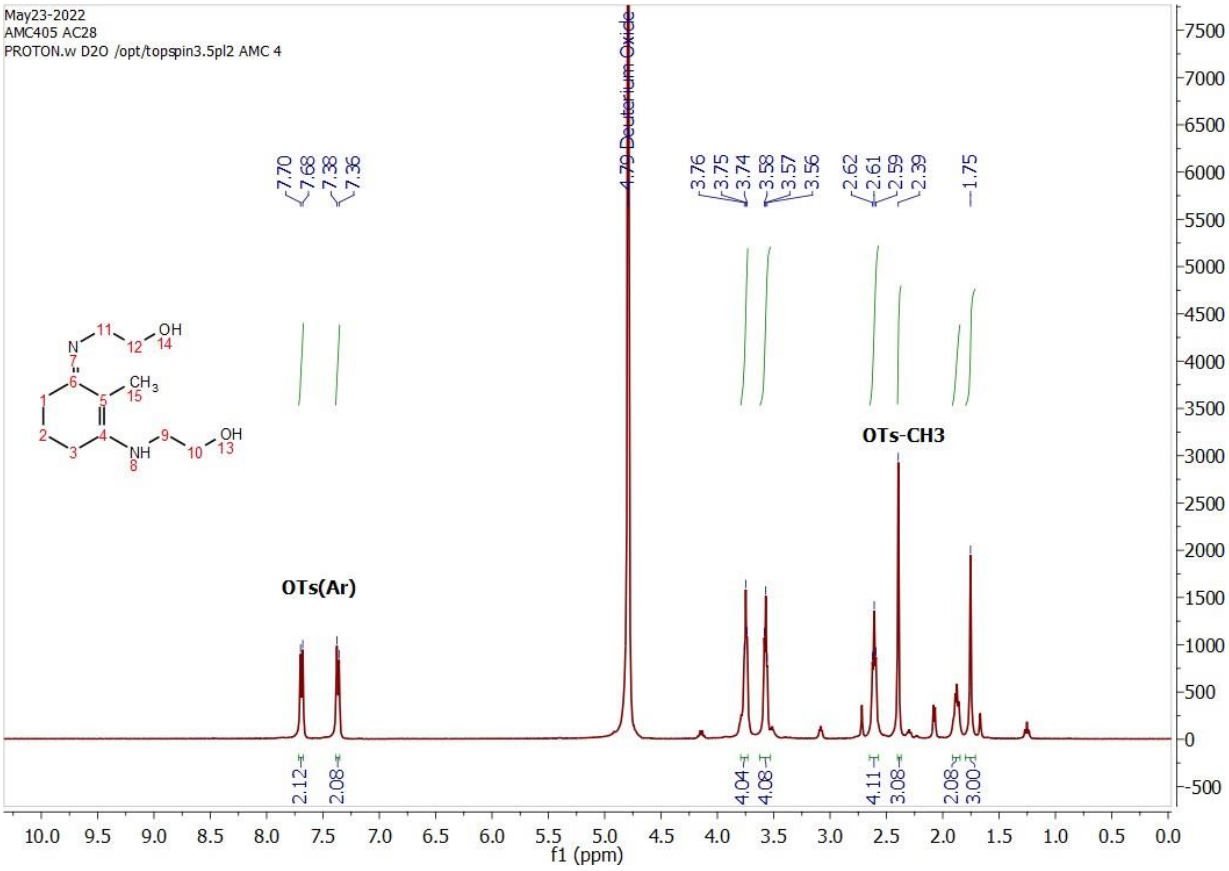

1H NMR of **(S)-2-Amino-3-phenylpropan-1-ol**

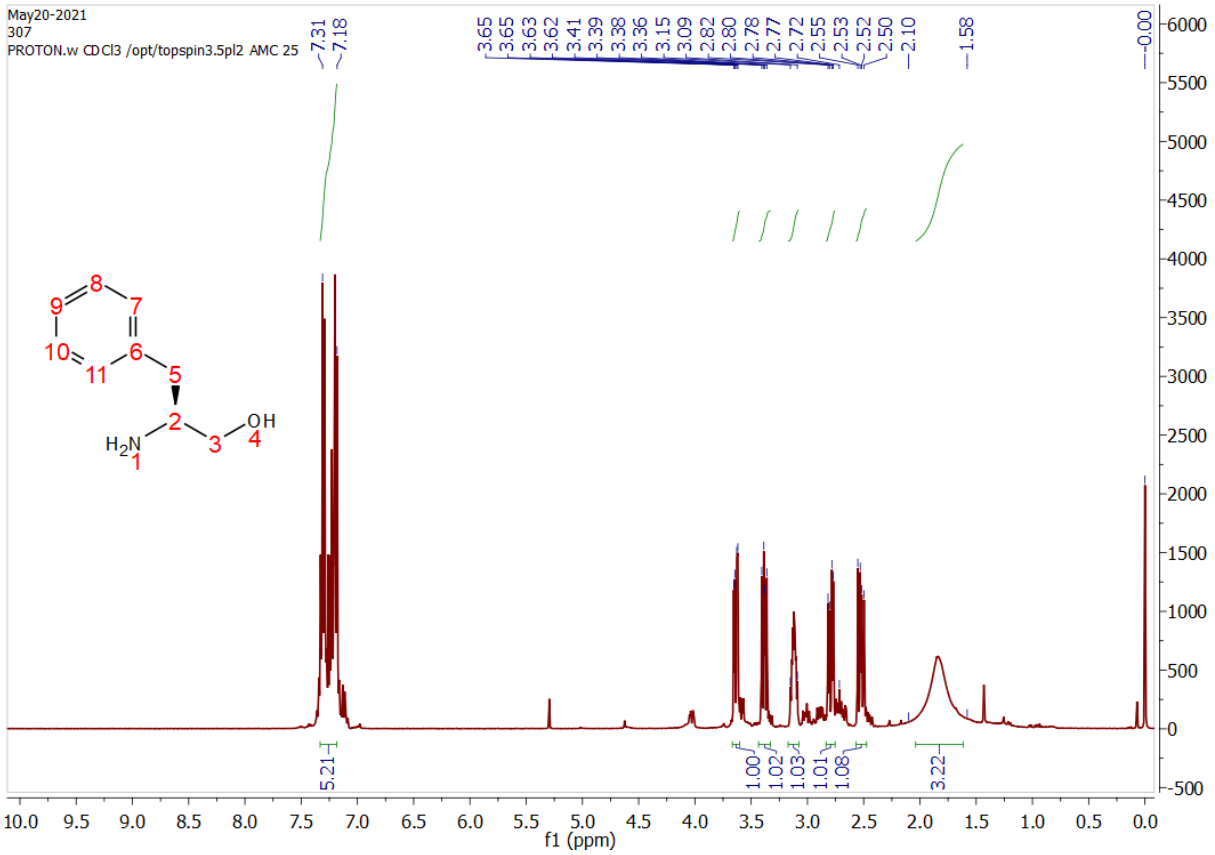

1H NMR of **1-hydroxy-N-(3-((1-hydroxy-3-phenylpropan-2-yl)amino)-2-methoxycyclohex-2-en-1-ylidene)-3-phenylpropan-2-aminium 4-methylbenzenesulfonate, AC33**

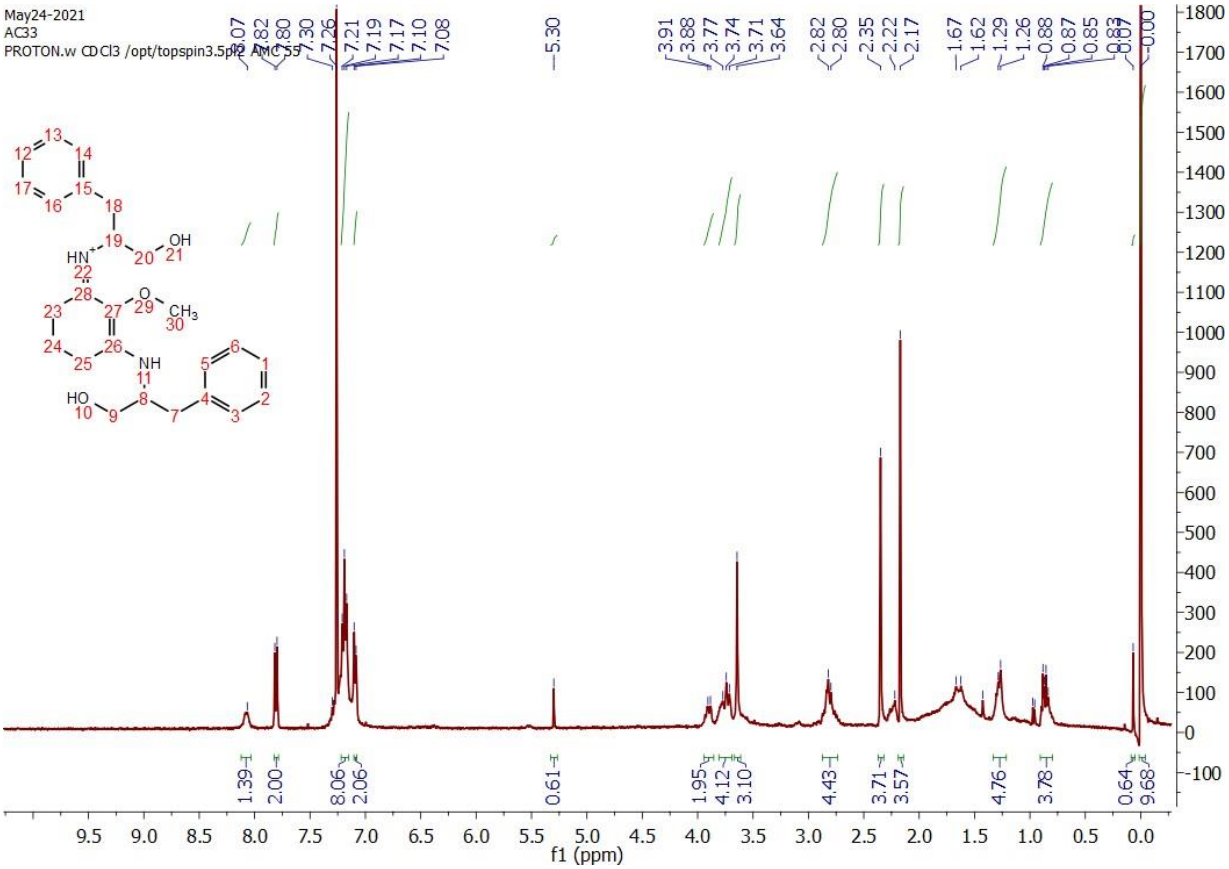

1H NMR of **5-hydroxy-N-(3-((5-hydroxypentyl)amino)cyclohex-2-en-1-ylidene)pentan-1-aminium tosylate, AC30**

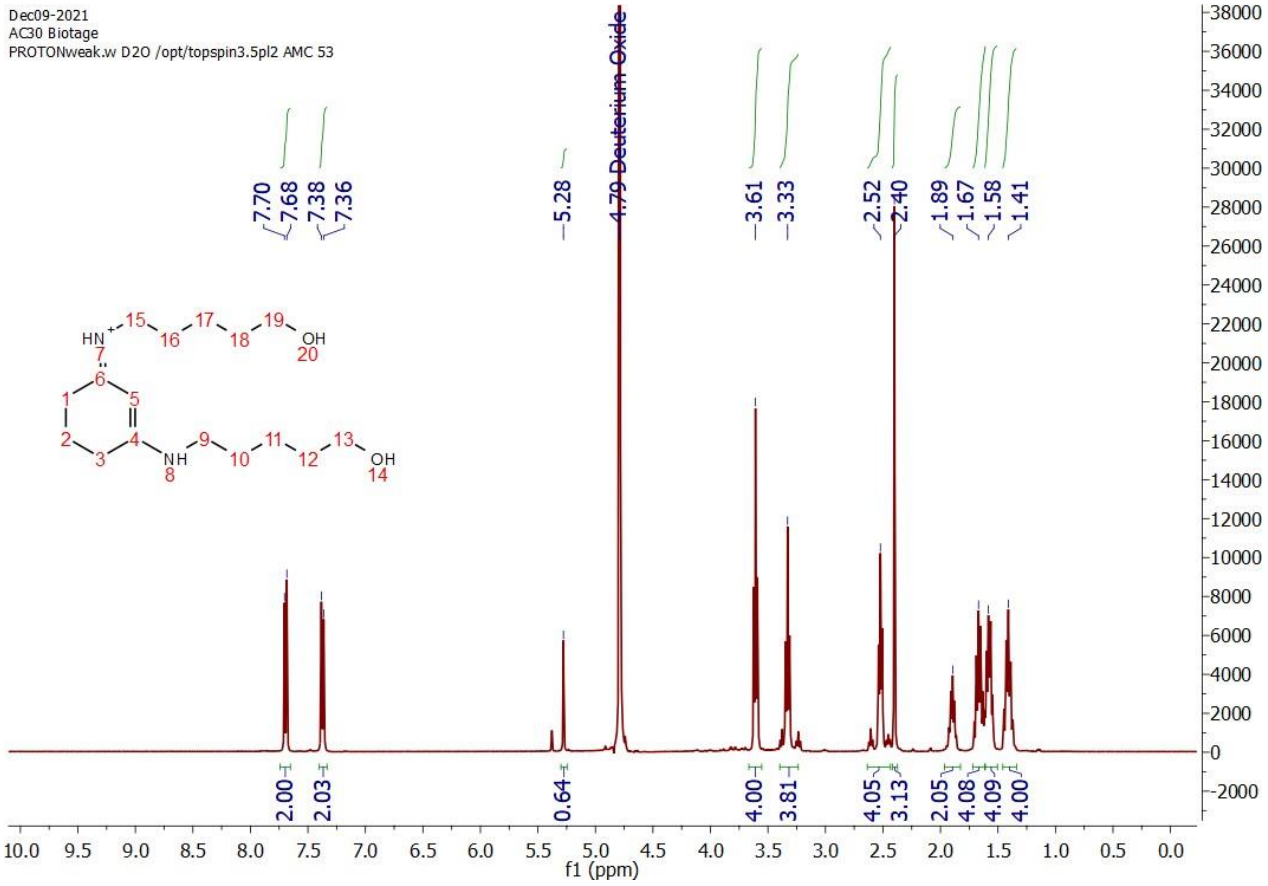

1H NMR of **5-hydroxy-N-(3-((5-hydroxypentyl)amino)-2-methoxycyclohex-2-en-1-ylidene)pentan-1-aminium tosylate, AC35**

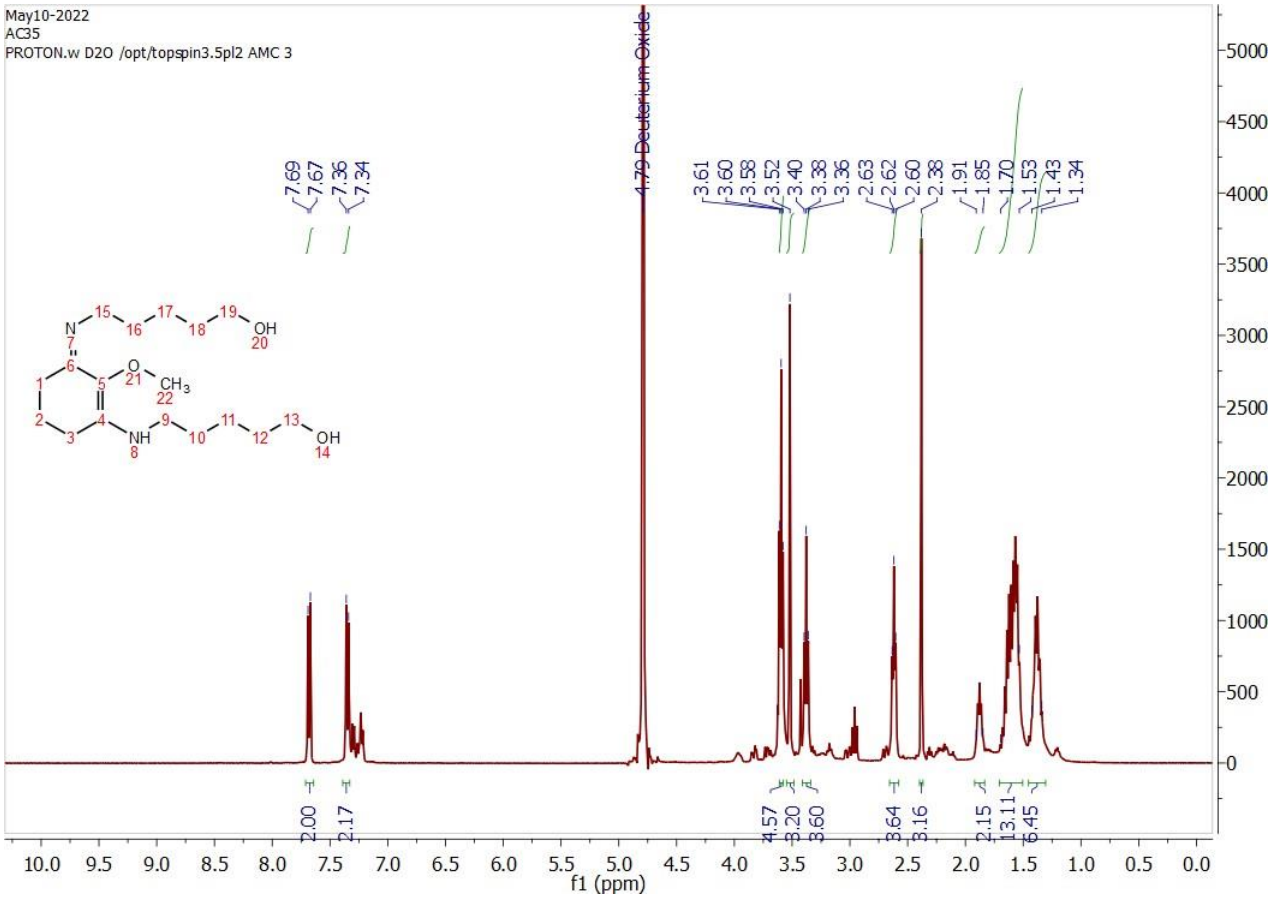

1H NMR of **4-methoxy-N-(3-((4-methoxyphenyl)amino)-2-methylcyclohex-2-en-1-ylidene)benzenaminium chloride, DS1**

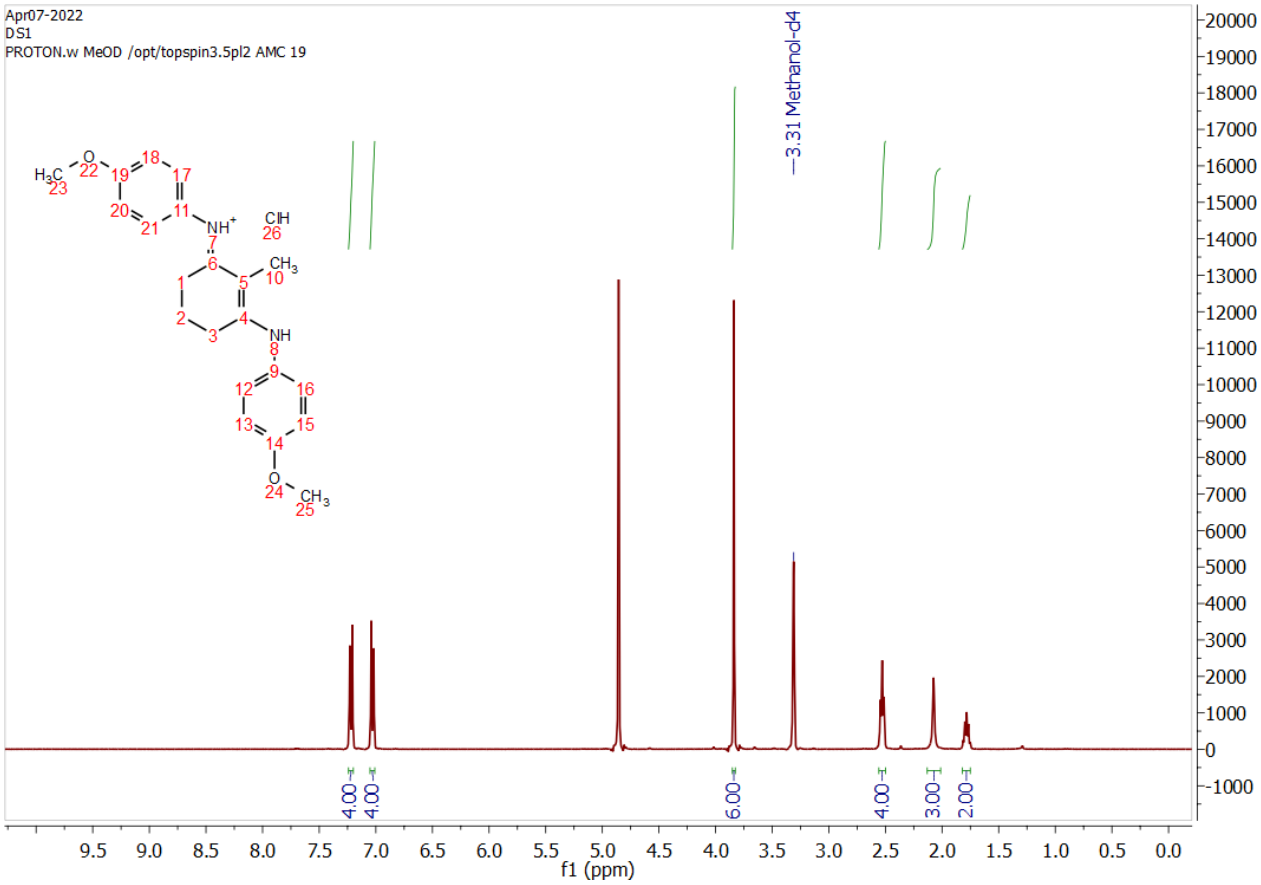

1H NMR of **N-(3-(cyclohexylamino)-2-methylcyclohex-2-en-1-ylidene)cyclohexanaminium chloride, DS2**

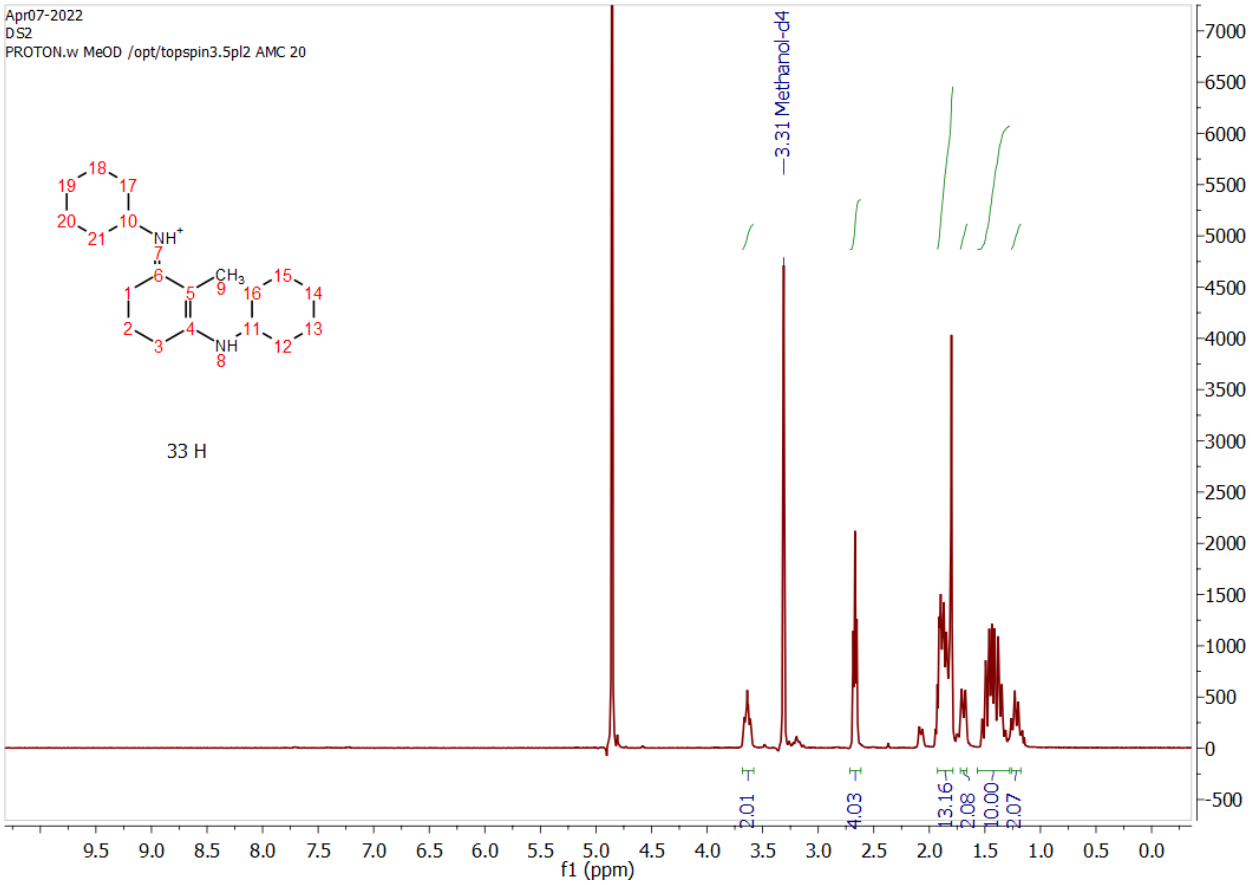

1H NMR of **porphyra-334**

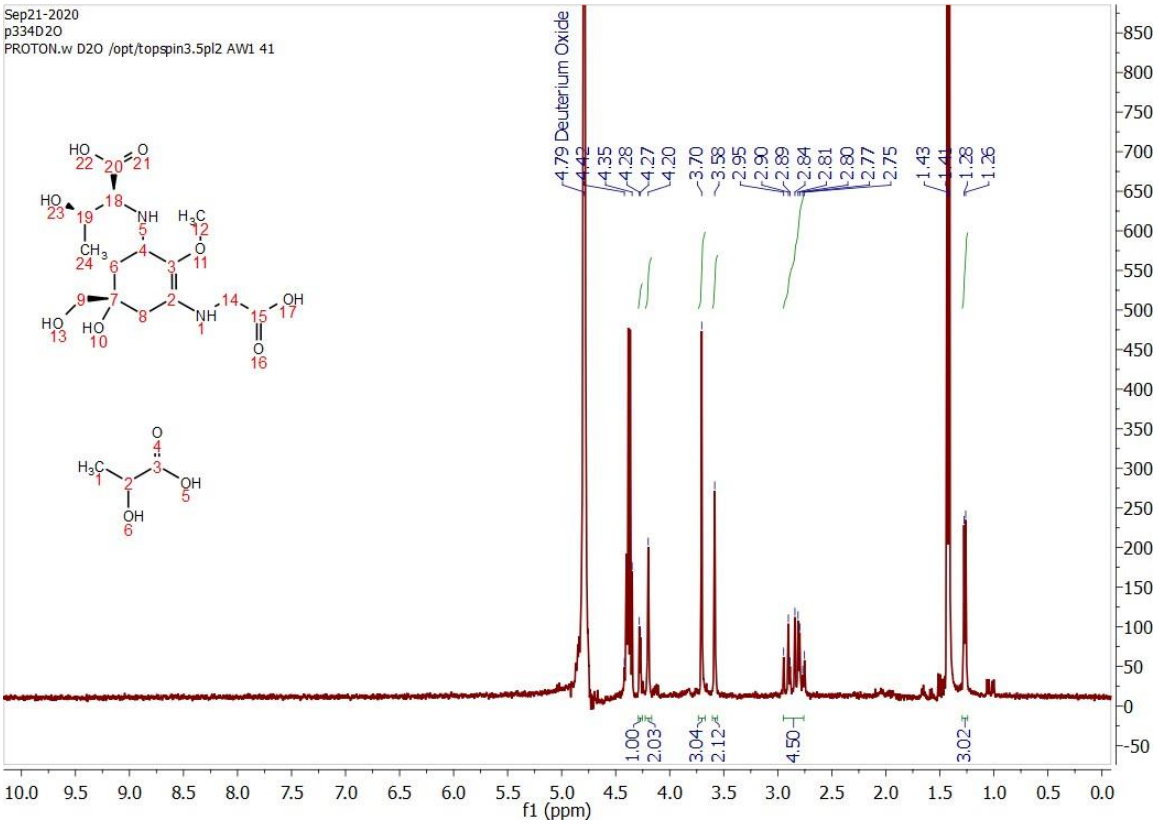

1H NMR of **4-(3-hydroxypropoxy)phenylethan-1-one**

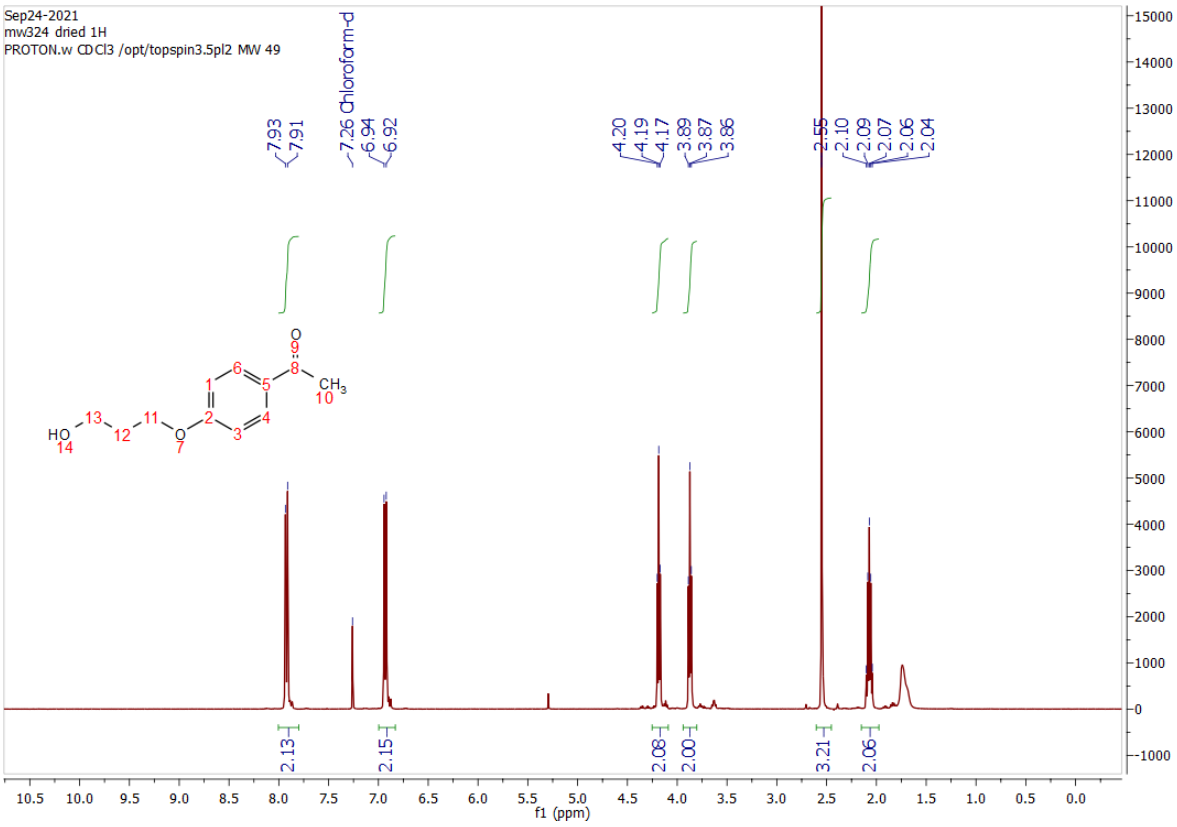

IR spectrum of **4-(3-hydroxypropoxy)phenylethan-1-one**

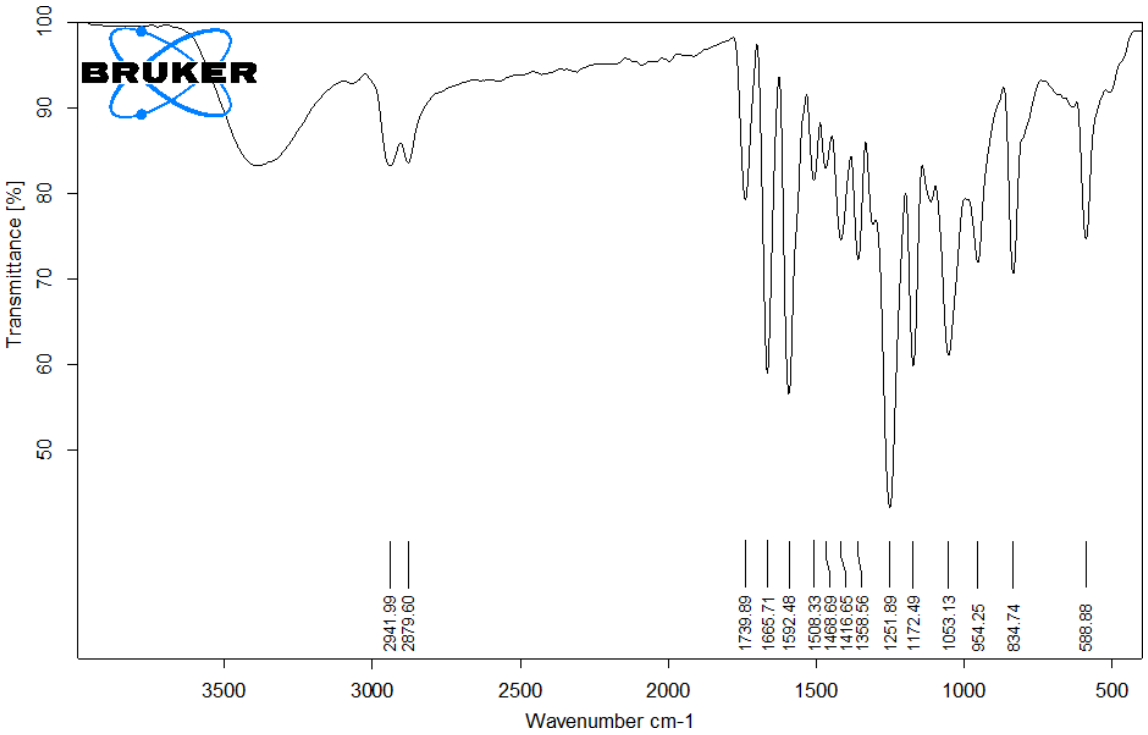

1H NMR of **4-(3-hydroxypropoxy)phenyl-3-phenylpropane-1,3-dione**

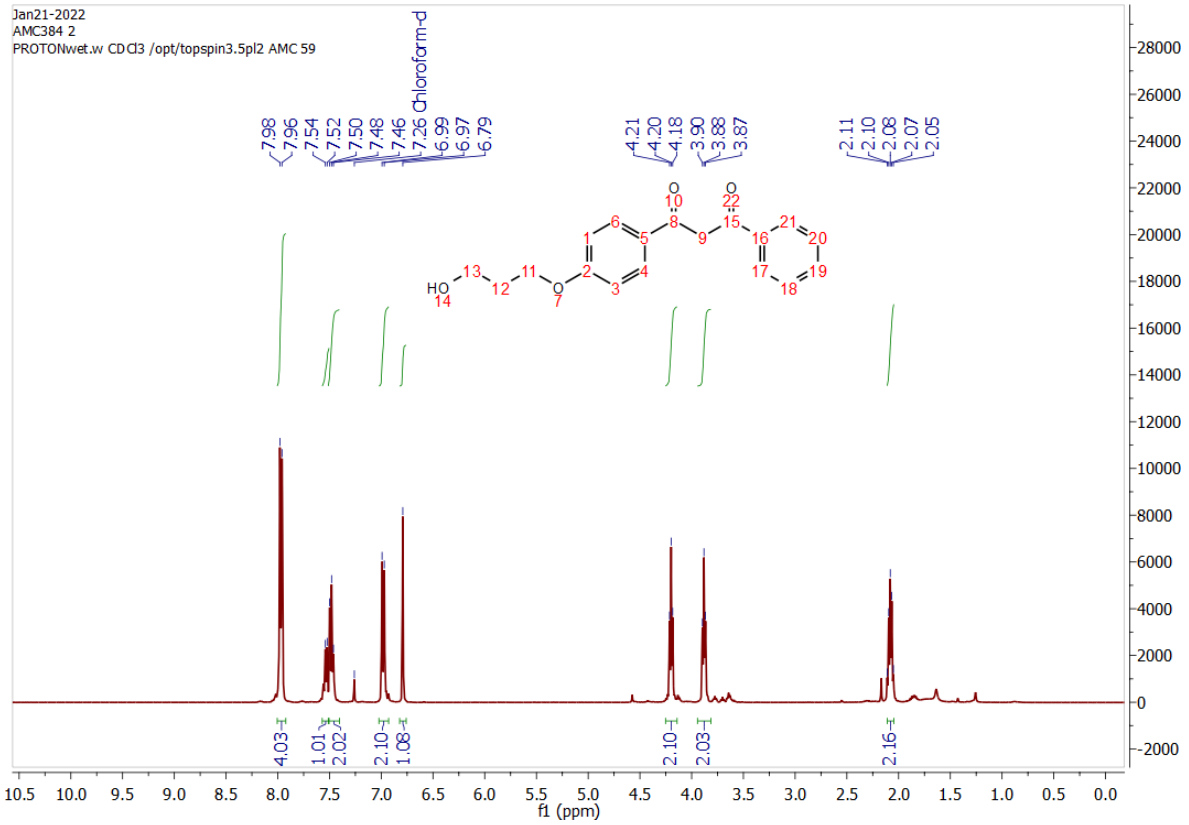

13C NMR of **4-(3-hydroxypropoxy)phenyl-3-phenylpropane-1,3-dione**

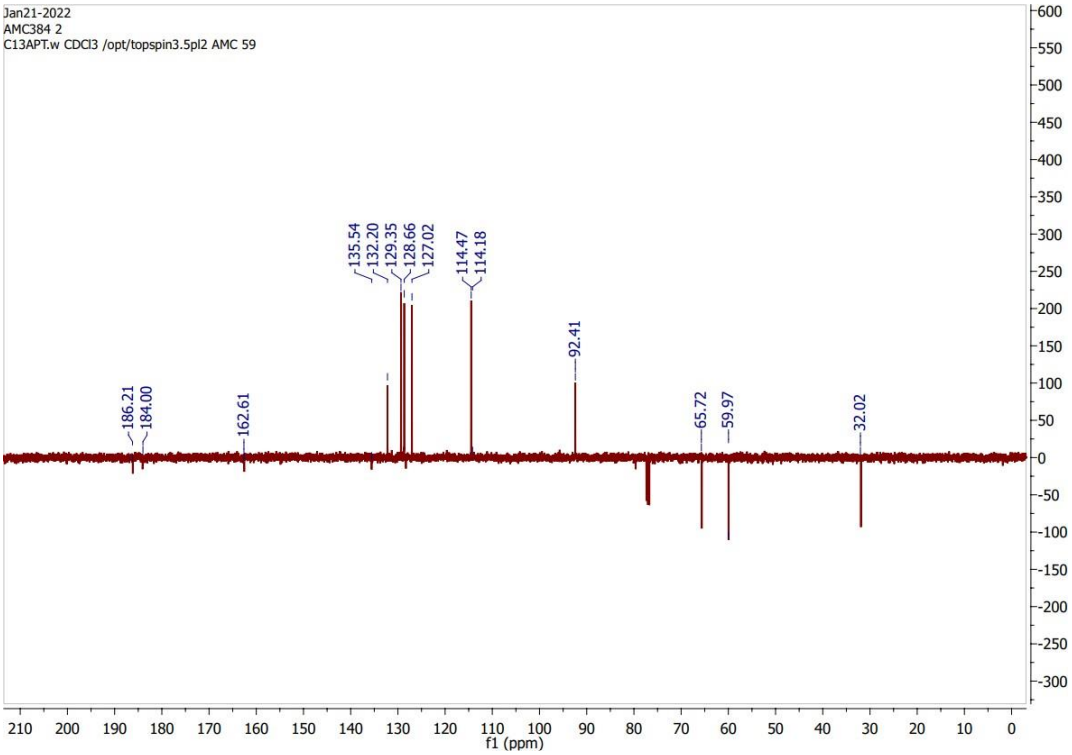

IR spectrum of **4-(3-hydroxypropoxy)phenyl-3-phenylpropane-1,3-dione**

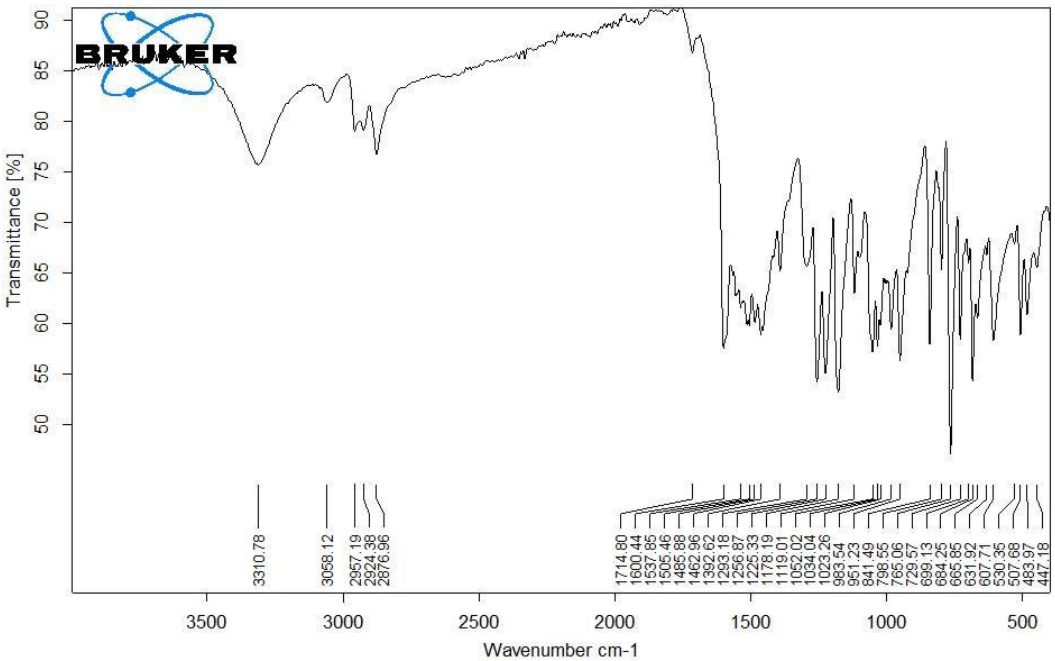

1H NMR of **1-(4-(*tert*-butyl)phenyl)-3-(4-(3-hydroxypropoxy)phenyl)propane-1,3-dione**

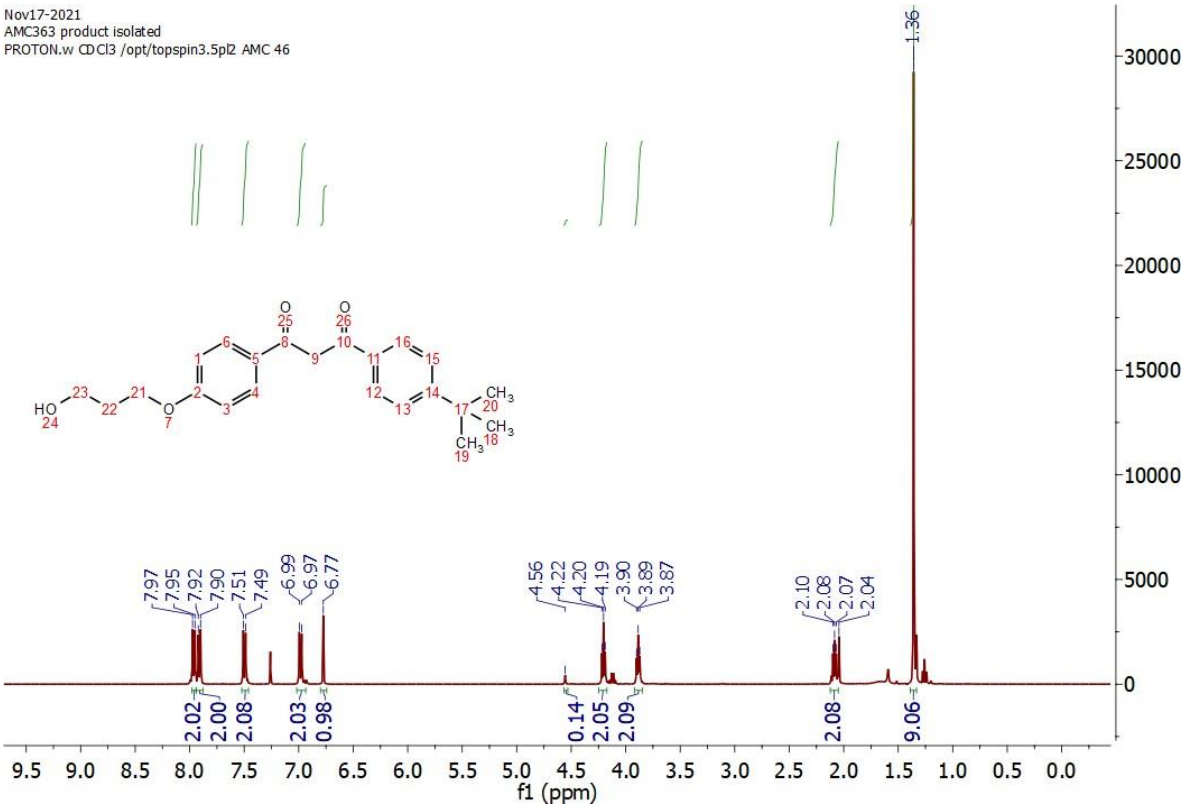

13C NMR of **1-(4-(*tert*-butyl)phenyl)-3-(4-(3-hydroxypropoxy)phenyl)propane-1,3-dione**

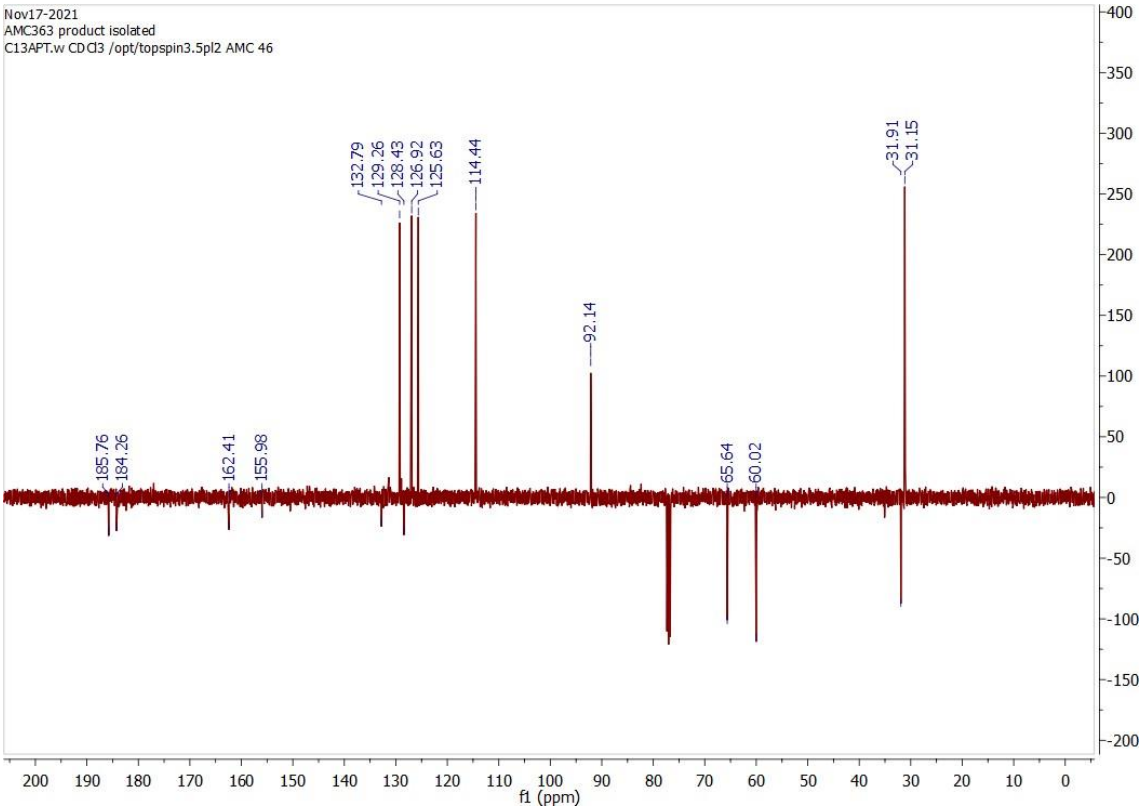

COSY of **1-(4-(*tert*-butyl)phenyl)-3-(4-(3-hydroxypropoxy)phenyl)propane-1,3-dione**

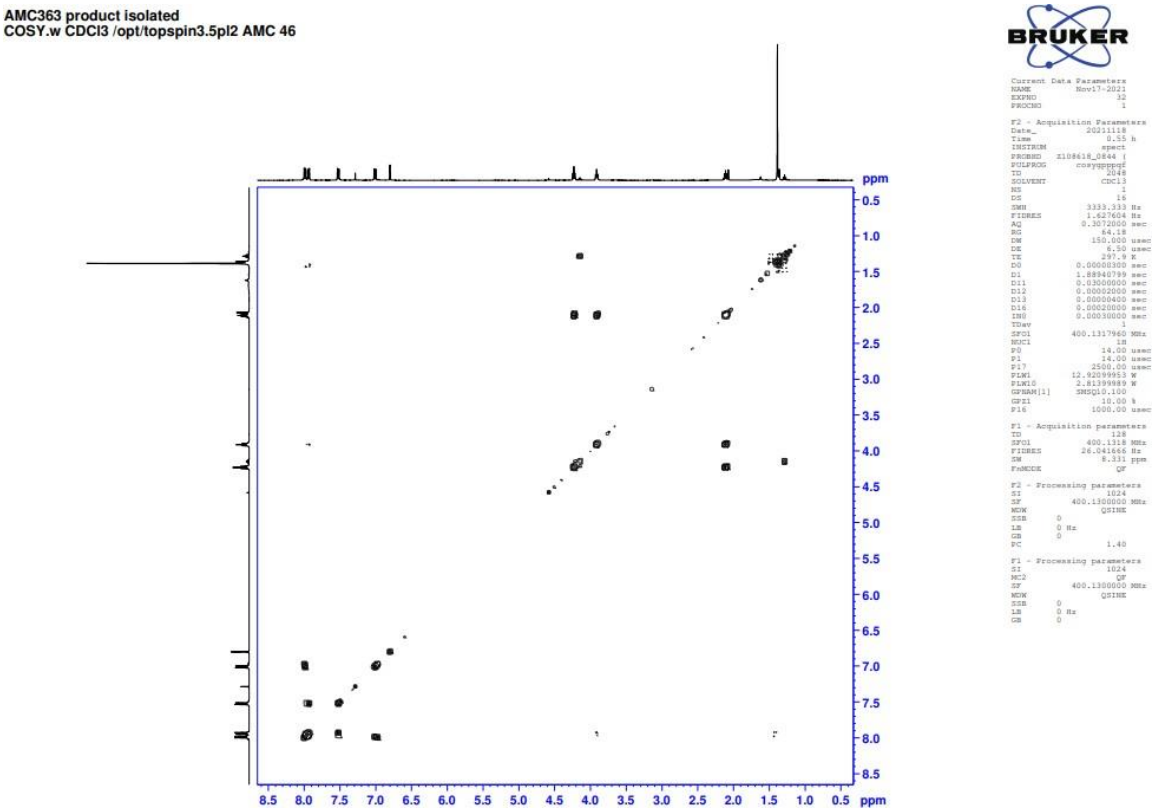

IR spectrum of **1-(4-(*tert*-butyl)phenyl)-3-(4-(3-hydroxypropoxy)phenyl)propane-1,3-dione**

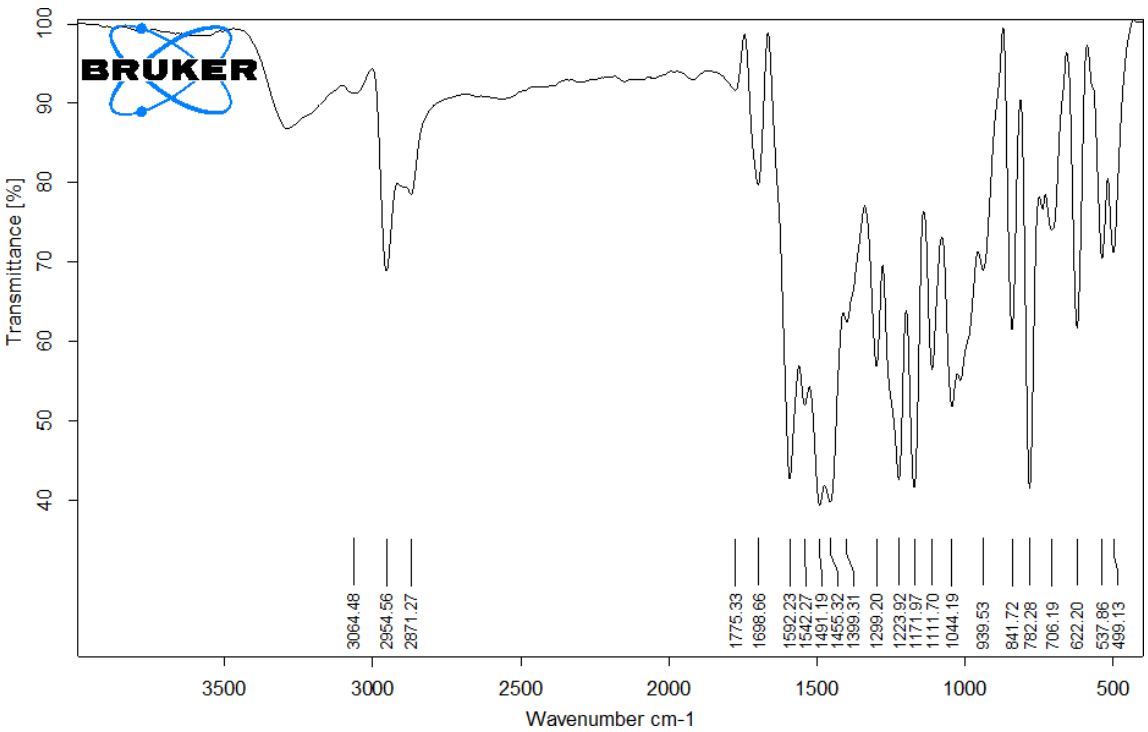

1H NMR of **1-(4-(3-hydroxypropoxy)phenyl)-3-(4-methoxyphenyl)propane-1,3-dione**

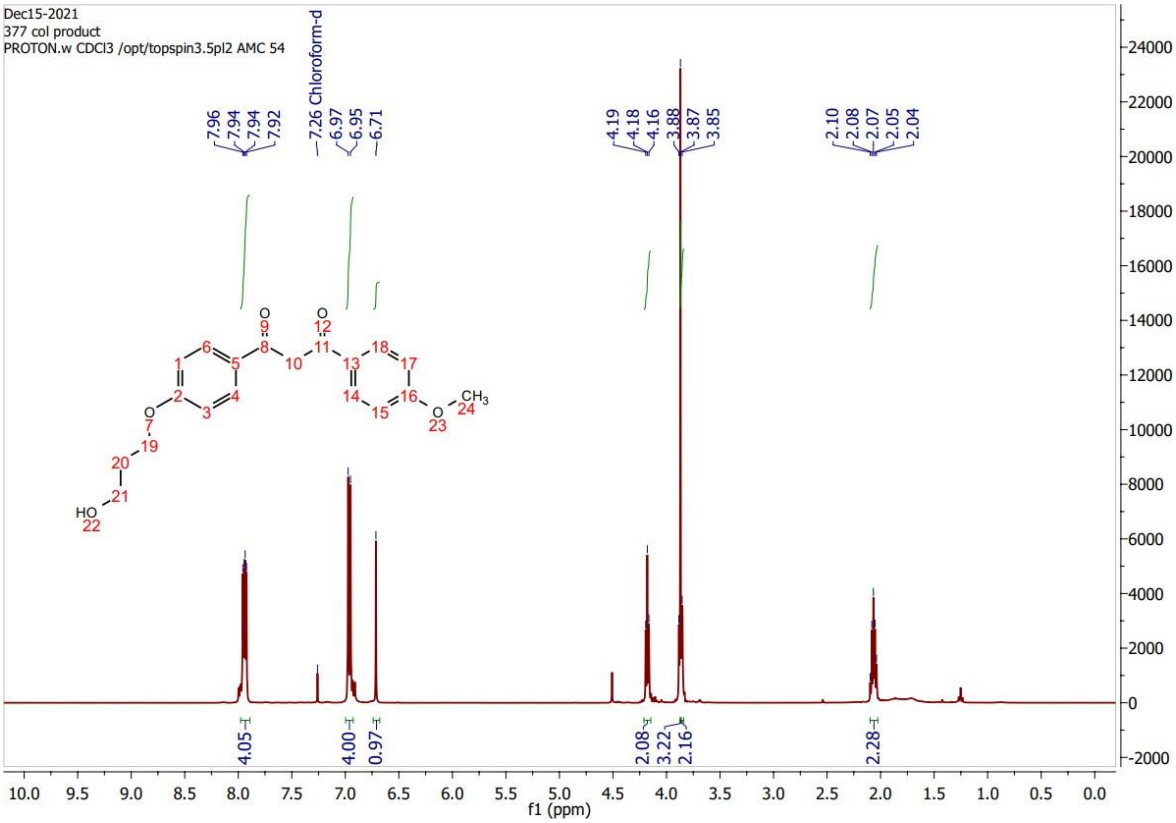

13C NMR of **1-(4-(3-hydroxypropoxy)phenyl)-3-(4-methoxyphenyl)propane-1,3-dione**

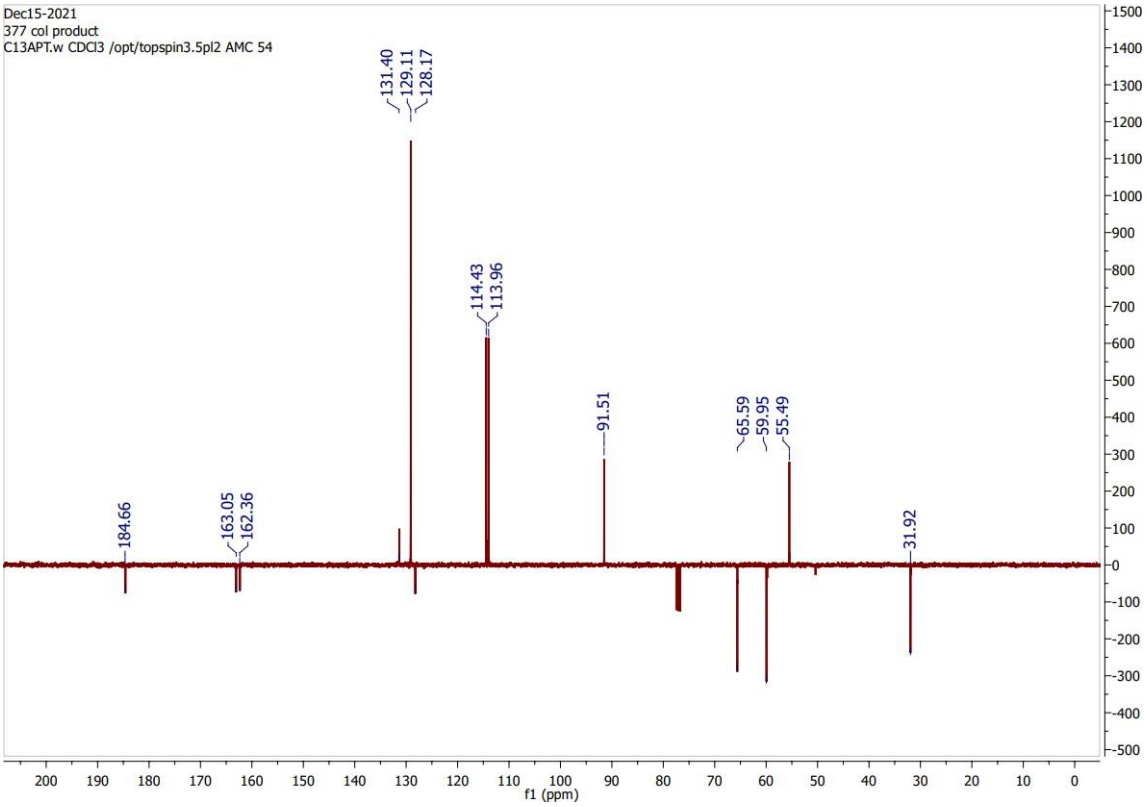

COSY of **1-(4-(3-hydroxypropoxy)phenyl)-3-(4-methoxyphenyl)propane-1,3-dione**

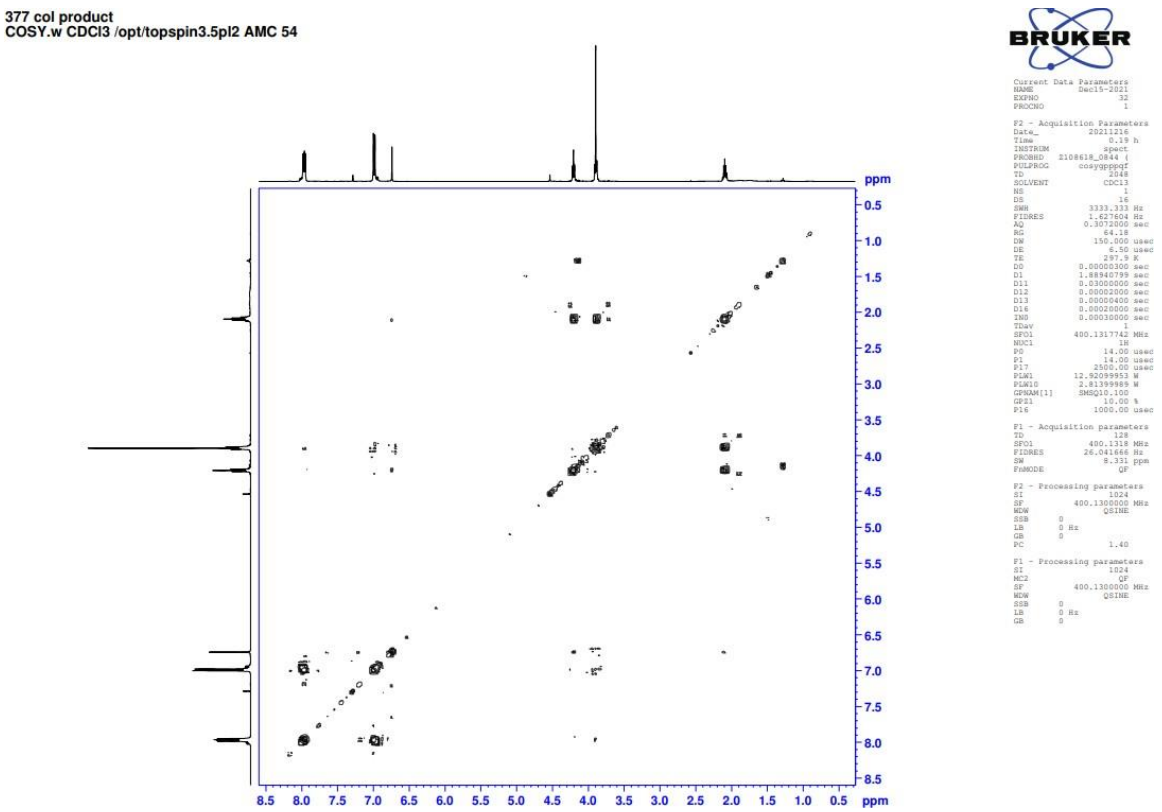

IR spectrum of **1-(4-(3-hydroxypropoxy)phenyl)-3-(4-methoxyphenyl)propane-1,3-dione**

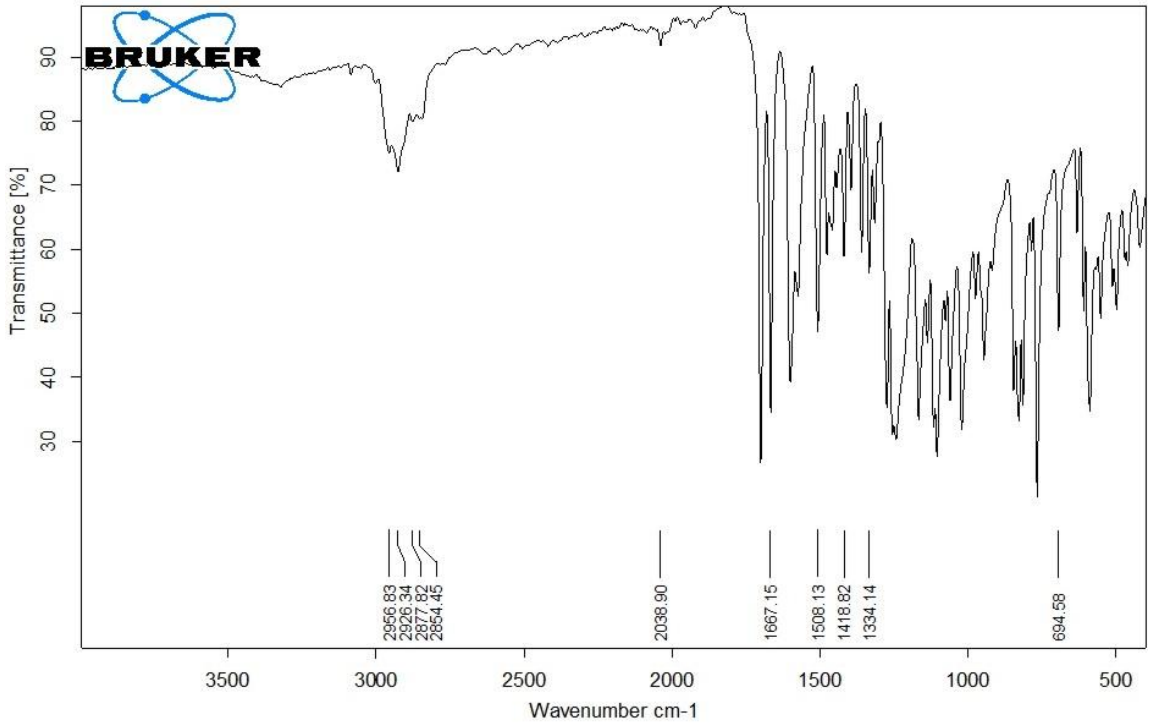

1H NMR of **1-(4-Chlorophenyl)-3-(4-(3-hydroxypropoxy)phenyl)propane-1,3-dione**

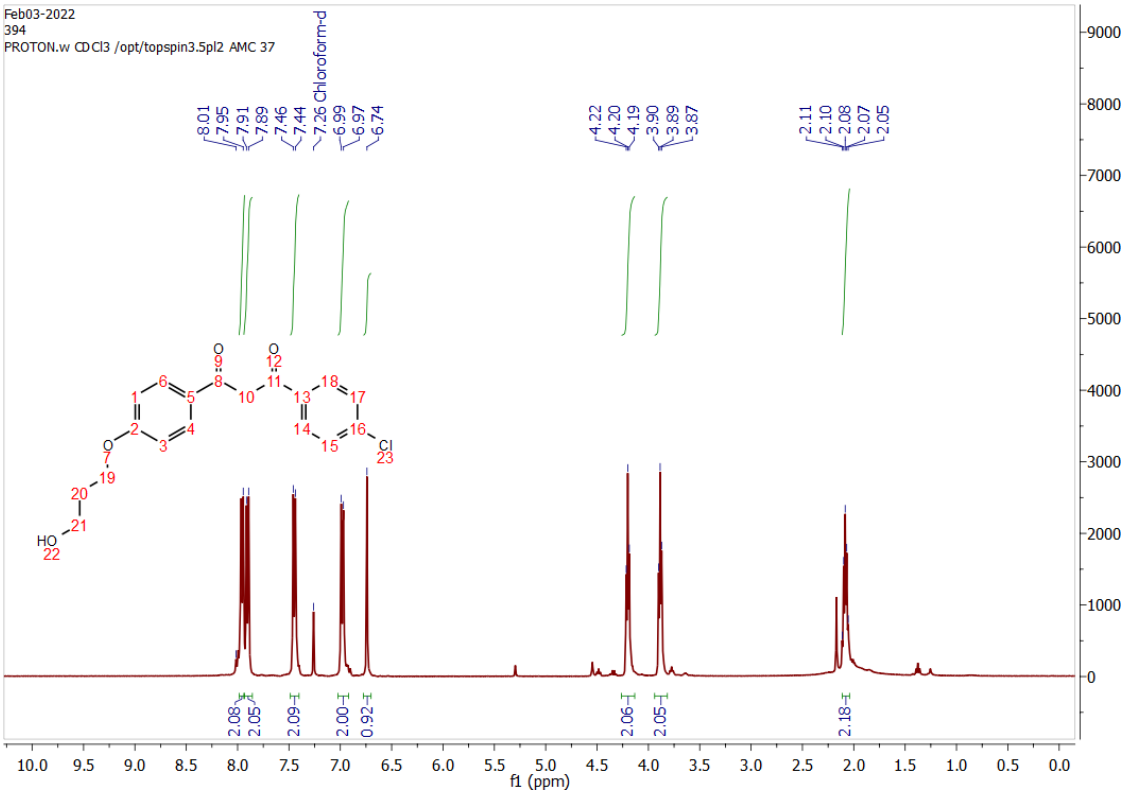

13C NMR of **1-(4-Chlorophenyl)-3-(4-(3-hydroxypropoxy)phenyl)propane-1,3-dione**

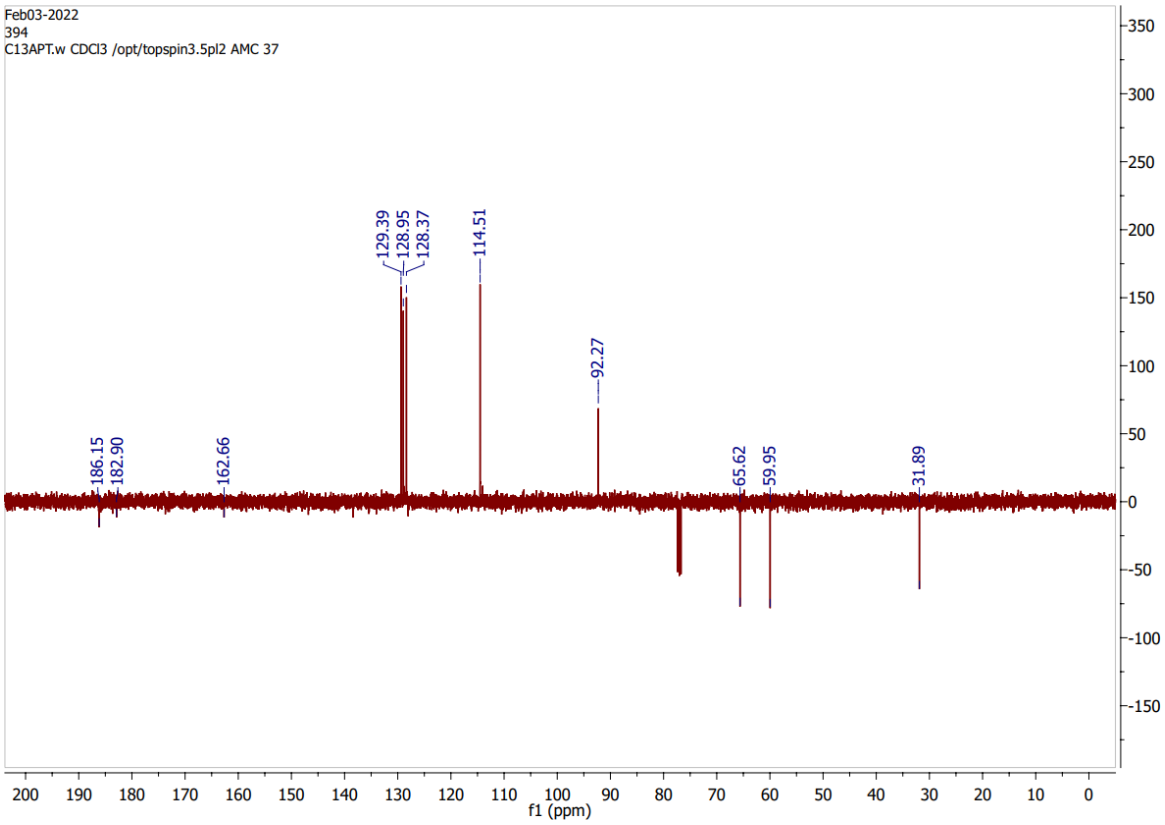

COSY of **1-(4-Chlorophenyl)-3-(4-(3-hydroxypropoxy)phenyl)propane-1,3-dione**

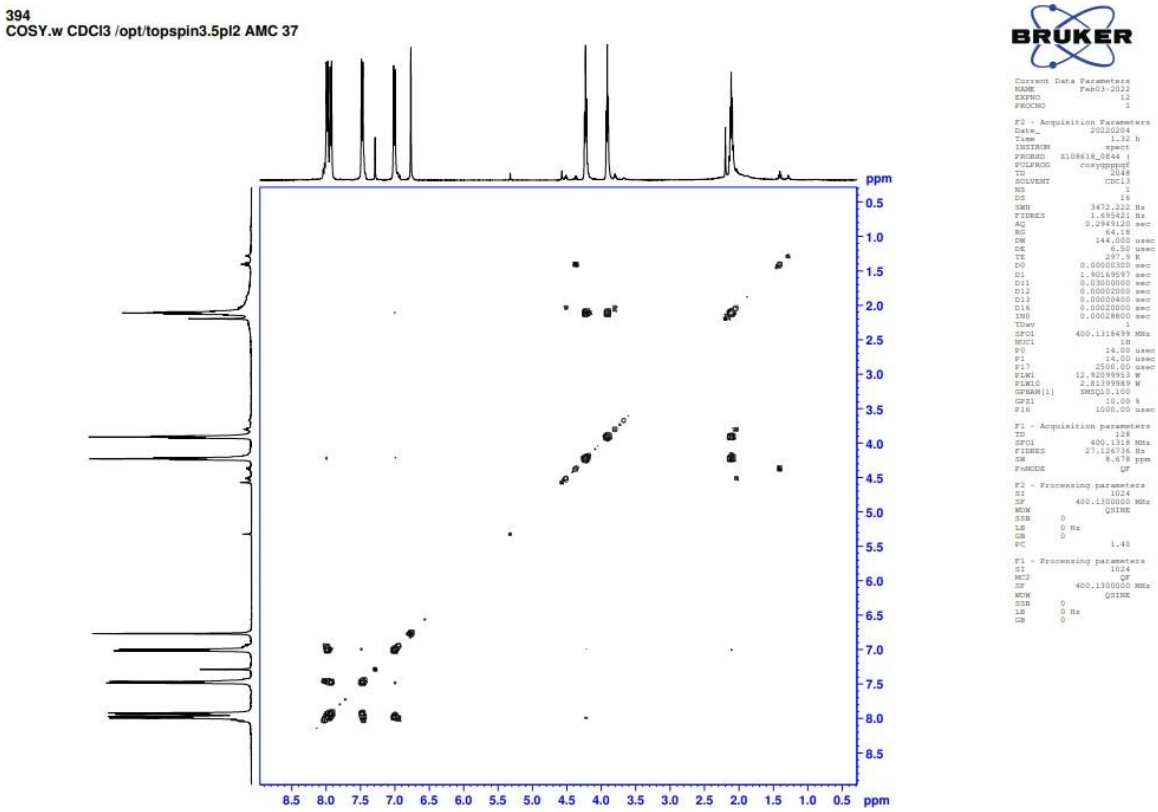

IR spectrum of **1-(4-Chlorophenyl)-3-(4-(3-hydroxypropoxy)phenyl)propane-1,3-dione**

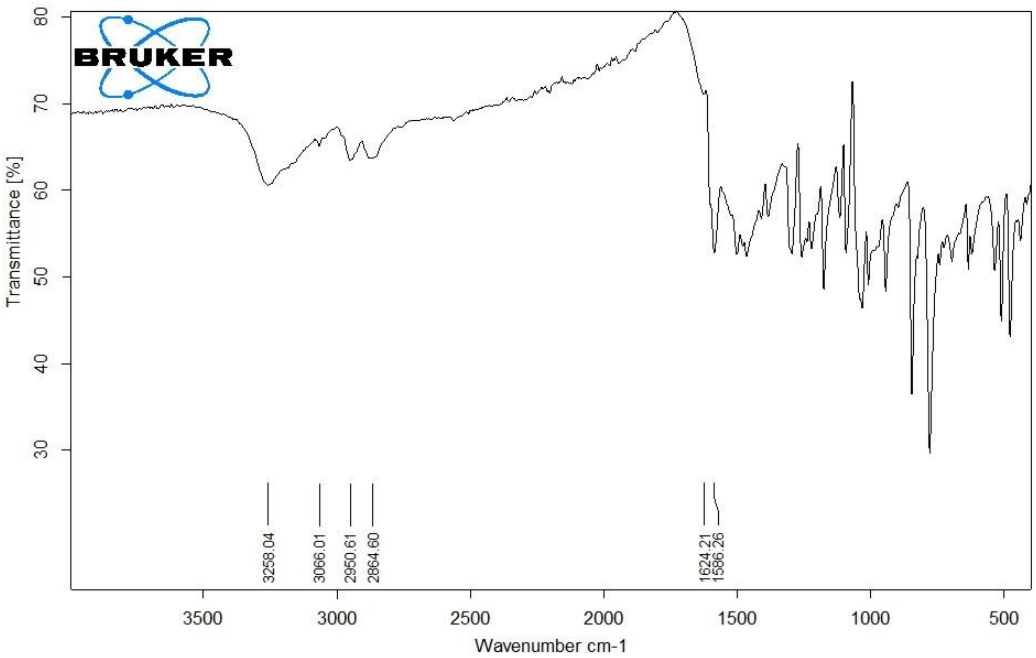

1H NMR of **2-Cyano-3,3-diphenylacrylic acid**

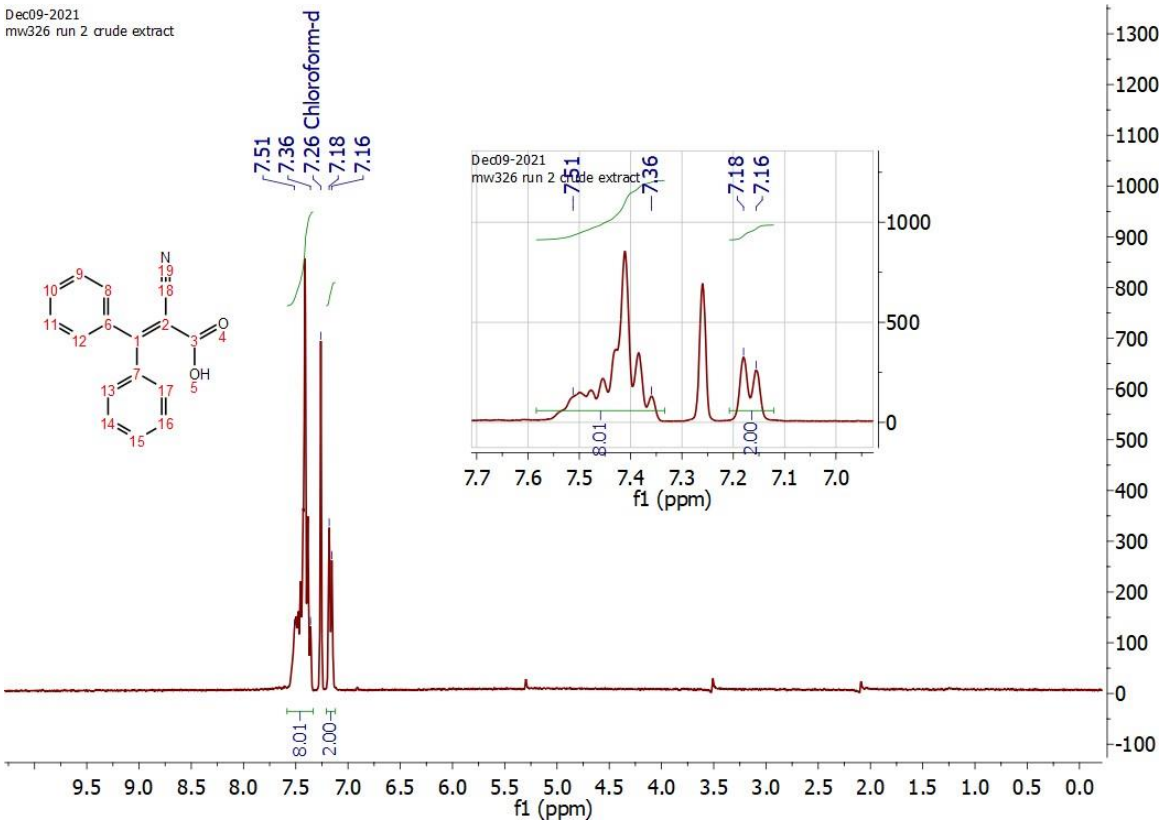

13C NMR of **2-Cyano-3,3-diphenylacrylic acid**

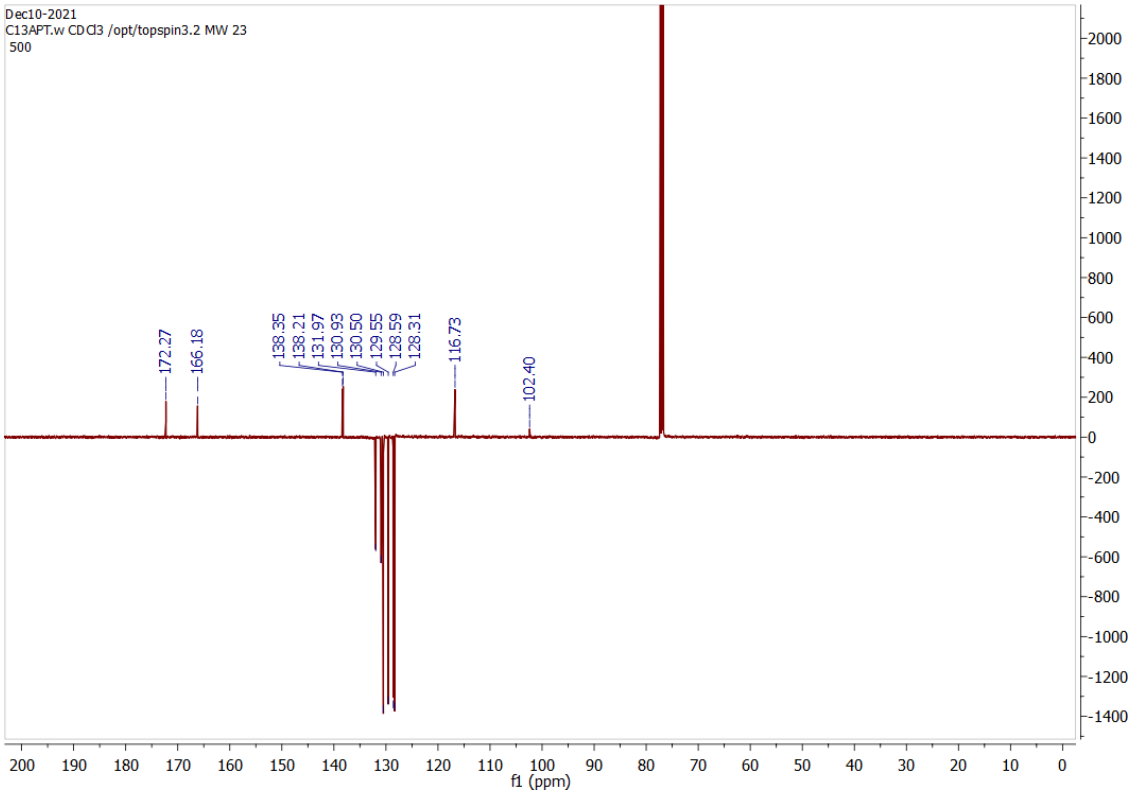

1H NMR of **methyl 4-methoxybenzoate**

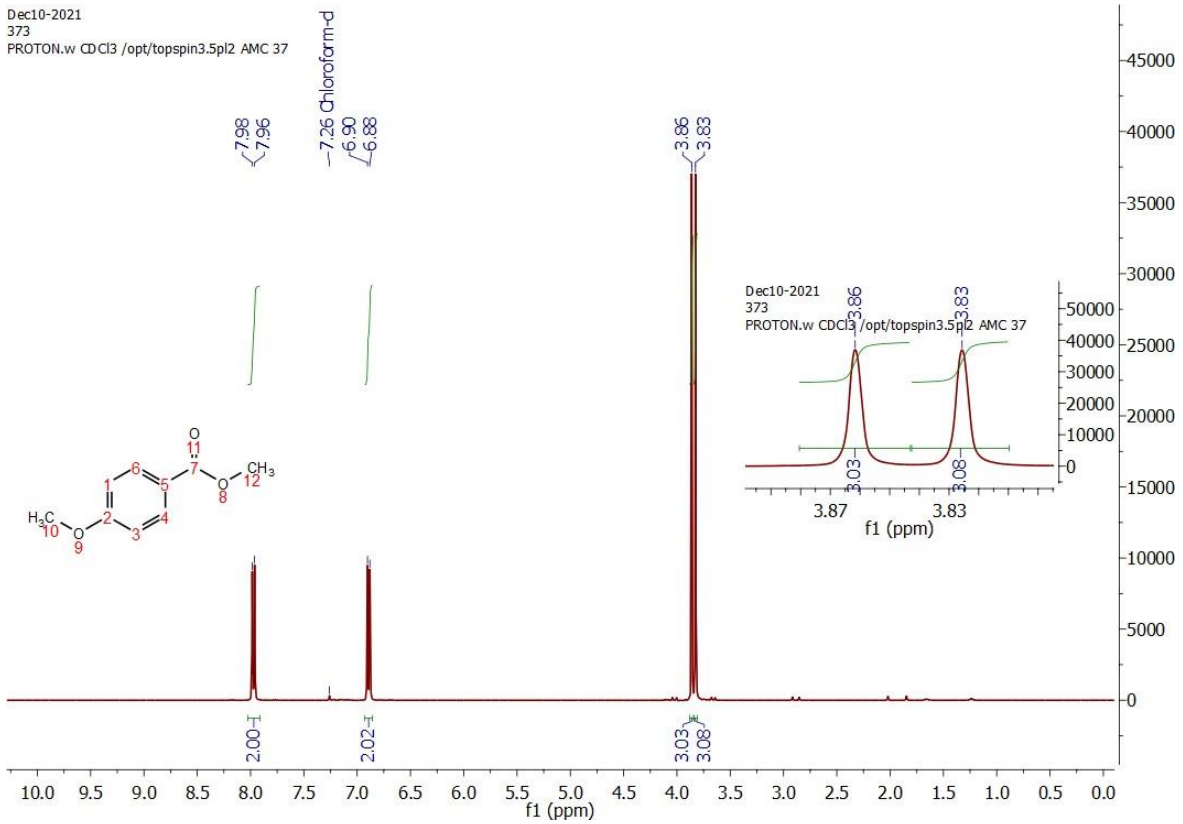

1H NMR of **ethyl 4-chlorobenzoate**

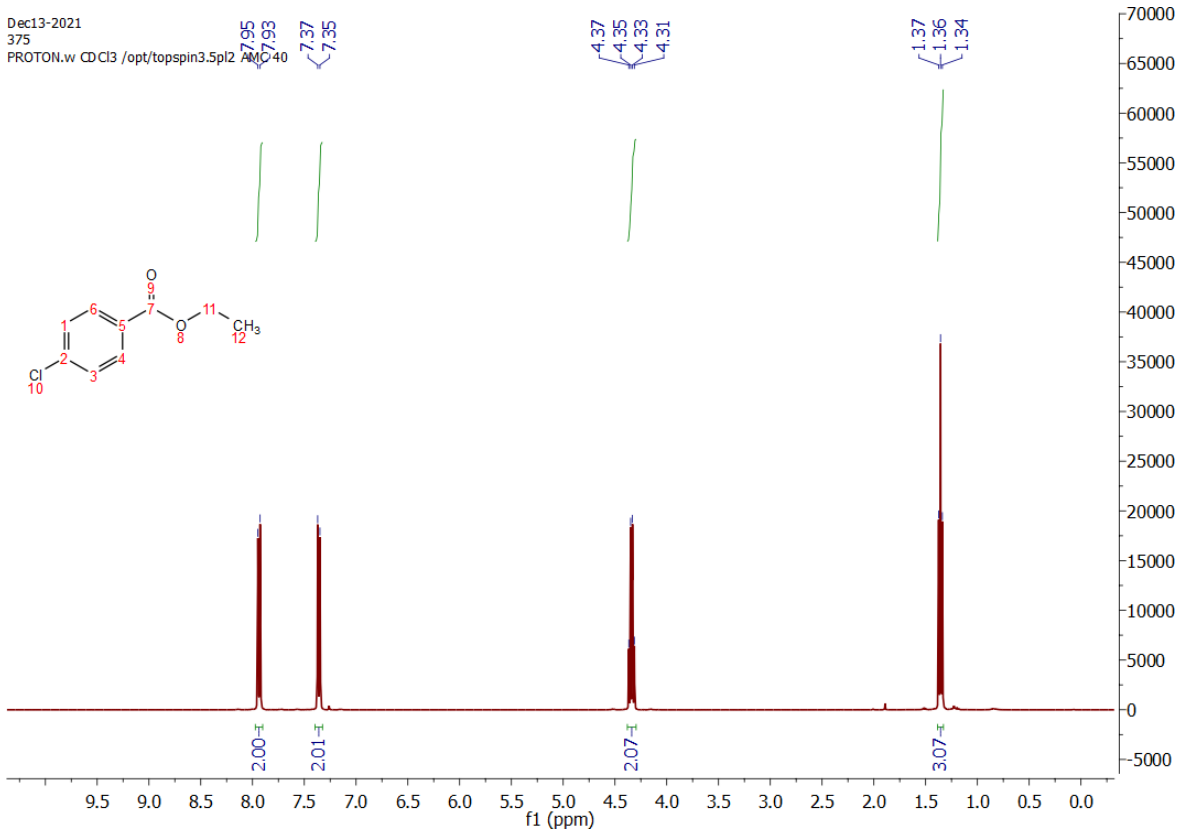

13C NMR of **ethyl 4-chlorobenzoate**

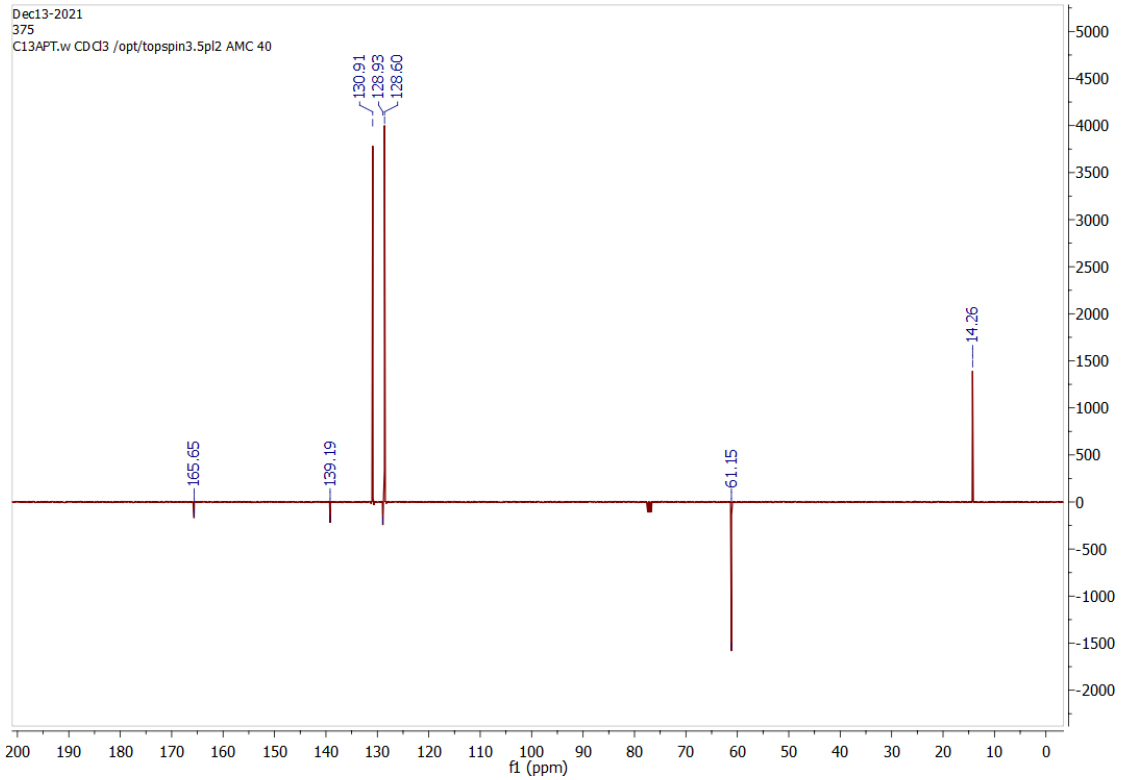

1H NMR of **3-(4-(3-Oxo-3-phenylpropanoyl)phenoxy)propyl 2-cyano-3,3-diphenylacrylate, "AVOCTO1"**

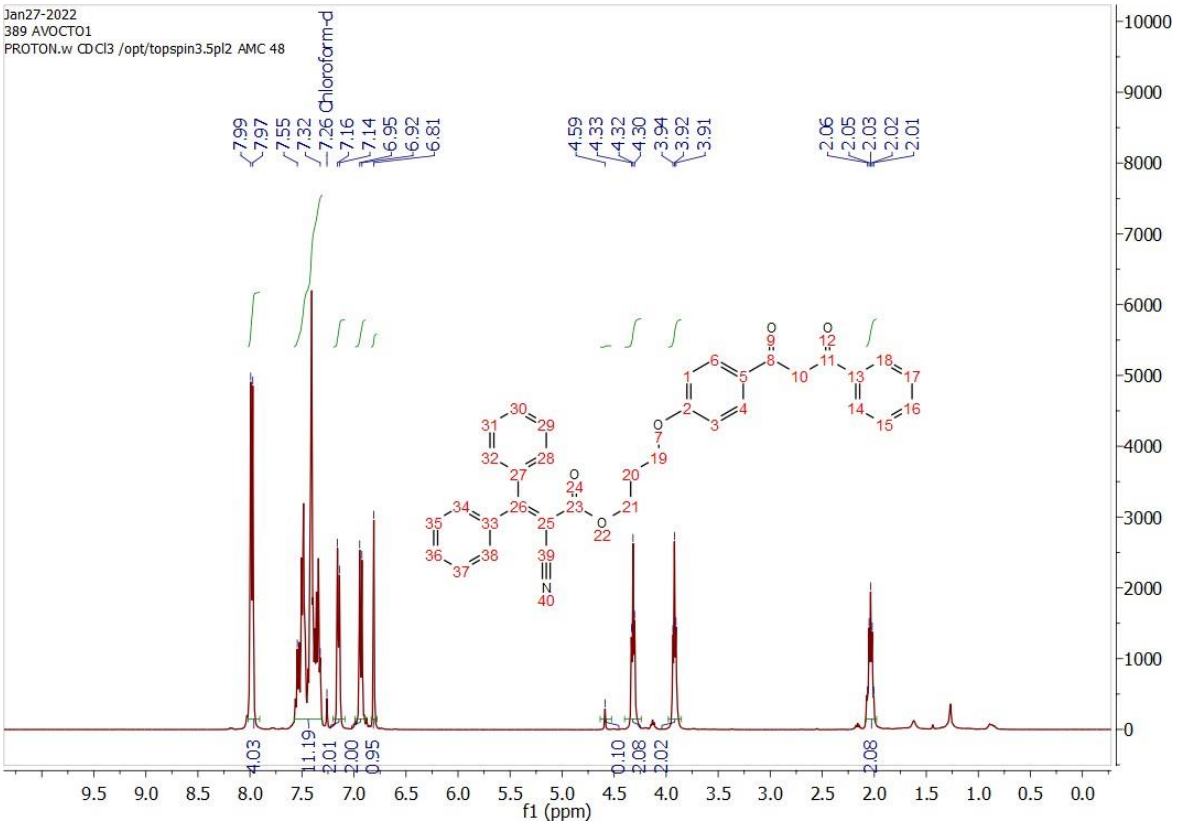

13C NMR of **AVOCTO1**

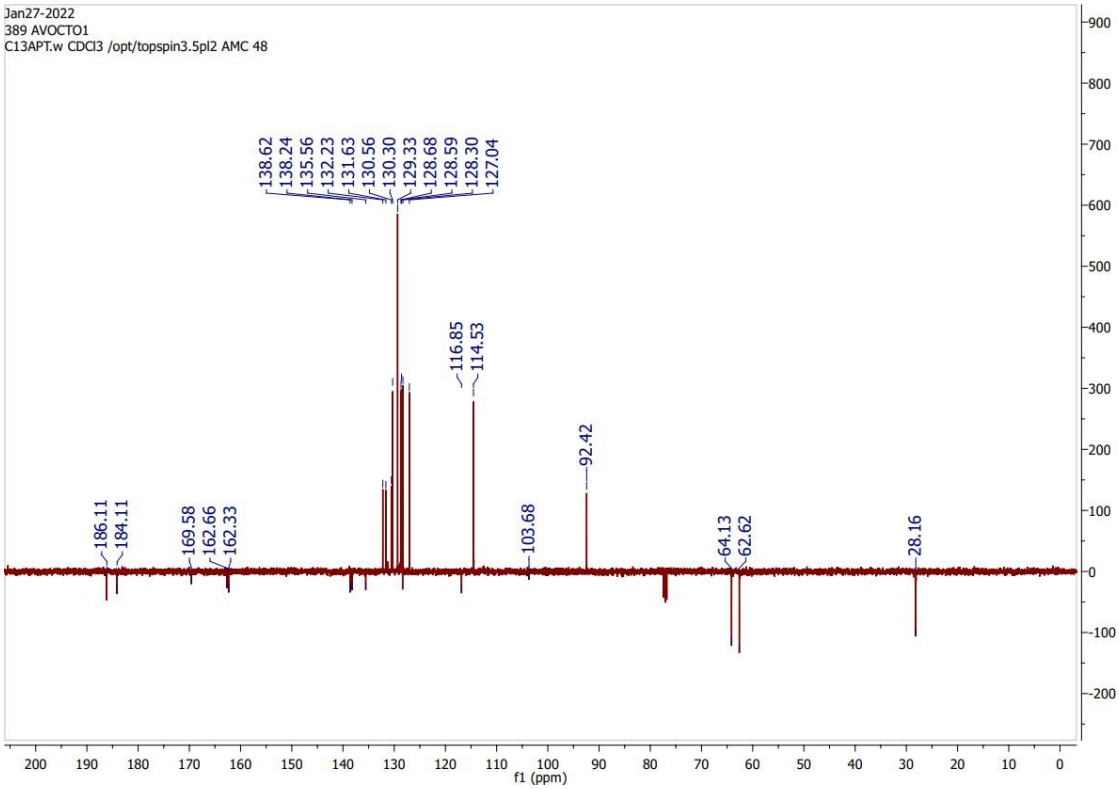

COSY of **AVOCTO1**

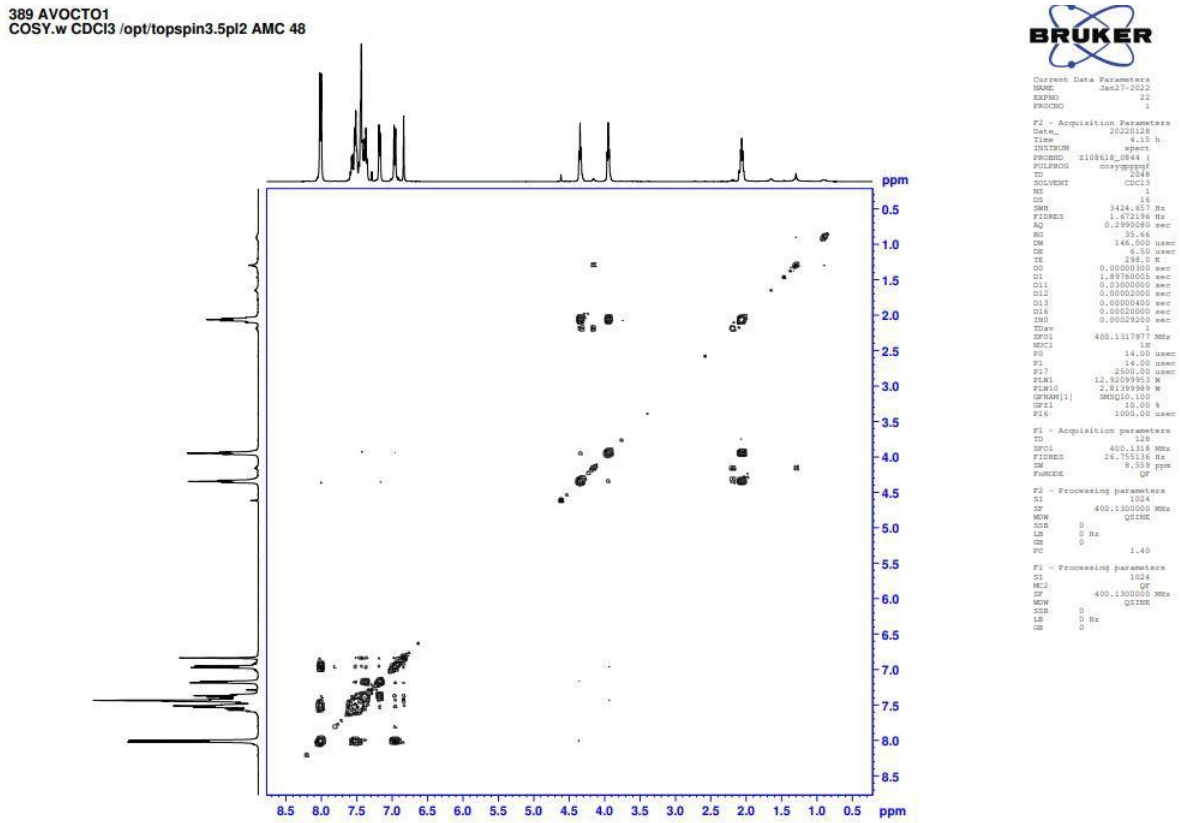

IR spectrum of **AVOCTO1**

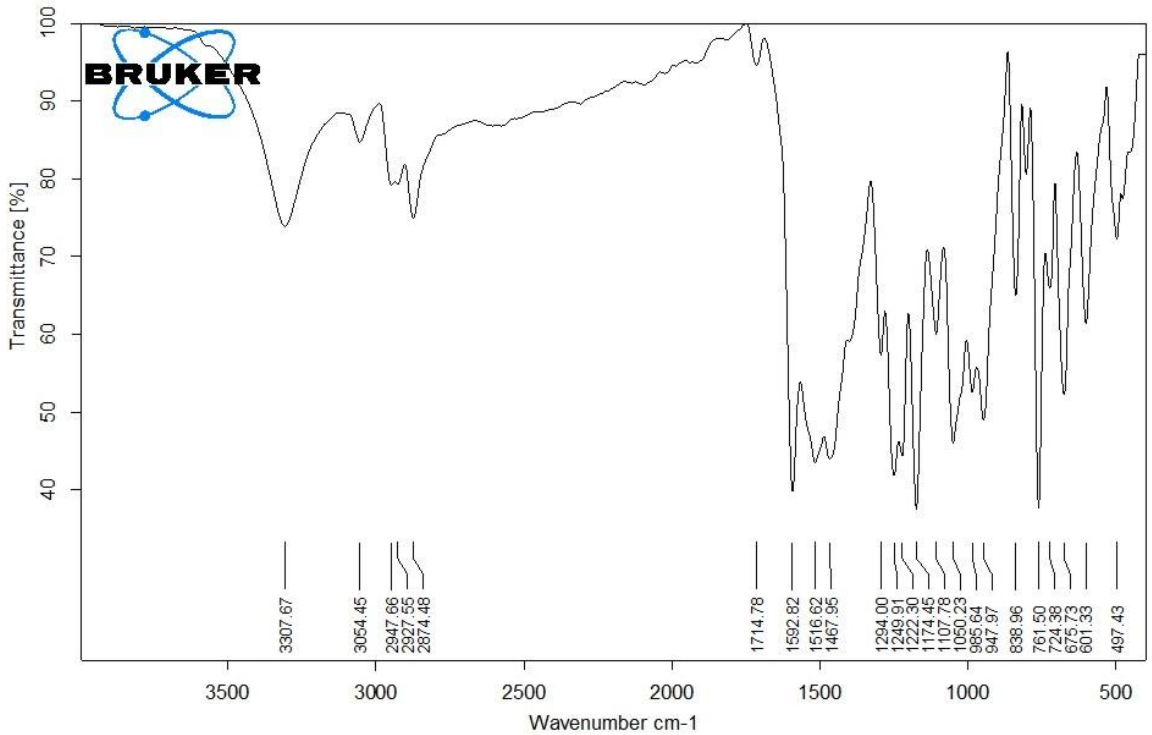

1H NMR of **3-(4-(3-(4-(*tert*-butyl)phenyl)-3-oxopropanoyl)phenoxy)propyl 2-cyano-3,3-diphenylacrylate, "AVOCTO2"**

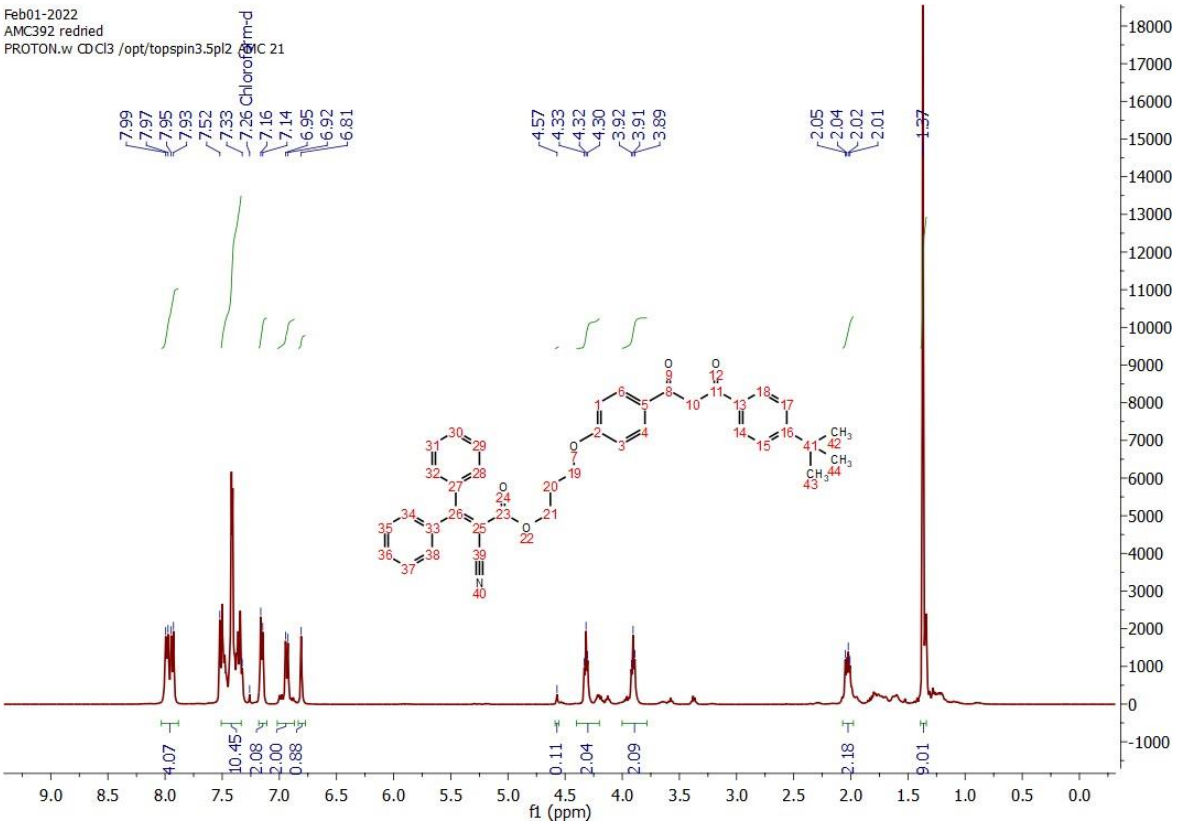

13C NMR of **AVOCTO2**

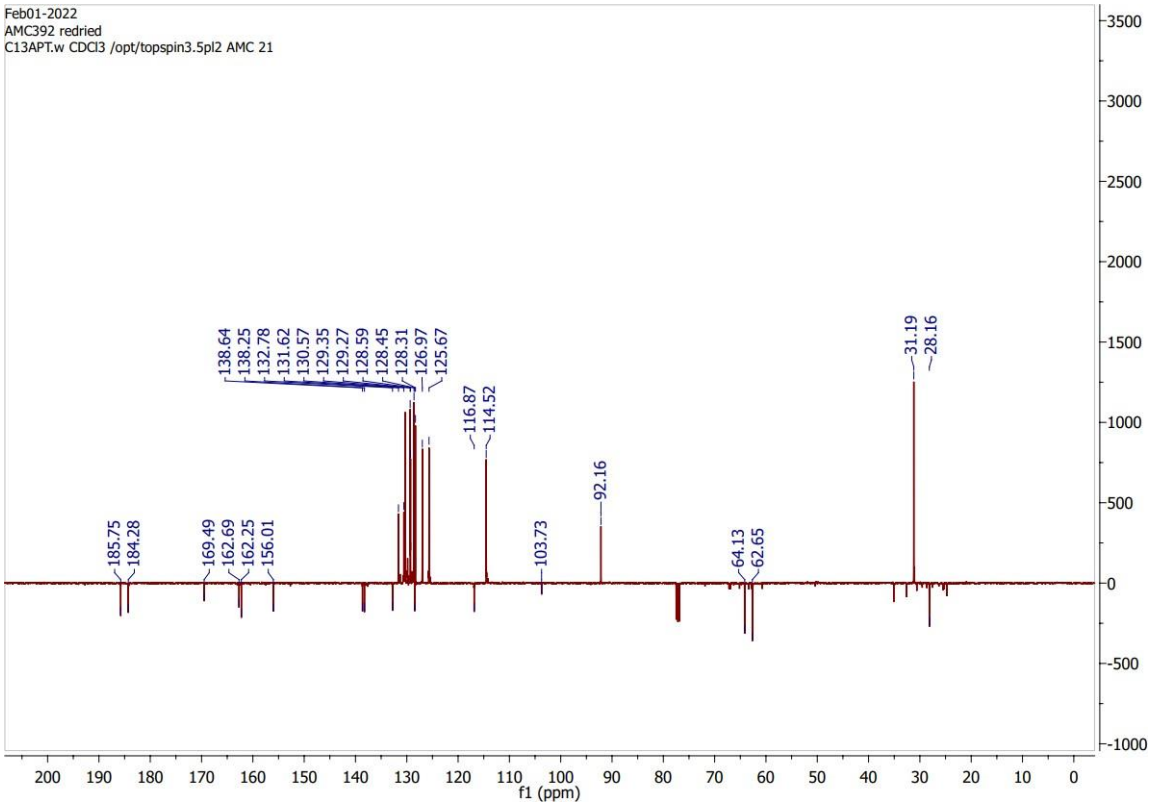

COSY of **AVOCTO2**

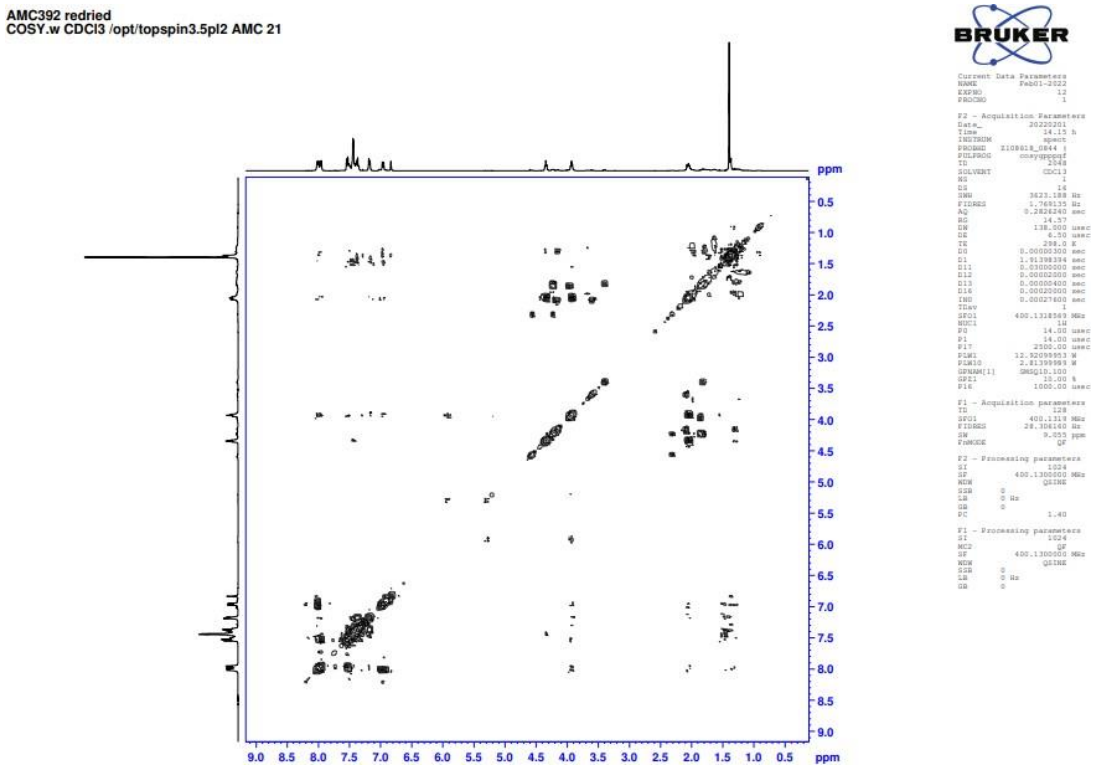

IR Spectrum of **AVOCTO2**

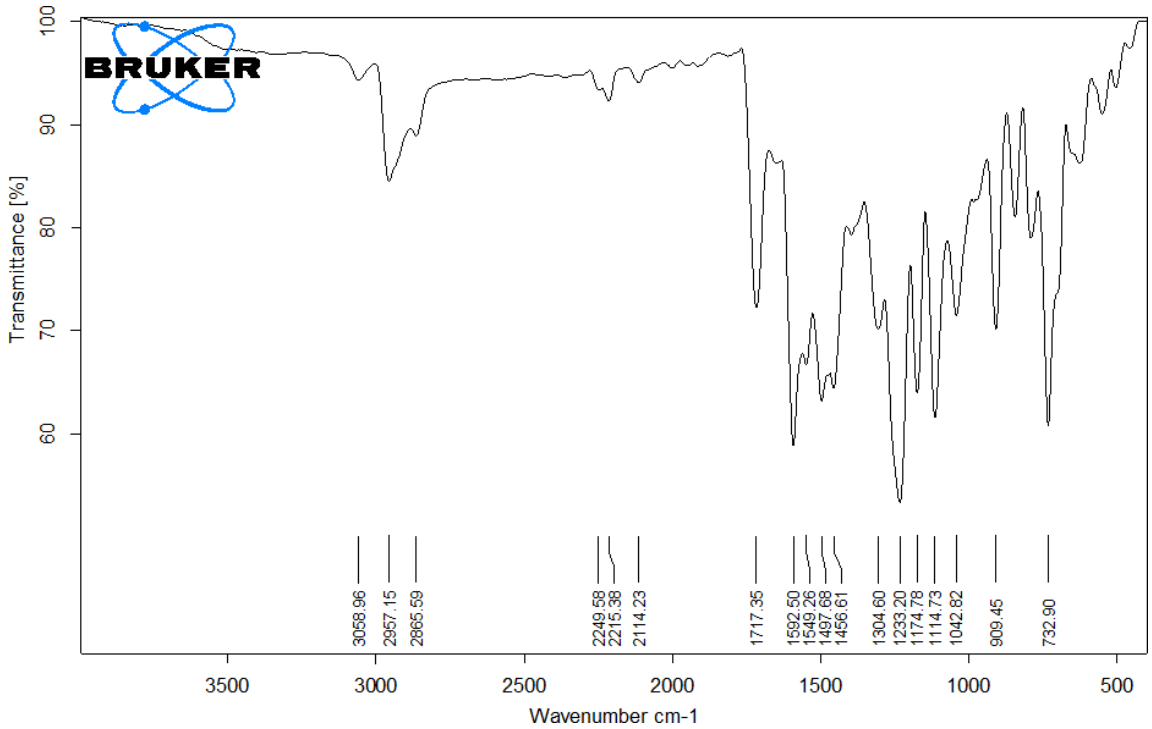

1H NMR of **3-(4-(2-Methyl-3-oxo-3-phenylpropanoyl)phenoxy)propyl 2-cyano-3,3-diphenylacrylate, "AVOCTO3"**

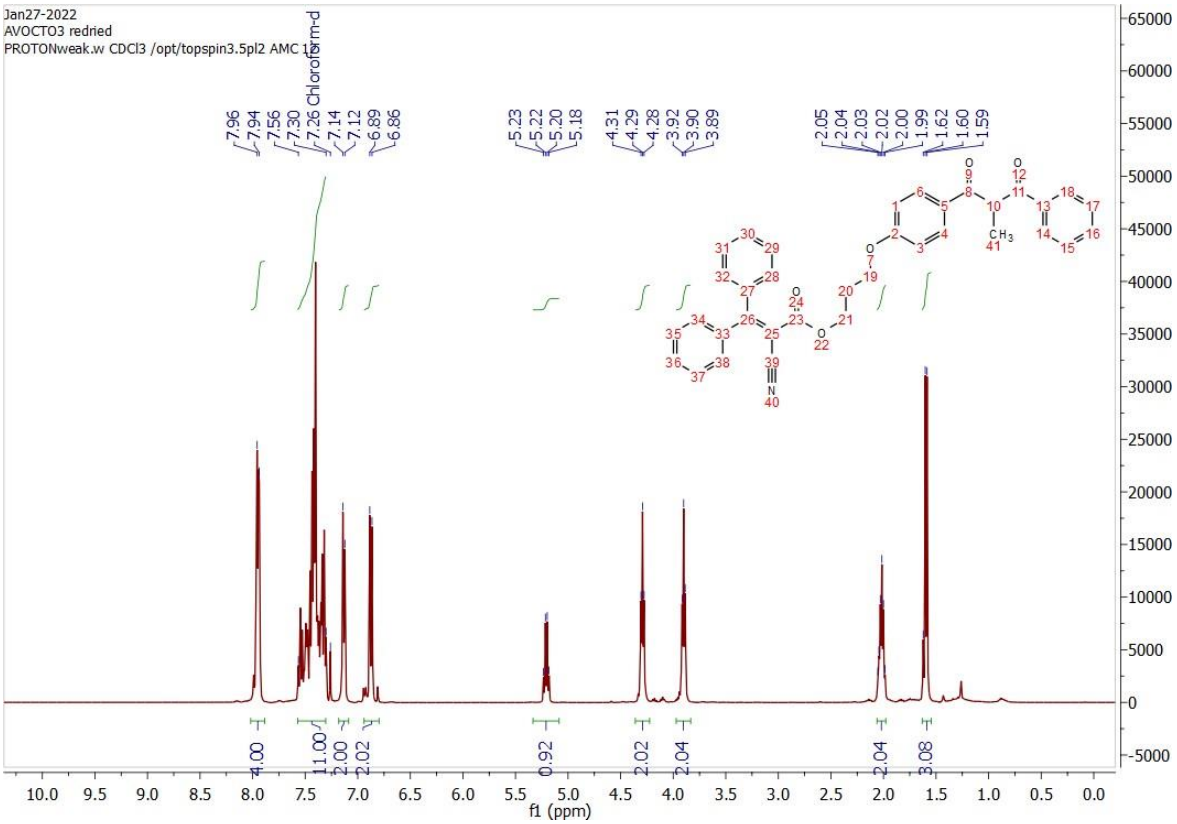

13C NMR of **AVOCTO3**

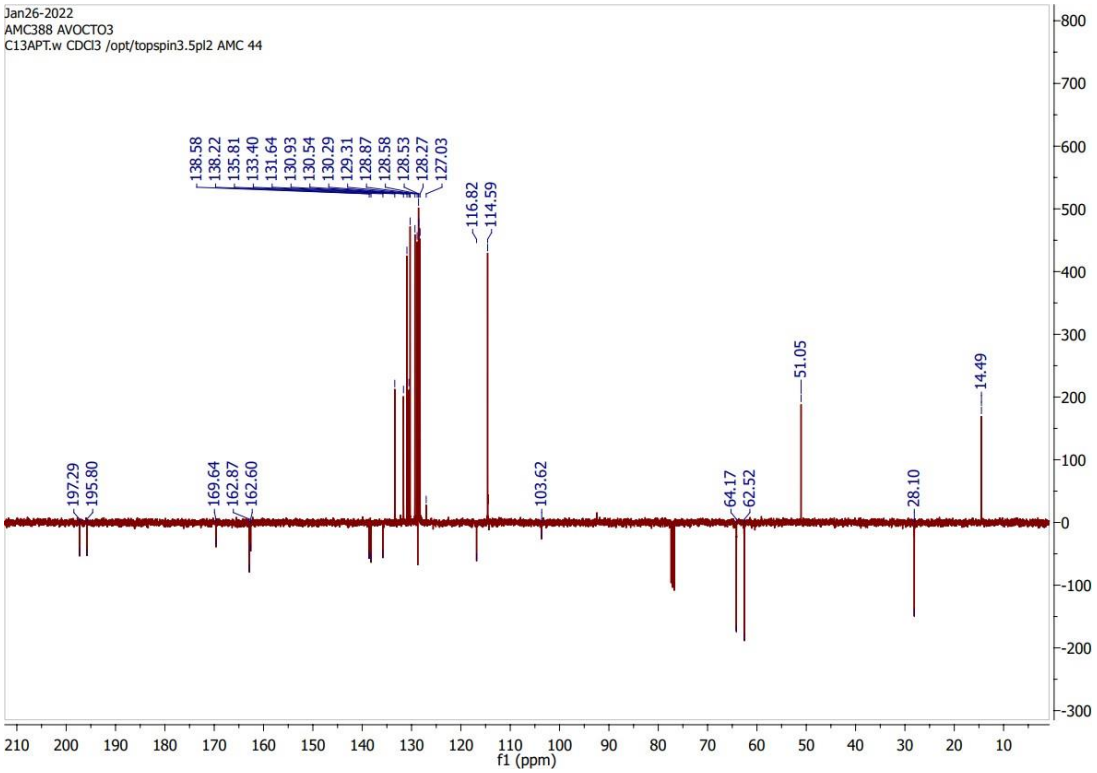

COSY of **AVOCTO3**

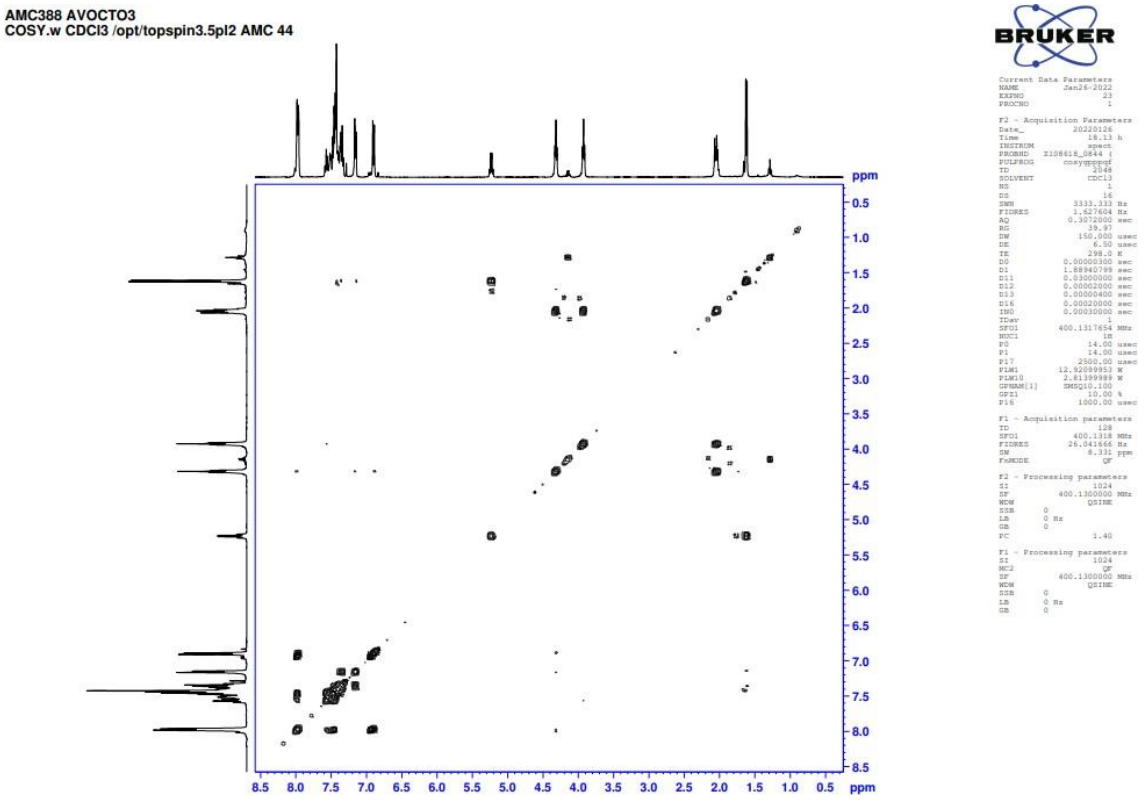

IR Spectrum of **AVOCTO3**

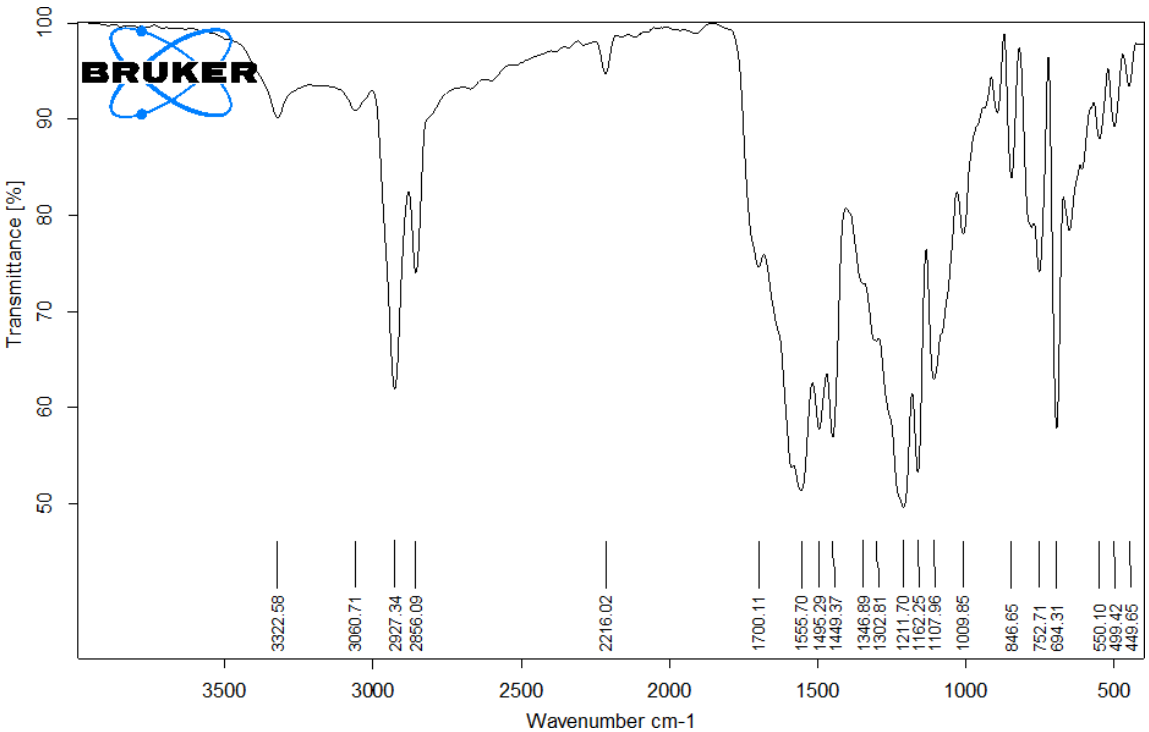

1H NMR of **3-(4-(3-(4-Methoxyphenyl)-3-oxopropanoyl)phenoxy)propyl 2-cyano-3,3-diphenylacrylate, "AVOCTO4"**

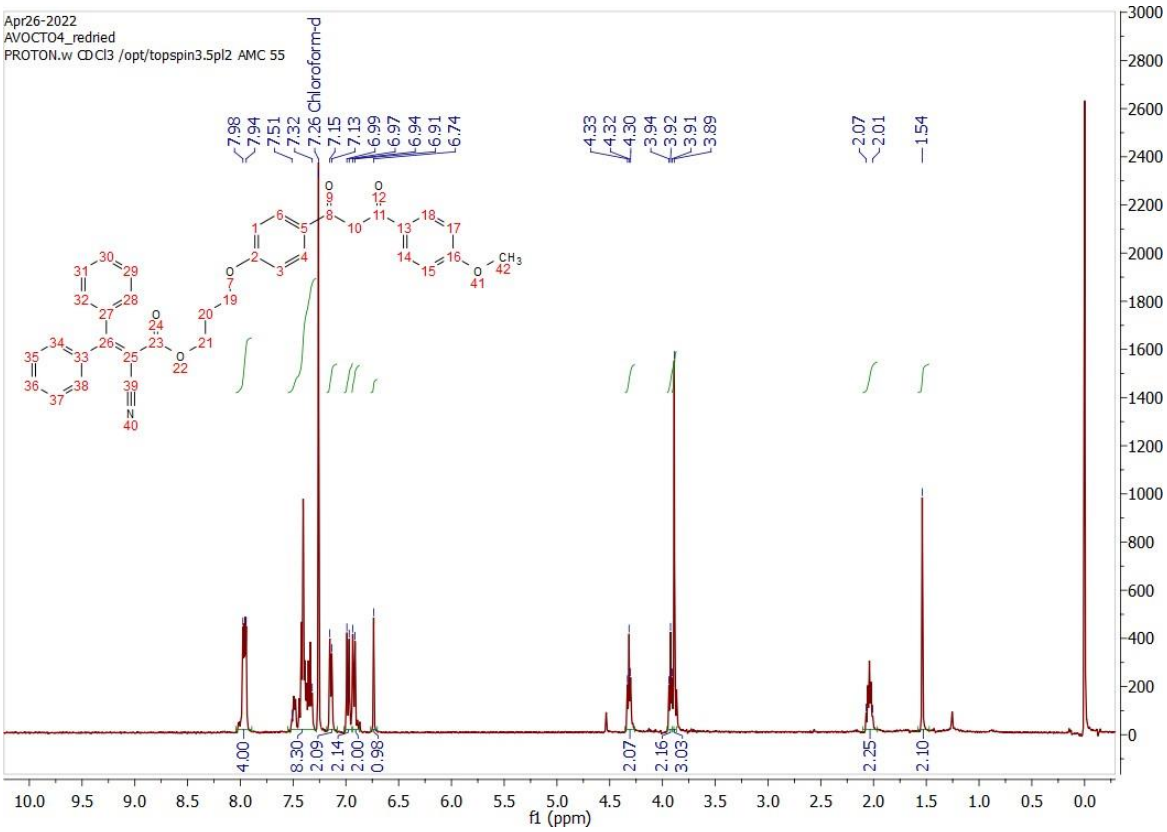

13C NMR of **AVOCTO4**

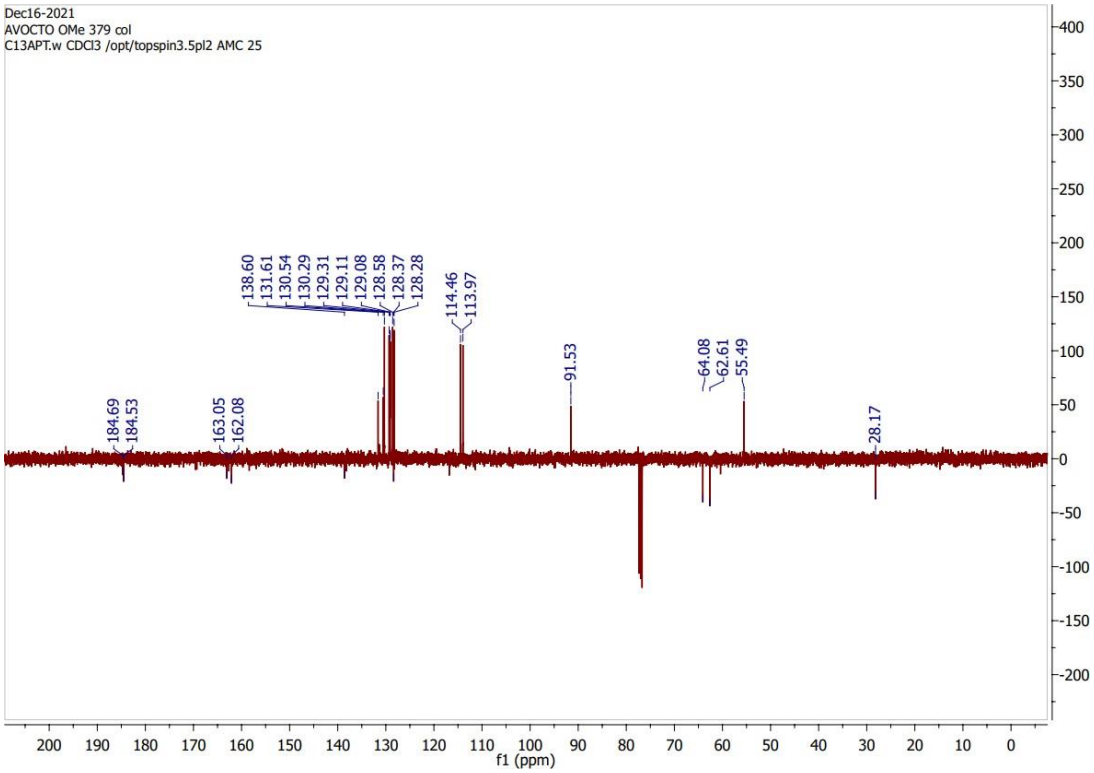

COSY of **AVOCTO4**

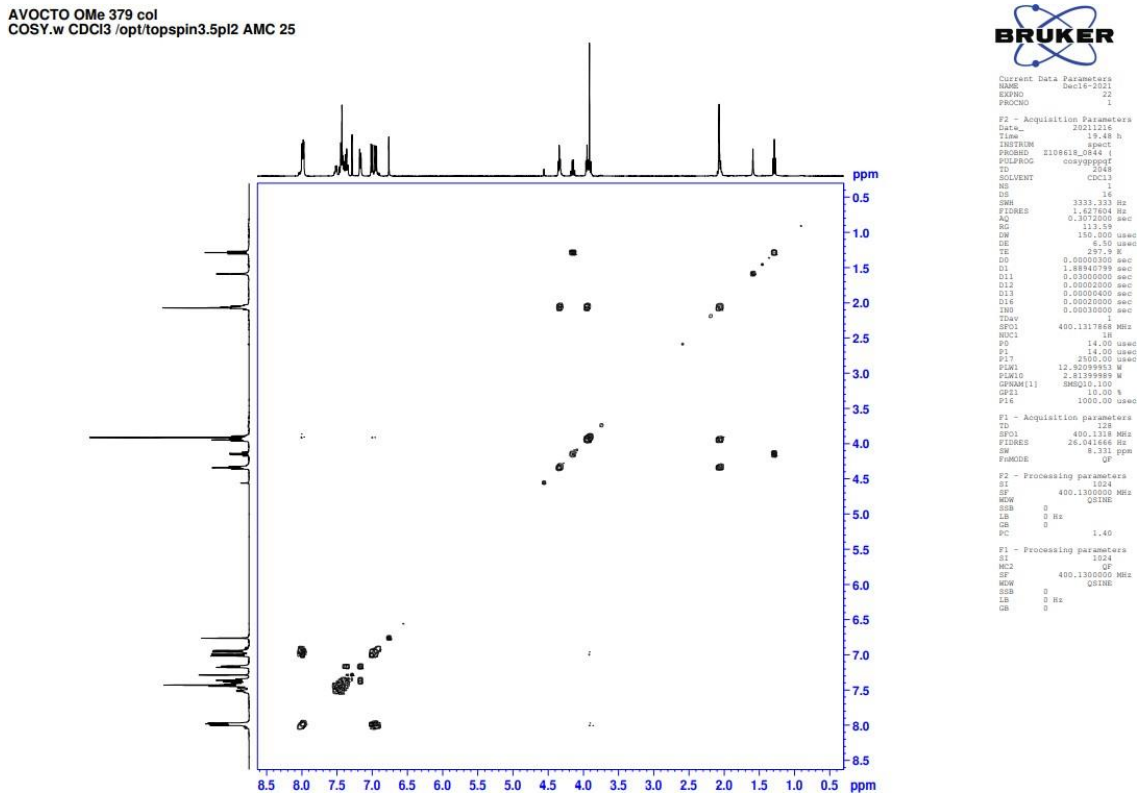

IR Spectrum of **AVOCTO4**

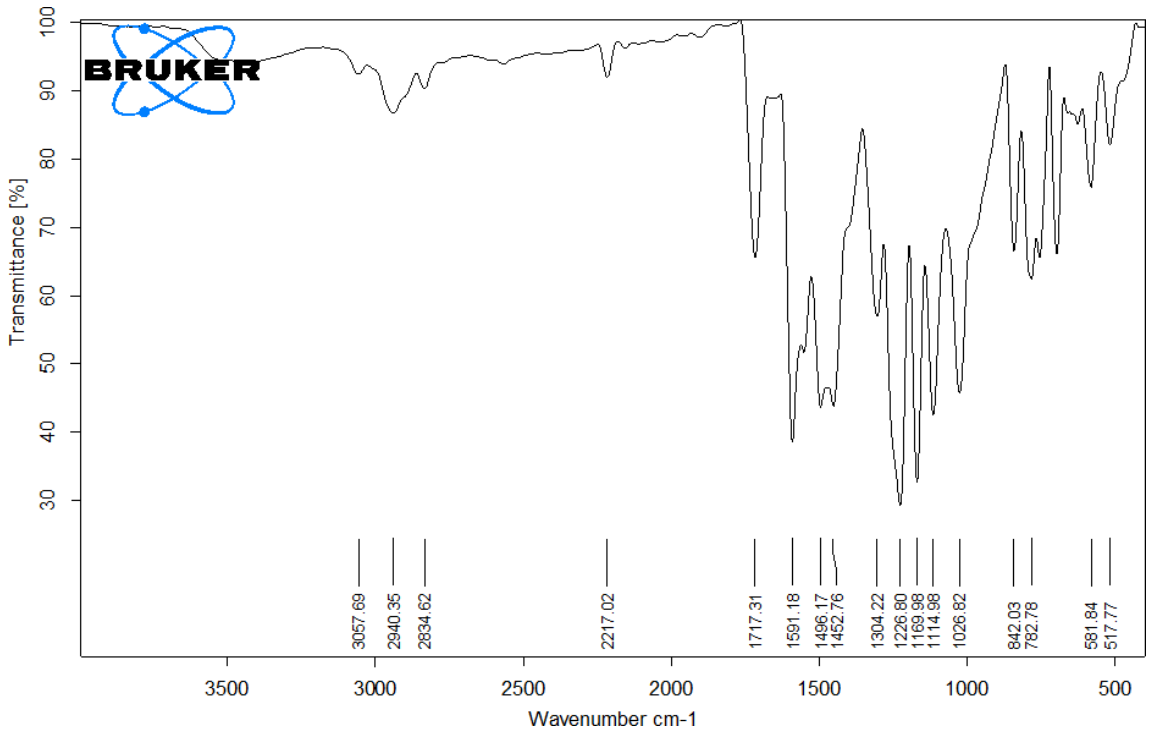

1H NMR of **3-(4-(3-(4-Chlorophenyl)-3-oxopropanoyl)phenoxy)propyl 2-cyano-3,3-diphenylacrylate, "AVOCTO5"**

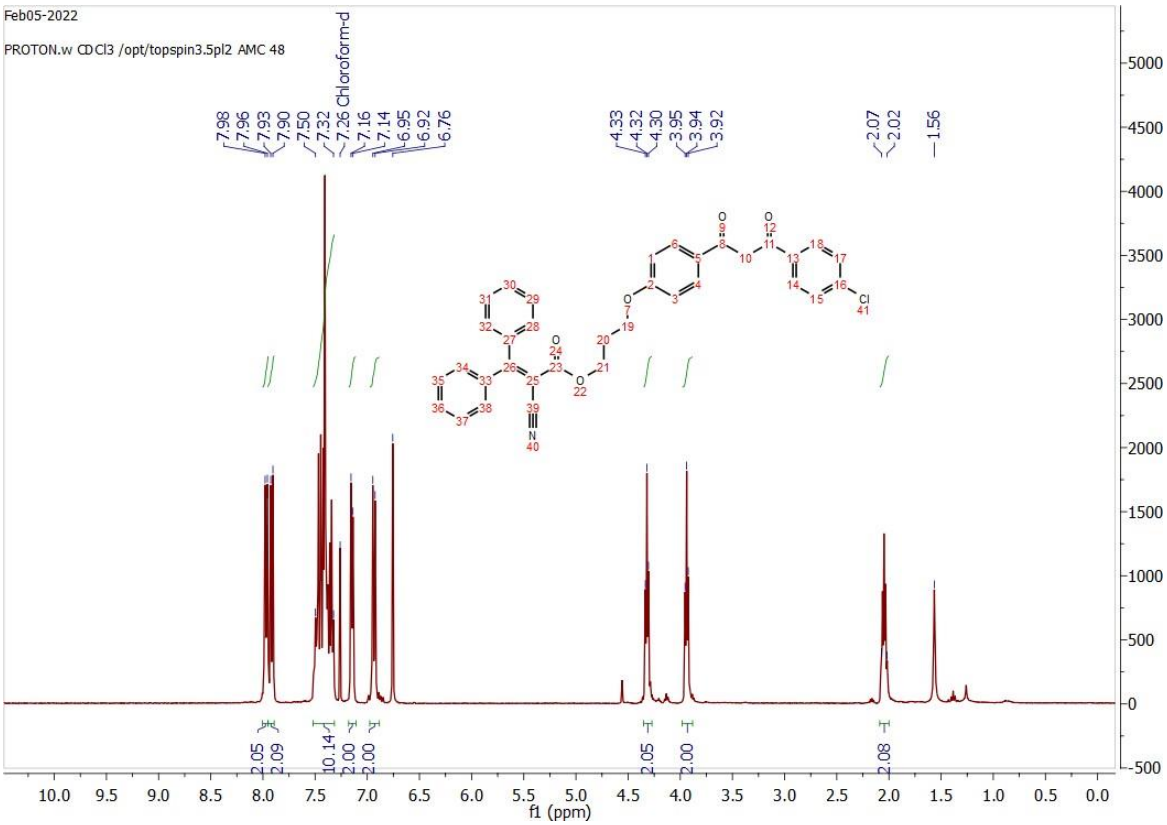

13C NMR of **AVOCTO5**

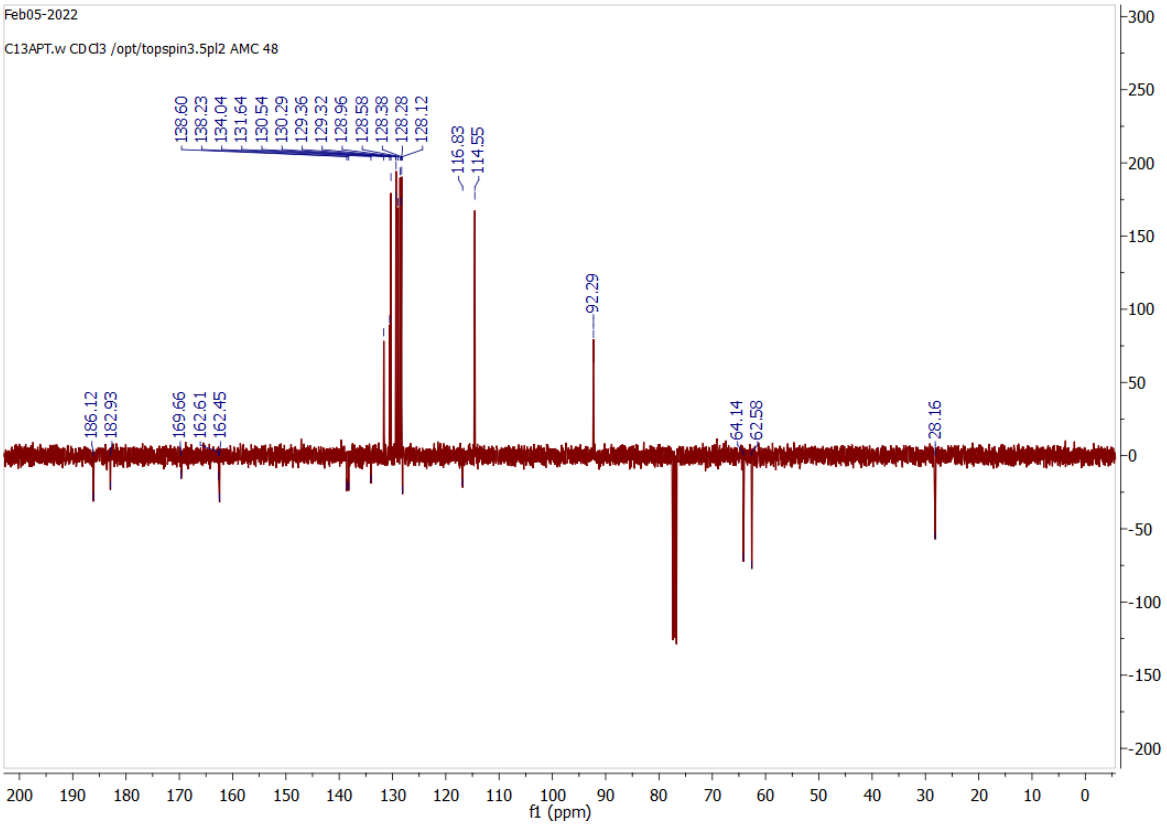

COSY of **AVOCTO5**

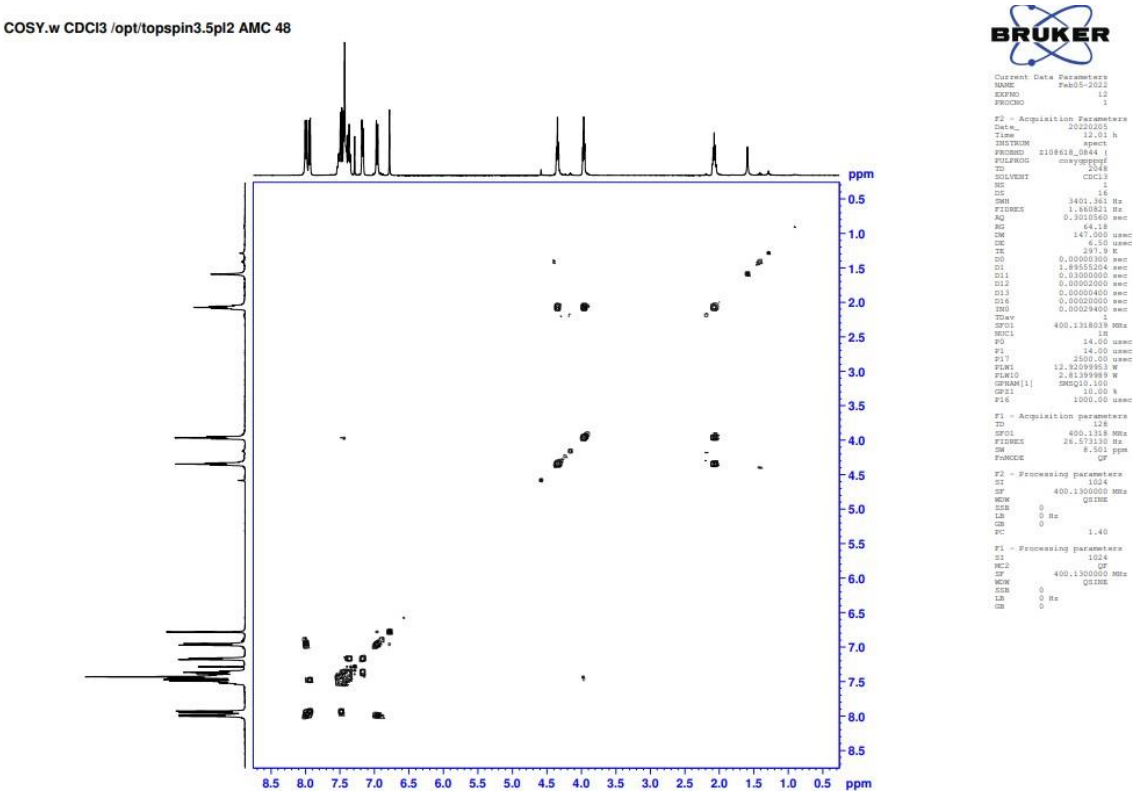

IR Spectrum of **AVOCTO5**

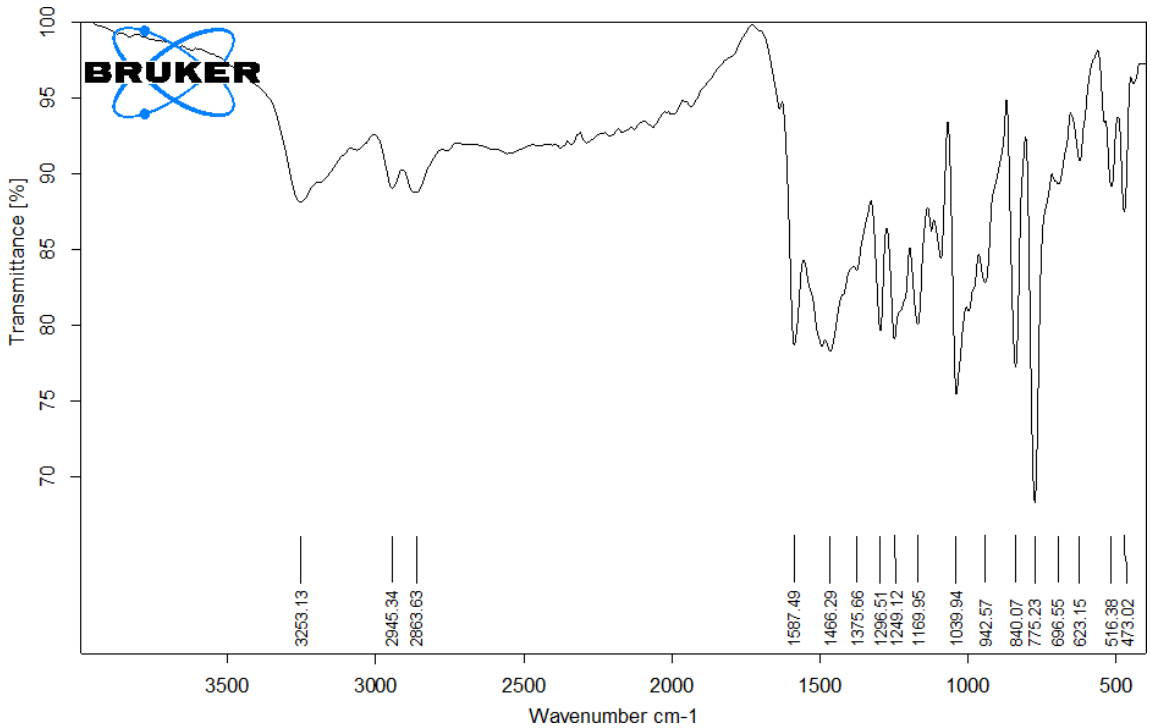

1H NMR of **1-(4-Chlorophenyl)-3-(4-methoxyphenyl)propane-1,3-dione**

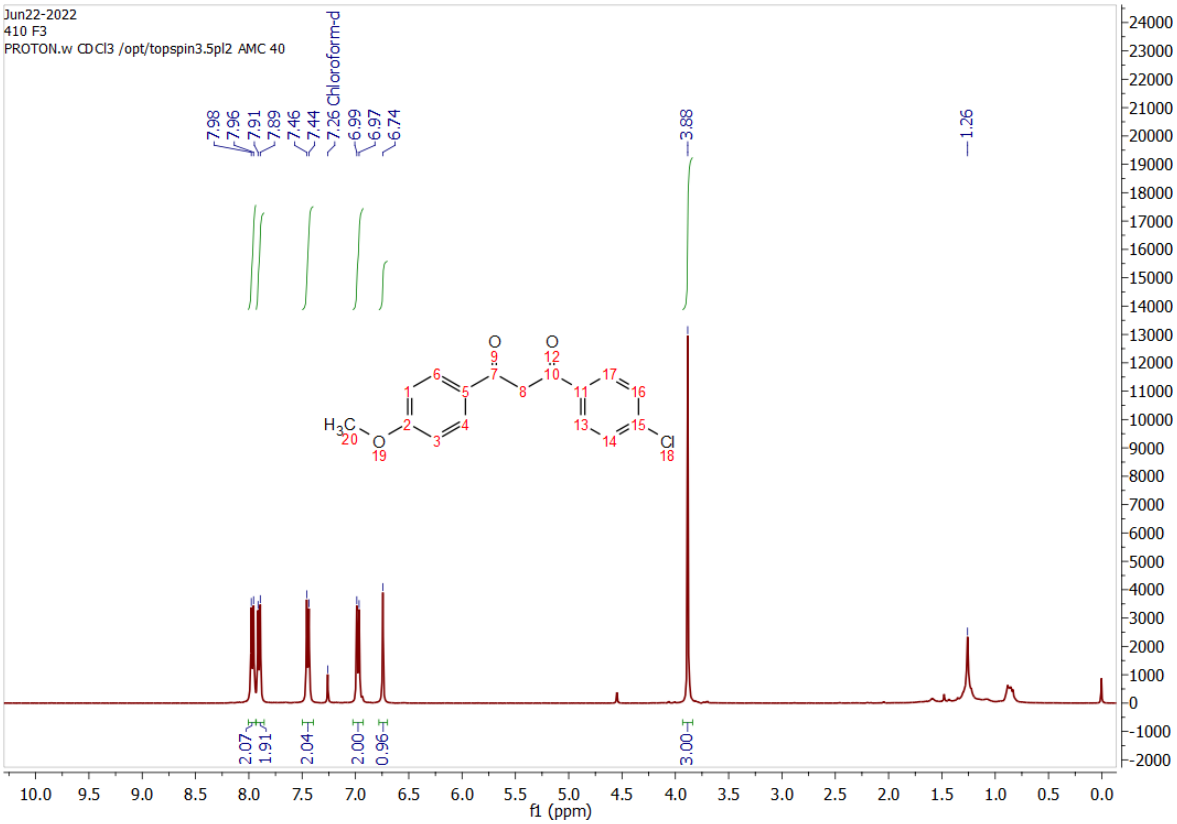

IR Spectrum of **1-(4-Chlorophenyl)-3-(4-methoxyphenyl)propane-1,3-dione**

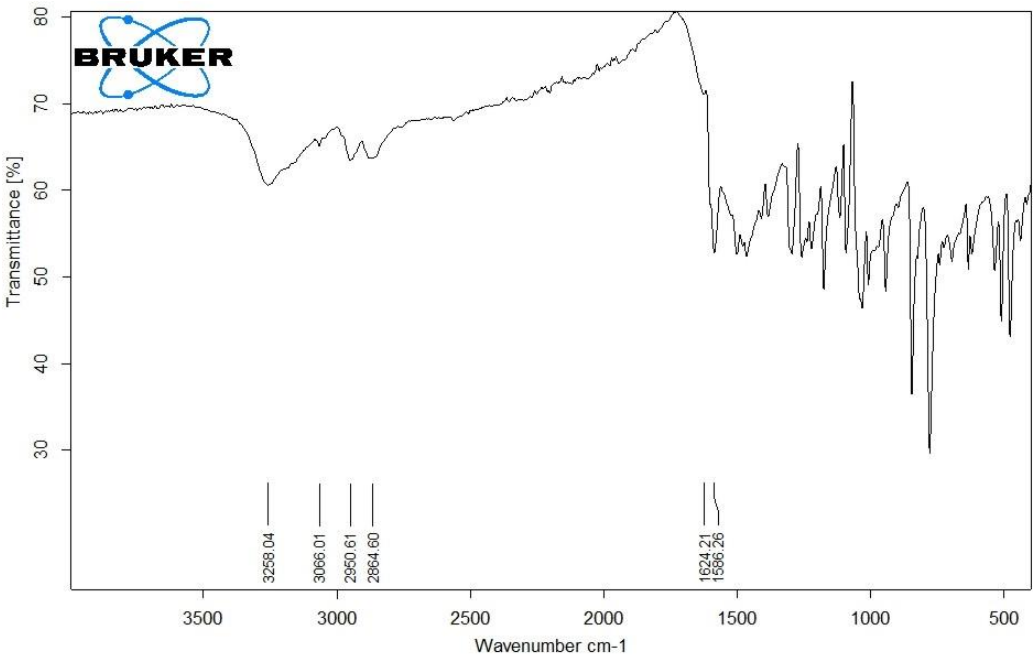

1H NMR of **1-(4-(Tert-butyl)phenyl)-3-(4-methoxyphenyl)-2-methylpropane-1,3-dione**

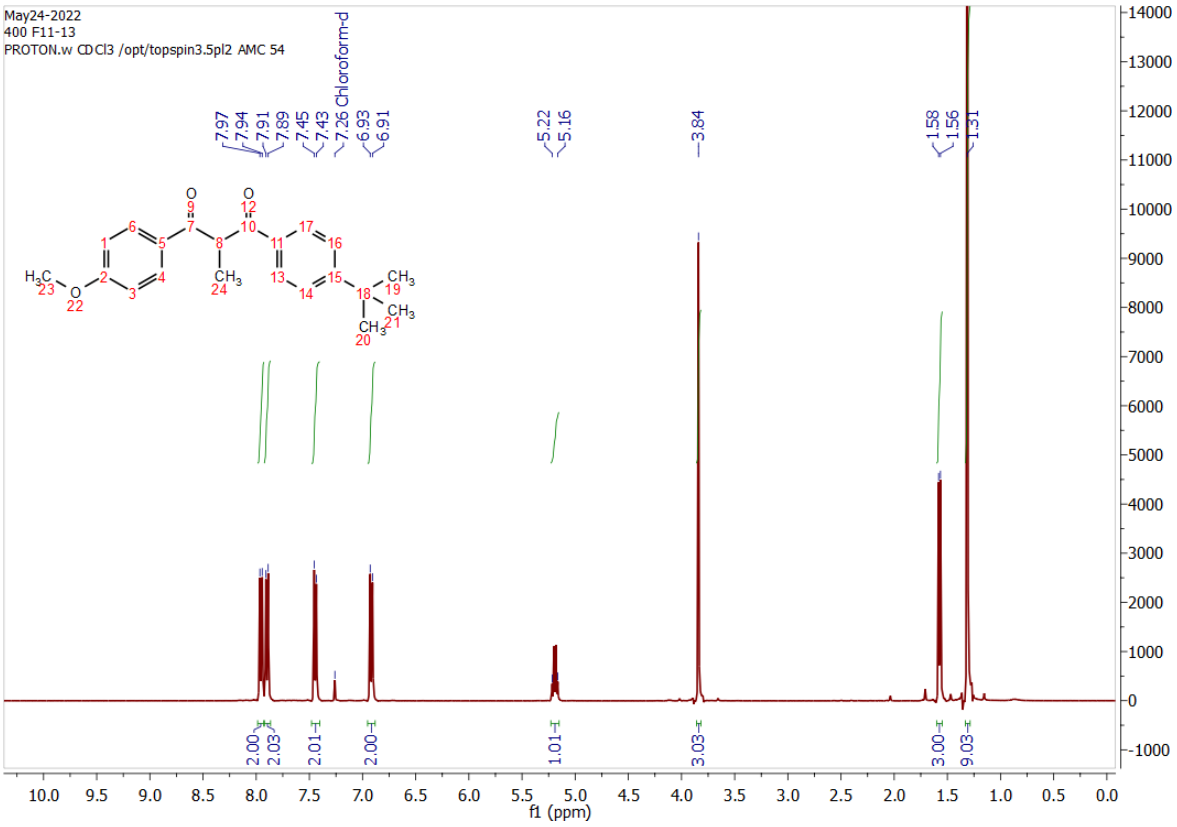

13C NMR of **1-(4-(Tert-butyl)phenyl)-3-(4-methoxyphenyl)-2-methylpropane-1,3-dione**

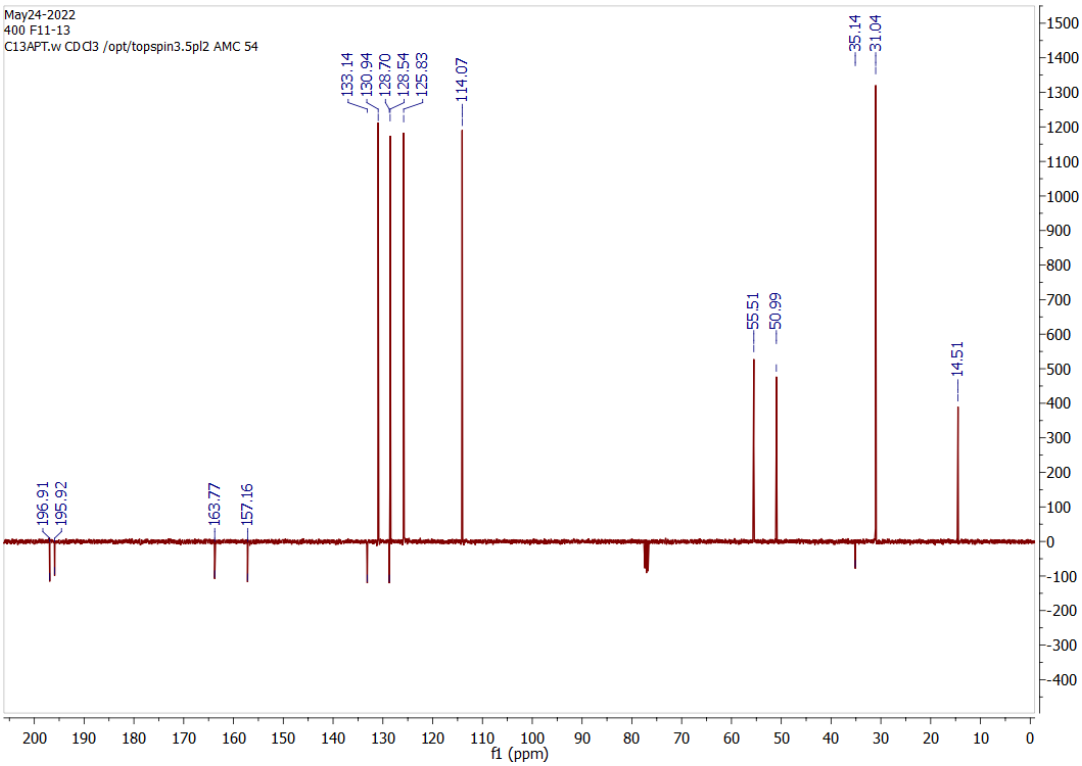

1H NMR of **(E)-3-(4-acetoxy-3,5-dimethoxyphenyl)acrylic acid**

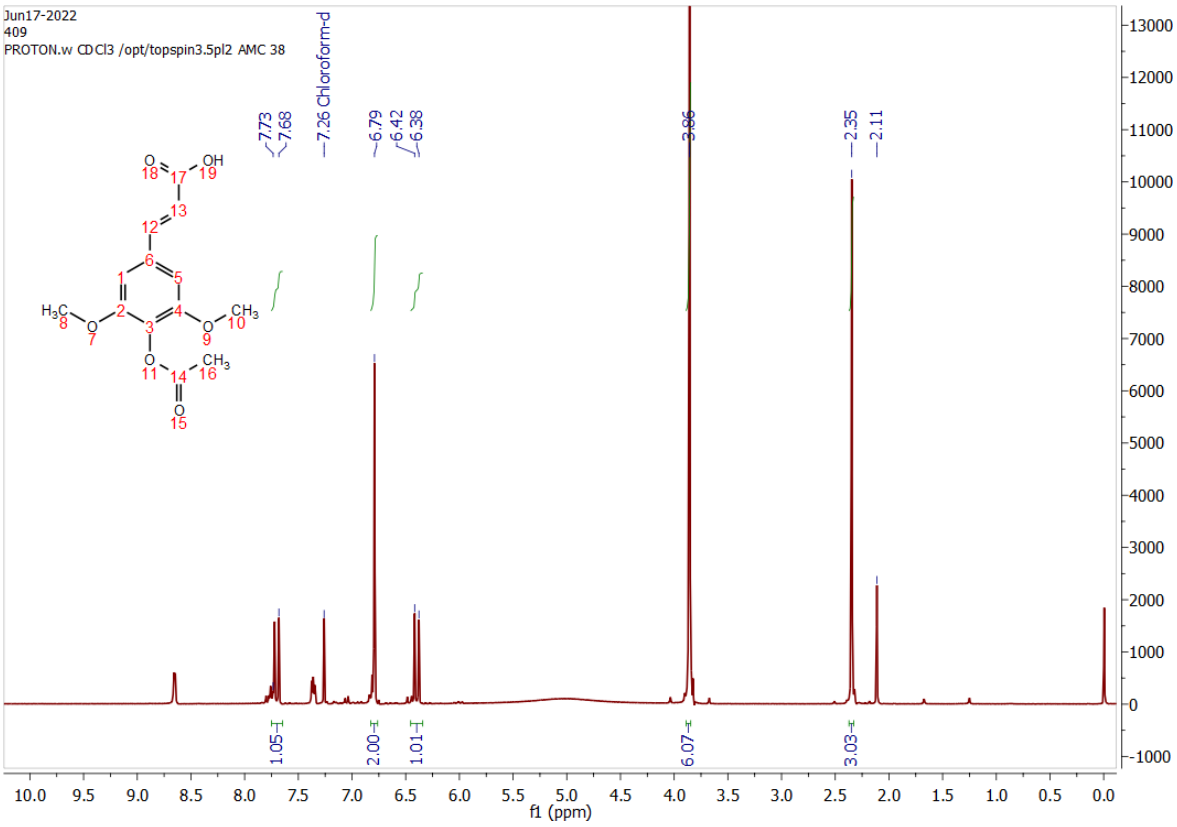

1H NMR of **3-(4-(3-oxo-3-phenylpropanoyl)phenoxy)propyl (E)-3-(4-acetoxy-3,5-dimethoxyphenyl)acrylate (OAc-AVOCINN)**

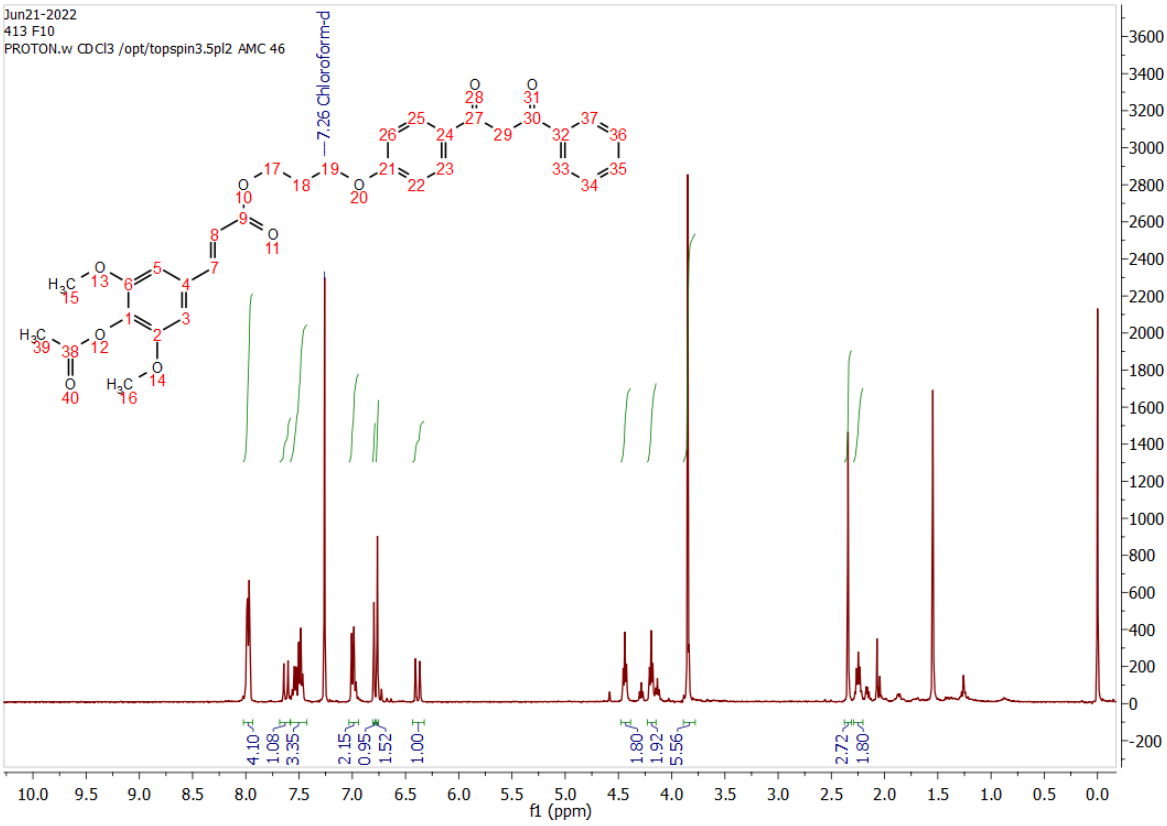

Detail of 1H NMR of **3-(4-(3-oxo-3-phenylpropanoyl)phenoxy)propyl (E)-3-(4-acetoxy-3,5-dimethoxyphenyl)acrylate (AVOCINN)**

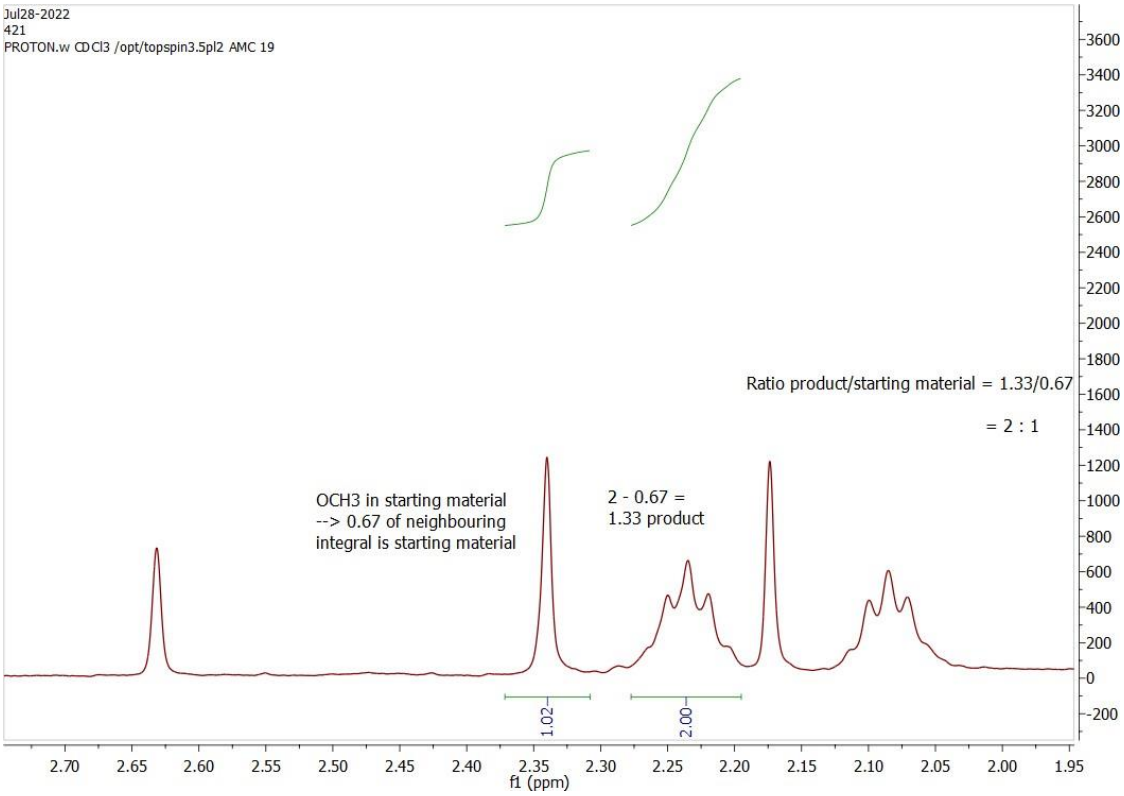

Comparison of 3 hour reflux and 24 hour reflux to starting material 1H NMR

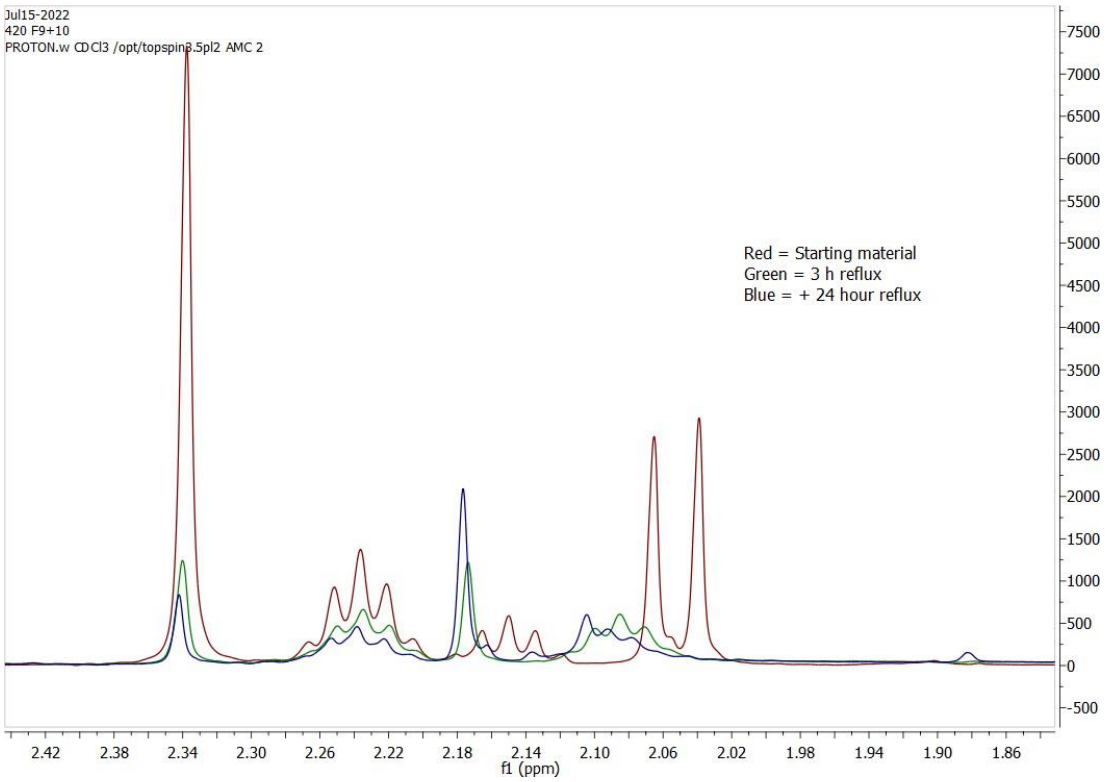

Compound Name	Type	Pubchem CID	λmax (nm)	ε ($M^{-1}.cm^{-1}$)	Molecular Formula	Exact Mass	SMILES	Fragments	Phylum	Antioxidant Activity	DOI 1	DOI 2	DOI 3
4-Deoxygadusol	Mycosporine-like amino-acid precursor	85926716	269	15.7	$C_8H_{12}O_5$	188.0685	OC(CC(CO)(O)C1)=C(OC)C1=O	66.9, 70.0, 85.3, 95.0, 113.4, 160.0, 175.2, 189.2	Cnidaria, Equinodermata, Lichen, Chordata	Yes	10.1007/s00726-015-2069-z	10.1016/S0040-4039(01)83784-9	10.1002/bscb.19800891212
Gadusol	Mycosporine-like amino-acid precursor	195955	268	12.4	$C_8H_{12}O_6$	204.0634	OC(CC(CO)(O)C1O)=C(OC)C1=O	58.3, 84.8, 117.5, 145.2, 160.0, 175.1, 203.7, 204.9, 205.4	Arthropoda Chordata Lichen	Yes	10.1007/s00726-015-2069-z	10.1002/bscb.19800891212	10.1042/bj1990741
Mycosporine-ethanolamine	Oxo-mycosporine		310		$C_{10}H_{17}NO_5$	231.1107	O=C1CC(CO)(O)CC(NCCO)=C1OC	-	Porifera		10.1246/cl.170490		
Mycosporine-glycine	Oxo-mycosporine	14444486	310	28.1	$C_{10}H_{15}NO_6$	245.0899	O=C1CC(CO)(O)CC(NCC(O)=O)=C1OC	57.1, 84.9, 100.1, 117.7, 143.9, 171.2, 231.7, 246.4	Arthropoda Chlorophyta, Chordata, etc.	Yes	10.1007/s00726-015-2069-z	10.1016/S0040-4039(01)83784-9	10.1002/rcm.8634
Mycosporine-alanine	Oxo-mycosporine		310	640	$C_{11}H_{17}NO_6$	259.1056	O=C1CC(CO)(O)CC(NC(C)C(O)=O)=C1OC	147, **171**, 42, 260,1	Cyanobacteria, Fungi	Yes	10.1016/0147-5975(92)90043-Q	10.1016/j.jphotobiol.2021.112302	

Mycosporine-β-alanine	Oxo-mycosporine		-	-	$C_{11}H_{17}NO_6$	259.1056	O=C1CC(CO)(O)CC(NCCC(O)=O)=C1OC	260.1	Cnidaria		10.3390/antiox4030603		
Mycosporine-serinol	Oxo-mycosporine	442866	310	27.27	$C_{11}H_{19}NO_6$	261.1212	O=C1CC(CO)(O)CC(NC(CO)CO)=C1OC	184, 194, 212.1, 216, 243.1, 262.1	Fungi, Cyanobacteria		10.1017/CBO9780511732263.015	10.1016/j.jchromb.2009.05.040	
Mycosporine-GABA	Oxo-mycosporine		310	28.9	$C_{12}H_{20}NO_6$	273.1212	O=C1CC(CO)(O)CC(NCCCC(O)=O)=C1OC	87.1, 137.1, 186.2, 274.1	Cyanobacteria, Dinoflagellata	Yes	10.1016/j.jphotobiol.2014.12.008	10.1002/rcm.8634	10.3390/antiox4030603
Mycosporine-serine	Oxo-mycosporine		310	-	$C_{11}H_{17}NO_7$	275.1005	O=C1CC(CO)(O)CC(NC(C(O)=O)CO)=C1OC	228, 236, 258, 276.1	Fungi		10.3390/antiox4030603	10.3390/antiox4030603	
Mycosporine-2	Oxo-mycosporine	101324823	310	-	$C_{13}H_{19}NO_6$	285.1212	O=C1CC(CO)(O)CC(N2C(CO)CCC2=O)=C1OC	286.1	Fungi		10.1016/0031-9422(81)85273-9		
Mycosporine-taurine	Oxo-mycosporine		309	28.1	$C_{10}H_{17}NO_7S$	295.0726	O=C1CC(O)(CO)CC(NCCS(=O)(O)=O)=C1OC	57.1, 186.2, 236.1, 263.3, 277.2, 296.2	Cnidaria, Cyanobacteria, Lichen		10.1007/s00726-015-2069-z	10.1007/BF00699229	10.1016/j.jphotobiol.2006.10.006
Normycosporine-glutamine	Oxo-mycosporine		320	-	$C_{12}H_{18}N_2O_7$	302.1114	OC1=C(NC(C(O)=O)CCC(N)=O)CC(CO)(O)CC1=O	303.1	Fungi		10.3390/antiox4030603	10.1016/S0031-9422(00)82614-X	
Mycosporine-ornithine	Oxo-mycosporine		310	-	$C_{13}H_{22}N_2O_6$	302.1478	O=C1CC(O)(CO)CC(NCCCC(C(O)=O)N)=C1OC	191.1, 235.2, 267.0, 303.2	Cyanobacteria		10.1002/rcm.8634	10.1128/AEM.01632-16	

Mycosporine-glutaminol	Oxo-mycosporine	101835613	310	12.542	$C_{13}H_{22}N_2O_6$	302.1478	O=C1CC(O)(CO)CC(NC(CO)CCC(N)=O)=C1OC	235, 267, 285, 303.2	Cyanobacteria, Fungi, Lichen		10.1515/znc-1985-9-1004	10.1016/S0031-9422(00)83866-2	
Normycosporine-glutamic acid (artifact)	Oxo-mycosporine		320	-	$C_{12}H_{17}NO_8$	303.0954	OC1=C(NC(C(O)=O)CCC(O)=O)CC(CO)(O)CC1=O	304.1	Fungi		10.1016/S0031-9422(00)82614-X		
Mycosporine-glutamicol	Oxo-mycosporine	9882880	310	17.248	$C_{13}H_{21}NO_7$	303.1318	O=C1CC(CO)(O)CC(NC(CO)CCC(O)=O)=C1OC	178, 210, 236, 258, 268, 286, 304.1	Fungi, Lichen		10.1016/S0031-9422(00)82614-X	10.1016/j.phytochem.2011.04.002	
Mycosporine-glutamine	Oxo-mycosporine	101835612	310	-	$C_{13}H_{20}N_2O_7$	316.1271	O=C1CC(CO)(O)CC(NC(C(O)=O)CCC(N)=O)=C1OC	317.1	Fungi		10.1016/S0031-9422(00)82614-X		
Mycosporine-lysine	Oxo-mycosporine		310	-	$C_{14}H_{24}N_2O_6$	316.1634	O=C1CC(CO)(O)CC(NCCCCC(N)C(O)=O)=C1OC	281.1, 317.2	Cyanobacteria		10.1128/AEM.01632-16		
Mycosporine-glutamic acid	Oxo-mycosporine	102095611	311	20.9	$C_{13}H_{19}NO_8$	317.1111	O=C1CC(CO)(O)CC(NC(C(O)=O)CCC(O)=O)=C1OC	225, 281, 299, 318.1	Fungi		10.1021/ja00206a059	10.1016/S0031-9422(00)82614-X	10.1016/S0031-9422(00)82419-X
Mycosporine-hydroxyglutamicol	Oxo-mycosporine	101805382	310	-	$C_{13}H_{21}NO_8$	319.1267	O=C1CC(CO)(O)CC(NC(CO)C(O)CC(O)=O)=C1OC	320.1	Lichen		10.1016/j.phytochem.2011.04.002		
Prasiolin	Oxo-mycosporine	132581102	324	12.393	$C_{13}H_{19}NO_9$	333.1060	O=C1C(O)C(CO)(O)CC(NC(CCC(O)=O)C(O)=O)=C1OC	334.1	Chlorophyta		10.1007/s00425-015-2396-z		

Palythine	Imino-mycosporine	16047608	320	35,500-36,200	$C_{10}H_{16}N_2O_5$	244.1059	N=C1CC(CO)(O)CC(NCC(O)=O)=C1OC	137.2, 168.2, 185.9, 198.9, 209.2, 230.2, 245.1	Arthropoda etc.	Yes	10.3390/md18010043	10.1002/rcm.8634	10.1007/BF01313484
N-methylpalythine (Aplysiapalythine C)	Imino-mycosporine		330	-	$C_{11}H_{18}N_2O_5$	258.1216	CNC1=C(OC)/C(CC(CO)(O)C1)=N/CC(O)=O	259.1	Cyanobacteria, Mollusca		10.1002/rcm.8634	10.1002/hlca.201100117	
Aplysiapalythine D	Imino-mycosporine		330	-	$C_{11}H_{18}N_2O_5$	258.1216	N=C1CC(CO)(O)CC(N(C)CC(O)=O)=C1OC	259.1	Cyanobacteria		10.1111/fwb.13627		
Dehydroxyl-usujirene	Imino-mycosporine		356	-	$C_{13}H_{19}N_2O_4$	267.1345		209, 224, 268.2	Cyanobacteria		10.1016/j.jphotobiol.2006.10.006		
N-ethylpalythine (Aplysiapalythine B)	Imino-mycosporine		332	-	$C_{12}H_{20}N_2O_5$	272.1372	OC(CC(NCC)=C/1OC)(CO)CC1=N/CC(O)=O	273.1	Mollusca, Rhodophyta		10.3390/md18010043	10.1002/hlca.201100117	10.1111/jpy.12827
Palythine-serine	Imino-mycosporine		320	10.5	$C_{11}H_{18}N_2O_6$	274.1165	N=C1CC(CO)(O)CC(NC(CO)C(O)=O)=C1OC	260, 275.1	Cnidaria, Cyanobacteria		10.1002/rcm.8634	10.1016/S0040-4039(97)01281-1	
Usujirene (cis isomer)	Imino-mycosporine		357	-	$C_{13}H_{20}N_2O_5$	284.1372	OC(CC(N/C=C\C)=C/1OC)(CO)CC1=N/CC(O)=O	197, 226, 241, 270, 285.1	Rhodophyta	Yes	10.3390/md18010043	10.3390/antiox4030603	
Palythene (trans isomer)	Imino-mycosporine		360	50	$C_{13}H_{20}N_2O_5$	284.1372	OC(CC(N/C=C/C)=C/1OC)(CO)CC1=N/CC(O)=O	139.1, 185.0, 197.3, 205.0,	Arthropoda etc.	Yes	10.1007/s00726-015-2069-z	10.3390/md18010043	10.1007/BF01313484

								223.0, 241.2, 285.0					
Mycosporine methylamine serine (N-methylmycosporine-serine)	Imino-mycosporine		325	16.6	$C_{12}H_{20}N_2O_6$	288.1321	OC(CC(NC(CO)C(O)=O)=C/1OC)(CO)CC1=N/C	274, 289.1	Cnidaria		10.1016/S0040-4039(97)01281-1		
Palythine–threonine	Imino-mycosporine		320	-	$C_{12}H_{20}N_2O_6$	288.1321	N=C1CC(CO)(O)CC(NC(C(C)O)C(O)=O)=C1OC	169, 172, 230, 245, 256, 274, 289.1	Cnidaria, Cyanobacteria		10.1002/rcm.8634	10.1016/j.jphotobiol.2008.12.001	10.3390/md11093124
Asterina-330	Imino-mycosporine	13194807	330	43.8	$C_{12}H_{20}N_2O_6$	288.1321	OC(CC(NCC(O)=O)=C/1OC)(CO)CC1=N/CCO	137, 167.8, 186.0, 198.4, 230.2, 243.1, 273.1, 289.2	Arthropoda Chlorophyta, etc.	Yes	10.1007/s00726-015-2069-z	10.3390/md18010043	10.3354/meps189035
Mycosporine-2-glycine	Imino-mycosporine	23427657	334		$C_{12}H_{18}N_2O_7$	302.1114	OC(CC(NCC(O)=O)=C/1OC)(CO)CC1=N/CC(O)=O	151.1, 164.1, 185.1, 200.1, 244.1, 288.1, 303.1	Bacillariophyta, Cnidaria, Cyanobacteria, Echinodermata, Mollusca, Rhodophyta	Yes	10.3390/md18010043	10.1007/BF00699229	10.1111/j.1574-6968.2002.tb11087.x

Palythinol	Imino-mycosporine	9948334	332	43.5	$C_{13}H_{22}N_2O_6$	302.1478	OC(CC(NCC(O)=O)=C/1OC)(CO)CC1=N/C(CO)C	102.2, 150.0, 186.1, 199.2, 243.2, 288.0, 303.5	Chlorophyta, Lichen, Phaeophyta, Porifera, Rhodophyta	No	10.1007/s00726-015-2069-z	10.3390/md18010043	10.1007/BF01313484
Asterina-methyl ester	Imino-mycosporine		330		$C_{13}H_{22}N_2O_6$	302.1478	OC(CC(NC(C)C(O)=O)=C/1OC)(CO)CC1=N/CCO	303.2	Dinoflagellata		10.1111/j.1529-8817.2011.01046.x		
N-isopropanolpalythine (Aplysiapalythine A)	Imino-mycosporine		332		$C_{13}H_{22}N_2O_6$	302.1478	OC(CC(NCC(O)=O)=C/1OC)(CO)CC1=N/CC(C)O	303.2	Mollusca, Rhodophyta		10.3390/md18010043	10.1002/hlca.201100117	
Mycosporine-methylamine-threonine	Imino-mycosporine		327	33.3	$C_{13}H_{22}N_2O_6$	302.1478	OC(CC(NC(C(C)O)C(O)=O)=C/1OC)(CO)CC1=N/C	303.2	Cnidaria, Rhodophyta		10.3390/md18010043	10.1016/0040-4039(95)00950-H	
Palythine-glutamine (Bostrychine-A)	Imino-mycosporine		322		$C_{13}H_{21}N_3O_6$	315.1430	N=C1CC(CO)(O)CC(NC(C(O)=O)CCC(N)=O)=C1OC	316.1	Rhodophyta		10.3390/md17060356		
Palythine-glutamic acid (Bostrychine-C)	Imino-mycosporine		322	22.351	$C_{13}H_{20}N_2O_7$	316.1271	N=C1CC(CO)(O)CC(NC(C(O)=O)CCC(O)=O)=C1OC	317.1	Rhodophyta		10.3390/md17060356		
Mycosporine-glycine-alanine	Imino-mycosporine	102110164	333	-	$C_{13}H_{20}N_2O_7$	316.1271	OC(CC(NCC(O)=O)=C/1OC)(CO)CC1=N/C(C(O)=O)C	186, 214, 258, 302, 317.1	Cyanobacteria, Rhodophyta		10.3390/md18010043	10.4490/algae.2020.35.5.19	
Palythenic acid	Imino-mycosporine	101016648	337	29.2	$C_{14}H_{20}N_2O_7$	328.1271	OC(CC(N/C(C(O)=O)=C/C)=C/1OC)(CO)C	138, 193, 197,	Dinoflagellata, Mollusca,	No	10.3390/md18010043	10.1002/rcm.8634	10.1007/s002270100654

							C1=N/CC(O)=O	205, 237, 268, 283, 296, 329.1	Rhodophyta				
Euhalothece-362	Imino-mycosporine	102182144	362	-	$C_{14}H_{22}N_2O_7$	330.1427	OC(CC(NC(C)C(O)=O)=C/1OC)(CO)CC1=N/C=C(CO)/O	213.1, 228.1, 242.1, 272.1, 316.1, 331.1	Cyanobacteria		10.1111/j.1574-6968.2002.tb11087.x	10.1111/j.1574-6968.2006.00203.x	
Mycosporine-glutamicol ethyl ester	Imino-mycosporine		310	21.295	$C_{15}H_{25}NO_7$	331.1631	O=C1CC(CO)(O)CC(NC(CO)CCC(OCC)=O)=C1OC	218, 264, 286, 314, 332.2	Fungi, Lichen				
Shinorine	Imino-mycosporine	101926676	334	44.668	$C_{13}H_{20}N_2O_8$	332.1220	OC(CC(NCC(O)=O)=C/1OC)(CO)CC1=N/C(C(O)=O)CO	137.1, 186.2, 230.0, 241.3, 255.0,	Arthropoda Bacillariophyta, etc.	No	10.1007/s00726-015-2069-z	10.3390/md18010043	10.1002/rcm.8634
Mycosporine-glycine-valine	Imino-mycosporine	101016647	335		$C_{15}H_{24}N_2O_7$	344.1584	OC(CC(NCC(O)=O)=C/1OC)(CO)CC1=N/C(C(O)=O)C(C)C	116.0, 118.1, 130.6, 183.9, 198.1, 268.2, 295.0, 313.0	Arthropoda, Cnidaria, Chordata, Echinodermata, Lichen, Mollusca, Porifera		10.1007/s00726-015-2069-z	10.1007/BF01313484	

Porphyra-334	Imino-mycosporine	91864535	334	42.3	$C_{14}H_{22}N_2O_8$	346.1376	OC(CC(NC(C(O)C)C(O)=O)=C/1OC)(CO)CC1=N/CC(O)=O	137, 151, 168, 186, 227, 243, 288, 303, 332, 347.1	Arthropoda Bacillariophyta, etc.	Yes	10.3390/md18010043	10.1002/rcm.8634	10.3354/meps189035
Mycosporine-serine-glycine methyl ester (Shinorine methyl ester)	Imino-mycosporine		332	-	$C_{14}H_{22}N_2O_8$	346.1376	OC(CC(NC(C)C(O)=O)=C/1OC)(CO)CC1=N/C(C(O)=O)CO	244, 269, 288, 314, 332, 347.3	Dinoflagellata		10.1111/jpy.12076		
Palythine-serine-sulfate	Imino-mycosporine		321	-	$C_{11}H_{18}N_2O_9S$	354.0733	N=C1CC(CS(=O)(OO)=O)(O)CC(NC(CO)C(O)=O)=C1OC	355.1	Cnidaria		10.1016/S0040-4039(97)00391-2		
Mycosporine-glycine-aspartic acid	Imino-mycosporine		333	-	$C_{14}H_{20}N_2O_9$	360.1169	OC(CC(NC(CC(O)=O)C(O)=O)=C/1OC)(CO)CC1=N/CC(O)=O	361.1	Arthropoda		10.1016/0305-0491(85)90457-2		
Mycosporine-threonine-β-alanine (Bostrychine-F)	Imino-mycosporine		332	44.994	$C_{15}H_{24}N_2O_8$	360.1533	OC(CC(NCCC(O)=O)=C/1OC)(CO)CC1=N/C(C(C)O)C(O)=O	361.2	Rhodophyta,		10.3390/md17060356		
Palythine-threonine-sulfate	Imino-mycosporine		321	-	$C_{12}H_{20}N_2O_9S$	368.0890	N=C1CC(CS(=O)(OO)=O)(O)CC(NC(C(C)O)	369.1	Cnidaria		10.1016/S0040-		

							C(O)=O)=C1OC				4039(97)00391-2		
Mycosporine-glycine-glutamic acid	Imino-mycosporine	102446627	330	43.9	$C_{15}H_{22}N_2O_9$	374.1325	OC(CC(NC(CC(O)=O)C(O)=O)=C/1OC)(CO)CC1=N/CC(O)=O	118.2, 176.0, 192.2, 228.3, 258.1, 297.1, 331.2, 375.3	Cnidaria, Lichen, Rhodophyta,		10.1007/s00726-015-2069-z	10.3390/md17060356	10.1016/S0742-8413(96)00135-1
Mycosporine-threamine-glutamic acid (Bostrychine-E)	Imino-mycosporine		333	21.618	$C_{16}H_{26}N_2O_8$	374.1689	OC(CC(NCC(O)C)=C/1OC)(CO)CC1=N/C(CCC(O)=O)C(O)=O	375.2	Rhodophyta,		10.3390/md17060356		
Catenellin e	Imino-mycosporine		320	-	$C_{13}H_{22}N_2O_9S$	382.1046	OC(CC(NCCS(O)(=O)=O)=C/1OC)(CO)CC1=N/C(C(O)=O)CO	383.1	Rhodophyta,		10.3390/md18010043	10.3390/md13106291	
M-343	Imino-mycosporine		343	-	-	386		387	Cyanobacteria,		10.1016/j.jphotobiol.2006.10.006		
Mycosporine-threonine-glutamine (Bostrychine-B)	Imino-mycosporine		335	36.155	$C_{17}H_{27}N_3O_9$	417.1747	OC(CC(NC(C(O)=O)CCC(N)=O)=C/1OC)(CO)CC1=N/C(C(O)=O)C(O)C	418.2	Rhodophyta,		10.3390/md17060356		
Mycosporine-threonine-glutamic	Imino-mycosporine		337	31.956	$C_{17}H_{26}N_2O_{10}$	418.1587	OC(CC(NC(C(O)=O)CCC(O)=O)=C/1OC)(	419.1	Rhodophyta,		10.3390/md17060356		

acid (Bostrychine-D)							CO)CC1=N/C(C(O)=O)C(O)C						
Klebsormidin B	Glycosylated Oxo-mycosporine		324	-	$C_{12}H_{19}NO_8$	305.1111	O=C1C(O)C(O)(CO)CC(N(C)C(C(O)=O)CO)=C1OC	306.1	Charophyta		10.3389/fmicb.2020.00499		
Klebsormidin A	Glycosylated Oxo-mycosporine		324	-	$C_{18}H_{29}NO_{13}$	467.1639	O=C1C(O)C(O)(CO)CC(N(C)C(C(O)=O)COC2OC(CO)C(O)C(O)C2O)=C1OC	468.2	Charophyta		10.3389/fmicb.2020.00499		
Hexose-palythine-serine	Glycosylated Imino-mycosporine		320	-	$C_{17}H_{28}N_2O_{11}$	436.1693	N=C1CC(O)(CO)CC(NC(COC2C(CO)OC(O)C(O)C2O)C(O)=O)=C1OC	142, 171, 207, 239, 241, 245, 257, 275, 378, 391, 407, 422, 437.2	Cyanobacteria,		10.1002/rcm.8634	10.1128/AEM.01633-16	
Hexose-bound palythine-threonine	Glycosylated Imino-mycosporine		322	-	$C_{18}H_{30}N_2O_{11}$	450.1850	OC(CC(NC(C(O)=O)C(C)O)=C1OC)(COC2OC(CO)C(O)C(O)C2O)CC1=N	185.2, 289.2, 349.2, 389.2, 407.2	Cyanobacteria,		10.1002/rcm.8634	10.3390/md11093124	
Pentose-bound shinorine	Glycosylated Imino-mycosporine		332	-	$C_{18}H_{28}N_2O_{12}$	464.1642	OC(C/1)(COC2OC(CO)C(O)C2O)CC(NC(C(O)=O)CO)=C(	211.3, 333.3, 377.1, 421.1, 465.1	Cyanobacteria,		10.1016/j.jphotobiol.2014.12.008		

							OC)C1=N\CC(O)=O						
Mycosporine-glutamino l-O-glucoside	Glycosylated Imino-mycosporine		310	25	$C_{19}H_{32}N_2O_{11}$	464.1642	OC(C/1)(COC2OC(CO)C(O)C2O)CC(NC(C(O)=O)CO)=C(OC)C1=N\CC(O)=O	303, 428, 446, 465.0	Fungi		10.1016/S0031-9422(00)82614-X	10.1002/yea.1148	10.1002/rcm.997
Mycosporine-glutamicol-O-glucoside (478 Da MAA)	Glycosylated Imino-mycosporine		310	25	$C_{19}H_{31}NO_{12}$	465.1846	O=C1CC(CO)(O)CC(NCC(COC2C(O)C(O)C(O)OC2CO)CC(O)=O)=C1OC	304, 466.2	Fungi		10.1002/rcm.997	10.1016/0031-9422(81)85272-7	
Hexose-shinorine	Glycosylated Imino-mycosporine		333	-	$C_{19}H_{30}N_2O_{13}$	494.1748	OC(C/1)(CO)CC(NCC(OC2C(CO)OC(O)C(O)C2O)=O)=C(OC)C1=N\C(C(O)=O)CO	186, 230, 265, 274, 287, 300, 303, 318, 333, 392, 436, 365, 480, 495.2	Cyanobacteria,		10.1128/AEM.01633-16		
Collemin A	Glycosylated Imino-mycosporine	10074531	311	34	$C_{19}H_{32}N_2O_{13}$	496.1904	OC(C(C(C(CO)O1)O)O)C1OC(C2O)NC(OC3C(C(O)=C(N)CC3CO)=O)C2OCCO	95.0, 198.1, 235.8, 300.2, 340.2, 409.1,	Lichen		10.1007/s00726-015-2069-z	10.1111/j.1432-1033.2004.03981.x	

								435.0, 497.2					
13-O-(β-galactosyl)-porphyra-334	Glycosylated Imino-mycosporine		334	-	$C_{20}H_{32}N_2O_{13}$	508.1904	OC(C/1)(CO)CC(NCC(O)=O)=C(OC)C1=N\C(C(O)=O)C(OC2OC(CO)C(O)C(O)C2O)C	347.1, 509.2	Cyanobacteria,	Yes	10.1016/j.jphotobiol.2017.05.019	10.3390/antiox4030603	
Hexose-bound porphyra-334	Glycosylated Imino-mycosporine		334	36.3	$C_{20}H_{32}N_2O_{13}$	508.1904	O[C@@](CC(NC(C(O)=O)C(C)O)=C/1OC)(COC2OC(CO)C(O)C(O)C2O)CC1=N/CC(O)=O	303.2, 347.2, 361.2, 421.2, 465.2, 509.2	Cyanobacteria,	Yes	10.3390/md11093124	10.3390/antiox4030603	
586-Da MAA	Glycosylated Imino-mycosporine		332	-	$C_{26}H_{42}N_4O_{11}$	586.2850	OC(C/1)(CO)CC(NCCCC(C(O)=O)NC2=C(OC)C(CC(CO)(O)C2)=O)=C(OC)C1=N\CCCC(N)C(O)=O	417.2, 428.2, 472.2, 499.3, 525.3, 543.3, 569.4, 587.3	Cyanobacteria,		10.1111/pre.12333		
Glycosylated Palythine-threonine (612-Da MAA)	Glycosylated Imino-mycosporine		324	28.2	$C_{24}H_{40}N_2O_{16}$	612.2378	OC(CC(NC(C(O)=O)C(C)OC1OC(CO)C(O)C(O)C1O)=C2OC)(COC3OC(CO)C(O)C(O)C3O)CC2=N	187.2, 289.2, 349.1, 389.2, 407.2, 451.2, 569.2, 613.2	Cyanobacteria,	Yes	10.3390/md11093124	10.3390/antiox4030603	
Nostoc-756 (756-Da MAA)	Glycosylated Imino-mycosporine		313	-	$C_{34}H_{52}N_4O_{15}$	756.3429	OC(C/1)(CO)CC(NCCCC(C(O)=O)NC2=C(OC)C(CC(CO)(O)C2)=O)=C(OC	454.1, 516.1, 552.1, 603.1, 639.1,	Cyanobacteria,		10.1111/pre.12333		

							)C1=N\CCCC(NC3=C(OC)C(CC(CO)(O)C3)=O)C(O)=O	657.1, 694.9, 757.2					
880-Da MAA	Glycosylated Imino-mycosporine		331	49.8	$C_{37}H_{60}N_4O_{20}$	880.3801	OC(C/1)(COC2OC(COC3OC(CO)C(O)C3O)C(O)C(O)C2O)CC(NCCCC(C(O)=O)NC4=C(OC)C(CC(CO)(O)C4)=O)=C(OC)C1=N\CCCC(N)C(O)=O	445.3, 489.3, 533.3, 737.4, 795.5, 837.5, 881.4	Cyanobacteria,	Yes	10.1016/j.jphotobiol.2014.12.008	10.3390/antiox4030603	
1050-Da MAA	Glycosylated Imino-mycosporine		312/340	58.8	$C_{45}H_{70}N_4O_{24}$	1050.4380	OC(C/1)(COC2OC(COC3OC(CO)C(O)C3O)C(O)C(O)C2O)CC(NCCCC(C(O)=O)NC4=C(OC)C(CC(CO)(O)C4)=O)=C(OC)C1=N\CCCC(NC5=C(OC)C(CC(CO)(O)C5)=O)C(O)=O	410.4, 437.1, 481.1, 501.0, 581.9, 722.3, 766.3, 963.4, 1051.4	Cyanobacteria,	Yes	10.1016/j.jphotobiol.2011.07.003	10.3390/antiox4030603	

8.3 Amino acid sequences

```
MDINTETEESSTESIIEFPLSETQRKAWFLSKLELQGCTDKIAFAIHWRQQVNVECLKQAFEIVIARHPSLHTAYRDKHGELVQQVLATTTAEIN
1         10        20        30        40        50        60        70        80        90

FVDASNWSEDKLKEKILDSSQHPFDLAVGSVVRMSLFSRTPTTHVLLLVVHCIASDTWGLLLLLDELLTLYHQLKSNTAISLSSLTSSYQDYVKQ
    100       110       120       130       140       150       160       170       180       190

EINLLNSPEGKQLGHYWQQYLAGELPTLELPSARSRSPIRSYKGACYKFSIAPDITDKVRYLAITEDVDLSTVVLSAFQLMLYRYTATENILVGL
        200       210       220       230       240       250       260       270       280

LPQRYQSEFKNVVGNFANSAVVKLAISGDVSFQRYLSQIQFAVAETIAHQAYPFPLLVRQLQLNSQLSHPPICQVGFAYHHLHELKIISKLFDEN
    290       300       310       320       330       340       350       360       370       380

FGELEYFEIPRQRTEFDLSLEILESQESLIGFLYYNSDLLDADTIARAAEHLQNLLVAIIANPQQLVARLPLLSDRE
        390       400       410       420       430       440       450       457
```

Amino acid sequence of the *Chlorogloeopsis fritschii* C domain

```
MDINTETETSHIQQANWFLYKFQPTGLSDKLSIAVRIKSPVDIKTIETTLQALTERHAILRSIYYEEDGQIIQKIRDTADIYLAKIDASSWSDEE
1         10        20        30        40        50        60        70        80        90

LNEQLSQRIKLPFNLENGSIFRACLFTRSATDYILVLTLHQIAADWESLLILVDDLVGIYESTINCKPPNLLPINKSYRDYIHQEVEFINSVEGK
    100       110       120       130       140       150       160       170       180       190

QIGKYWRENLADDLPVLELPTTSPRPSMRTYDGAAIKFTINPELTQQLKQLVKTQGVTIEEILLAVFKVLLYRYTGEQDILVALLQKRANRLLFE
        200       210       220       230       240       250       260       270       280

QVVGNFNNVTVARQAISATIKFTDLLNQVRQQLFELDRYQNYPFSLLIQELKSYTLSHPPICQVAFGYSQLDKLFNAQEIDIEYYEIPQQKVDFE
    290       300       310       320       330       340       350       360       370       380

LSLEVTDLQSYSLGYFKYNTDILEAETVAKIAEHFQNLLTAFVANPDTPVGKLPMLSDGE
        390       400       410       420       430       440
```

Amino acid sequence of the *Moorea producens* C domain